Role of Pax8 and thyroid hormones in metabolic homeostasis

CABIMER,

Department of Regeneration and Cell therapy.

Thesis presented by Livia López Noriega for the degree of Doctor of Philosophy.

Seville, 11 May 2018

Directors:

Alejandro Martín Montalvo

Benoit Gauthier

Tutor:

Benoit Gauthier

ABSTRACT

Two independent studies indicated that PAX8 could play a role in glucose homeostasis and pancreatic islet physiology. Pax8 expression was reported in murine islets during gestation while a genome-wide study associated a polymorphism nearby PAX8 with type 2 diabetes. In addition, Pax8 is necessary for the synthesis of thyroid hormones, which are known to exert profound effects in whole body metabolism. Herein, we show that PAX8 protects pancreatic islets from apoptosis and have identified a detrimental polymorphism that may be associated with gestational diabetes as well as gestational thyroid dysfunction. However, Pax8 +/- female mice did not develop glucose intolerance during pregnancy and displayed normal circulating T4 levels at 5 months old. In contrast to females, Pax8 +/- male mice showed decreased T4 levels in blood. However, these mice were 8 months old; suggesting that the reduction in circulating T4 levels in Pax8 +/- animals may be developed with advancing age. Interestingly, untreated Pax8 +/- male mice showed glucose intolerance and insulin resistance, while T4 supplementation rescued the phenotype. Therefore, our results indicate that the alterations observed in glucose homeostasis are due to reduced T4 levels in circulation. Noteworthy, insulin signaling was preferentially impaired in the liver of Pax8 +/- male mice, where ROS production was found significantly increased. We next sought to investigate whether T4 supplementation could enhance glucose homeostasis in healthy wild type animals. Remarkably, T4 treatment was found to enhance glucose clearance and increase insulin expression in pancreatic islets. Basal circulating insulin concentration was also higher in T4-treated mice, which could be explained by an upregulation of glucokinase expression in pancreatic islets from these animals. Importantly, T4 supplementation also increased circulating insulin levels and insulin content in pancreatic islets in a model of experimental autoimmune diabetes. In addition, T4 supplementation improved the survival rate of mice treated with streptozotocin. Therefore, our results indicate that reduced circulating T4 levels are associated with impaired glucose homeostasis whereas T4 supplementation enhances glucose clearance and blunts the onset of experimental autoimmune diabetes.

TABLE OF CONTENTS

LIST OF FIGURES

LIST OF ABREVIATIONS

ABTS	2,2'-azino-bis (3-ethylbenzothiazoline-6-sulphonic acid
ACC	Acetyl-CoA carboxylase
AgRP	Agouti-related peptide
AMPK	AMP-activated protein kinase
APC	antigen presenting cells
APS	adapter protein containing PH and Src homology 2 domains
ARX	Aristaless related homeobox
AS160	AKT substrate of 160 kDa
ATP	Adenosine triphosphate
BAT	Brown adipose tissue
BCL-2	B-cell lymphoma 2
BIRC5	Baculoviral IAP Repeat-Containing 5
BMR	Basal metabolic rate
BSA	Bovine serum albumin
cAMP	cyclic AMP
CAP	c-Cbl associated protein
CaRT	cocaine- and amphetamine-regulated transcript
CD36	fatty acid translocase cluster determinant 36
CoQ	Coenzyme Q
CPE	Carboxypeptidase E
CPT1	carnitine palmitoyl transferase 1
D1/D2/D3	Deiodinase 1/ deiodinase 2/ deiodinase 3
DAB	3,3′-diaminobenzidine
DAG	diglycerides
DIT	diiodotyrosine
DM	Diabetes Mellitus
DTNB	5,5'-Dithiobis-(2-Nitrobenzoic Acid)
EAD	Experimental autoinmune diabetes
E2F1	E2F transcription factor 1
ER	Endoplasmic reticulum

$FADH_2$	Flavin adenine dinucleotide
FASN	Fatty acid synthase
FATP	fatty acid transport protein
FBS	Fetal Bovine Serum
FOXO	Forkhead box O
GAD 65	glutamic acid decarboxylase 65
GAP	GTPase-activating protein
GCK	Glucokinase
GDM	Gestational Diabetes Mellitus
GFP	Green fluorescence protein
GLUT	Glucose transporter
G6Pase	Glucose-6-phosphatase
GPD	glycerophosphate dehydrogenase
GSIS	Glucose stimulated insulin secretion
GSK3β	Glycogen synthase kinase 3 beta
α-GSU	α-glycoprotein hormone subunit
GTD	Gestational thyroid dysfunction
GSV	GLUT4 storage vesicles
HbA1c	Glycated haemoglobin
HBSS	Hanks balance salt solution
HDL	high density lipoprotein
HFD	Hight-fat diet
HIF-1α	Hypoxia inducible factor-1α
HPLC	high performance liquid chromatography
HPT	hypothalamus-pituitary-thyroid
4-HNE	4-hydroxy-2-nonenal
IA-2	islet antigen-2
IFN-γ	Interferon-γ
IL-1β	interleukin-1β
IL-6	Interleukin-6
IPA	Ingenuity Pathway Analysis
IPPTT	Intraperitoneal pyruvate tolerance test

IR	Insulin receptor
IRD	Inner ring deiodination
IRS	Insulin Receptor substrate
ITT	Insulin tolerance test
JNK	Jun NH_2-terminal kinase
KRBH	Krebs-Ringer bicarbonate-HEPES buffer
K_{ATP}	ATP-sensitive K^+ channel
LDL/VLDL	Low density lipoprotein/vey low density lipoprotein
MafA	Maf basic leucine-zipper transcription factor A
MAPK	mitogen-activated protein kinase
ME	malic enzyme
MHC	Major Histocompatibility Complex
MIT	monoiodotyrosine
MLK3	Mixed-lineage protein kinase 3
MOI	Multiplicity of infection
MODY	Maturity onset of the diabetes of the young
MT-COX II	mitochondrial encoded cytochrome c oxidase subunit 2
MT-ND2	mitochondrial encoded NADH dehydrogenase 2
MTP	mitochondrial trifunctional protein
MTT	3-(4,5-dimethylthiazol-2-yl)-2,5-diphenyltetrazolium bromide
mTOR	mammalian target of rapamycin
mTORC2	mammalian target of rapamycin complex 2
NADH	Nicotinamide adenine dinucleotide
NAFLD	Non-alcoholic fatty liver disease
NF-κB	Nuclear factor kappa B
NGN3	Neurogenin 3
NIS	sodium/iodide symporter
NPY	Neuropeptide Y
OGTT	Oral glucose tolerance test
ORD	Outer ring deiodination
OXPHOS	Oxidative phosphorylation

PAX	Paired box gene
PBS	Phosphate Buffered Saline
PC	Protein convertase
PCR	Polymerase chain reaction
PDE3B	Phosphodiesterase 3B
PDK1	3-phosphoinositide-dependent protein kinase-1
PDX1	Pancreatic and duodenal homeobox 1
PEPCK	Phosphoenolpyruvate carboxykinase
PFKFB1	6-phosphofructo-2-kinase/fructose-2,6-bisphosphatase 1
PGC1α	Peroxisome proliferator-activated receptor γ coactivator-1α
PH	Pleckstrin homology
PI3K	Phosphoinositide 3-kinase
PIP_2	Phosphatidylinositol 4,5-bisphosphate
PIP_3	Phosphatidylinositol (3,4,5)-triphosphate
PKC	Protein kinase C
PLC	phospholipase C
PM	Plasma membrane
POMC	proopiomelanocortin
PP2A	Protein phosphatase 2
ROS	Reactive Oxygen species
RT	Room temperature
RXR	Retinoid X receptor
SABC	HRP-Streptavidin Conjugate
SDS	Sodium dodecyl sulfate
SH2	Src-homology 2
SFFV	Spleen Focus-Forming Virus
SOD	Superoxide dismutases
SNARE	Soluble N-ethylmaleimide-sensitive factor attachment protein receptor
SNAP23	Synaptsomal associated protein 23
SNP	Single nucleotide polymorphisms
SREBP-1c	Sterol regulatory element binding protein -1c

STX4	Syntaxin 4
STZ	Streptozotocin
Syts	Synaptotagmins
T2	3,5-diiodo-L-thyronine
T3	Triiodothyronine
T4	Levothyroxine
T1DM	Type 1 diabetes mellitus
T2DM	Type 2 diabetes mellitus
TAC	Transcriptome analysis console
TCA	Tricarboxylic acid
Tfam	Mitochondrial transcription factor A
Tg	Thyroglobulin
TBST	Tris-buffered saline 1X +0.1% Tween
TEMED	N,N,N’,N’-tetramethylethylenediamine
TH	Thyroid hormone
Th	T helper cells
Thf	follicular T helper cells
TMB	3,3',5,5'-Tetramethylbenzidine
TNF-α	Tumour necrosis factor-α
Tph	Tryptophan hydroxylase
TPO	Thyroperoxidase
TR	Thyroid hormone receptor
TRα1	Thyroid hormone receptor-α1
TRβ1	Thyroid hormone receptor-β1
TRβ2	Thyroid hormone receptor-β2
TRE	Thyroid-hormone response elements
TRH	Thyrotropin-releasing hormone
TSH	Thyroid stimulating hormone
Tunel	terminal deoxynucleotidyl transferase dUTP nick end labelling
UCP	uncoupling protein
VAMP2	Vesicle-associated protein 2
WAT	White adipose tissue

WT	Wild-type
ZnT8	Zinc transporter 8

I. INTRODUCTION

1.1. Pancreatic regulation of glucose homeostasis

Glycaemic control is exquisitely regulated by hormones secreted by the pancreas, which exert effects on multiple target tissues. The pancreas has two principal functions: 1) to facilitate the digestion (exocrine pancreas) and 2) to control glucose homeostasis (endocrine pancreas) (Röder et al., 2016). The exocrine function is mediated by acinar cells that secrete digestive enzymes such as amylase, pancreatic lipase and trypsinogen, through the pancreatic duct into the upper small intestine. The endocrine function is achieved through the secretion of different hormones by the islet of Langerhans. These micro-organs are clusters of endocrine cells (50-3000 cells) that are found scattered throughout the pancreas and account only for 1-2% of the volume or weight of the entire gland (Figure 1).

There are five different types of endocrine cells within pancreatic islets: glucagon-producing α-cells, insulin-producing β-cells, somatostatin-producing δ-cells, pancreatic polypeptide-producing PP-cells and ghrelin-producing ε-cells (Figure 1) (Röder et al., 2016, Rutter et al., 2015). The distribution and abundance of the different cell types varies among species. In rodents, the core of the islet is composed by β-cells (60-80% of the total islet), whereas α-cells (10-20% of the total islet cells), δ-cells and PP-cells (~5% of the total islet cells) as well as ε-cells (<1% of the total islet cells) are located preferentially in the periphery. In contrast, in humans, the different cell types are scattered and the ratio between α- and β- cells is higher. Actually, the final structure of human pancreatic islets is believed to result from the folding of a trilaminar sheet composed by a single layer of β-cells surrounded by two layers of α-cells. This organization is believed to promote

greater contact between α- and β- cells, which may contribute to an enhanced regulation of insulin secretion (Dolenšek et al., 2015).

The five types of endocrine cells arise from the same population of endocrine precursors, characterized by the expression of the transcription factor Neurogenin 3 (Ngn3). Indeed, Ngn3 deficiency results in the loss of all pancreatic endocrine cell types. These endocrine precursors are differentiated into the 5 different cell types according to the expression/repression of several transcription factors (Cano et al., 2014). For instance, the opposing activities of paired box gene 4 (Pax4) and aristaless related homeobox (Arx) are essential in the cell fate choice between α and β cell lineages. Pax4 silencing leads to the loss of β- and δ- cells and an increase in α-cell number. In contrast, Arx inactivation results in the complete loss of α-cells and an increase in β- and δ- cell numbers (Collombat et al., 2003). Furthermore, ectopic expression of Pax4 and/or inactivation of Arx in α-cells, promotes the trans-differentiation of these cells into β-cells (Courtney et al., 2013, Collombat et al., 2009). Once cell fate has been established, subsequent expression of several transcription factors is needed for complete cell maturation and maintenance of specific cell function. In this regard, the expression of the Maf basic leucine-zipper transcription factor A (MafA) is needed for proper maturation of β-cells, but is not required for β-cell fate specification. Actually, MafA knock-out mice have normal pancreatic islets at birth but become hyperglycaemic with age (He et al., 2014). Other genes, such as paired box gene 6 (Pax6), play a role not only in the differentiation of progenitor cells to specific endocrine cell types, but also in maintaining the proper functionality of adult endocrine cells, including α- and β- cells (Gosmain et al., 2012).

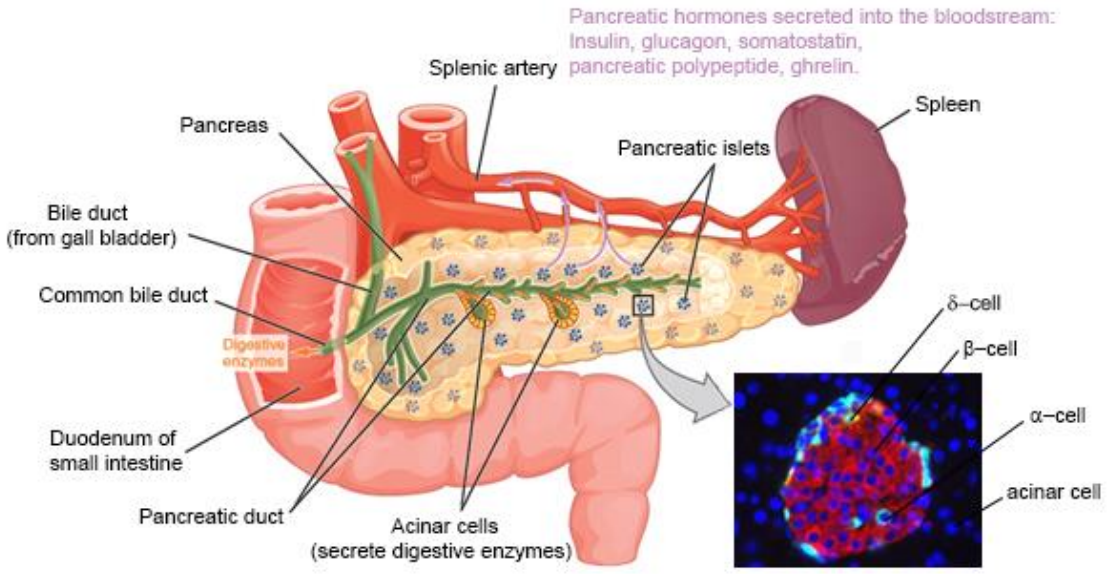

Figure 1. Representation of the pancreas anatomy. The majority of the gland is composed by acinar cells, while endocrine cells are found forming island-like structures scattered through the organ. Representative immunofluorescence image of a pancreatic section from a wild type mouse showing insulin (β-cells), glucagon (α-cells) and somatostatin (δ-cells). Modified from (Röder et al., 2016).

Each of the hormones secreted by the different cell types have a distinct function. Glucagon is secreted in response to low circulating glucose concentration in order to stimulate glycogenolysis and gluconeogenesis in the liver (Thorel et al., 2011). In contrast, insulin is released when glucose levels in blood are high to promote glucose uptake in its target tissues as well as to inhibit hepatic glucose production (Samuel and Shulman, 2016). Somatostatin inhibits both insulin and glucagon, preventing large fluctuates in blood glucose levels (Hauge-Evans et al., 2009). Pancreatic polypeptide acts as a long-term satiety signal and inhibits glucagon release (Aragon et al., 2015), whereas ghrelin inhibits insulin release and stimulates appetite (Dezaki, 2013). The coordinated action of the different hormones, particularly glucagon and insulin, maintains the

concentration of circulating glucose within a narrow physiological range of 4–6 mM (Röder et al., 2016).

1.1.1 Insulin biosynthesis and secretion

The biologically active form of insulin is a monomer with a molecular weight of 5.8 kDa composed by two chains bound by three disulphide bonds. The "A" chain is 21 amino acids long, while the "B" chain consists in 30 amino acids. However, insulin gene encodes a 110 amino acids protein called pre-proinsulin. This protein contains a N-terminal signal that promotes its translocation to the endoplasmic reticulum (ER), where the N-terminal is removed by a signal peptidase (Fu et al., 2013, De Meyts, 2004). The product, so-called proinsulin, is further processed within the ER, where the disulphide bonds are formed and the protein is folded into its native three-dimensional structure (Sun et al., 2015). Proinsulin is then transported to the Golgi apparatus, where it is finally cleaved into insulin and C-peptide by the prohormone convertases PC1/3 and PC2 as well as carboxypeptidase E (CPE) (Liu et al., 2015). Both, insulin and C-peptide are stored in secretory granules. In rodents, β-cells contain approximately 13,000 insulin granules and each granule stores approximately 200,000 molecules of insulin. However, insulin content within β-cells is dynamic, and varies in response to several stimuli. Indeed, insulin biosynthesis is rapidly induced in response to glucose at both, transcriptional and posttranscriptional levels. Therefore, insulin content in β-cells increases in the presence of nutrients and decreases during nutrient deprivation (Fu et al., 2013).

Although insulin secretion can be induced to some extent by free fatty acids and amino acids, the main stimuli to trigger insulin secretion is the increase in circulating

glucose concentration (Fu et al., 2013, Röder et al., 2016). In rodents, β-cells only express the glucose transporter 2 (GLUT2), whereas in humans the main glucose transporter found in β-cells is GLUT1 (although they also express GLUT3 and GLUT2) (McCulloch et al., 2011). After entering into the β-cell, glucose is phosphorylated by glucokinase (GCK). This hexokinase responds to changes in circulating glucose, acting as a glucose sensor, and is the rate-limiting enzyme for glycolysis in β-cells. There are two main characteristics that differentiate GCK from other hexokinases: 1) its low affinity for glucose and 2) it is not inhibited by its product (Kaufman et al., 2015, Fu et al., 2013). Interestingly, mutations in this gene resulting in increased enzyme activity are associated not only with a lower threshold for glucose induced insulin secretion, but also with an increase in β-cell proliferation and apoptosis (Kassem et al., 2010). In contrast, inactivating mutations in the gene that encodes for GCK cause hyperglycaemia (MODY 2) (Gloyn et al., 2004, Gloyn et al., 2005). Once glucose is phosphorylated, it follows the glycolytic pathway, producing two molecules of pyruvate. Pyruvate is then transferred into the mitochondria, and it is subsequently metabolized to acetyl coenzyme A by the pyruvate dehydrogenase complex. Then, acetyl coenzyme A enters into the tricarboxylic acid (TCA) cycle to produce nicotinamide adenine dinucleotide (NADH) and flavin adenine dinucleotide ($FADH_2$) to feed the mitochondrial electron transport chain for the production of adenosine triphosphate (ATP) in the mitochondrial complex V. The subsequent increase in ATP:ADP ratio leads to the closure of the ATP-sensitive K^+(K_{ATP}) channels, which promotes the depolarization of the plasma membrane and the opening of voltage-dependent Ca^{2+} channels. The following increase of Ca^{2+} concentration within β-cells induces the fusion of the insulin granules with the plasma membrane followed by

the secretion of their content. The fusion of the secretory granules with the plasma membrane is mediated by a number of proteins belonging to the family of the soluble N-ethylmaleimide-sensitive factor attachment protein receptor (SNARE) proteins. SNARE proteins form the so-called SNARE complex together with Sec1/Munc18-like protein. In addition, synaptotagmins (Syts) proteins, that act as Ca^{2+} sensors, are attached to SNARE complexes and induce the fusion of the secretory vesicles to the plasma membrane when bound to Ca^{2+} (Figure 2) (Gauthier and Wollheim, 2008).

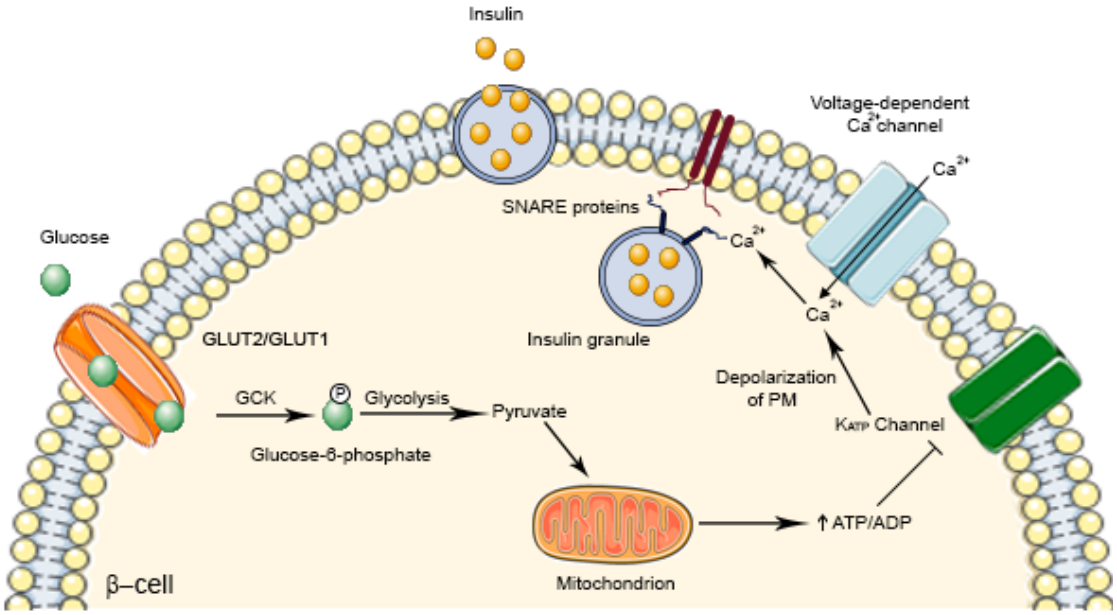

Figure 2. Schematic representation of insulin secretion in β-cells. Glucose enters into the β-cell by GLUT2 in mice or GLUT1/GLUT2 in humans. Afterwards, it is phosphorylated by GCK into glucose-6-phosphate which is metabolized during glycolysis to form pyruvate. Pyruvate is translocated to the mitochondria where is used to produce acetyl coenzyme A for the TCA cycle, which produces the substrate for the production of ATP by the respiratory chain. The increase in ATP/ADP results in the closure of K_{ATP} channels and subsequent depolarization of the plasma membrane as well as opening of the voltage-dependent Ca^{2+} channels. The increased concentration of intracellular Ca^{2+}, induces the fusion of the insulin granules with the plasma membrane (PM) and the subsequent release of insulin. The figure was generated using images from Servier Medical Art.

Insulin secretion is biphasic, with a first peak of insulin secretion five minutes after the glucose stimuli, and a second phase in which insulin is secreted in a slower and constant manner (Röder et al., 2016, Dolai et al., 2016). During the first phase, insulin is secreted from a small pool of granules already pre-docked to the plasma membrane (so-called readily releasable pool). In contrast, during the second phase, secretory vesicles from a reserve pool within β-cells must be translocated and subsequently docked to the plasma membrane. Interestingly, the proteins that form the SNARE complex from the pre-docked secretory vesicles (Syn-1A, VAMP2, and Munc18a) are distinct from the ones found in the reserve pool (Syn-3, VAMP8, and Munc18b), while Syt-7 seems to be the major Ca^{2+} sensor in both cases (Dolai et al., 2016, Henquin, 2009). The second phase is, at least to some extent, independent of the closure of the K_{ATP} channels, being stimulated by intermediates of the TCA cycle, NADPH and glutamate that act as amplifying signals for glucose induced insulin secretion (Henquin, 2009, Fu et al., 2013, Maechler and Wollheim, 1999).

1.1.2 Insulin action in main metabolic tissues.

The main target tissues of insulin are: skeletal muscle, white adipose tissue (WAT), liver, brain, β-cells, kidneys and macrophages. The first three are often referred as peripheral tissues and have been the most widely studied in terms of insulin signalling. Insulin exerts its effects on target tissues via Insulin Receptor (IR), which becomes auto-phosphorylated on tyrosine residues upon binding with its ligand (Haeusler et al., 2017). Subsequently, IR substrate (IRS) proteins, are recruited and phosphorylated on multiple tyrosine residues by the active IR. IRS1 phosphorylation on tyrosine residues generate binding sites for proteins containing Src-homology 2 (SH2) domains, such as

phosphoinositide 3-kinase (PI3K). The binding of the two SH2 domains in the regulatory subunits of PI3K to IRS1 results in activation of its catalytic subunit. Active PI3K phosphorylates phosphatidylinositol 4,5-bisphosphate (PIP_2) to form the lipid second messenger phosphatidylinositol (3,4,5)-triphosphate (PIP_3). Then, 3-phosphoinositide-dependent protein kinase-1 (PDK1) is recruited to the plasma membrane and binds to PIP_3 through its Pleckstrin homology (PH) domain. The binding of PDK1 to PIP_3, induces a conformational change in PDK1 that is necessary for its access to substrates, including AKT. AKT is also recruited to the plasma membrane by its PH domain, where it is activated by its phosphorylation at Thr308 by PDK1 and at Ser473 by mammalian target of rapamycin complex 2 (mTORC2) (Boucher et al., 2014, Bayascas, 2010).

In the skeletal muscle and WAT, one of the principal actions of insulin is to induce the translocation of GLUT4 to the plasma membrane, promoting glucose uptake. In the absence of insulin, only 5% of the total GLUT4 is found at the plasma membrane, with the majority of this protein located in specific GLUT4 storage vesicles (GSVs), endosomes and the trans-Golgi network. Insulin induced translocation of GLUT4 to the plasma membrane is mediated by two different pathways: 1) PI3K dependent pathway downstream AKT phosphorylation and 2) The APS–insulin signalling pathway (Leto and Saltiel, 2012).

1) The PI3K dependent pathway, which has been observed in adipocytes as well as in skeletal muscle, requires the phosphorylation of the AKT substrate of 160 Kda (AS160) Rab GTPase-activating protein (GAP) by AKT. AS160 protein maintains in the GDP-bound inactivate state a number of Rab proteins (Rab8A, Rab10 and Rab14) that are located in GSVs. AKT phosphorylation inhibits AS160

GAP activity, allowing its target Rab proteins to change to the GTP-bound activate state and thus triggering translocation of GSVs (Osorio-Fuentealba et al., 2013, Gonzalez and McGraw, 2006, Mîinea et al., 2005). Moreover, AKT also regulates the fusion of GSVs with the plasma membrane. GSV fusion is mediated by SNARE complexes formed by the vesicle-associated protein 2 (VAMP2), syntaxin 4 (STX4), which is localized in the plasma membrane, and synaptsomal associated protein 23 (SNAP23). AKT phosphorylates the protein Synip, which is normally bound to STX4, interfering with its interaction with VAMP2 in the approaching vesicle. AKT phosphorylation decreases Synip affinity to STX4, thus allowing it to interact with VAMP2 and inducing GSV fusion (Figure 3) (Leto and Saltiel, 2012).

2) The APS–insulin signalling pathway has only been shown to be necessary for GLUT4 translocation in adipocytes, while its role in skeletal muscle is unclear (Leto and Saltiel, 2012). This pathway is mediated by IR direct phosphorylation of the adapter protein containing PH and SH2 domains (APS) on Tyr-618. APS, which is constitutively bound to c-Cbl associated protein (CAP), promotes the phosphorylation of the CAP/c-Cbl complex on Tyr-700 and Tyr-774. Once phosphorylated, the CAP/Cbl complex migrates to lipid rafts in the plasma membrane and recruits the CrK/C3G complex to this microdomain. Subsequently, C3G activates a member of the RHO-family of small GTPases, TC10 (Katsanakis and Pillay, 2005). TC10 has been reported to be needed in adipocytes for insulin induced actin rearrangements that are crucial for GLUT4 translocation (Figure 3) (JeBailey et al., 2004).

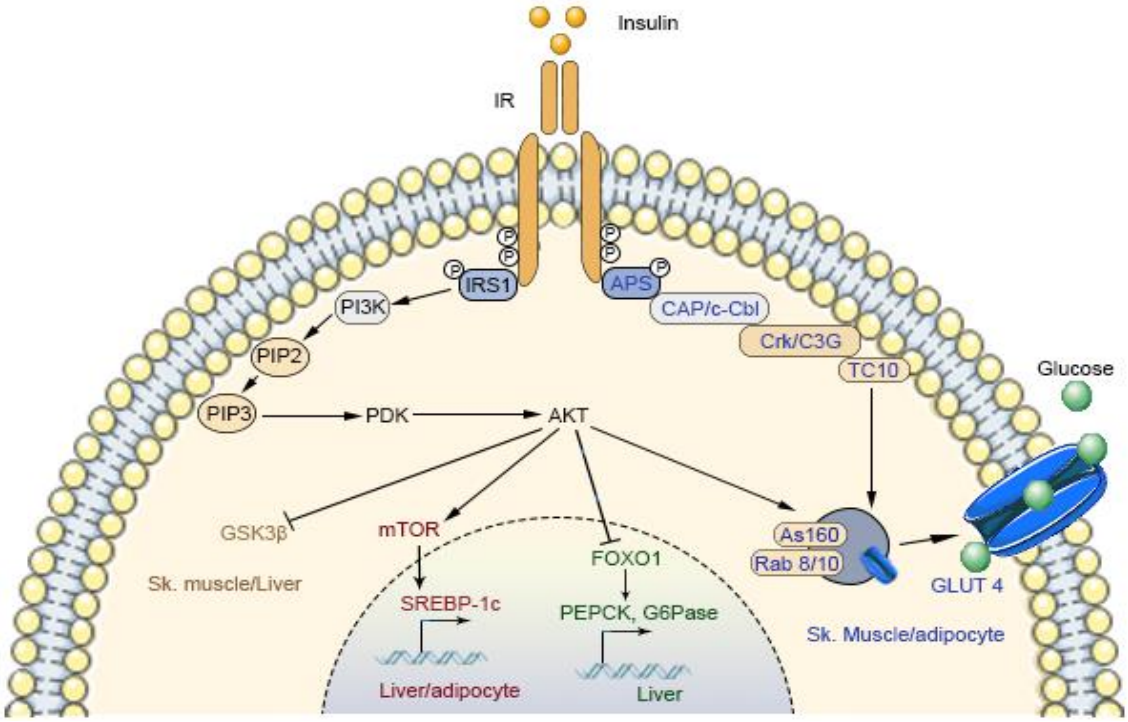

Figure 3. Schematic representation of insulin signalling in peripheral tissues. In Skeletal muscle insulin promotes GLUT4 translocation and subsequent glucose uptake as well as glycogen synthesis. In adipocytes, insulin induces glucose uptake as well as lipogenesis. In liver, insulin inhibits gluconeogenesis and promotes lipogenesis. The figure was generated using images from Servier Medical Art.

Another important effect of insulin in WAT is to inhibit lipolysis. Insulin induced inhibition of lipolysis is mediated by PI3K. Phosphorylated AKT activates phosphodiesterase 3B (PDE3B), leading to increased degradation of cyclic AMP (cAMP), which otherwise activates lipolytic enzymes (Ahmed et al., 2010).

Moreover, insulin induces lipid synthesis in both WAT and liver. This is mediated by AKT activation of mammalian target of rapamycin (mTOR) and subsequent induction of sterol regulatory element binding protein -1c (SREBP-1c) expression (Blüher et al., 2002, Xu et al., 2013) (Figure 3). SREBP-1c is considered as a master transcriptional regulator of fatty acid and triglyceride synthesis, since it regulates the expression of

several genes involved in lipid synthesis such as fatty acid synthase (FASN) (Figure 3) (Xu et al., 2013). Of note, in adipocytes, insulin may also increase FASN expression directly without affecting SREBP-1c expression (Palmer et al., 2002).

In the liver, one of the principal functions of insulin is to inhibit hepatic glucose production. During fasting, hepatic glucose production is fundamental to maintain circulating glucose levels within it physiological range and to avoid hypoglycaemia. In contrast, upon feeding, inhibition of hepatic glucose production by insulin is necessary to prevent hyperglycaemia. Glucose is produced in the liver by two processes: 1) gluconeogenesis, which is the formation of glucose from pyruvate/lactate and 2) glycogenolysis, which is the breakdown of glycogen to produce glucose (Sharabi et al., 2015). Insulin inhibition of hepatic glucose production is mediated by activated AKT, which phosphorylates FOXO1, resulting in its translocation from the nucleus to the cytoplasm. Therefore, AKT effectively inhibits the transcription of FOXO1 target genes, including those needed for gluconeogenesis, such as phosphoenolpyruvate carboxykinase (PEPCK) and glucose-6-phosphatase (G6Pase) (Li et al., 2010) (Figure 3). Additionally, although the major suppressor of glycogenolysis is glucose itself, insulin has also been shown to inhibit glycogenolysis in human hepatocytes (Petersen et al., 2017). Activated AKT also phosphorylates and inhibits Glycogen synthase kinase 3 beta (GSK3β), which is an inhibitor of glycogen synthase. Therefore, AKT effectively activates glycogen synthase and promotes glycogen synthesis in both liver and skeletal muscle (Haeusler et al., 2017, Samuel and Shulman, 2016) (Figure 3). Finally, insulin also induces the expression of GCK, the rate-limiting enzyme for glucose utilization in the liver, and promotes glycolysis (the pathway by which glucose is metabolized to generate pyruvate).

Actually, insulin promotes the dephosphorylation and subsequent activation of 6-phosphofructo-2-kinase/fructose-2,6-bisphosphatase 1 (PFKFB1), which is a key enzyme involved in glycolysis (Noguchi et al., 2013).

In β-cells, insulin has been suggested to promote both β-cell proliferation and survival though the PI3K-AKT pathway (Haeusler et al., 2017, Samuel and Shulman, 2016). Transgenic mice expressing a constitutively active form of AKT specifically in β-cells exhibit increased β-cell mass due to β-cell hyperplasia and increased number of pancreatic islets. Furthermore, the constitutively active form of AKT protected β-cells from Streptozotocin (STZ) induced apoptosis (Tuttle et al., 2001). In addition, insulin contributes to maintain the differentiated state of β-cells through AKT mediated inhibition of FOXO1. Actually, FOXO1 has been shown to negatively regulate the expression of the pancreatic and duodenal homeobox 1 (Pdx1). gene, a transcription factor required for normal β-cell function (Talchai et al., 2012).

Insulin has also been proposed to promote macrophage survival through the upregulation of the antiapoptotic protein B-cell lymphoma 2 (Bcl-2) (Rask-Madsen and Kahn, 2012, Mauer et al., 2010). Interestingly, insulin has been reported to activate nuclear factor kappa B (NF-κB), which induces Bcl-2 expression, inhibiting apoptosis in macrophages isolated from obese mice (San José et al., 2009, Hill et al., 2015). On the other hand, insulin mediated AKT activation and subsequent inhibition of FOXO1 may also regulate the secretion of pro-inflammatory cytokines by macrophages. Actually, FOXO1 upregulation in activated macrophages increases interleukin-1β (IL-1β) expression (Su et al., 2009).

In the brain insulin action reduces food intake by decreasing the expression of the orexigenic neuropeptides Agouti-related peptide (AgRP) and neuropeptide Y (NPY), as well as by increasing the expression of anorexigenic neuropeptides proopiomelanocortin (POMC) and cocaine- and amphetamine-regulated transcript (CaRT). In addition, insulin action in the brain affects body temperature. Keinridders et al. showed that insulin injections into the preoptic area of the brain in rodents can activate brown adipose tissue (BAT) and increase body temperature, whereas the effect is lost in neuron specific IR knock-out mice (Kleinridders et al., 2014).

1.2 Diabetes Mellitus

Diabetes Mellitus (DM) is a major health problem worldwide. According to the World Health Organization, there are approximately 422 million people suffering the deleterious effects of DM and it is predicted to become the 7th leading cause of death in the world by the year 2030 (World Health organization). This metabolic disease is characterized by the dysregulation of glucose homeostasis and hyperglycaemia. The diagnostic criteria for diabetes include fasting circulating glucose levels higher than 7 mmol/L (126 mg/dl), abnormal glucose-tolerance during an oral glucose tolerance test (OGTT) and increased glycated haemoglobin (HbA1C), which indicates the average of circulating glucose concentration over 3 months, (*e.g.* equal or greater than 6.5%) (Atkinson et al., 2014).

Increased levels of circulating glucose long term lead to several complications such as retinopathy, nephropathy, neuropathy (microvascular), ischemic heart disease,

peripheral vascular disease, cerebrovascular disease (macrovascular), blindness and lower limb amputation (Cade, 2008, Organization, 2015, World Health organization).

The most prevalent types of DM are: 1) type I, 2) type II and 3) gestational diabetes. Additionally, there are also other subtypes of DM, known as "maturity onset of the diabetes of the young" (MODY), neonatal diabetes, "mitochondrial related diabetes and deafness" and "latent autoimmune diabetes in adults" (Gloyn et al., 2005, Gloyn et al., 2004, Siddiqui et al., 2015, Vandenouweland et al., 1994).

1.2.1 Type 1 diabetes mellitus

Type 1 diabetes mellitus (T1DM), is an autoimmune disease caused by a direct attack of immune cells that selectively destroys pancreatic β-cells, resulting in the development of hyperglycaemia. Currently, there is no cure for T1DM, and patients largely rely on insulin treatment to maintain circulating glucose levels constant.

Normally, the progress of this disease is preceded by a long latency period (over several months or years), where patients are asymptomatic but still present several autoantibodies against islet autoantigens such as insulin, glutamic acid decarboxylase 65 (GAD 65), islet antigen-2 (IA-2) and Zinc transporter 8 (ZnT8) (Paschou et al., 2017). Antibody production by B cells is mainly dependent on the action of a subset of CD4+ CXCR5+ T helper cells, so-called follicular T helper cells (Thf), that are crucial for the development of the disease (Viisanen et al., 2017, Walker and von Herrath, 2016). Pancreatic islets from T1DM patients are infiltrated with Thfs together with other T helper cells (Th1 and Th17), B cells, macrophages and antigen presenting cells (APCs). This infiltration of immune cells, so-called insulitis, is a major hallmark of T1DM. Th1 and

Th17, which are the most abundant cell types within insulitis, play a crucial role in inducing β-cell apoptosis via the secretion of pro-inflammatory cytokines such as tumour necrosis factor -α (TNF-α), interferon-γ (IFNγ) and IL-1β as well as granzyme B and perforin (Walker and von Herrath, 2016, Li et al., 2014, Atkinson et al., 2014). However, infiltration of immune cells in pancreatic islets does not always lead to diabetes. In fact, it has been suggested that in non-autoimmune prone individuals, initial islet infiltration may promote repair and regeneration of β-cells (Hill et al., 2007).

Compelling data indicate that both genetic and environmental factors are required for the development and progression of T1DM. To date, more than 50 loci have been associated with increased susceptibility to this disease. The main genes associated with increased risk of T1DM are located on chromosome 6 within the Major Histocompatibility Complex (MHC), which accounts for 40-50% of the genetic predisposition to this disease (Paschou et al., 2017). The incidence of T1DM is increasing rapidly, without any significant change in the genetic pool, indicating a strong environmental component. In this regard, infections with *Helicobacter Pylori* or the hepatitis A virus have been associated with a protective role against T1DM, whereas other viral infections, specially enteroviruses, are considered as triggers of the disease (Kondrashova and Hyöty, 2014).

1.2.2 Type 2 diabetes Mellitus

Type 2 diabetes mellitus (T2DM) is characterized by insulin resistance in peripheral tissues coupled to a decrease in insulin secretion due to β-cell dedifferentiation and apoptosis (Donath and Halban, 2004). This type of diabetes is the most prevalent

form, accounting for 80-90% of all the cases worldwide (World Health organization). Additionally, its incidence is increasing rapidly mainly due to the increase in obesity, which is a major risk factor for T2DM together with aging. There are several mechanisms by which obesity promotes insulin resistance (Ye, 2013).

First, obesity is associated with a chronic low-grade inflammation. Indeed, an increase of pro-inflammatory cytokines such as TNF-α, IL-1β and interleukin-6 (IL-6) have been reported in both WAT and the circulation of obese patients as well as in animal models for obesity (Ye, 2013). TNF-α activates the Jun NH_2-terminal kinase (JNK) which phosphorylates IRS-1 at the serine 307, impairing tyrosine phosphorylation by IR (Aguirre et al., 2000). Moreover, IL-1β downregulates IRS-1 expression at the transcriptional level in adipocytes (Figure 4) (Jager et al., 2007). The increase in pro-inflammatory cytokines is partially explained by the increase in macrophage infiltrations in WAT observed during obesity. Actually, reducing macrophage infiltrations in WAT has been found to enhance insulin sensitivity (Ye, 2013).

Moreover, lipotoxicity has been shown to induce insulin resistance in both liver and skeletal muscle. The main function of adipose tissue is to store fatty acids. Nevertheless, when the storage ability of adipocytes is overwhelmed, ectopic accumulation of lipids in the liver and skeletal muscle occurs, leading to inflammation, apoptosis and insulin resistance. In addition, adipocytes that have reached their maximal expansion capacity also present insulin resistance. The most common lipid species within ectopic fat depositions in both skeletal muscle and liver are triglycerides.

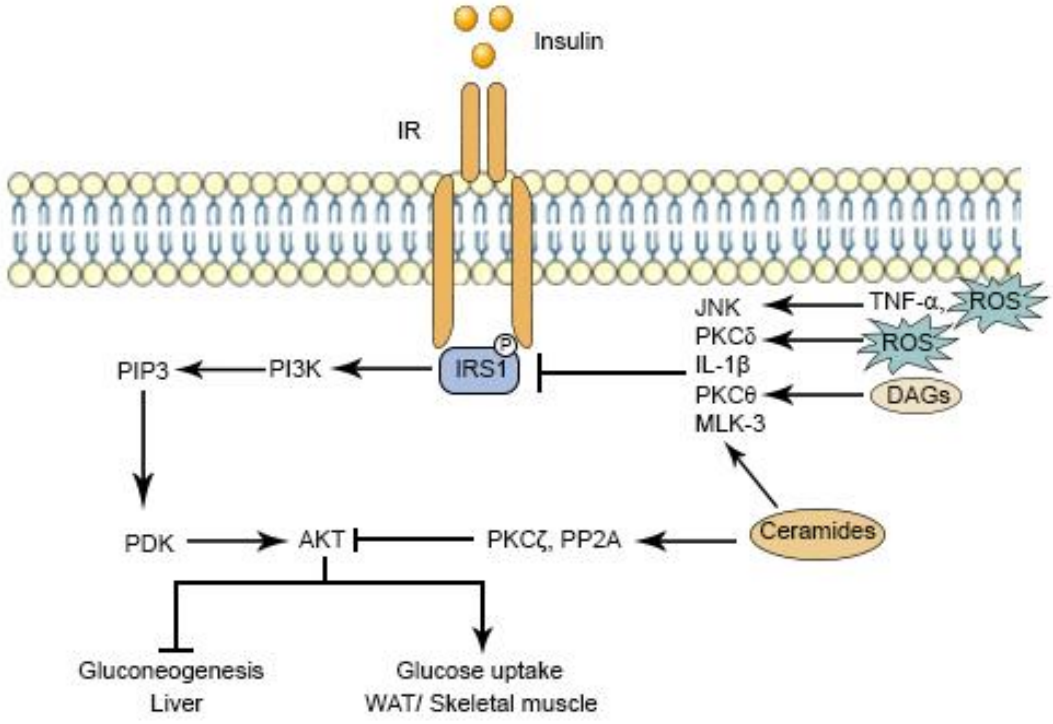

Figure 4. Schematic representation of the main contributors to insulin resistance. Cytokines inhibit insulin signalling at the IRS1 level. DAGs also inhibit the phosphorylation of IRS-1 by the insulin receptor, whereas ceramides inhibit AKT phosphorylation. Moreover, ROS inhibit insulin signalling in a process mediated by JNK and PKCδ activation. Inhibition of insulin signalling results in enhanced gluconeogenesis in the liver and impaired glucose uptake in the skeletal muscle and WAT. The figure was generated using images from Servier Medical Art.

However, other lipid intermediates such as diglycerides (DAG) and ceramides, are believed to play a more important role in the development of insulin resistance (Brøns and Grunnet, 2017). DAGs activate protein kinase C Θ (PKCΘ), which phosphorylates IRS-1 at Ser1101, impairing IR-dependent tyrosine phosphorylation of IRS-1 and thus insulin signalling (Jelenik et al., 2017). Likewise, ceramides may inhibit IRS-1 phosphorylation via the activation of Mixed-lineage protein kinase 3 (MLK3), which in turns activates JNK. In addition, ceramides also reduce AKT phosphorylation by

activating protein phosphatase 2 (PP2A). Moreover, ceramides bind and activate PKCζ, which phosphorylates a serine or threonine residue (depending on the AKT isoform) at the site 34 in the PH domain of AKT, preventing its recruitment to the plasma membrane (Figure 4) (Galadari et al., 2013).

In the liver, insulin resistance involves the inhibition of the AKT-FOXO1 branch, whereas the mTOR/SREBP-1c branch that induces lipogenesis may be less affected, contributing to the accumulation of fatty acids in this tissue (Czech, 2017). Additionally, ectopic accumulation of lipids in both liver and skeletal muscle may result from an increased uptake of fatty acids due to continued lipid excess uptake and/or to a reduced rate of the beta-oxidation of fatty acids (Brøns and Grunnet, 2017). In this regard, several studies indicate that insulin resistance is associated with mitochondrial dysfunction, although there are contradictory results (Rector et al., 2010, Holmström et al., 2012, Jelenik et al., 2017, Brøns and Grunnet, 2017, Richardson et al., 2005). Rector *et al.* showed that OLEFT rats (a model for obesity and T2DM) had reduced hepatic mitochondrial content even before the appearance of insulin resistance (Rector et al., 2010). Likewise, mitochondrial function in both liver and soleus muscle was altered in db/db mice, which are a model for obesity and T2DM (Holmström et al., 2012). Additionally, lipid infusions in healthy humans were reported to decrease the expression of Peroxisome proliferator-activated receptor γ coactivator-1α (PGC1α), which is involved in mitochondrial biogenesis (Richardson et al., 2005). In contrast, an independent study failed to detect any alteration in the expression of PGC1α in young healthy subjects after high-fat diet (HFD) feeding (Brøns and Grunnet, 2017). Moreover, Jelenik *et al.* did not detect mitochondrial dysfunction in two different models of hepatic

steatosis with insulin resistance. Conversely, they observed a temporary increase in β-oxidation and TCA cycle–linked maximal respiratory capacity, which was later associated with an increase in reactive Oxygen species (ROS) production (Jelenik et al., 2017). In a different study, Pereira et al. found that lipid infusions induced hepatic insulin resistance in a process dependent of ROS production (Pereira et al., 2014). Interestingly, ROS have been shown to activate JNK and PKCδ, which phosphorylate IRS1 at Ser307 and Ser357 respectively, thus inhibiting insulin signalling (Ye, 2013, Waraich et al., 2008, Pereira et al., 2014). In addition, 4-hydroxy-2-nonenal (4-HNE), which results from ROS attack on the double bonds of polyunsaturated fatty acids (lipid peroxidation), has been found to impair insulin signalling in the skeletal muscle of mice (Pillon et al., 2012).

The classic paradigm stablishes that insulin resistance is the first step in the development of T2DM, followed by an increase of insulin production by β-cells in an attempt to maintain glucose levels under physiological range. During this period, patients exhibit hyperinsulinemia but not hyperglycaemia. Although there are compelling evidences that support this model, there are also several studies that indicate that hyperinsulinemia is the first step in the development of T2DM. According to the later model, over-nutrition would itself enhance insulin secretion by β-cells, which would result in hyperinsulinemia and this would cause insulin resistance. This hypothesis is supported by data indicating that hyperinsulinemia induces inflammatory pathways that lead to insulin resistance in peripheral tissues (Shanik et al., 2008, Marín-Juez et al., 2014, Vikram and Jena, 2010). Indeed, reducing hyperinsulinemia by STZ or diazoxide treatment in obese mice, results in decreased WAT inflammation and enhanced insulin sensitivity. Nonetheless, it should be noted that the two hypotheses are not mutually

exclusive and probably act in parallel. In this scenario, hyperinsulinemia firstly induced by insulin resistance, further increases insulin resistance, propelling the vicious cycle of T2DM (Czech, 2017).

The last step in the pathogenesis of T2DM, is the reduction of insulin secretion due to β-cell dedifferentiation/dysfunction and apoptosis. There is still an interesting debate regarding the relative contribution of β-cell mass loss and β-cell dysfunction to the development of the disease (Martinez-Sanchez et al., 2016). Apoptosis of β-cells in T2DM is caused, at least in part, by an increase in ROS production resulting from the increased metabolic activity of β-cells in the pre-diabetic state characterized by hyperinsulinemia (Elumalai et al., 2017, Tachibana et al., 2015). Nonetheless, increased ROS may impair β-cell function by promoting MafA degradation as well as by interfering with the DNA binding capacity of Pdx1 (Gerber and Rutter, 2017). Moreover, hyperglycaemia itself promotes the dedifferentiation of β-cells, since it has been shown to reduce the expression of genes required for proper β-cell function such as Pdx1 and Pax6, whereas it enhances the expression of the endocrine progenitor marker Ngn3 (Brereton et al., 2016). Therefore, T2DM is the result of insulin resistance coupled to β-cell apoptosis, dedifferentiation and dysfunction.

1.2.3 Gestational diabetes

Gestational diabetes mellitus (GDM), defined as diabetes appearing specifically during pregnancy, is a relatively common disease that affects approximately 10% of all pregnancies. Importantly, GDM is associated with several health complications for both mother and foetus, such as preeclampsia, perinatal hypoglycaemia, respiratory distress

syndrome and macrosomia (Pasek and Gannon, 2013). Moreover, women with GDM are seven times more likely to develop T2DM later on in life (Pasek and Gannon, 2013) and their offspring are also at increased risk for the development of obesity and T2DM (Chiefari et al., 2017).

During pregnancy, several maternal adaptations are required in order to secure the viability of the mother and the fetus. The immune system of the mother must adapt to tolerate the fetus while maintaining efficient immune responses (Le Bouteiller and Bensussan, 2017). Moreover, inflammation is increased to promote insulin resistance in the mother in order to assure nutrient flow to the growing foetus. This increase in inflammation is caused, at least to some extent, by the expansion and functional changes that occur in WAT during gestation. Actually, during pregnancy there is an increase in several serum adipokines, such as leptin, whereas adiponectin is decreased (Rojas-Rodriguez et al., 2015, Vivas et al., 2016). In order to counterbalance insulin resistance and prevent maternal hyperglycaemia (GDM), the endocrine pancreas must adapt (Figure 5) (Chiefari et al., 2017). This adaptation consists in the augmentation of insulin secretion via both β-cell enhanced functionality (enhanced glucose-induced insulin secretion) and β-cell mass expansion.

Seminal reports have established the transcriptional profile of murine pancreatic islets during pregnancy. Genes modulated during pregnancy include the two isoforms of the serotonin producing enzyme tryptophan hydroxylase (Tph1 and Tph2), genes involved in placental lactogens signalling such as the prolactin receptor, proliferative markers such as Ki67 and pro-survival genes such as Baculoviral IAP Repeat-Containing 5 (Birc5) (Rieck et al., 2009). Remarkably, disruption of the serotonin receptors Htr2b

and Htr3 prevent β-cell mass expansion and enhanced glucose induced insulin secretion during gestation, respectively, leading to the development of GDM in mice (Kim et al., 2010, Ohara-Imaizumi et al., 2013). These studies highlight the importance of both mechanisms in the pathogenesis of GDM. In addition, several studies have found that single nucleotide polymorphisms (SNPs) in genes that regulate β-cell function, such as GCK, are associated with higher risk of GDM (Zhang et al., 2013). Although these studies indicate a strong genetic component in the pathogenesis of GDM, environmental factors may also be involved in the development of the disease. In this regard, viral infections, such as hepatitis B, have been associated with an increased risk of developing GDM (Lao et al., 2007).

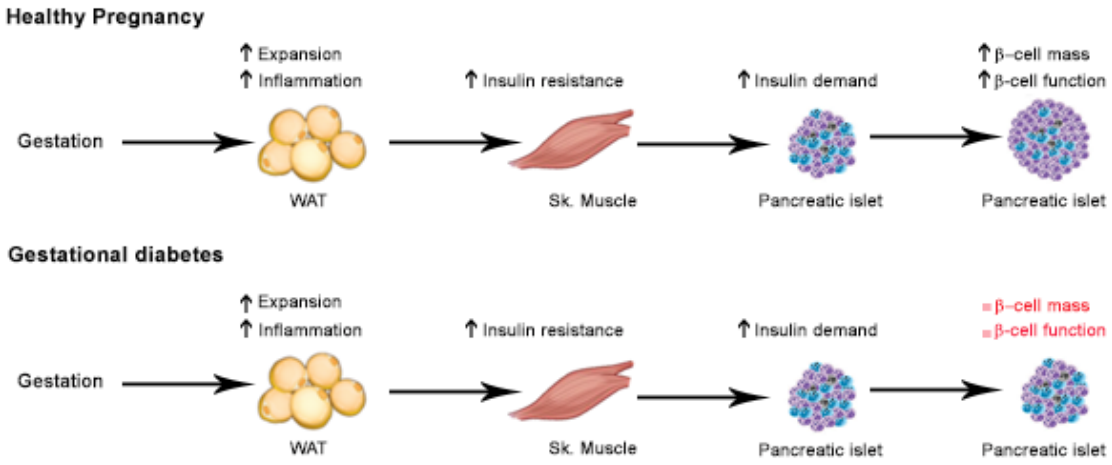

Figure 5. Schematic representation of the pathogenesis of GDM. During pregnancy, there is an increase of inflammation due, at least in part, to the expansion and functional changes in WAT. Inflammation promotes the appearance of insulin resistance. GDM develops when pancreatic islets are unable to adapt to the increased insulin demand.

1.3 Pax genes

Paired box genes (Pax) are a family of transcription factors characterized by the presence of a 128-aminoacid DNA binding domain called the "paired domain". This gene

family is subdivided into four groups, according to the presence or absence of an octapeptide domain and the presence, absence or truncation of a homeodomain (Figure 6). The paired domain consists of two subdomains, each of which structurally resembles a helix–turn–helix motif. The homeodomain is a highly conserved 60-amino acid helix-loop-helix DNA-binding domain, commonly found in genes involved in animal development such as HOX genes. On the other hand, the octapeptide motif consists in an 8-amino acid motif that may facilitate transcriptional inhibitory activity (Lang et al., 2007, Robson et al., 2006).

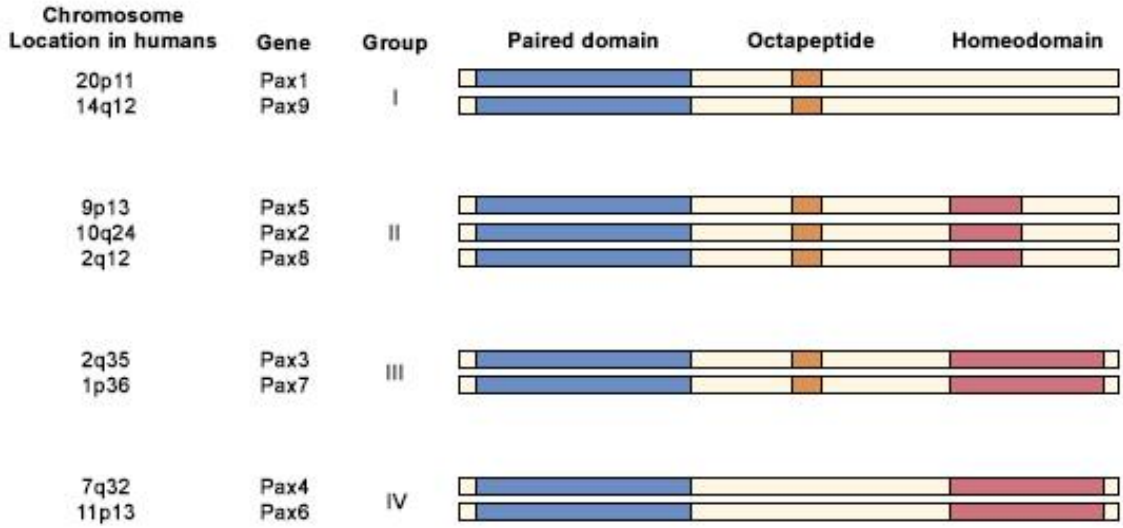

Figure 6. Classification of the Pax gene family according to the presence and structure of its domains. Group I is defined by the presence of the octapeptide motif and the absence of the homeodomain. Groups II and III, which are considered as tumour promoting, exhibit both an octapeptide domain and the homeodomain, although the homeodomain of group II is truncated. Members of the subgroup IV, Pax4 and Pax6, are characterized by the absence of the octapeptide domain.

These transcription factors are involved in early animal development and play a crucial role in organogenesis, tissue specification and cell differentiation. Actually, Pax genes are normally expressed during development and their expression is downregulated

in adult tissues. However, specific Pax genes remain expressed in the central nervous system, thymus, thyroid, kidney and the endocrine pancreas (Lang et al., 2007, Robson et al., 2006).

1.3.1 Pax genes expressed in pancreatic islets

Members of the group IV, Pax4 and Pax6, which lack the octapeptide domain, are essential for the organogenesis and maturation of pancreatic islets. Overexpression of Pax4 has been shown to protect against hyperglycaemia induced by STZ and against an experimental model of autoimmune diabetes (Mellado-Gil et al., 2016, He et al., 2011). However, Pax4 overexpression also decreases insulin secretion and promotes a dedifferentiated state through the repression of MafA (He et al., 2011). Pax6 deletion in β-cells during adulthood causes the development of hyperglycaemia in mouse and reduces the expression of genes essential for β-cell function such as MafA and Ins2 (Mitchell et al., 2017). Furthermore, expression of the group II member, Pax2, has been detected in human islets and during murine pancreatic development, reaching its maximal expression around E12.5. A detailed study of the pancreases of $Pax2^{1Neu}$ mutant mice at E18.5, revealed that these mice have an increased volume of β-cells (note that total number was not measured), accompanied by an increase in the total area occupied by pancreatic islets. Nevertheless, the architecture of pancreatic islets, differentiation of α- and β- cells as well as insulin and glucagon content were not affected. Although further studies are required to confirm the role of Pax2 in pancreatic islet physiology, the mild effect of Pax2 deficiency on the pancreas could stem from the compensatory role of other Pax genes expressed in this organ.

1.3.2 Pax8

Pax8, which belongs to group II, is expressed during development in the midbrain–hindbrain boundary in early central nervous system, the inner ear, kidney, urogenital tract, placenta and thyroid (Harter et al., 2015, Bouchard et al., 2010, Mittag et al., 2007, Tong et al., 2009, Ferretti et al., 2005). In contrast, in adult tissues it is only expressed in thyroid and kidney (Ferretti et al., 2005, Tong et al., 2009). Of particular importance is the role of Pax8 in thyroid development, where it is needed for the thyroid follicle formation. The thyroid follicle is the structural and functional unit of the thyroid gland and comprises a single layer of follicular cells enclosing a central lumen where thyroid hormones (THs) are synthesized and stored (Ferretti et al., 2005). Moreover, Pax8 expression is maintained in adult thyroid follicular cells and is required for the expression of thyroid specific genes, including thyroglobulin (Tg), thyroperoxidase (TPO), and sodium/iodide symporter (NIS), which are essential for the synthesis of active THs (Marotta et al., 2014, Arauchi et al., 2017). Remarkably, Pax8 knock-out mice die at weaning (around 21-26 days old), but thyroxine (T4) supplementation allows these mice to survive until 6 months of life (Mansouri et al., 1998, Christ et al., 2004). Likewise, in humans, heterozygous mutations in Pax8 are associated with hypothyroidism (Montanelli and Tonacchera, 2010). In addition, Pax8 null mutant mice are infertile due to defects in the urogenital tract and have structural and functional abnormalities in the outer and middle ear, despite T4 supplementation (Mittag et al., 2007, Christ et al., 2004, Wistuba et al., 2007). Major defects in other tissues such as the kidney or the midbrain-hindbrain region have not been observed. This fact is most likely explained by a partial redundancy of the highly homologous Pax2 and Pax5 genes (Mittag et al., 2007, Wistuba et al., 2007).

Pax8 is also found in a translocation mutation t(2;3)(q13;p25) that results in a fusion protein with peroxisome proliferator-activated receptor γ (PPARγ) to form what has been termed the PAX8-PPARγ oncogene. This oncogene is associated with follicular thyroid carcinomas and adenomas (Raman and Koenig, 2014). Additionally, Pax8 is aberrantly expressed in the majority of thyroid adenocarcinomas as well as in other cancers such as Wilms tumours, renal, ovarian and placental cancers (Robson et al., 2006). Pax8 has also been proposed as a biomarker for pancreatic neuroendocrine tumours (PNTs) (Sangoi et al., 2011). However, it was later shown that this gene is not expressed in PNTs, since previous studies reporting its expression in PNTs used a polyclonal antibody that cross reacted with Pax6 (Lorenzo et al., 2011). A specific monoclonal antibody for Pax8 did not reveal Pax8 expression in PNTs, which was consistent with the data from Q-RT-PCR that did not detect Pax8 transcripts in murine islets, while scarcely detected them in human islets. Therefore, these results raised serious concerns on the reliability of the use of Pax8 as a marker for PNTs (Lorenzo et al., 2011).

The role of Pax8 in tumorous cells is to promote cell replication and survival. In this sense, Pax8 has been shown to interact with the promoter of E2F transcription factor 1 (E2F1), which acts as an activator for G1/S transition. Silencing of Pax8 in renal, thyroid and ovarian cancers, causes cell cycle arrest that ultimately leads to senescence of tumorous cells (Li et al., 2011). Pax8 has also been reported to activate the transcription of the anti-apoptotic proto-oncogene Bcl-2 in the kidney, which inhibits the permeabilization of the mitochondrial membrane and subsequent apoptosis (Hewitt et al., 1997). In addition, all the Pax proteins that belong to the group II (Pax2, Pax5 and Pax8)

inhibit the transcription of the tumour suppressor gene p53 by binding its first exon, resulting in the promotion of cell survival (Stuart et al., 1995).

Interestingly, several studies indicate that Pax8 may be involved in the regulation of glucose homeostasis. A genome wide study reported that a SNP in the vicinity of this gene was correlated to higher prevalence of developing T2DM in an Afro-American population (Elbein et al., 2009). In parallel, another study revealed that Pax8 is also robustly expressed in murine pancreatic islets during pregnancy, a situation in which there is an increase in β-cell proliferation and survival in order to adapt to the high insulin demands produced by the presence of the foetus (Rieck et al., 2009). Previous work from our lab, confirmed that Pax8 expression is strongly induced during pregnancy in murine pancreatic islets, with a major peak at day 14 of gestation, after the induction of proliferation of pancreatic islet cells *in vivo* (Karnik et al., 2007, Kim et al., 2010, Jiménez Moreno, 2015). Remarkably, the expression profile of Pax8 during pregnancy differed from Tph1, another pregnancy-induced gene involved in the biosynthesis of serotonin, which promotes β-cell proliferation and enhances glucose induced insulin secretion (Kim et al., 2010, Jiménez Moreno, 2015). In addition, prolactin treatment induced the expression of Pax8 in human islets, with a major peak at 72 hours, also differing from Tph1 expression and induction of proliferation (Jiménez Moreno, 2015).

The fact that Pax8 is expressed in pancreatic islets during gestation suggests that this gene might be expressed as a part of the machinery that promotes beta-cell proliferation, functionality and/or survival during pregnancy. Unfortunately, the physiological implications of the induction of Pax8 and of the genes transcriptionally regulated by itself in pancreatic islets during pregnancy are unknown. In order to address

this issue, our lab performed a transcriptional analysis of murine pancreatic islets overexpressing Pax8. Interestingly, a large number of up-regulated genes in murine Pax8 overexpressing islets (Rsad2, Cxcl10, Ifit3, Iigp1, Ddx60 and Ifit1) belong to the interferon inducible gene network. Consistently, Pax8 was shown to modulate canonical pathways involved in immune response and cellular proliferation. Moreover, a further analysis of annotated "Diseases and Functions" associated the transcriptional profile of islets over-expressing Pax8 to several immune-related diseases, endocrine/metabolic disorders and cell cycle/cell death/cancer (Jiménez Moreno, 2015).

Curiously, a heterozygous novel Pax8 mutation associated with congenital hypothyroidism was identified in a Portuguese family of Azores and the only pregnant female of this family harbouring this Pax8 mutation developed gestational diabetes (Jiménez Moreno, 2015). This polymorphism consists in the substitution of proline to arginine at codon 25 (P25R) located in the paired domain, and results in impaired functionality (Carvalho et al., 2013). As mentioned before, Pax8 is required for THs production. Interestingly, both subclinical hypothyroidism and low concentration of circulating THs have been associated with the development of GDM (Guzman-Gutierrez et al., 2014, Karakosta et al., 2012, Tudela et al., 2012). Therefore, current evidences suggest that Pax8 might be involved in diabetogenesis and glucose homeostasis, either directly by its expression in pancreatic islets, indirectly via the action of THs or due to a combination of both. However, the role of Pax8 in pancreatic islets physiology and glucose homeostasis has not been studied yet.

1.4 Thyroid hormones

The main THs produced by the thyroid gland are triiodothyronine (T3) and T4 (Schweizer et al., 2017). The synthesis of THs occur in structures called thyroid follicles, which are formed by a monolayer of polarized follicular cells that are organized in a tri-dimensional ovoid structure surrounding the follicle lumen. The interior of the follicle, so-called colloid, contains high levels of the protein Tg. The first step in TH synthesis is the iodide oxidation and incorporation into tyrosine residues of Tg. Then, tyrosine residues are further oxidized to form monoiodotyrosine (MIT) and diiodotyrosine (DIT), which are combined to form T4 and T3 in a process mediated by the enzyme TPO. The final step involves the cleavage of Tg within vesicles containing proteolytic enzymes in order to produce the final forms of T3 and T4 that are secreted (Figure 7A) (Ortiga-Carvalho et al., 2016, Carvalho and Dupuy, 2017).

TH production and secretion, and thus, circulating TH levels, are tightly regulated under physiological conditions by the hypothalamus-pituitary-thyroid (HPT)-axis. The hypothalamus secretes thyrotropin-releasing hormone (TRH) that stimulates the transcription of the α-glycoprotein hormone subunit (α-GSU) and βTSH genes in the anterior pituitary. These two genes encode for the two subunits that form thyrotropin, also called thyroid-stimulating hormone (TSH). TSH then stimulates the production of T4 and T3 in the thyroid, which in turn inhibit both TRH and TSH synthesis (Figure 7B) (Ortiga-Carvalho et al., 2016). Alterations in this regulatory mechanism may result in the appearance of hypothyroidism (low TH levels, high TSH) or hyperthyroidism (high TH levels, low TSH), both of which lead to serious health complications.

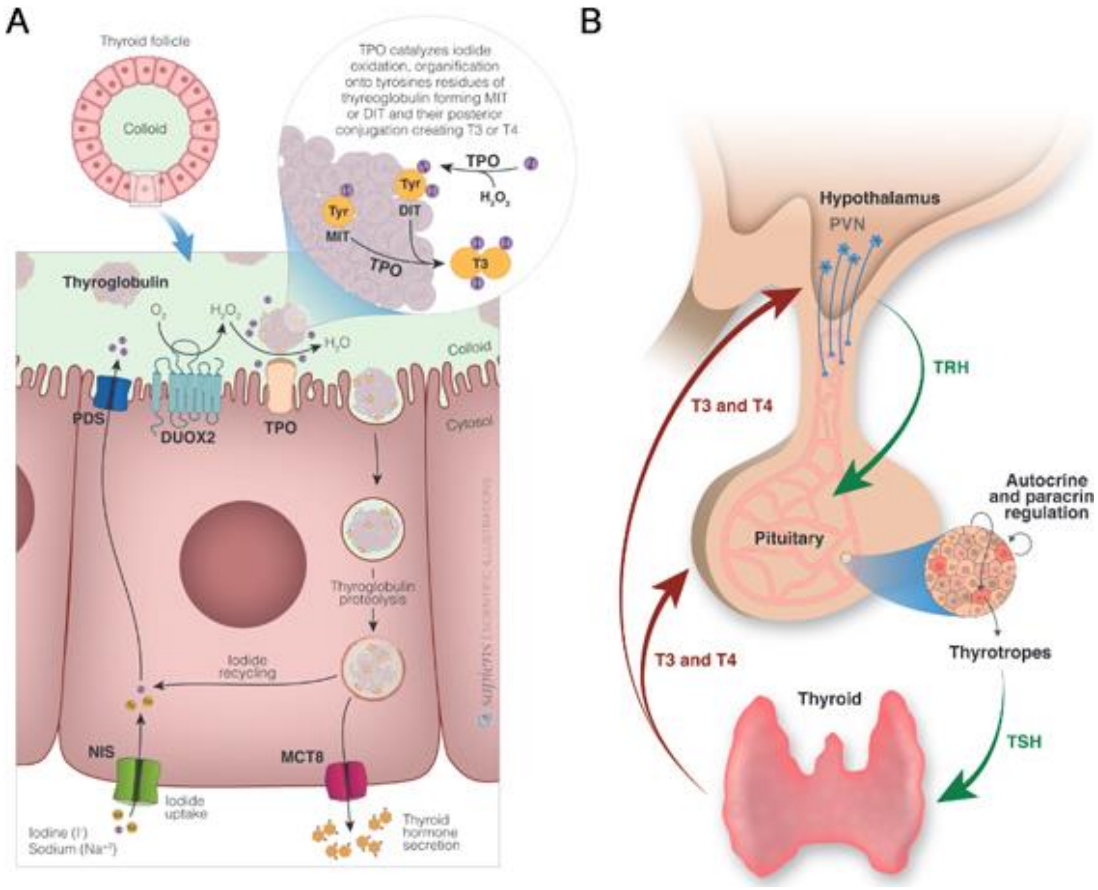

Figure 7. Thyroid hormones synthesis and regulation by the HPT axis. (A) THs are produced after the uptake of iodide by NIS in a process that involves the iodination of the tyrosyl residues of Tg. **(B)** TH levels in circulation are mainly regulated by the HPT axis, that involves TRH stimulation of TSH synthesis and subsequent induction of THs synthesis. THs then inhibit both TRH and TSH production in a negative feedback loop. From (Ortiga-Carvalho et al., 2016).

In humans, 80% of the THs secreted by the thyroid gland is T4 and 20% is T3, while in rodents approximately 50% of the THs secreted is T4 and 50% is T3 (van der Spek et al., 2017). T4 has a half-life in circulation of approximately 6 days, while T3 has a half-life of 1 day (Grozinsky-Glasberg et al., 2006), thus T4 is more stable than T3 in circulation. T4 is converted by deiodinase enzymes into T3 within cells. There are 3 types of deiodinases (D1, D2 and D3), which differ in in their pattern of expression within

tissues. D1 is able to remove an iodine atom from both the outer and the inner ring of THs, D2 only deiodinases the outer ring, while D3 only acts on the inner ring. T3 can be further deiodinased to form 3,5-diiodo-L-thyronine (T2) (Figure 8) (van der Spek et al., 2017). Classically, it has been considered that T3 is the active form, since it binds to nuclear thyroid hormone receptors (TR) with greater affinity than T4 or T2. However, several studies indicate that, both T4 and T2 may have important biological effects in several tissues, specially through non-genomic actions that do not involve the binding of THs to TR (Senese et al., 2014, Schroeder and Privalsky, 2014).

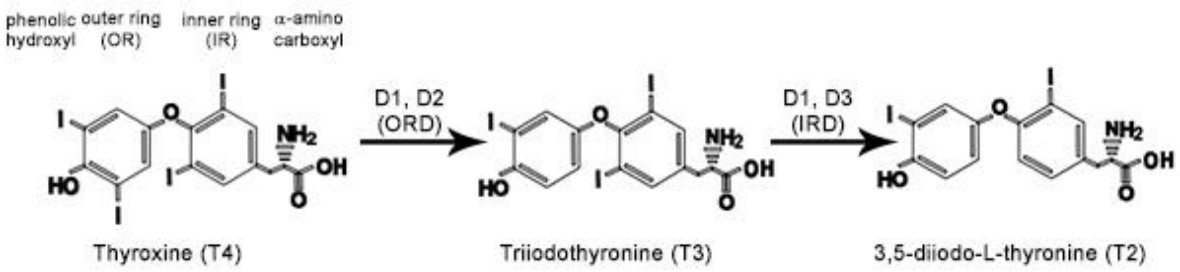

Figure 8. Deiodination of thyroid hormone isoforms. Deiodination of the outer ring of T4 by D1 or D2 produces the active form T3, which can be further deiodinase in the inner ring by D1 or D3 to produce T2. The functional groups as well as the outer and inner rings are labelled in T4. IRD: inner ring deiodination; ORD: outer ring deiodination.

1.4.1 Genomic actions of thyroid hormones

The classic, genomic mechanism of THs action is mediated by nuclear TRs. TRs are encoded by two genes, THRA and THRB, located on chromosomes 17 and 3, respectively. THRA encodes for the thyroid hormone receptor-α1 (TRα1), which is the major isoform expressed in heart, brain, bone and intestine, although lower levels of expression are also found in skeletal muscle and liver, among others. TRβ1 is the major isoform expressed in the liver, kidney, and thyroid, although to a lesser extent is also

present in brain, heart, thyroid, skeletal muscle, lungs, and spleen. TRβ2 is expressed in the hypothalamus, pituitary, and retina, and is involved in the regulation of the HPT axis (Senese et al., 2014, Lanni et al., 2016). These receptors act as transcription factors upon binding with its ligand. They contain multiple functional domains, including a DNA-binding domain. The DNA-binding domain is highly conserved and interacts with specific DNA segments that are known as "thyroid-hormone response elements" (TREs). TRs interact with TREs, which are normally formed by doublets of the half-site AGGCTA, as homodimers or forming heterodimers with the retinoid X receptor (RXR). Normally, TRs are bound to these sequences in DNA independently of THs. However, interaction of THs with TR causes conformational changes in TR and subsequent activation/suppression of target genes (Paquette et al., 2014).

1.4.2 Nongenomic actions of thyroid hormones

THs have been shown to exert non-genomic actions that are rapid in onset (minutes to hours) compared to transcriptional dependent mechanisms. These non-genomic actions are dependent on TRs located at the plasma membrane, cytoplasm and/or the mitochondria.

The thyroid receptor at the plasma membrane is located on the integrin αvβ3 and activates mitogen-activated protein kinase (MAPK) through phospholipase C (PLC) and protein kinase C (PKC) as well as PI3K via Src kinase (Davis et al., 2016, Cheng et al., 2010). Moreover, PI3K is also activated by non-genomic actions of THs by truncated forms of TRs found in the cytoplasm. Activated MAPK and PI3K by non-genomic actions of THs have been shown to promote angiogenesis via the induction of hypoxia inducible

factor-1α (HIF-1α) expression and to modulate Ca^{2+} and Na^{2+} concentration within cells via the modulation of the activity of Ca^{2+} ATPase and Na^{2+} ATPase (Lin et al., 2012, Davis et al., 2016). Furthermore, activation of PI3K results in the phosphorylation of AKT and subsequent translocation of GLUT4 to the plasma membrane in the skeletal muscle and adipocytes (Senese et al., 2014, Davis et al., 2016). MAPK activation by THs results in the induction of proliferation of several cell types, including human bone cells, epicardial progenitor cells, embryo hepatocytes and several types of cancer cells (Deng et al., 2017, Davis et al., 2016, Alisi et al., 2004).

In the mitochondria, there are two truncated TRα1 receptors with molecular masses of 43 and 28 kDa, thus so-called p43 and p28, respectively. The function of p28 is still unknown, while p43 binds to TRE sequences within the mitochondrial DNA. Therefore, p43 induces the expression of several mitochondrial genes, such as cytochrome c oxidase subunit 2 (MT-COX II) and mitochondrial encoded NADH dehydrogenase 2 (MT-ND2). As a consequence, p43 increases mitochondrial activity (Wrutniak-Cabello et al., 2017, Casas et al., 2008).

1.4.3 The role of thyroid hormones in differentiation and maturation of metabolic tissues

THs play a significant role in the differentiation of the vast majority of somatic cells (Sirakov et al., 2013, Obregon, 2008). Interestingly, during the last years, extensive research has focused on the role of THs in the differentiation, maturation and functionality of several metabolic tissues (Obregon, 2008, Bloise et al., 2017, Mastracci and Evans-Molina, 2014). In this regard, T3 modulates the expression of several genes whose

expression is dramatically increased during adipocyte differentiation, including glycerophosphate dehydrogenase (GPD), malic enzyme (ME) and PEPCK (Obregon, 2008). Likewise, physiological levels of THs are important for the normal pattern of different types of fibre distribution in skeletal muscle. Skeletal muscle is composed of two main types of different fibres, classified according to twitch speed: type I, so-called slow fibres and type II, so-called fast fibres. Remarkably, hypothyroid rats present a delay in the switch to adult myosin in fast fibres, but not in slow ones. Indeed, T3 has been shown to play a crucial role in the transition of neonatal fibre to type II (Bloise et al., 2017). Furthermore, T3 supplementation enhances postnatal pancreatic islet development via the induction of MafA and attenuates hyperglycaemia in STZ-treated as well as in leptin-receptor deficient mice (Aguayo-Mazzucato et al., 2013, Lin and Sun, 2011, Verga Falzacappa et al., 2011). In addition, T3 administration increases the expression of endocrine markers in acinar and ductal cell lines as well as in pancreatic explants (Misiti et al., 2005, Aïello et al., 2014). Remarkably, newly developed in vitro protocols aiming to differentiate human embryonic stem cells towards insulin-secreting β-cells, use T3 in specific steps of the differentiation protocol (Pagliuca et al., 2014, Rezania et al., 2014). These data indicate that THs are involved in the differentiation and the maturation of pancreatic precursor cells into functional endocrine cells.

1.4.4 Effects of thyroid hormones in metabolism

One of the main physiological roles of THs is the regulation of basal metabolic rate (BMR), defined here as the rate of energy expenditure per time at rest, which accounts for about 60–75% of the calories burned in a healthy subject (Johannsen et al., 2012). Remarkably, BMR is the main source of energy expenditure in humans and a reduced

BMR is associated with weight gain and obesity (Mullur et al., 2014). Specifically, THs increase oxygen consumption, while reducing the maximal capacity to produce ATP (Johannsen et al., 2012).

Mitochondria are the main site of ATP synthesis, which is coupled to oxygen consumption via dissipation of the proton electrochemical gradient that occurs across the inner mitochondrial membrane, where the respiratory chain is located. The respiratory chain (or electron transport chain) is composed by 4 complexes. Complex I (NADH-ubiquinone oxidoreductase) oxidises NADH to form NAD^+ and reduces coenzyme Q (CoQ). Complex II (succinate-ubiquinone-oxidoreductase) catalyses the oxidation of succinate to also reduce CoQ. Complex III (ubiquinone cytochrome c-reductase) uses the electrons donated by CoQ to reduce cytochrome c, which transfers electrons from complex III to complex IV. Complex IV (cytochrome c-oxidase) reduces O_2, forming H_20. During this process, superoxide is produced, mainly at complexes I and III, and it is converted to hydrogen peroxide by superoxide dismutases (SOD) (Figure 9A) (Zhong and Yin, 2015). The electrons transport is accompanied by the transfer of protons (H^+) from the mitochondrial matrix to the intermembrane space at complexes I, III, and IV, which creates an electrochemical gradient ($\Delta\psi m$). Protons re-enter into the mitochondrial matrix through complex V, which uses the proton-motive force to generate ATP from ADP and inorganic phosphate (Lanni et al., 2016). Noteworthy, some protons re-enter the mitochondrial matrix by other means, lowering $\Delta\psi m$ without producing ATP. This proton flux across the inner mitochondrial membrane that is not translated into ATP synthesis is called proton leak (Figure 9A). Proton leak has been shown to be important for energy dissipation in the form of heat and accounts for a significant part of the BMR in animals.

The main proteins contributing to proton leak are uncoupling proteins 1, 2, 3 and 4 (UCP1, UCP2 UCP3 and UCP4). UCP1 is mainly expressed in brown adipose tissue and is involved in thermogenesis. UCP2 and UCP3 are expressed in several tissues, including WAT, skeletal muscle and liver, while UCP4 is almost exclusively expressed in the brain with low levels of expression in the spinal cord and medulla (Rousset et al., 2004, Lindquist et al., 2017, Lanni et al., 2003, Andrews et al., 2005). Interestingly, UCP2, UCP3 and UCP4 have been shown to decrease ROS generation in several cell types including L6-muscle cells and neurons (Lanni et al., 2003, Andrews et al., 2005, Nabben et al., 2008). In this sense, uncoupling is thought to lead to greater oxygen consumption and reduce the proton motive force by reducing the mitochondrial membrane potential, which subsequently reduces ROS production. Moreover, it has been suggested that UCP2 can also act as a channel, promoting the transport of mitochondrial ROS to the cytosol where they can be reduced by antioxidant defensive mechanisms. Consistent with a role of UCP2 in decreasing ROS production, UCP2 null mice have decreased lifespan compared to WT mice (Andrews and Horvath, 2009).

THs enhance mitochondrial respiration by both genomic and non-genomic actions (Figure 9B). Genomic actions involve the induction of expression of genes such as the nuclear-encoded mitochondrial transcription factor A (TFAM) and PGC1-α. TFAM binds to mtDNA to regulate the transcription of several mitochondrial genes and PGC1α is considered a master regulator of mitochondrial biogenesis (Lanni et al., 2016). In addition, as mentioned before, THs bind to p43 within the mitochondria to induce the expression of several mitochondrial genes, including COXII and ND2 (Figure 9B) (Casas et al., 2008).

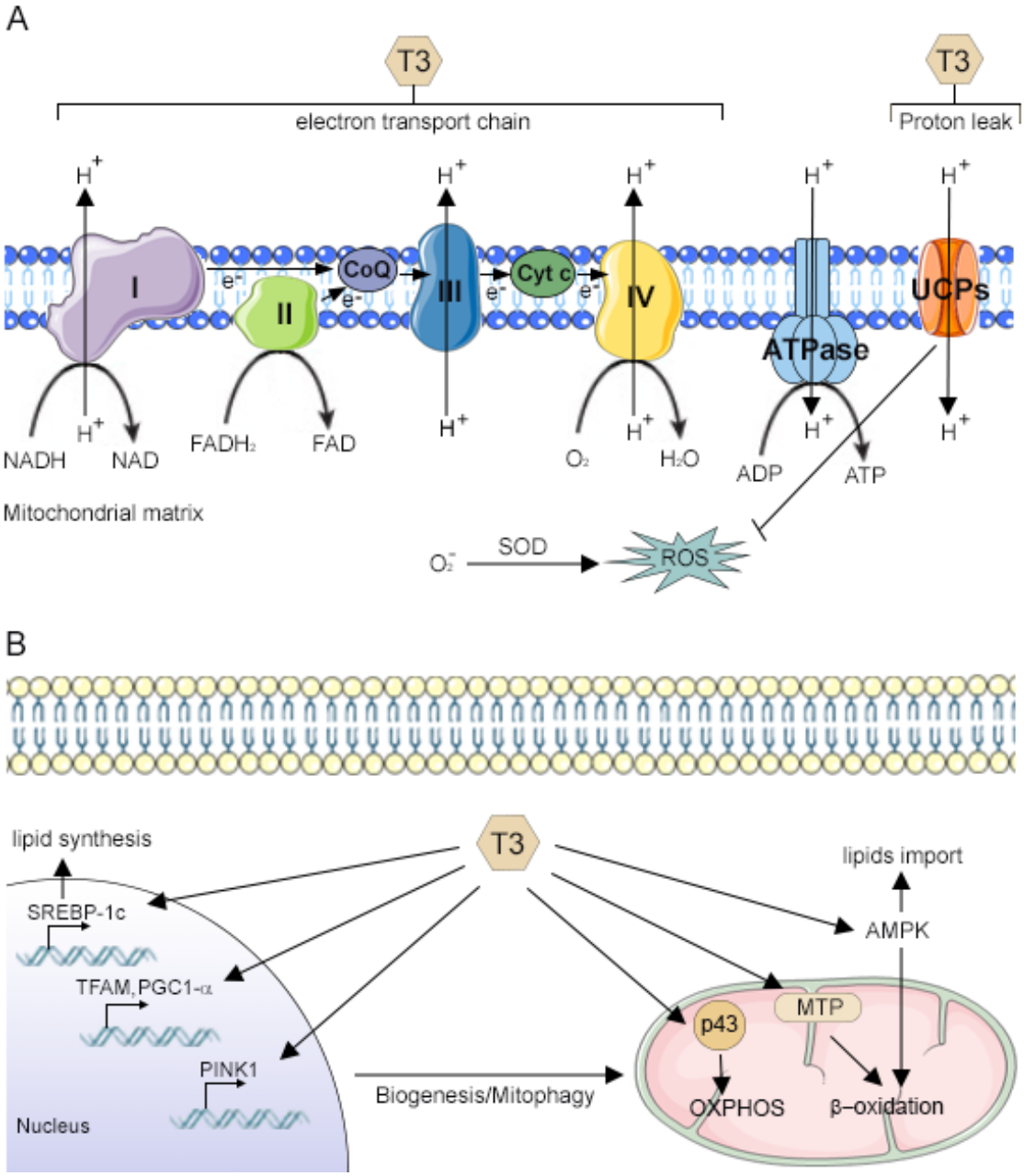

Figure 9. Schematic representation of the main effects of thyroid hormones in cellular metabolism. (A) THs increase oxidative phosphorylation (OXPHOS), but also decrease the efficiency of ATP production and ROS production during mitochondrial respiration by inducing UCPs expression. (**B)** THs promote mitochondrial biogenesis and mitophagy. In addition, they increase both lipid synthesis and lipid catabolism. The figure was generated using images from Servier Medical Art.

In contrast, THs also decrease the efficiency of mitochondrial respiration, since they induce the expression of UCP1, UCP2 and UCP3 (Lanni et al., 2003). Since UCP2 and UCP3 have antioxidant capacities, the induction of these proteins by THs also indicate a role of these hormones in the redox state of the mitochondria. Actually, Chi *et al.* found that treatment with T3 supressed the development of hepatocellular carcinoma by lowering ROS production, while hypothyroidism induced by 0.02% methimazole and 0.1% sodium perchlorate treatment accelerated the development of this type of cancer in hepatic HBx transgenic mice. Noteworthy, the authors found that T3 treatment enhanced mitochondrial turnover by inducing both mitochondrial biogenesis and mitophagy. As a result, the quality of cellular mitochondria was improved and ROS production was reduced (Chi et al., 2017).

Maintaining a healthy population of mitochondria is also relevant for a proper lipid metabolism, since the majority of fatty acid β-oxidation occurs within this organelle. THs promote lipid synthesis via the activation of mTOR, which induces the expression of SREBP-1c, a master regulator of lipid synthesis. However, one of the most widely studied effects of THs is the reduction of cholesterol and lipid levels (Damiano et al., 2017, Finan et al., 2016). On the other side, hypothyroidism is strongly associated with non-alcoholic fatty liver disease (NAFLD), while the use of THs and thyromimetics is a promising strategy to treat it (Finan et al., 2016, Ferrandino et al., 2017).

Fatty acids are converted into fatty acyl-CoA within cells in order to use them as fuel for mitochondrial metabolism by β-oxidation, or for other purposes, such as membrane synthesis. AMP-activated protein kinase (AMPK) acts as a sensor of the energy status of the cell and, depending on its activity, acyl-CoA would be used to

produce energy or would be stored. Remarkably, THs induce the activating phosphorylation of AMPK (Thr 172), which in turns promotes the membrane localization of fatty acid transport protein (FATP) and fatty acid translocase cluster determinant 36 (CD36), enhancing fatty acids uptake to the cell. Moreover, phosphorylated AMPK inhibits the enzyme acetyl-CoA carboxylase (ACC) via Ser79 phosphorylation, which catalyses the synthesis of malonyl-CoA from acetyl-CoA. Malonyl-CoA inhibits the carnitine palmitoyl transferase 1 (CPT1), a protein needed for the entrance of fatty acyl-CoA into the mitochondria. In addition to cytoplasmic AMPK, several reports have suggested that direct targets of THs within mitochondria can also increase β-oxidation rate (Sayre and Lechleiter, 2012) (Figure 9B). In this regard, Chocron et al., showed that T3 promotes the stabilization of the mitochondrial trifunctional protein (MTP), which catalyses the last three reactions (hydration, dehydrogenation, and cleavage) of the β-oxidation of long fatty acids (Chocron et al., 2012). Through these mechanisms, both T3 and T2 have been shown to increase fatty acid oxidation. This may explain why THs decrease lipid content in tissues, such as skeletal muscle and liver, despite increasing fatty acid import (through FATP and CD36) and lipid synthesis by inducing SREBP1c expression (Lombardi et al., 2012, Damiano et al., 2017).

In addition to reducing lipid content in several tissues, THs have also been shown to induce several beneficial changes in whole body metabolism, such as weight loss, reduction of serum cholesterol and triglycerides (Moreno et al., 2011). However, both hypothyroidism and hyperthyroidism have been associated with metabolic problems, such as T2DM. Hypothyroidism is associated with decreased glucose absorption by the intestinal tract, insulin synthesis and glucose disposal. In contrast, hyperthyroidism

correlates with increased glucose production and secretion by the liver, hyperinsulinemia and insulin resistance (Duntas et al., 2011). Therefore, the effect of THs in metabolic homeostasis need to be further studied.

II. OBJECTIVES

Hypothesis: We hypothesize that Pax8 might be involved in diabetogenesis and glucose homeostasis, either directly by its expression in pancreatic islets, indirectly via the action of thyroid hormones or due to a combination of both. In addition, we also hypothesize that T4 supplementation may have a beneficial effect on glucose homeostasis.

The main objective of this thesis is to determine the role of Pax8 and thyroid hormones in metabolic homeostasis and diabetogenesis. In order to do that, the following specific aims are addressed:

1. Determine the role of Pax8 in pancreatic islet physiology and the development of gestational diabetes.
2. Determine the role of Pax8 deficiency in the development of T2DM in male aging mice.
3. Determine the effect of T4 supplementation in healthy C57BL/6 mice as well as in the RIP/B7.1 and STZ models of experimental diabetes.

III. MATERIALS & METHODS

3.1 Mice management

Procedures involving the use of live animals were approved by the CABIMER Animal Committee and performed in accordance with the Spanish law on animal use RD 53/2013 and the EU Directive 2010/63/EU for animal experiments. Animals were housed in individually ventilated cages (Tecniplast, Buguggiate, Italy) (one to five mice per cage) in a specific pathogen-free facility and kept under controlled environmental conditions (12 hours-light–dark cycle, 23 ± 1 °C with 30–50% relative humidity). Mice were provided with standard rodent chow (Envigo, TD2914), unless stated otherwise, and sterilized tap water *ad libitum.* For the HFD study, a chow enriched with 65% of fat was used (Envigo, TD06414).

3.2 Experimental groups

C57BL/6J mice were used as the control wild type (WT) group in all the studies. Likewise, all the transgenic mice used in this thesis have a C57BL/6J genetic background. Pax8 knockout mice were obtained from Infrafrontiers mouse repositorium, Italy. These animals were originated by the replacement of the second exon of Pax8 gene with a neomycin cassette (Mansouri et al., 1998). RIP-B7.1 mice were supplied by Dr Bernhard O. Boehm (Ulm University Medical Centre, Ulm, Germany). These mice express the B7.1 costimulatory protein under the rat insulin promoter (RIP-B7.1) (Pechhold et al., 2003).

Mouse genotyping was performed by PCR in a 0.4 mm tail sample obtained at day 10 after birth. Extraction and amplification of genomic DNA was performed using the REDExtract-N-AmpTM Tissue PCR Kit (Sigma-Aldrich; 031M6112) and the

specific primers used for the polymerase chain reaction (PCR) are outlined in table 1 (Mellado-Gil et al., 2016, Yang et al., 2012).

For pregnancy studies, WT and Pax8 +/- females between 3 and 6 months of age were used. Pax8 -/- female mice could not be used since they are infertile despite T4 supplementation (Mittag et al., 2007). All the metabolic tests were performed at day 14 of pregnancy, where the peak in Pax8 expression in pancreatic islets is found. Mating of animals was conducted overnight in a ratio of 1 male to 3-4 females. Successful mating was confirmed by the presence of a vaginal mucous plug the following morning. In some cases, (7.5 μg/g) of Poly I:C (double stranded RNA), which mimics a viral infection, was injected intraperitoneally from pregnancy day 1 to 5 and 8 to 14 (Figure 10A) (Moriyama et al., 2002).

Table 1. Primers used for mice genotyping.

Gene	Sequence
Pax8	5'-GGATGTGGAATGTGTGCGAGG-3' 5'-GCTAAGAGAAGGTGGATGAGAG-3' 5'-GATGCTGCCAGTCTCGTAG-3'
RIP-B7.1	5´-CAAACAACAGCCTTACCTTCGG-3' 5´-GCCTCCAAAACCTACACATCCT-3'

In order to study the role of Pax8 in the development of T2DM, WT, Pax8 +/- and Pax8 -/- male mice, supplemented or not with T4, were used. T4 supplementation was initiated at postnatal day 1 by giving a subcutaneous injection of 18 ng/g of T4 until weaning. After weaning 5 μg/ml of T4 was administrated in the drinking water. All the metabolic tests were carried out between 7 to 9 months of age. Rotarod and wirehang tests were performed in mice ranging from 9 to 15 months old. Moreover, animals were weighted monthly. A cohort of animals was sacrificed after 16 hours of fasting at 9

months old by cervical dislocation and tissues were harvested for further analysis (Figure 10B). A group of WT and Pax8 +/- male mice were fed with HFD from the second or third month of life. In this cohort fed with HFD, metabolic tests were performed between 6-8 months of life and euthanization was performed at 7-8 months old (Figure 10C).

In order to study the effect of T4 supplementation in glucose homeostasis in healthy mice, WT female mice treated or not with T4 were used. Animals were injected subcutaneously with 18 ng/g of T4 from postnatal day 1 until weaning. After weaning, 50 μg/ml of T4 was administrated in the drinking water. Metabolic tests were performed between 2 to 4 months of age and tissues were harvested at 6 months of age (Figure 10D). All animals were fasted for 16 hours prior euthanization by cervical dislocation. In addition, 4 animals per group received an intraperitoneal dose of 0.75 U/Kg per body weight of insulin 15 minutes prior sacrifice. For experiments related to experimental autoimmune diabetes (EAD), transgenic RIP-B7.1 mice were used. T4 supplementation (5 μg/ml of T4 in the drinking water) was started at 6 weeks of age. EAD was triggered by intramuscular immunization at 8 weeks of age with 50 μg of pC1/ppins plasmid DNA (1 μg/μl) containing the pre-proinsulin II. At 11 weeks of age, animals were killed by cervical dislocation (Figure 10E). For experiments related to chemically induced diabetes mellitus, thirty-four-week-old male C57BL/6 mice were treated with T4 (5 μg/ml of T4 in the drinking water) during two weeks. After 2 weeks of T4 treatment, experimental diabetes mellitus was triggered by two intraperitoneal injections (one each day for two consecutive days) of STZ (150 mg/kg). STZ was dissolved in 10 mM Na-citrate buffer (pH 4.5) each day (Verga Falzacappa et al., 2011). Mice were killed if circulating glucose levels were above 500 mg/dl for more than 96 hours (Figure 10F).

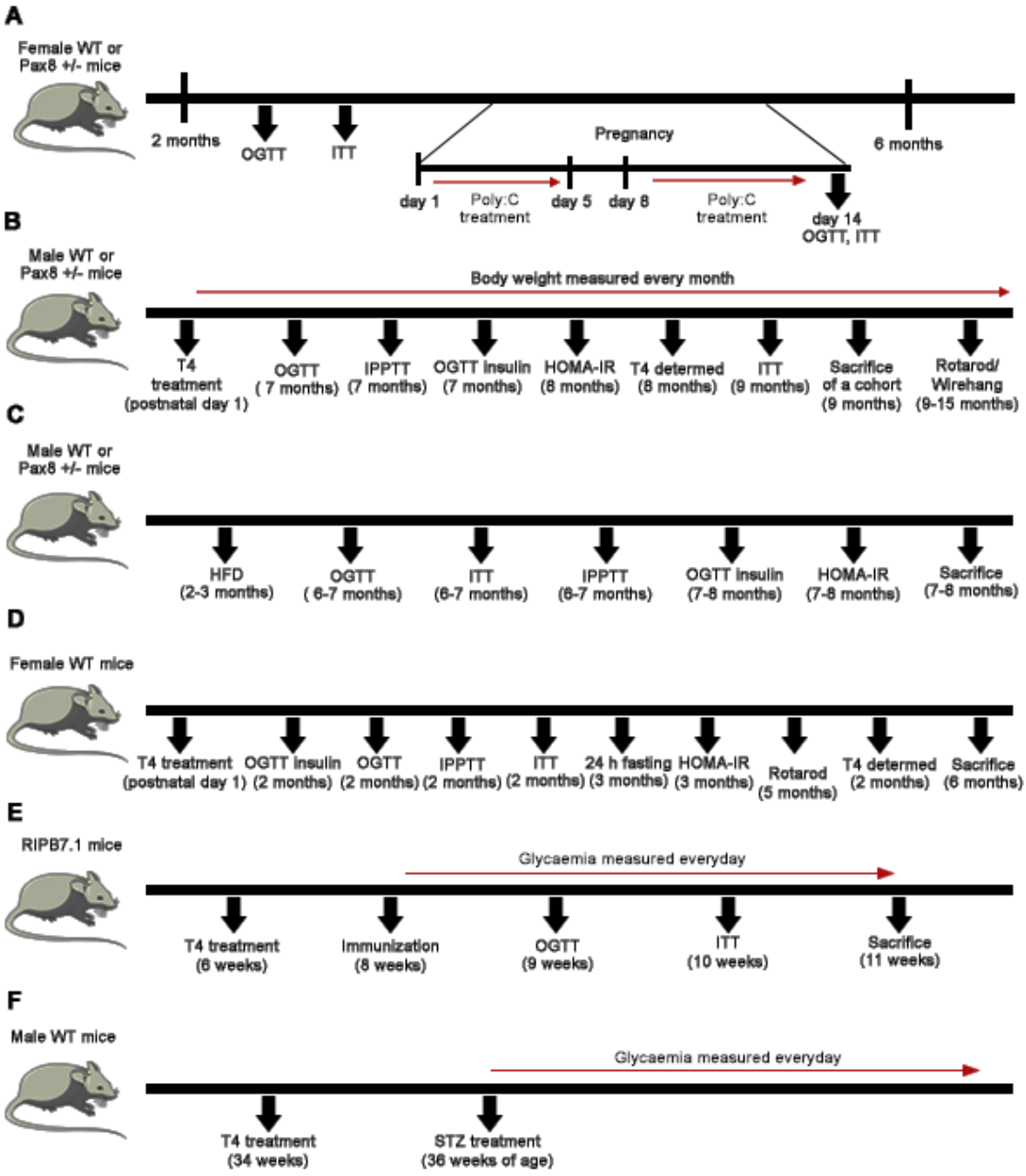

Figure 10. Experimental groups used in this thesis and metabolic tests performed. (A) Pregnancy studies. **(B-C)** Study on Pax8 deficiency in males on standard diet (B) and on HFD (C). **(D)** Effect on T4 supplementation in healthy mice. (**E)** Effect on T4 supplementation in the RIP-B7.1 model of EAD. (**F)** Effect of T4 supplementation on mice treated with STZ.

3.3 T4 determination

To determine T4 concentration in serum, blood was collected by tail venepuncture in eppendorfs and incubated for 30 minutes at room temperature (RT) in order to let blood clot. Afterwards, blood was centrifuged at 4000 x g during 20 minutes and serum was collected into new tubes. T4 levels were determined using the total T4 enzyme immunoassay test kit (MP Biomedicals, 07BC-1007), according to the manufacturer's instructions. Briefly, 25 µl of serum were placed into the antibody-coated wells and incubated with 100 µl of the conjugate reagent at RT for 1 hour. After washing with distilled water 5 times, 100 µl of 3,3',5,5'-Tetramethylbenzidine (TMB) were added for colour development and incubated for 20 minutes at RT in the dark. Then, stop solution was added and absorbance was read at 450 nm using a Varioskan Flash spectrophotometer (Thermo Scientific).

3.4 α-GSU determination.

To determine α-GSU levels, blood was collected by tail venepuncture in EDTA covered tubes and centrifuged immediately at 4 ºC during 20 minutes at 4000 x g to obtain plasma. Then, α-GSU was determined using a commercially available kit following the manufacturer's instructions (Abbexa, abx 254594). First, samples were diluted 1:100 in the sample diluent buffer and placed into the ELISA plate after performing two washing steps. The plate was incubated for 90 minutes at 37 ºC and two further washes were performed. Next, 100 µl of the biotin-conjugated antibody working solution were added into each well and incubated for 60 minutes at 37 ºC. After washing three more times, HRP-Streptavidin Conjugate (SABC) solution was added and left for 30 minutes at 37

ºC. 5 washing steps were conducted before adding TMB solution and then the plate was incubated for 15 minutes at 37 ºC in the dark. Finally, 50 µl of the stop solution were added and absorbance was measured at 450 nm using a Varioskan flash spectrophotometer (Thermo Scientific).

3.5 Oral glucose tolerance test (OGTT)

OGTTs were performed at 4 post meridiem (p.m.). Animals were fasted 6 hours prior the experiment and received an oral dose of glucose (3 g/kg of body weight) by gavage. Blood glucose levels were determined by tail venepuncture using a glucose meter Optimum Xceed (Abbott) at 0, 15, 30, 60 and 120 minutes after the glucose load. For insulin measurements, blood was collected in EDTA covered tubes at times 0, 15 and 30 minutes after the glucose load. Subsequently, blood was centrifuged at 4000 x g during 20 minutes at 4 ºC and plasma was collected. Insulin was determined by ELISA (CrystalChem, 90080), according to the manufacturer's instructions (Martin-Montalvo et al., 2013).

3.6 Insulin tolerance test (ITT)

ITTs were performed at 1 p.m. and animals were fasted 3 hours prior the experiment. In the studies where females were used, animals received an intraperitoneal insulin injection of 0.75 $U \cdot Kg^{-1}$ of body weight. In contrast, males received an insulin injection of 1.5 $U \cdot Kg^{-1}$ of body weight. Blood glucose levels were then determined by tail venepuncture using a glucose meter Optimum Xceed (Abbott) at 0, 15, 30, 60 and 120 minutes after the insulin injection (Martin-Montalvo et al., 2013).

3.7 Intraperitoneal pyruvate tolerance test (IPPTT)

IPPTs were performed at 4 p.m. after mice were fasted for the previous 6 hours. Mice received an intraperitoneal injection of 2 g/kg of body weight of sodium pyruvate (Sigma-Aldrich). Blood glucose was determined by tail venepuncture using a glucose meter Optimum Xceed (Abbott) at 0, 15, 30, 60 and 120 minutes after the pyruvate load.

3.8 24 hours fasting

For the 24 hours fasting study, animals were fasted from 8 p.m. and glucose levels were measured at 0, 4, 6, 12, 16, 20 and 24 hours during fasting by tail venepuncture using a glucose meter Optimum Xceed (Abbott).

3.9 Homeostatic model assessment: insulin resistance (HOMA-IR)

In order to determine the HOMA-IR, glucose levels were measured by tail venepuncture using a glucose meter Optimum Xceed (Abbott) at 16 hours of fasting. At this time, blood was also collected in EDTA covered tubes and centrifuged at 4000 x g during 20 minutes to obtain plasma. Insulin was measured in plasma by ELISA (CrystalChem, 90080), according to the manufacturer's instructions. Glucose and insulin levels were then used to estimate insulin resistance by the HOMA2 Calculator available from Oxford website (Levy et al., 1998).

3.10 HbA1c

HbA1c levels were determined in blood samples using Hemoglobin A1c (HbA1c) Assay kit (CrystalChem, 80099), according to the manufacturer's protocol. Briefly, 5 µl

of whole blood samples were incubated with a lysis buffer for 10 minutes to completely lyse the red blood cells. Then, 25 µl of the lysate was incubated in a microplate together with 160 µl of protease buffer for 5 minutes at 37 ºC. After that incubation, a first absorbance measurement was taken at 700 nm. An enzyme solution (70 µl) was further added and final absorbance at 700 nm was measured using a Varioskan flash spectrophotometer (Thermo Scientific) after another 5 minutes of incubation at 37 ºC.

3.11 Rotarod

Results from rotarod tests are presented as the time to fall from an accelerating rotarod (4–40 rpm over 5 minutes). Mice were given a 1-minute habituation trial at 4 rpm on the day before the experiment. Results shown are the averages of three trials per mouse (Mitchell et al., 2014).

3.12 Wirehang

For wirehang test, mice were allowed to grip a horizontal 1-mm wire with four paws up to 60 seconds and the latency to fall from the wire was determined. Three different trials were performed with each mouse (Gomez et al., 1997).

3.13 Energy intake determination

In order to determine the daily energy intake, 150 g of chow were placed in each individual cage (n = 5 wt; n = 6 Pax8 +/-). After each week, the weight of the remaining chow was measured for individual cages and mouse chow was added to reach 150 g. The total amount of chow consumed every week was then divided by the total number of mice in each cage. In order to determine the fasting-induced energy intake, animals were fasted

overnight. Then, animals were individualized and 10 g were placed in each cage. The amount of chow consumed by each animal was measured after 4 and 8 hours (Sun et al., 2016).

3.14 Determination of the content of lipid in faeces.

In order to determine faecal lipid content, the bedding of each cage was collected after two days in a new, clean cage. The faeces were handpicked and dried at 55 ºC for 3 days. Then, 5 ml of 0.9 % NaCl were added to 1000 mg of powdered dried faeces. After vortex, 5 ml of a solution 2:1 of chloroform-methanol was added. Once centrifuged for 10 minutes at 1000 x g, the liquid bottom phase that contained the lipids was taken, dried and weighted (Kraus et al., 2015).

3.15 Transaminases determination

Blood obtained by tail venepuncture was used to measure serum glutamic oxaloacetic (GOT), and serum glutamic-pyruvic transaminase (GPT). A drop of blood was placed in a strip for each transaminase, Reflotron GPT (ALT) (10745138) and Reflotron GOT (AST) (100745120), and measured using reflotron plus (Roche).

3.16 Cholesterol determination

Cholesterol and concentrations of high-density lipoprotein (HDL) as well as Low-density/very low-density lipoprotein (LDL/VLDL) in serum were determined using the EnzyChrom AF HDL and LDL/VLDL Assay kit (BioAssay Systems, E2HL-100), according to manufacturer's instructions. First, 20 µl of serum were mixed by vortex with 20 µl of precipitation reagent. After centrifuging the samples at 9500 x g for 5 minutes,

HDL was obtained from the supernatant. The pellet was resuspended in PBS to measure LDL concentration. Subsequently, 24 µl of each fraction were diluted in 96 µl of assay buffer. Total cholesterol was obtained by diluting 12 µl of serum in 108 µl of assay buffer. Next, 50 µl of each dilution were placed into a 96-well plate and incubated for 30 minutes at RT together with 50 µl of a working solution containing the enzyme mix and dye reagent. Finally, absorbance was read at 570 nm using a Varioskan flash spectrophotometer (Thermo Scientific).

3.17 Triglyceride determination

Triglycerides were determined using an EnzyChrom Triglyceride Assay Kit (BioAssay Systemsm, ETGA-200). In order to measure the concentration of triglycerides in plasma, samples were diluted 5-fold in Milli-Q water. In order to determine triglyceride content within liver and gastrocnemius, tissues were homogenized in 5% Triton-X100 (Sigma-Aldrich) using a mortar and pestle. The supernatant was taken after centrifuging at 18000 x g during 5 minutes. Next, 10 µl of samples were placed into a 96 well together with 100 µl of the working reagent (containing 100 µl of assay buffer, 2 µl of enzyme mix, 5 µl of lipase, 1µl of ATP and 1 µl of dye reagent). The plate was then incubated for 30 minutes at RT and the absorbance was measured at 570 nm using a Varioskan flash spectrophotometer (Thermo Scientific).

3.18 Lipidomics

In order to determine the different composition of fatty acids in WAT, liver and skeletal muscle, 20 mg of each tissue was weighted and homogenized using a polytron (PRO250 Homogenizer, PRO Scientific) in 350 µl of a solution 3:2 of hexane-

isopropanol, 0,1% BHT (Hara and Radin, 1978). Tissues were then incubated overnight at 4 ºC and, subsequently, 250 µl of sodium sulphate were added. After centrifugation at 2000 x g for 80 seconds the upper hexane rich layer was analysed for different lipid species by gas chromatography by Enrique Force's group at Instituto de la Grasa.

3.19 Isolation of islets

Mice were sacrificed by cervical dislocation and pancreatic islets were isolated by injecting 0.7 mg/ml of collagenase type V (Sigma-Aldrich) into the pancreas by cannulation of the Winsur duct. After the extraction, the pancreas was incubated for 10 minutes at 37 ºC in a water bath. Then, islets were handpicked (Jimenez-Moreno et al., 2015).

3.20 Human islets

Human islets were kindly provided by Dr. D. Bosco (The Cell Isolation and Transplantation Centre, Department of Surgery, Geneva, Switzerland) and were cultured in CMRL-1066 (Cellgro) supplemented with 10% FBS, 100 U/ml penicillin, 100 µg/ml streptomycin and 100 µg/ml gentamycin (Sigma-Aldrich) (Jimenez-Moreno et al., 2015). The characteristics of the donors used for this thesis are outlined in table 2.

Table 2. Donors from which human pancreatic islets were obtained.

Donor	Islet Viability	Islet Purity	Islet Size	Average Islet Size
Number #1	80 %	80 %	50-400 µm	100-200 µm
Number #2	80 %	80 %	50-400 µm	100-200 µm
Number #3	88 %	88 %	50-400 µm	100-200 µm
Number #4	90 %	70 %	50-400 µm	100-200 µm
Number #5	95 %	90 %	50-400 µm	100-200 µm
Number #6	95 %	90 %	50-400 µm	100-200 µm

3.21 Lentivirus production

For production of lentiviruses, 6×10^6 Hek293T cells were seeded into a 100 mm Petri dish (Nunc) and cultured for 24 hours. Then, cells were transfected with 2.29 ug/per plate of the transfer vector pHRSIN, harbouring or not the gene of interest (human PAX8 or murine Pax8) under the Spleen Focus-Forming Virus (SFFV) promoter and the green fluorescent protein (GFP) marker under the constitutive ubiquitin promoter, already available in our laboratory (Jimenez Moreno, 2015). Transfection was then performed using the LipoD293 DNA In Vitro Transfection Reagent (SignaGen Laboratories) (45 µl per plate). In addition, two human immunodeficiency virus packaging plasmids were added at the following concentrations: pCMVDR8.91 (1.53 µg/ per plate) and pVSVG (0.76 µg/ per plate). Lentiviruses were harvested 72 hours post-transfection, passed through a 0.45 µm Millex-HV filter (Merck Millipore), and concentrated by ultracentrifugation in an Optima TM L-100K ultracentrifuge at 87300 x g for 90 minutes at 4 ºC in a swinging rotor SW-28 (Beckman-Coulter). Virus particles were resuspended in serum-free DMEM (Invitrogen) and stored at −80 °C until used. In order to determine lentiviral particle titers, Hek293T cells were seeded at a confluence of 10^5 cells, in a twelve-well plate. Then, lentiviral particles were added and titer was estimated by flow cytometry 72 hours post-infection (FACSCalibur, BD Biosciences) (Jimenez-Moreno et al., 2015).

3.22 Transduction of pancreatic islets

Freshly isolated islets were cultured for 3 hours for recovery in 2.5 ml of complete RPMI medium (Sigma) supplemented with 10% Fetal Bovine Serum (FBS) (Sigma), 100

U/ml penicillin, 100 µg/ml streptomycin (Sigma-Aldrich), 2 mM glutamine (Sigma-Aldrich), 1 mM sodium pyruvate (Sigma-Aldrich), 50 µM β-mercaptoethanol (Gibco) and HEPES 10 mM (Gibco). Then, islets were incubated with 1000 µl of warm (37 ºC) 0.5 X trypsin-EDTA (250 mg/L trypsin; 0.48 mM EDTA) for 3 minutes in a cell culture incubator (37 ºC, 5% CO_2). The 0.5 X trypsin-EDTA was prepared from Trypsin-EDTA 10 X (5000 mg/l trypsin; 9.6 mM EDTA) (Gibco) diluted in Hanks Balanced Salt Solution (HBSS) 1 X (Gibco). In order to inhibit trypsin activity, 1000 µl of RPMI complete medium were added and islets were centrifuged at 50 x g for 2 minutes. Afterwards, the supernatant was removed and islets were resuspended in 100 µl of serum free RPMI. Lentiviruses were added at multiplicity of infection (MOI) 20, assuming that a single islet has 1000 cells. Pancreatic islets were incubated over-night in a cell culture incubator (37 ºC, 5% CO2) and medium was changed to 200-500 µl of complete RPMI medium (Jimenez-Moreno et al., 2015). For optimal lentiviral transduction and viability of islets, experiments were carried out at 72 hours post-infection.

3.23 Transcriptomic analysis by RNA microarray

Total RNA from at least 200 islets of 3 different donors transduced either with a lentiviral vector harbouring PAX8 or GFP (control) was extracted using the RNeasy Micro Kit (Qiagen, 74034), according to the manufacturer's instructions. Briefly, islets were homogenized in 350 µl of RLT lysis buffer containing β-mercaptoethanol (10 µl of β-mercaptoethanol in 1 ml RLT buffer) using a syringe. After centrifuging for 3 minutes at 20000 x g the supernatant was taken and 1 volume of ethanol 70% was added. The sample, was next transferred to a RNeasy MinElute spin column placed in a 2 ml collection tube and centrifuged for 15 s at ≥ 8000 x g. The spin column was further

centrifuged 15 s at 8000 x g after adding 350 µl of RW1 buffer, which is used to wash membrane-bound RNA. Subsequently, 80 µl of a DNase solution were added and incubated for 15 minutes at RT. Then, 350 µl of RW1 buffer were added and the spin column was centrifuged for 15 s at 8000 x g. Next, 500 µl of RPE buffer, which is also used to wash membrane-bound RNA, were added. After another centrifugation for 15 s at 8000 x g, 500 µl of 80% ethanol were added and the spin column was centrifuged for 2 minutes at 8000 x g. Total RNA was eluted in 14 µl of RNase free water.

Subsequent microarray was performed by the Genomic core facility of CABIMER using standard protocols. Briefly, 20 ng of total cRNA per sample were hybridized to GeneChip Human Gene 2.0 ST (Affymetrix) and the signal reading was performed with the Scanner 3000 7G (Affymetrix). Data were processed with the software Affymetrix GeneChip Command Console 2.0, generating the *CEL files (containing the hybridization raw data) and *CHP files (containing the normalized data). SST-RMA (Signal Space Transformation-Robust Microarray Analysis) was the method followed for the normalization, since it makes a background correction and a normalization, enabling the expression comparisons. Results were analysed using the platform Ingenuity Pathway Analysis (IPA) (Ingenuity, USA) as well as the transcriptome analysis console (TAC) software (Affimetrix) by personnel from our laboratory.

3.24 MTT (3-(4,5-dimethylthiazol-2-yl)-2,5-diphenyltetrazolium bromide) assay

Groups of 35 islets were handpicked to determine the metabolic activity of the islets using a Cell Proliferation Kit I (MTT), according to the manufacturer's protocol (Roche, Spain). Briefly, islets were incubated with 0.5% MTT for 4 hours. Then, blue

formazan crystals were solubilized overnight with 100 µl of solubilization solution. Optical density was determined at 550 nm with a reference wavelength of 650 nm, using a Varioskan Flash spectrophotometer (Thermo Scientific) (Jimenez-Moreno et al., 2015).

3.25 Glucose stimulated insulin secretion (GSIS)

GSIS was performed to assess islet functionality. Groups of 10 islets were washed in 500 µL of Krebs-Ringer bicarbonate-HEPES buffer (KRBH) (140 mM NaCl, 3.6 Mm KCl, 0.5 mM NaH_2PO_4, 0.5 mM $MgSO_4$, 1.5 mM $CaCl_2$, 2 mM $NaHCO_3$, 10 mM HEPES, 0.1 % bovine serum albumin (BSA)) and pre-incubated at 37 °C for 45 minutes in 300 µl of the same buffer. Islets were then centrifuged and KRBH buffer was discarded. Subsequently, fresh KRBH supplemented with 2.5 mM glucose was added and islets were incubated for 30 minutes. Then, buffer was harvested (basal insulin secretion) and 500 µL of KRBH supplemented with 22 mM glucose were added. Islets were incubated for an additional 30 minutes at 37 °C and the buffer was harvested (glucose induced insulin secretion). Insulin levels were measured using a mouse insulin ELISA kit according to the manufacturer's instructions (Crystal Chem, 90080). Stimulation index was expressed as the ratio of insulin levels at 22 mM glucose divided by insulin levels at 2.5 mM glucose (Mellado-Gil et al., 2016).

3.26 Cell death determination

Groups of 10 islets were handpicked to determine the degree of apoptosis using a Cell death detection ELISA plus kit, according to the manufacturer's instructions (Roche, Spain). Briefly, islets were lysed with 200 µl of a lysis buffer and centrifuged at 200 x g for 10 minutes. Then, 20 µl of the supernatant was placed into the ELISA plaque and

incubated for 2 hours with 80 µl of the immunoreagent. After the incubation period, samples were washed three times with the incubation buffer and incubated for 10 minutes with 2,2'-azino-bis (3-ethylbenzothiazoline-6-sulphonic acid (ABTS) solution for colour development. Optical density was determined at 405 nm with a reference wavelength of 490 nm using a Varioskan Flash spectrophotometer (Thermo Scientific).

3.27 Genetic screening

PAX8 genetic screening was performed in collaboration with Dr. José Moreno at La Paz hospital in Madrid. In order to determine whether PAX8 genetic variants could be associated with the development of GDM in concurrence with gestational thyroid dysfunction (GTD), a strict selective inclusion criterion was used to define the human cohort of study:

1. Patients presented hypothyroidism: Free levothyroxine T4 < 0.90 ng/dl or TSH > 2.5 mU/l during first trimester of pregnancy or TSH > 3 mU/l during the second/third trimesters of pregnancy of non-autoimmune nature (negative presence of circulating Tg and TPO antibodies).
2. Patients were diagnosed with GDM by OGTT under internationally accepted criteria.
3. Patients reported family history of non-autoimmune hypothyroidism and/or T2DM.

Exclusion criteria were:

1. Patients not taking iodine supplements.
2. Obese patients (BMI> 30).

After obtaining written informed consent, blood was collected and genomic DNA was extracted from peripheral leukocytes utilizing the Chemagen DNA Blood Kit in the

Chemagic TM automated system (Perking Elmer). The entire coding sequence of the human PAX8 gene was amplified by PCR under standard conditions. Primers are described in table 2. DNA sequencing was performed in an ABI370 Sequencer and analysed with Sequencher. The study was approved by the Local Ethical Committee.

3.28 PAX8 site directed mutagenesis and cloning of PAX8 variants

The human and murine PAX8 wild type variants cloned into the pHRSIN DUAL-GFP easy vector were already available in our laboratory. Polymorphisms on PAX8 (P25R and T356M) were introduced using a technical service provided by GenScript (Piscataway, NJ) in the pGEM-T easy vector.

The pGEM-T easy vectors containing PAX8 variants and the PCDNA3.1 vector (already available in our laboratory) were digested with 0.5 µl of BamHI and NotI overnight at 4 ºC. Correct digestion was analysed by electrophoresis in a 0.5% agarose gel dissolved in TBE 1X and containing 0.1 µg/l of ethidiumbromide. DNA fragments were then obtained from the agarose gel and purified using the QIAquick Gel Extraction Kit (Qiagen, 28704), according to manufacturer's instructions. For ligation, 17.5 ng of the inserts were ligated with 50 ng of the PCDNA3.1 vector following a molar ratio of 1:3. Reaction was catalysed by 1 µl of T4 DNA ligase (Promega) and was left for 1 hour at 37 ºC. Then, DNA was added to 50 µl of competent cells. The bacteria were maintained on ice for 15 minutes before receiving a heat shock at 42 °C for 1 minute. The cells were then incubated for 30 minutes at 37 °C with constant shaking in LB Broth. Next, cells were plated on a warm LB/agar plate with ampicillin. Successful colonies were selected and correct ligation was first verified by digestion. Moreover, the correct sequence of all

PAX8 constructs was verified by direct sequencing using the service provided by the CNIO (Madrid).

3.30 Luciferase reporter assay

The Luciferase reporter assay was performed at La Paz hospital in collaboration with Dr. José Moreno's group. Briefly, the human thyroglobulin gene promoter (hTg), which is a PAX8 target, was subcloned into the firefly luciferase reporter plasmid. Then it was transfected in HEK293T cells along with expression vectors for the Thyroid Transcription Factor 1 (TTF1; also known as NKX2.1) in combination with PAX8Wt, T356M or P25R using the FuGENE6 reagent (Promega Biotech Iberica, Madrid, Spain). To correct for transfection efficiency, Renilla-encoding pRL-CMV vector was co-transfected in all cases. Cellular extracts were collected 48 hours post-transfection, and Dual-Luciferase Reporter Assay (Promega) was performed according to the manufacturer's instructions. The ratio between the luciferase and Renilla activities was expressed relative to the ratio obtained in cells transfected with reporter and empty expression vector (pcDNA3).

3.31 PAX8 variants stability and subcellular localization

MCF-7 cells, which do not express PAX8, were grown in DMEM medium supplemented with 10% FBS and 1% penicillin and streptomycin (Invitrogen).

In order to study the protein stability of PAX8 variants, 3 x 10^5 MCF-7 cells were seeded in 6 well plates and transiently transfected using the PCDNA3.1 constructs 24 hours later. For transfection in 6 well plates, 4 μg of DNA and 10 μl of lipofectamine

2000 (Invitrogen) both resuspended in 250 µl of Optimem medium were used for each well. 24 hours after transfection, 80 µg/ml of cycloheximide were added. Cells were frozen in liquid nitrogen and processed for protein extraction to perform western blots at the following times: 24 hours after transfection and before cycloheximide treatment (referred as time 0 h); 48 hours post transfection and thus 24 hours after cycloheximide treatment (referred as time 24 h); 72 hours post transfection and 48 hours post cycloheximide treatment (referred as time 48 h).

To determine whether the subcellular localization of PAX8 variants was affected, $3x10^4$ MCF-7 cells were seeded in 12 mm diameter glass coverslips (Menzel-Glaser) in 24 well plates. Transfection was performed 24 hours later using 1.6 µg of DNA and 2 µl of lipofectamine 2000 (Invitrogen), both resuspended in 50 µl of Optimem medium. 24 hours post transfection, cells were washed with PBS 1X 3 times and fixed with 100% Methanol at -20 ºC for immunofluorescence.

3.32 Western blots

Cells and tissues were lysed in radioimmunoprecipitation assay buffer (RIPA buffer: 20 mM Tris-HCl, 150 mM NaCl, 1 mM Na_2-EDTA, 1 mM EGTA, 1% NP-40, 1% sodium deoxycholate) with 1% Phosphatase Inhibitor Cocktails (P0044 and P5725, Sigma-Aldrich), 1% Protease Inhibitor Cocktail (P8340, Sigma-Aldrich) and 1% Deacetylation Inhibition Cocktail (SC-362323, Santa Cruz Biotechnology). Cells were lysed in 50 µl of RIPA buffer per well using a syringe, whereas approximately 10 mg of tissues were homogenized using a Polytron (PRO250 Homogenizer, PRO Scientific) in

250 μL of RIPA buffer per sample. The resulting lysates were centrifuged at 20.000 x g for 10 minutes (4 ºC) and supernatants were harvested.

Colorimetric assessment at 595 nm using a Varioskan Flash (Thermo Scientific) with Quick Start™ Bradford 1x Dye Reagent (BioRad) was used to determine the concentration of protein samples. A series of known concentrations of BSA were used for the calculation of a standard absorbance-concentration curve.

Protein solutions were prepared with Laemmli loading buffer (4% SDS, 10% 2-mercaptoethanol, 20% glycerol, 0.004% bromophenol blue, 0.125 M Tris HCl, pH 6.8) and then heated at 95 ºC during 4-5 minutes. SDS-PAGE (sodium dodecyl sulfate polyacrylamide gel electrophoresis) was performed under reducing conditions at constant voltage (100 V) in 1.5 mm 12% polyacrylamide gels with discontinuous buffer system. The polyacrylamide gels had two differentiated parts: the stacking gel (5% polyacrylamide, 0.1% SDS, 125 mM Tris-HCl, 0.1% ammonium persulfate, 0.025% TEMED (N,N,N',N'-tetramethylethylenediamine), pH 6.8); and the resolving gel (12% polyacrylamide, 0.1% SDS, 375 mM Tris-HCl, 0.1% ammonium persulfate, 0.025% TEMED, pH 8.8). The stacking gel promotes the compaction of the proteins at the same level (the Kohlrausch frontier), enabling an equal beginning of the protein migration through the resolving gel. In each gel, 20 μg of proteins were loaded per well.

Transference from gel to nitrocellulose membrane was performed with Trans-Blot Turbo Transfer System (Bio-Rad), following predetermined Bio-Rad protocols. To check equal and appropriate loading and transference, ponceau staining was made (0.1% Ponceau S (w/v) in 5% acetic acid). Then, membranes were blocked with Tris-buffered

saline 1X +0.1% Tween (TBST), containing 4% of BSA shaking at 50 rpm for 1 hour in a Heidolph Rotamax 120 shaker. Afterwards, primary antibody incubation was made overnight on rotation at 4 ºC in TBST-BSA 4%. The antibodies used are outlined in table 3. Next day, membranes were washed for 15 minutes 3 times with TBST containing 4% of skim milk. Horseradish peroxidase (HRP)-conjugated secondary antibody incubation was then made for 1 hour in TBST-milk 4% (Table 3). Then, membranes were washed three times for 15 minutes each with TBST-milk 4% and three times with TBST. The development was made using Clarity Western ECL Substrate (Bio-rad).

3.33 Immunohistochemistry

3.33.1 Immunofluorescence in cultured cells

After fixing the cells with 100% methanol at -20 ºC, cells were washed 3 times with Phosphate Buffered Saline (PBS) 1X (8 g NaCl, 0.2 g KCl, 1.44 g Na_2HPO_4, 0.24 g KH_2PO_4, pH 7.4, adjust to 1 L with H_2O) for 5 minutes (each wash) and blocked with PBS + 0.2% Tween, containing 2% of BSA for 45 minutes. Then, cells were incubated with the corresponding primary antibodies diluted in PBS + 0.2% Tween-BSA 2% overnight at 4 ºC (Table 3). The next day, cells were washed with PBS 1X three times for 5 minutes each and incubated with matching secondary antibodies conjugated with fluorophores diluted in PBS + 0.2% Tween for 1 hour at RT (Table 3). After performing three washing steps with PBS 1X, nuclear counterstaining was performed by DAPI staining (10 µg/ml; Sigma-Aldrich) diluted 1:1000 in PBS for 5 minutes at RT. Finally, cells were washed three times with PBS for 5 minutes each and mounted using DAKO fluorescent mounting medium (Dako).

3.33.2 Immunofluorescence and immunohistochemistry in tissues and cultured islets

Tissues were fixed in 4% of paraformaldehyde for 24 hours at 4 ºC, while approximately 100 mouse islets were fixed in 10% Formalin (Panreac Appli. Chem) for 48 hours at RT. Subsequently, islets were mixed with approximately 100 µl of 150-300 µm diameter Affi-Gel blue beads (Bio-Rad) and included in warm (70 ºC) HistoGel (Thermo Scientific) (Cozar-Castellano et al., 2004). Histogel containing the islet-bead mixture or tissues were then embedded in paraffin following the standard procedures of CABIMER Histology Core facility.

Paraffin blocks were sectioned (5 µm thickness) using a microtome Leica RM 2255 (Leica Microsystems) and mounted on SuperFrost Plus slides (Menzel-Glaser). Sections were deparaffinized/rehydrated in the oven at 60 ºC for 15 minutes followed by immersion in decreasing concentrations of ethanol (Xylene 5 minutes/2 x; Ethanol 100% 1 minute/2 x; Ethanol 96% 1 minute; Ethanol 80% 1 minute; Ethanol 70% 1 minute; Distilled water 5 minutes/2 x). After deparaffinization and rehydration, sections were subjected to heat-induced antigen retrieval. Antigen retrieval was performed in 10 mM sodium citrate buffer (pH 6.0) either in an autoclave for 10 minutes at 121 ºC or in the microwave in 3 cycles of 3 minutes (with 2 minutes at RT between heating cycles) at 800 W, avoiding the boiling of the buffer. Samples were cold down in the same solution for 20 minutes at RT. For Horseradish peroxidase (HRP) immunohistochemistry, endogenous peroxidase was blocked by incubating sections with a solution of 3% hydrogen peroxide for 15 minutes. After washing with PBS1 X for 3 times, blocking was performed with PBS + 0.2% Triton containing 3% of Donkey serum (Sigma-Aldrich) (for immunofluorescence) or 3% BSA (for immunohistochemistry) for 1 hour at RT. Primary

antibodies at the indicated dilutions were added in PBS + 0.2% Triton X-100 containing 1% BSA and incubated overnight at 4 ºC in a dark humid chamber (Table 3). Subsequently, sections were washed with PBS, followed by PBS + 0.2% Triton X-100 and PBS for 5 minutes each. Then, samples were incubated with secondary antibodies (Table 3) diluted in PBS + 0.2% Triton X-100 containing 0.1% BSA for 1 hour at RT in a dark humid chamber. For immunofluorescence, nuclear counterstaining was performed by DAPI staining (10 μg/ml; Sigma-Aldrich) diluted 1:1000 in PBS for 5 minutes at RT and sections were mounted using DAKO fluorescent mounting medium (Dako). For immunohistochemistry, visualization of the immunoreaction was performed using Vectastain Elite ABC (Vector Laboratories) and 3,3′-diaminobenzidine (DAB) substrate (Vector Laboratories), according with the manufacturer's instructions. The colour reaction was stopped and sections were washed 3 times with PBS 1X. Dehydration of the tissues was subsequently performed by placing the slides in an ascending ethanol series (70%, 80%, 90%, 96%, 2×100% ethanol for 1 minute each one) and through two changes of xylene for 1 and 5 minutes, respectively. Then, sections were mounted with DPX (Sigma-Aldrich) and air-dried. After intensity quantification, sections were counterstained with hematoxylin (Merck).

Table 3. Antibodies used in this thesis.

Antibody	Dilution	Vendor	Catalog number
Anti-Ki67	1:150	Leica Microsystems	NCL-L-Ki67-MM1
Biotin-rabbit anti-mouse	1:300	Sigma-Aldrich	B8520
Alexa fluor 555 donkey anti-mouse	1:800	Thermofisher	A31579
Alexa fluor 647 donkey anti-rabbit	1:800	Thermofisher	A31573
Alexa fluor 488 donkey anti-goat	1:800	Thermofisher	A11055

Anti-insulin (H-86)	1:500	Santa Cruz Biotecnology	SC9168
Anti-insulin	1:500	Sigma-Aldrich	I2018
Anti-somastotatin	1:100	Santa Cruz Biotechnology	SC-7819
Anti-glucagon	1:100	Sigma-Aldrich	G2654
Anti-glucokinase	1:50	Santa Cruz Biotechnology	SC-7908
Anti-Pax8	1:100 WB 1:20 IF	Abcam	Ab124445
Anti-cleaved caspase 3	1:150	Cell Signaling	9661S
Anti-GFP	1:200	Abcam	Ab6673
Anti-MAFA	1:200	Bethyl Laboratories	IHC-00352
Anti-β-catenin	1:200	Cell signaling	9582
Anti-IR-β	1:200	Santacruz Biotechnology	SC-711
Anti-IRS1	1:200	Santacruz Biotechnology	SC-599
Anti-pTyr 632 IRS1	1:200	Santacruz Biotechnology	SC-17196
Anti-PI3K	1:1000	Cell Signaling	4292
Anti-pSer473 AKT	1:500	Cell Signaling	9271
Anti-AKT	1:1000	Cell Signaling	9272
Anti-pSer256 FOXO1	1:300	Cell Signaling	9461
Anti-FOXO1	1:1000 WB; 1:100 IF	Cell Signaling	2880
Anti-GSK3β	1:200	Santacruz Biotechnology	SC-9166
Anti-pThr202/pTyr204 ERK	1:1000	Cell Signaling	9106
Anti-ERK	1:1000	Cell Signaling	9102
Anti-GAPDH	1:1000	Cell Signaling	2118
Anti-β-actin	1:5000	Sigma-Aldrich	A2228
Anti-pThr172 AMPK	1:1000	Cell Signaling	2535
Anti-AMPK	1:1000	Cell Signaling	2532
Anti-LC3B	1:1000	Cell Signaling	2775
Anti-UCP2	1:200	Santa Cruz Biotechnology	SC-6526
Anti-VDAC	1:1000	Abcam	15895
Anti-PGC1α	1:1000	Santa Cruz Biotechnology	SC-517380
Anti-4HNE	1:1000	Millipore	393206
HRP-goat anti-rabbit	1:5000	Sigma-Aldrich	A0545
HRP-rabbit anti-mouse	1:5000	Sigma-Aldrich	A9044
HRP-mouse anti-goat	1:5000	Santa Cruz Biotechnology	sc-2354

3.34 Tunel assay

For the terminal deoxynucleotidyl transferase dUTP nick end labelling (Tunel) staining, the InSitu Cell Death Detection Kit, Fluorescein was used according to manufacturer's instructions (Sigma-Aldrich). Briefly, paraffin sections were deparaffinized/rehydrated as previously described and incubated for 15 minutes at RT with Proteinase K. Then, slides were rinsed with PBS 1X 3 times for 5 minutes each and incubated for 30 minutes at RT in Tris-HCl, 0.1 M pH 7.5, containing 3% BSA and 20% FBS. Afterwards, 50 µl per section of Tunel reaction mixture were added. After 1 hour of incubation in a humid chamber, slides were washed with PBS 1X 3 times during 5 minutes each. Then, slides were incubated with a primary antibody overnight, and the protocol described above for immunofluorescence was continued.

3.35 Hematoxylin and eosin staining

Paraffin sections were deparaffinized/rehydrated as previously described and slides were immersed into hematoxylin (Merck) for 4 minutes. Then, sections were rinsed with abundant tap water. Subsequently, slides were placed in acid ethanol for approximately 5-10 seconds and further rinsed with tap water. Samples were immersed in eosin (Merck) for 2 minutes followed by another washing step with tap water. Finally, sections were dehydrated as described above and mounted with DPX (Sigma-Aldrich).

3.36 Electron Microscopy

For electron microscopy, tissues were fixed in 4% PFA with 2% glutaraldehyde in PBS for 72 hours at 4 ºC (Hinova-Palova et al., 2014). Then, they were washed with

PBS three times and stored in PBS with 0.2% sodium azide. Images were taken at the Príncipe Felipe Institute in Valencia core facility by Mario Soriano.

3.37 Image Quantifications

Western blots were quantified with ImageJ software and normalized to the corresponding housekeeping gene (GAPDH). Likewise, the intensity of DAB immunohistochemical staining and the area of adipocytes were quantified using ImageJ software. Quantifications of cell number/percentage were performed manually using adobe photoshop.

3.38 Mitochondrial electron transport chain activities

In order to measure the activity of mitochondrial complexes and superoxide generation, 10 mg of liver and gastrocnemius of WT and Pax8 +/- mice were used. Tissues were homogenized using a glass conical tissue grinder in 250 µl of a sucrose homogenization buffer 250 mM pH 7.4 (0.121 g of Tris, 0.15 g of KCL, 0.038 g of EDTA and 4.27 g of sucrose in 50 ml of distilled water) (Spinazzi et al., 2012).

3.38.1 Complex I+III activity

15 µg of gastrocnemius extracts or 50 µg of liver extracts were incubated for 2 minutes in a 1ml cuvette containing 765 or 755 µl of distilled water, respectively, in order to induce an osmotic shock. Subsequently, 100 µl of potassium phosphate buffer (0.5 M, pH 7.5), 20 µl of fatty acid-free BSA (50 mg/ ml), 30 µl of KCN (10 mM) (Sigma-Aldrich) and 50 µl of oxidized cytochrome c (1mM) (Millipore) were added. After mixing with a pipette a first read at 550 nm was taken for 2 minutes using a DU-800

spectophotometer (Beckman Coulter). The reaction was then started by adding 20 µl of NADH (10 mM) (Sigma-Aldrich) and the increase in absorbance was measured at 550 nm for 3 minutes using a DU-800 spectrophotometer (Beckman Coulter). The specific activity was calculated assuming a extinction coefficient for reduced cytochrome c of 18.5 mM^{-1} cm^{-1} (Spinazzi et al., 2012).

3.38.2 Complex II+III activity

15 µg of gastrocnemius or 50 µg of liver extracts were incubated for 10 minutes in a 1-ml cuvette containing 860 or 850 µl of distilled water (respectively), 40 µl of potassium phosphate buffer (0.5 M, pH 7.5), 30 µl of KCN (10 mM) (Sigma-Aldrich) and 25 µl of succinate (40 mM) (Sigma-Aldrich). The reaction was started by adding 50 µl of oxidized cytochrome c (1 mM) (Millipore). Then the increase in absorbance at 550 nm was measured for 3 minutes using a DU-800 spectophotometer (Beckman Coulter). The specific activity was calculated assuming a extinction coefficient for reduced cytochrome c of 18.5 mM^{-1} cm^{-1} (Spinazzi et al., 2012).

3.38.3 Superoxide generation

50 µg of gastrocnemius extracts or 100 µg of liver extracts were incubated for 2 minutes in 735 µl of distilled water. Subsequently, 100 µl of potassium phosphate buffer (0.5 M, pH 7.5), 20 µl of fatty acid-free BSA (50 mg/ ml), 30 µl of KCN (10 mM) (Sigma-Aldrich) and 50 µl of partially acetylated cytochrome c (1mM) (Sigma-Aldrich) were added. After mixing with a pipette a first read at 550 nm was taken for 2 minutes using a DU-800 spectophotometer (Beckman Coulter). The reaction was then started by adding 20 µl of a solution containing equal amounts of NADH (10 mM) and succinate (400 mM)

and the increase in absorbance was measured at 550 nm for 3 minutes using a DU-800 spectrophotometer (Beckman Coulter). The specific activity was calculated assuming an extinction coefficient of 18.5 mM^{-1} cm^{-1} (Martin-Montalvo et al., 2013).

3.38.4 Citrate synthase

15 μg of gastrocnemius extracts or 50 μg of liver extracts were added to a 1-ml cuvette containing 320 or 310 μl of distilled water, 500 μl of Tris (200 mM, pH 8.0) with 0.2% of Triton X-100 (Sigma-Aldrich), 100 μl of 5,5'-Dithiobis-(2-Nitrobenzoic Acid) (DTNB) (Sigma-Aldrich), and 15 μl of acetyl coenzyme A (10 mM) (Sigma-Aldrich). After mixing with a pipette, the baseline activity was measured at 412 nm for 2 minutes. Then, the reaction was started by adding 50 μl of oxaloacetic acid (10 mM) and absorbance was read at 412 nm for 3 minutes using a DU-800 spectrophotometer (Beckman Coulter). The specific activity was calculated assuming a extinction coefficient of 13.6 mM^{-1} cm^{-1} (Spinazzi et al., 2012).

3.39 RT- PCRs

Total RNA was extracted from frozen skeletal muscle and liver samples using the Easy-blue RNA extraction kit (Intron Biotechnologies). Briefly, tissues were homogenized using a Polytron (PRO250 Homogenizer, PRO Scientific) in 200 μl of easy-BLUE (Trizol). Then, 40 μl of Chloroform were added, vortex, and the sample was centrifuged at 18000 x g at 4 ºC for 10 minutes. The upper layer was transferred into another tube where isopropanol was added (80 μl) and incubated for 10 minutes at RT. After centrifuging samples at 18000 x g for 10 minutes at 4 ºC, the supernatant was removed and 75 % ethanol was added to the RNA pellet. Finally, another centrifugation

step was performed, the pellet was air-dried and diluted in 20 µl of RNase free water. For islet experiments RNA was extracted using the RNeasy Micro Kit (Qiagen), according to manufacturer's instructions. Complementary DNA (cDNA) was synthesized using random hexamers (Roche) and Superscript II Reverse transcriptase (Invitrogen).

Genomic DNA for mitochondrial DNA determinations, was extracted using the DNeasy Blood & tissue kit (QIAGEN, 60504), according to manufacturer's protocol. Briefly, ~5 mg of gastrocnemius and livers from WT and Pax8 +/- animals were lysed in 180 µl of ATL buffer and 20 µl of proteinase K, mixed by vortexing and incubated overnight at 56 ºC. After vortex, 200 µl of the buffer AL and 200 µl of ethanol (96-100%) were added and mixed by vortexing thoroughly. Then, samples were transferred to the DNeasy Mini spin column and centrifuged at 6000 x g for 1 minute. Next, 500 µl of buffer AW1 were added. After centrifuging at 6000 x g for 1 minute, 500 µl of buffer AW2 were added. Subsequently, the spin column was centrifuged for 3 minutes at 20000 x g in order to dry the membrane. Finally, in order to elute the DNA, 100 µl of buffer AE were added directly into the membrane, incubated for 1 minute at RT and centrifuged for 1 minute at 6000 x g.

The RT-PCR was performed on individual cDNAs or genomic DNA (for the mitochondrial DNA determination) using SYBR green (Roche). Primer sequences are presented in Table 4. The mRNA expression was calculated by the $2^{-\Delta\Delta CT}$ method and normalized to the expression of β-actin or RPS29.

Table 4. Primers used for RT-PCR in this thesis.

Gene	Forward primer sequence	Reverse primer sequence
Mouse PAX8	5'-GTTTGAGCGGCAGCATTAC-3'	5'- GTAAGGGCAGTGGGTACAGC-3'
Human Pax8	5´-CCCCCTACTCCTCCTACAGC-3´	5´-GGCCTTGATGTGGAACTGTAA-3´
Mouse INS1	5′-CCTGTTGGTGCACTTCCTAC-3′	5′-TGCAGTAGTTCTCCAGCTGG-3
Mouse INS2	5′-GCAGCACCTTTGTGGTTCCC-3′	5′-TGCAGTAGTTCTCCAGCTGG-3
Mouse MAFA	5′-CAGCAGCGGCACATTCTG-3′	5′-GCCCGCCAACTTCTCGTAT-3′
Mouse IR-β	5'-ACCCTGGACCCAATACGC-3'	5'-CCATTGGGGTCAGAGGGG-3'
Mouse IRS1	5'-GGCAGGGGAGGACTTGAG-3'	5'-CTGCCTCGGAGTTCAGCT-3'
Mouse AKT	5'-AGGTAGCTGTCAACAAGGCA-3'	5'–CTTGCCGAGGAGTTTGAGA–3'
Mouse FOXO1	5'–GAGAAGAGGCTCACCCTGTC–3'	5'-ACAGATTGTGGCGAATTGAA-3'
Mouse GSK3-β	5'-CCGGCTAACACCACTGGA-3'	5'-GTCCACGGTCTCCAGCAT-3'
Mouse ERK	5'-GCTCACCCTTACCTGGAACA-3'	5'-GGACCAGATCCAAAAGGACA-3'
Mouse GLUT2	5'-TGACTGGAGCCCTCTTGATG-3'	5'-CACTTCGTCCAGCAATGATGA-3'
Mouse GCK	5'-CTTCACCTTCTCCTTCCCTG-3'	5'-ATCTCAAAGTCCCCTCTCCT-3'
Mouse G6Pase	5'-TCTTGTGGTTGGGATTCTGG-3'	5'-CGGATGTGGCTGAAAGTTTC-3'
Mouse LPK	5'-AGTCTTCCCCTTGCTCTACC-3'	5'-AATCACCAGATCACCAACTCG-3'
Mouse PEPCK	5'-CCATCCCAACTCGAGATTCTG-3'	5'-CTGAGGGCTTCATAGACAAGG-3'
GAPDH	5'-CACCAACTGCTTAGCCCC-3'	5'-TCTTCTGGGTGGCAGTGATG-3'
Mouse LDH	5'-AGTCTCCCGTGCATCCTCAA-3'	5'-AGGGTGTCCGCACTCTTCCT-3'
Mouse mtND1	5´-CCTATCACCCTTGCCATCAT-3´	5´-GAGGCTGTTGCTTGTGTGAC-3´
Mouse PECAM	5'-ATGGAAAGCCTGCCATCATG-3	5'-TCCTTGTTGTTCAGCATCAC-3'

Mouse PGC1α	5'–GGGTCAGAGGAAGAGATAAAGTTG–3'	5'–CACCAAACCCACAGAAAACAG–3'
Mouse PGC1β	5'–GTGATAAAACCGTGCTTCTGG–3'	5'–GGTGTTCGGTGAGATTGTAGAG–3'
Mouse RPS29	5'-GGAGTCACCCACGGAAGTT-3'	5'-CATGTTCAGCCCGTATTTGC-3'
Mouse UCP2	5'-GCTTGGGATCCTGGAACGT-3'	5'-GGCAGCCATTAGGGCTCTTT-3'
Mouse SREBP1c	5'-GCATGCCATGGGCAAGTAC-3'	5'–AGCATCTCCTGCGCACTCA–3'
Mouse SREBP2	5'- ACCGGTCCTCCATCAACG-3'	5'- CCAGGTCGATGCCCTTCA-3'
Mouse FASN	5'-TCCTGAATCAGCCCACG-3'	5'-ACACCCATGAGCGAGTCC-3'
Mouse SOCS2	5'-GTAAGGGCAGTGGGTACAGC-3'	5'-GGTAAAGGGAGTCCCCAGA-3'
Mouse IL-1β	5'-AACTGTTGGTGAGGAATGTGG-3'	5'-GGTCCTGTCCCTCTTGTTTTCA-3'
Mouse TNF-α	5'-CCCTCACACTCAGATCATCTTCT-3'	5'-GCTACGACGTGGGCTACAG-3'
Mouse CPT1	5'-AGACAAGAACCCCAACATCC-3'	5'-CAAAGGTGTCAAATGGGAAGG-3'
Mouse LCAD	5'-GGTGGAAAACGGAATGAAAGG-3'	5'-GGCAATCGGACATCTTCAAG-3'
Mouse MCAD	5'-TGTTAATCGGTGAAGGAGCAG-3'	5'-CTATCCAGGGCATACTTCGTG-3'
Mouse ATP5a1	5'-CATTGGTGATGGTATTGCGC-3'	5'-TCCCAAACACGACAACTCC-3'
Mouse COX5	5'-ACCCTAATCTAGTCCCGTCC-3'	5'–CAGCCAAAACCAGATGACAG–3'
Mouse UQCRC1	5'-ATCAAGGCACTGTCCAAGG-3'	5'-TCATTTTCCTGCATCTCCCG-3'
Mouse NDUFAB5	5'-GGACCGAGTTCTGTATGTCTTG-3'	5'-AAACCCAAATTCGTCTTCCATG-3'
Mouse β-ACTIN	5'-GGACCAGATCCAAAAGGACA-3'	5'-GCTCACCCTTACCTGGAACA-3'

3.40 Statistical analysis

For comparisons between two groups, statistical significance was calculated using non-paired two-tailed student's t-test using Excel software, except in the case were values were normalized to 1, in which a Mann-Whitney Rank Sum Test was performed. For comparisons between more than 2 groups a one-way ANOVA or two-way ANOVA tests were performed. If values were relativized to 1, ANOVA on ranks (Kurstal-Wallis) was performed. For metabolic tests (OGTT, ITT etc), repeated measurements two-way ANOVA tests were performed. Except for the t-tests, all the statistical analyses were performed using Graph Pad (Prism 6) and/or SigmaPlot 12.5 software. For all analyses, p-value < 0.05 was considered statistically significant. Errors are represented as the standard error of the mean (SEM). Plots were designed with the software SigmaPlot 12.5.

IV. RESULTS

AIM 1: Determine the role of Pax8 in pancreatic islet physiology and the development of gestational diabetes.

N.B: Results presented herein are part of a manuscript entitled "A novel association of a mutation in PAX8 with Gestational Diabetes Mellitus underlies the transient role of this transcription factor in human islet survival" currently under revision in Diabetes in which I am second author.

4.1.1 Apoptotic signalling is modulated upon PAX8 over-expression in pancreatic islets

In order to investigate cellular processes modulated by PAX8 and its target genes in human pancreatic islets, a microarray was performed using human pancreatic islets transduced with GFP (mock) or PAX8. Principal Component Analysis (PCA) demonstrated a clear effect of PAX8 over-expression on the transcriptional profile of human pancreatic islets (Figure 11A). As expected, the most up-regulated gene was PAX8, indicating the efficiency of lentiviral-mediated PAX8 over-expression. Additionally, translationally controlled tumour protein (TPT1) and HSPA1A were found among the most induced genes in PAX8 over-expressing human pancreatic islets (Figure 11B). Remarkably, TPT1 has been shown to inhibit apoptosis by promoting p53 degradation, while HSPA1A belongs to the *heat shock protein*70 gene family and also has antiapoptotic properties (Amson et al., 2011, Boia-Ferreira et al., 2017, Dulin et al., 2012). Moreover, other upregulated genes in PAX8 overexpressing islets, such as DNAJC22 and CCT6A, encode for chaperones involved in proper protein folding. A comparison of the microarray performed in human pancreatic islets with the previous one preformed on murine islets (see introduction), revealed that the most upregulated genes and the functional enriched pathways were species specific. However, some genes, such as the serotonin receptor HTR3B, were regulated similarly in human and murine islets overexpressing PAX8 (Figure 11C).

Remarkably, the analysis of human islets revealed changes in apoptosis and WNT signalling, which is involved in organogenesis and stem cell proliferation (Figure 11D) (Komiya and Habas, 2008). In addition, further analysis using IPA software

of annotated "Diseases and Functions" associated preferentially the transcriptional profile of human islets over-expressing PAX8 to several endocrine/metabolic disorders and cell cycle/cell death/cancer (Figure 11E). Of note, IPA software does not discern between potential protections or predisposition to the disease. The overall interpretation of these results is that the induction of PAX8 expression in human pancreatic islets exerts profound modulations in apoptotic signalling.

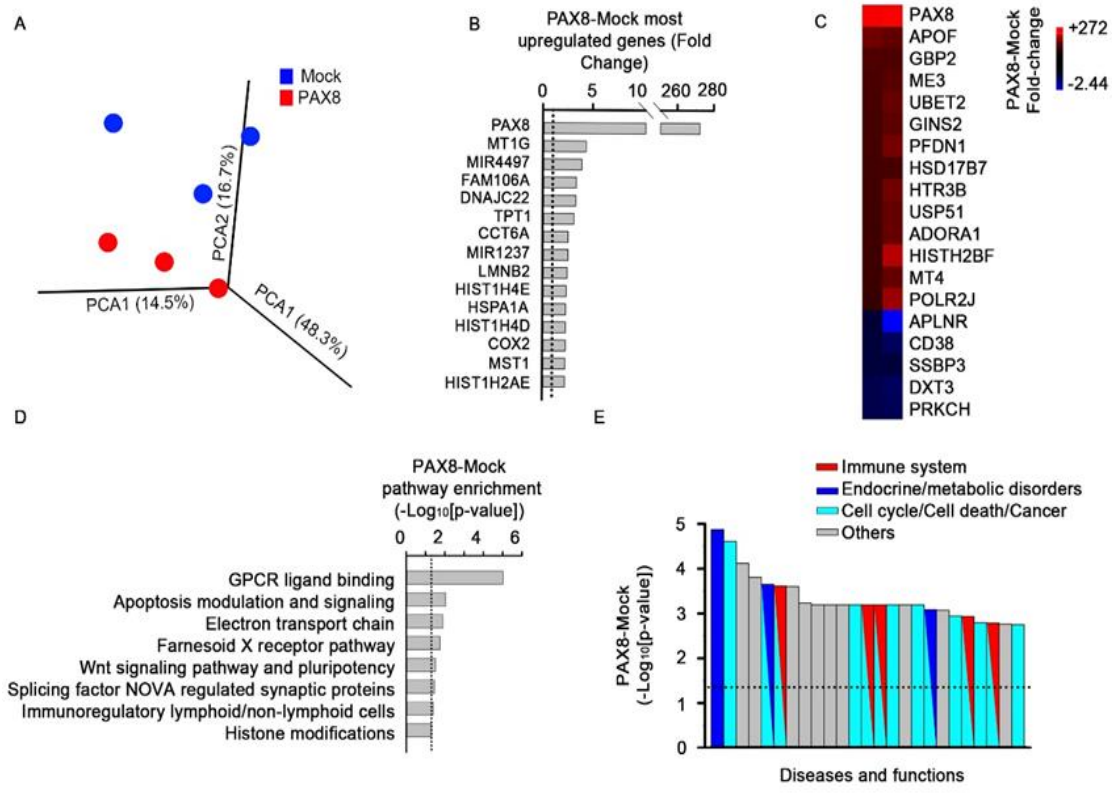

Figure 11. PAX8 overexpression in pancreatic islets modulates apoptotic signalling and endocrine/metabolic disorders. (A) PCA analysis. **(B)** Most upregulated genes in human islets over-expressing PAX8. **(C)** Heat map depicting the expression values of shared significantly modulated genes in murine and human pancreatic islets over-expressing PAX8. **(D)** Canonical pathways modulated by PAX8 over-expression in human pancreatic islets**. (E)** Diseases associated with PAX8 over-expression. n = 3 per group.

4.1.2 PAX8 over-expression reduces apoptosis in murine and human pancreatic islets

In order to further investigate the physiological role of PAX8 in pancreatic islets, freshly isolated murine pancreatic isles were transduced with an “empty” lentivirus (mock), a Pax8 (murine) lentivirus or a PAX8 (human) lentivirus (Figure 12A-B). Islet metabolic activity, determined by MTT, was similar in both Pax8-transduced and PAX8-transduced murine pancreatic islets when compared to mock-transduced murine pancreatic islets (GFP:100 % vs. Pax8:117 ± 35 % and PAX8: 98 ± 14 %, p-value = 0.584 one-way ANOVA on ranks) (Figure 12C). Additionally, islet functionality, determined by glucose-stimulated insulin secretion (GSIS), was unaffected upon Pax8 or PAX8 transduction of murine pancreatic islets (GFP: 2.65 ± 0.4-fold induction vs. Pax8: 2.65 ± 0.53-fold induction and PAX8: 2.52 ± 0.82-fold induction, p-value = 0.985 one-way ANOVA) (Figure 12D).

In contrast, consistent with the microarray data, the over-expression of both PAX8 and Pax8 in murine pancreatic islets produced a reduction on apoptosis, as determined by cell death ELISA (GFP: 100% vs. Pax8: 63 ± 11% and PAX8: 77 ± 7%, p-value = 0.008, one-way ANOVA on ranks) (Figure 12E). Likewise, human pancreatic islets transduced with the human PAX8 lentivirus also exhibited reduced apoptosis when compared to mock-transduced human islets (GFP: 100% vs. PAX8: 81 ± 0.46%, p-value = 0.001 Mann Whitney Rank Sum test), suggesting that the anti-apoptotic role of PAX8 in pancreatic islets is evolutionarily conserved between mice and humans (Figure 12F). In addition, immunohistochemical determination of cleaved-caspase 3 expressing cells confirmed the

reduction on the percentage of apoptotic cells in murine pancreatic islets (GFP: 17 ± 1.6% vs. Pax8: 8.47 ± 2.23%, p-value = 0.035 t-test two tailed) (Figure 12 G-H).

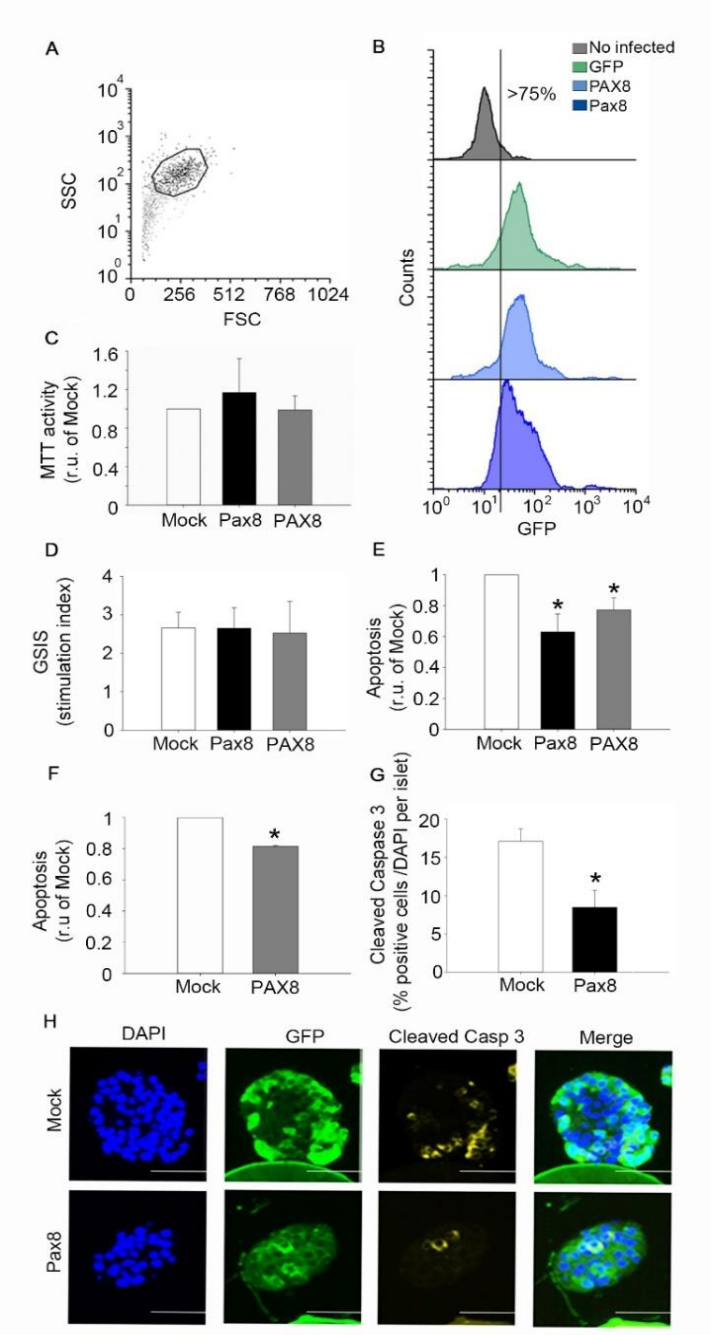

Figure 12. Lentiviral mediated PAX8 over-expression reduces apoptosis in human and murine pancreatic islets. Human or murine pancreatic islets were transduced with mock (GFP control), murine Pax8 (Pax8) or human Pax8 (PAX8) lentiviral vectors. **(A, B)** Determination of the transduction efficiency by flow cytometry. **(A)** Population of cells analysed according to

their size (FSC) and granularity (SSC). FSC: forward scattered light. SSC: side scattered light. **(B)** Flow cytometry histograms showing the number of events plotted against GFP fluorescence. The line indicates the threshold for positivity. **(C)** Determination of metabolic activity using the MTT assay in murine islets. n = 4-7 per condition. **(D)** Determination of GSIS in murine islets. n = 3-4 per condition. **(E)** Determination of the degree of apoptosis measured by ELISA in murine islets. n = 5-8 per group. **(F)** Determination of apoptosis rate by ELISA in human islets. n = 3 per group. **(G)** Determination of the percentage of cleaved Caspase 3 positive cells in murine pancreatic islets. n = 3 per group. **(H)** Representative images of GFP (marker of positive transduction) and cleaved Caspase 3 staining in murine pancreatic islets. Immunofluorescence followed by DAPI staining. Scale bar = 50 μm. Data is represented as the mean ± SEM. * $p < 0.05$ compared to mock transduced islets, one-way ANOVA on ranks (Krustal-Wallis) in panels C and E, one-way ANOVA in panel D, Mann Whitney Rank Sum test in panel F and t-test two tailed applied to panel G.

4.1.3 A novel PAX8 detrimental polymorphism associates with GDM and GTD

Our results indicating that Pax8 expression is induced in islets during gestation and that it promotes β-cell survival, suggest that this transcription factor may be involved in β-cell adaptation during pregnancy. Moreover, GTD has been associated with GDM and PAX8 is essential for proper thyroid function (Tudela et al., 2012, Guzman-Gutierrez et al., 2014, Karakosta et al., 2012). Therefore, it is tempting to speculate that detrimental polymorphisms in PAX8 may be associated with GDM. In order to address this possibility, our collaborators at La Paz Hospital conducted a genetic screening (see materials and methods for selective criteria) in patients with GDM and GTD. Interestingly, exon sequencing analysis of PAX8 locus in a patient cohort of 7 families, identified a woman in pedigree 3 bearing a novel heterozygous variant (c.1067C>T). This missense mutation causes a threonine to methionine substitution at codon 356 (p.T356M), located at the carboxyterminal region of the protein (Figure 13A-B). The location of the mutation on PAX8 is unusual, since almost all the thyroid relevant PAX8 polymorphisms known are located at the N-terminal DNA-binding domain. Importantly, the index patient was diagnosed with GTD and GDM in her 4 pregnancies. In addition, her father, who

also harbours the mutation, was diagnosed with pre-diabetes (HbA1c = 6.7%) at the age of 55. Likewise, several family members of the pedigree were diagnosed with T2DM and/or non-autoimmune hypothyroidism, although they were not accessible for genotyping (Figure 13A). To rule out the possibility of a common polymorphism in PAX8, the presence of PAX8-T356M was searched in 100 alleles from individuals of the same genetic background. None of these individuals harboured the PAX8-T356M variant (Method of Arbitrary Function <0.00034). Moreover, this mutation has not been documented in the Exome Variant Server (http://evs.gs.washington.edu/EVS/) or the dbSNP (http://www.ncbi.nlm.nih.gov/snp/), further indicating that PAX8-T356M is not a common PAX8 variant. Remarkably, an *in silico* analysis using SIFT, PolyPhen and PredictSNP software suggested that this polymorphism might be deleterious (Table 5).

Table 5. In silico prediction scores for the PAX8 p.T356M (c.1067C>T) variant.

SIFT	PolyPhen-2	PredictSNP
0.04-damaging[1]	0.882-possibly damaging[2]	51%-deleterious[3]

- [1] Prediction score from <0.05 (probably damaging) to >0.05 (probably tolerated). http://sift.jcvi.org/
- [2] Prediction score from 0 (probably benign) to 1 (probably damaging). http://genetics.bwh.harvard.edu/pph2
- [3] Expected accuracy score. https://loschmidt.chemi.muni.cz/predictsnp1

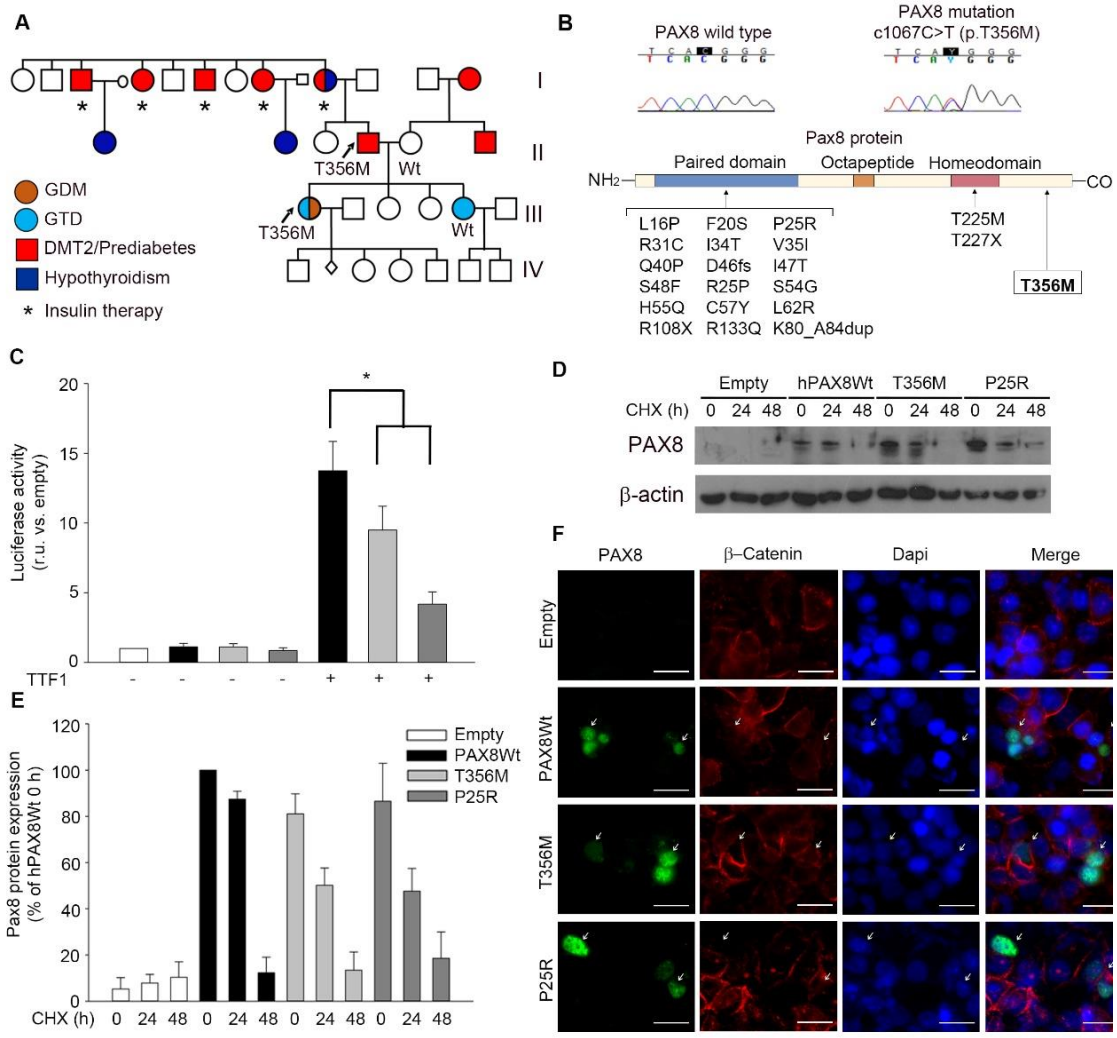

Figure 13. The novel PAX8-T356M variant identified in the genetic screening is pathogenic but does not affect protein stability or subcellular localization. **(A)** Representative image of the family pedigree with gestational diabetes as well as T2DM and hypothyroidism in several generations. The arrow indicates the index case. **(B)** Sequencing chromatogram of the mutation in the index patient and wild type sequence in a healthy relative as well as schematic representation of PAX8 protein with annotated known mutations, including T356M. **(C)** Luciferase reporter assay. n = 3 per group. **(D)** Representative western blots showing PAX8-Wt, PAX8-T356M, and PAX8-P25R protein levels in transfected MCF-7 cells at times 0, 24 and 48 hours after cycloheximide treatment (80 µg/ml). n = 3 per condition. **(E)** Densitometric analysis of western blots shown in panel D. **(F)** Representative immunofluorescence image of MCF-7 cells transfected with PAX8-Wt, PAX8-T356M or PAX8-P25R showing the subcellular localization of each PAX8 variant. n = 3 per condition. Data are represented as the mean ± SEM, * p-value < 0.05 compared to PAX8 Wt one-way ANOVA test.

We next focused to determine whether mutations on PAX8 associated with GDM affect the functionality of this transcription factor. To this end, our collaborators at La paz hospital analysed by luciferase reporter assay the transactivation potential of wild-type PAX8 (Pax8-Wt), PAX8-T356M and PAX8-P25R (see the introduction) on the Tg gene promoter. Importantly, PAX8-P25R was previously shown to lack DNA binding capacity while retaining nuclear localization (Carvalho et al., 2013). Remarkably, transfection with PAX8-T356M or PAX8-P25R variants resulted in decreased luciferase activity compared to Pax8-Wt, indicating that both variants have compromised transcriptional activity (Figure 13C). However, protein stability, as determined by protein levels after cycloheximide treatment, and the subcellular localization of GDM-associated PAX8 variants were similar to those of wild-type PAX8 (Figure 13D-F).

4.1.4 Female Pax8 +/- mice do not develop GDM

In order to determine whether Pax8 deficiency is associated with GDM in an animal model, we next performed several metabolic tests in WT and Pax8 +/- female mice under regular physiological conditions and at day 14 of pregnancy (when there is a peak in Pax8 expression in murine pancreatic islets). Pax8 -/- mice could not be used since they are infertile despite T4 supplementation.

Surprisingly, non-pregnant Pax8 +/- female mice showed decreased levels of circulating glucose 30 minutes after a glucose load compared to non-pregnant WT female mice (Figure 14A). However, no significant differences between genotypes were found at any other time point measured during the OGTT and in the area under the curve (AUC) for this experiment (Figure 14A-B). Likewise, no significant differences between

genotypes were found at any time point measured during the ITT and thus in the AUC for this experiment (Figure 14C-D). Interestingly, Pax8 +/- pregnant mice had increased circulating glucose levels compared to Pax8 +/- non-pregnant mice at 15 and 30 minutes after the insulin injection. The same tendency could be observed between non-pregnant and pregnant WT mice, which could suggest that there is indeed some degree of insulin resistance during pregnancy in both genotypes.

Since Pax8 overexpression in murine pancreatic islets modulated several genes within the interferon pathway (see introduction), we speculated that Pax8 may be involved in immune signalling. Remarkably, viral infections have been associated with increased risk of developing GDM (Lao et al., 2007). Therefore, we next investigated whether Pax8 +/- female mice were more prone to develop GDM when challenged with Poly I:C (double stranded RNA that mimics viral infections). To this end, we performed an OGTT at day 14 of pregnancy in WT and Pax8 +/- mice who received intraperitoneal injections of Poly I:C from pregnancy days 1-5 and 8-14. No differences were observed in glucose clearance between treated Pax8 +/- mice and WT animals, while significant differences where observed 30 minutes after the glucose load between non-pregnant mice from both genotypes and their counterparts during pregnancy (Figure 14E). These results suggest that Poly I:C treatment may contribute to the development of glucose intolerance during pregnancy. However, no differences were observed in the AUC between the different experimental groups (Figure 14F).

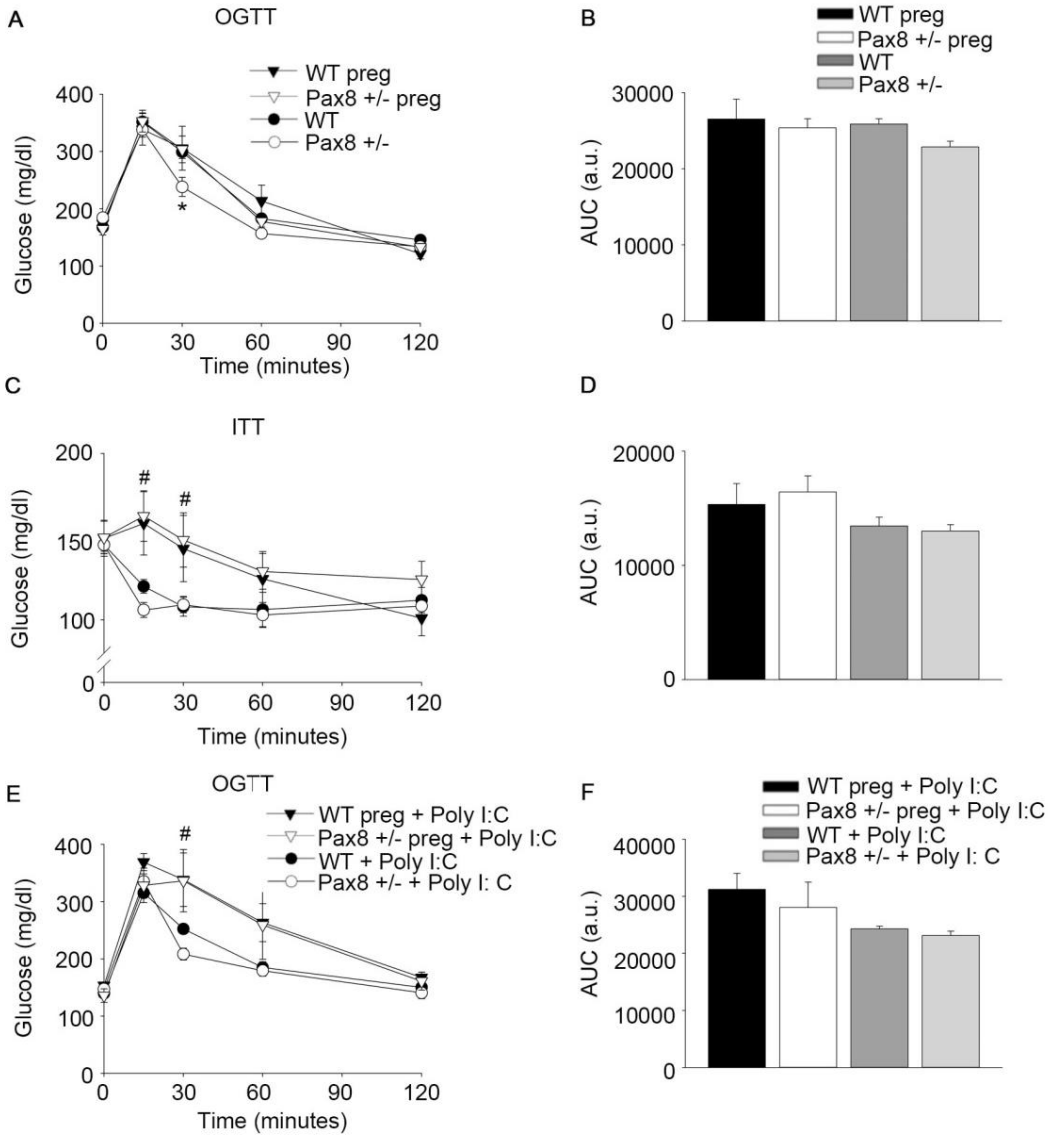

Figure 14. Pax8 +/- female mice exhibit normal glucose tolerance during pregnancy. (A) Circulating glucose levels during an OGTT. n = 11 WT, n = 8 Pax8 +/-, n = 8 WT pregnant, n = 11 Pax8 +/- pregnant. **(B)** AUC for the OGTT. (**C)** Glucose levels in blood during an ITT. n = 10 WT, n = 9 Pax8 +/-, n = 5 WT pregnant, n = 9 Pax8 +/- pregnant. (**D)** AUC for the ITT. **(E)** Circulating glucose levels during an OGTT performed in animals treated with Poly I:C. n = 7 WT + Poly I:C, n = 5 for all the remaining experimental groups. **(F)** AUC for the OGTT performed in mice treated with Poly I:C. Data are represented as the mean ± SEM. * p-value < 0.05 between WT and Pax8 +/- mice. # p-value < 0.05 between non-pregnant and pregnant mice from the same genotype. Repeated measurements two-way ANOVA in A, C and E. Two-way ANOVA in B, D and F.

Noteworthy, circulating T4 levels were similar between Pax8 +/- and WT female mice (WT: 5.16 ± 0.21 μg/dl vs. Pax8: 4.92 ± 0.17 μg/dl, p-value = 0.407 t-test two tailed) (Figure 15), which could suggest a potential genetic compensation for Pax8 haploinsufficiency. However, it is also important to note that T4 levels were not measured during pregnancy.

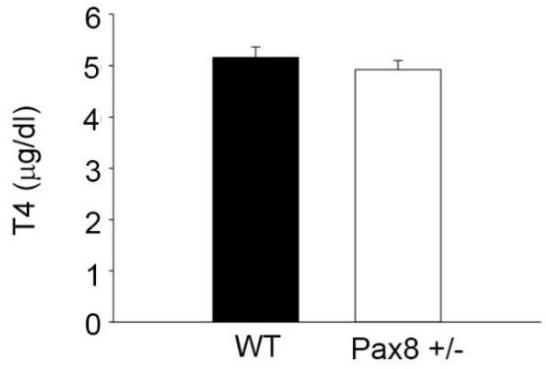

Figure 15. Pax8 +/- female mice have similar circulating T4 levels than WT. Circulating T4 levels of WT and Pax8 +/- female mice at 5 months old. n = 6 per group. No significant differences were observed in a t-test two tailed (p-value = 0.407).

AIM 2: Determine the role of Pax8 deficiency in the development of T2DM in male aging mice.

N.B: Results presented herein are part of a manuscript currently under preparation in which I am first author. Running title: **“**The thyroid hormone axis in metabolic health”.

4.2.1 Pax8 +/- male mice exhibit reduced circulating T4 levels

The analysis of our pedigree might suggest an association of PAX8-T356M with prediabetes/T2DM (Figure 13A). Moreover, a polymorphism nearby PAX8 was associated with T2DM in an Afro-American population by a genome wide study (Elbein et al., 2009). Therefore, we next investigated whether a deficiency in Pax8 could be associated with T2DM in mice. To this end, we studied the metabolic status in WT, Pax8 +/- and Pax8 -/- male mice.

In contrast to females, untreated Pax8 +/- male mice displayed reduced T4 levels in blood compared to WT animals (WT: 3.71 ± 0.10 µg/dl vs. Pax8 +/-: 3.33 ± 0.12 µg/dl, p-value = 0.029 t-test two tailed) (Figure 16). Nonetheless, these mice were 8 months old, suggesting that the reduction in circulating T4 levels in Pax8 +/- mice may be developed with advancing age.

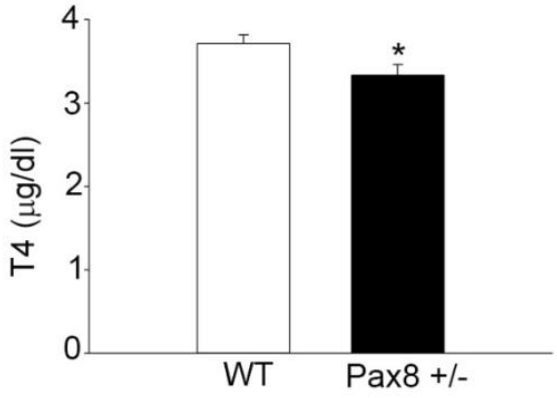

.

Figure 16. Pax8 +/- male mice exhibit reduced circulating T4 levels. T4 levels in serum from WT and Pax8 +/- male mice. n = 23 WT, n = 15 Pax8 +/-. Data are represented as the mean ± SEM. * p-value < 0.05 t-test two tailed.

Importantly, no differences in T4 levels have been observed in Pax8 +/- mice compared to WT at postnatal days 7, 21 and postnatal week 22 (Glaschke et al., 2010).

However, Mansouri et al. observed an increase in TSH levels in Pax8 +/- mice and $Pax8^{+/-}TR\alpha1^{-/-}$ mice (which also have a deficiency in the thyroid hormone receptor α1) exhibit decreased T4 levels around weaning (Mansouri et al., 1998, Mittag et al., 2005)

4.2.2 Pax8 +/- male mice show glucose intolerance and insulin resistance

In order to determine whether Pax8 deficiency affects metabolic homeostasis and whether it is due to its effect in TH concentration, we performed several metabolic tests in WT and Pax8 +/- male mice supplemented or not with T4 from postnatal day 1 (18 ng/g of body weight per day by subcutaneous injections) until weaning, followed by T4 administration in the drinking water (5 μg/ml *ad libitum*). Importantly, the treatment increased circulating T4 levels in both genotypes (WT: 3.71 ± 0.10 μg/dl vs. WT+T4: 12.77 ± 1.62 μg/dl, p-value < 0.0001 and Pax8 +/-: 3.33 ± 0.12 μg/dl vs. Pax8 +/-+T4: 14.85 ± 2.83 μg/dl, p-value < 0.0001, t-test two tailed).

Untreated Pax8 +/- male mice exhibited glucose intolerance, as determined by increased glucose levels at times 15 and 30 minutes after a glucose load and an increased AUC during the OGTT (WT: 25217 ± 894 arbitrary units (a.u.) vs. Pax8 +/-: 30715 ± 916 a.u., p-value = 0.008 two-way ANOVA). In contrast, no differences were found in circulating glucose levels between WT and Pax8 +/- animals treated with T4 (Figure 17A-B). Insulin levels during the OGTT were not affected in untreated Pax8 +/- mice, whereas Pax8 +/- mice treated with T4 had a lower peak of insulin secretion 15 minutes after the glucose load and a lower AUC for the experiment (WT: 195 ± 41 a.u. vs. Pax8 T4: 95 ± 11 a.u., p-value = 0.035 two-way ANOVA) (Figure 17C-D).

We next performed an IPPTT to investigate whether gluconeogenesis was affected in Pax8 +/- mice. Untreated Pax8 +/- mice had increased glucose levels in blood compared to untreated WT animals at 60 and 120 minutes after the pyruvate load and an increased AUC during the IPPTT (WT: 21919 ± 1273 a.u. vs. Pax8 +/-: 28168 ± 1941 a.u., p-value = 0.0153 two-way ANOVA) (Figure 17E-F). Of note, this increase in the last time points with an unaffected peak during the IPPTT may be indicative of insulin resistance rather than enhanced gluconeogenesis. Consistent with that, untreated Pax8 +/- animals displayed severe insulin resistance, as determined by increased glucose levels in blood 30, 60 and 120 minutes after an intraperitoneal insulin injection, and increased AUC during the ITT (WT: 13451 ± 955 a.u. vs. Pax8: 20277 ± 618 a.u., p-value < 0.0001 two-way ANOVA) (Figure 17G-H). Importantly, significant differences in the OGTT, IPPTT and ITT between untreated Pax8 +/- and WT male mice were maintained even when values where relativized by basal glucose levels (Figure 18A-C).

Further confirming insulin resistance, untreated Pax8 +/- mice had an increased value for the HOMA-IR index (WT: 2.84 ± 0.42 a.u. vs. Pax8 +/-: 4.40 ± 0.13 a.u., p-value = 0.006 two-way ANOVA) (Figure 19A-C). Importantly, no significant differences were observed between Pax8 +/- male mice treated with T4 and untreated WT mice in the ITT or the HOMA-IR, demonstrating that T4 supplementation prevents the development of insulin resistance in Pax8 +/- mice (Figure 17G-H and 19A-C). Moreover, untreated Pax8 +/- male mice exhibited increased levels of HbA1c (WT: 5.7 ± 0.55% vs. Pax8 +/-: 7.02 ± 0.43%, p-value = 0.0207 two-way ANOVA), which indicates long term-increased glucose levels in blood (Figure 19D).

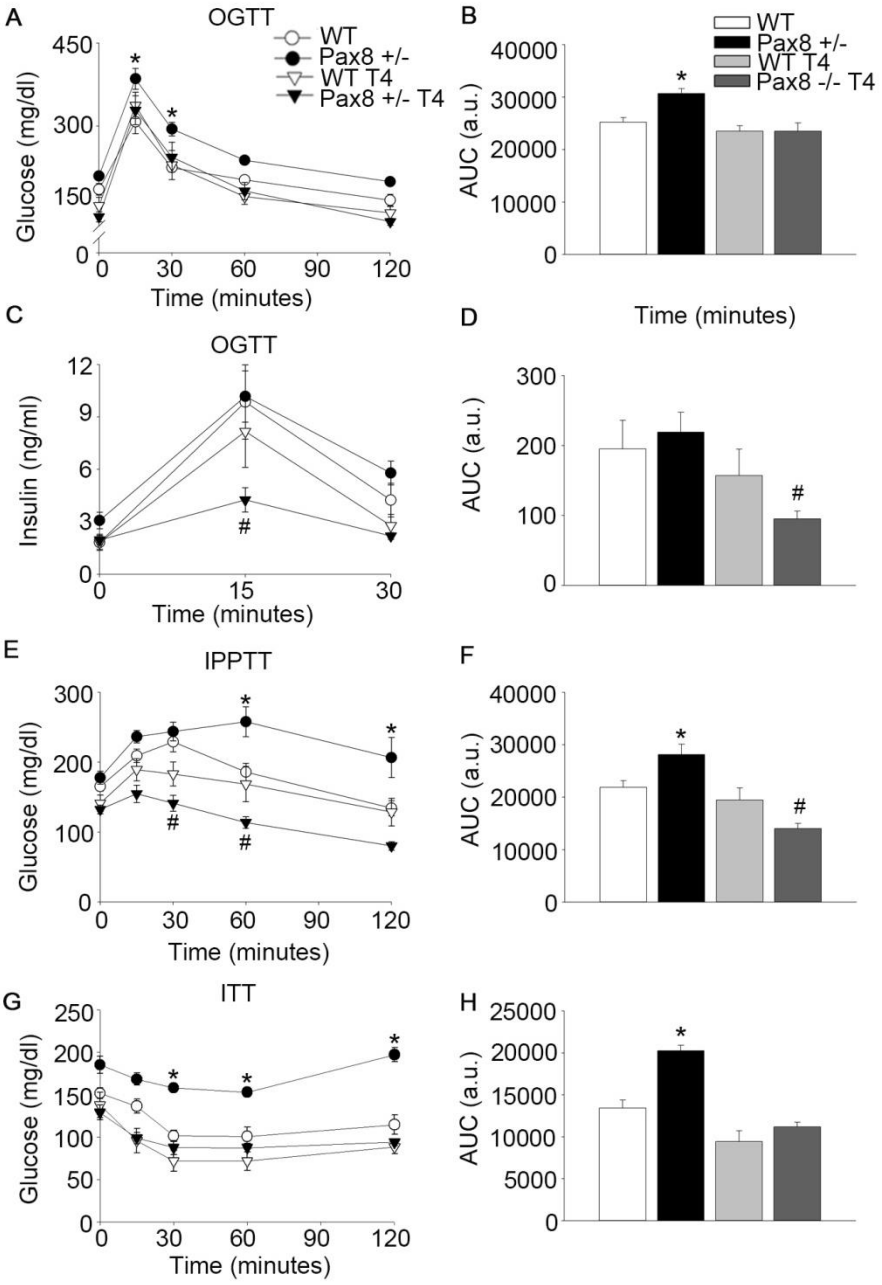

Figure 17. Untreated Pax8 +/- male mice exhibit glucose intolerance and insulin resistance. (A) Circulating glucose levels during an OGTT. n = 8 per group. **(B)** AUC for the OGTT. **(C)** Circulating insulin levels during an OGTT. n = 8 per group. **(D)** AUC for the insulin levels in the OGTT. **(E)** Circulating glucose levels during an IPPTT. n = 8 per group. **(F)** AUC for the IPPTT. **(G)** Circulating glucose levels during an ITT. n = 8 per group. **(H)** AUC for the ITT. Data are represented as the mean ± SEM. * p-value < 0.05 between untreated WT and untreated Pax8 +/- mice. # p-value < 0.05 between untreated WT and Pax8 +/- mice treated with T4. Repeated measurements two-way ANOVA in A, C, E and G and two-way ANOVA in all the other panels.

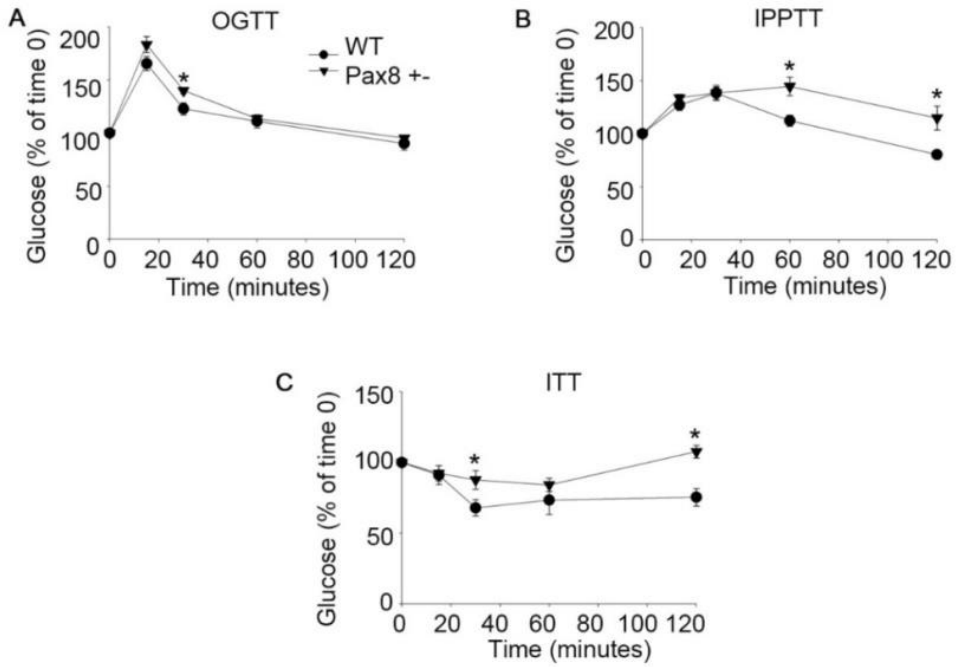

Figure 18. Glucose levels in metabolic tests expressed as percentage of basal glucose. (A) Glucose concentration in blood during the OGTT expressed as the percentage of basal glucose. n = 8 per group. **(B)** Glucose concentration in blood during the IPPTT expressed as the percentage of basal. n = 8 per group. **(C)** Glucose concentration in blood during the ITT expressed as the percentage of basal. n = 8 per group. * p-value < 0.05 Mann-Whitney Rank Sum test.

Consistent with the insulin resistance observed in metabolic tests, western blots performed in liver extracts of untreated WT and Pax8 +/- mice revealed a decrease in pSer473 AKT (WT: 100 ± 5.84% vs. Pax8 +/-: 82.57 ± 3.63%, p-value = 0.039 t-test two tailed), while total AKT levels were not altered (Figure 19E and G). In contrast, pSer473 AKT levels were increased in gastrocnemius extracts of Pax8 +/- mice compared to WT (WT: 100 ± 11.36% vs. Pax8 +/-: 138.31 ±11.72%, p-value = 0.040 t-test two tailed), while no differences were observed in total AKT levels (Figure 19F and H). Therefore, our results suggest an impairment of insulin signalling preferentially in the liver of Pax8 +/- male mice.

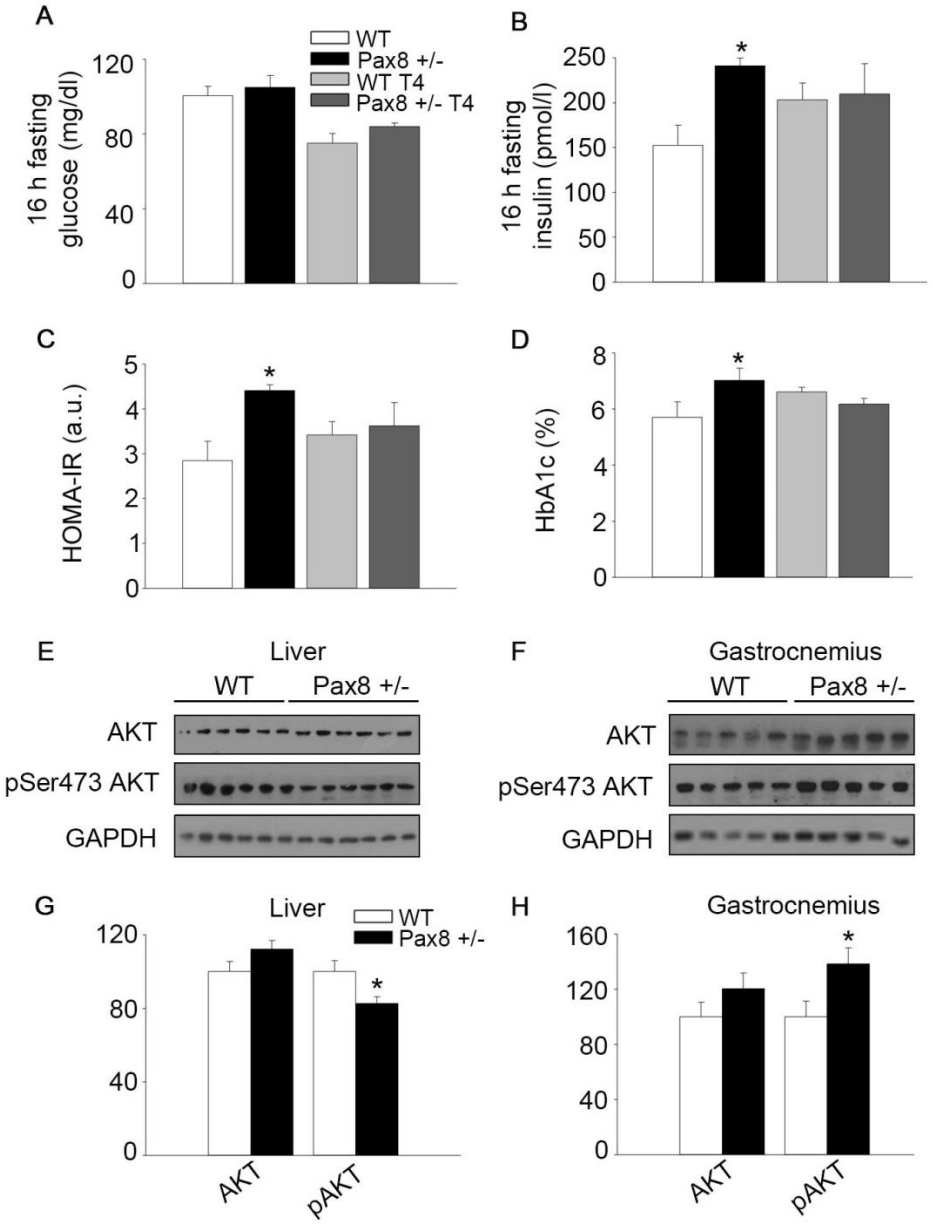

Figure 19. Pax8 +/- male mice exhibit increased HOMA-IR index and impaired insulin signalling in liver. (A) Glucose levels in blood after 16 hours of fasting. n = 8 per group. **(B)** Circulating insulin levels after 16 hours of fasting. n = 8 per group. **(C)** HOMA-IR. n= 8 per group. **(D)** Percentage of HbA1c. n = 7 per group. **(E)** Western blots showing total AKT and pSer473 AKT in liver extracts of untreated WT and Pax8 +/- mice. **(F)** Western blots showing AKT and pSer473 AKT in gastrocnemius extracts of untreated WT and Pax8 +/- mice. **(G)** Densitometric analysis of western blots shown in panel E. n = 6 per group. **(H)** Densitometric analysis of western blots shown in panel F. n = 6 per group. Mice were fasted 16 hours prior sacrifice. Data are represented as the mean ± SEM. * p-value < 0.05. Two-way ANOVA in panels A-D. T-test two tailed in panels G-H.

Next, we analysed the pattern of expression of Pax8 by RT-PCR in main metabolic tissues during adulthood in WT animals, in order to determine whether a deficiency of Pax8 expression in any metabolic tissue could contribute to the phenotype observed. However, Pax8 expression was not detected in any of the main metabolic tissues tested as compared to kidney (Figure 20). These results further indicate that the phenotype observed is mainly due to lower circulating T4 levels.

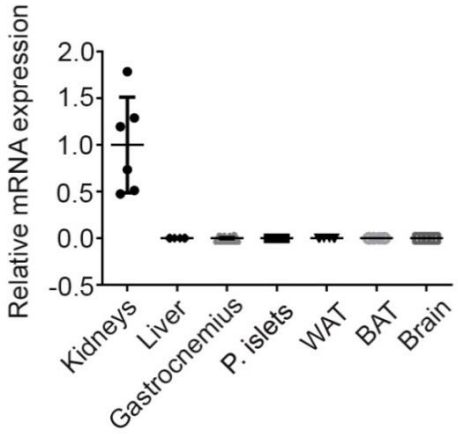

Figure 20. Pax8 expression is not detected in main metabolic tissues during adulthood. Relative mRNA expression of Pax8 in main metabolic tissues compared to kidney expression. Kidneys: n = 6; Liver: n = 6; Gastrocnemius: n = 6; Pancreatic islets: n = 3; WAT: n = 6; BAT: n = 6; Brain: n = 6. Data are represented as the mean ± SEM.

4.2.3 Pancreatic islets from Pax8 -/- and Pax8 +/- mice are normally developed

THs are known to promote postnatal pancreatic islet development and maturation through MafA (Aguayo-Mazzucato et al., 2013). Moreover, we and others have shown that Pax8 expression is induced during gestation in pancreatic islets, suggesting that Pax8 could be expressed in the endocrine compartment of the pancreas under different metabolic circumstances. Therefore, it is tempting to speculate that the lack of one or two alleles of Pax8 could result in abnormal islet architecture. In order to determine whether pancreatic islets of Pax8 +/- and Pax8 -/- mice are affected, we carried out

immunohistochemical analyses determining insulin, glucagon and somatostatin positive cells in pancreatic sections from WT, Pax8 +/- and Pax8 -/- male mice at postnatal day 21. No significant differences were found between experimental groups in the percentage of these endocrine cells within pancreatic islets. Moreover, the overall morphology of pancreatic islets was similar between different genotypes (Figure 21A-D).

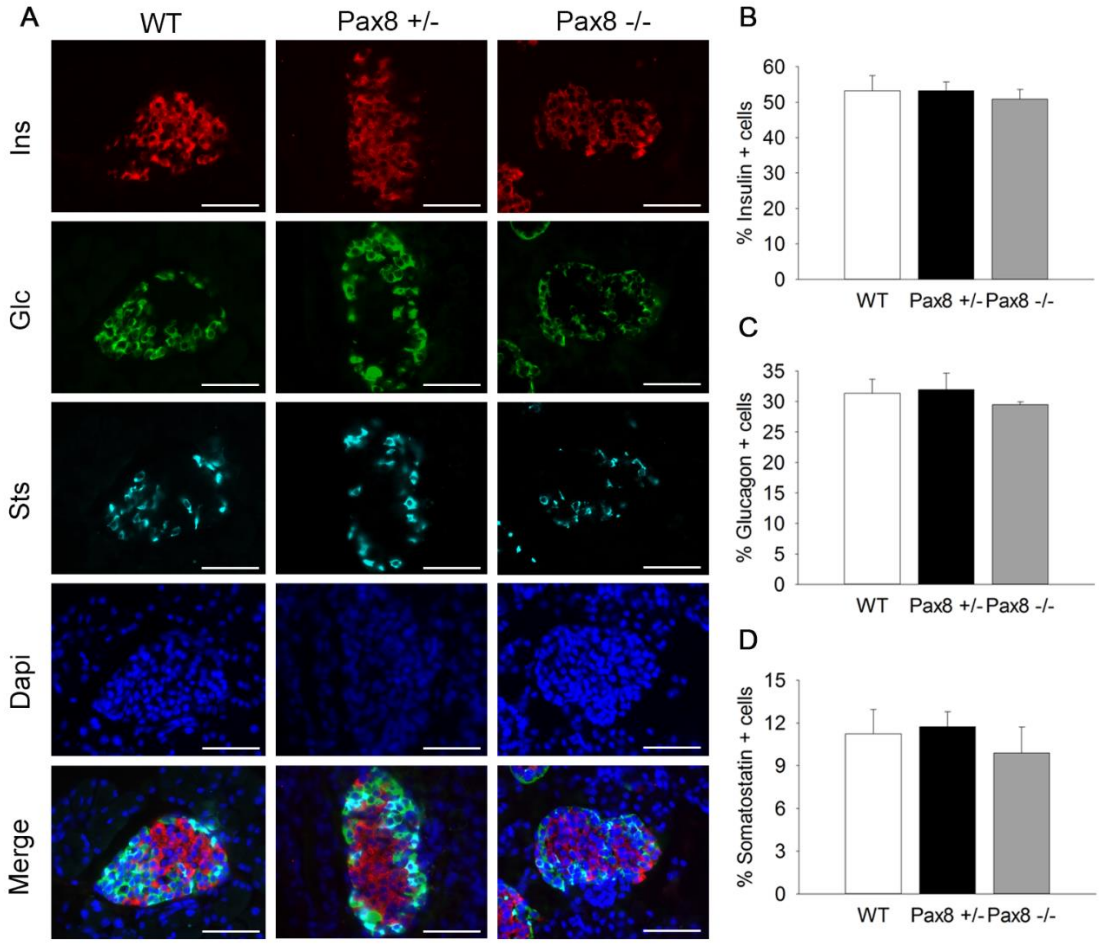

Figure 21. Pancreatic islets from WT, Pax8 +/- and Pax8 -/- animals exhibit similar morphology. (A) Representative immunofluorescence images of pancreatic sections from untreated WT, Pax8 +/- and Pax8 -/- male mice at postnatal day 21. n = 4 per group. **(B)** Percentage of insulin positive cells within the islet. n = 4 per group. **(C)** Percentage of glucagon positive cells within the islet. n = 4 per group. **(D)** Percentage of somatostatin positive cells within the islet. n = 4 per group. In all cases, at least 1000 endocrine cells per animal were counted. Data are represented as the mean ± SEM.

4.2.4 Pax8 +/- male mice exhibit increased body weight

Remarkably, untreated Pax8 +/- male mice exhibited increased body weight compared to WT between 7 to 13 months old, while animals treated with T4 from both genotypes displayed reduced body weight from month 6 until they died due to T4 toxicity around 12-16 months of age (Figure 22).

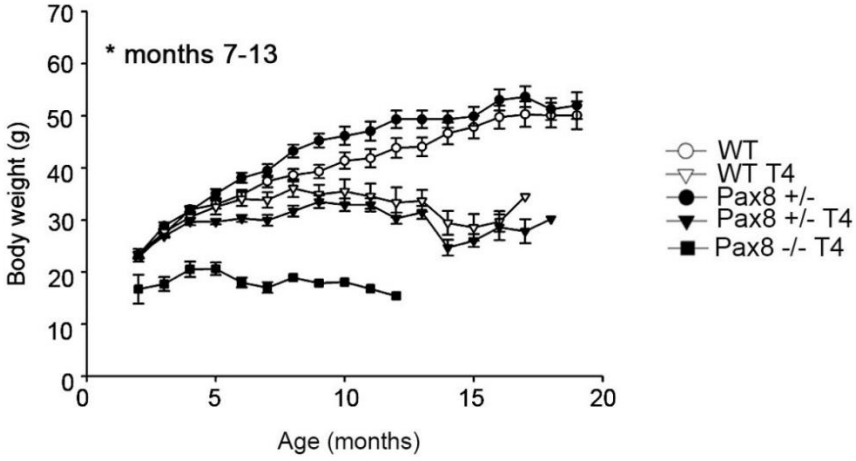

Figure 22. Untreated Pax8 +/- male mice exhibit increased body weight. Body weights (g) of WT and Pax8 +/- male mice treated or not with T4 as well as Pax8 -/- mice treated with T4. Note that untreated Pax8 -/- mice die at weaning. Data are represented as the mean ± SEM. * p-value < 0.05 Repeated measurements two-way ANOVA.

At 9 months of age (when a cohort of untreated WT and Pax8 +/- mice were sacrificed) the WAT of Pax8 +/- mice was heavier than the WAT from WT animals (WT: 1.123 ± 0.23 g vs. Pax8 +/-: 1.77 ± 0.15 g, p-value = 0.043, t-test two tailed), even when relativized by total body weight (WT: 3.01 ± 0.49% of body weight, Pax8 +/-: 4.43 ± 1.99% of body weight, p-value = 0.033 t-test two tailed) (Figure 23A-B). Consistent with this, a strong tendency towards increased adipocyte area was observed in Pax8 +/- male mice at this age (WT: 1644 ± 200 μm^2 vs. Pax8 +/-: 3194 ± 458 μm^2, p-value = 0.13 t-test two tailed) (Figure 23C-D). However, the lipidomic analysis did not reveal any

differences between Pax8 +/- and WT mice in the composition of different fatty acid species within WAT (Figure 23E).

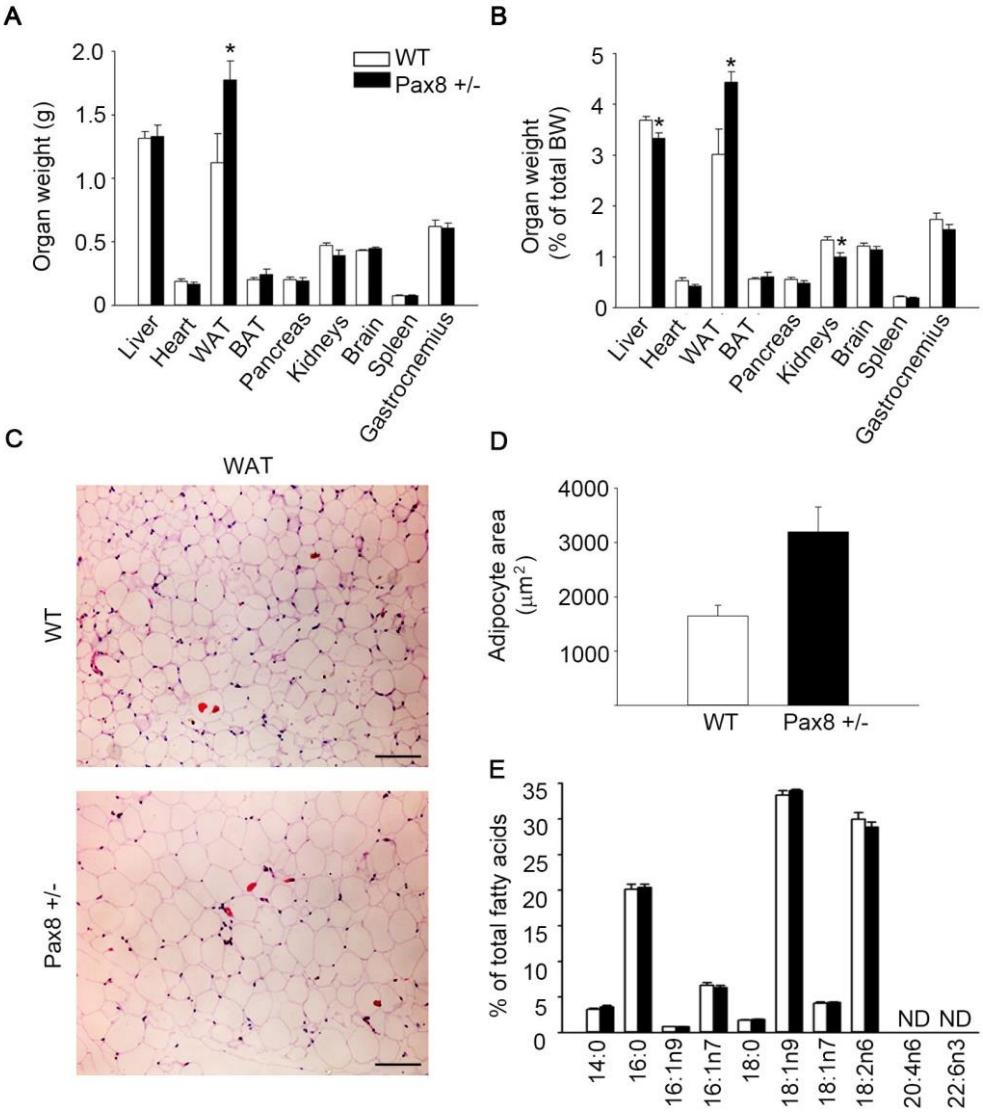

Figure 23. Untreated Pax8 +/- male mice exhibit increased WAT weight. (A) Organs and tissues weight at 9 months of age. n = 6 per group. **(B)** Organs and tissue weight at 9 months of age relativized by total body weight. n = 6 per group. **(C)** Representative images of hematoxylin and eosin staining of WAT sections. n = 3 WT, n = 2 Pax8 +/-. Scale bar = 100 μm. **(D)** Quantification of adipocyte area. n = 3 WT, n = 2 Pax8 +/-. **(E)** Lipidomic analysis depicting percentage of lipid species in WAT. n = 6 per group. Data are represented as the mean ± SEM. * p-value < 0.05 t-test two tailed.

4.2.5 Pax8 +/- male mice exhibit compromised performance on rotarod and wirehang tests

Despite having increased body and WAT weight, untreated Pax8 +/- male mice did not show increased daily energy intake. In contrast, fasting induced energy intake was reduced when compared to WT animals (WT: 5.05 ± 0.22 kcal/8hours, Pax8 +/-: 3.85 ± 0.29 kcal/8hours, p-value = 0.003 t-test two tailed) (Figure 24A-B). Moreover, faecal lipid content was similar in both genotypes (Figure 24C).

Surprisingly, no significant differences were found in plasma triglycerides, while total cholesterol was decreased in Pax8 +/- mice compared to WT (WT: 122 ± 9.53 mg/dl vs. Pax8 +/-: 87 ± 6.99 mg/dl, p-value = 0.012, t-test two tailed) (Figure 24D and E). However, this was due to a reduction in the high-density lipoprotein (HDL) fraction (WT: 86 ± 4.10 mg/dl vs. Pax8 +/-: 60 ± 4.07 mg/dl, p-value < 0.0001 t-test two tailed) (Figure 24E). Next, we measured glutamic oxaloacetic transaminase (GOT) and glutamic-pyruvic transaminase (GPT) in serum as markers of liver damage. Unexpectedly, Pax8 +/- animals exhibited decreased levels of GPT, while no differences were observed in GOT levels (Figure 24F-G). In order to determine the overall health status of Pax8 +/- mice, animals were challenged on rotarod and wirehang tests. Pax8 +/- mice performed poorly on rotarod test, as determined by the reduced time (s) in falling from an accelerating rotarod (WT: 111 ± 2.82 s vs. Pax8 +/-: 88.7 ± 5.25 s, p-value = 0.0005 t-test two tailed) (Figure 24H). Similarly, a significantly shorter latency to fall in Pax8 +/- mice was observed in the wirehang test (WT: 25.7 ± 2.3 s vs. Pax8 +/-: 11.9 ± 2.03 s, p-value < 0.0001 t-test two tailed) (Figure 24I). Therefore, our results suggest that Pax8 +/- male mice exhibit an overall unhealthy status.

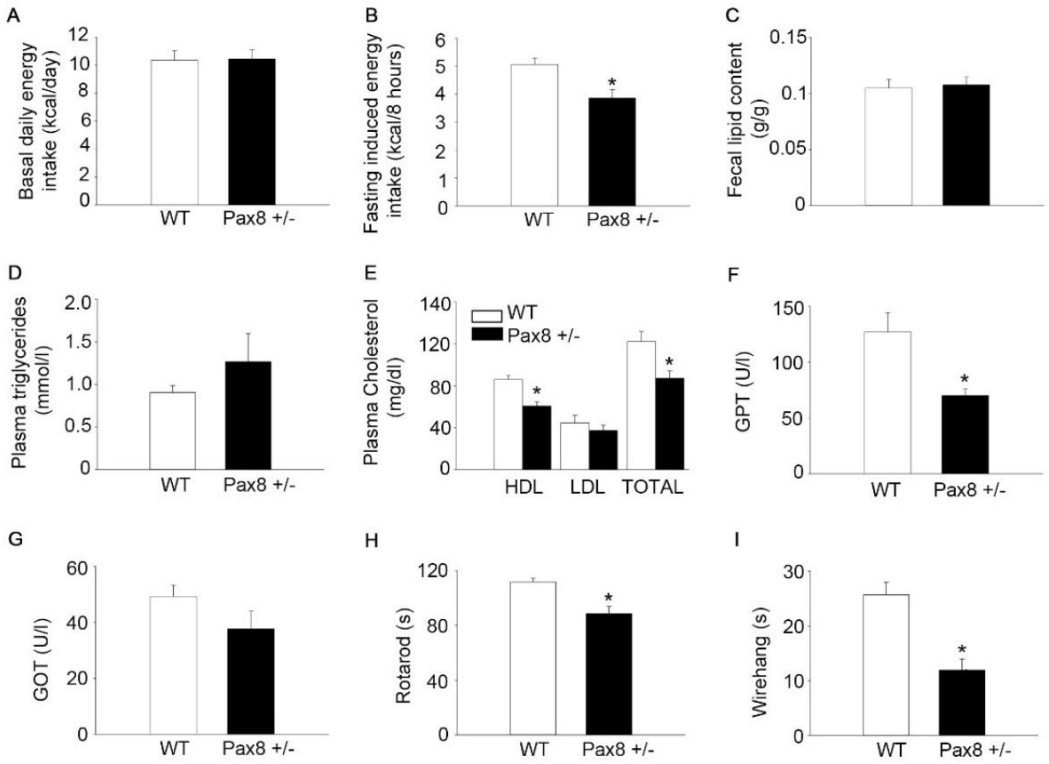

Figure 24. Untreated Pax8 +/- male mice exhibit lower HDL content in plasma and perform poorly in rotarod and wirehang tests. (A) Basal Daily energy intake. n = 5 cages WT, n = 4 cages Pax8 +/-. (**B)** Fasting induced energy intake. n = 20 WT, n = 14 Pax8 +/-. (**C)** Lipid content in faeces. n = 7 WT, n = 6 Pax8 +/-. (**D)** Triglycerides concentration in plasma. n = 18 WT, n = 13 Pax8 +/-. (**E)** Total cholesterol in plasma and HDL as well as LDL levels. n = 6 per group. (**F)** Serum levels of GPT. n = 7 per group. (**G)** Serum levels of GOT. n = 7 per group. (**H)** Time to fall from an accelerating rotarod in seconds (s). n = 27 WT, n = 20 Pax8 +/-. (**I)** Time to fall in wirehang test (s). n = 27 WT, n = 20 Pax8 +/-. Data are represented as the mean ± SEM. * p-value < 0.05 t test-two tailed.

4.2.6 Pax8 +/- male mice exhibit increased triglyceride content in both liver and skeletal muscle

Hematoxylin and eosin analyses of the liver of Pax8 +/- animals revealed that Pax8 +/- animals displayed increased lipid content in this tissue. Accordingly, triglyceride content was increased in the liver of Pax8 +/- mice compared to WT (WT: 33.77 ± 5.49 nmol/mg of protein vs. Pax8 +/-: 57.17 ± 3.62 nmol/mg of protein, p-value = 0.007 t-test

two tailed) (Figure 25A-B). Likewise, the intramuscular lipid content in the gastrocnemius of Pax8 +/- animals was increased as observed by hematoxylin and eosin staining as well as by triglyceride determination (WT: 14.77 ± 4.26 nmol/mg of protein vs. Pax8 +/: 28.01 ± 2.15 nmol/mg of protein, p-value = 0.033 t-test two tailed) (Figure 25A and C).

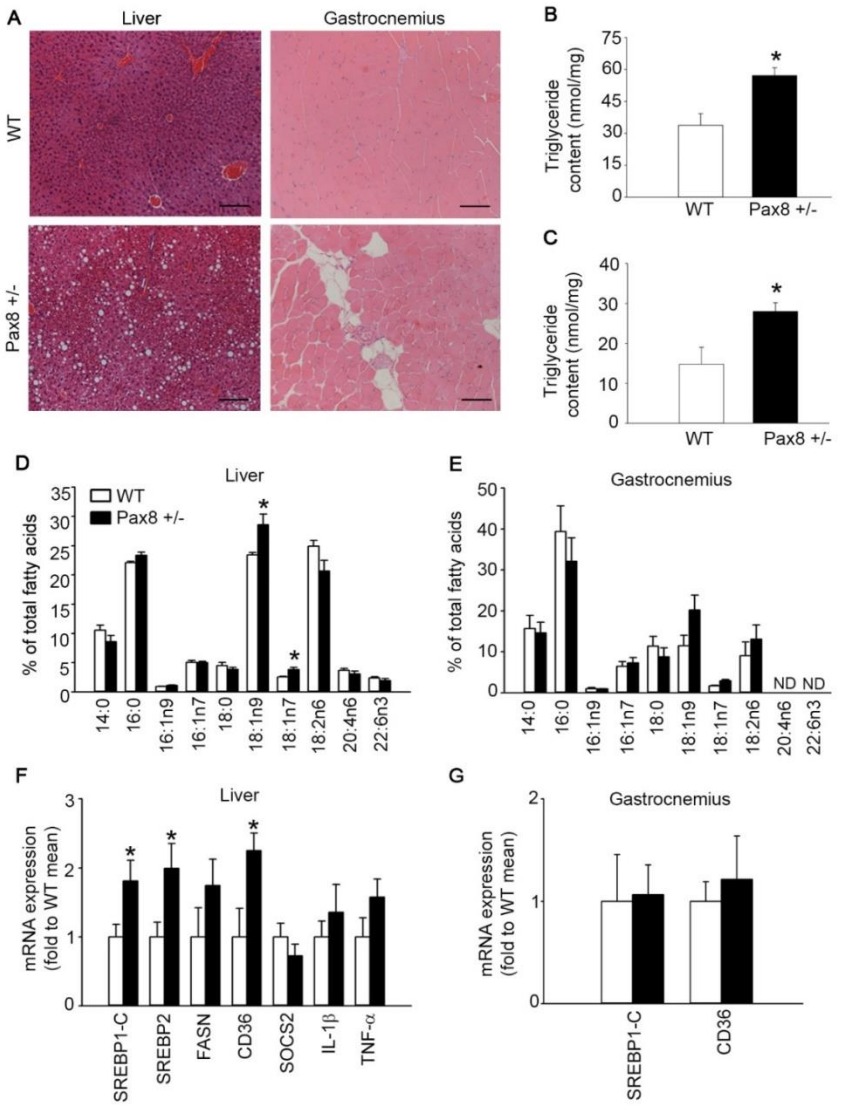

Figure 25. Pax8 +/- mice exhibit increased triglyceride content in both liver and gastrocnemius. (A) Representative images of haematoxylin and eosin staining of liver and gastrocnemius sections from WT and Pax8 +/- mice. n = 6 per group. Scale bar = 100 μm. **(B)** Triglyceride content per mg of protein in liver. n = 6 WT, n = 4 Pax8 +/-. **(C)** Triglyceride

content per mg of protein in gastrocnemius. n = 5 WT, n = 4 Pax8 +/-. **(D)** Lipidomic analysis depicting percentages of the different species of fatty acids in livers of WT and Pax8 +/- mice. n = 5 WT, n = 6 Pax8 +/-. **(E)** Lipidomic analysis depicting percentages of the different species of fatty acids in gastrocnemius of WT and Pax8 +/- mice. n = 6 per group. **(F)** mRNA expression of genes involved in lipid synthesis/import and inflammation in livers from WT and Pax8 +/- mice. SREBP1-c: n = 6 per group; SREBP2: n = 6 per group; FASN: n = 6 per group; CD36: n = 6 WT, n = 5 Pax8 +/-; LDLR: n = 4 WT, n = 6 Pax8 +/-; SOCS2: n = 4 WT, n = 6 Pax8 +/-; IL-1β: n = 5 WT, n = 6 Pax8 +/-; TNF-α: n = 5 WT, n = 6 Pax8 +/. **(G)** mRNA expression of genes involved in lipid synthesis/import in gastrocnemius from WT and Pax8 +/- mice. SREBP1-c: n = 6 WT, n = 5 Pax8 +/-; CD36: n = 5 WT, n = 6 Pax8 +/-. Data are represented as the mean ± SEM. * p-value < 0.05 t-test two tailed.

Moreover, the lipidomic analysis revealed a significant increase in the percentage of 18:1n9 and 18:1n7 fatty acid species in livers from Pax8 +/- mice compared to WT, while no significant differences were observed in gastrocnemius (Figure 25D-E). Remarkably, the expression of SREBP-1c and CD36, which are involved in lipid synthesis and lipid uptake into the cell, respectively, was induced in livers but not gastrocnemius of Pax8 +/- mice (Figure 25F-G). However, no significant differences were observed in pro-inflammatory markers such as IL-1β in the liver of Pax8 +/- mice (Figure 25F).

4.2.7 Superoxide production is increased in livers from Pax8 +/- male mice, although mitochondrial content is not affected

Both mitochondrial dysfunction and increased activity have been associated with insulin resistance (Holmström et al., 2012, Jelenik et al., 2017). In addition, mitochondria are the major site of β-oxidation. Therefore, we next investigated whether mitochondria content and function were affected in Pax8 +/- male mice compared to WT.

Surprisingly, the expression of medium chain acyl-CoA dehydrogenase (MCAD), which catalyses the first step in β-oxidation of medium chain fatty acids, was increased

in livers of Pax8 +/- mice compared to WT. In contrast, no differences were observed in mRNA levels of CPT1 and LCAD, which are involved in the import of fatty acids into the mitochondria and long chain fatty acid β-oxidation, respectively (Figure 26A) (Sayre and Lechleiter, 2012, Huang et al., 2014).

Interestingly, both ATP synthase subunit α (ATP5a) and PGC1-α expression were increased in liver but not gastrocnemius of Pax8 +/- mice compared to WT (Figure 26A-D). In contrast, UCP2 expression was decreased in the liver of Pax8 +/- mice as determined by both RT-PCR and western blots (WT: 100 ± 12.58 % vs. Pax8 +/-: 58.32 ± 13.81%, p-value = 0.049), while no differences were observed in gastrocnemius extracts (Figure 26A-F). The increase in ATP5a coupled to a decrease in UCP2 levels could suggest that ATP production is enhanced in the liver of Pax8 +/- mice. Consistent with this hypothesis, pThr172 AMPK protein levels, which indicate the energetic status of the cell, were reduced in liver (WT: 100 ± 28.61% vs. Pax8 +/-: 22.90 ± 7.21%, p-value = 0.042 t-test two-tailed) but not in gastrocnemius extracts of Pax8 +/- mice compared to WT. However, no differences were found in total AMPK protein levels in any metabolic tissue tested (Figure 26C-F).

Noteworthy, mRNA levels of genes encoding for proteins found at mitochondrial complexes were not altered in either liver or gastrocnemius of Pax8 +/- mice compared to WT (Figure 26A-B). Likewise, no differences were observed in VDAC protein levels, indicating that mitochondrial content is not affected in these tissues (Figure 26C-F).

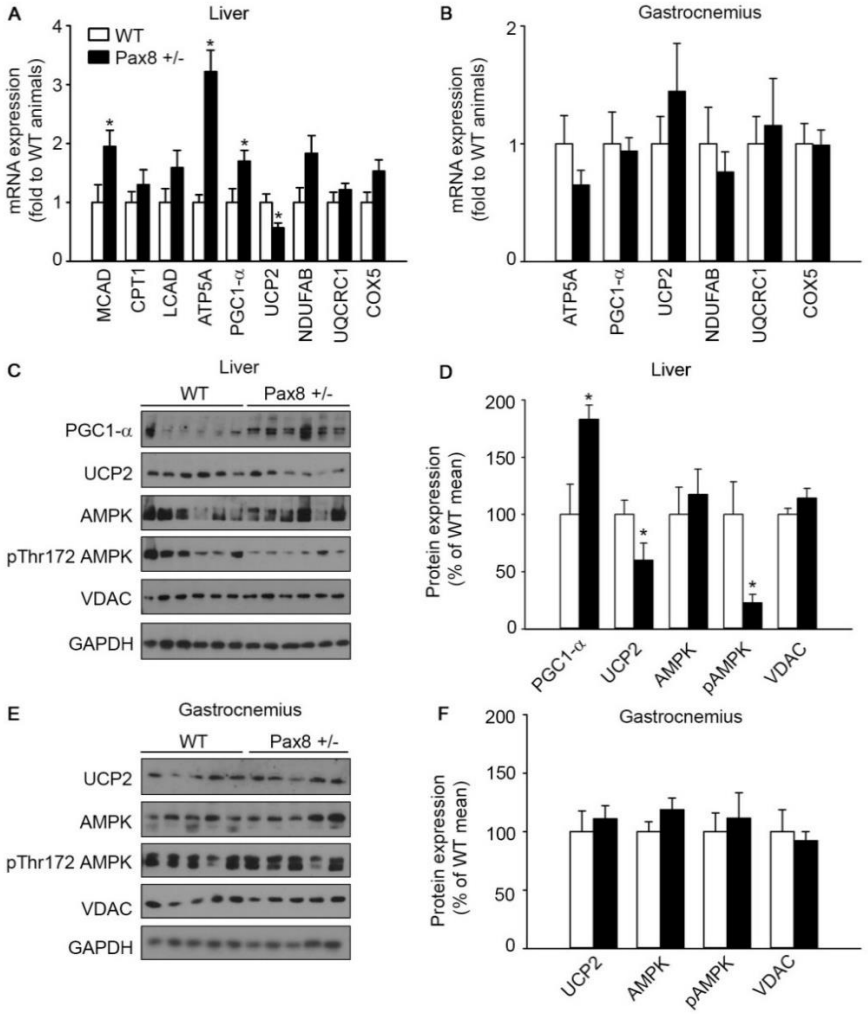

Figure 26. Pax8 +/- mice exhibit increased ATP5A and PGC1-α expression in the liver, while UCP2 is downregulated. (A) mRNA expression of genes involved in β-oxidation, mitochondrial biogenesis and function in the liver of WT and Pax8 +/- mice. CPT1: n = 5 WT, n = 6 Pax8 +/-; LCAD: n = 6 per group; MCAD: n = 6 per group; NDUFAB = n = 6 per group; UQCRC1: n = 6 per group; COX5: n = 6 per group; ATP5a: n = 5 WT, n = 6 Pax8 +/-; PGC1α: n = 6 per group; UCP2: n = 5 per group. **(B)** mRNA expression of genes involved in mitochondrial biogenesis and function in gastrocnemius of WT and Pax8 +/- mice. NDUFAB: n = 5 WT, n = 4 Pax8 +/-; UQCRC1: n = 6 WT, n = 5 Pax8 +/-; COX5: n = 5 WT, n = 4 Pax8 +/-; ATP5a: n = 5 WT, n = 4 Pax8 +/-; PGC1α: n = 5 WT, n = 4 Pax8 +/-; UCP2: n = 5 per group. **(C)** Western blots showing proteins involved in mitochondrial biogenesis/function as well as AMPK and its phosphorylated isoform in livers of WT and Pax8 +/- mice. n = 6 per group. **(D)** Densitometric analysis of western blots shown in panel C. **(E)** Western blots showing proteins involved in mitochondrial function as well as AMPK and its phosphorylated isoform in gastrocnemius of WT and Pax8 +/- mice. n = 5 per group. **(F)** Densitometric analysis of western blots shown in panel E. Data are represented as the mean ± SEM. * p-value < 0.05 t-test two tailed.

Consistent with these results, mitochondrial DNA content to nuclear DNA ratio was not altered in any of the metabolic tissues tested (Figure 27A-B). In addition, electron microscopy images of gastrocnemius from WT and Pax8 +/- mice revealed normal mitochondrial appearance (Figure 27C).

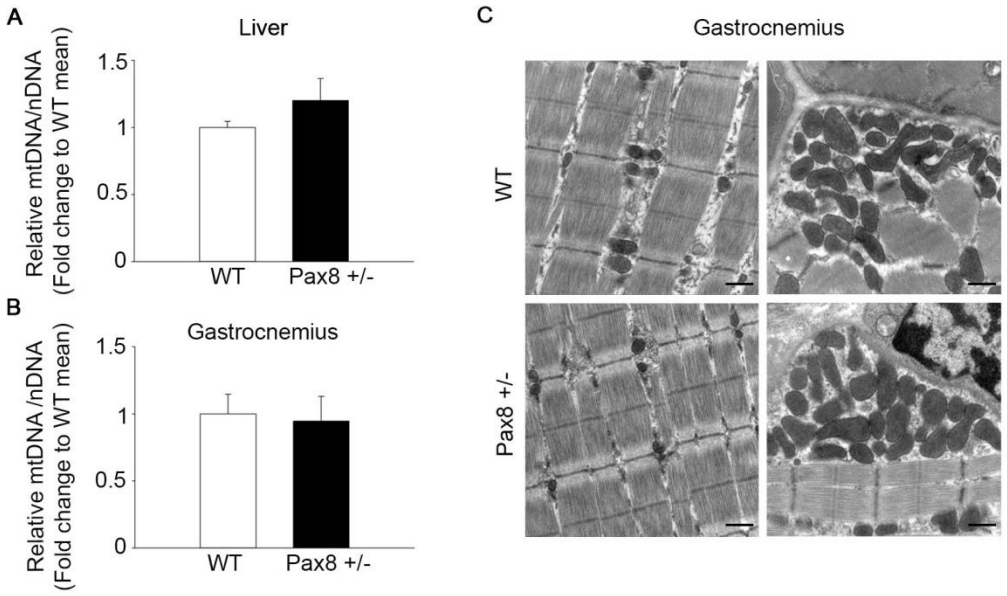

Figure 27. Mitochondrial DNA content is not affected in liver and gastrocnemius of Pax8 +/- mice. (A) Relative mitochondrial DNA content in livers of WT and Pax8 +/- mice. n = 6 per group. **(B)** Relative mitochondrial DNA content in gastrocnemius of WT and Pax8 +/- mice. n = 6 per group. **(C)** Electron microscopy images of gastrocnemius of WT and Pax8 +/- mice showing normal mitochondrial appearance. n = 6 per group. Scale bar = 500 nm. Data are represented as the mean ± SEM.

Further confirming that mitochondrial content is not altered in these tissues, citrate synthase activity was not affected in either liver or gastrocnemius extracts of Pax8 +/- mice (Figure 28A-B). Likewise, no significant differences were observed between genotypes in the specific activities of complexes I+III and II+III in both liver and gastrocnemius (Figure 28C-J). However, superoxide generation in the liver of Pax8 +/- animals was significantly increased (WT: 7.2 ± 0.2 nmol/mg·min vs. Pax8 +/-: 8.5 ± 0.3 nmol/mg·min, p-value = 0.009 t-test two tailed), even when relativized to citrate synthase

activity (WT: 0.0386 ± 0.0024 nmol/mg·min vs. Pax8 +/-: 0.0454 ± 0.0017 nmol/mg·min, p-value = 0.046 t-test two tailed) (Figure 28K-L). In contrast, superoxide generation in gastrocnemius extracts of Pax8 +/- and WT mice was similar (Figure 28M-N).

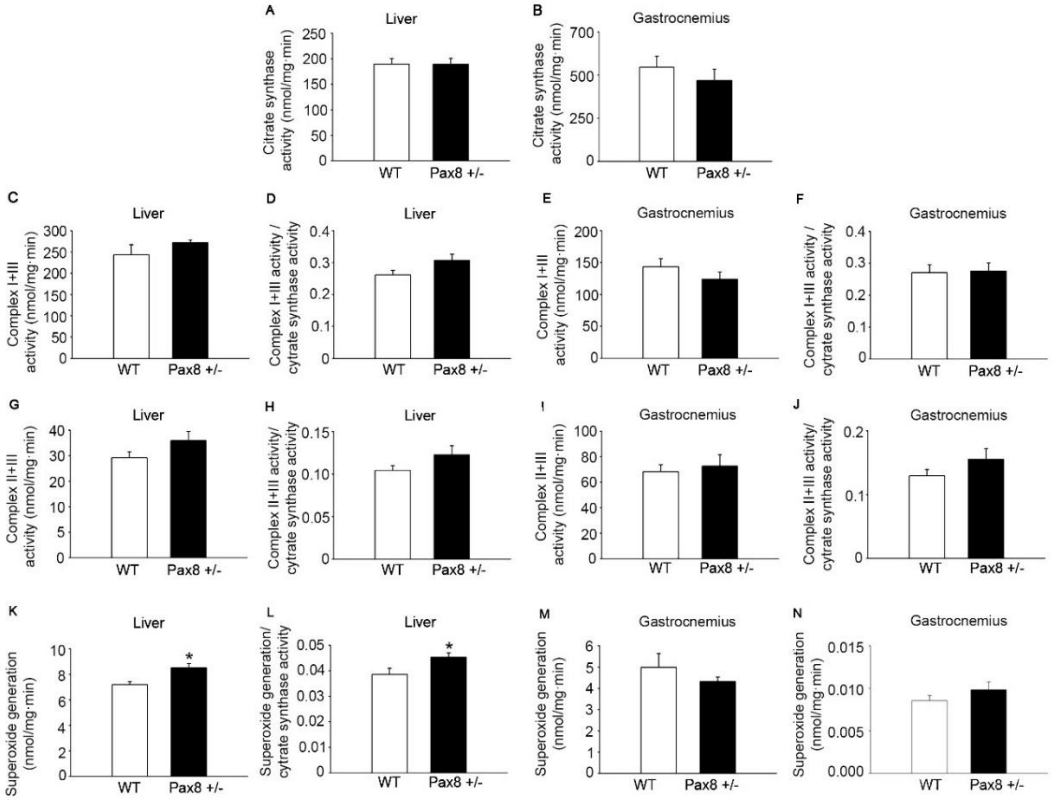

Figure 28. Superoxide generation is increased in livers of Pax8 +/- mice. (A) Citrate synthase activity in liver extracts of WT and Pax8 +/- mice. n = 6 per group. **(B)** Citrate synthase activity in gastrocnemius extracts of WT and Pax8 +/- mice. n = 6 per group. **(C)** Complex I+III activity in liver extracts of WT and Pax8 +/- mice. n = 6 per group. **(D)** Complex I+III activity shown in panel C relativized to citrate synthase activity shown in A. **(E)** Complex I+III activity in gastrocnemius extracts of WT and Pax8 +/-mice. n = 6 per group. **(F)** Complex I+III activity shown in panel E relativized to citrate synthase activity shown in B. **(G)** Complex II+III activity in liver extracts of WT and Pax8 +/- mice. n = 6 per group. **(H)** Complex II+III activity shown in panel G relativized to citrate synthase activity shown in A. **(I)** Complex II+III activity in gastrocnemius extracts of WT and Pax8 +/- mice. n = 6 per group. **(J)** Complex II+III activity shown in panel I relativized to citrate synthase activity shown in B. **(K)** Superoxide generation in liver extracts of WT and Pax8 +/- mice. n = 6 per group. **(L)** Superoxide generation shown in panel K relativized to citrate synthase activity shown in A. **(M)** Superoxide generation in gastrocnemius extracts of WT and Pax8 +/- mice. n = 5 WT, n = 6 Pax8 +/-. **(N)** Superoxide generation shown in panel M relativized to citrate synthase activity shown in B. Data are represented as the mean ± SEM. * p-value < 0.05 t-test two tailed.

Determinations by western blot of 4-HNE, which results from lipid peroxidation, revealed a significant increase in both liver (WT: 100 ± 6.033% vs. 132.50 ± 8.88%, p-value = 0.014 t-test two tailed) and gastrocnemius (WT: 100 ± 3.39% vs. Pax8 +/-: 128.63 ± 7.76%, p-value = 0.016 t-test two tailed) of Pax8 +/- mice compared to WT (Figure 29A-D).

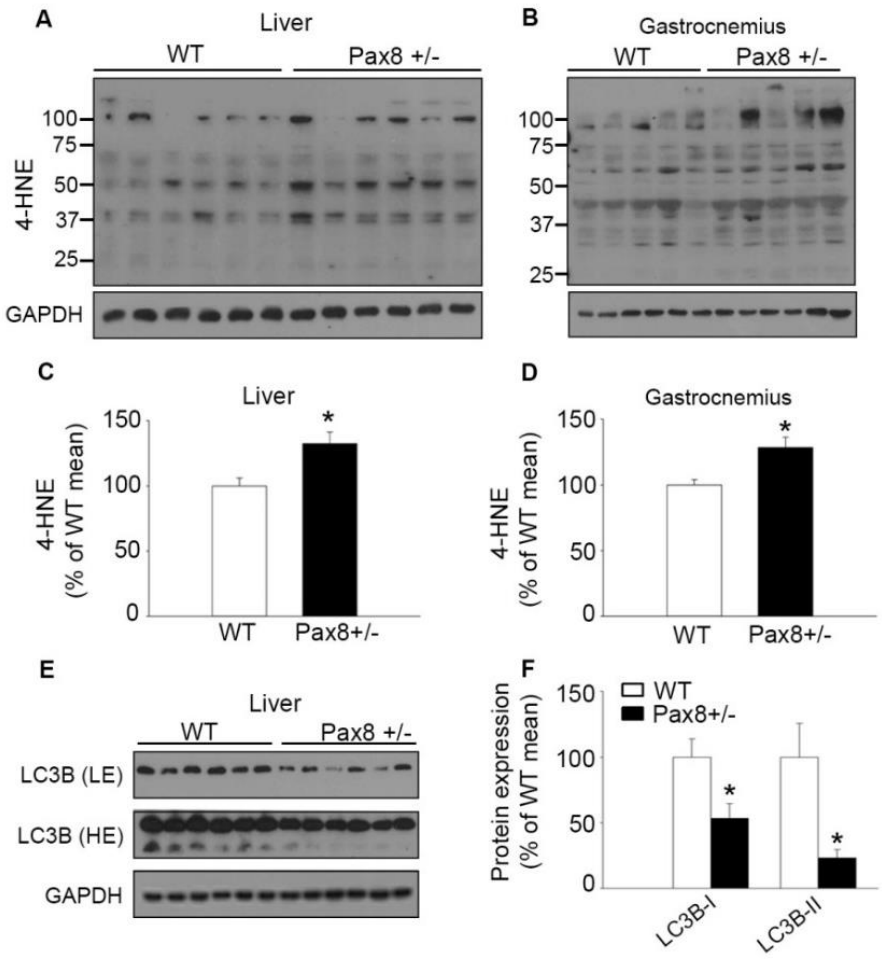

Figure 29. Pax8 +/- mice exhibit increased 4-HNE in liver and gastrocnemius. (A) Western blot showing 4-HNE staining in liver extracts of WT and Pax8 +/- mice. n = 6 per group. **(B)** Western blot showing 4-HNE staining in gastrocnemius extracts of WT and Pax8 +/- mice. n = 5 per group. **(C)** Densitometric analysis of the western blot shown in panel A. **(D)** Densitometric analysis of the western blot shown in panel B. **(E)** Western blots showing LC3B (LC3B-I = 16 kDa and LC3B-II = 14 kDa) in liver extracts of WT and Pax8 +/- mice. LE = Low exposure. HE = High exposure. n = 6 per group. **(F)** Densitometric analysis of western blots shown in E. Data are represented as the mean ± SEM. * p-value < 0.05 t-test two tailed.

Remarkably, protein levels of LC3B-I and LC3B-II were dramatically reduced in liver extracts of Pax8 +/- mice (WT: 100 ±13.82% vs. Pax8 +/-: 53.26 ± 11.16%, p-value = 0.026 t-test two tailed and WT: 100 ± 25.84% vs. Pax8 +/-: 23.26 ± 6.42%, p-value = 0.004 t-test two tailed, respectively). Likewise, there was a tendency towards a decreased ratio LC3BII/LC3BI (WT: 0.99 ± 0.16% vs. Pax8: 0.56 ± 0.16%, p-value = 0.086 t-test two tailed), indicating that autophagy may be impaired in the liver of Pax8 +/- mice (Figure 29E-F).

4.2.8 Pax8 +/- male mice fed in HFD do not exhibit exacerbated glucose intolerance or insulin resistance

In order to investigate whether the phenotype observed in Pax8 +/- mice was further exacerbated by an environmental stressor, we determined the effects of HFD feeding in Pax8 +/- mice. Importantly, circulating T4 levels were significantly reduced in Pax8 +/- mice compared to WT mice feed in HFD (WT: 3.28 ± 0.26 µg/dl vs. Pax8 +/-: 2.62 ± 0.14µg/dl, p-value = 0.047 t-test two tailed) (Figure 30).

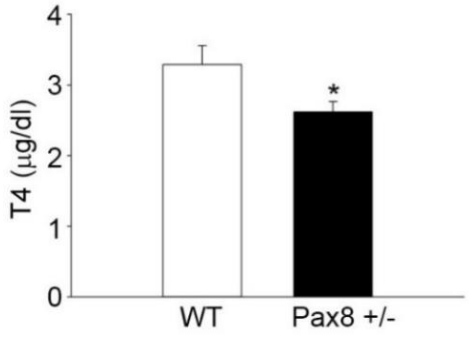

Figure 30. Pax8 +/- in HFD exhibit reduced circulating T4 levels. T4 levels in serum from WT and Pax8 +/- male mice in HFD at 7 months of life. n = 8 WT, n = 9 Pax8 +/-. Data are represented as the mean ± SEM. * p-value < 0.05 t-test two tailed.

However, Pax8 +/- mice in HFD did not exhibit increased body weight compared to WT mice in HFD and no differences were observed in fasting induced energy intake (Figure 31A-B).

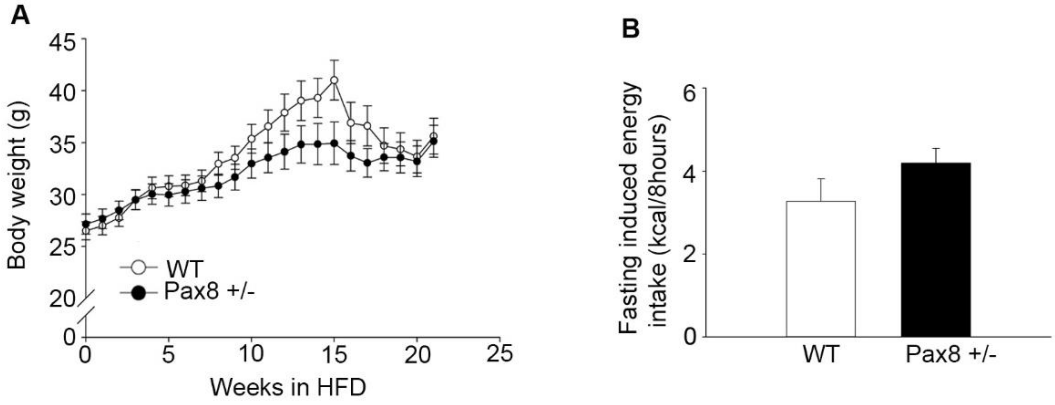

Figure 31. HFD feeding does not exacerbate body weight gain in Pax8 +/- mice. **(A)** Body weights (g) of WT and Pax8 +/- mice during weeks in HFD. HFD was started at 2-3 months of age. n = 15 WT, n = 13 Pax8 +/-. **(B)** Fasting induced energy intake in WT and Pax8 +/- mice fed in HFD. n = 8 WT, n = 9 Pax8 +/-. Data are represented as the mean ± SEM.

Glucose levels during the OGTT between different genotypes remained similar, whereas a tendency towards decreased levels of circulating insulin was observed 15 minutes after a glucose load in Pax8 +/- mice compared to WT (WT: 8.49 ± 2.47 ng/ml vs. Pax8 +/-: 4.58 ± 1.05 ng/ml, p-value = 0.073 t-test two tailed) (Figure 32A-D). Remarkably, glucose levels were lower at all the time points measured after a pyruvate load in Pax8 +/- animals compared to WT (Figure 32E). Therefore, the AUC for the IPPTT was reduced (WT: 42061 ± 1820 a.u. vs. Pax8 +/-: 33.072 ± 3617 a.u., p-value = 0.0163) (Figure 32F). However, no significant differences were observed during the ITT (Figure 32G-H), in the HOMA-IR or in the percentage of HbA1c between different genotypes fed on HFD (Figure 33A–D).

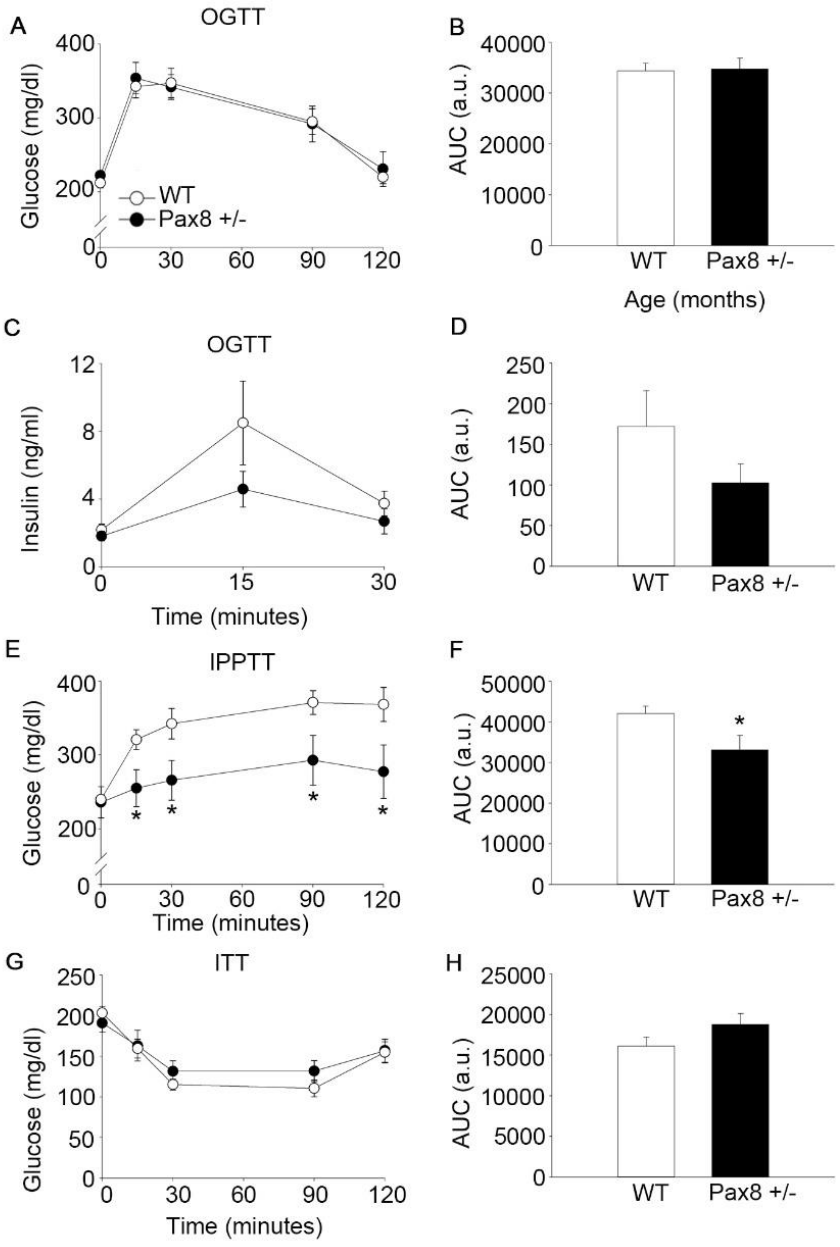

Figure 32. Pax8 +/- mice in HFD exhibit similar glucose tolerance than WT mice in HFD. **(A)** Circulating glucose levels during an OGTT. n = 13 WT, n = 11 Pax8 +/-. **(B)** AUC for glucose levels during the OGTT. **(C)** Insulin levels in plasma during an OGTT. n = 8 per group. **(D)** AUC for insulin levels during the OGTT. **(E)** Circulating glucose levels during the IPPTT. n = 13 WT, n = 10 Pax8 +/-. **(F)** AUC for the IPPTT. **(G)** Glucose levels in blood during the ITT. n = 9 per group. **(H)** AUC for the ITT. Data are represented as the mean ± SEM. * p-value <0.05 repeated measurements two-way ANOVA in panels A, C, E and G. T-test two tailed in panels B, D, F and H.

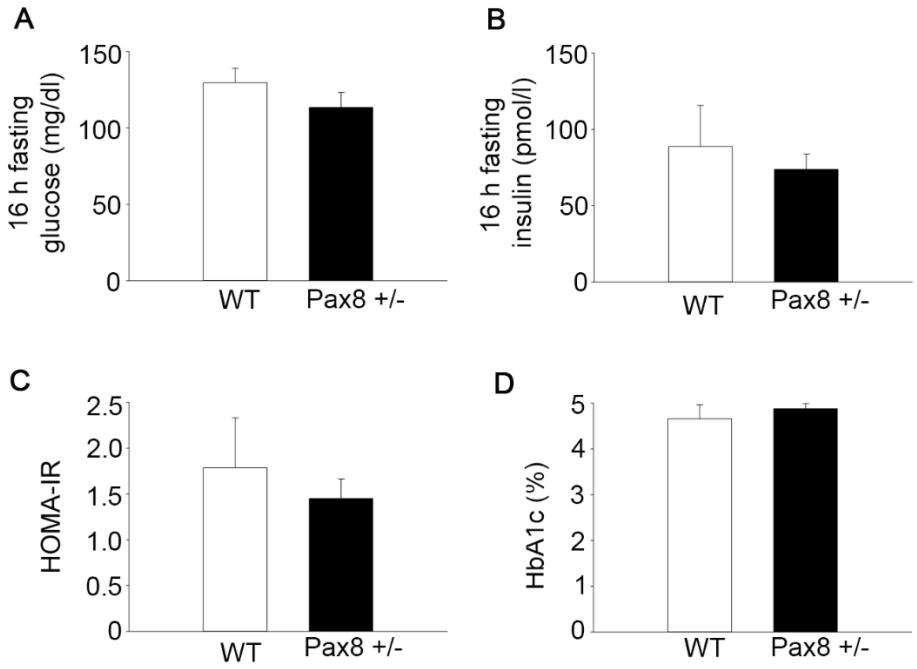

Figure 33. HFD feeding does not exacerbate insulin resistance in Pax8 +/- mice. (A) Glucose levels in blood after 16 hours of fasting. n = 8 per group. **(B)** Circulating insulin after 16 hours of fasting. n = 8 per group. **(C)** HOMA-IR. n = 8 per group. **(D)** Percentage of HbA1c n = 8 per group. Data are represented as the mean ± SEM.

Importantly, Pax8 +/- male mice fed on HFD exhibited an extremely unhealthy appearance, even though glucose tolerance and insulin resistance were similar to control group on HFD. Moreover, the reduced circulating glucose levels shown during the IPPTT by Pax8 +/- male mice in HFD (i.e. impaired gluconeogenesis), could reflect a hepatic dysfunction.

AIM 3: Determine the effect of T4 supplementation in healthy C57BL/6 mice as well as in the RIP-B7.1 and STZ models of experimental diabetes.

N.B. Results presented herein are published in an article entitled: “Levothyroxine enhances glucose clearance and blunts the onset of experimental type 1 diabetes mellitus in mice”, published in the British Journal of Pharmacology in which I am first author.

4.3.1 T4 supplementation effectively increases circulating T4 levels

Since according to our previous results reduced circulating T4 levels are associated with glucose intolerance and insulin resistance, we next investigated whether T4 supplementation could have a beneficial effect on glucose homeostasis. In order to determine the metabolic effects of T4 supplementation in mice, we treated female wild-type C57BL/6 mice with T4 from postnatal day 1 (18 ng/g of body weight per day by subcutaneous injections) until weaning, followed by T4 administration in the drinking water (50 $\mu g.ml^{-1}$ *ad libitum*) until 24-weeks of age, when mice were euthanized. Importantly, the treatment increased circulating T4 concentration (UT: 5.091 ± 0.168 µg/dl vs. T4: 17.73 ± 0.644 µg/dl, p-value < 0.0001 t-test two tailed) (Figure 34A).

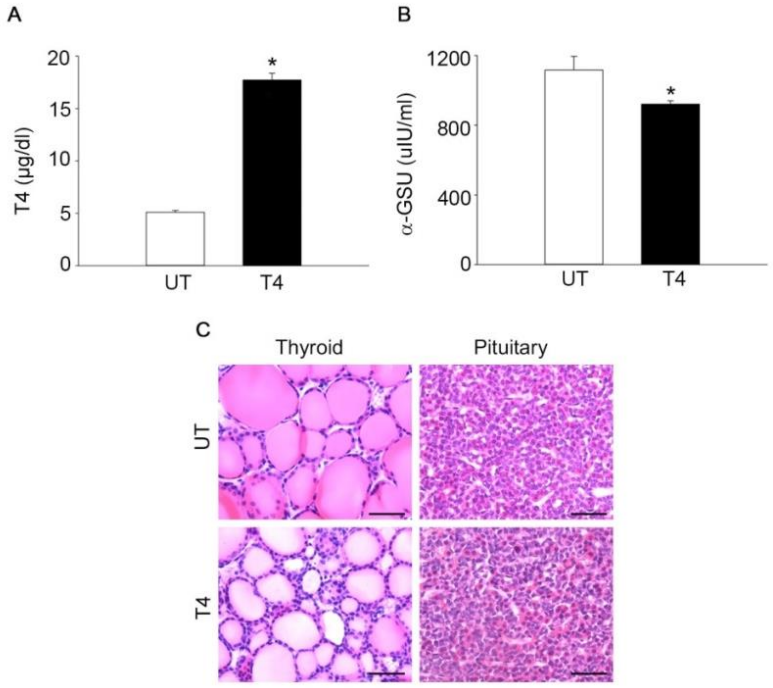

Figure 34. Circulating T4 levels are increased upon T4 treatment. (A) Circulating T4 levels in untreated and T4-treated mice. n = 7 UT, n = 8 T4. **(B)** Plasma levels of the α-GSU subunit of pituitary hormones. n = 7 UT, n = 8 T4. **(C)** Representative images of the histological analysis of the thyroid and pituitary from untreated and T4-treated mice. Thyroid: n = 6 UT, n = 7 T4. Pituitary: n = 5 UT, n = 6 T4. Scale bar = 100 µm. UT: untreated; T4: treated with T4. Data are represented as the mean ± SEM. * p-value < 0.05 t-test two tailed.

Consistent with this, plasma levels of the α-GSU subunit of pituitary hormones, such as TSH, were concomitantly reduced in T4-treated mice (UT: 1116 ± 77 uIU/ml vs. T4: 921 ± 18 uIU/ml, p-value = 0.045 t-test two tailed) (Figure 34B). Noteworthy, histological examinations of the thyroid and the pituitary revealed no major macroscopic changes in tissue morphology. However, thyroid sections of T4-treated mice had a slightly less intense staining of the colloid in the lumen of the follicle, suggestive of reduced endogenous thyroglobulin content (Figure 34C).

4.3.2 T4 supplementation enhances glucose clearance in healthy C57BL/6 mice

Glucose tolerance was enhanced by T4 supplementation as determined by reduced glucose levels in blood at all time points measured after a glucose load and a lower AUC during the OGTT (UT: 27581 ± 1081 a.u. vs. T4: 19333 ± 597 a.u., p-value < 0.0001 t-test two tailed) (Figure 35A-B). Noteworthy, significant differences in circulating glucose during the OGTT were maintained even when glucose levels were expressed as the percentage of basal glucose (Figure 36A). Basal circulating insulin levels in the OGTT were higher in T4-treated mice, while at 15-30 minutes post-glucose load insulin levels were similar to those of untreated animals. However, the increase in basal circulating levels were enough to increase the AUC (UT: 28.87 ± 1.97 a.u. vs. T4: 37.60 ± 3.17 a.u., p-value = 0.03 t-test two tailed) (Figure 35C-D). In order to determine whether gluconeogenesis was affected, animals were challenged with an intraperitoneal pyruvate injection (IPPTT). Glucose levels were lower at all the time points measured during the IPPTT, as it was the AUC (UT: 25532 ± 899 a.u. vs. T4: 7925 ± 628 a.u., p-value < 0.0001 t-test two tailed) (Figure 35E-F). However, differences were lost when values were relativized to basal glucose (Figure 36B).

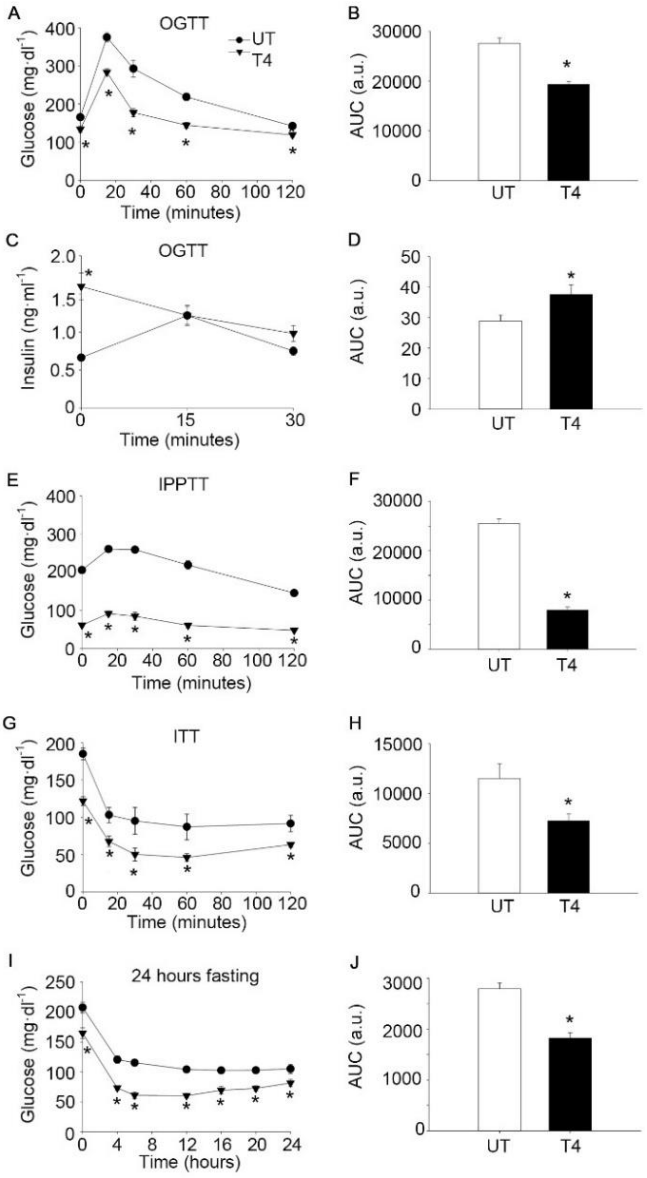

Figure 35. T4 enhances glucose clearance in wild-type C57BL/6 mice. (A) Glucose concentration in blood after an oral glucose load (OGTT). n = 13 per group. **(B)** AUC of glucose levels during the OGTT. **(C)** Plasma levels of insulin after an oral glucose load (OGTT). n = 7 UT, n = 8 T4. **(D)** AUC of insulin levels during OGTT. **(E)** Glucose concentration in blood after an intraperitoneal pyruvate load (IPPTT). n = 7 UT, n = 8 T4. **(F)** AUC of glucose levels during the IPPTT. **(G)** Glucose concentration in blood after an intraperitoneal insulin injection (ITT). n = 12 UT, n = 13 T4. **(H)** AUC of glucose levels during the ITT. **(I)** Glucose concentration in blood during a 24-hour fasting period. n = 7 UT, n = 8 T4. **(J)** AUC of glucose levels during the 24-hour fasting period. UT: untreated; T4: treated with T4. Data are represented as the mean ± SEM. * p-value < 0.05 t-test two tailed.

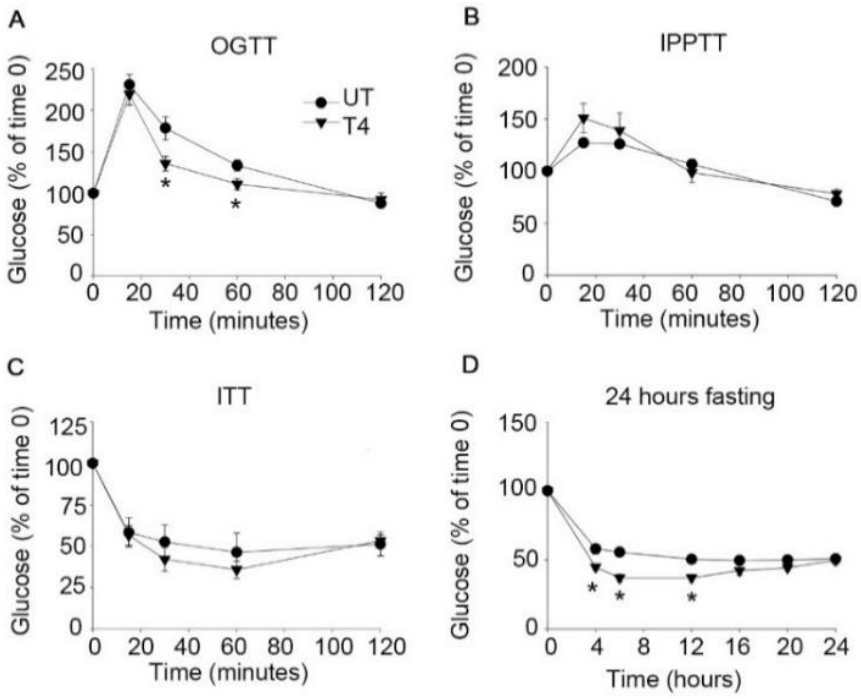

Figure 36. Glucose levels in metabolic test expressed as percentage of basal glucose. (A) Glucose concentration in blood during the OGTT expressed as the percentage of basal (time 0) glucose. n = 13 per group. **(B)** Glucose concentration in blood during the IPPTT expressed as the percentage of basal glucose. n = 7 UT, n = 8 T4. **(C)** Glucose concentration in blood during the ITT expressed as the percentage of basal glucose. n = 12 UT, n = 13 T4. **(D)** Glucose concentration in blood during a 24-hour fasting period expressed as the percentage of basal glucose. n = 7 UT, n = 8 T4. UT: untreated; T4: treated with T4. Data are represented as the mean ± SEM. * p-value < 0.05 Mann-Whitney Rank Sum test.

The AUC for the ITT was also lower in T4-treated animals compared to untreated mice (UT: 11515 ± 1502 a.u. vs. T4: 7280 ± 680 a.u., p-value = 0.021 t-test two tailed), since circulating glucose levels were significantly lower at any time point measured during the experiment (Figure 35 G-H). However, differences were related to the lower basal glucose, as determined by the lack of significant differences when glucose levels were expressed as the percentage of basal glucose (Figure 36C). We next measured circulating glucose levels during a 24-hour fasting period. Glucose levels were significantly reduced in T4-treated mice at any time point measured during the

experiment, as it was the AUC (UT: 2794 ± 117 a.u. vs. T4: 1825 ± 105 a.u., p-value < 0.0001 t-test two tailed) (Figure 35I-J and 36D). Consistent with the high insulin levels determined during the basal time of the OGTT (6-hour fasting), circulating insulin levels were also higher at 16-hours of fasting; while glucose levels were lower (Figure 37A-B).

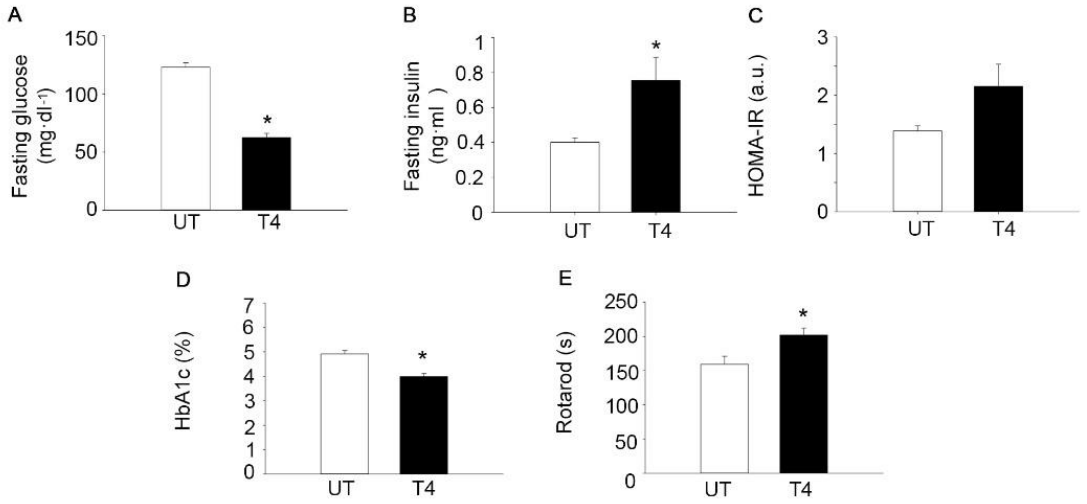

Figure 37. T4 treatment decreases HbA1c levels. (A) Circulating glucose levels after 16 hours of fasting. n = 7 UT, n = 8 T4. **(B)** Circulating insulin levels after 16 hours of fasting. n = 7 UT, n = 8 T4. **(C)** HOMA-IR. n = 7 UT, n = 8 T4. **(D)** Percentage of HbA1c in blood. n = 9 UT, n = 14 T4. **(E)** Time to fall from an accelerating rotarod. n = 12 UT, n = 18 T4. UT: Untreated; T4: T4-treated. Data are represented as the mean ± SEM. * p < 0.05 compared to untreated mice t-test two tailed.

Interestingly, despite the lower glucose levels during the ITT, a trend towards increased HOMA-IR was found in T4-treated mice (UT: 1.38 ± 0.08 a.u. vs. T4: 2.15 ± 0.37 a.u., p-value = 0.08 in t-test two-tailed) (Figure 37C). Supporting the long-term reduction of glucose levels in mice treated with T4, the percentage of HbA1c was found to be lower (UT: 4.91 ± 0.13% vs. T4: 3.99 ± 0.12%, p-value < 0.0001) (note that the untreated group is within the healthy physiological range) (Figure 37D). Taken together, these results indicate that T4 supplementation reduces dramatically glucose concentration

in blood, which is associated with increased circulating insulin. Furthermore, rotarod performance was improved by T4, indicating the overall healthy status of T4-treated mice (Figure 37E).

Additionally, at 6 months of age, body weight was slightly reduced in T4-treated mice compared to untreated animals (Figure 38A), although energy intake was similar in both experimental groups, even when divided by body weight (Figure 38B-C). Noticeably, at time of euthanization, WAT weight was reduced in T4-treated mice (Figure 38D-E). In contrast, several organs, including BAT, heart and liver were found to be heavier in T4-treated mice, even when divided by body weight (Figure 38D-E).

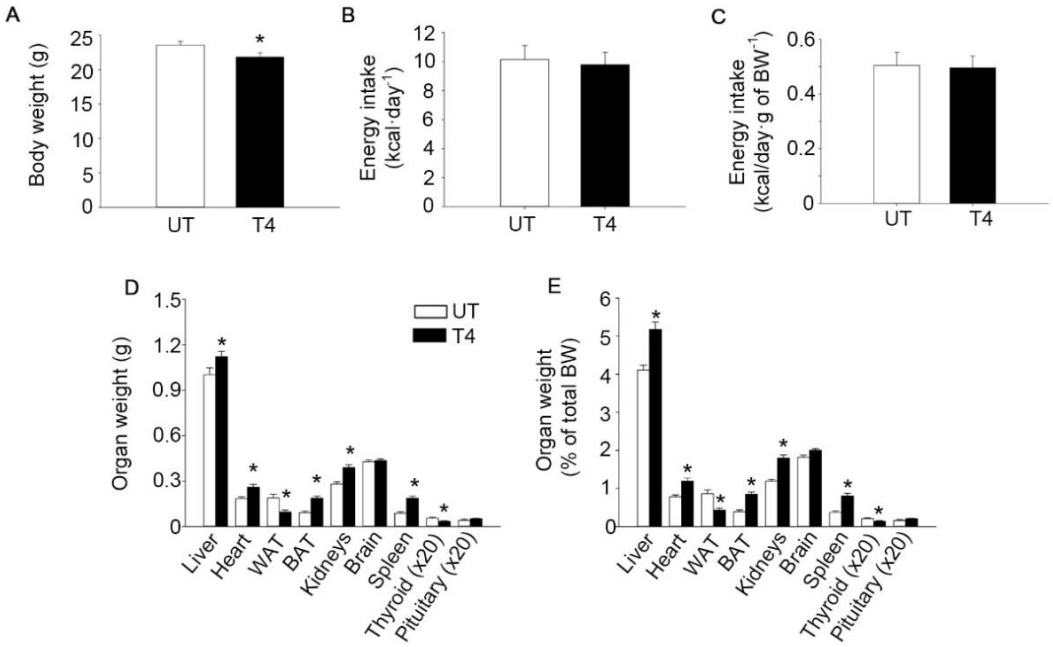

Figure 38. T4 supplementation reduces body weight. (A) Body weight. Age = 24 weeks. n = 12 UT, n = 18 T4. **(B)** Energy intake. Age = 8 weeks. n = 7 UT, n = 8 T4. **(C)** Energy intake shown in (B) relativized to body weight shown in (A). **(D)** Organs weight. Age = 24 weeks. For liver, heart, WAT, BAT, kidney, brain and spleen n = 12 UT, n = 18 T4. For thyroid and pituitary n = 6 UT, n = 7 T4. **(E)** Organs weight divided by body weight. Age = 24 weeks. For liver, heart, WAT, BAT, kidney, brain and spleen n = 12 UT, n = 18 T4. For thyroid and pituitary n = 6 UT, n = 7 T4. UT: Untreated; T4: T4-treated. Data are represented as the mean ± SEM. * $p < 0.05$ compared to untreated mice t-test two tailed.

4.3.3 T4 supplementation increases β-cell insulin content

The increase in circulating insulin levels observed in T4-treated mice indicated a potential effect of the hormone on pancreatic islets. Accordingly, immunohistochemical analysis revealed that insulin staining, as determined by mean intensity, was higher in pancreatic sections of T4-treated mice compared to control animals (UT: 29.92 ± 4.01 a.u. vs. T4: 47.46 ± 3.08 a.u., p-value = 0.009 in t-test two tailed), while glucagon was unaffected (Figure 39A-C). Increased insulin content in the islets of T4-treated mice was further confirmed by ELISA determination using freshly isolated pancreatic islets (UT: 410 ± 39.14 ng per 10 islets vs. T4: 769 ± 118 ng per 10 islets, p-value = 0.022 in t-test two tailed) (Figure 39D). Remarkably, GCK expression was also increased in pancreatic islets from T4-treated animals as determined by mean intensity in immunohistochemical analysis (UT: 22.14 ± 1.61 a.u. vs. T4: 36.82 ± 4.68 a.u., p-value = 0.01 in t-test two tailed) and mRNA expression (UT: 1 ± 0.03 vs. T4: 1.87 ± 0.17, p-value = 0.004 in t-test two tailed) (Figure 39E-F).

Determinations of mRNA expression by real-time PCR also revealed an increase in AKT expression, while no significant differences were observed between different experimental groups in the expression of MafA and FOXO1, which are markers of β-cell differentiation/maturation (Figure 39F) (Aguayo-Mazzucato et al., 2013, Kikuchi et al., 2012). Moreover, immunofluorescence analysis revealed that the subcellular localization of both MafA and FOXO1 was unaffected in T4-treated animals (Figure 39G and I).

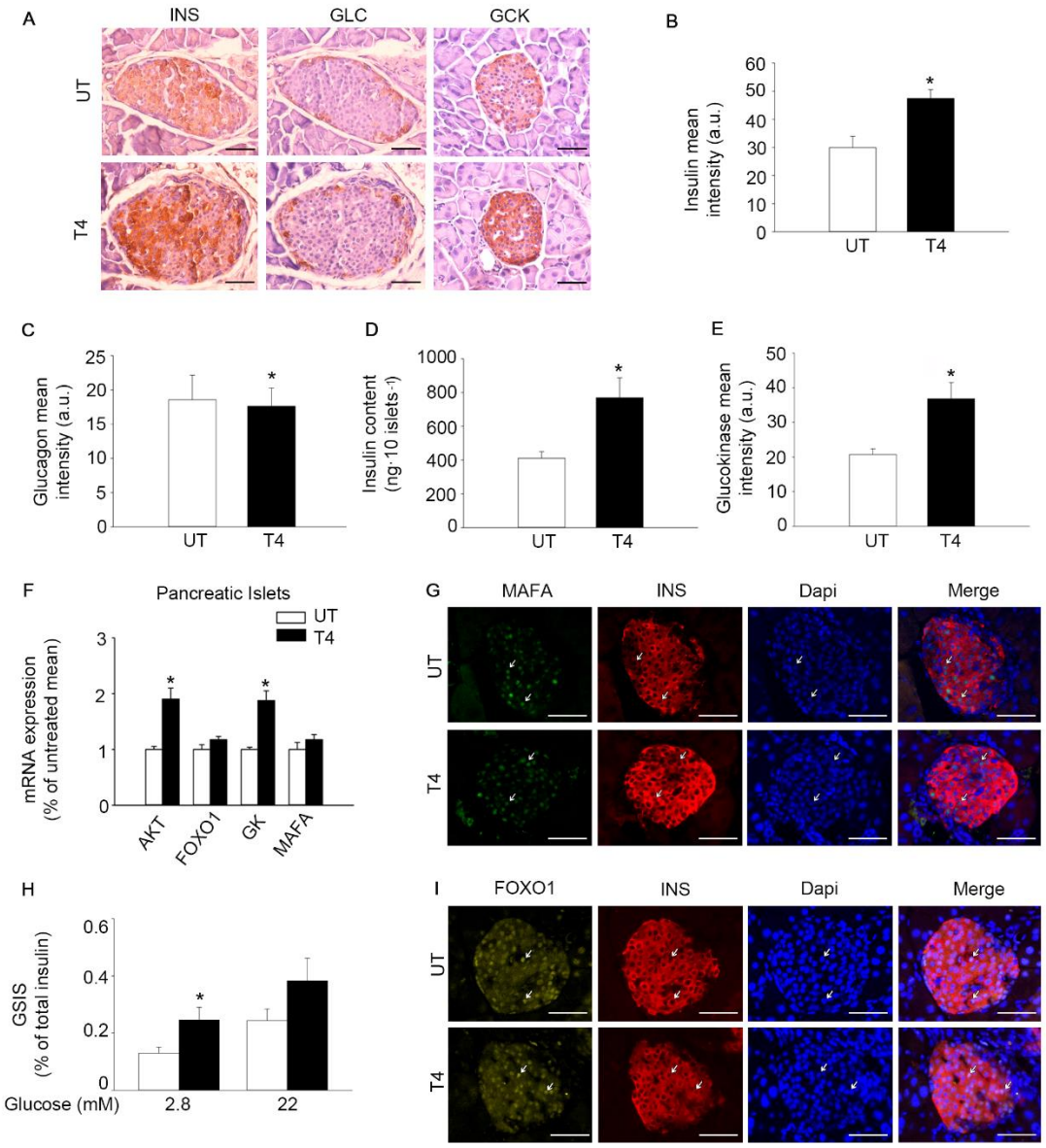

Figure 39. T4 increases insulin and GCK expression in pancreatic islets. (A) Representative images of insulin (INS), glucagon (GLC) and GCK staining in pancreases from mice treated or not with T4. DAB staining followed by hematoxylin counterstaining. **(B)** Quantification of insulin staining (mean intensity). n = 5 per group. **(C)** Quantification of glucagon staining (mean intensity). n = 5 per group. **(D)** Determination of pancreatic islet insulin content by ELISA. n = 6 UT, n = 7 T4. **(E)** Quantification of GCK staining (mean intensity). n = 6 per group. **(F)** Determination of messenger RNA (mRNA) levels of genes involved in pancreatic islet metabolism. Values were normalized to islets isolated from untreated mice. n = 6 UT, n = 5 T4. **(G)** Representative images of MafA and insulin immunofluorescence staining. n = 5 per group. **(H)** Determination of GSIS. n = 6 UT, n = 7 T4. **(I)** Representative images of FOXO1 and INS immunofluorescence staining. n = 6 UT, n = 7 T4. UT: untreated mice, T4: mice treated with T4. Data are represented as the mean ± SEM. * $p < 0.05$ compared to untreated mice t-test two tailed.

Remarkably, GSIS assays performed in islets isolated from untreated and T4-treated mice determined that insulin secretion was increased in T4-treated mice when islets were cultured under low glucose (2.8 mM) conditions (UT: 0.13 ± 0.02% of total insulin vs. T4: 0.27 ± 0.03% of total insulin, p-value = 0.021 in t-test two tailed). However, differences in insulin secretion under high glucose (22 mM) conditions did not reach statistical significance (Figure 39H).

4.3.4 T4 supplementation enhances β-cell turnover

Immunohistochemical analyses performed in pancreatic islets revealed that β-cell proliferation, defined here as the percentage of Ki67 positive cells within the insulin-expressing cell population, was increased in T4-treated animals when compared to untreated mice (UT: 0.14 ± 0.033% vs. T4: 0.56 ± 0.075%, p-value = 0.002 in t-test two tailed) (Figure 40A-B). As opposed to β-cells, non-insulin-expressing pancreatic endocrine cells showed similar proliferation in untreated and T4-treated mice (percentage of Ki67 positive cells in islet residing non-insulin expressing cells) (Figure 40C). Interestingly, the percentage of apoptotic cells, determined by Tunel staining, was also increased by T4 administration specifically in the β-cell population (UT: 0.05 ± 0.11% vs. T4: 1.19 ± 0.23%, p-value = 0.049 in t-test two-tailed) (Figure 40D-F). Therefore, our results indicate that T4 supplementation effectively promotes β-cell turnover in healthy WT animals by increasing both β-cell proliferation and apoptosis.

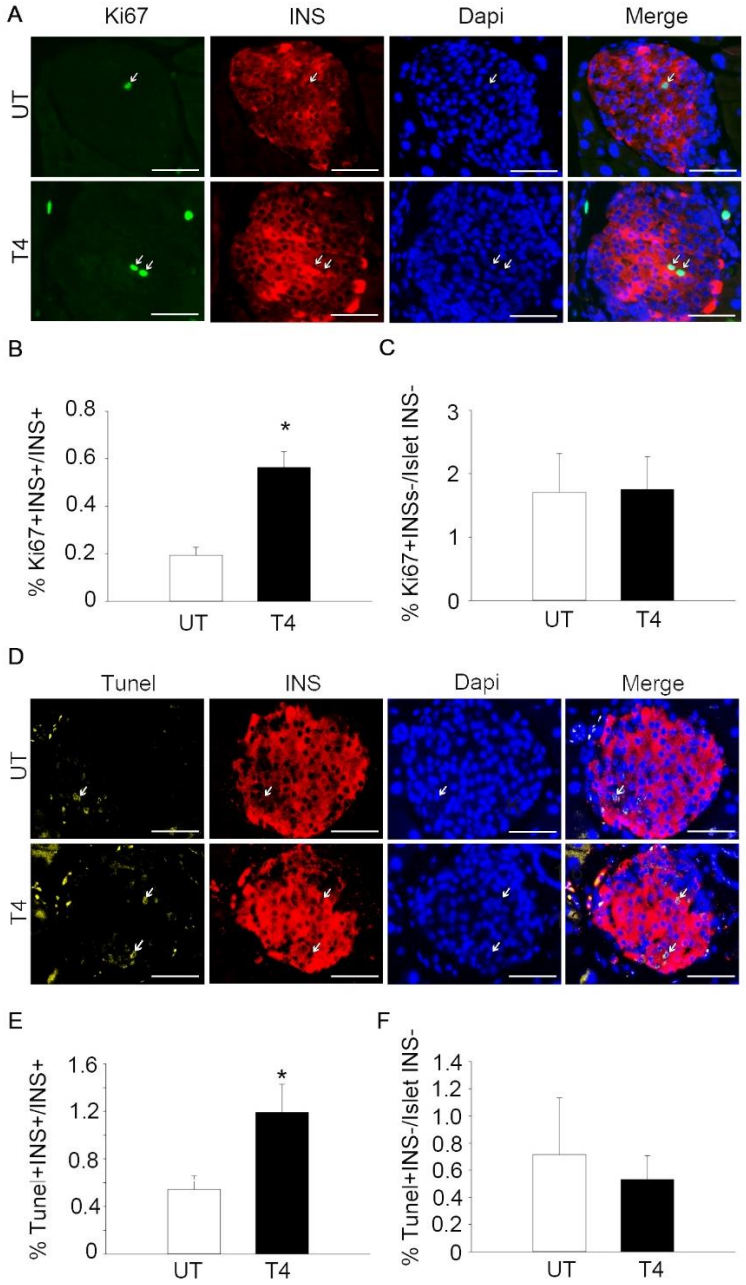

Figure 40. T4 induces β-cell proliferation and apoptosis. (A) Representative immunofluorescence image of pancreatic islets from untreated and T4-treated mice showing Ki67 and insulin (INS). **(B)** Quantification of the percentage of Ki67+ INS+ cells. n = 5 per group. **(C)** Quantification of Ki67+INS- cells. n = 5 per group. **(D)** Representative immunofluorescence image of pancreatic islets of T4-treated mice showing Tunel staining. **(E)** Quantification of Tunel + INS+ cells. n = 5 per group. **(F)** Quantification of Tunel + INS- cells. n = 5 per group. In all cases, at least 1000 endocrine cells per animal were counted. UT: untreated mice. T4: mice treated with T4. Data are represented as the mean ± SEM. * p-value < 0.05 t-test two tailed.

4.3.5 T4 induces the activation of IRS1-AKT signalling in insulin-target tissues

In order to determine the underlying mechanism of T4 action in insulin-target tissues, we determined mRNA expression by semi-quantitative real-time PCR of several genes involved in the insulin signalling pathway. We found that the transcript levels of AKT and FOXO1 were over-expressed in both the skeletal muscle and the liver of T4-treated mice (Figure 41A-B). Consistent with these data, protein extracts of both, T4-treated liver and skeletal muscle, exhibited increased protein levels of total AKT, FOXO1 as well as IRS1 and GSK3-β (Figure 41C-E). Moreover, the phosphorylated isoforms of several members of the insulin signalling such as pTyr632 IRS1, pSer473 AKT and pSer256 FOXO1, were significantly increased in both, skeletal muscle and liver lysates isolated from T4-treated mice (Figure 41C-E). Remarkably, ERK phosphorylation at Thr202/Tyr204 in skeletal muscle was reduced in T4-treated samples, indicating the specificity of the effect of T4 supplementation in the IRS1-AKT branch of the insulin signalling. In order to determine whether T4 supplementation could also increase the maximal activation of the IRS1-AKT axis of the insulin signalling, a cohort of mice was treated with insulin (0.75 $UI.kg^{-1}$ of body weight) 15 minutes prior sacrifice (Figure 41F-H). No differences on insulin-stimulated phosphorylation of Ser473 AKT levels were found, indicating that maximal insulin-induced AKT activation is not affected by T4-treatment.

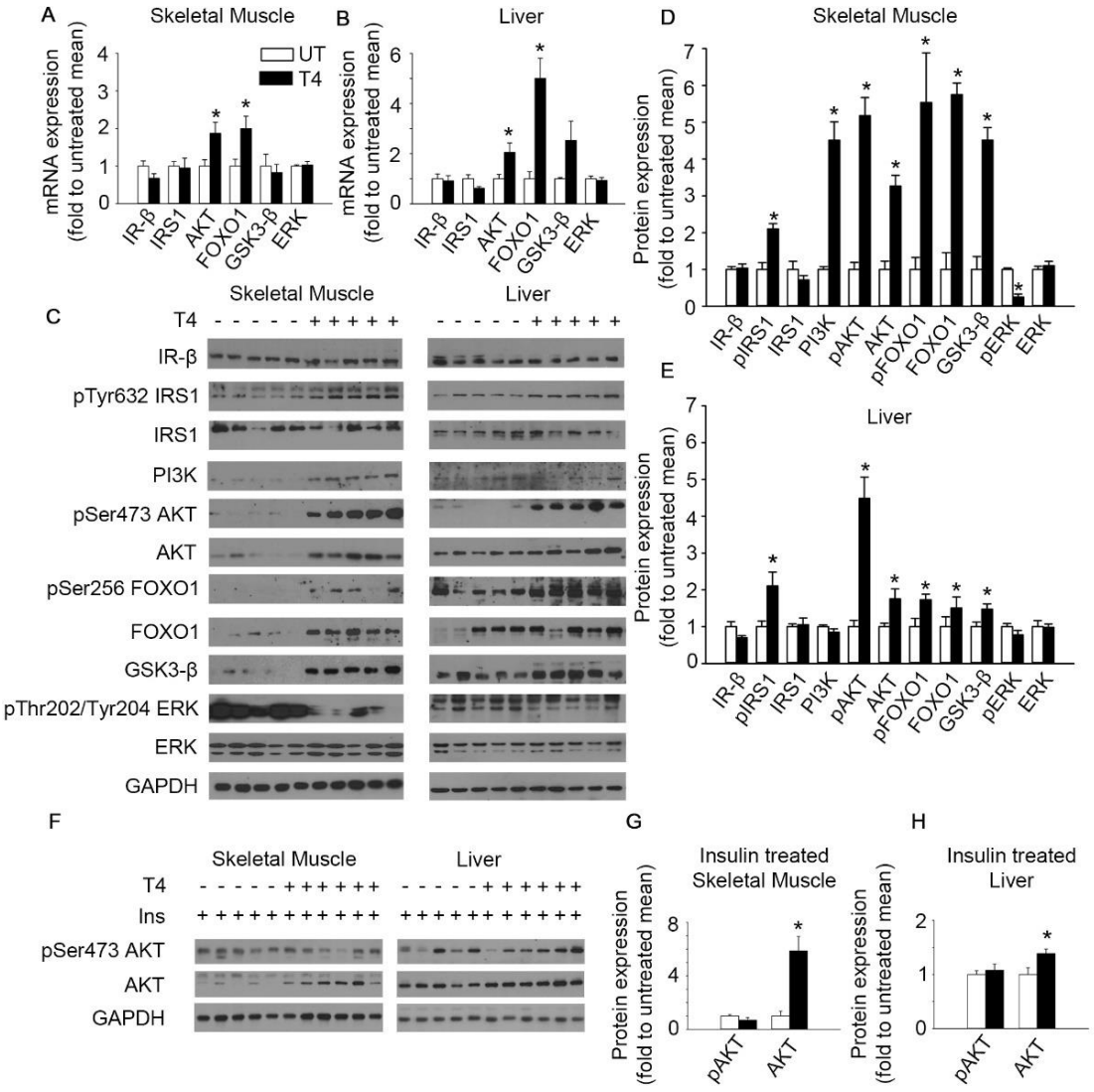

Figure 41. T4 activates insulin signalling in skeletal muscle and liver. (A) Determination of mRNA levels of several members of the insulin pathway in the skeletal muscle of mice treated or not with T4. IR-β: n = 5 per group; IRS1: n = 6 per group; AKT: n = 5 per group; FOXO1: n = 6 per group; GSK3-β: n = 6 per group; ERK: n= 6 per group. **(B)** Determination of mRNA levels of several members of the insulin pathway in the liver. IR-β: n = 6 UT, n = 5 T4; IRS1: n = 6 UT, n = 5 T4; AKT: n = 6 per group; FOXO1: n = 6 UT, n = 5 T4; GSK3-β: n = 5 per group; ERK: n = 6 UT, n = 5 T4. **(C)** Western blots indicating activation of insulin signalling in the skeletal muscle and liver of T4-treated mice. n = 5 per group. **(D)** Densitometric analysis of western blots performed in skeletal muscle extracts shown in panel C. **(E)** Densitometric analysis of western blots performed in liver extracts shown in panel C. **(F)** Representative images of western blots showing the maximal activation of insulin signalling in T4-treated and untreated mice challenged with an insulin injection 15 minutes prior euthanization. **(G)** Densitometric analysis of western blots performed in skeletal muscle extracts shown in F. n =

5 UT, n = 6 T4. **(H)** Densitometric analysis of western blots performed in liver extracts shown in F. n = 5 UT, n = 6 T4. UT: Untreated; T4: T4-treated. Mice were fasted for 16 hours prior euthanization and in all cases values were normalized to untreated mice. Data are represented as the mean ± SEM. * $p < 0.05$ compared to untreated mice t-test two tailed. The undergraduate/master's students Alvaro Jesus Narbona and Juan Luis Araujo have contributed to perform the western blots and RT-PCRs presented in this figure.

We next investigated whether T4 treatment also modulated the expression of genes involved in glucose utilization (e.g. increased glycolysis and gluconeogenesis) as well as mitochondrial biogenesis and uncoupling by real time PCR in both skeletal muscle and liver. Remarkably, the expression of PEPCK, which is involved in gluconeogenesis, was found increased in the liver of T4-treated mice. Additionally, genes involved in mitochondrial biogenesis (PGC1α) and uncoupling of the respiratory chain (UCP2), were increased in both liver and skeletal muscle extracts from T4-treated mice compared to control animals (Figure 42A-B).

Taken together, these results suggest that T4-induced high insulin levels in circulation drive to sustained activation of the IRS1-AKT signalling and subsequent increase in glucose uptake in insulin target tissues to maintain their high metabolic requirements. Supporting these data, a significant increase on phosphorylated Thr172 AMPK, which indicates a starvation-like status, was found in T4-treated skeletal muscle extracts. Noteworthy, this regulation was not detected in liver samples, suggesting that T4 modulates energy metabolism differently in the liver and the gastrocnemius (Figure 42C-E).

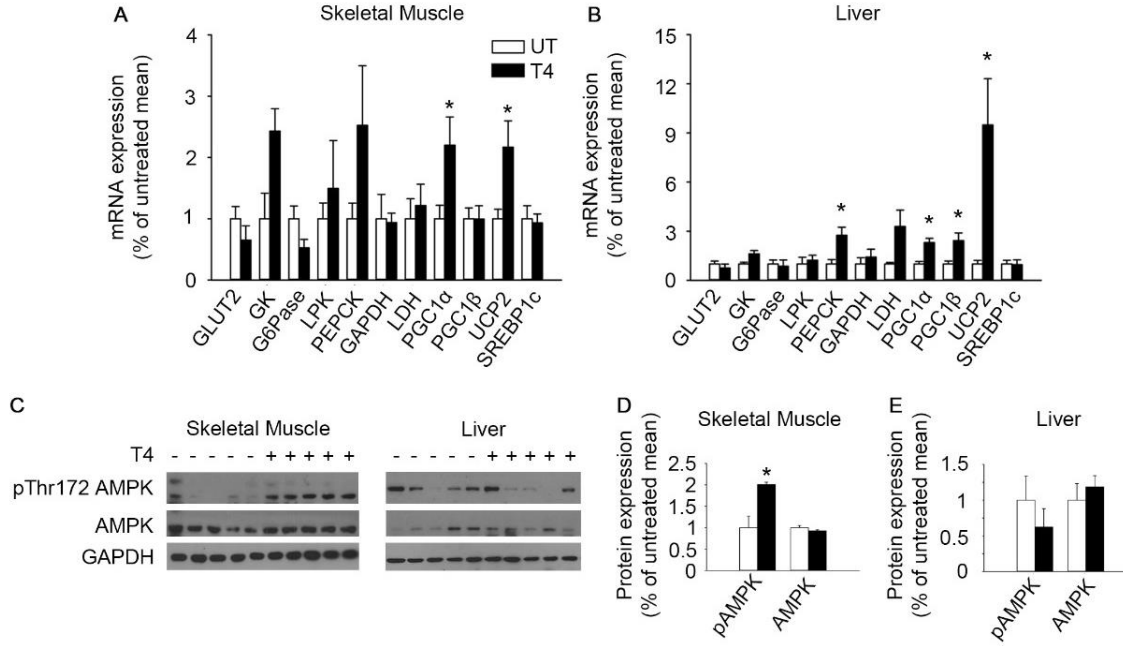

Figure 42. T4 supplementation increases the expression of genes involved in mitochondrial biogenesis and induces a starving-like status in skeletal muscle. (A) Determination of mRNA levels of genes involved in energy metabolism in the skeletal muscle of untreated and T4-treated mice. GLUT2: n = 5 UT, n = 6 T4; GK: n = 5 UT, n = 6 T4; G6Pase: n = 5 UT, n =6 T4; LPK: n = 5, n = 6 T4; PEPCK: n = 5 UT, n = 6 T4; GAPDH: n = 6 per group; LDH: n = 5 UT, n = 6 T4; PGC1α: n = 6 per group; PGC1β: n = 6 per group; UCP2: n = 5 per group; SREBP1c: n = 5 UT, n = 6 T4. **(B)** Determination of mRNA levels of genes involved in energy metabolism in the liver. GLUT2: n = 5 UT, n = 6 T4; GK: n = 5 per group; G6Pase: n = 5 UT, n = 6 T4; LPK: n = 5 UT, n = 6 T4; PEPCK: n = 5 UT, n = 6 T4; GAPDH: n = 6 UT, n = 5 T4; LDH: n = 5 per group; PGC1α: n = 5 UT, n = 6 T4; PGC1β: n = 6 per group; UCP2: n = 6 UT, n = 5 T4; SREBP1c: n = 6 UT, n = 5 T4. **(C)** Western blots indicating activation of AMPK in skeletal muscle and liver. n = 5 per group. Mice were fasted for 16 hours prior euthanization and all values are relativized to control group. **(D, E)** Densitometric analysis of western blots shown in panel C. UT: untreated; T4: treated with T4. Data are represented as the mean ± SEM. * p- value < 0.05 t-test two tailed.

4.3.6 T4 supplementation improves glycaemic control in the RIP-B7.1 model of EAD

Given the effects of T4 supplementation in the promotion of β-cell proliferation and the increase of circulating insulin levels in healthy C57BL/6 mice, we next sought to determine whether T4 supplementation could blunt the onset of T1DM in the RIP-B7.1 model of EAD (Mellado-Gil et al., 2016a, Harlan et al., 1994). To this end, RIP-B7.1

mice were treated with T4, (5 μg.ml^{-1} in the drinking water) starting at 6-weeks of age. RIP-B7.1 mice were immunized at 8-weeks of age to trigger the autoimmune attack to the β-cells. Determination of circulating T4 levels revealed a significant increase in T4-treated RIP-B7.1 when compared to untreated RIP-B7.1 immunized mice (RIP-B7.1 UT: 4.09 ± 0.16 μg/dl vs. RIP-B7.1 T4: 6.68 ± 0.28 μg/dl, p-value <0.0001 t-test two-tailed) (Figure 43). Moreover, similar to healthy wild type C57BL/6 mice (Figure 38D-E), the weight of several organs, including BAT, was found to be higher at the time of euthanization (5 weeks of T4-treatment; 11-weeks of age) (Figure 44A). However, differences on the weight of WAT were not apparent.

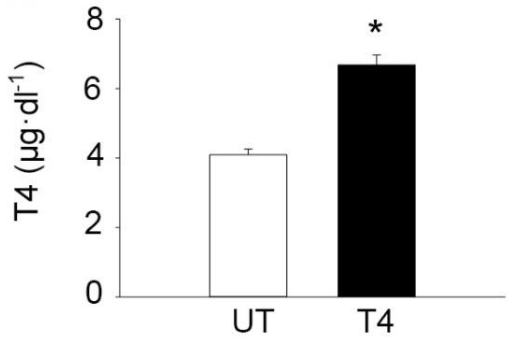

Figure 43. **T4 treatment increases circulating T4 in RIP-B7.1 mice**. Circulating T4 levels in untreated and T4-treated RIP-B7.1 mice. n = 9 UT, n = 8 T4. UT: untreated; T4: treated with T4. Data are represented as the mean ± SEM. * p-value < 0.05 in t-test two tailed.

Since, there is a decline in weight associated with diabetes progression in mice, RIPB7.1 mice were weighted every week (Huang et al., 2011). Noticeably, T4-treated immunized RIP-B7.1 mice gained weight over the course of the experiment, while control (untreated) immunized RIP-B7.1 mice reached a plateau. Thus, body weights were significantly different from week 4 of T4-treatment, 2 weeks post-immunization (Figure 44B).

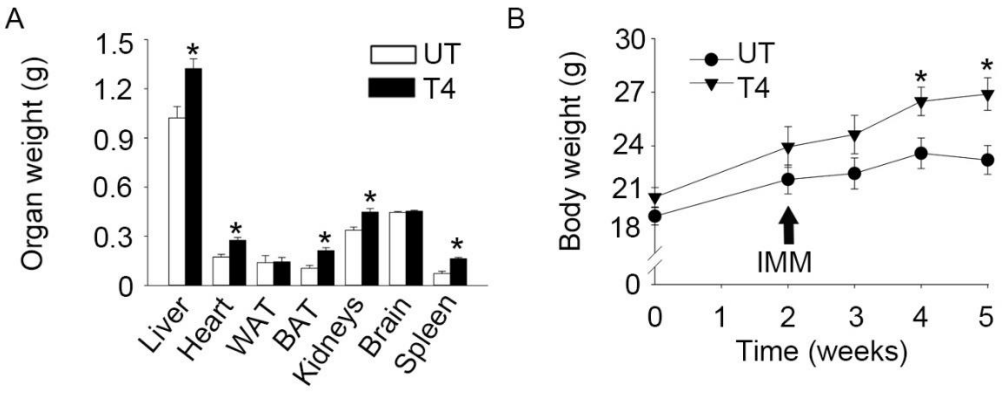

Figure 44. T4 supplementation alters organ weight and prevents body weight decline that follows hyperglycaemia in RIPB7.1 mice. (A) Organ weight in RIPB7.1 mice treated or not with T4. n = 6 UT, n = 9 T4-treated. **(B)** Body weight. n = 8 UT, n = 9 T4. Data are represented as the mean ± SEM. * p-value < 0.05.

In order to determine the effect of T4 supplementation in the pathogenesis of EAD, several metabolic tests were performed. T4-treated immunized RIP-B7.1 mice exhibited enhanced glucose clearance compared to untreated immunized RIP-B7.1 mice at 2 weeks post-immunization and 4 weeks of T4 treatment as determined by differences at several time points measured during an OGTT and a lower AUC for the experiment (Figure 45A-B). An ITT performed 3 weeks post-immunization and 5 weeks after T4 treatment, indicated that circulating glucose was significantly lower in T4-treated immunized RIP-B7.1 mice at any time point during the experiment (Figure 45C-D). However, these differences were clearly derived from the lower basal glucose levels found in T4-treated RIP-B7.1 immunized mice compared to untreated immunized RIP-B7.1 mice. Post-prandial glucose determinations revealed significant differences from 1-week post-immunization. Indeed, untreated immunized RIP-B7.1 animals developed severe hyperglycaemia at 3-weeks post-immunization, while T4-treated immunized RIP-B7.1 mice remained normoglycemic (Figure 45E). Remarkably, postprandial circulating

insulin was dramatically increased in T4-treated RIP-B7.1 immunized mice (UT RIP-B7.1: 0.51 ± 0.11 ng/ml vs. T4 RIP-B7.1: 3.36 ± 0.48, p-value = 0.0004 t-test two tailed) (Figure 45F), which was accompanied with increased phosphorylation of the IRS1 at Tyr 632 in the liver (Figure 46).

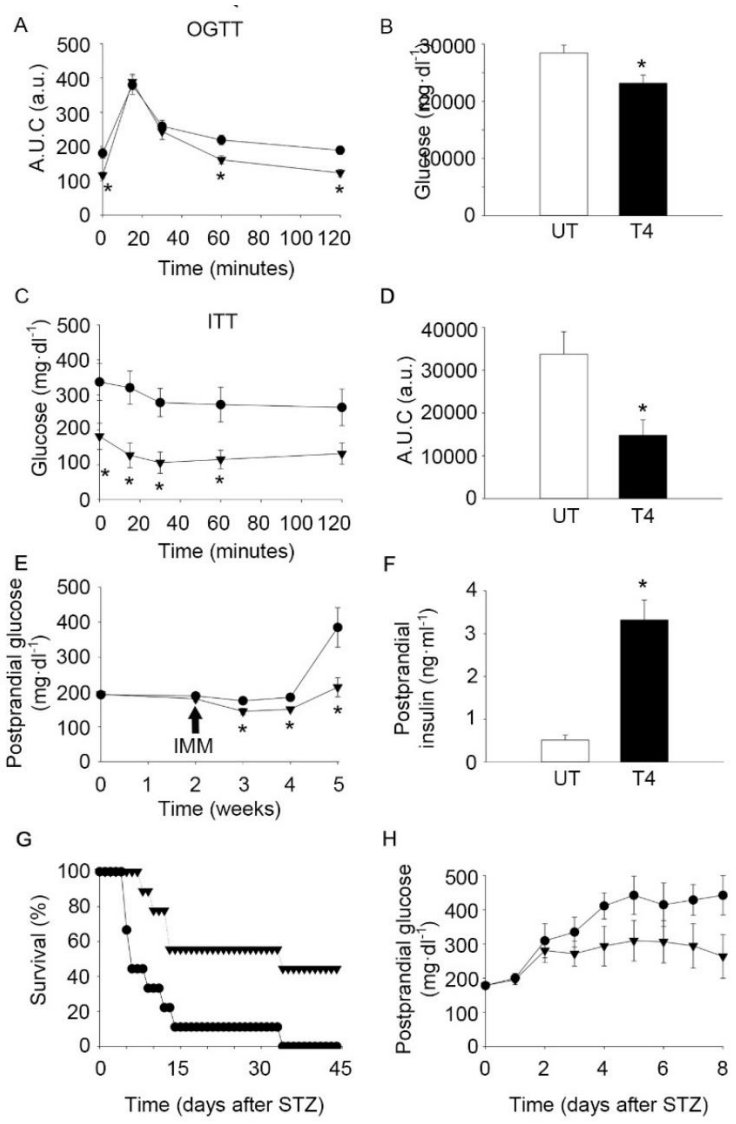

Figure 45. T4 supplementation blunts the onset of EAD in RIPB-7.1 mice and increases the survival in C57BL/6 mice treated with STZ. (A) Glucose concentration in blood during an OGTT at 4 weeks of T4-treatment on RIP-B7.1 mice. n = 8 UT, n = 9 T4. (**B)** AUC of glucose levels during the OGTT. (**C)** Glucose concentration in blood during an ITT at 5 weeks of T4-treatment on RIP-B7.1 mice. n = 7 UT, n = 9 T4. (**D)** AUC of glucose levels during the ITT. (**E)** Postprandial glucose concentration in blood on RIP-B7.1 mice. n = 8 UT, n = 9 T4.

(**F)** Postprandial circulating insulin levels. n = 7 UT, n = 8 T4. (**G)** Survival of C57BL/6 mice challenged with STZ. n = 9 per group. (**H)** Postprandial glucose concentration in blood on C57BL/6 mice challenged with STZ. Alive animals were included. UT: Untreated; T4: T4-treated; IMM: Immunization. Arrows indicate the time of immunization. Data are represented as the mean ± SEM. * p < 0.05 compared to untreated mice, t-test two tailed. A LogRank survival test was applied to survival curves

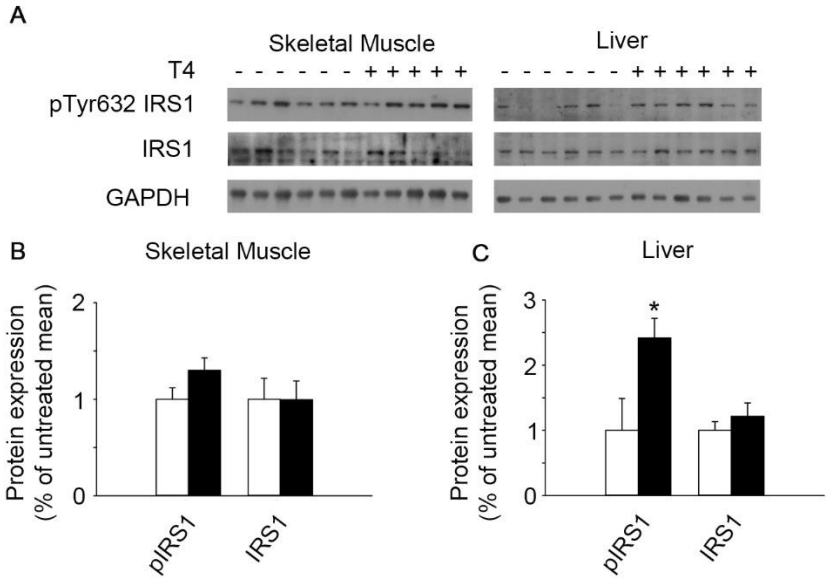

Figure 46. T4 supplementation increases pThyr632 in the liver of RIP-B7.1 mice. (A) Western blots showing phospho-tyrosine 632 IRS1, total IRS1 and GAPDH, used as loading control, in the skeletal muscle and liver of T4-treated mice. Skeletal muscle n = 6 UT, n= 5 T4. Liver n = 6 per group. **(B)** Densitometric analysis of the western blots performed in skeletal muscle extracts shown in panel A. **(C)** Densitometric analysis of the western blots performed in liver extracts shown in panel A. Values were normalized to control group. UT: Untreated; T4: T4-treated. Data are represented as the mean ± SEM. * p < 0.05 compared to untreated mice, t-test two tailed.

Next, we investigated whether T4 supplementation could improve glucose homeostasis in a different mouse model of experimental diabetes, such as STZ treatment. To this end, male wild-type C57BL/6 mice were treated with T4, (5 μg.ml-1 in the drinking water) starting 2 weeks prior 2 consecutive intraperitoneal injections of STZ (150 mg/kg) (Verga Falzacappa et al., 2011). Importantly, the average survival of control STZ treated mice was 8 days, whereas the T4-treated group achieved a mean survival of 34 days, including some mice that survived to STZ (P<0.01, χ2=7,689) (Figure 45G).

Furthermore, postprandial glucose levels showed a trend towards reduced glycemia in T4-treated mice (Figure 45H). Taken together, our results indicate that T4 blunts the onset of T1DM in the RIP-B7.1 model of EAD and promotes survival in STZ-induced experimental DM.

4.3.7 T4 supplementation increases insulin expression in pancreatic islets and β-cell proliferation in immunized RIP-B7.1 mice

In order to determine the underlying effects of T4 supplementation on the pancreas of an animal model for EAD, we next performed immunohistochemical analysis in pancreatic sections from untreated and T4-treated immunized RIP-B7.1 mice. Remarkably, T4-treated mice exhibited a marked increase in insulin expression, as determined by the mean intensity of DAB staining (RIPB-7.1 UT: 5.04 ± 0.93 a.u. vs. 11.37 ± 1.46 a.u., p-value = 0.006 t-test two tailed) with no significant variation in glucagon levels (Figure 47A-C). Noteworthy, both values were considerably lower compared to healthy C57BL/6 mice.

We next investigated whether T4 could also increase the proliferation of β-cells in the RIP-B7.1 model of EAD. Interestingly, the abundance of islet-residing Ki67 positive cells was increased in immunized RIP-B7.1 mice when compared to healthy C57BL/6 mice, indicating that islet-residing immune cells and/or pancreatic endocrine cells proliferate under the immune attack. Nonetheless, T4-treated immunized RIP-B7.1 mice exhibited a marked increase in proliferating β-cells when compared to untreated immunized RIP-B7.1 mice (RIPB-7.1 UT: 2.95 ± 1.28% vs. RIPB-7.1 T4: 7.57 ± 1.49%, p-value = 0.041 t-test two tailed) (Figure 47D-E). As expected, the immune attack

increased the percentage of apoptotic β-cells in both, T4-treated and untreated immunized RIP-B7.1 mice (Figure 47F-G). However, no differences in the percentage of apoptotic β-cells were observed between T4-treated and untreated immunized RIP-B7.1 mice. These results suggest that increased β-cell proliferation might be the underlying mechanism by which T4 blunts the onset of EAD in RIP-B7.1 mice.

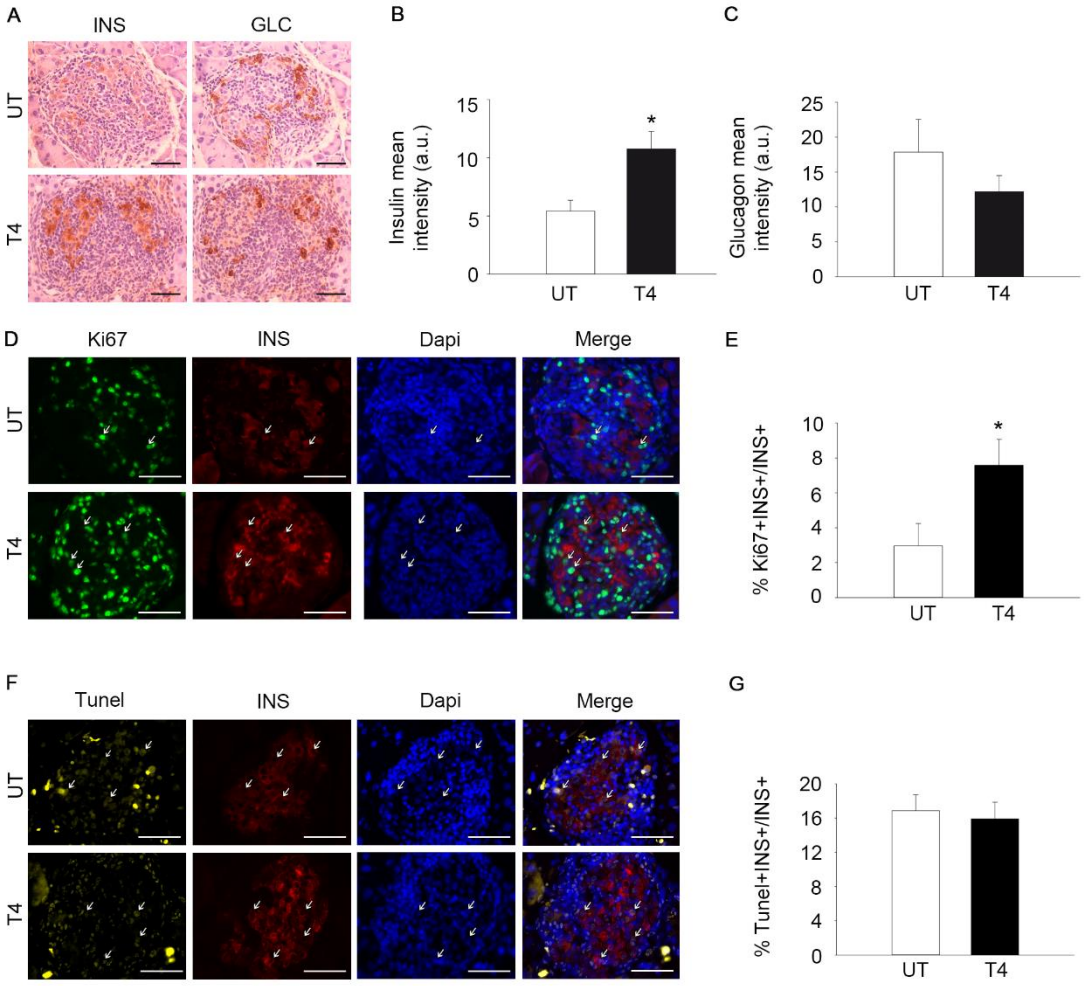

Figure 47. T4 increases insulin expression and enhances β-cell proliferation in the RIP-B7.1 model of EAD. (A) Representative images of insulin (INS) and glucagon (GLC) staining in pancreases from immunized RIPB7.1 mice treated or not with T4. DAB staining followed by hematoxylin counterstaining. **(B)** Quantification of insulin staining (mean intensity). n = 6 UT, n = 5 T4. **(C)** Quantification of glucagon staining (mean intensity). n = 6 UT, n = 5 T4. **(D)** Representative images of Ki67 and insulin staining in pancreases from immunized RIP-B7.1 mice treated or not with T4. Immunofluorescence followed by Dapi staining. **(E)**

Percentage of Ki67+Insulin+ cells over total insulin+ cells. n = 5 per group. **(F)** Representative images of Tunel and insulin staining in pancreases from immunized RIP-B7.1 mice treated or not with T4. Immunofluorescence followed by Dapi staining. **(G)** Percentage of Tunel+Insulin+ cells over total insulin+ cells. n = 5 per group. UT: Untreated; T4: T4-treated. Scale bar = 50 μm. Arrows indicate representative positive staining. Data are represented as the mean ± SEM. * $p < 0.05$ compared to untreated mice t-test two tailed.

In order to determine whether T4 supplementation could blunt the onset of EAD via an effect on the immune system, we next quantified the degree of insulitis in untreated and T4-treated immunized RIPB-7.1 mice. Noticeably, pancreatic islets from both experimental groups showed the same degree of immune infiltrations (Figure 48).

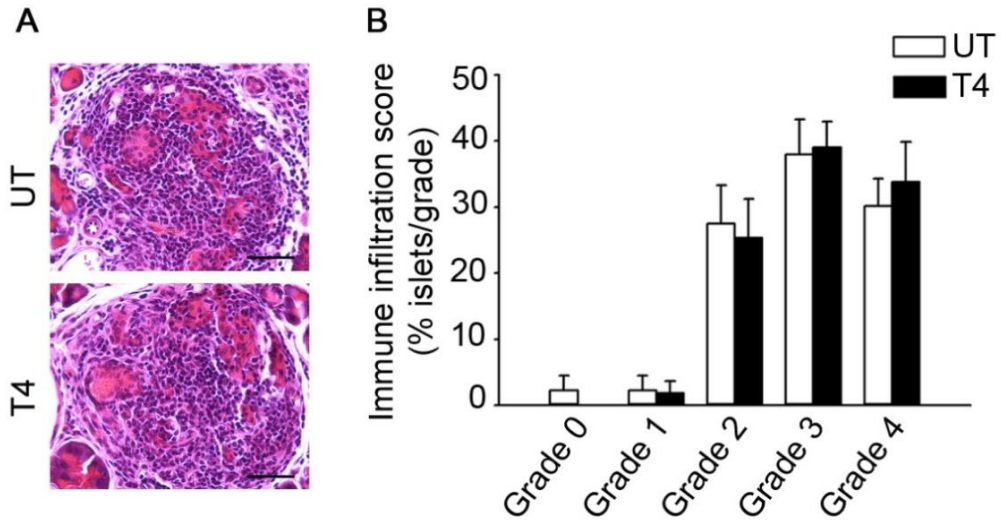

Figure 48. T4-treated and untreated immunized RIP-B7.1 mice show similar degree of insulitis. (A) Representative images of immune infiltrations in T4-treated and untreated immunized RIP-B7.1 mice. **(B)** Insulitis was scored as grade 0–4 according to the percentage of infiltrated islet area (0: 0%; 1: <10%; 2: >10% and <55%; 3: >55% and <75%; 4: >75%). Scale bar = 50 μm. n = 5 per group. UT: Untreated; T4: T4-treated. Data are represented as the mean ± SEM. * p-value < 0.05 compared to untreated mice t-test two tailed.

In summary, our results suggest that T4 supplementation blunts the onset of EAD by increasing β-cell proliferation and insulin content, without affecting the degree of insulitis.

V. DISCUSSION

The uncover of novel target genes capable to induce the regeneration and/or protection of β-cells represents a promising strategy to develop novel therapies to treat DM. During pregnancy the endocrine pancreas is challenged to adapt to a situation of high metabolic demand. Consequently, several genes are induced to increase β-cell functionality, proliferation and protection (Rieck et al., 2009). This phenomenon represents a unique example of rapid and reversible β-cell mass adaptation occurring in mammalian physiology. Therefore, genes induced during pregnancy are candidate target genes to treat DM. Moreover, deficiencies in those genes may cause gestational diabetes, thus they can be potential biomarkers for this disease. One of such genes is PAX8, which expression in the endocrine pancreas of mice has only been detected during pregnancy. Previous work from our laboratory showed that there is a major peak in the expression of Pax8 in pancreatic islets at day 14 of gestation, after the initiation of islet cell proliferation, which might suggest that PAX8 does not play a significant role in the induction of β-cell replication. Remarkably, PAX8 expression was also induced *in vitro* in human pancreatic islets upon prolactin treatment, suggesting that PAX8 might be a downstream target of placental lactogens during gestation (Jiménez Moreno, 2015).

Herein we found that the expression of the Htr3b subunit of the serotonin receptor Htr3 was induced in both, murine and human pancreatic islets over-expressing PAX8. Noteworthy, Htr3 knock-out mice develop gestational diabetes due to the inability of β-cells to increase its functionality (i.e. decrease the glucose threshold for GSIS) (Ohara-Imaizumi et al., 2013). However, PAX8 over-expression in islets did not enhance metabolic activity or GSIS. In contrast, both murine and human pancreatic islets over-expressing PAX8 were shown to be protected from apoptosis. Importantly, protection

from apoptosis has been shown to be crucial for the proper adaptation of β-cells during pregnancy. Indeed, β-cell-specific knockout mice for the anti-apoptotic gene survivin, display glucose intolerance due to attenuated β-cell expansion during pregnancy (Rieck et al., 2009, Xu et al., 2015, Rieck and Kaestner, 2010). Therefore, based on our data, we speculate that PAX8 could be involved in the protection of β-cells from apoptosis, which might be especially important in the pro-inflammatory milieu that occurs during pregnancy. Interestingly, the anti-apoptotic attributes of PAX8 have been described in other cell types as well as in cancer (Di Palma et al., 2013, Hewitt et al., 1997). Actually, lack of Pax8 expression has been associated with increased apoptosis in the cardiomyocytes of Pax8 homozygous knockout mice (Yang et al., 2012). Therefore, our findings suggest that specific interventions targeting at PAX8 in pancreatic endocrine cells could be explored to enhance islet cell survival.

Our hypothesis suggesting that PAX8 may act as a pro-survival gene in islets during gestation is supported by the identification and functional characterization of a novel PAX8 mutation (p.T356M) associated with GDM and GTD. The transcription factor PAX8 contains a paired domain and a homeodomain, which allows DNA-binding, as well as an octapeptide with homology to the engrailed-type repressor sequence (Poleev et al., 1997, Kozmik et al., 1993, Buisson et al., 2015). The majority of inactivating PAX8 mutations described have been located in the highly conserved DNA-binding paired domain (amino acids 9-137) (Liu et al., 2017, Montanelli and Tonacchera, 2010b). However, PAX8-T356M is located at the c-terminal region of the protein and does not affect the paired domain, the octapeptide or the homeodomain. Interestingly, while the capacity of DNA-binding would not be expected to be compromised in this variant,

promoter transactivation assays determined that the functionality of PAX8-T356M is suboptimal. Noteworthy, PAX8-T356M protein stability and subcellular localization were not altered compared to PAX8-Wt. Therefore, it is tempting to speculate that this variant is ineffective *in vivo* due to altered protein interactions with co-factors involved in the regulation of Pax8 transcriptional activity (Di Palma et al., 2008). Of note, other mutations in PAX8 that do not affect the paired homeodomain-binding sites, but exhibit impaired DNA binding capacity and loss of transcriptional activity, have already been described in the literature (Montanelli and Tonacchera, 2010b). To date, detrimental PAX8 polymorphisms in heterozygosis have been reported to be the genetic cause of thyroid dysfunction and urogenital malformations (Esperante et al., 2008, Carvalho et al., 2013b, Al Taji et al., 2007). However, no associations of PAX8 polymorphisms and glucose disorders during pregnancy have been established. In this thesis, we have shown for first time a possible association between PAX8 and GDM as well as GTD, suggesting that this transcription factor could be used as a genetic marker for both pathologies. Nonetheless, in order to properly confirm this association a larger cohort of patients should be studied.

Compelling evidences in animal models indicate that Pax8 is expressed in different organs such as thyroid, brain and the excretory system during development (Plachov et al., 1990). In adulthood, Pax8 expression is restricted to the kidney and the thyroid, with barely to undetectable expression levels in the endocrine pancreas (Plachov et al., 1990, Lorenzo et al., 2011). Homozygous Pax8 knockout mice show severe hypothyroidism and die around weaning, unless they are supplemented with T4. Furthermore, despite T4 hormone supplementation, Pax8 knockout mice are infertile due

to defects in the urogenital tract (Mittag et al., 2009, Mansouri et al., 1998 Mittag et al., 2007). Therefore, in order to determine the physiological role of Pax8 in glucose homeostasis during pregnancy, we used female Pax8 +/- mice. Curiously, female Pax8 +/- mice did not develop glucose intolerance or insulin resistance during pregnancy when compared to WT pregnant mice. Moreover, no significant differences were observed between pregnant WT and Pax8 +/- mice when challenged with Poly I:C (double stranded RNA that mimics viral infections), although animals from both genotypes treated with Poly I: C displayed glucose intolerance when compared to treated non-pregnant mice. As opposed to humans harbouring detrimental PAX8 polymorphisms in heterozygosis, to date heterozygous Pax8 mice have not been reported to exhibit any overt phenotype (Mansouri et al., 1998). In this context, a dominant negative effect of the protein has been proposed as the possible explanation of the human phenotype, suggesting that a detrimental copy of PAX8 might be in fact more deleterious than the simply lack of one functional allele (Liu et al., 2017, Mansouri et al., 1998). Remarkably, female Pax8 +/- mice showed similar levels of circulating T4 when compared to WT animals, although they were not measured during pregnancy. In this sense, THs have been shown to be involved in postnatal pancreatic islet development and are known to have profound effects on metabolism. Moreover, there is an association between subclinical hypothyroidism and GDM (Tudela et al., 2012). Therefore, the possibility that TH deficiency contributes to the association between detrimental PAX8 polymorphisms and GDM cannot be excluded.

A genome-wide association study detected a SNP in the vicinity of PAX8 with a strong association with T2DM in an Afro-American population (Elbein et al., 2009). In

addition, the analysis of our pedigree might suggest an association between the new detrimental polymorphism and prediabetes/T2DM. Therefore, it is tempting to speculate that PAX8 expression may be physiologically relevant in the control of glucose metabolism beyond the scope of pregnancy. In order to investigate this possibility, we studied metabolic homeostasis in WT and Pax8 +/- male mice. Noteworthy, Pax8 +/- mice had significantly, but moderately, reduced levels of circulating T4. Therefore, metabolic tests were performed in animals from both genotypes supplemented or not with T4 in order to determine whether the effect of Pax8 deficiency on metabolic homeostasis was due to the restricted levels of THs. Remarkably, untreated Pax8 +/- male mice displayed increased body weight, glucose intolerance and severe insulin resistance, while T4 supplementation rescued the phenotype. Thus, the phenotype observed appeared to be caused by the reduced levels of circulating T4 found. Remarkably, an increase in body weight in untreated Pax8 +/- animals is consistent with the lower BMR (defined as the rate of energy expenditure per time at rest) associated with hypothyroidism. In addition, untreated Pax8 +/- animals exhibited an overall unhealthy status.

The architecture and proportion of endocrine cells were similar in WT and Pax8 +/- as well as Pax8 -/- animals at postnatal day 21, excluding the possibility that a major defect in pancreatic islet development would account for the phenotype. Moreover, insulin secretion after a glucose load was not affected in untreated Pax8 +/- mice, suggesting that the phenotype observed is caused by an effect of THs mainly in peripheral tissues. Indeed, we observed an increase in WAT weight and a tendency to increased adipocyte size, which are correlated with insulin resistance. Furthermore, we found that Pax8 +/- animals accumulated higher lipid content in the liver and had increased

intramuscular lipid depositions. Since ectopic lipid depositions are strongly correlated with insulin resistance, this could contribute to the dysregulation in glucose homeostasis and insulin resistance observed in Pax8 +/- male mice. In addition, 4-HNE, which results from lipid peroxidation and has also been associated with insulin resistance, was increased in both the liver and the gastrocnemius of Pax8 +/- mice. In contrast, superoxide production was found increased specifically in the liver. Furthermore, protein levels of UCP2, which has been reported to possess antioxidant properties, were also reduced specifically in the liver of Pax8 +/- mice (Andrews et al., 2005, Andrews and Horvath, 2009). These results indicate an increase in ROS levels in the liver of Pax8 +/- mice, which may cause hepatic insulin resistance. Consistent with this, insulin signalling was preferentially impaired in the liver of Pax8 +/- mice, as determined by the decrease in AKT phosphorylation found in this tissue. Moreover, our results also suggest that autophagy may be impaired in the liver of Pax8 +/- mice, which may cause an accumulation of damaged proteins/organelles. Remarkably, T3 supplementation has been reported to reduce ROS production in the liver of hepatic HBx transgenic mice (mouse model for hepatocellular carcinoma) by enhancing mitochondrial turnover and thus improving the quality of cellular mitochondria (Chi et al., 2017). Therefore, it is tempting to speculate that the reduced circulating T4 levels found in Pax8 +/- mice underlies an increase in ROS production in the liver that impairs insulin signalling in this organ.

Whereas mild hypothyroidism causes insulin resistance and glucose intolerance, supplementation with TH provides undeniably positive benefits for metabolic health, attenuating hyperglycaemia in STZ-treated and leptin-receptor deficient mice (Lin and Sun, 2011; Verga Falzacappa et al., 2011; Shoemaker et al., 2012). Therefore, THs or

their analogues could represent a promising therapeutic approach for the treatment of metabolic complications. However, the detrimental effects of high circulating levels of THs (thyrotoxicosis) are well known. Patients suffering thyrotoxicosis exhibit a pleiotropy of symptoms that include life-threatening disorders such as cardiovascular collapse and thyroid storm, among others (Bahn et al., 2011; Garmendia Madariaga et al., 2014). Moreover, there is an association between hyperthyroidism and insulin resistance. Indeed, in healthy subjects there is a positive correlation between increased HOMA-IR and increased TH levels, even within physiological range (Duntas et al., 2011). These risks have precluded the investigation of potential therapies based on the use of THs to treat metabolic disorders.

In this thesis, we show that a level of T4 supplementation increases insulin concentration in blood and enhances glucose clearance, while maintaining an overall healthy status in wild-type C57BL/6 mice. In addition, our results indicate that T4 supplementation increases insulin content in pancreatic β-cells. Previous reports had demonstrated that the T3-TR complex induces MafA transcription through direct binding to TH response elements located in the MafA promoter (Aguayo-Mazzucato et al., 2013). Moreover, MafA is known to bind to the insulin promoter, inducing insulin expression (Olbrot et al., 2002; Matsuoka et al., 2004), providing a plausible molecular mechanism by which T4 supplementation enhances insulin expression in pancreatic β-cells. However, as opposed to a previous study using 7-day-old mice, our immunohistochemical analysis in pancreatic sections from healthy adult mice indicated that MafA is already predominantly located in the nucleus of pancreatic β-cells and T4 supplementation does not further promote the nuclear localization of this transcription factor. Therefore, our

results suggest that T4 supplementation in adulthood increases insulin content by other pathways different from the presence/absence of MafA in the nucleus (Aguayo-Mazzucato et al., 2013).

Islets isolated from mice treated with T4 exhibited a marked increase in GCK gene and protein expression. Remarkably, an upregulation of GCK expression may contribute to the increased insulin secretion found under fasting conditions, as observed in GSIS tests, since enhanced GCK activity has been previously shown to lower the glucose threshold that stimulates insulin secretion (Weinhaus et al., 2007; Kassem et al., 2010). Increased circulating insulin in T4-treated animals activated the IRS1-Akt axis of insulin signalling, suggesting that glucose uptake is increased in insulin target tissues. T4 is known to increase the basal metabolic rate by inducing the expression of several mitochondrial uncoupling proteins, such as UCP2 (Lanni et al., 2003; Ramadan et al., 2011). As a result of increased mitochondrial uncoupling, mitochondrial efficiency is lower (defined here as the amount of nutrients used to produce one molecule of ATP) and heat production is increased (note that BAT weight in T4-treated animals was increased). In order to adapt to this situation, T4-treated cells require higher amounts of nutrients to maintain their metabolism. Therefore, it is tempting to speculate that insulin expression and secretion in pancreatic islets under fasting conditions is enhanced in mice treated with T4 to allow nutrient uptake by insulin-target tissues. Supporting this hypothesis, we found that, as opposed to untreated animals, in which a significant increase in insulin levels was promoted by a glucose bolus, insulin levels in T4-treated mice were already maximal prior glucose load, suggesting that the insulin secretion machinery is already active. Moreover, our results also indicate that β-cell proliferation and apoptosis are specifically

increased in mice treated with T4. Remarkably, increased GCK activity has been associated to increased β-cell proliferation and apoptosis. Therefore, the increase in GCK expression induced by T4 administration might contribute to the enhancement of β-cell turnover, promoting the existence of a highly insulin-expressing β-cell population, which actively secretes insulin into the circulation under basal conditions (Kassem et al., 2000; Kassem et al., 2010).

Given the age of the animals, the length of the treatment (~24 weeks at the end of the experiment, which represents ~25% of an average lifespan of this mouse strain) and the mouse chow used in this study (a standard healthy diet), we do not believe that the increase of insulin expression in pancreatic β-cells found in T4-treated mice was indicative of over-stimulation of β-cells, as found in prediabetic individuals. However, since hyperinsulinemia itself has been shown to promote insulin resistance, we cannot exclude the possibility that a longer T4 treatment could cause insulin resistance, which would resemble the phenomenon observed in hyperthyroid patients. However, the analysis of insulin-target tissues indicated that the higher insulin concentration in blood is able to activate the IRS1-Akt axis of the insulin signalling pathway. Previous reports have indicated that T4 exerts non-genomic effects by activating specifically PI3K and its downstream targets (Lin and Sun, 2011). Although we cannot exclude that non-genomic T4 actions contribute to the activation of PI3K and its downstream targets in vivo, we found that T4 supplementation activates insulin signalling as early as the level of IRS1, as shown by the increase in pTyr632-IRS1 in skeletal muscles and livers of T4-treated mice. Remarkably, we found that both T4-supplemented and control mice treated with insulin at the end of the experiment, reached the same level of AKT activation (pSer473-

AKT levels). Therefore, our results suggest that high insulin levels *per se* are responsible for T4-mediated AKT activation. Hence, although the major effects of reduced circulating T4 levels were observed in peripheral tissues, the main target of T4 supplementation seems to be the endocrine pancreas (Figure 49).

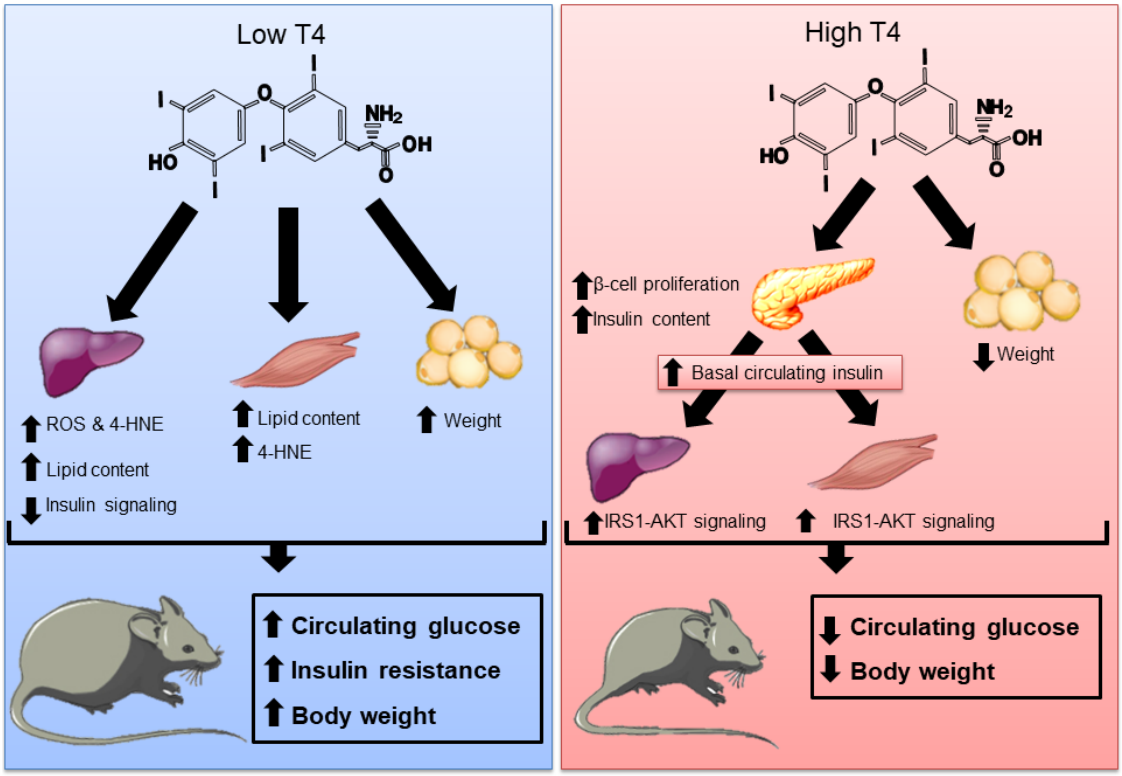

Figure 49. Schematic representation of the effects of reduced and increased circulating T4 levels in metabolism. Reduced circulating T4 levels in mice are associated with glucose intolerance, insulin resistance and increased body weight. In contrast, T4 supplementation enhances glucose homeostasis and decreases body weight in healthy mice.

In this thesis, we also show that T4 supplementation blunts the onset of T1DM using the RIP-B7.1 model of EAD and increases survival in STZ-induced experimental diabetes in wild-type C57BL/6 mice. Previous research has determined that during the onset of T1DM, β-cell proliferation is increased in an attempt to compensate β-cell loss

(Willcox et al., 2010). In this regard, we observed that, although immune infiltration and the percentage of apoptotic β-cells is similarly augmented in untreated or T4-treated pancreases during the immune attack, β-cell proliferation is remarkably increased in T4-treated RIP-B7.1 mice. This process presumably leads to compensation for β-cell loss, allowing the production and secretion of enough insulin to maintain normoglycemia. Actually, both insulin content and postprandial circulating insulin levels were significantly increased in T4-treated immunized RIPB-7.1 mice. Our experimental design initiated T4 supplementation 2 weeks prior to induction of diabetes mellitus (immunization or STZ treatment), as these research models (EAD and STZ) are very aggressive and a significant percentage of mice die within the first 2 weeks after the induction of diabetes. In order to evaluate a possible therapeutic benefit, experiments aiming to determine whether T4 supplementation after the onset of T1DM could improve glucose homeostasis would be required. Notwithstanding, our results indicate that interventions based on the use of THs or thyromimetics could open novel venues for the treatment of T1DM. Although novel treatments including the use of T4 supplementation might not be optimal for the treatment of metabolic diseases due to side effects, certain newly developed thyromimetics could affect specific cell types or organs that could benefit from these actions of THs, resulting in the improvement of metabolic homeostasis, while avoiding side effects (Shoemaker et al., 2012; Coppola et al., 2014; Finan et al., 2016). Although the profound systemic effects of T4-administration in mice suggest that THs and thyromimetics might be useful in ameliorating the abnormal metabolism in diabetic patients, the identification of the underlying mechanisms that are critical for the

observed improvements on glucose control and potential long-term toxic effects must be addressed before results in mice could be extrapolated to humans.

VI. CONCLUSIONS

1. PAX8 over-expression protects pancreatic islets cells from apoptosis and does not have an effect in metabolic activity or GSIS.
2. A novel PAX8 variant (PAX8-T356M) is associated with GTD and GDM.
3. PAX8-T356M exhibit compromised functional activity on the activation of Tg promoter.
4. Pax8 +/- female mice exhibit normal circulating T4 levels at 5 months of age.
5. Pax8 +/- female mice do not display glucose intolerance or insulin resistance during pregnancy.
6. Pax8 +/- male mice exhibit reduced circulating T4 levels at 8 months of life.
7. Pax8 +/- male mice exhibit increased body weight from 7 to 13 months of life.
8. Pax8 +/- male mice display glucose intolerance and insulin resistance.
9. AKT phosphorylation is reduced in the liver of Pax8 +/- male mice.
10. Pax8 +/- male mice exhibit increased triglyceride content in the liver as well as intramuscular lipid depositions.
11. There is an increase in superoxide generation in the liver of Pax8 +/- male mice, while mitochondrial content is not altered.
12. T4 supplementation enhances glucose clearance in WT mice.
13. T4 supplementation increases insulin content in pancreatic islets of WT mice.

14. T4 supplementation increases GCK expression in pancreatic islets of WT mice.

15. Insulin secretion at low glucose concentrations *in vitro* is increased in pancreatic islets of WT mice treated with T4.

16. T4 supplementation increases β-cell proliferation and apoptosis in pancreatic islets from healthy mice.

17. T4 supplementation blunts the onset of T1DM in the RIPB-7.1 model of EAD and increases survival in mice challenged with STZ.

18. T4 supplementation increases insulin content and β-cell proliferation in the pancreatic islets of RIPB-7.1 mice.

VII. BIBLIOGRAPHY

Aguayo-Mazzucato, C., Zavacki, A. M., Marinelarena, A., Hollister-Lock, J., El Khattabi, I., Marsili, A., Weir, G. C., Sharma, A., Larsen, P. R. and Bonner-Weir, S. (2013) 'Thyroid hormone promotes postnatal rat pancreatic beta-cell development and glucose-responsive insulin secretion through MAFA', *Diabetes,* 62(5), pp. 1569-80.

Aguirre, V., Uchida, T., Yenush, L., Davis, R. and White, M. F. (2000) 'The c-Jun NH(2)-terminal kinase promotes insulin resistance during association with insulin receptor substrate-1 and phosphorylation of Ser(307)', *J Biol Chem,* 275(12), pp. 9047-54.

Ahmed, K., Tunaru, S., Tang, C., Müller, M., Gille, A., Sassmann, A., Hanson, J. and Offermanns, S. (2010) 'An autocrine lactate loop mediates insulin-dependent inhibition of lipolysis through GPR81', *Cell Metab,* 11(4), pp. 311-9.

Al Taji, E., Biebermann, H., Limanova, Z., Hnikova, O., Zikmund, J., Dame, C., Gruters, A., Lebl, J. and Krude, H. (2007) 'Screening for mutations in transcription factors in a Czech cohort of 170 patients with congenital and early-onset hypothyroidism: identification of a novel PAX8 mutation in dominantly inherited early-onset non-autoimmune hypothyroidism', *Eur J Endocrinol,* 156(5), pp. 521-9.

Alisi, A., Spagnuolo, S., Napoletano, S., Spaziani, A. and Leoni, S. (2004) 'Thyroid hormones regulate DNA-synthesis and cell-cycle proteins by activation of PKCalpha and p42/44 MAPK in chick embryo hepatocytes', *J Cell Physiol,* 201(2), pp. 259-65.

Amson, R., Pece, S., Lespagnol, A., Vyas, R., Mazzarol, G., Tosoni, D., Colaluca, I., Viale, G., Rodrigues-Ferreira, S., Wynendaele, J., Chaloin, O., Hoebeke, J., Marine, J. C., Di Fiore, P. P. and Telerman, A. (2011) 'Reciprocal repression between P53 and TCTP', *Nat Med,* 18(1), pp. 91-9.

Andrews, Z. B., Diano, S. and Horvath, T. L. (2005) 'Mitochondrial uncoupling proteins in the CNS: in support of function and survival', *Nat Rev Neurosci,* 6(11), pp. 829-40.

Andrews, Z. B. and Horvath, T. L. (2009) 'Uncoupling protein-2 regulates lifespan in mice', *Am J Physiol Endocrinol Metab,* 296(4), pp. E621-7.

Aragon, F., Karaca, M., Novials, A., Maldonado, R., Maechler, P. and Rubi, B. (2015) 'Pancreatic polypeptide regulates glucagon release through PPYR1 receptors

expressed in mouse and human alpha-cells', *Biochimica Et Biophysica Acta-General Subjects*, 1850(2), pp. 343-351.

Arauchi, A., Matsuura, K., Shimizu, T. and Okano, T. (2017) 'Functional Thyroid Follicular Cells Differentiation from Human-Induced Pluripotent Stem Cells in Suspension Culture', *Front Endocrinol (Lausanne)*, 8, pp. 103.

Atkinson, M. A., Eisenbarth, G. S. and Michels, A. W. (2014) 'Type 1 diabetes', *Lancet*, 383(9911), pp. 69-82.

Aïello, V., Moreno-Asso, A., Servitja, J. M. and Martín, M. (2014) 'Thyroid hormones promote endocrine differentiation at expenses of exocrine tissue', *Exp Cell Res*, 322(2), pp. 236-48.

Bayascas, J. R. (2010) 'PDK1: the major transducer of PI 3-kinase actions', *Curr Top Microbiol Immunol*, 346, pp. 9-29.

Bloise, F. F., Cordeiro, A. and Ortiga-Carvalho, T. M. (2017) 'Role of thyroid hormone in skeletal muscle physiology', *J Endocrinol*.

Blüher, M., Michael, M. D., Peroni, O. D., Ueki, K., Carter, N., Kahn, B. B. and Kahn, C. R. (2002) 'Adipose tissue selective insulin receptor knockout protects against obesity and obesity-related glucose intolerance', *Dev Cell*, 3(1), pp. 25-38.

Boia-Ferreira, M., Basílio, A. B., Hamasaki, A. E., Matsubara, F. H., Appel, M. H., Da Costa, C. R. V., Amson, R., Telerman, A., Chaim, O. M., Veiga, S. S. and Senff-Ribeiro, A. (2017) 'TCTP as a therapeutic target in melanoma treatment', *Br J Cancer*, 117(5), pp. 656-665.

Bouchard, M., de Caprona, D., Busslinger, M., Xu, P. and Fritzsch, B. (2010) 'Pax2 and Pax8 cooperate in mouse inner ear morphogenesis and innervation', *BMC Dev Biol*, 10, pp. 89.

Boucher, J., Kleinridders, A. and Kahn, C. R. (2014) 'Insulin receptor signaling in normal and insulin-resistant states', *Cold Spring Harb Perspect Biol*, 6(1).

Brereton, M. F., Rohm, M. and Ashcroft, F. M. (2016) 'β-Cell dysfunction in diabetes: a crisis of identity?', *Diabetes Obes Metab*, 18 Suppl 1, pp. 102-9.

Brøns, C. and Grunnet, L. G. (2017) 'MECHANISMS IN ENDOCRINOLOGY: Skeletal muscle lipotoxicity in insulin resistance and type 2 diabetes: a causal mechanism or an innocent bystander?', *Eur J Endocrinol,* 176(2), pp. R67-R78.

Buisson, I., Le Bouffant, R., Futel, M., Riou, J. F. and Umbhauer, M. (2015) 'Pax8 and Pax2 are specifically required at different steps of Xenopus pronephros development', *Dev Biol,* 397(2), pp. 175-90.

Cade, W. T. (2008) 'Diabetes-related microvascular and macrovascular diseases in the physical therapy setting', *Phys Ther,* 88(11), pp. 1322-35.

Cano, D. A., Soria, B., Martín, F. and Rojas, A. (2014) 'Transcriptional control of mammalian pancreas organogenesis', *Cell Mol Life Sci,* 71(13), pp. 2383-402.

Carvalho, A., Hermanns, P., Rodrigues, A.-L., Sousa, I., Anselmo, J., Bikker, H., Cabral, R., Pereira-Duarte, C., Mota-Vieira, L. and Pohlenz, J. (2013) 'A New PAX8 Mutation Causing Congenital Hypothyroidism in Three Generations of a Family Is Associated with Abnormalities in the Urogenital Tract', *Thyroid,* 23(9), pp. 1074-1078.

Carvalho, D. P. and Dupuy, C. (2017) 'Thyroid hormone biosynthesis and release', *Mol Cell Endocrinol,* 458, pp. 6-15.

Casas, F., Pessemesse, L., Grandemange, S., Seyer, P., Gueguen, N., Baris, O., Lepourry, L., Cabello, G. and Wrutniak-Cabello, C. (2008) 'Overexpression of the mitochondrial T3 receptor p43 induces a shift in skeletal muscle fiber types', *PLoS One,* 3(6), pp. e2501.

Cheng, S. Y., Leonard, J. L. and Davis, P. J. (2010) 'Molecular aspects of thyroid hormone actions', *Endocr Rev,* 31(2), pp. 139-70.

Chi, H. C., Chen, S. L., Lin, S. L., Tsai, C. Y., Chuang, W. Y., Lin, Y. H., Huang, Y. H., Tsai, M. M., Yeh, C. T. and Lin, K. H. (2017) 'Thyroid hormone protects hepatocytes from HBx-induced carcinogenesis by enhancing mitochondrial turnover', *Oncogene,* 36(37), pp. 5274-5284.

Chiefari, E., Arcidiacono, B., Foti, D. and Brunetti, A. (2017) 'Gestational diabetes mellitus: an updated overview', *J Endocrinol Invest,* 40(9), pp. 899-909.

Chocron, E. S., Sayre, N. L., Holstein, D., Saelim, N., Ibdah, J. A., Dong, L. Q., Zhu, X., Cheng, S. Y. and Lechleiter, J. D. (2012) 'The trifunctional protein mediates thyroid hormone receptor-dependent stimulation of mitochondria metabolism', *Mol Endocrinol,* 26(7), pp. 1117-28.

Christ, S., Biebel, U. W., Hoidis, S., Friedrichsen, S., Bauer, K. and Smolders, J. W. (2004) 'Hearing loss in athyroid pax8 knockout mice and effects of thyroxine substitution', *Audiol Neurootol,* 9(2), pp. 88-106.

Collombat, P., Mansouri, A., Hecksher-Sorensen, J., Serup, P., Krull, J., Gradwohl, G. and Gruss, P. (2003) 'Opposing actions of Arx and Pax4 in endocrine pancreas development', *Genes Dev,* 17(20), pp. 2591-603.

Collombat, P., Xu, X., Ravassard, P., Sosa-Pineda, B., Dussaud, S., Billestrup, N., Madsen, O. D., Serup, P., Heimberg, H. and Mansouri, A. (2009) 'The ectopic expression of Pax4 in the mouse pancreas converts progenitor cells into alpha and subsequently beta cells', *Cell,* 138(3), pp. 449-62.

Courtney, M., Gjernes, E., Druelle, N., Ravaud, C., Vieira, A., Ben-Othman, N., Pfeifer, A., Avolio, F., Leuckx, G., Lacas-Gervais, S., Burel-Vandenbos, F., Ambrosetti, D., Hecksher-Sorensen, J., Ravassard, P., Heimberg, H., Mansouri, A. and Collombat, P. (2013) 'The Inactivation of Arx in Pancreatic alpha-Cells Triggers Their Neogenesis and Conversion into Functional beta-Like Cells', *Plos Genetics,* 9(10).

Cozar-Castellano, I., Takane, K. K., Bottino, R., Balamurugan, A. N. and Stewart, A. F. (2004) 'Induction of beta-cell proliferation and retinoblastoma protein phosphorylation in rat and human islets using adenovirus-mediated transfer of cyclin-dependent kinase-4 and cyclin D1', *Diabetes,* 53(1), pp. 149-59.

Czech, M. P. (2017) 'Insulin action and resistance in obesity and type 2 diabetes', *Nat Med,* 23(7), pp. 804-814.

Damiano, F., Rochira, A., Gnoni, A. and Siculella, L. (2017) 'Action of Thyroid Hormones, T3 and T2, on Hepatic Fatty Acids: Differences in Metabolic Effects and Molecular Mechanisms', *Int J Mol Sci,* 18(4).

Davis, P. J., Goglia, F. and Leonard, J. L. (2016) 'Nongenomic actions of thyroid hormone', *Nat Rev Endocrinol,* 12(2), pp. 111-21.

De Meyts, P. (2004) 'Insulin and its receptor: structure, function and evolution', *Bioessays,* 26(12), pp. 1351-62.

Deng, S. B., Jing, X. D., Wei, X. M., Du, J. L., Liu, Y. J., Qin, Q. and She, Q. (2017) 'Triiodothyronine promotes the proliferation of epicardial progenitor cells through the MAPK/ERK pathway', *Biochem Biophys Res Commun,* 486(2), pp. 372-377.

Dezaki, K. (2013) 'Ghrelin function in insulin release and glucose metabolism', *Endocrine development,* 25, pp. 135-43.

Di Palma, T., de Cristofaro, T., D'Ambrosio, C., Del Prete, D., Scaloni, A. and Zannini, M. (2008) 'Poly(ADP-ribose) polymerase 1 binds to Pax8 and inhibits its transcriptional activity', *J Mol Endocrinol,* 41(5), pp. 379-88.

Di Palma, T., Filippone, M. G., Pierantoni, G. M., Fusco, A., Soddu, S. and Zannini, M. (2013) 'Pax8 has a critical role in epithelial cell survival and proliferation', *Cell Death Dis,* 4, pp. e729.

Dolai, S., Xie, L., Zhu, D., Liang, T., Qin, T., Xie, H., Kang, Y., Chapman, E. R. and Gaisano, H. Y. (2016) 'Synaptotagmin-7 Functions to Replenish Insulin Granules for Exocytosis in Human Islet β-Cells', *Diabetes,* 65(7), pp. 1962-76.

Dolenšek, J., Rupnik, M. S. and Stožer, A. (2015) 'Structural similarities and differences between the human and the mouse pancreas', *Islets,* 7(1), pp. e1024405.

Donath, M. Y. and Halban, P. A. (2004) 'Decreased beta-cell mass in diabetes: significance, mechanisms and therapeutic implications', *Diabetologia,* 47(3), pp. 581-589.

Dulin, E., García-Barreno, P. and Guisasola, M. C. (2012) 'Genetic variations of HSPA1A, the heat shock protein levels, and risk of atherosclerosis', *Cell Stress Chaperones,* 17(4), pp. 507-16.

Duntas, L. H., Orgiazzi, J. and Brabant, G. (2011) 'The interface between thyroid and diabetes mellitus', *Clin Endocrinol (Oxf),* 75(1), pp. 1-9.

Elbein, S. C., Das, S. K., Hallman, D. M., Hanis, C. L. and Hasstedt, S. J. (2009) 'Genome-Wide Linkage and Admixture Mapping of Type 2 Diabetes in African American

Families From the American Diabetes Association GENNID (Genetics of NIDDM) Study Cohort', *Diabetes,* 58(1), pp. 268-274.

Elumalai, S., Karunakaran, U., Lee, I. K., Moon, J. S. and Won, K. C. (2017) 'Rac1-NADPH oxidase signaling promotes CD36 activation under glucotoxic conditions in pancreatic beta cells', *Redox Biol,* 11, pp. 126-134.

Esperante, S. A., Rivolta, C. M., Miravalle, L., Herzovich, V., Iorcansky, S., Baralle, M. and Targovnik, H. M. (2008) 'Identification and characterization of four PAX8 rare sequence variants (p.T225M, p.L233L, p.G336S and p.A439A) in patients with congenital hypothyroidism and dysgenetic thyroid glands', *Clin Endocrinol (Oxf),* 68(5), pp. 828-35.

Ferrandino, G., Kaspari, R. R., Spadaro, O., Reyna-Neyra, A., Perry, R. J., Cardone, R., Kibbey, R. G., Shulman, G. I., Dixit, V. D. and Carrasco, N. (2017) 'Pathogenesis of hypothyroidism-induced NAFLD is driven by intra- and extrahepatic mechanisms', *Proc Natl Acad Sci U S A,* 114(43), pp. E9172-E9180.

Ferretti, E., Arturi, F., Mattei, T., Scipioni, A., Tell, G., Tosi, E., Presta, I., Morisi, R., Lacroix, L., Gulino, A., Russo, D., Damante, G. and Filetti, S. (2005) 'Expression, regulation, and function of paired-box gene 8 in the human placenta and placental cancer cell lines', *Endocrinology,* 146(9), pp. 4009-15.

Finan, B., Clemmensen, C., Zhu, Z., Stemmer, K., Gauthier, K., Müller, L., De Angelis, M., Moreth, K., Neff, F., Perez-Tilve, D., Fischer, K., Lutter, D., Sánchez-Garrido, M. A., Liu, P., Tuckermann, J., Malehmir, M., Healy, M. E., Weber, A., Heikenwalder, M., Jastroch, M., Kleinert, M., Jall, S., Brandt, S., Flamant, F., Schramm, K. W., Biebermann, H., Döring, Y., Weber, C., Habegger, K. M., Keuper, M., Gelfanov, V., Liu, F., Köhrle, J., Rozman, J., Fuchs, H., Gailus-Durner, V., Hrabě de Angelis, M., Hofmann, S. M., Yang, B., Tschöp, M. H., DiMarchi, R. and Müller, T. D. (2016) 'Chemical Hybridization of Glucagon and Thyroid Hormone Optimizes Therapeutic Impact for Metabolic Disease', *Cell,* 167(3), pp. 843-857.e14.

Fu, Z., Gilbert, E. R. and Liu, D. (2013) 'Regulation of insulin synthesis and secretion and pancreatic Beta-cell dysfunction in diabetes', *Curr Diabetes Rev,* 9(1), pp. 25-53.

Galadari, S., Rahman, A., Pallichankandy, S., Galadari, A. and Thayyullathil, F. (2013) 'Role of ceramide in diabetes mellitus: evidence and mechanisms', *Lipids Health Dis,* 12, pp. 98.

Gauthier, B. R. and Wollheim, C. B. (2008) 'Synaptotagmins bind calcium to release insulin', *Am J Physiol Endocrinol Metab,* 295(6), pp. E1279-86.

Gerber, P. A. and Rutter, G. A. (2017) 'The Role of Oxidative Stress and Hypoxia in Pancreatic Beta-Cell Dysfunction in Diabetes Mellitus', *Antioxid Redox Signal,* 26(10), pp. 501-518.

Glaschke, A., Glösmann, M. and Peichl, L. (2010) 'Developmental changes of cone opsin expression but not retinal morphology in the hypothyroid Pax8 knockout mouse', *Invest Ophthalmol Vis Sci,* 51(3), pp. 1719-27.

Gloyn, A. L., Odili, S., Zelent, D., Buettger, C., Castleden, H. A., Steele, A. M., Stride, A., Shiota, C., Magnuson, M. A., Lorini, R., d'Annunzio, G., Stanley, C. A., Kwagh, J., van Schaftingen, E., Veiga-da-Cunha, M., Barbetti, F., Dunten, P., Han, Y., Grimsby, J., Taub, R., Ellard, S., Hattersley, A. T. and Matschinsky, F. M. (2005) 'Insights into the structure and regulation of glucokinase from a novel mutation (V62M), which causes maturity-onset diabetes of the young', *J Biol Chem,* 280(14), pp. 14105-13.

Gloyn, A. L., Pearson, E. R., Antcliff, J. F., Proks, P., Bruining, G. J., Slingerland, A. S., Howard, N., Srinivasan, S., Silva, J., Molnes, J., Edghill, E. L., Frayling, T. M., Temple, I. K., Mackay, D., Shield, J. P. H., Sumnik, Z., van Rhijn, A., Wales, J. K. H., Clark, P., Gorman, S., Aisenberg, J., Ellard, S., Njolstad, P. R., Ashcroft, F. M. and Hattersley, A. T. (2004) 'Activating mutations in the gene encoding the ATP-sensitive potassium-channel subunit Kir6.2 and permanent neonatal diabetes', *New England Journal of Medicine,* 350(18), pp. 1838-1849.

Gomez, C. M., Maselli, R., Gundeck, J. E., Chao, M., Day, J. W., Tamamizu, S., Lasalde, J. A., McNamee, M. and Wollmann, R. L. (1997) 'Slow-channel transgenic mice: a model of postsynaptic organellar degeneration at the neuromuscular junction', *J Neurosci,* 17(11), pp. 4170-9.

Gonzalez, E. and McGraw, T. E. (2006) 'Insulin signaling diverges into Akt-dependent and -independent signals to regulate the recruitment/docking and the fusion of GLUT4 vesicles to the plasma membrane', *Mol Biol Cell,* 17(10), pp. 4484-93.

Gosmain, Y., Katz, L. S., Masson, M. H., Cheyssac, C., Poisson, C. and Philippe, J. (2012) 'Pax6 is crucial for β-cell function, insulin biosynthesis, and glucose-induced insulin secretion', *Mol Endocrinol,* 26(4), pp. 696-709.

Grozinsky-Glasberg, S., Fraser, A., Nahshoni, E., Weizman, A. and Leibovici, L. (2006) 'Thyroxine-triiodothyronine combination therapy versus thyroxine monotherapy for clinical hypothyroidism: meta-analysis of randomized controlled trials', *J Clin Endocrinol Metab,* 91(7), pp. 2592-9.

Guzman-Gutierrez, E., Veas, C., Leiva, A., Escudero, C. and Sobrevia, L. (2014) 'Is a low level of free thyroxine in the maternal circulation associated with altered endothelial function in gestational diabetes?', *Frontiers in Pharmacology,* 5.

Haeusler, R. A., McGraw, T. E. and Accili, D. (2017) 'Biochemical and cellular properties of insulin receptor signalling', *Nat Rev Mol Cell Biol*.

Hara, A. and Radin, N. S. (1978) 'Lipid extraction of tissues with a low-toxicity solvent', *Anal Biochem,* 90(1), pp. 420-6.

Harlan, D. M., Hengartner, H., Huang, M. L., Kang, Y. H., Abe, R., Moreadith, R. W., Pircher, H., Gray, G. S., Ohashi, P. S., Freeman, G. J. and et al. (1994) 'Mice expressing both B7-1 and viral glycoprotein on pancreatic beta cells along with glycoprotein-specific transgenic T cells develop diabetes due to a breakdown of T-lymphocyte unresponsiveness', *Proc Natl Acad Sci U S A,* 91(8), pp. 3137-41.

Harter, P. N., Baumgarten, P., Zinke, J., Schilling, K., Baader, S., Hartmetz, A. K., Schittenhelm, J., Beschorner, R., Liebner, S., Schulte, D., Plate, K. H., Gutwein, P., Korshunov, A., Pfister, S. M., Jones, D. T., Doberstein, K. and Mittelbronn, M. (2015) 'Paired box gene 8 (PAX8) expression is associated with sonic hedgehog (SHH)/wingless int (WNT) subtypes, desmoplastic histology and patient survival in human medulloblastomas', *Neuropathol Appl Neurobiol,* 41(2), pp. 165-79.

Hauge-Evans, A. C., King, A. J., Carmignac, D., Richardson, C. C., Robinson, I. C. A. F., Low, M. J., Christie, M. R., Persaud, S. J. and Jones, P. M. (2009) 'Somatostatin Secreted by Islet delta-Cells Fulfills Multiple Roles as a Paracrine Regulator of Islet Function', *Diabetes,* 58(2), pp. 403-411.

He, K. H., Juhl, K., Karadimos, M., El Khattabi, I., Fitzpatrick, C., Bonner-Weir, S. and Sharma, A. (2014) 'Differentiation of pancreatic endocrine progenitors reversibly blocked by premature induction of MafA', *Dev Biol,* 385(1), pp. 2-12.

He, K. H. H., Lorenzo, P. I., Brun, T., Jimenez Moreno, C. M., Aeberhard, D., Vallejo Ortega, J., Cornu, M., Thorel, F., Gjinovci, A., Thorens, B., Herrera, P. L., Meda,

P., Wollheim, C. B. and Gauthier, B. R. (2011) 'In Vivo Conditional Pax4 Overexpression in Mature Islet beta-Cells Prevents Stress-Induced Hyperglycemia in Mice', *Diabetes*, 60(6), pp. 1705-1715.

Henquin, J. C. (2009) 'Regulation of insulin secretion: a matter of phase control and amplitude modulation', *Diabetologia*, 52(5), pp. 739-51.

Hewitt, S. M., Hamada, S., Monarres, A., Kottical, L. V., Saunders, G. F. and McDonnell, T. J. (1997) 'Transcriptional activation of the bcl-2 apoptosis suppressor gene by the paired box transcription factor PAX8', *Anticancer Research*, 17(5A), pp. 3211-3215.

Hill, A. A., Anderson-Baucum, E. K., Kennedy, A. J., Webb, C. D., Yull, F. E. and Hasty, A. H. (2015) 'Activation of NF-κB drives the enhanced survival of adipose tissue macrophages in an obesogenic environment', *Mol Metab*, 4(10), pp. 665-77.

Hill, N. J., Stotland, A., Solomon, M., Secrest, P., Getzoff, E. and Sarvetnick, N. (2007) 'Resistance of the target islet tissue to autoimmune destruction contributes to genetic susceptibility in Type 1 diabetes', *Biol Direct*, 2, pp. 5.

Hinova-Palova, D. V., Landzhov, B., Dzhambazova, E., Minkov, M., Edelstein, L., Malinova, L., Paloff, A. and Ovtscharoff, W. (2014) 'Neuropeptide Y immunoreactivity in the cat claustrum: A light- and electron-microscopic investigation', *J Chem Neuroanat*, 61-62, pp. 107-19.

Holmström, M. H., Iglesias-Gutierrez, E., Zierath, J. R. and Garcia-Roves, P. M. (2012) 'Tissue-specific control of mitochondrial respiration in obesity-related insulin resistance and diabetes', *Am J Physiol Endocrinol Metab*, 302(6), pp. E731-9.

Huang, Li, T., Li, X., Zhang, L., Sun, L., He, X., Zhong, X., Jia, D., Song, L., Semenza, G. L., Gao, P. and Zhang, H. (2014) 'HIF-1-mediated suppression of acyl-CoA dehydrogenases and fatty acid oxidation is critical for cancer progression', *Cell Rep*, 8(6), pp. 1930-1942.

Huang, H. H., Farmer, K., Windscheffel, J., Yost, K., Power, M., Wright, D. E. and Stehno-Bittel, L. (2011) 'Exercise increases insulin content and basal secretion in pancreatic islets in type 1 diabetic mice', *Exp Diabetes Res*, 2011, pp. 481427.

Jager, J., Grémeaux, T., Cormont, M., Le Marchand-Brustel, Y. and Tanti, J. F. (2007) 'Interleukin-1beta-induced insulin resistance in adipocytes through down-

regulation of insulin receptor substrate-1 expression', *Endocrinology*, 148(1), pp. 241-51.

JeBailey, L., Rudich, A., Huang, X., Di Ciano-Oliveira, C., Kapus, A. and Klip, A. (2004) 'Skeletal muscle cells and adipocytes differ in their reliance on TC10 and Rac for insulin-induced actin remodeling', *Mol Endocrinol*, 18(2), pp. 359-72.

Jelenik, T., Kaul, K., Séquaris, G., Flögel, U., Phielix, E., Kotzka, J., Knebel, B., Fahlbusch, P., Hörbelt, T., Lehr, S., Reinbeck, A. L., Müller-Wieland, D., Esposito, I., Shulman, G. I., Szendroedi, J. and Roden, M. (2017) 'Mechanisms of Insulin Resistance in Primary and Secondary Nonalcoholic Fatty Liver', *Diabetes*, 66(8), pp. 2241-2253.

Jimenez-Moreno, C. M., Herrera-Gomez, I. G., Lopez-Noriega, L., Lorenzo, P. I., Cobo-Vuilleumier, N., Fuente-Martin, E., Mellado-Gil, J. M., Parnaud, G., Bosco, D., Gauthier, B. R. and Martin-Montalvo, A. (2015) 'A Simple High Efficiency Intra-Islet Transduction Protocol Using Lentiviral Vectors', *Curr Gene Ther*, 15(4), pp. 436-46.

Jiménez Moreno, C. M. (2015) *Role of Pax4 and Pax8 in pancreatic islets physiology and patophysiology.* Biochemistry and chemical engineering doctoral program., Universidad Pablo de Olavide.

Johannsen, D. L., Galgani, J. E., Johannsen, N. M., Zhang, Z., Covington, J. D. and Ravussin, E. (2012) 'Effect of short-term thyroxine administration on energy metabolism and mitochondrial efficiency in humans', *PLoS One*, 7(7), pp. e40837.

Karakosta, P., Alegakis, D., Georgiou, V., Roumeliotaki, T., Fthenou, E., Vassilaki, M., Boumpas, D., Castanas, E., Kogevinas, M. and Chatzi, L. (2012) 'Thyroid dysfunction and autoantibodies in early pregnancy are associated with increased risk of gestational diabetes and adverse birth outcomes', *J Clin Endocrinol Metab*, 97(12), pp. 4464-72.

Karnik, S. K., Chen, H., McLean, G. W., Heit, J. J., Gu, X., Zhang, A. Y., Fontaine, M., Yen, M. H. and Kim, S. K. (2007) 'Menin controls growth of pancreatic beta-cells in pregnant mice and promotes gestational diabetes mellitus', *Science*, 318(5851), pp. 806-9.

Kassem, S., Bhandari, S., Rodríguez-Bada, P., Motaghedi, R., Heyman, M., García-Gimeno, M. A., Cobo-Vuilleumier, N., Sanz, P., Maclaren, N. K., Rahier, J.,

Glaser, B. and Cuesta-Muñoz, A. L. (2010) 'Large islets, beta-cell proliferation, and a glucokinase mutation', *N Engl J Med,* 362(14), pp. 1348-50.

Katsanakis, K. D. and Pillay, T. S. (2005) 'Cross-talk between the two divergent insulin signaling pathways is revealed by the protein kinase B (Akt)-mediated phosphorylation of adapter protein APS on serine 588', *J Biol Chem,* 280(45), pp. 37827-32.

Kaufman, B. A., Li, C. and Soleimanpour, S. A. (2015) 'Mitochondrial regulation of β-cell function: maintaining the momentum for insulin release', *Mol Aspects Med,* 42, pp. 91-104.

Kikuchi, O., Kobayashi, M., Amano, K., Sasaki, T., Kitazumi, T., Kim, H. J., Lee, Y. S., Yokota-Hashimoto, H., Kitamura, Y. I. and Kitamura, T. (2012) 'FoxO1 gain of function in the pancreas causes glucose intolerance, polycystic pancreas, and islet hypervascularization', *PLoS One,* 7(2), pp. e32249.

Kim, H., Toyofuku, Y., Lynn, F. C., Chak, E., Uchida, T., Mizukami, H., Fujitani, Y., Kawamori, R., Miyatsuka, T., Kosaka, Y., Yang, K., Honig, G., van der Hart, M., Kishimoto, N., Wang, J., Yagihashi, S., Tecott, L. H., Watada, H. and German, M. S. (2010) 'Serotonin regulates pancreatic beta cell mass during pregnancy', *Nat Med,* 16(7), pp. 804-8.

Kleinridders, A., Ferris, H. A., Cai, W. and Kahn, C. R. (2014) 'Insulin action in brain regulates systemic metabolism and brain function', *Diabetes,* 63(7), pp. 2232-43.

Komiya, Y. and Habas, R. (2008) 'Wnt signal transduction pathways', *Organogenesis,* 4(2), pp. 68-75.

Kondrashova, A. and Hyöty, H. (2014) 'Role of viruses and other microbes in the pathogenesis of type 1 diabetes', *Int Rev Immunol,* 33(4), pp. 284-95.

Kozmik, Z., Kurzbauer, R., Dorfler, P. and Busslinger, M. (1993) 'Alternative splicing of Pax-8 gene transcripts is developmentally regulated and generates isoforms with different transactivation properties', *Mol Cell Biol,* 13(10), pp. 6024-35.

Kraus, D., Yang, Q. and Kahn, B. B. (2015) 'Lipid Extraction from Mouse Feces', *Bio Protoc,* 5(1).

Lang, D., Powell, S. K., Plummer, R. S., Young, K. P. and Ruggeri, B. A. (2007) 'PAX genes: Roles in development, pathophysiology, and cancer', *Biochemical Pharmacology,* 73(1), pp. 1-14.

Lanni, A., Moreno, M. and Goglia, F. (2016) 'Mitochondrial Actions of Thyroid Hormone', *Compr Physiol,* 6(4), pp. 1591-1607.

Lanni, A., Moreno, M., Lombardi, A. and Goglia, F. (2003) 'Thyroid hormone and uncoupling proteins', *FEBS Lett,* 543(1-3), pp. 5-10.

Lao, T. T., Chan, B. C., Leung, W. C., Ho, L. F. and Tse, K. Y. (2007) 'Maternal hepatitis B infection and gestational diabetes mellitus', *J Hepatol,* 47(1), pp. 46-50.

Le Bouteiller, P. and Bensussan, A. (2017) 'Up-and-down immunity of pregnancy in humans', *F1000Res,* 6, pp. 1216.

Leto, D. and Saltiel, A. R. (2012) 'Regulation of glucose transport by insulin: traffic control of GLUT4', *Nat Rev Mol Cell Biol,* 13(6), pp. 383-96.

Levy, J. C., Matthews, D. R. and Hermans, M. P. (1998) 'Correct homeostasis model assessment (HOMA) evaluation uses the computer program', *Diabetes Care,* 21(12), pp. 2191-2.

Li, C. G., Nyman, J. E., Braithwaite, A. W. and Eccles, M. R. (2011) 'PAX8 promotes tumor cell growth by transcriptionally regulating E2F1 and stabilizing RB protein', *Oncogene,* 30(48), pp. 4824-4834.

Li, M., Song, L. J. and Qin, X. Y. (2014) 'Advances in the cellular immunological pathogenesis of type 1 diabetes', *J Cell Mol Med,* 18(5), pp. 749-58.

Li, S., Brown, M. S. and Goldstein, J. L. (2010) 'Bifurcation of insulin signaling pathway in rat liver: mTORC1 required for stimulation of lipogenesis, but not inhibition of gluconeogenesis', *Proc Natl Acad Sci U S A,* 107(8), pp. 3441-6.

Lin, H. Y., Tang, H. Y., Davis, F. B., Mousa, S. A., Incerpi, S., Luidens, M. K., Meng, R. and Davis, P. J. (2012) 'Nongenomic regulation by thyroid hormone of plasma membrane ion and small molecule pumps', *Discov Med,* 14(76), pp. 199-206.

Lin, Y. and Sun, Z. (2011) 'Thyroid hormone potentiates insulin signaling and attenuates hyperglycemia and insulin resistance in a mouse model of type 2 diabetes', *Br J Pharmacol,* 162(3), pp. 597-610.

Lindquist, C., Bjørndal, B., Rossmann, C. R., Tusubira, D., Svardal, A., Røsland, G. V., Tronstad, K. J., Hallström, S. and Berge, R. K. (2017) 'Increased hepatic mitochondrial FA oxidation reduces plasma and liver TG levels and is associated with regulation of UCPs and APOC-III in rats', *J Lipid Res,* 58(7), pp. 1362-1373.

Liu, M., Sun, J., Cui, J., Chen, W., Guo, H., Barbetti, F. and Arvan, P. (2015) 'INS-gene mutations: from genetics and beta cell biology to clinical disease', *Mol Aspects Med,* 42, pp. 3-18.

Liu, S., Wang, X., Zou, H., Ge, Y., Wang, F., Wang, Y., Yan, S., Xia, H. and Xing, M. (2017) 'Identification and characterization of novel PAX8 mutations in Congenital Hypothyroidism(CH) in a Chinese population', *Oncotarget,* 8(5), pp. 8707-8716.

Lombardi, A., De Matteis, R., Moreno, M., Napolitano, L., Busiello, R. A., Senese, R., de Lange, P., Lanni, A. and Goglia, F. (2012) 'Responses of skeletal muscle lipid metabolism in rat gastrocnemius to hypothyroidism and iodothyronine administration: a putative role for FAT/CD36', *Am J Physiol Endocrinol Metab,* 303(10), pp. E1222-33.

Lorenzo, P. I., Jimenez Moreno, C. M., Delgado, I., Cobo-Vuilleumier, N., Meier, R., Gomez-Izquierdo, L., Berney, T., Garcia-Carbonero, R., Rojas, A. and Gauthier, B. R. (2011) 'Immunohistochemical assessment of Pax8 expression during pancreatic islet development and in human neuroendocrine tumors', *Histochemistry and Cell Biology,* 136(5), pp. 595-607.

Maechler, P. and Wollheim, C. B. (1999) 'Mitochondrial glutamate acts as a messenger in glucose-induced insulin exocytosis', *Nature,* 402(6762), pp. 685-9.

Mansouri, A., Chowdhury, K. and Gruss, P. (1998) 'Follicular cells of the thyroid gland require Pax8 gene function', *Nature Genetics,* 19(1), pp. 87-90.

Marotta, P., Amendola, E., Scarfo, M., De Luca, P., Zoppoli, P., Amoresano, A., De Felice, M. and Di Lauro, R. (2014) 'The paired box transcription factor Pax8 is essential for function and survival of adult thyroid cells', *Molecular and Cellular Endocrinology,* 396(1-2), pp. 26-36.

Martin-Montalvo, A., Mercken, E. M., Mitchell, S. J., Palacios, H. H., Mote, P. L., Scheibye-Knudsen, M., Gomes, A. P., Ward, T. M., Minor, R. K., Blouin, M. J., Schwab, M., Pollak, M., Zhang, Y., Yu, Y., Becker, K. G., Bohr, V. A., Ingram, D. K., Sinclair, D. A., Wolf, N. S., Spindler, S. R., Bernier, M. and de Cabo, R. (2013) 'Metformin improves healthspan and lifespan in mice', *Nat Commun,* 4, pp. 2192.

Martinez-Sanchez, A., Rutter, G. A. and Latreille, M. (2016) 'MiRNAs in β-Cell Development, Identity, and Disease', *Front Genet,* 7, pp. 226.

Marín-Juez, R., Jong-Raadsen, S., Yang, S. and Spaink, H. P. (2014) 'Hyperinsulinemia induces insulin resistance and immune suppression via Ptpn6/Shp1 in zebrafish', *J Endocrinol,* 222(2), pp. 229-41.

Mastracci, T. L. and Evans-Molina, C. (2014) 'Pancreatic and Islet Development and Function: The Role of Thyroid Hormone', *J Endocrinol Diabetes Obes,* 2(3).

Mauer, J., Chaurasia, B., Plum, L., Quast, T., Hampel, B., Blüher, M., Kolanus, W., Kahn, C. R. and Brüning, J. C. (2010) 'Myeloid cell-restricted insulin receptor deficiency protects against obesity-induced inflammation and systemic insulin resistance', *PLoS Genet,* 6(5), pp. e1000938.

McCulloch, L. J., van de Bunt, M., Braun, M., Frayn, K. N., Clark, A. and Gloyn, A. L. (2011) 'GLUT2 (SLC2A2) is not the principal glucose transporter in human pancreatic beta cells: implications for understanding genetic association signals at this locus', *Mol Genet Metab,* 104(4), pp. 648-53.

Mellado-Gil, J. M., Jimenez-Moreno, C. M., Martin-Montalvo, A., Alvarez-Mercado, A. I., Fuente-Martin, E., Cobo-Vuilleumier, N., Lorenzo, P. I., Bru-Tari, E., de Gracia Herrera-Gomez, I., Lopez-Noriega, L., Perez-Florido, J., Santoyo-Lopez, J., Spyrantis, A., Meda, P., Boehm, B. O., Quesada, I. and Gauthier, B. R. (2016) 'PAX4 preserves endoplasmic reticulum integrity preventing beta cell degeneration in a mouse model of type 1 diabetes mellitus', *Diabetologia,* 59(4), pp. 755-65.

Misiti, S., Anastasi, E., Sciacchitano, S., Verga Falzacappa, C., Panacchia, L., Bucci, B., Khouri, D., D'Acquarica, I., Brunetti, E., Di Mario, U., Toscano, V. and Perfetti, R. (2005) '3,5,3'-Triiodo-L-thyronine enhances the differentiation of a human pancreatic duct cell line (hPANC-1) towards a beta-cell-Like phenotype', *J Cell Physiol,* 204(1), pp. 286-96.

Mitchell, R. K., Nguyen-Tu, M. S., Chabosseau, P., Callingham, R. M., Pullen, T. J., Cheung, R., Leclerc, I., Hodson, D. J. and Rutter, G. A. (2017) 'The transcription factor Pax6 is required for pancreatic β cell identity, glucose-regulated ATP synthesis, and Ca2+ dynamics in adult mice', *J Biol Chem*, 292(21), pp. 8892-8906.

Mitchell, S. J., Martin-Montalvo, A., Mercken, E. M., Palacios, H. H., Ward, T. M., Abulwerdi, G., Minor, R. K., Vlasuk, G. P., Ellis, J. L., Sinclair, D. A., Dawson, J., Allison, D. B., Zhang, Y., Becker, K. G., Bernier, M. and de Cabo, R. (2014) 'The SIRT1 activator SRT1720 extends lifespan and improves health of mice fed a standard diet', *Cell Rep*, 6(5), pp. 836-43.

Mittag, J., Friedrichsen, S., Heuer, H., Polsfuss, S., Visser, T. J. and Bauer, K. (2005) 'Athyroid Pax8-/- mice cannot be rescued by the inactivation of thyroid hormone receptor alpha1', *Endocrinology*, 146(7), pp. 3179-84.

Mittag, J., Friedrichsen, S., Strube, A., Heuer, H. and Bauer, K. (2009) 'Analysis of hypertrophic thyrotrophs in pituitaries of athyroid Pax8-/- mice', *Endocrinology*, 150(9), pp. 4443-9.

Mittag, J., Winterhager, E., Bauer, K. and Gruemmer, R. (2007) 'Congenital hypothyroid female Pax8-deficient mice are infertile despite thyroid hormone replacement therapy', *Endocrinology*, 148(2), pp. 719-725.

Montanelli, L. and Tonacchera, M. (2010) 'Genetics and phenomics of hypothyroidism and thyroid dys- and agenesis due to PAX8 and TTF1 mutations', *Molecular and Cellular Endocrinology*, 322(1-2), pp. 64-71.

Moreno, M., Silvestri, E., De Matteis, R., de Lange, P., Lombardi, A., Glinni, D., Senese, R., Cioffi, F., Salzano, A. M., Scaloni, A., Lanni, A. and Goglia, F. (2011) '3,5-Diiodo-L-thyronine prevents high-fat-diet-induced insulin resistance in rat skeletal muscle through metabolic and structural adaptations', *FASEB J*, 25(10), pp. 3312-24.

Moriyama, H., Wen, L., Abiru, N., Liu, E., Yu, L., Miao, D., Gianani, R., Wong, F. S. and Eisenbarth, G. S. (2002) 'Induction and acceleration of insulitis/diabetes in mice with a viral mimic (polyinosinic-polycytidylic acid) and an insulin self-peptide', *Proc Natl Acad Sci U S A*, 99(8), pp. 5539-44.

Mullur, R., Liu, Y. Y. and Brent, G. A. (2014) 'Thyroid hormone regulation of metabolism', *Physiol Rev*, 94(2), pp. 355-82.

Mîinea, C. P., Sano, H., Kane, S., Sano, E., Fukuda, M., Peränen, J., Lane, W. S. and Lienhard, G. E. (2005) 'AS160, the Akt substrate regulating GLUT4 translocation, has a functional Rab GTPase-activating protein domain', *Biochem J*, 391(Pt 1), pp. 87-93.

Nabben, M., Hoeks, J., Briedé, J. J., Glatz, J. F., Moonen-Kornips, E., Hesselink, M. K. and Schrauwen, P. (2008) 'The effect of UCP3 overexpression on mitochondrial ROS production in skeletal muscle of young versus aged mice', *FEBS Lett*, 582(30), pp. 4147-52.

Noguchi, R., Kubota, H., Yugi, K., Toyoshima, Y., Komori, Y., Soga, T. and Kuroda, S. (2013) 'The selective control of glycolysis, gluconeogenesis and glycogenesis by temporal insulin patterns', *Mol Syst Biol*, 9, pp. 664.

Obregon, M. J. (2008) 'Thyroid hormone and adipocyte differentiation', *Thyroid*, 18(2), pp. 185-95.

Ohara-Imaizumi, M., Kim, H., Yoshida, M., Fujiwara, T., Aoyagi, K., Toyofuku, Y., Nakamichi, Y., Nishiwaki, C., Okamura, T., Uchida, T., Fujitani, Y., Akagawa, K., Kakei, M., Watada, H., German, M. S. and Nagamatsu, S. (2013) 'Serotonin regulates glucose-stimulated insulin secretion from pancreatic β cells during pregnancy', *Proc Natl Acad Sci U S A*, 110(48), pp. 19420-5.

Organization, W. H. (2015) *Diabetes Program* 2015).

Ortiga-Carvalho, T. M., Chiamolera, M. I., Pazos-Moura, C. C. and Wondisford, F. E. (2016) 'Hypothalamus-Pituitary-Thyroid Axis', *Compr Physiol*, 6(3), pp. 1387-428.

Osorio-Fuentealba, C., Contreras-Ferrat, A. E., Altamirano, F., Espinosa, A., Li, Q., Niu, W., Lavandero, S., Klip, A. and Jaimovich, E. (2013) 'Electrical stimuli release ATP to increase GLUT4 translocation and glucose uptake via PI3Kγ-Akt-AS160 in skeletal muscle cells', *Diabetes*, 62(5), pp. 1519-26.

Pagliuca, F. W., Millman, J. R., Guertler, M., Segel, M., Van Dervort, A., Ryu, J. H., Peterson, Q. P., Greiner, D. and Melton, D. A. (2014) 'Generation of Functional Human Pancreatic beta Cells In Vitro', *Cell*, 159(2), pp. 428-439.

Palmer, D. G., Rutter, G. A. and Tavaré, J. M. (2002) 'Insulin-stimulated fatty acid synthase gene expression does not require increased sterol response element binding protein 1 transcription in primary adipocytes', *Biochem Biophys Res Commun*, 291(3), pp. 439-43.

Paquette, M. A., Atlas, E., Wade, M. G. and Yauk, C. L. (2014) 'Thyroid hormone response element half-site organization and its effect on thyroid hormone mediated transcription', *PLoS One*, 9(6), pp. e101155.

Paschou, S. A., Papadopoulou-Marketou, N., Chrousos, G. and Kanaka-Gantenbein, C. (2017) 'On type 1 diabetes mellitus pathogenesis', *Endocr Connect*.

Pasek, R. C. and Gannon, M. (2013) 'Advancements and challenges in generating accurate animal models of gestational diabetes mellitus', *American Journal of Physiology-Endocrinology and Metabolism*, 305(11), pp. E1327-E1338.

Pechhold, K., Karges, W., Blum, C., Boehm, B. O. and Harlan, D. M. (2003) 'Beta cell-specific CD80 (B7-1) expression disrupts tissue protection from autoantigen-specific CTL-mediated diabetes', *J Autoimmun*, 20(1), pp. 1-13.

Pereira, S., Park, E., Mori, Y., Haber, C. A., Han, P., Uchida, T., Stavar, L., Oprescu, A. I., Koulajian, K., Ivovic, A., Yu, Z., Li, D., Bowman, T. A., Dewald, J., El-Benna, J., Brindley, D. N., Gutierrez-Juarez, R., Lam, T. K., Najjar, S. M., McKay, R. A., Bhanot, S., Fantus, I. G. and Giacca, A. (2014) 'FFA-induced hepatic insulin resistance in vivo is mediated by PKCδ, NADPH oxidase, and oxidative stress', *Am J Physiol Endocrinol Metab*, 307(1), pp. E34-46.

Petersen, M. C., Vatner, D. F. and Shulman, G. I. (2017) 'Regulation of hepatic glucose metabolism in health and disease', *Nat Rev Endocrinol*, 13(10), pp. 572-587.

Pillon, N. J., Croze, M. L., Vella, R. E., Soulère, L., Lagarde, M. and Soulage, C. O. (2012) 'The lipid peroxidation by-product 4-hydroxy-2-nonenal (4-HNE) induces insulin resistance in skeletal muscle through both carbonyl and oxidative stress', *Endocrinology*, 153(5), pp. 2099-111.

Plachov, D., Chowdhury, K., Walther, C., Simon, D., Guenet, J. L. and Gruss, P. (1990) 'Pax8, a murine paired box gene expressed in the developing excretory system and thyroid gland', *Development*, 110(2), pp. 643-51.

Poleev, A., Okladnova, O., Musti, A. M., Schneider, S., Royer-Pokora, B. and Plachov, D. (1997) 'Determination of functional domains of the human transcription factor PAX8 responsible for its nuclear localization and transactivating potential', *Eur J Biochem,* 247(3), pp. 860-9.

Raman, P. and Koenig, R. J. (2014) 'Pax-8-PPAR-gamma fusion protein in thyroid carcinoma', *Nature Reviews Endocrinology,* 10(10), pp. 616-623.

Rask-Madsen, C. and Kahn, C. R. (2012) 'Tissue-specific insulin signaling, metabolic syndrome, and cardiovascular disease', *Arterioscler Thromb Vasc Biol,* 32(9), pp. 2052-9.

Rector, R. S., Thyfault, J. P., Uptergrove, G. M., Morris, E. M., Naples, S. P., Borengasser, S. J., Mikus, C. R., Laye, M. J., Laughlin, M. H., Booth, F. W. and Ibdah, J. A. (2010) 'Mitochondrial dysfunction precedes insulin resistance and hepatic steatosis and contributes to the natural history of non-alcoholic fatty liver disease in an obese rodent model', *J Hepatol,* 52(5), pp. 727-36.

Rezania, A., Bruin, J. E., Arora, P., Rubin, A., Batushansky, I., Asadi, A., O'Dwyer, S., Quiskamp, N., Mojibian, M., Albrecht, T., Yang, Y. H. C., Johnson, J. D. and Kieffer, T. J. (2014) 'Reversal of diabetes with insulin-producing cells derived in vitro from human pluripotent stem cells', *Nature Biotechnology,* 32(11), pp. 1121-1133.

Richardson, D. K., Kashyap, S., Bajaj, M., Cusi, K., Mandarino, S. J., Finlayson, J., DeFronzo, R. A., Jenkinson, C. P. and Mandarino, L. J. (2005) 'Lipid infusion decreases the expression of nuclear encoded mitochondrial genes and increases the expression of extracellular matrix genes in human skeletal muscle', *J Biol Chem,* 280(11), pp. 10290-7.

Rieck, S. and Kaestner, K. H. (2010) 'Expansion of beta-cell mass in response to pregnancy', *Trends in Endocrinology and Metabolism,* 21(3), pp. 151-158.

Rieck, S., White, P., Schug, J., Fox, A. J., Smirnova, O., Gao, N., Gupta, R. K., Wang, Z. V., Scherer, P. E., Keller, M. P., Attie, A. D. and Kaestner, K. H. (2009) 'The Transcriptional Response of the Islet to Pregnancy in Mice', *Molecular Endocrinology,* 23(10), pp. 1702-1712.

Robson, E. J. D., He, S. J. and Eccles, M. R. (2006) 'A PANorama of PAX genes in cancer and development', *Nature Reviews Cancer,* 6(1), pp. 52-62.

Rojas-Rodriguez, R., Lifshitz, L. M., Bellve, K. D., Min, S. Y., Pires, J., Leung, K., Boeras, C., Sert, A., Draper, J. T., Corvera, S. and Moore Simas, T. A. (2015) 'Human adipose tissue expansion in pregnancy is impaired in gestational diabetes mellitus', *Diabetologia,* 58(9), pp. 2106-14.

Rousset, S., Alves-Guerra, M. C., Mozo, J., Miroux, B., Cassard-Doulcier, A. M., Bouillaud, F. and Ricquier, D. (2004) 'The biology of mitochondrial uncoupling proteins', *Diabetes,* 53 Suppl 1, pp. S130-5.

Rutter, G. A., Pullen, T. J., Hodson, D. J. and Martinez-Sanchez, A. (2015) 'Pancreatic β-cell identity, glucose sensing and the control of insulin secretion', *Biochem J,* 466(2), pp. 203-18.

Röder, P. V., Wu, B., Liu, Y. and Han, W. (2016) 'Pancreatic regulation of glucose homeostasis', *Experimental & Molecular Medicine*, 48. DOI: doi:10.1038/emm.2016.6.

Samuel, V. T. and Shulman, G. I. (2016) 'The pathogenesis of insulin resistance: integrating signaling pathways and substrate flux', *J Clin Invest,* 126(1), pp. 12-22.

San José, G., Bidegain, J., Robador, P. A., Díez, J., Fortuño, A. and Zalba, G. (2009) 'Insulin-induced NADPH oxidase activation promotes proliferation and matrix metalloproteinase activation in monocytes/macrophages', *Free Radic Biol Med,* 46(8), pp. 1058-67.

Sangoi, A. R., Ohgami, R. S., Pai, R. K., Beck, A. H., McKenney, J. K. and Pai, R. K. (2011) 'PAX8 expression reliably distinguishes pancreatic well-differentiated neuroendocrine tumors from Heal and pulmonary well-differentiated neuroendocrine tumors and pancreatic acinar cell carcinoma', *Modern Pathology,* 24(3), pp. 412-424.

Sayre, N. L. and Lechleiter, J. D. (2012) 'Fatty acid metabolism and thyroid hormones', *Curr Trends Endocinol,* 6, pp. 65-76.

Schroeder, A. C. and Privalsky, M. L. (2014) 'Thyroid hormones, t3 and t4, in the brain', *Front Endocrinol (Lausanne),* 5, pp. 40.

Schweizer, U., Towell, H., Vit, A., Rodriguez-Ruiz, A. and Steegborn, C. (2017) 'Structural aspects of thyroid hormone binding to proteins and competitive

interactions with natural and synthetic compounds', *Mol Cell Endocrinol,* 458, pp. 57-67.

Senese, R., Lasala, P., Leanza, C. and de Lange, P. (2014) 'New avenues for regulation of lipid metabolism by thyroid hormones and analogs', *Front Physiol,* 5, pp. 475.

Shanik, M. H., Xu, Y., Skrha, J., Dankner, R., Zick, Y. and Roth, J. (2008) 'Insulin resistance and hyperinsulinemia: is hyperinsulinemia the cart or the horse?', *Diabetes Care,* 31 Suppl 2, pp. S262-8.

Sharabi, K., Tavares, C. D., Rines, A. K. and Puigserver, P. (2015) 'Molecular pathophysiology of hepatic glucose production', *Mol Aspects Med,* 46, pp. 21-33.

Siddiqui, K., Musambil, M. and Nazir, N. (2015) 'Maturity onset diabetes of the young (MODY)-History, first case reports and recent advances', *Gene,* 555(1), pp. 66-71.

Sirakov, M., Skah, S., Nadjar, J. and Plateroti, M. (2013) 'Thyroid hormone's action on progenitor/stem cell biology: new challenge for a classic hormone?', *Biochim Biophys Acta,* 1830(7), pp. 3917-27.

Spinazzi, M., Casarin, A., Pertegato, V., Salviati, L. and Angelini, C. (2012) 'Assessment of mitochondrial respiratory chain enzymatic activities on tissues and cultured cells', *Nat Protoc,* 7(6), pp. 1235-46.

Stuart, E. T., Haffner, R., Oren, M. and Gruss, P. (1995) 'LOSS OF P53 FUNCTION THROUGH PAX-MEDIATED TRANSCRIPTIONAL REPRESSION', *Embo Journal,* 14(22), pp. 5638-5645.

Su, D., Coudriet, G. M., Hyun Kim, D., Lu, Y., Perdomo, G., Qu, S., Slusher, S., Tse, H. M., Piganelli, J., Giannoukakis, N., Zhang, J. and Dong, H. H. (2009) 'FoxO1 links insulin resistance to proinflammatory cytokine IL-1beta production in macrophages', *Diabetes,* 58(11), pp. 2624-33.

Sun, J., Cui, J., He, Q., Chen, Z., Arvan, P. and Liu, M. (2015) 'Proinsulin misfolding and endoplasmic reticulum stress during the development and progression of diabetes', *Mol Aspects Med,* 42, pp. 105-18.

Sun, Y., Yang, Y., Qin, Z., Cai, J., Guo, X., Tang, Y., Wan, J., Su, D. F. and Liu, X. (2016) 'The Acute-Phase Protein Orosomucoid Regulates Food Intake and Energy Homeostasis via Leptin Receptor Signaling Pathway', *Diabetes,* 65(6), pp. 1630-41.

Tachibana, K., Sakurai, K., Yokoh, H., Ishibashi, T., Ishikawa, K., Shirasawa, T. and Yokote, K. (2015) 'Mutation in insulin receptor attenuates oxidative stress and apoptosis in pancreatic beta-cells induced by nutrition excess: reduced insulin signaling and ROS', *Horm Metab Res,* 47(3), pp. 176-83.

Talchai, C., Xuan, S., Lin, H. V., Sussel, L. and Accili, D. (2012) 'Pancreatic β cell dedifferentiation as a mechanism of diabetic β cell failure', *Cell,* 150(6), pp. 1223-34.

Thorel, F., Damond, N., Chera, S., Wiederkehr, A., Thorens, B., Meda, P., Wollheim, C. B. and Herrera, P. L. (2011) 'Normal glucagon signaling and β-cell function after near-total α-cell ablation in adult mice', *Diabetes,* 60(11), pp. 2872-82.

Tong, G. X., Yu, W. M., Beaubier, N. T., Weeden, E. M., Hamele-Bena, D., Mansukhani, M. M. and O'Toole, K. M. (2009) 'Expression of PAX8 in normal and neoplastic renal tissues: an immunohistochemical study', *Mod Pathol,* 22(9), pp. 1218-27.

Tudela, C. M., Casey, B. M., McIntire, D. D. and Cunningham, F. G. (2012) 'Relationship of subclinical thyroid disease to the incidence of gestational diabetes', *Obstet Gynecol,* 119(5), pp. 983-8.

Tuttle, R. L., Gill, N. S., Pugh, W., Lee, J. P., Koeberlein, B., Furth, E. E., Polonsky, K. S., Naji, A. and Birnbaum, M. J. (2001) 'Regulation of pancreatic beta-cell growth and survival by the serine/threonine protein kinase Akt1/PKBalpha', *Nat Med,* 7(10), pp. 1133-7.

van der Spek, A. H., Fliers, E. and Boelen, A. (2017) 'The classic pathways of thyroid hormone metabolism', *Mol Cell Endocrinol,* 458, pp. 29-38.

Vandenouweland, J. M. W., Lemkes, H., Trembath, R. C., Ross, R., Velho, G., Cohen, D., Froguel, P. and Maassen, J. A. (1994) 'MATERNALLY INHERITED DIABETES AND DEAFNESS IS A DISTINCT SUBTYPE OF DIABETES AND ASSOCIATES WITH A SINGLE-POINT MUTATION IN THE MITOCHONDRIAL TRNA(LEU(UUR)) GENE', *Diabetes,* 43(6), pp. 746-751.

Verga Falzacappa, C., Mangialardo, C., Madaro, L., Ranieri, D., Lupoi, L., Stigliano, A., Torrisi, M. R., Bouchè, M., Toscano, V. and Misiti, S. (2011) 'Thyroid hormone T3 counteracts STZ induced diabetes in mouse', *PLoS One*, 6(5), pp. e19839.

Viisanen, T., Ihantola, E. L., Näntö-Salonen, K., Hyöty, H., Nurminen, N., Selvenius, J., Juutilainen, A., Moilanen, L., Pihlajamäki, J., Veijola, R., Toppari, J., Knip, M., Ilonen, J. and Kinnunen, T. (2017) 'Circulating CXCR5+PD-1+ICOS+ Follicular T Helper Cells Are Increased Close to the Diagnosis of Type 1 Diabetes in Children With Multiple Autoantibodies', *Diabetes*, 66(2), pp. 437-447.

Vikram, A. and Jena, G. (2010) 'S961, an insulin receptor antagonist causes hyperinsulinemia, insulin-resistance and depletion of energy stores in rats', *Biochem Biophys Res Commun*, 398(2), pp. 260-5.

Vivas, Y., Díez-Hochleitner, M., Izquierdo-Lahuerta, A., Corrales, P., Horrillo, D., Velasco, I., Martínez-García, C., Campbell, M., Sevillano, J., Ricote, M., Ros, M., Ramos, M. P. and Medina-Gomez, G. (2016) 'Peroxisome proliferator activated receptor gamma 2 modulates late pregnancy homeostatic metabolic adaptations', *Mol Med*, 22.

Walker, L. S. and von Herrath, M. (2016) 'CD4 T cell differentiation in type 1 diabetes', *Clin Exp Immunol*, 183(1), pp. 16-29.

Waraich, R. S., Weigert, C., Kalbacher, H., Hennige, A. M., Lutz, S. Z., Häring, H. U., Schleicher, E. D., Voelter, W. and Lehmann, R. (2008) 'Phosphorylation of Ser357 of rat insulin receptor substrate-1 mediates adverse effects of protein kinase C-delta on insulin action in skeletal muscle cells', *J Biol Chem*, 283(17), pp. 11226-33.

Wistuba, J., Mittag, J., Luetjens, C. M., Cooper, T. G., Yeung, C. H., Nieschlag, E. and Bauer, K. (2007) 'Male congenital hypothyroid Pax8-/- mice are infertile despite adequate treatment with thyroid hormone', *J Endocrinol*, 192(1), pp. 99-109.

World Health organization, D. U. *Diebetes Program*. Available at: http://www.who.int/diabetes/en/.

Wrutniak-Cabello, C., Casas, F. and Cabello, G. (2017) 'Mitochondrial T3 receptor and targets', *Mol Cell Endocrinol*, 458, pp. 112-120.

Xu, X., So, J. S., Park, J. G. and Lee, A. H. (2013) 'Transcriptional control of hepatic lipid metabolism by SREBP and ChREBP', *Semin Liver Dis,* 33(4), pp. 301-11.

Xu, Y., Wang, X., Gao, L., Zhu, J., Zhang, H., Shi, H., Woo, M. and Wu, X. (2015) 'Prolactin-stimulated survivin induction is required for beta cell mass expansion during pregnancy in mice', *Diabetologia,* 58(9), pp. 2064-73.

Yang, D., Lai, D., Huang, X., Shi, X., Gao, Z., Huang, F., Zhou, X. and Geng, Y. J. (2012) 'The defects in development and apoptosis of cardiomyocytes in mice lacking the transcriptional factor Pax-8', *Int J Cardiol,* 154(1), pp. 43-51.

Ye, J. (2013) 'Mechanisms of insulin resistance in obesity', *Front Med,* 7(1), pp. 14-24.

Zhang, C., Bao, W., Rong, Y., Yang, H., Bowers, K., Yeung, E. and Kiely, M. (2013) 'Genetic variants and the risk of gestational diabetes mellitus: a systematic review', *Hum Reprod Update,* 19(4), pp. 376-90.

Zhong, H. and Yin, H. (2015) 'Role of lipid peroxidation derived 4-hydroxynonenal (4-HNE) in cancer: focusing on mitochondria', *Redox Biol,* 4, pp. 193-9.

VIII. APPENDIX

Send Orders for Reprints to reprints@benthamscience.ae

436 *Current Gene Therapy,* **2015,** *15,* **436-446**

A Simple High Efficiency Intra-Islet Transduction Protocol Using Lentiviral Vectors

Carmen María Jiménez-Moreno[1], Irene de Gracia Herrera-Gomez[1], Livia López-Noriega[1], Petra Isabel Lorenzo[1], Nadia Cobo-Vuilleumier[1], Esther Fuente-Martín[1], José Manuel Mellado-Gil[1], Géraldine Parnaud[2], Domenico Bosco[2], Benoit Raymond Gauthier[1,*] and Alejandro Martín-Montalvo[1,*]

[1]*Pancreatic Islet Development and Regeneration Unit, Department of Stem Cells, CABIMER-Andalusian Center for Molecular Biology and Regenerative Medicine, Avenida Américo Vespucio, Parque Científico y Tecnológico Cartuja 93, 41092 Sevilla, Spain;* [2]*Cell Isolation and Transplantation Center, Department of Surgery, Geneva University Hospitals and University of Geneva Rue Michel-Servet 1, 1211 Geneva, Switzerland*

Abstract: Successful normalization of blood glucose in patients transplanted with pancreatic islets isolated from cadaveric donors established the proof-of-concept that Type 1 Diabetes Mellitus is a curable disease. Nonetheless, major caveats to the widespread use of this cell therapy approach have been the shortage of islets combined with the low viability and functional rates subsequent to transplantation. Gene therapy targeted to enhance survival and performance prior to transplantation could offer a feasible approach to circumvent these issues and sustain a durable functional β-cell mass *in vivo*. However, efficient and safe delivery of nucleic acids to intact islet remains a challenging task. Here we describe a simple and easy-to-use lentiviral transduction protocol that allows the transduction of approximately 80 % of mouse and human islet cells while preserving islet architecture, metabolic function and glucose-dependent stimulation of insulin secretion. Our protocol will facilitate to fully determine the potential of gene expression modulation of therapeutically promising targets in entire pancreatic islets for xenotransplantation purposes.

Keywords: Diabetes Mellitus, Gene transfer, Infection, Lentivirus, Pancreatic islet, Transduction.

INTRODUCTION

Type 1 Diabetes Mellitus (T1DM) is one of the most common multifactorial endocrine and metabolic diseases in childhood resulting in persistent hyperglycaemia. Currently, approximately 490,000 children have been diagnosed with T1DM and 78,000 children under the age of 15 are estimated to develop T1DM annually worldwide [1]. More alarmingly, a recent epidemiological study has revealed that the incidence rate of T1DM in children in the United Sates has increased dramatically by 29% between 1985 and 2004 surpassing by 18 times the incidence of Type 2 Diabetes Mellitus (T2DM) in the white population [2]. The most common form of T1DM results from the breakdown of β-cell-specific self-tolerance by T-lymphocytes precipitating an autoimmune attack and eradication of insulin-producing cells [3]. Strong genetic and environmental factors contribute to the onset of T1DM [4]. Existing treatments for T1DM are primarily focused on insulin supplementation. However, despite the beneficial effects of life-long insulin therapy on glucose homeostasis, insulin administration does not eliminate severe diabetic complications such as retinopathy, nephropathy as well as cardiovascular and cerebrovascular diseases [5].

In the past 10 years, clinical islet transplantation has gained much attention as a cell replacement therapy for restoring the functional β-cell mass. Unfortunately, the limited supply of islets from donors has failed to meet demands imposed by the ever-growing number of T1DM patients. An additional major hurdle has been the lack of durability of islet function with insulin independency in less than 10% of patients 5 years after transplantation [6, 7]. Furthermore, several post-transplant events, such as instant blood mediated inflammatory reaction and cytokine cascade, seriously affect the long-term functionality of islets [8-11]. *Ex vivo* genetic modifications of islets to enhance cell function and survival prior to transplantation have been successfully demonstrated in animal models [12, 13]. This strategy can ultimately increase islet viability and performance providing a tangible approach to improve human islet transplantation and long-term insulin independence. Although protocols designed to modulate gene expression have been extensively used in single cells, the complexity of pancreatic islets has impeded successful gene delivery. Indeed, due to its tridimensional structure, β-cells embedded within the core of islets are sequestered from any significant contact with the remote environment [14-19]. During the last years, several

*Address correspondence to these co-senior authors at the Pancreatic Islet Development and Regeneration Unit, Department of Stem Cells, CABIMER-Andalusian Center for Molecular Biology and Regenerative Medicine, Avenida Américo Vespucio, Parque Científico y Tecnológico Cartuja 93, 41092 Sevilla, Spain; Tel: 0034 954 468 004; Fax: 0034 954 461 664;
E-mails: benoit.gauthier@cabimer.es and alejandro.martinmontalvo@cabimer.es

1875-5631/15 $58.00+.00

non-viral strategies for genetic modification of islet cells, such as electroporation, microporation, gene gun particle bombardment, cationic liposomes and polymeric particles, have been investigated [15, 19-21]. Unfortunately, in most cases those techniques provided low gene transfer efficiencies and the difficulty of reproducing these protocols have hindered their broad use to allow optimized islet gene transfer. More recently, *ex vivo* infection of islets was proposed in order to conduct mechanistic studies and also to transfer therapeutically promising genes or alleles prior to islet xenotransplantation [22]. Adenoviral vectors have been used with this purpose since the efficiency of infection in non-dividing cells is greater than other vectors and their epichromosomal location reduces the probability of conferring insertional mutations. The efficiency of the majority of adenovial-based infection protocols has been found to be limited to only ~7-30 % of islet cells and infected cells were mostly located in the periphery of the islet [14, 15]. Although several studies reported infection of 30-90 % of islet cells throughout the whole islet [14, 23, 24] excessive viral dosage were used which may cause cytotoxicity [14, 25, 26]. Alternatively, genetic modifications of adenoviral vectors such as the inclusion of Arg-Gly-Asp motif were attempted to enhance transduction efficiency up to ~80 % of islet cells at 10 Plaque Forming Units (PFU) per cell [15]. Unfortunately, the drawback for adenoviral transduction was the methodological difficulties of these experimental protocols and the transient modulation of gene expression [23, 27].

The use of lentiviral vectors in gene therapy has become a powerful tool to safely deliver genetic material with the purpose to rectify molecular defects, enhance functional performance or increase viability of cells. Major advantages of lentiviral vectors include the capacity to infect both dividing and non-dividing cells using repeated dosing, genome integration and long-term expression as well as low immunogenicity [28]. Currently, 89 gene therapy clinical trials using lentiviral vectors are ongoing [29] focusing predominantly on the treatment of primary immunedeficiencies [30]. Transduction protocols using lentiviruses have also been developed for islet infection yielding similar efficiency than adenoviral vectors (~3-50 % of β -cells) [14, 16-18, 31-33]. Given the tremendous attributes of lentiviral vectors combined with their current use in clinical trials, we set out to develop a simple and optimal lentiviral transduction protocol for intact human and mouse pancreatic islets with the long-term goal to apply this protocol for gene therapy in islets prior to transplantation without compromising their integrity and functionality.

MATERIALS AND METHODS

Consumables

Reagents and materials used in this study along with reference numbers and companies of purchase are outlined in Table **1**.

Animals

Male mice (c57bl/6, 12 week-old) were purchased from Janvier Labs (Le Genest-Saint-Isle, France). Mice experimentations were approved by the CABIMER Animal Committee and performed in accordance with the Spanish law on animal use RD 53/2013.

Table 1. List of reagents and materials used in this study.

Product	Vendor	Catalog Number
50 x 9 mm Petri dishes	BD Falcon	351006
Affi-Gel blue beads	Bio-Rad	153-7301
Bovine Serum Albumin	Sigma-Aldrich	A3294
CalPhos mammalian transfection kit	ClonTech	631312
CMRL-1066	Cellgro	99-663-CV
Collagenase	Roche	C9263
DAKO fluorescent mounting medium	Dako	S3023
DAPI	Sigma-Aldrich	32670
Donkey serum	Sigma-Aldrich	D9663
Fetal Bovine Serum	Sigma-Aldrich	F7524
Formaldehyde	Panreac AppliChem	252931
Gentamycin	Sigma-Aldrich	G1397
Glutamine	Sigma-Aldrich	G7513
Hanks Balanced Salt Solution 1X	Gibco	14170088
HEPES	Gibco	15630-056
HistoGel	Thermo Scientific	R904012
micro-Plate 96 welllibiTreat	IBIDI	89626
Millex-HV filter 0.45 μm	Merck Millipore	SLHV033RS
PBS	Sigma-Aldrich	P5368
Penicillin/Streptomycin	Sigma-Aldrich	P4333
Polystyrene Round-bottom tube	BD Falcon	352058
RPMI-1640	Sigma-Aldrich	R0883
Sodium pyruvate	Sigma-Aldrich	S8636
SuperFrost Plus slides	Menzel-Glaser	J1800AMNZ
Trypsin-EDTA 10 X	Gibco	15400054
β-mercaptoethanol	Gibco	31350-10

Islets Procuration and Culture

Mice were sacrificed by cervical dislocation and pancreatic islets were isolated using the collagenase digestion procedure with subsequent handpicking as previously described [34]. Prior to culture islets were washed with Phosphate Buffered Saline (PBS) containing 100 U/ml penicillin and 100 μg/ml streptomycin to minimize post-isolation contami-

nations. Subsequently islets were cultured in mouse Complete Media (CM) comprised of RPMI 1640 supplemented with 10 % FBS, 100 U/ml penicillin, 100 µg/ml streptomycin, 2 mM glutamine, 1 mM sodium pyruvate, 50 µM β-mercaptoethanol and 10 mM HEPES. Isolated human islets were either kindly provided by the Cell Isolation and Transplantation Centre (Geneva, Switzerland) or purchased from Tebu-bio (Le Perray En Yvelines, France). Characteristics of human islet preparations are included in Table **S1**. Islets were cultured in human Complete Media (CM) composed of CMRL-1066 supplemented with 10 % FBS, 100 U/ml penicillin, 100 µg/ml streptomycin, 2 mM L-glutamine and 100 µg/ml gentamycin.

Lentivirus Generation

We opted for the dual-promoter lentivirus, pHRSIN DUAL-GFP also known as pHRSIN-CSGWdINotIpUbEm (kindly supplied by Dr. Pintor-Toro, CABIMER, Spain) to conduct our studies [35]. This vector allows the cloning and expression of a Gene Of Interest (GOI) under the control of the SFFV promoter while the constitutive *Ubiquitin* (Ubi) promoter regulates expression of the reporter GFP. Lentivirus amplification and purification was performed by seeding 5×10^6 Hek293T cells into a 100 mm Petri dish and subsequently transfected 24 hours later with: 1) 15 µg of vector, 2) 10 µg the HIV packaging plasmids pCMVDR8.91 and 3) 5 µg of HIV packaging plasmids pVSVG (also known as pMDG). Transient DNA transfection was performed using the CalPhos transfection mammalian kit according to the manufacturer's recommendations. Viral particles were harvested 72 hours post-transfection, purified using a 0.45 µm Millex-HV filter, and concentrated by ultracentrifugation in an Optima™ L-100K ultracentrifuge at 87300 x g for 90 minutes at 4º C in a swinging bucket rotor SW-28 (Beckman-Coulter, Spain). Virus particles were resuspended in serum-free DMEM (Invitrogen), distributed in aliquots, snapped frozen in liquid nitrogen, and stored at −80 °C. Viral titer was estimated by transducing Hek293T cells with increasing amounts of pHRSIN DUAL-GFP followed by flow cytometry (FACSCalibur, BD Biosciences, Spain) analysis to determine the PFU/ml based on GFP emission.

Live Imaging and Flow Cytometry

An ImageXpress Micro System (Molecular Devices) was used to monitor GFP fluorescence in living islets. To this end, approximately 20 transduced human or mouse islets were seeded in µ-Plate 96 welllibiTreat plate in a final volume of 200 µl of CM. Islets were cultured for 4 days at 37º C and images (fluorescence or phase contrast) were automatically captured daily and processed using the MetaXpress software. In parallel, islet transduction efficiency was estimated by flow cytometry. In brief, approximately 20 islets were transferred into 5 ml polystyrene Round-bottom tube in a final volume of 50 µl of CM. Islets were disaggregated using 1 X trypsinization for 5 minutes at 37º C and subsequently centrifuged at 200 x g for 5 minutes. Cells were resuspended in 300 µl of PBS and the number of GFP positive cells was estimated as compared to non-infected cells.

Islet Processing and Immunocytochemistry

Islet embedding was performed according to the protocol developed by Cozar-Castellano *et al.* [36]. In brief, approximately 200 human or murine islets were fixed in 10 % formaldehyde at room temperature for 48 hours. Islets were then washed three times in distilled water prior to adding warm (70° C) HistoGel containing 100 µl of 150-300 µm diameter Affi-Gel blue beads. After cooling, Histogel containing the islet-bead mixture was embedded in paraffin following the standard procedures of the CABIMER Histology Core Facility. Paraffin blocks were sectioned (5 µm thickness) using a microtome Leica RM 2255 (Leica Microsystems, Spain). Sections were mounted on SuperFrost Plus slides. After every 10 sections, a slide was stained with hematoxylin-eosin to confirm islet integrity and presence of islets. Sections were deparaffinized/rehydrated at 60˚ C for 20 minutes followed by immersion in decreasing concentrations of ethanol (Xylene 5 minutes/2 x; Ethanol 100 % 1 minute/2 x; Ethanol 96 % 1 minute; Ethanol 80 % 1 minute; Ethanol 70 % 1 minute; Distilled water 2 minutes/2 x). After deparaffinization and rehydration, sections were subjected to heat-induced antigen retrieval using 10 mM sodium citrate buffer (pH 6.0) in the microwave in 3 cycles of 3 minutes at 800 W avoiding boiling of the buffer, with 2 minutes at room temperature between heating cycles. Samples were cold down in the same solution for 20 minutes at room temperature. After washing with PBS, samples were incubated in PBS + 0.5 % Triton X-100 and then washed again with PBS. Blocking was performed with PBS + 0.2 % Triton X-100 containing 1 % Bovine Serum Albumin (BSA) and 3 % Donkey serum for 1 hour at room temperature. Primary antibodies (Table **2**) at the indicated dilutions were added in PBS + 0.1 % Triton X-100 containing 1 % BSA and 3 % Donkey serum and incubated overnight at 4˚ C in a dark humid chamber. Subsequently, sections were washed with PBS for 5 minutes, PBS + 0.2 % Triton X-100 for 5 minutes and PBS for 5 minutes. Samples were then incubated with secondary antibodies (Table **2**) diluted in PBS + 0.2 % Triton X-100 containing 0.1 % BSA for 1 hour at room temperature in a dark humid chamber. Nuclear counterstaining was performed by DAPI staining diluted 1:1000 in PBS for 5 minutes at room temperature. Finally, samples were washed three times with PBS for 5 minutes each and sections were mounted using DAKO fluorescent mounting medium. Wide-field immunofluorescence microscopy was performed using a Leica microscope (AF6000) (Leica, England). Images were taken at 40X magnification. Confocal images were acquired using a Leica confocal microscope (TCS SP5). The images were scanned under a HCX PL APO lambda blue 63X/ 1.4 OIL objective. To analyze the whole section, each sample was analyzed using a spatial series through the Z axis. Each spatial series was composed of approximately 5-7 optical sections with a size of 0.8 µm and a 3D projection of each z-stack was performed using three sections.

Viability and Functional Assay

Islet viability subsequent to transduction was assessed in groups of 35 islets using the Cell Proliferation Kit I (MTT) according to the manufacturer´s recommendations (Roche, Spain). Optical density was determined at 550 nm with a reference wavelength of 650 nm using a Varioskan Flash

Table 2. List of antibodies used in this study.

Antibody	Dilution	Vendor	Catalog Number
Anti-GFP	1:200	Abcam	Ab6673
Anti-insulin (H-86)	1:500	Santa Cruz	SC9168
Anti-insulin	1:500	Sigma-Aldrich	I2018
Anti-glucagon	1:150	Sigma-Aldrich	G2654
Anti-glucagon	1:200	Cell Signaling	2760S
Anti-cleaved caspase-3	1:150	Cell Signaling	9661
Alexa fluor 488 donkey anti-goat	1:800	Invitrogen	A11055
Alexa fluor 555 donkey anti-mouse	1:800	Life technologies	A31579
Alexa fluor 647 donkey anti-rabbit	1:800	Life technologies	A31573

spectrophotometer (Thermo Scientific, Spain). In parallel, glucose stimulated insulin secretion was performed to assess the functional integrity of islets. Groups of 10 islets were washed in 500 µL of Krebs-Ringer bicarbonate-HEPES buffer (KRBH) (140 mM NaCl, 3.6 mM KCl, 0.5 mM NaH_2PO_4, 0.5 mM $MgSO_4$, 1.5 mM $CaCl_2$, 2 mM $NaHCO_3$, 10 mM HEPES, 0.1% BSA) and pre-incubated at 37° C for 45 minutes in 300 µl of the same buffer. Islets were then centrifuged and KRBH buffer was discarded. Subsequently, fresh KRBH supplemented with 2.5 mM glucose was added and islets were incubated for 30 minutes. Next, buffer was harvested (basal insulin secretion) and 500 µL of KRBH supplemented with 16.8 mM glucose was added. Islets were incubated for an additional 30 minutes at 37° C and then buffer was harvested (induced insulin secretion). Insulin levels were measured using a mouse or human insulin enzyme immunoassay kit (Mercodia AB, Spain) according to the manufacturer´s instructions. Stimulation index was expressed as the ratio of insulin levels at 16.8 mM glucose divided by insulin levels at 2.5 mM glucose.

Statistical Analysis

Results are expressed as the mean± SEM. Statistical differences were estimated by two-tailed unpaired student's *t*-test. *Indicates statistical significance, p value <0.05.

RESULTS

Elaboration of a High Efficiency Transduction Protocol in Mouse Islets

Modulation of gene expression has been particularly challenging in the context of whole pancreatic islets as compared to cell lines due to their three dimensional structure composed of approximately 1000 to 2000 compacted cells. Sophisticated protocols such as *in vivo* perfusion or microporation using adeno and lenti viruses claim to have successfully and homogenously transduced up to 70% islet cells [24]. As these protocols may be cumbersome to carry out or simply not always feasible (i.e. *in vivo* perfusion of human islets) we sought to develop a readily accessible and friendly

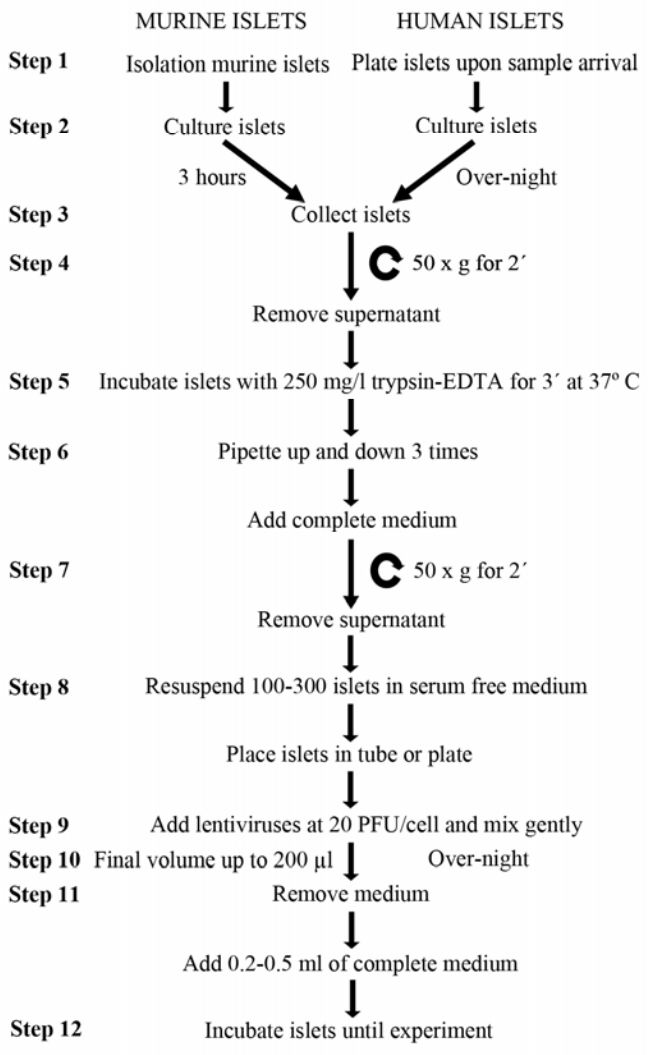

Fig. (1). Optimized protocol for lentiviral-mediated islet infection. Summarized scheme of the transduction protocol described in Box **1**.

BOX 1. OPTIMIZED ISLET INFECTION PROTOCOL

Step 1. Isolation of fresh murine islets by collagenase digestion (0.7-0.9 mg/ml) and subsequent handpicking (for human samples go to step 2).
Step 2. Culture islets for 3 hours in 50 x 9 mm Petri dishes in 2.5 ml of complete RPMI. For human samples, place islets upon sample arrival in 100 x 9 mm Petri dishes and culture them over-night in 10 ml of complete CMRL-1066.
Step 3. Collect medium and islets from the plate in a 15 ml falcon tube.
Step 4. Centrifuge islets at 50 x g for 2 minutes and remove supernatant.
Step 5. Incubate islets with 1000µl of warm (37º C) 0.5 X trypsin- Ethylenediaminetetraacetic acid (EDTA) (250 mg/l trypsin; 0.48 mM EDTA) for 3 minutes in a cell culture incubator (37º C, 5 % CO2). For trypsin-EDTA preparation: Aliquots of 0.5 % Trypsin-EDTA 10 X (5000 mg/l; 9.6 mM EDTA) are diluted in Hanks Balanced Salt Solution (HBSS) 1 X to obtain a final concentration of 0.5 X trypsin-EDTA (250 mg/l; 0.48 mM EDTA)).
Step 6. Pipette up and down 3 times slowly and carefully with a 1000 µl tip using a micropipette and subsequently add 1000 µl of complete RPMI for murine islets or complete CMRL-1066 for human islets.
Step 7. Centrifuge islets at 50 X g for 2 minutes and remove supernatant.
Step 8. Resuspend 100-300 islets in serum free RPMI (for murine islets) or serum free CMRL-1066 (for human islets). Place islets in a polystyrene Round-bottom tube or in a µ-Plate 96 welllibiTreat culture plate depending on the desired experiment. Note that final volume must not exceed 200 µl.
Step 9. Add lentiviruses at 20 Plaque Forming Units per cell (PFU/cell), assuming that a single islet has 1000 cells. Note that final volume must not exceed 200 µl and virus concentration must be in the range of 1.5-5 x10^4 PFU/µl. Resuspend islets by gently tapping the polystyrene Round-bottom tube or the µ-Plate 96 welllibiTreat culture plate three times.
Step 10. Incubate islets over-night in cell culture incubator (37º C, 5 % CO2) for optimal lentiviral transduction.
Step 11. Remove medium and add 200-500 µl of complete RPMI (for murine islets) or CMRL-1066 (for human islets).
Step 12. Incubate islets at 37º C in a cell culture incubator (37º C, 5 % CO2) until the optimal timing for the desired experiment is achieved.

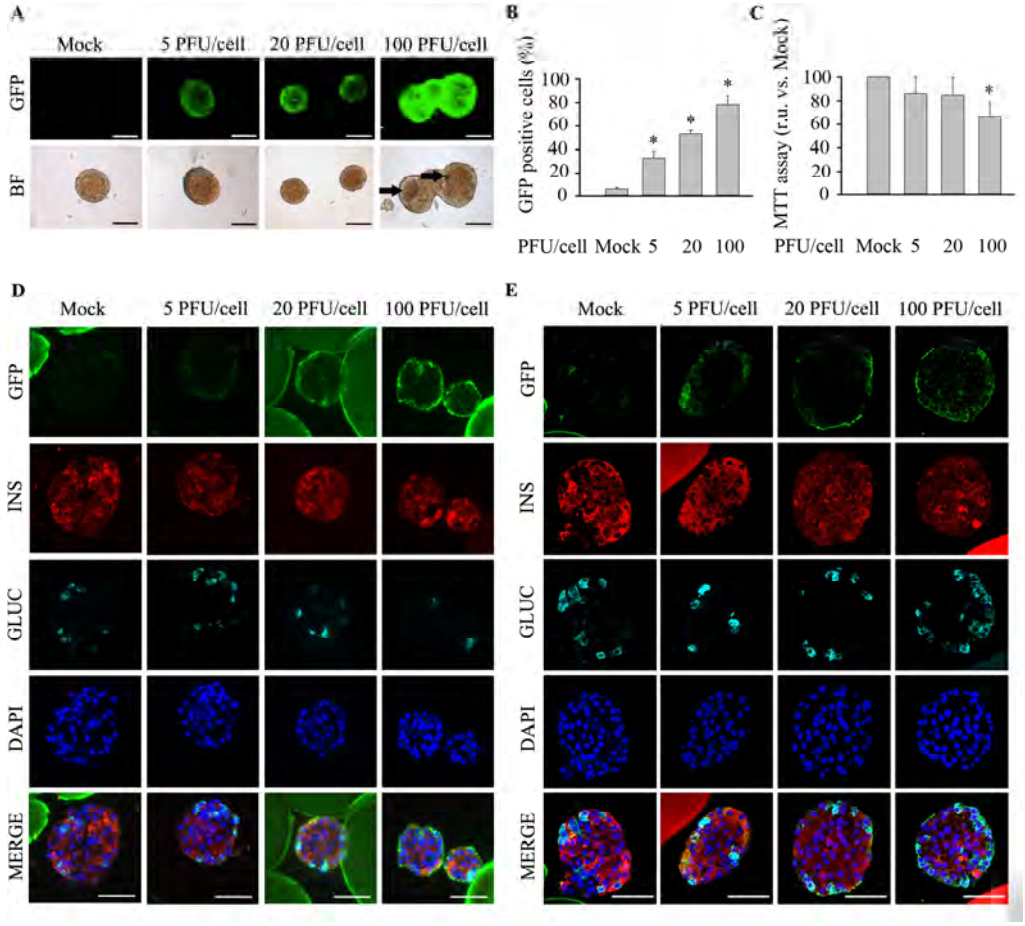

Fig. (2). High pHRSIN DUAL-GFP PFU/cell levels compromise islet viability with sub-optimal islet transduction efficiency. Freshly isolated murine islets were exposed to increasing PFU/cell of pHRSIN DUAL-GFP. Non-transduced islets (Mock) were used as control. **(A)** Representative images of *ex vivo* cultured entire live transduced islets. Top; GFP expression was assessed by fluorescence acquisition using an ImageXpress Microsystem. Low; Bright field images. Images were captured at 4 days post-infection. Arrows indicate necrotic areas. Scale-bars indicate 100 µm. *n=4* experiments per condition. **(B)** Transduction efficiency, defined as the percentage of islet cells expressing GFP, was determined by flow cytometry in disaggregated islets at 4 days post-infection. *n=6* per condition. **(C)** Determination of islet metabolic activity using the MTT assay at 4 days post-infection *n=4-6* per condition. **(D-E)** Representative immunofluorescence images of Affi-Gel bead-embedded pancreatic islets 4 days post-infection. Antibodies against GFP (green), insulin (red) and glucagon (cyan) were employed. Of note, in some instances the Affi-Gel beads, emitted a non specific fluorescent signal along with GFP (Green) and insulin (red). (**D**) Wide-field fluorescence microscopy. (**E**) Confocal microscopy. Scale-bars, 50 µm. *n=3* per condition. Data are represented as the mean ± SEM. * $p < 0.05$ versus control non-transduced islets.

user lentiviral protocol (BOX **1** and Fig. **1**). Consistent with previous reports, the mere exposure of islets to increasing PFU/cell of pHRSIN DUAL-GFP resulted in enhanced GFP fluorescence from living islets corroborating with a greater number of islet cells expressing GFP, as assessed by flow cytometry of dispersed islets (Fig. **2A-B**). However, the 100 PFU/cell that achieved 80% infection efficiency also considerably reduced islet viability (Fig. **2C**) with the appearance of necrotic cells in the islet core (Fig. **2A**, arrows). Intriguingly, wide-field and confocal immunocytochemistry revealed that even at high PFU/cell cells at the periphery were preferentially infected (e.g. GFP positive) (Fig. **2D-E**). In an attempt to increase accessibility to cells sequestered within the core to viral particles without compromising viability, we mildly loosen up islet cells using either 1X (500 mg/L trypsin; 0.96 mM EDTA) or 0.5X (250 mg/L trypsin; 0.48 mM EDTA) trypsin-EDTA for 3 minutes prior to transduction. Both trypsin concentrations improved the number of GFP-expressing islet cells at either 5 or 20 PFU/cell (Fig. **3A-B**). Flow cytometry of disaggregated islets confirmed that the number of GFP-positive cells infected at 5 PFU/cell increased from ~30% in control islets to ~50% in islets pretreated with trypsin independent of its concentration (Fig. **3B**). Similarly, 20 PFU/cell resulted in 80% of cells expressing GFP independent of trypsin concentrations (Fig. **3B**). Unexpectedly, 1X trypsin jeopardized viability of cells in all conditions (Fig. **3C**). High-resolution confocal microscopy confirmed that 0.5X trypsin-EDTA facilitated infection of cells residing within the islet core (Fig. **3D**). We next sought to determine the temporal evolution of GFP expression subsequent to transduction using 0.5X trypsin. In order to expose islets to minimal amount of viral particles, we also assessed the transduction efficiency of 7 and 10 PFU/cell. For each viral dosage, the percentage of GFP-positive cells remained relatively constant over the 10 day period (Fig. **4A-B**). Of note, at day 10, non-infected (mock) islet cells emit low levels of fluorescent, indicative of auto-fluorescence produced by apoptotic cells [37]. Consistent with this premise, islet architecture was strongly compromised at day 10 with signs of necrosis as compared to islets 4 days post infection (Fig. **4C**). In some instances, bacterial contamination was also observed 10 days after transduction (data not shown). Islets transduced at 20 PFU/cell consistently presented ~80% of islet cells at day 4 post-infection, as compared to all other PFU/cell tested (Fig. **4B**). GFP immunostaining was detected homogeneously throughout the islet co-localizing with both insulin as well as glucagon-positive cells 4 days post-infections (Fig. **4D-E**). More importantly at this time point, neither islet viability (Fig. **4F**) nor function, as measured by glucose-induced insulin secretion (Fig. **4G**), were altered at 20 PFU/cell as compared to 5, 7, 10 PFU/cell or control non-transduced islets. Furthermore, the apoptotic rate, as assessed by cleaved-caspase 3 immunostaining, was identical in both control and 4 days post-transduction islets indicating, that the protocol is not detrimental for islet health (Fig. **4H-I**) In summary, our data indicate that 80% of mouse islet cells express GFP 4 days after exposure to a short and mild trypsin treatment and to a viral dosage of 20 PFU/cell.

Transduction Protocol Validation in Human Islet

We next validated our transduction protocol in human islets. Live human islets revealed intense GFP expression without apparent ultra-structural abnormalities 4 days post transduction (Fig. **5A**). Consistent with mouse islets, approximately 70 to 80% of islet cells were GFP-positive, as determined by flow cytometry of dispersed islets (Fig. **5B**). Remarkably, the viability and functionality of transduced islets were not altered (Fig. **5C-D**). Finally, GFP immunostaining assessed by wide-field and confocal microscopy was detected homogeneously throughout islets co-localizing with both insulin and glucagon (Fig. **5E-F** and Supplemental Fig. **1**). Taken together, our data indicate that the proposed protocol is easy, reliable and allows the transduction of the majority of cells residing in entire islets from murine and human origin.

DISCUSSION

Given the indispensable role of pancreatic islets in glucose homeostasis, the modulation of gene expression in transplanted islets could be a promising approach to boost islet performance and durability for the treatment of T1DM [38, 39]. In this context, non-viral strategies, such as electroporation, gene gun particle bombardment, cationic liposomes and polymeric particles, have been developed for genetic modification of islet cells [15, 19-21]. Unfortunately, these techniques provide only low to intermediate gene transfer efficiencies, limiting their applicability. In contrast, published adenovial-based infection protocols claim to have successfully transduced up to 90 % of islet cells using high viral doses [14, 15, 23, 25-27]. Although promising, these protocols are technically challenging to perform. Moreover, these protocols result in transient expression and frequently induce cell toxicity. Alternatively, lentiviral vectors have emerged as an alternative strategy to modulate gene expression in intact islets. Up to 50 % of β cells in intact islets have been efficiently transduced without adverse viability effects [14, 16-18, 31-33]. Based on these initial successes, we have devised an easy-to-use and reproducible protocol that bestows a significant improvement of murine and human islet transduction efficiency. In summary, our optimized easy-to-use transduction protocol resulted in an infection efficiency of ~70-80 % of cells within intact murine and human islets without compromising health. In the optimization of our protocol three non-mutually exclusive parameters were considered: 1) PFU/cell, 2) islet architecture, and 3) time post-transduction. Consistent with other reports, we found that high PFU/cell (e.g. 100 PFU/cell or greater) increased transduction efficiency but to the detriment of islet cell function and survival [14, 25, 26]. The negative impact of high virus dosage has also been substantiated *in vivo* xenotransplantation studies [15]. We established that a 20 PFU/cell was the optimal viral dosage reaching 50 % cell infection in intact islets without jeopardizing either viability or function. This PFU/cell is substantially lower to those (100-1000 PFU/cell) previously utilized in another published protocol [25]. Addition of a mild 0.5X trypsin-EDTA treatment to facilitate core accessibility greatly improved transduction efficiency while preserving islet health and function, reaching approximately 80 % of the islet cell population. Interestingly, 1X trypsin-EDTA affected cell viability. Pro-distension agents such as collagenase and triton-X-100 were also found to increase infection efficiency yet compromised islet functionality [14, 23]. Thus, although these treatments seemingly appear to be

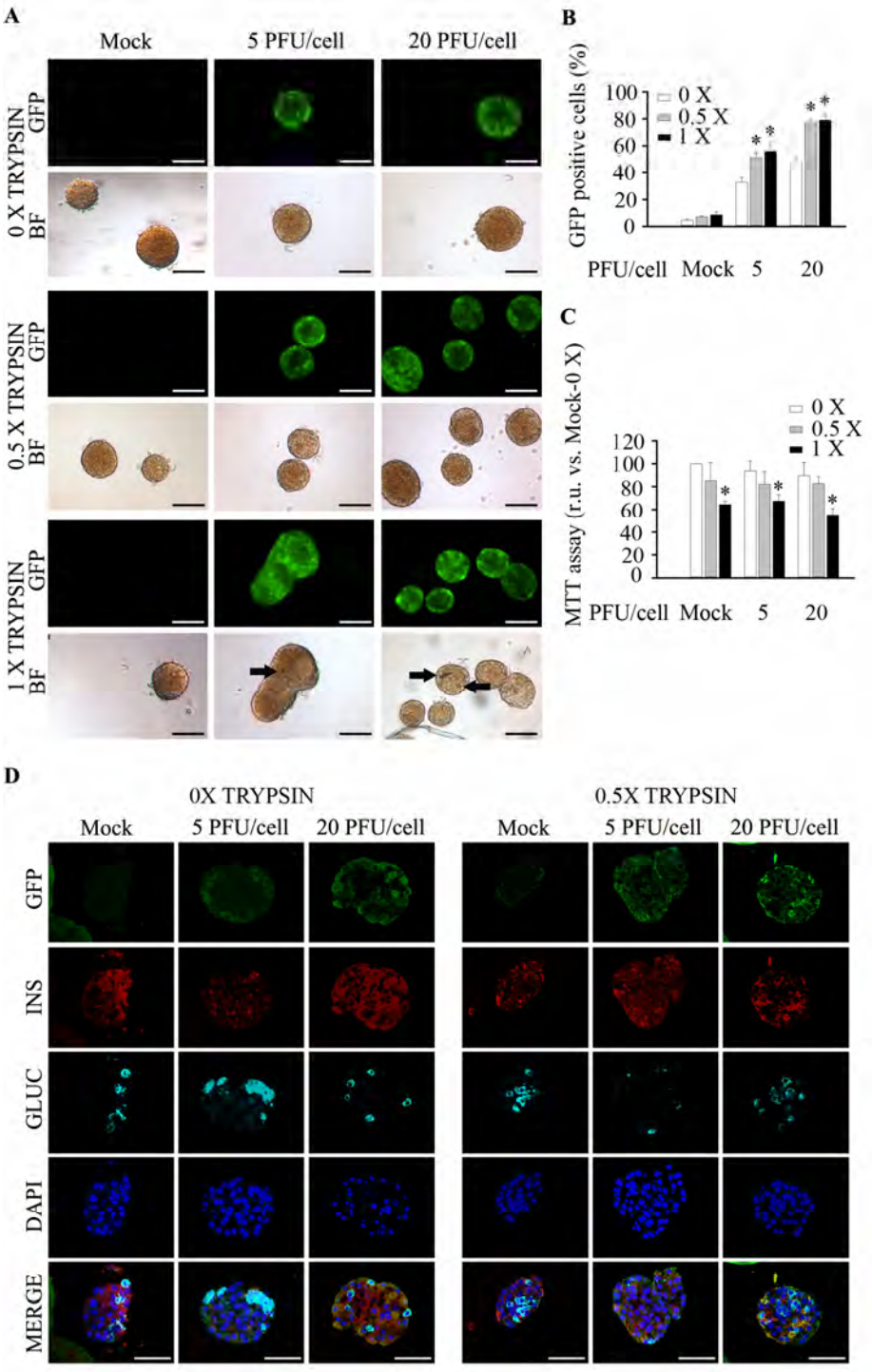

Fig. (3). A Mild Trypsin-EDTA treatment increases transduction efficiency in murine islets. Freshly isolated murine islets were treated or not with two concentrations of trypsin-EDTA prior transduction or not with pHRSIN DUAL-GFP. **(A)** Representative images of live islets exhibiting GFP fluorescence subsequent to treatment: Top; GFP expression was assessed by fluorescence acquisition using an ImageXpress Microsystem. Low; Bright field images. Images were captured at 4 days post-infection. Arrows indicate necrotic areas. Scale-bars 100 µm. *n=4* experiments per condition. **(B)** Transduction efficiency in trypsin-EDTA treated islets was determined by flow cytometry in disaggregated islets at 4 days post-infection. *n=3-8* per condition. **(C)** Determination of islet metabolic activity using the MTT assay 4 days post-infection. *n=4* per condition. **(D)** Representative confocal immunofluorescence images of Affi-Gel bead-embedded pancreatic islets 4 days post-infection with or without 0.5X trypsin-EDTA treatment. Antibodies against GFP (green), insulin (red) and glucagon (cyan) were employed. Of note, in some instances the Affi-Gel beads, emitted a non specific fluorescent signal along with GFP (green). Scale-bars, 50 µm. *n=3* per condition. 0 X: Untreated; 0.5 X: 0.5 X trypsin-EDTA treatment (250 mg/l trypsin; 0.48 mM EDTA); 1 X: 1 X trypsin-EDTA treatment (500 mg/l; 0.96 mM EDTA). Data are represented as the mean ± SEM. * $p < 0.05$ versus control non-transduced trypsin-EDTA untreated islets.

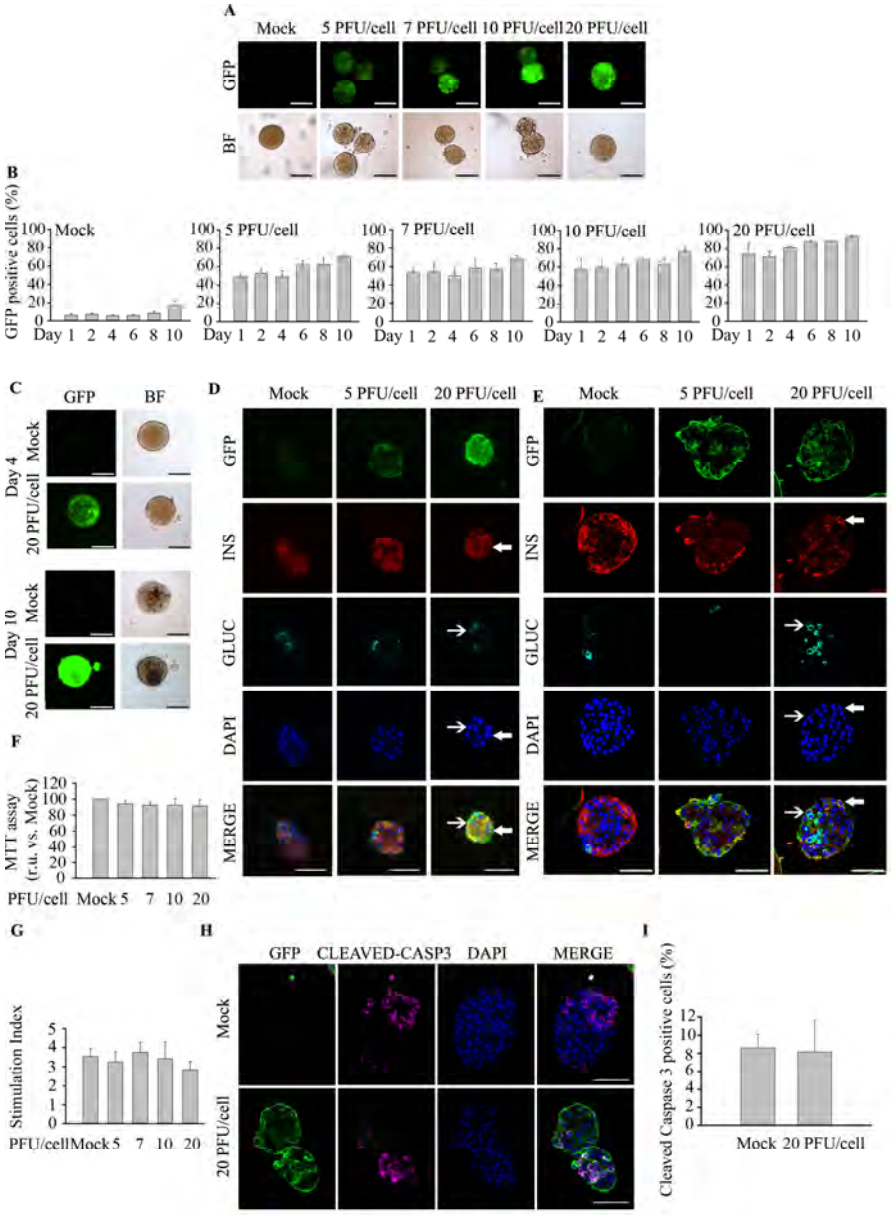

Fig. (4). Mild trypsinization combined with 20 PFU/cell represents the optimal infection protocol for murine islets. Freshly isolated murine islets were treated with 0.5 X trypsin-EDTA (250 mg/l; 0.48 mM EDTA) and subsequently exposed to increasing **PFU/cell** of pHRSIN DUAL-GFP. **(A)** Representative images of GFP fluorescence emitted from live islets: Top; GFP expression was assessed by fluorescence acquisition using an ImageXpress Microsystem. Low; Bright field images. Images were captured at 4 days post-infection. Scale-bars 100 µm. *n=4* experiments per condition. **(B)** Transduction efficiency in 0.5 X trypsin-EDTA treated islets at different days after transduction was determined by flow cytometry in dispersed islets. *n=4* per condition. **(C)** Representative images of live islets exhibiting GFP fluorescence 4 and 10 days post-treatment: Top; GFP expression was assessed by fluorescence acquisition using an ImageXpress Microsystem. Low; Bright field images. Scale-bars 100 µm. *n=4* experiments per condition. **(D-E)** Representative immunofluorescence images of Affi-Gel bead-embedded pancreatic islets trypsin-treated and transduced or not with pHRSIN DUAL-GFP. Antibodies against GFP (green), insulin (red) and glucagon (cyan) were employed. Images were captured in samples fixed at 4 days post-infection using either wide-field fluorescence microscopy (**D**) or confocal microscopy (**E**). Of note, in some instances the Affi-Gel beads, emitted a non specific fluorescent signal along with GFP (green) and insulin (red). Filled arrows indicate transduced cells expressing insulin; Non-filled arrows indicate transduced cells expressing glucagon. Scale-bars 50 µm. *n=3* per condition. **(F)** Determination of islet metabolic activity subsequent to a 0.5 X trypsin-EDTA treatment followed by transduction with 20 **PFU/cell**. A MTT assay was performed 4 days post-infection. *n=3-4* per condition. **(G)** Glucose-stimulated insulin secretion was assessed in islet treated with 0.5 X trypsin-EDTA followed by transduction with increasing amount of pHRSIN DUAL-GFP. **(H)** Representative immunofluorescence images of Affi-Gel bead-embedded pancreatic islets 0.5X trypsin-treated and transduced or not with pHRSIN DUAL-GFP. Antibodies against GFP (green) and cleaved Caspase 3 (magenta). Images were captured in samples fixed at 4 days post-infection using confocal fluorescence microscopy. *n=3* per condition. **(I)** Determination of apoptosis rate by quantification of cleaved caspase 3 positive cells in islets 0.5X trypsin-EDTA-treated and transduced or not with pHRSIN DUAL-GFP. *n=3* per condition. Data are represented as the mean ± SEM of *n=3*. * $p < 0.05$ versus control non-transduced 0.5 X trypsin-EDTA treated islets.

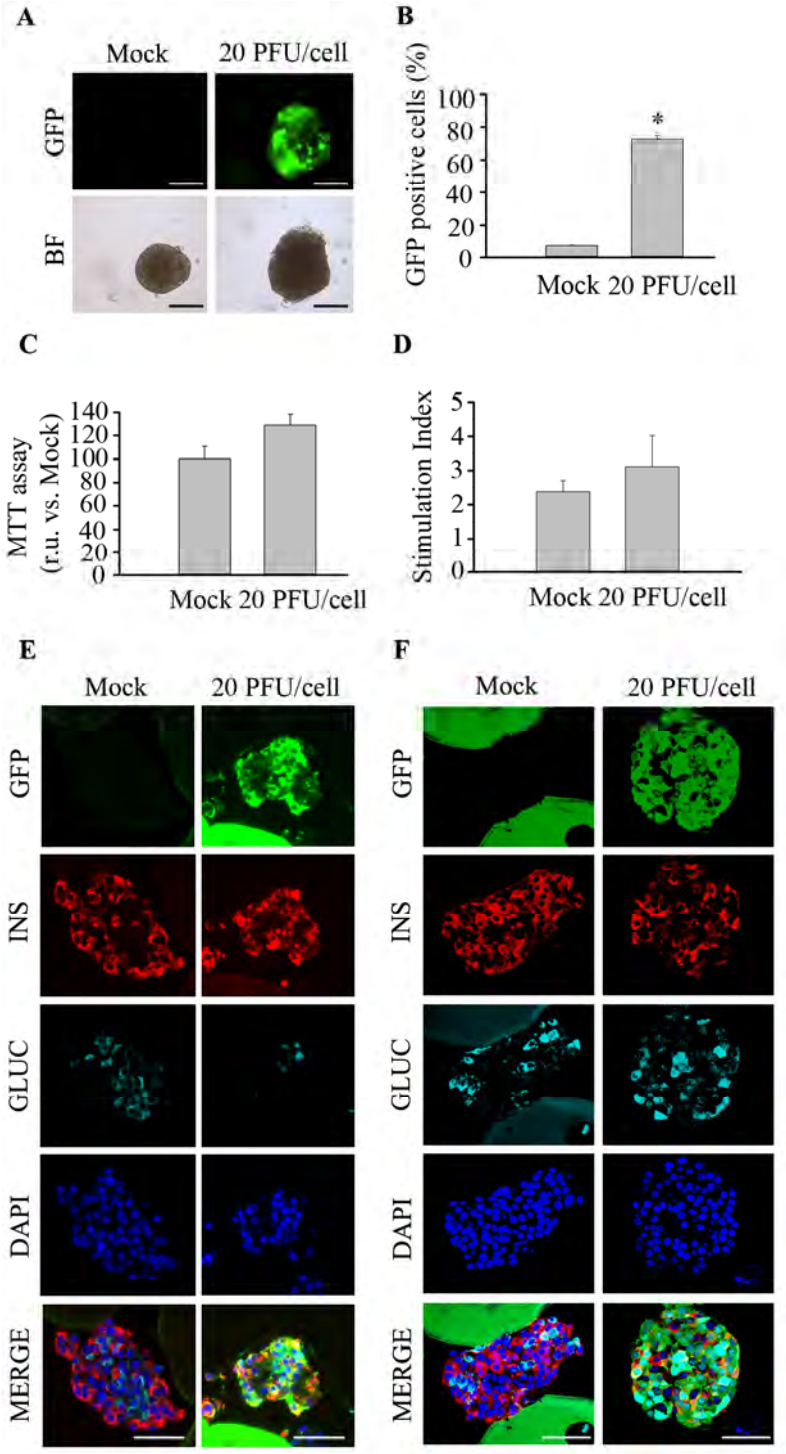

Fig. (5). Human islets are efficiently transduced using the optimized protocol. Human islets obtained from cadaveric donors were initially treated with 0.5 X trypsin-EDTA (250 mg/l trypsin; 0.48 mM EDTA) and then transduced with pHRSIN DUAL-GFP at 20 PFU/cell. **(A)** Live imaging reveals GFP expression in human islets 4 days post-infection: Top; GFP expression, assessed by fluorescence acquisition using an ImageXpress Microsystem, Bottom; Bright field images. Scale-bars 100 µm. *n=3* per condition. **(B)** Transduction efficiency in 0.5 X trypsin-EDTA treated islets was determined by flow cytometry of dispersed islets at 4 days post-transduction with 20 PFU/cell. *n=3* per condition. **(C)** Islet metabolic activity was assessed using the MTT assay. *n=3* per condition. (**D**) Glucose-stimulated insulin secretion was assessed in either control islets or islet treated with 0.5 X trypsin-EDTA followed by transduction with 20 PFU/cell of pHRSIN DUAL-GFP. *n=3* per condition. **(E-F)** Co-immunostaining of GFP (green), insulin (red) and glucagon (cyan) was performed on sections from Affi-Gel bead-embedded human pancreatic islets subsequent to treatment. Images were captured in samples fixed at 4 days post-infection using wide-field fluorescence microscopy (**E**) or confocal microscopy (**F**). Scale-bars 50µm. *n=3* per condition. Data are represented as the mean ± SEM. * $p < 0.05$ versus control non-transduced 0.5 X trypsin-EDTA treated islets.

beneficial, it is of utmost importance to verify that islet function and viability are preserved post-treatment. We also found that time post infection was another critical parameter to the successful outcome of the experiment. Indeed, we established that islet integrity and health is maintained up to 4 days post transduction.

Although islet cell transplantation has demonstrated many clinical successes to date, more work is necessary to further improve its efficacy and universalize this treatment to the vast majority of T1DM patients and to allow long-term insulin independency. From the results shown in this report, we speculate that human islets infected with our protocol may provide a venue to improve health and function prior to transplantation and prevent post-transplantation dismay. Indeed, human islets presented normal metabolic activity and functionality, marked insulin and glucagon expression and normal islet architecture, suggesting that the proposed protocol for islet infection does not compromise human islet health. Therefore, lentiviral-mediated gene expression modulation using this protocol could be therapeutically promising to generate a functional and stable islet transplanted mass in humans.

CONCLUSION

Here we present a protocol that represents a reliable easy-to-use procedure to transduce efficiently human and mouse islets with the dual purpose of studying the impact of therapeutic genes in islet physiology and ultimately facilitating the universalization of islet infection prior transplantation. The stable integrating nature of lentiviral vectors supports the notion that lentiviral-mediated gene transfer might be an optimal method to improve islet function for the treatment of T1DM [40]. In this sense, the value of potential benefits based on the modulation of gene expression in entire islets warrants further experimentation to determine the applicability of our protocol for islet infection prior transplantation.

LIST OF ABREVIATIONS

BSA	=	Bovine Serum Albumin
CM	=	Complete Media
GOI	=	Gene Of Interest
KRBH	=	Krebs-Ringer bicarbonate-HEPES buffer
PFU/cell	=	Plaque Forming Units per cell
PBS	=	Phosphate Buffered Saline
T1DM	=	Type 1 Diabetes Mellitus
T2DM	=	Type 2 Diabetes Mellitus
Ubi	=	Ubiquitin

CONFLICT OF INTEREST

The authors confirm that this article content has no conflict of interest.

ACKNOWLEDGEMENTS

This work was funded by grants from the Consejería de Salud, Fundación Pública Andaluza Progreso y Salud, Junta de Andalucía (PI-0727-2010 to B.R.G.), Consejería de Economía, Innovación y Ciencia (P10.CTS.6359 to B.R.G.) and the Ministerio de Economía y Competitividad, Instituto de Salud Carlos III co-funded by Fondos FEDER (PI10/00871 and PI13/00593 to B.R.G). A.M-M. is a recipient of a Miguel Servet grant (CP14/00105) from the Instituto de Salud Carlos III co-funded by Instituto de Salud Carlos III and FEDER. N.C.V is supported by a JDRF subsidy (17-2013-372 to B.R.G.). Human islets were provided through the JDRF award 31-2012-783 (ECIT Islet for Basic Research program). We thank Cindy Cruz-Zambrano at the CABIMER Histology Core Facility for excellent technical assistance in embedding and sectioning of islet samples. We thank I. Cózar for kindly providing the protocol for islet embedding. We thank Dr. Collins and Dr. Pintor-Toro for kindly providing the pHRSIN-DUAL-GFP lentiviral vector.

CM J-M, IG H-G, L L-N, PI L, N C-V, E F-M, JM M-G and A M-M performed the experiments; G P and D B isolated and provided human pancreatic islets. CM J-M, BR G and A M-M designed the study and wrote the manuscript.

SUPPLEMENTARY MATERIAL

Supplementary material is available on the publishers Web site along with the published article.

REFERENCES

[1] Atlas, I (2014). IDF Atlas. vol. March12th 2014: http://www.idf.org/diabetesatlas.

[2] Lipman, TH, Levitt Katz, LE, Ratcliffe, SJ, *et al.* (2013). Increasing incidence of type 1 diabetes in youth: twenty years of the Philadelphia Pediatric Diabetes Registry. *Diabetes care* **36**: 1597-1603.

[3] Tisch, R, and Wang, B (2008). Dysrulation of T cell peripheral tolerance in type 1 diabetes. *Advances in immunology* **100**: 125-149.

[4] Redondo, MJ, and Eisenbarth, GS (2002). Genetic control of autoimmunity in Type I diabetes and associated disorders. *Diabetologia* **45**: 605-622.

[5] Roglic, G, and Unwin, N (2010). Mortality attributable to diabetes: estimates for the year 2010. *Diabetes Res Clin Pract* **87**: 15-19.

[6] Ludwig, B, Reichel, A, Kruppa, A, Ludwig, S, *et al.* (2015). Islet transplantation at the Dresden diabetes center: five years' experience. *Horm Metab Res = Horm- und Stoffwechselforschung = Horm et metab* **47**: 4-8.

[7] Ryan, EA, Paty, BW, Senior, PA, Bigam, D, *et al.* (2005). Five-year follow-up after clinical islet transplantation. *Diabetes* **54**: 2060-2069.

[8] Johansson, H, Lukinius, A, Moberg, L, Lundgren, T, *et al.* (2005). Tissue factor produced by the endocrine cells of the islets of Langerhans is associated with a negative outcome of clinical islet transplantation. *Diabetes* **54**: 1755-1762.

[9] Saito, Y, Goto, M, Maya, K, Ogawa, N, *et al.* (2010). Brain death in combination with warm ischemic stress during isolation procedures induces the expression of crucial inflammatory mediators in the isolated islets. *Cell transplant* **19**: 775-782.

[10] Shapiro, AM, Lakey, JR, Ryan, EA, Korbutt, GS, *et al.* (2000). Islet transplantation in seven patients with type 1 diabetes mellitus using a glucocorticoid-free immunosuppressive regimen. *New Eng j med* **343**: 230-238.

[11] Tjernberg, J, Ekdahl, KN, Lambris, JD, *et al.* B (2008). Acute antibody-mediated complement activation mediates lysis of pancreatic islets cells and may cause tissue loss in clinical islet transplantation. *Transplantation* **85**: 1193-1199.

[12] Hwang, HJ, Lee, M, Park, JH, Jung, *et al.* (2015). Improved islet transplantation outcome by the co-delivery of siRNAs for iNOS and 17beta-estradiol using an R3V6 peptide carrier. *Biomaterials* **38**: 36-42.

[13] Wu, H, Panakanti, R, Li, F, and Mahato, RI (2010). XIAP gene expression protects beta-cells and human islets from apoptotic cell death. *Mol pharma* **7**: 1655-1666.

[14] Barbu, AR, Bodin, B, Welsh, M, Jansson, L, and Welsh, N (2006). A perfusion protocol for highly efficient transduction of intact pancreatic islets of Langerhans. *Diabetologia* **49**: 2388-2391.

[15] Bilbao, G, Contreras, JL, Dmitriev, I, Smyth, CA, *al.* (2002). Genetically modified adenovirus vector containing an RGD peptide in the HI loop of the fiber knob improves gene transfer to nonhuman primate isolated pancreatic islets. *American journal of transplantation : off j Am Soc Transplant Am Soc Transplant Surgeons* **2**: 237-243.

[16] Gallichan, WS, Kafri, T, Krahl, T, *et al.* (1998). Lentivirus-mediated transduction of islet grafts with interleukin 4 results in sustained gene expression and protection from insulitis. *Human gene therapy* **9**: 2717-2726.

[17] Giannoukakis, N, Mi, Z, Gambotto, A, Eramo, M, *et al.* (1999). Infection of intact human islets by a lentiviral vector. *Gene ther* **6**: 1545-1551.

[18] Leibowitz, G, Beattie, GM, Kafri, T, Cirulli, V, *et al.* (1999). Gene transfer to human pancreatic endocrine cells using viral vectors. *Diabetes* **48**: 745-753.

[19] Rodriguez Rilo, HL, Paljug, WR, Lakey, JR, *et al.* (1998). Biolistic bioengineering of pancreatic beta-cells with fluorescent green protein. *Transplantation proceedings* **30**: 465-468.

[20] Mahato, RI, Henry, J, Narang, AS, Sabek, O, *et al.* (2003). Cationic lipid and polymer-based gene delivery to human pancreatic islets. *Mol ther : j Am Soc Gene Ther* **7**: 89-100.

[21] Bartlett, R, Denis, M, *et al.* (1998). Introduction of immunomodulatory genes into isolated pancreatic islets via biolistic particle bombardment. *Transpl proceedings* **30**: 452.

[22] Levine, F (1997). Gene therapy for diabetes: strategies for beta-cell modification and replacement. *Diabetes/metab rev* **13**: 209-246.

[23] Takahashi, R, Ishihara, H, Takahashi, K, Tamura, A, *et al.* (2007). Efficient and controlled gene expression in mouse pancreatic islets by arterial delivery of tetracycline-inducible adenoviral vectors. *J mol endocrin* **38**: 127-136.

[24] Lefebvre, B, Vandewalle, B, Longue, J, Moerman, E, *et al.* (2010). Efficient gene delivery and silencing of mouse and human pancreatic islets. *BMC biotechno* **10**: 28.

[25] Kvell, K, Nguyen, TH, Salmon, P, Glauser, F, M, *et al.* (2005). Transduction of CpG DNA-stimulated primary human B cells with bicistronic lentivectors. *Mol ther : j Am Soc Gene Ther* **12**: 892-899.

[26] Rajalingam, K, Al-Younes, H, Muller, A, *et al.* (2001). Epithelial cells infected with Chlamydophila pneumoniae (Chlamydia pneumoniae) are resistant to apoptosis. *Infection and immunity* **69**: 7880-7888.

[27] Diraison, F, Motakis, E, Parton, LE, Nason, *et al.* (2004). Impact of adenoviral transduction with SREBP1c or AMPK on pancreatic islet gene expression profile: analysis with oligonucleotide microarrays. *Diabetes* **53 Suppl 3**: S84-91.

[28] Hughes, A, Jessup, C, Drogemuller, C, *et al.* (2010). Gene therapy to improve pancreatic islet transplantation for Type 1 diabetes mellitus. *Curr diabetes rev* **6**: 274-284.

[29] Worldwide, GTCT (2014). Gene Therapy Clinical Trials Worldwide. vol. 2014: http://www.abedia.com/wiley/vectors.php.

[30] Farinelli, G, Capo, V, Scaramuzza, S, and Aiuti, A (2014). Lentiviral vectors for the treatment of primary immunodeficiencies. *J inherited metab disease* **37**: 525-533.

[31] Kobinger, GP, Deng, S, Louboutin, JP, Vatamaniuk, M, *et al.* (2004). Transduction of human islets with pseudotyped lentiviral vectors. *Human gene ther* **15**: 211-219.

[32] Fenjves, ES, Ochoa, MS, Cechin, S, *et al.* (2008). Protection of human pancreatic islets using a lentiviral vector expressing two genes: cFLIP and GFP. *Cell transplantation* **17**: 793-802.

[33] Chou, FC, and Sytwu, HK (2009). Overexpression of thioredoxin in islets transduced by a lentiviral vector prolongs graft survival in autoimmune diabetic NOD mice. *J biomed sci* **16**: 71.

[34] Brun, T, Franklin, I, St-Onge, L, Biason-Lauber, A, *et al.* (2004). The diabetes-linked transcription factor PAX4 promotes {beta}-cell proliferation and survival in rat and human islets. *J cell biol* **167**: 1123-1135.

[35] Moreno-Mateos, MA, Espina, AG, Torres, B, *et al.* (2011). PTTG1/securin modulates microtubule nucleation and cell migration. *Mol biol cell* **22**: 4302-4311.

[36] Cozar-Castellano, I, Takane, KK, Bottino, R, (2004). Induction of beta-cell proliferation and retinoblastoma protein phosphorylation in rat and human islets using adenovirus-mediated transfer of cyclin-dependent kinase-4 and cyclin D1. *Diabetes* **53**: 149-159.

[37] Dittmar, R, Potier, E, van Zandvoort, M, *et al.* (2012). Assessment of cell viability in three-dimensional scaffolds using cellular auto-fluorescence. *Tissue engineering Part C, Methods* **18**: 198-204.

[38] Nicolau, C, Le Pape, A, Soriano, P, *et al.* (1983). *In vivo* expression of rat insulin after intravenous administration of the liposome-entrapped gene for rat insulin I. *PNAS USA* **80**: 1068-1072.

[39] Li, W, Wu, W, Song, H, Wang, F, Li, H, Chen, L, *et al.* (2014). Targeting Nrf2 by dihydro-CDDO-trifluoroethyl amide enhances autophagic clearance and viability of beta-cells in a setting of oxidative stress. *FEBS lett* **588**: 2115-2124.

[40] Jiang, H, Hester, G, Liao, L, *et al.* (2011). Mechanisms by which HIV envelope minimizes immunogenicity. *Immunologic res* **49**: 147-158.

Received: February 06, 2014 **Revised: June 08, 2015** **Accepted: June 16, 2015**

SCIENTIFIC REPORTS

OPEN

PAX4 Defines an Expandable β-Cell Subpopulation in the Adult Pancreatic Islet

Received: 22 June 2015
Accepted: 01 October 2015
Published: 27 October 2015

Petra I. Lorenzo[1], Esther Fuente-Martín[1], Thierry Brun[2], Nadia Cobo-Vuilleumier[1], Carmen María Jimenez-Moreno[1], Irene G. Herrera Gomez[1], Livia López Noriega[1], José Manuel Mellado-Gil[1], Alejandro Martin-Montalvo[1], Bernat Soria[3,4] & Benoit R. Gauthier[1]

PAX4 is a key regulator of pancreatic islet development whilst in adult acute overexpression protects β-cells against stress-induced apoptosis and stimulates proliferation. Nonetheless, sustained PAX4 expression promotes β-cell dedifferentiation and hyperglycemia, mimicking β-cell failure in diabetic patients. Herein, we study mechanisms that allow stringent PAX4 regulation endowing favorable β-cell adaptation in response to changing environment without loss of identity. To this end, PAX4 expression was monitored using a mouse bearing the enhanced green fluorescent protein (GFP) and cre recombinase construct under the control of the islet specific pax4 promoter. GFP was detected in 30% of islet cells predominantly composed of PAX4-enriched β-cells that responded to glucose-induced insulin secretion. Lineage tracing demonstrated that all islet cells were derived from PAX4$^+$ progenitor cells but that GFP expression was confined to a subpopulation at birth which declined with age correlating with reduced replication. However, this GFP$^+$ subpopulation expanded during pregnancy, a state of active β-cell replication. Accordingly, enhanced proliferation was exclusively detected in GFP$^+$ cells consistent with cell cycle genes being stimulated in PAX4-overexpressing islets. Under stress conditions, GFP$^+$ cells were more resistant to apoptosis than their GFP$^-$ counterparts. Our data suggest PAX4 defines an expandable β-cell sub population within adult islets.

During embryogenesis, both the exocrine and endocrine compartment of the pancreas arises through the interplay of numerous transcription factors that will temporally and spatially bestow the fate of the various cell lineages[1]. Among these, the paired homeodomain nuclear factor Pax4 is indispensable for the generation of islet cell progenitors and subsequent β-cell maturation. Although detectable, PAX4 expression in adult islet β-cells is low as compared to its embryonic expression[2]. In contrast, aberrantly high expression levels for this transcription factor are detected in human insulinomas, lymphomas, head and neck squamous cell carcinomas as well as in breast cancer cells[3–5]. A distinctive attribute of *Pax4* is that mutations and polymorphisms in this gene are associated with both Type 1 and 2 Diabetes Mellitus (T1DM and T2DM), as well as with maturity onset diabetes of the young (MODY) in several ethnic populations[2], with a strong prominence in the Asian population[6–11]. *Pax4* gene variations also predispose to Ketosis-prone diabetes in populations of West African ancestry[12]. Paradoxically, *Pax4* polymorphisms were also linked to longevity in the Korean population[13].

[1]Pancreatic Islet Development and Regeneration Unit, Department of Stem Cells, CABIMER-Andalusian Center for Molecular Biology and Regenerative Medicine, Seville, Spain. [2]Department of Cell Physiology and Metabolism, University of Geneva, Geneva, Switzerland. [3]Cellular Therapy of Diabetes Mellitus and its Complications, Department of Stem Cells, CABIMER-Andalusian Center for Molecular Biology and Regenerative Medicine, Seville, Spain;. [4]CIBERDEM, Instituto Carlos III, Madrid, Spain. Correspondence and requests for materials should be addressed to P.I.L. (email: petra.lorenzo@cabimer.es) or B.R.G. (email: benoit.gauthier@cabimer.es)

Since a hallmark of both T1DM and T2DM, independent of etiology, is the gradual loss of the functional insulin-producing β-cell mass, we and others have demonstrated that PAX4 is not only essential for islet development[14] but also for survival and expansion of adult β-cells[15,16]. In mice, conditional overexpression of PAX4 in β-cells was shown to protect animals against streptozotocin (STZ)-induced hyperglycemia and isolated islets against cytokines induced apoptosis. In contrast, animals expressing the diabetes-linked mutant variant R121W (R129W in mice) were more susceptible to develop hyperglycemia and β-cell death upon STZ treatment. Interestingly, sustained expression of PAX4 *in vivo* resulted in loss of islet structure and insulin secretion with the concomitant appearance of a $BrdU^+/PDX1^+/INSULIN^-$ cell subpopulation suggesting dedifferentiation of β-cells that potentially acquire a proliferative phenotype[17]. Intriguingly, β-cell dedifferentiation characterized by the loss of INSULIN granules and re-expression of the pancreatic endocrine progenitor marker NGN3 was also recently reported in various animal models of T2DM[18,19]. Restoration of functional β-cells was achieved upon normalization of blood glucose levels using insulin therapy indicating that the hyperglycaemic milieu favoured survival through loss of β-cell identity at the expense to attempt rescuing glucose homeostasis[19]. The potential implication of PAX4 in this process was recently connoted through data demonstrating that transcript levels for this factor were increased in islets isolated from T2DM donors[20]. The correlation between PAX4 expression levels and the phenotypic state of β-cells led us to characterize *in vivo* PAX4 regulation within the islets under various physiological and pathophysiological conditions. To this end, we took advantage of a transgenic mouse model expressing both the enhanced green fluorescence protein (GFP) and the *Cre* recombinase under the control of the pancreatic islet specific *Pax4* gene promoter region[21] to monitor in real time the endogenous expression pattern of PAX4 under various metabolic conditions. We demonstrate that within mature islets endogenous PAX4 marks predominantly a subset of islet β-cells, which on one hand is more susceptible to expansion in response to increased insulin demands such as pregnancy, while on the other hand, is more resistant to stress-induced apoptosis.

Results

PAX4 is heterogeneously expressed within adult mice pancreatic islet cells. Previous studies performed *in vitro* as well as *in vivo* have shown that acute PAX4 expression is important for β-cell survival and/or expansion while chronic expression triggers dedifferentiation and tumour formation[3–5,15,17,22]. In order to elucidate the mechanism by which β-cells fine tune PAX4 expression without shedding identity and ultimately inducing hyperglycemia we took advantage of a transgenic mouse model expressing both the *Gfp* and the *Cre* cDNAs under the transcriptional control of an optimal *Pax4* gene promoter sequence (pPax4-*Cre*-IRES-*Egfp* mice)[23]. The latter minimal promoter fragment was shown to direct islet specific expression of the *pax4* gene mimicking the full-length promoter[21,24]. The pPax4-*Cre*-IRES-*Egfp* transgenic animals display normal islet architecture as well as glucose homeostasis during their life span thereby providing a powerful model to monitor endogenous levels of PAX4 through GFP fluorescence. Live imaging of whole islets derived from these mice revealed that only a fraction of cells emitted detectable levels of GFP fluorescence, revealing potential cell heterogeneity in PAX4 expression (Fig. 1a). To validate this premise, cell suspensions were prepared from islets derived from either wild type C57BL/6 or pPax4-*Cre*-IRES-*Egfp* mice and the various cell populations were discriminated by size or complexity against fluorescence intensity using flow cytometry (Fig. 1b). This approach revealed that $14.79 \pm 4.06\%$ of total islet cells expressed GFP whereas $25.48 \pm 6.57\%$ of the total β-cell population expressed GFP (Fig. 1c). Despite GFP expression only in a subset of islet cells, genomic amplification confirmed transgene integration in both GFP^+ and GFP^- subpopulations reinforcing the premise that the *Pax4* gene promoter driving GFP expression was only active in a subpopulation of islet cells (Fig. 1d). Consistent with the latter, endogenous *Pax4* transcript levels were 5-fold enriched in the GFP^+ cell subpopulation (Fig. 1e). Of note, the average Ct value of Pax4 in GFP^+ cells was approximately 29 while the Ct values for the Cyclophilin control gene was 22. Henceforth, this cell population will be denoted as $GFP/PAX4^+$. In order to further characterize this $GFP/PAX4^+$ subpopulation, we next assess expression levels of the β-cell markers Pdx1 and Insulin. Transcript levels for either gene remained relatively constant in both subpopulations (Fig. 1e). Consistent with the latter, immunostaining of PDX1 revealed expression of the transcription factor in the vast majority of $GFP/PAX4^+$ cells as well as in the GFP^- cells (Supplementary Fig. S1). As DNA methylation is associated with transcriptional silencing of *Pax4*[3,20], we assessed the methylation status of the 11 GpC sites found within the 409 bp promoter region (Fig. 1f). This region was hypomethylated in both the $GFP/PAX4^+$ and GFP^- subpopulations as well as in MIN6 cells that expressed high levels of PAX4 (Fig. 1f). Thus the methylation profile cannot account for differential GFP expression within the two subpopulations. Interestingly, both $GFP/PAX4^+$ and GFP^- subpopulations displayed similar insulin secretion in response to glucose alone or in combination with IBMX/forskolin indicating that GFP/PAX4-expressing cells retained functionality under normal physiological conditions (Fig. 1g). Taken together these data suggest that PAX4 expression is restricted to a subpopulation of cells phenotypically and functionally similar to β-cells.

PAX4 expression is gradually confined to a subset of islet cells with age, correlating with decreased proliferation. To assess in more detail the spatial distribution as well as to determine the specific cell types expressing GFP within islets, we performed immunohistochemistry analysis of pancreas sections derived from pPax4-*Cre*-IRES-*Egfp* adult mice (Fig. 2). Co-immunostaining using an

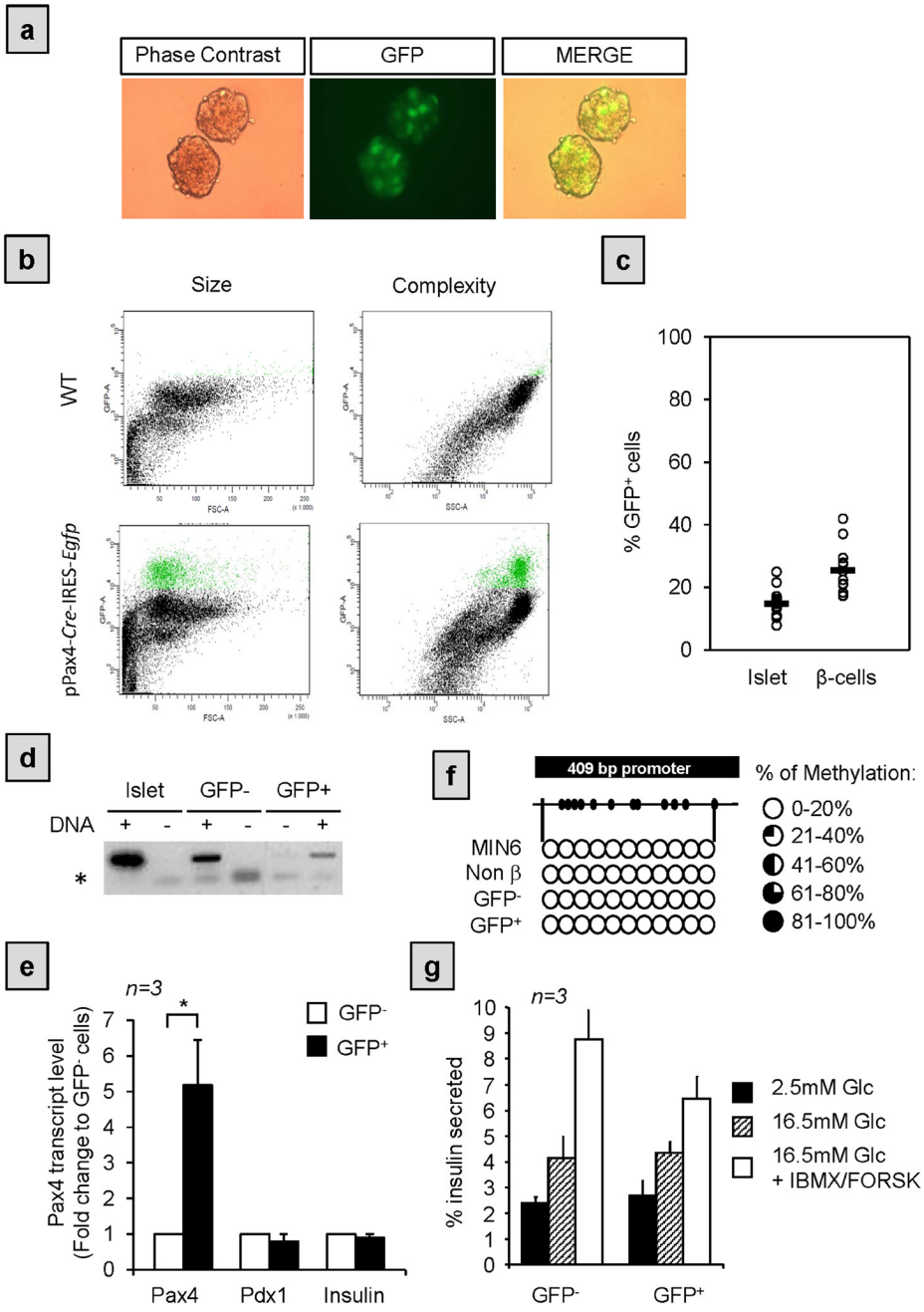

Figure 1. GFP is expressed in a subset of islet cells that are enriched in Pax4 mRNA. (**a**) Phase contrast and fluorescence microscopy images of intact live islets isolated from pPax4-*Cre*-IRES-*Egfp* mice showing GFP fluorescence only in a subset of islet cells. (**b**) Representative cytometer plots corresponding to dispersed adult islets from C57BL/6 wild type (WT)(upper panels) and pPax4-*Cre*-IRES-*Egfp* (lower panels) mice. Plots represent GFP fluorescence (Y axis) vs. cell size (X axis left plots) or cell complexity (X axis right plots). GFP expressing cells (green) display similar size and complexity as the β-cells. (**c**) Quantification of the cytometry analysis. Each dot corresponds to an independent analysis using islet pools from at least 3 animals and presented either per islet or per β-cell population. (**d**) Agarose gel electrophoresis of PCR-amplified *gfp* fragment confirming transgene insertion in both GFP^+ and GFP^- islet cell populations (DNA +). Negative controls for PCR are indicated as DNA -. Non-specific primer-dimers are denotes as *. (**e**) Fold change in Pax4, Pdx1 and Insulin transcript levels in sorted GFP^+ cells relative to the levels detected in the GFP^- fraction. *T-Student: $p < 0.05$. (**f**) Bisulfite sequencing analysis of the 409 bp *pax4* gene promoter region. The analysis was performed in parallel in MIN6 cells and in the different sorted islet cell populations, showing in all of them less than 20% methylation for each of the CpG sites. (**g**) Insulin secretion was assessed in 30 min static incubations in response to 2.5 mM (black bars) and 16.5 mM glucose alone (hashed bars) or in combination with 1 μM IBMX/forskolin (white bars). Insulin released was quantified by ELISA and expressed as a percentage of total cellular insulin content. Results are the mean ± SE from 3 independent experiments conducted on either GFP^+ or GFP^- pooled fractions, performed in duplicates.

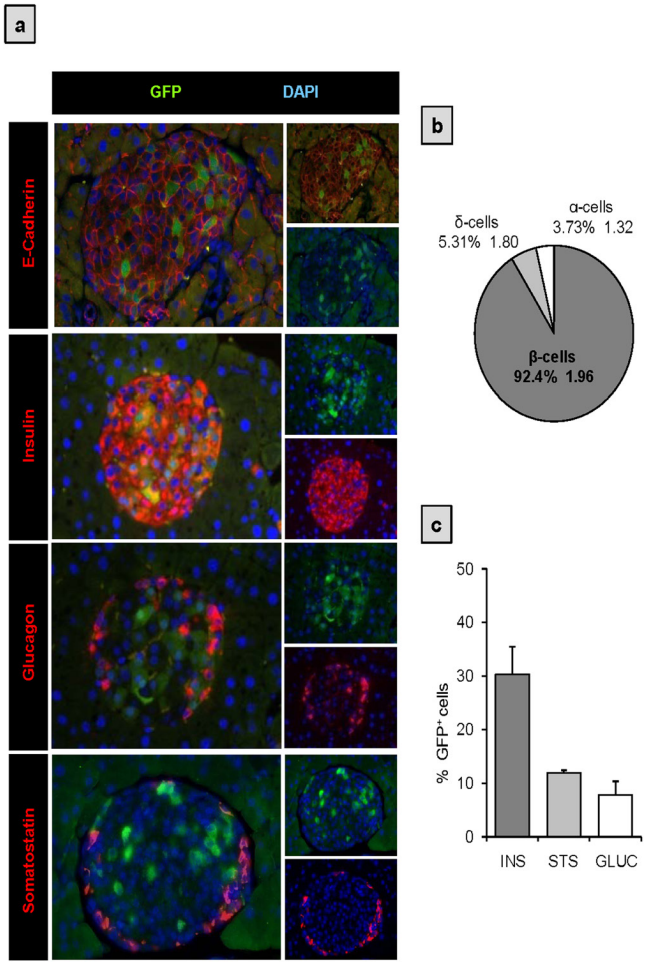

Figure 2. GFP expression predominantly co-localizes with insulin-producing β-cells in adult islets. (**a**) Immunohistochemistry analysis of paraffin sections from adult pPax4-*Cre*-IRES-*Egfp* mice pancreas. Representative microscopy images for co-immunofluorescent labeling of GFP (green) together with E-CADHERIN (for cellular delimitation) or with the pancreatic islet cell markers INSULIN (red), GLUCAGON (red) or SOMATOSTATIN (red). Nuclei counterstaining was performed using DAPI (blue). (**b**) Quantitative analysis (average ± SE) of the GFP^+ cell population composition. (**c**) Quantification of the percentage of $INSULIN^+$, $GLUCAGON^+$ and $SOMATOSTATIN^+$ cells that co-express GFP (average ± SE). Sections (2 to 4) from 3 to 5 independent animals with an average of 15 islets and 1400 cells per animal were used for quantifications.

antibody against the cell membrane protein E-CADHERIN along with an anti-GFP sera, clearly established the presence of a GFP/$PAX4^+$cell subset randomly distributed within islets (Fig. 2a). Analysis of GFP co-expression with markers of different islet cell types revealed that more than 90% of the GFP/$PAX4^+$ subpopulation were insulin-expressing cells (Fig. 2a,b) and comprised approximately 30% of the total β-cell population (Fig. 2c). However, 3.73 ± 1.32% and 5.31 ± 1.80% of GFP/$PAX4^+$ cells co-immunostained for GLUCAGON and SOMATOSTATIN respectively (Fig. 2a,b), representing roughly 6% and 10% of the total α- and δ-cell populations (Fig. 2c).

To determine the fate of GFP/$PAX4^+$ cells after birth, we performed lineage-tracing experiments. To this end, pPax4-*Cre*-IRES-*Egfp* mice were crossed to mice carrying the *Rosa26*;lox-stop-lox;*LacZ* reporter (R26R). In double transgenic animals (pPax4-*Cre*-IRES-*Egfp*;R26R), Pax4 promoter driven expression of CRE should result in the excision of the lox-stop-lox cassette hence permanently activating the *LacZ* gene in all PAX4-expressing cells along with their downstream progeny. Accordingly, β-Galactosidase (β-Gal) staining was detected in all islet cells at postnatal day 1 (P1) and remained constant until the age of 53 weeks (Fig. 3a, upper panels). Reciprocally, INSULIN, GLUCAGON and SOMATOSTATIN co-localized with β-Gal (Fig. 4a) substantiating previous findings that PAX4 expression is induced early on during development in endocrine progenitors that give rise to all islet cells[25]. These results also demonstrate that despite possible limitations of minimal promoter studies, the *pax4* gene promoter used in this transgenic mouse model is sufficient to recapitulate endogenous PAX4 expression during pancreas development and in adulthood. In contrast to β-Gal staining throughout the whole islet, GFP expression was detected

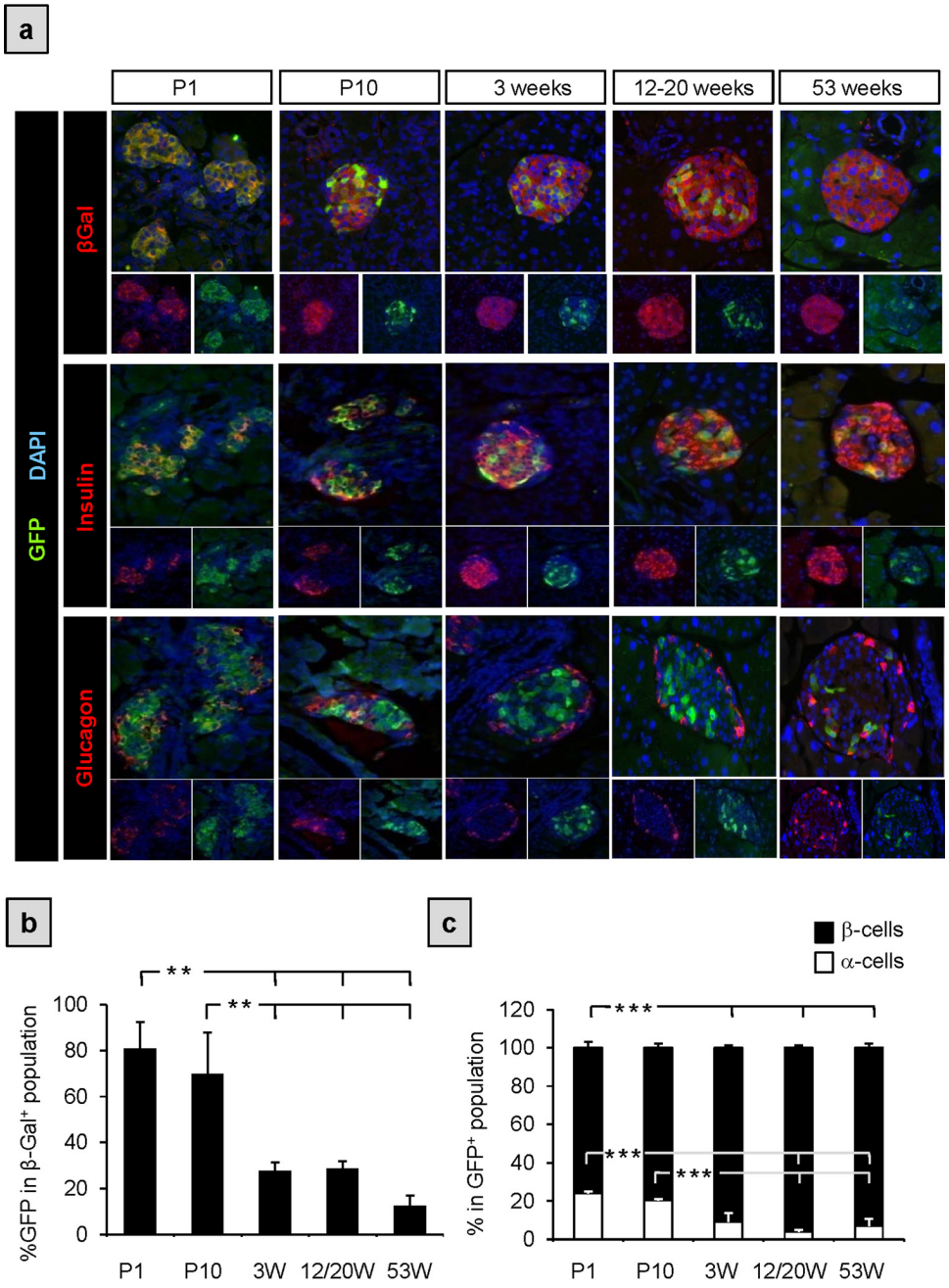

Figure 3. Lineage tracing analysis reveals an age dependent decrease in the GFP/Pax4$^+$subpopulation. (**a**) Representative images from IHC of paraffin sections of pPax4-*Cre*-IRES-*EgfpXRosa26*;lox-stop-lox;*LacZ* mice at the indicated ages. Co-immunodetection of GFP (green) along with β-GAL (red, upper panels), INSULIN (red middle panels) or GLUCAGON (red lower panels). Nuclei counterstaining was performed using DAPI (blue). (**b**) Quantification of β-Gal cells that co-express GFP at the indicated ages (average ± SE). (**c**) Quantitative analysis (average ± SE) of GFP$^+$ cells within the β- and α-cell populations. Sections (2 to 4) from 3 to 5 animals with an average of 10 islets and 900 cells per animal were used for quantifications. **ANOVA:$p < 0.01$; ***ANOVA:$p < 0.001$.

in approximately 70 to 80% of these cells at P1 as well as P10 and was thereafter restricted to 30% of β-Gal$^+$ cells by the age of 3-weeks (Fig. 3a,b). This fraction of GFP/PAX4$^+$ cells remained relatively constant during adulthood until the age of 1 year (53 weeks) at which point GFP expression was further reduced to 15% of β-Gal$^+$ cells (Fig. 3a,b). Noteworthy, this decrease in GFP/PAX4$^+$ population correlated with the age-dependent reduction in the ratio of proliferating islet cells, from 6.37 ± 1.97% at P10 to 0.81 ± 0.27% in adult mice and further decrease to 0.6 ± 0.1% in aged animals (data not shown). As expected, INSULIN$^+$ cells encompassed the majority of the GFP/PAX4$^+$ population during adulthood (Fig. 3a,c). However during early postnatal stages, P1 and P10, the percentage of GFP/PAX4$^+$

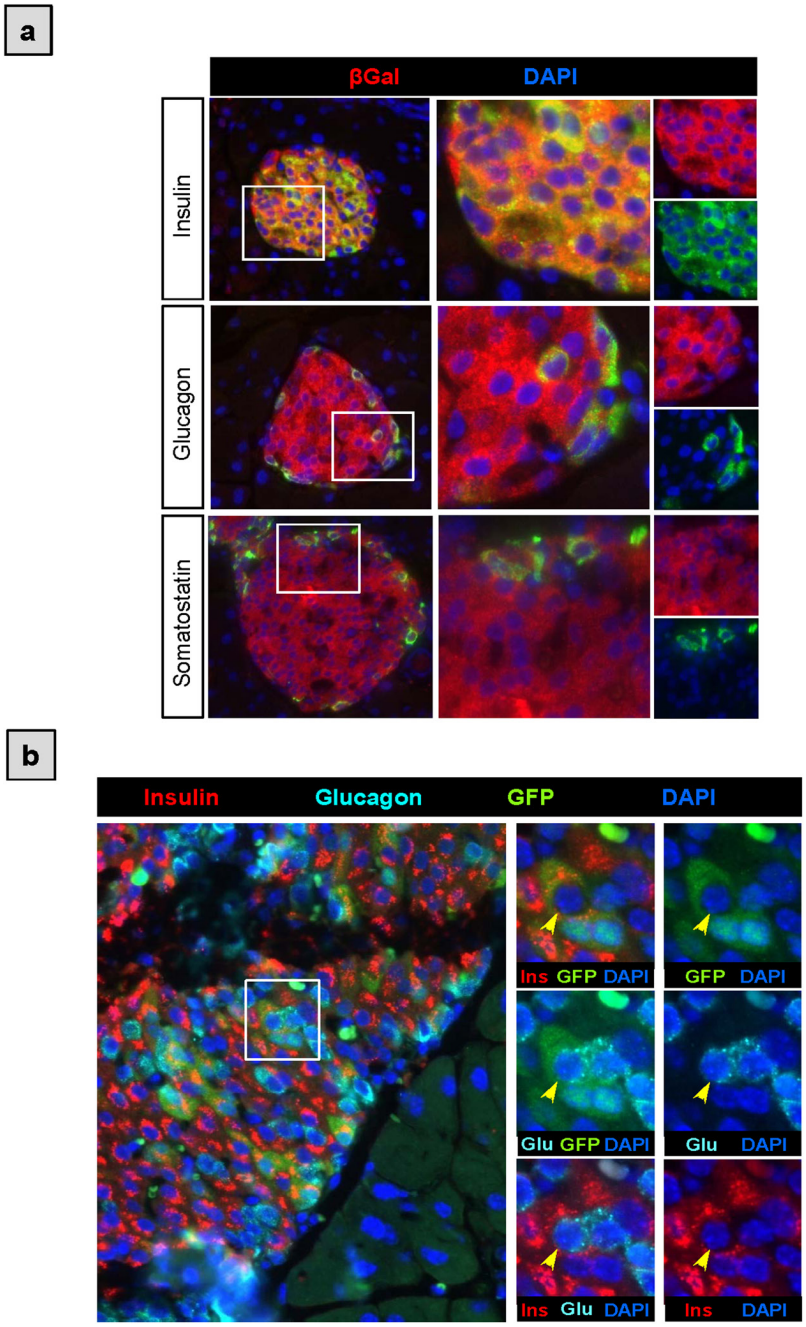

Figure 4. GFP/PAX4$^+$ cells contribute to all endocrine cell progeny. (**a**) Co-immunohistochemical analysis of β-Gal (red) along with INSULIN, GLUCAGON and SOMATOSTATIN (green) on pancreatic paraffin sections from adult pPax4-*Cre*-IRES-*Egfp*X*Rosa26*;lox-stop-lox;*LacZ* mice. Nuclei were stained with DAPI (blue). (**b**) Triple-immunostaining for INSULIN (red) GLUCAGON (cian) and GFP (green). Inset with yellow arrows delineate a representative GFP/PAX4$^+$ cell co-expressing INSULIN and GLUCAGON. Nuclei were stained with DAPI (blue).

cells that co-express GLUCAGON was approximately 20%, decreasing with maturity to approximately 3% in adult animals (Fig. 3a,c). Of note, we also detected rare glucagon/insulin co-expressing GFP/PAX4$^+$ cells (Fig. 4b) indicative of either an early bi-hormonal precursor pool or trans-differentiation of GLUCAGON/GFP/PAX4$^+$ cells towards a β-cell phenotype. Together, these lineage-tracing experiments show that PAX4 gives rise to all endocrine cells during development and that its expression subsequently becomes restricted to a fraction of islet cells predominantly composed of β-cells with residual expression in some α- and δ-cells as well as in rare bi-hormonal (GLUCAGON/INSULIN) expressing cells.

Symbol	Gene Description	fold change	p value
Errfi1	ERBB receptor feedback inhibitor 1	2.254	0.020
Cdkn1a	cyclin-dependent kinase inhibitor 1A (p21)	1.956	0.011
Ccnb2	cyclin B2	1.478	0.012
Ccna2	cyclin A2	1.447	0.001
Myc	myelocytomatosis oncogene	1.412	0.003
Cdk5	cyclin-dependent kinase 5	1.368	0.002
Trp53	transformation related protein 53	1.361	0.013
Ccnd3	cyclin D3	1.339	0.034
Ccnd1	cyclin D1	1.275	0.026
Hdac1	histone deacetylase 1	1.272	0.042
Pcna	proliferating cell nuclear antigen	1.271	0.032
Otub2	OTU domain, ubiquitin aldehyde binding 2	1.262	0.047

Table 1. Significantly up-regulated cell cycle genes after Pax4 overexpression.

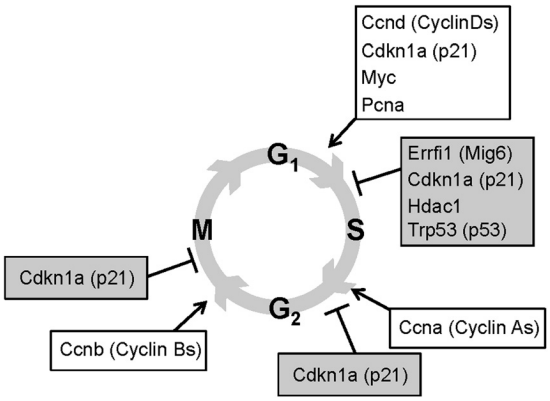

Figure 5. PAX4 regulates cell cycle genes. Schematic representation of PAX4 regulated cell cycle activators (white boxes) and inhibitors (grey boxes) as determined by RNA microarray analysis performed on PAX4 overexpressing islets (GSE62846).

PAX4 primes cell cycle genes correlating with the preferential expansion of the GFP/PAX4$^+$ cell subset during pregnancy. The fraction of replicative β-cells drastically decreases with age correlating with the observed decline in GFP/PAX4$^+$cells (Fig. 3). The association of these two events combined with our previous finding that PAX4 induces cell replication[15] prompt us to investigate whether the GFP/PAX4$^+$ subpopulation could represent the β-cell replicative unit of the islet. A recent gene expression analysis conducted on PAX4 overexpressing islets revealed a significant functional enrichment in the cell cycle pathway. A more detailed *in silico* gene analysis within this pathway disclosed that PAX4 induced the expression of both cell cycle activators such as CYCLIN A2, B2, D1 and D3, CMYC, HDAC and PCNA as well cell cycle inhibitors such as P21, P53, OTUB2 and ERRFI1 (Table 1). These data suggest that PAX4 defines a proliferation permissive β-cell subpopulation primed to expansion only under conditions that alleviate cell cycle brakes (Fig. 5). To validate this hypothesis, we assessed the replicative capacity as well as expansion of the GFP/PAX4$^+$ islet cell subset during pregnancy, a physiological condition associated with intense β-cell replication[26]. Immunohistochemical analysis, using antibodies against GFP, INSULIN and GLUCAGON, were performed on pancreas sections derived from pregnant pPax4-*Cre*-IRES-*Egfp* mice sacrificed at 10.5, 12.5, 14.5 and 17.5 days *post coitum* (*dpc*) (Fig. 6). In agreement with previous studies[27], islet-cell proliferation peaked at 12.5 *dpc* (Fig. 6e). Consistent with the latter, a significant transient increase in the overall number of GFP/PAX4$^+$ cells was observed, reaching 45 ± 3% of total islet cell population by 12.5 *dpc* and decreasing thereafter to 19 ± 1% by 17.5 *dpc* (Fig. 6a,b). Accordingly, 52 ± 3% of β-cells were GFP/PAX4$^+$ while 20 ± 6% of α-cells expressed GFP by 12.5 *dpc* (Fig. 6a,b). Consistent with the expansion of the GFP/PAX4$^+$ cell subpopulation, a

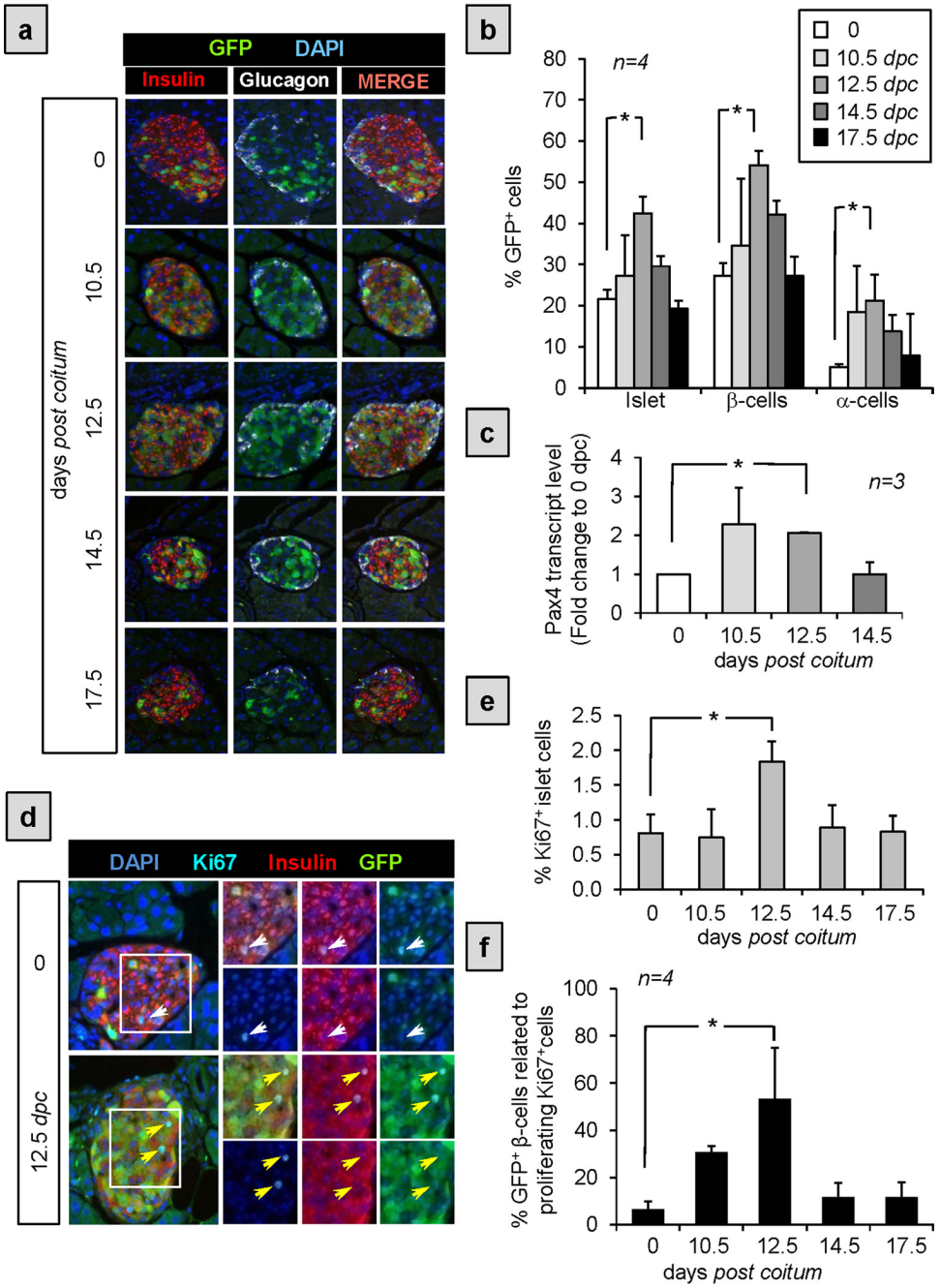

Figure 6. The GFP/PAX4$^+$subpopulation is transiently increased during pregnancy. (**a**) Representative composite images of pancreas sections obtained from pregnant pPax4-*Cre*-IRES-*Egfp* females that were co-immunostained for GFP (green), INSULIN (red) and GLUCAGON (white). Nuclei counterstaining was performed using DAPI (blue). (**b**) Cell quantification of percent GFP/PAX4$^+$ cells distributed within the total islet cell, β-cell and α-cell population. (**c**) Fold change in endogenous Pax4 mRNA levels measured by qt-RT-PCR in whole islets from pregnant C57BL/6 mice. (**d**) Representative composite images of pancreas sections obtained from control and 12.5 *dpc* pPax4-*Cre*-IRES-*Egfp* females that were triple-immunostained for GFP (green), INSULIN (red) and KI67 (cian). Nuclei counterstaining was performed using DAPI (blue). Insets depict KI67$^+$/GFP$^-$ cells (white arrow) and KI67$^+$/GFP$^+$ cells (yellow arrow). (**e**) Quantitative analysis (average ± SE) of the proliferative, Ki67$^+$ cells during pregnancy. (**f**) Cell quantification represented as the percentage of GFP$^+$β-cells among the total amount of proliferating KI67$^+$cells. Data show the mean ± SE of 3 to 5 animals with an average of 15 islets and 1200 cells per animal were used for quantifications.*ANOVA:$p < 0.05$ as compared to day 0.

transient increase in endogenous Pax4 transcript levels was also detected in whole islets of pregnant mice reaching maximal levels of 2-fold at 12.5 *dpc* as compared to islets isolated from non-pregnant females (Fig. 6c). We next assessed cell proliferation within the GFP/PAX4$^+$ and GFP$^-$ subpopulations. To this end, immunostaining for the proliferation marker Ki67 along with GFP and INSULIN was performed on sections of pregnant mice pancreas (Fig. 6d). In adult non-pregnant mice, $6 \pm 3\%$ of Ki67$^+$ cells were insulin expressing GFP/PAX4$^+$ (Fig. 6f) while $58 \pm 6\%$ were GFP$^-$ β-cells. However, in pregnant mice by 12.5 *dpc* the number of GFP/PAX4$^+$ β-cells dramatically increased to $55 \pm 20\%$ of the Ki67$^+$ proliferating cell population (Fig. 6f) whereas replication of GFP$^-$ β-cells remained relatively constant (data not shown). This increase was transient as by 17.5 *dpc* proliferation of the GFP/PAX4$^+$ population regressed to control values. Taken together our results suggest that although the fraction of proliferating GFP/PAX4$^+$ β-cells is lower than that of the GFP$^-$ β-cell fraction in control animals, GFP/PAX4$^+$ β-cells are more permissive to proliferation and expansion upon conditions stimulating β-cell replication such as during pregnancy.

GFP/PAX4$^+$ islet cells are more resistant to stress-induced apoptosis. High levels of PAX4 were also shown to protect β-cells against stress-induced apoptosis as well as to act as a survival factor in INS-1E insulinoma cells[2,15,17]. This PAX4-mediated protective effect was recently correlated to improve calcium and endoplasmic reticulum (ER) homeostasis (Mellado-Gil *et al.*, manuscript submitted). This data led us to postulate that GFP/PAX4$^+$ cells within islets would be more resistant to apoptosis as compared to their GFP$^-$ counterpart. To validate this assumption, islets isolated from pPax4-*Cre*-IRES-*Egfp* mice were cultured in the presence of thapsigargin (THAP), an inhibitor of ubiquitous ER Ca^{2+}-ATPases that induces ER-stress dependent apoptosis. Cleaved-CASPASE-3 immunostaining revealed a significant 2-fold enrichment in apoptotic GFP$^-$ cells within THAP-treated islets as compared to untreated controls, while no significant increase in apoptosis was discerned in GFP/PAX4$^+$ cells (Fig.7a,b). In order to substantiate these findings in a more physiological context, pPax4-*Cre*-IRES-*Egfp* mice were treated with streptozotocin (STZ), an agent that specifically destroys β-cells. Animals were sacrificed 24 hours post-STZ treatment prior to the development of hyperglycemia with the aim to clearly discriminate the impact of STZ on the two GFP subpopulations. As anticipated, the number of GFP/PAX4$^+$ cells remained relative constant while the overall β-cell population drastically decreased from 70 to 30% of all islet cells in STZ-treated mice (Fig. 7c,d). A more detailed analysis of the various β-cell populations based on GFP expression pattern revealed that the decrease in β-cell mass predominantly stemmed from the loss of GFP$^-$cells while GFP/PAX4$^+$β-cells were refractory to STZ-mediated destruction (Fig. 7e). Of note, we did not observed any gender specific effect of STZ on the two distinct subpopulations. However, a slight increase in the percentage of INSULIN$^-$ cells in the GFP/PAX4$^+$ subpopulation was discerned upon STZ treatment (Fig. 7e) potentially as a result of either re-expression of PAX4 in α-cells or loss of β-cell entity. Immunofluorescence analysis revealed that the percentage of GFP/PAX4$^+$ cells among glucagon expressing cells remained relatively constant after STZ treatment (Supplementary Fig. S2) suggesting that INSULIN$^+$/GFP/PAX4$^+$ cells were undergoing de-differentiation resulting in the loss of INSULIN expression.

Discussion

Our work establishes the existence of a *bona fide* PAX4-enriched cell subpopulation nested within pancreatic islets that can, on one hand expand in periods of increased functional demands, and on the other hand exhibit improved viability in response to pathophysiological situations. These results foster the prospect that PAX4, a critical regulator of embryonic β-cell development, maintains plasticity within a pool of cells in adult islets concealed predominantly as β-cells. These cells are dispersed throughout the islet without any apparent niche. Heterogeneity among islet β-cells has been well documented and first described by Pipeleers as the sociobiology of pancreatic β-cells[28]. Consistent with the notion of an islet β-cell progenitor reservoir contributing to this heterogeneity, several studies using reporter constructs to track the fate of β-cells either *in vitro* or *in vivo*, revealed the existence of at least three distinct subpopulations of β-cells within human and mouse islets[29–31]. Of particular interest was the characterization of a proliferative immature PDX1$^+$/INSULIN^{low} β-cell subpopulation that comprised approximately 15 to 25% of all islet cells and that expressed higher levels of PAX4[32]. This cell population is reminiscent to that of PDX1$^+$/INSULIN^{low}/BrdU$^+$ β-cells characterized in PAX4 over-expressing mice[17] as well as to the endogenous GFP/PAX4$^+$ cell fraction described herein. Nonetheless, GSIS was normal in GFP/PAX4$^+$ cells whereas it was impaired in both PAX4 over-expressing islets and in the reported PDX1$^+$/INSULIN^{low} β-cell subpopulation[17,32]. As the insulin content of both GFP/PAX4$^+$ and GFP$^-$ cells was identical (as assessed for GSIS presented in Fig. 1g), we propose that pending environmental cues expression levels of PAX4 will define the fate, state and functionality of endogenous islet cells. Such premise is reinforced by the fact that some of the GFP/PAX4$^+$ cells express SOMATOSTATIN, GLUCAGON or INSULIN and GLUCAGON together, resembling embryonic cell fate commitment process, where dual hormone cells have been detected[33,34].

Our data reconcile divergent views regarding an ongoing debate on whether β-cell expansion involves an elusive progenitor cell pool or proceeds through self-duplication of resident β-cells[35–37]. Consistent with self-duplication advocates, we find that under normal conditions, both GFP/PAX4$^+$and GFP$^-$ β-cells are prone to proliferation, a state that is gradually impaired with age[38]. However, in physiological

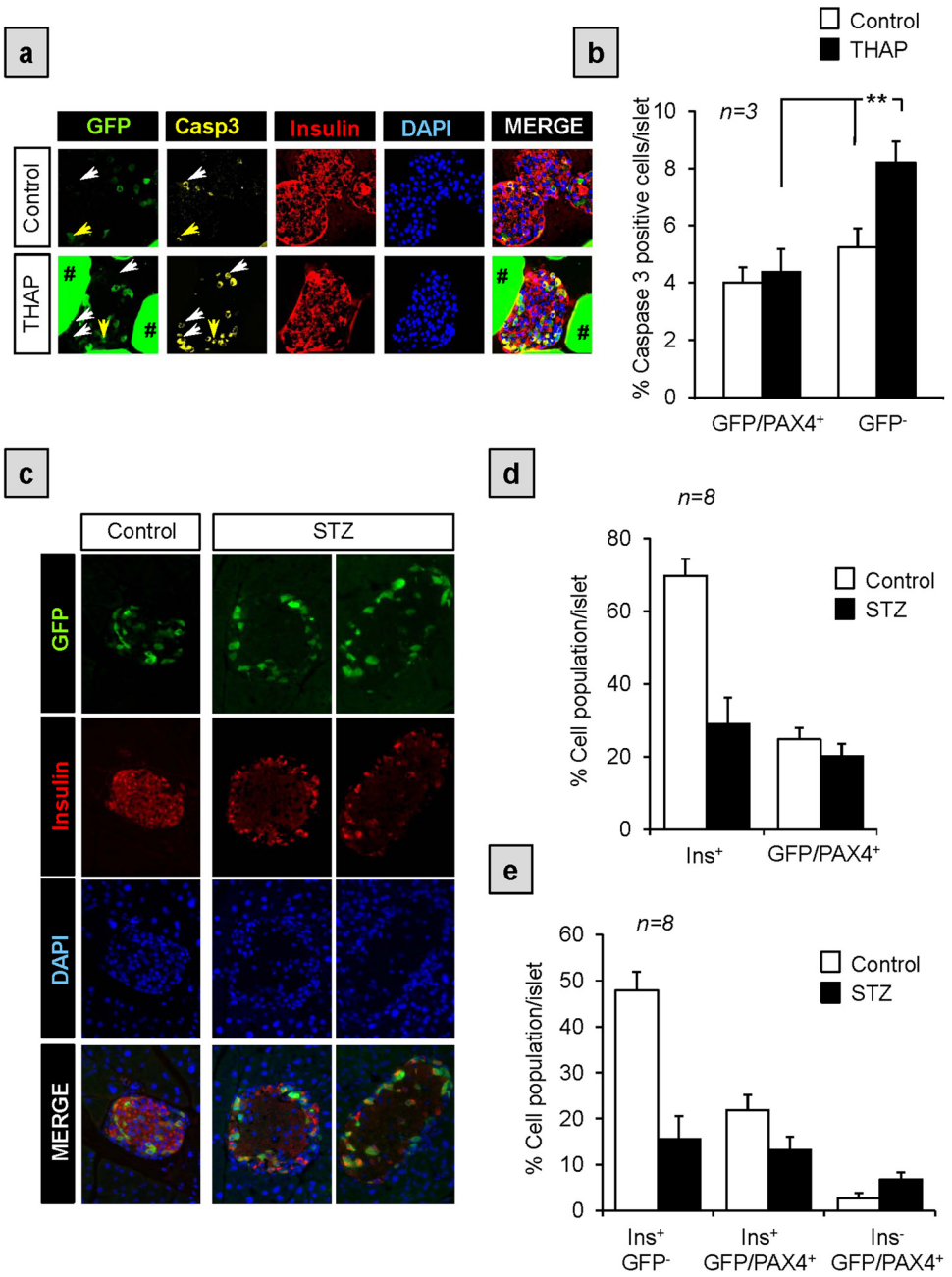

Figure 7. GFP/PAX4$^+$ cells are more resistant to apoptosis than their GFP/PAX4$^-$ counterparts. (**a**) Immunofluorescent detection of GFP (green), cleaved-CASPASE 3 (yellow), and INSULIN (red) as well as DAPI nuclear staining (blue) in islets isolated from pPax4-*Cre*-IRES-*Egfp* and treated *in vitro* for 24 hours with thapsigargin (THAP). Arrows depict examples of GFP$^-$/cleaved caspase 3$^+$ cells. Non-specific GFP labeling of Affi-Gel® beads used for islet mounting is denoted by #. (**b**) Cell quantification represented as the percentage of cleaved caspase 3-positive cells in either GFP/PAX4$^+$or GFP$^-$ cells treated or not with thapsigargin. Data show the mean ± SE of 3 independent experiments, each representing at least 10 islets and 1000 cells per conditions. **ANOVA:$p < 0.01$. (**c**) pPax4-*Cre*-IRES-*Egfp* mice were injected (*i.p.*) with STZ (200 mg/kg body weight) to promote β-cell apoptosis and pancreas extracted 24 hours post treatment. Animals were normoglycemic at this time point. Pancreas sections were then co-immunostained for GFP (green) and INSULIN (red). (**d**) The number of INSULIN$^+$ and GFP/PAX4$^+$cells were counted and results presented as the percentage of total islet cells. (**e**) Percentage of GFP$^-$ and GFP/PAX4$^+$ cells between INSULIN$^+$ and INSULIN$^-$ cells. Data show the mean ± SE of 8 independent animals, each representing an average of 15 islets and 1500 cells per animal.

situation evoking an increase in the β-cell mass, as during pregnancy, we witnessed a specific enrichment in the replication of GFP/PAX4$^+$ cells as compared to the GFP$^-$ cells advocating in favor of the recruitment of a specialized plastic β-cell pool. This specific mobilization could be a consequence of GFP/PAX4$^+$ cells being permissive to cell proliferation as revealed by increased cell cycle genes in equivalent PAX4-overexpressing islet cells. A similar cell cycle re-entry dependent permissive state was recently reported for islets conditionally overexpressing the connective tissue growth factor[39]. Hence, our study demonstrates that both GFP/PAX4$^+$ and GFP$^-$ β-cells are susceptible to basal proliferation but that only the fraction, defined by expression levels of PAX4, are permissive to increased replication pending stimuli. However, this capacity to proliferate declines with age as assessed by both a decrease in the GFP/PAX4$^+$ subpopulation as well as in cell replication correlating with increased failure to adapt β-cell mass with age[40].

Additional members of the *pax* gene family have been shown to convey similar proliferative and survival phenotypes within adult tissues. For example, PAX6 is essential for the production and subsequent maintenance of progenitor cells in the adult hippocampal dentate gyrus while PAX7 expression is critical for survival and plasticity of adult skeletal muscle satellite cells in response to environmental cues[41,42]. In addition, PAX3 expressing melanocytic progenitor cells are permissive to injury signals for re-entry into cell cycle and initiate regeneration whereas PAX2 re-activation is essential for kidney injury repair[43,44]. Interestingly, *pax* genes have arisen from a single gene during the early metazoan era emphasizing a common ancestral function among the *pax* members including PAX4. This function that pre-dates gene duplication most likely relates to the capability of expressing host cells to respond to a dynamic environment[45]. The latter also includes increased survival in response to hostile settings, a premise also demonstrated by the ability of the GFP/PAX4$^+$ cell subset to preferentially resist STZ and thapsigargin-mediated apoptosis as compared to GFP$^-$ cells.

Recent studies suggest that in the diabetic state β-cells revert to NGN3$^+$/MAFA$^-$/INSULIN$^-$ progenitor-like cells rather than undergoing massive apoptosis[18,19,46]. Re-differentiation of dedifferentiated cells was possible following insulin therapy[19]. Interestingly, we previously demonstrated that PAX4 transcript levels are induced by high glucose and are dramatically increased in islets obtained from T2DM donors correlating with increased survival[2,15]. Chronic PAX4 expression was also shown to lead to MAFA and INSULIN repression reminiscent of the progenitor-like cells induced by the diabetic milieu[19]. Of particular interest is the finding that NGN3 was increased in islet overexpressing PAX4. Taken together, it is tempting to speculate that under pathophysiological conditions, acute increased in PAX4 expression will initially protect cells while sustained expression will induce dedifferentiation towards a 'progenitor phenotype' as an adaptive mechanism to protect cells against a hostile environment. In support of this viewpoint, we observed a small increase in INSULIN$^-$ cells within the GFP/PAX4$^+$ subpopulation subsequent to STZ treatment (Fig. 7e) while others have reported robust increases in PAX4 expression levels in islets of STZ-treated mice[47]. Once the threat is neutralized, repression of PAX4, by mechanisms independent of DNA methylation, will promote re-differentiation towards a β-cell phenotype.

Pax4 could be considered a 'selfish gene' safeguarding survival of the fittest cell population within islets[48]. Indeed, by exquisitely fine tuning its levels in response to the microenvironment, PAX4 will act as a rheostat in defining the phenotypic characteristic of islet cells to best adapt to their new surroundings. Functional impairment associated with PAX4-dependent re-entry into cell cycle would have little consequence short term on glucose homeostasis, as the predominant β-cell mass would remain quiescent and functional. Disparity in the impact of *pax4* gene mutations on the incidence of diabetes could potentially be rationalized by the outcome of gene-environment interaction, which will dictate fitness of β-cells. In conclusion, strategies to fine-tune PAX4 expression levels may constitute a promising approach to simultaneously expand while blocking dedifferentiation of the functional β-cell mass with the aim to salvage hyperglycemia in diabetic patients.

Methods

Animals. Mice were maintained on a normal light/dark cycle and studied under conditions approved by the Institutional Animal Care Committee of CABIMER. Methods associated with animals were carried out in accordance with the approved guidelines.The pPax4-*Cre*-IRES-*Egfp* mice, kindly provided by Dr. P. Gruss (Max Planck Institute, Gottingen, DE), were back crossed to C57BL/6 mice (Jackson Laboratory). Animals were genotyped with the REDExtract-N-Amp kit (Sigma-Aldrich, Madrid, Spain) using specific primers that can be obtained upon request. Lineage tracing experiments were conducted on the progeny of pPax4-*Cre*-IRES-*Egfp* mice bred to *Rosa26*;lox-stop-lox;*LacZ* mice. For *in vivo* cell death analysis, adult (3–4 months) pPax4-*Cre*-IRES-*Egfp* mice (average body weight 25 g) were treated with a single high-dose of streptozotocin (STZ: 200 mg/kg body weight) by intraperitoneal injection. STZ was dissolved in 0.1 M sodium citrate buffer and injected within 5 min of dissolution. Blood glucose levels from tail vein samples were determined prior to and 24 hours after STZ injection using a Precision Xceed glucometer (Abbott, Madrid, Spain).

Mouse Islet Isolation and Treatment. Mouse pancreatic islets were isolated by intraductal collagenase as described elsewhere[17]. Islets were maintained overnight in 11.1 mM glucose/RPMI-1640 (Life Technologies, Madrid, Spain) supplemented with 10% fetal bovine serum (Sigma), 100 Units/ml penicillin and 100 μg/ml streptomycin (Sigma), 2 mM glutamine (Life Technologies), 10 mM hepes (Life

Technologies), 1 mM sodium pyruvate (Sigma), and 50 μM β-mercaptoethanol (Life Technologies). In some instances, GFP fluorescence from living islets was captured using and Image-Xpress device (Molecular devices, Spain). Composition of the various islet cell subpopulations was assessed by flow cytometry (FACSCalibur, BD Biosciences) while isolation of GFP^+ and GFP^- islet cells was achieved using FACS (FACSAria,BD Biosciences) and FACSDiva software (BD Biosciences). Briefly, isolated islets from adult (3–4 months) C57BL/6 WT mice and pPax4-*Cre*-IRES-*Egfp* mice were dispersed by trypsinization, resuspended in PBS containing 25 mM Hepes and 2.5 mM EDTA and filtered through cell strainer caps (70 μm). Using fluorescence-activated sorting, β-cells were separated from non-β-cells based on their size (FSC channel) and autofluorescence (FL-1 channel-GFP), as previously described[49]. Purified subpopulations were plated on an 804G matrix rich in laminin for 24 hours to improve cell viability prior to insulin secretion assay. The latter was performed by incubating cells for 30 min in Krebs-Ringer bicarbonate Hepes buffer containing 2.5, 16.5 mM glucose or a mixture of 16.5 mM glucose/1 μM forskolin/100 μM isobutylmethylxanthine (IBMX). Supernatants were collected and cells lysed in 1 mM acetic acid/ethanol. Secreted and total cellular content of insulin were assessed using an ELISA kit (Linco, St Charles, MO). For *in vitro* thapsigargin-induced cell death assessment, groups of 150 islets were incubated or not during 24 hours with 1 μM thapsigargin. Islets were then embedded according to the protocol of Cozar-Castellano *et al.*[50] and processed for IHC analysis.

RNA Isolation and Quantitative PCR. RNA was extracted from GFP^+ and GFP^- islet cells using the RNeasy micro Plus kit (Qiagen Iberia S.L., Madrid Spain). After quantification and analysis of the RNA integrity using a 2100 bioanalyzer (Agilent-Eukaryote Total RNA Nano Series), 100 to 200 ng RNA was used for cDNA synthesis using Super Script II RT (Life Technologies) and Anchored OligodT as primers. For RNA extraction from whole islets, RNeasy micro Plus kit (Qiagen Iberia S.L., Madrid Spain) was used. Between 800 ng and 1 μg of RNA was employed for cDNA synthesis using Super Script II RT (Life Technologies) and Anchored OligodT as primers. Quantitative PCR was performed using a 7500 Real-Time PCR System (Applied Biosystems). Specific primers for the analyzed genes (Pax4, Pdx1 and Insulin) were designed to span an intron in order to avoid genomic DNA amplification. The housekeeping genes β-actin and cyclophilin were used as control.

RNA Microarray. Labeled cRNA samples were prepared from pools of at least 100 islets isolated from Pax4/rtTA transgenic animals (8-week old females) treated or not with DOX as previously described[17]. Three independent preparations of cRNA per group were then hybridized to the GeneChip Mouse Gene 1.0 ST Array chip (Affymetrix, Santa Clara, CA) using standard protocols of the Genomic Core Facility of CABIMER. Analysis of the transcriptome profiling is described elsewhere (Mellado Gil *et al.*, Manuscript submitted). Raw data are accessible in the Gene Expression Omnibus database under accession number GSE62846.

Bisulfite Sequencing. DNA was extracted from MIN6 cells as well as from FACS purified non-β, GFP^+ and GFP^- subpopulations. Bisulfite conversion of unmethylated C to U was performed using "Cells-to-CpG Bisulfite Conversion" kit (Life Technologies) following guidelines of the manufacturer. Converted DNA was amplified using MyTaqHS DNA polymerase (Bioline, Paris, France) along with specific primers for the region of interest on the *pax4* gene promoter. Amplicons were purified using QIAquick PCR purification kit (Qiagen Iberia S.L.), cloned into the pGEMT vector and transformed into DH5α *E. Coli* bacteria. At least 20 colonies per DNA region and cell subpopulation were sequenced and analyzed using the BiQ Analyzer software.

Immunohistochemistry. For paraffin sections, pancreata were dissected and fixed overnight in 4% paraformaldehyde at 4 °C. Dehydration, embedding, and sectioning at 5 μm thickness were performed by the Histology platform of CABIMER. Sections were rehydrated in decreasing ethanol concentration solutions and subjected to heat-induced antigen retrieval in 10 mM sodium citrate buffer pH 6. Sections were then blocked in PBS containing 5% donkey serum and 0.2%TritonX100 for 1 h at room temperature. Primary antibodies were incubated overnight at 4 °C in PBS 1% BSA 0.2% TritonX100, except for GFP antibody that was incubated in PBS 0.1% BSA 0.2% TritonX100. The following primary antibodies and dilutions were used: Goat anti-GFP 1:200 (Abcam), mouse anti-INSULIN 1:500 (Sigma), rabbit anti-INSULIN 1:100 (Santa Cruz), mouse anti-GLUCAGON 1:150 (Sigma), mouse anti-PDX1 1:150 (Hybridoma bank), rabbit anti-SOMATOSTATIN 1:150 (Santa Cruz), goat anti-SOMATOSTATIN 1:100 (Santa Cruz), mouse anti-E-CADHERIN 1:250 (BD Transduction laboratories), mouse anti-Ki67 1:150 (Novocastra), rabbit anti-Ki67 1:150 (Pierce-Thermo Scientific), rabbit anti-β-GAL1:500 (MP Biomedicals) and rabbit anti-cleaved CASPASE-3 1:150 (Cell Signaling). Secondary antibodies were incubated for 1 hour at room temperature at a 1:800 dilution in PBS 0.2% TritonX100. The following secondary antibodies were employed: Alexa Fluor 488 donkey anti-goat, Alexa Fluor 555 donkey anti-mouse and Alexa Fluor 647 donkey anti-rabbit (Life Technologies). Counterstaining was performed with 5 μg/ml DAPI (Life Technologies) and slides finally mounted using fluorescent mounting medium (DAKO). Epifluorescence microscopy images were taken with a Leica DM6000B microscope. For image quantification, slides from 4 to 8 animals per time point were studied with an average of 15 islets per animal.

Statistical Analysis. Results are expressed as mean ± SE. Statistical differences were estimated using a 2-tailed Student's test for comparison between 2 groups and 1-way ANOVA for more that 2 groups, with Scheffe's F test for post-hoc analysis.

References

1. Carrasco, M. *et al.* in *Islets of Langerhans* Vol. 1 (ed Shahidul Islam) Ch. 6 109–129 (Springer, 2015).
2. Brun, T. & Gauthier, B. R. A focus on the role of Pax4 in mature pancreatic islet beta-cell expansion and survival in health and disease. *J. Mol. Endocrinol.* **40,** 37–45 (2008).
3. Li, Y. *et al.* Aberrant DNA demethylation in promoter region and aberrant expression of mRNA of PAX4 gene in hematologic malignancies. *Leuk. Res.* **30,** 1547–1553 (2006).
4. Miyamoto, T. *et al.* Expression of dominant negative form of PAX4 in human insulinoma. *Biochem. Biophys. Res. Commun.* **282,** 34–40 (2001).
5. Zhang, J. *et al.* Transcriptional control of PAX4-regulated miR-144/451 modulates metastasis by suppressing ADAMs expression. *Oncogene*. doi: 10.1038/onc.2014.259 (2014).
6. Gong, Z. C. *et al.* NeuroD1 A45T and PAX4 R121W polymorphisms are associated with plasma glucose level of repaglinide monotherapy in Chinese patients with type 2 diabetes. *Br. J. Clin. Pharmacol.* **74,** 501–509 (2012).
7. Jo, W., Endo, M., Ishizu, K., Nakamura, A. & Tajima, T. A Novel PAX4 Mutation in a Japanese patient with maturity-onset diabetes of the young. *Tohoku J. Exp. Med.* **223,** 113–118 (2011).
8. Cho, Y. S. *et al.* Meta-analysis of genome-wide association studies identifies eight new loci for type 2 diabetes in east Asians. *Nat. Genet.* **44,** 67–72 (2012).
9. Plengvidhya, N. *et al.* PAX4 mutations in Thais with maturity onset diabetes of the young. *J. Clin. Endocrinol. Metab.* **92,** 2821–2826 (2007).
10. Tokuyama, Y., Matsui, K., Ishizuka, T., Egashira, T. & Kanatsuka, A. The Arg121Trp variant in PAX4 gene is associated with beta-cell dysfunction in Japanese subjects with type 2 diabetes mellitus. *Metabolism* **55,** 213–216 (2006).
11. Zhang, Y. *et al.* [Association between A1168C polymorphism in PAX4 gene and type 1 diabetes in Han Chinese]. *Zhongguo Yi Xue Ke Xue Yuan Xue Bao* **29,** 370–373 (2007).
12. Mauvais-Jarvis, F. *et al.* PAX4 gene variations predispose to ketosis-prone diabetes. *Hum. Mol. Genet.* **13,** 3151–3159 (2004).
13. Park, J. W. *et al.* Candidate gene polymorphisms for diabetes mellitus, cardiovascular disease and cancer are associated with longevity in Koreans. *Exp. Mol. Med.* **41,** 772–781 (2009).
14. Sosa-Pineda, B., Chowdhury, K., Torres, M., Oliver, G. & Gruss, P. The Pax4 gene is essential for differentiation of insulin-producing beta cells in the mammalian pancreas. *Nature* **386,** 399–402 (1997).
15. Brun, T. *et al.* The diabetes-linked transcription factor Pax4 promotes beta-cell proliferation and survival in rat and human islets. *J. Cell Biol.* **167,** 1123–1135 (2004).
16. Lu, J. *et al.* Pax4 paired domain mediates direct protein transduction into mammalian cells. *Endocrinology.* **148,** 5558–5565 (2007).
17. Hu He, K. H. *et al. In vivo* conditional pax4 overexpression in mature islet beta cells prevents stress-induced hyperglycemia in mice. *Diabetes* **60,** 1705–1715 (2011).
18. Talchai, C., Xuan, S., Lin, H. V., Sussel, L. & Accili, D. Pancreatic beta cell dedifferentiation as a mechanism of diabetic beta cell failure. *Cell.* **150,** 1223–1234 (2012).
19. Wang, Z., York, N. W., Nichols, C. G. & Remedi, M. S. Pancreatic beta cell dedifferentiation in diabetes and redifferentiation following insulin therapy. *Cell Metab.* **19,** 872–882 (2014).
20. Brun, T. *et al.* The diabetes-linked transcription factor Pax4 is expressed in human pancreatic islets and is activated by mitogens and GLP-1. *Hum. Mol. Genet.* **17,** 478–489 (2008).
21. Brink, C. & Gruss, P. DNA sequence motifs conserved in endocrine promoters are essential for Pax4 expression. *Dev. Dyn.* **228,** 617–622 (2003).
22. Brun, T., Duhamel, D. L., Hu He, K. H., Wollheim, C. B. & Gauthier, B. R. The transcription factor Pax4 acts as a survival gene in the insulinoma INS1E cells. *Oncogene* **26,** 4261–4271 (2007).
23. Wellershaus, K. *et al.* A new conditional mouse mutant reveals specific expression and functions of connexin36 in neurons and pancreatic beta-cells. *Exp. Cell. Res.* **314,** 997–1012 (2008).
24. Brink, C., Chowdhury, K. & Gruss, P. Pax4 regulatory elements mediate beta cell specific expression in the pancreas. *Mech. Dev.* **100,** 37–43 (2001).
25. Greenwood, A. L., Li, S., Jones, K. & Melton, D. A. Notch signaling reveals developmental plasticity of Pax4(+) pancreatic endocrine progenitors and shunts them to a duct fate. *Mech. Dev.* **124,** 97–107 (2007).
26. Migliorini, A., Bader, E. & Lickert, H. Islet cell plasticity and regeneration. *Mol. Metab*. **3,** 268–274 (2014).
27. Rieck, S. & Kaestner, K. H. Expansion of beta-cell mass in response to pregnancy. *Trends Endocrinol. Metab.* **21,** 151–158 (2010).
28. Pipeleers, D. The biosociology of pancreatic B cells. *Diabetologia* **30,** 277–291 (1987).
29. Katsuta, H. *et al.* Subpopulations of GFP-marked mouse pancreatic beta-cells differ in size, granularity, and insulin secretion. *Endocrinology* **153,** 5180–5187 (2012).
30. Szabat, M., Johnson, J. D. & Piret, J. M. Reciprocal modulation of adult beta cell maturity by activin A and follistatin. *Diabetologia* **53,** 1680–1689 (2010).
31. Smukler, S. R. *et al.* The adult mouse and human pancreas contain rare multipotent stem cells that express insulin. *Cell Stem Cell* **8,** 281–293 (2011).
32. Szabat, M., Luciani, D. S., Piret, J. M. & Johnson, J. D. Maturation of adult beta-cells revealed using a Pdx1/insulin dual-reporter lentivirus. *Endocrinology* **150,** 1627–1635 (2009).
33. Collombat, P. *et al.* The ectopic expression of Pax4 in the mouse pancreas converts progenitor cells into alpha and subsequently beta cells. *Cell* **138,** 449–462 (2009).
34. Al-Hasani, K. *et al.* Adult duct-lining cells can reprogram into beta-like cells able to counter repeated cycles of toxin-induced diabetes. *Dev. Cell* **26,** 86–100 (2013).
35. Bonner-Weir, S. *et al.* Beta-cell growth and regeneration: replication is only part of the story. *Diabetes* **59,** 2340–2348 (2010).
36. Dor, Y., Brown, J., Martinez, O. I. & Melton, D. A. Adult pancreatic beta-cells are formed by self-duplication rather than stem-cell differentiation. *Nature* **429,** 41–46 (2004).
37. Teta, M., Rankin, M. M., Long, S. Y., Stein, G. M. & Kushner, J. A. Growth and regeneration of adult beta cells does not involve specialized progenitors. *Dev. Cell* **12,** 817–826 (2007).
38. Teta, M., Long, S. Y., Wartschow, L. M., Rankin, M. M. & Kushner, J. A. Very slow turnover of beta-cells in aged adult mice. *Diabetes* **54,** 2557–2567 (2005).
39. Riley, K. G. *et al.* Connective tissue growth factor modulates adult beta-cell maturity and proliferation to promote beta-cell regeneration in mice. *Diabetes* **64,** 1284–1298 (2015).

40. Rankin, M. M. & Kushner, J. A. Adaptive beta-cell proliferation is severely restricted with advanced age. *Diabetes* **58,** 1365–1372 (2009).
41. Maekawa, M. *et al.* Pax6 is required for production and maintenance of progenitor cells in postnatal hippocampal neurogenesis. *Genes Cells* **10,** 1001–1014 (2005).
42. Seale, P. *et al.* Pax7 is required for the specification of myogenic satellite cells. *Cell* **102,** 777–786 (2000).
43. Nishimura, E. K. *et al.* Dominant role of the niche in melanocyte stem-cell fate determination. *Nature* **416,** 854–860 (2002).
44. Huang, B. *et al.* WT1 and Pax2 re-expression is required for epithelial-mesenchymal transition in 5/6 nephrectomized rats and cultured kidney tubular epithelial cells. *Cells Tissues Organs* **195,** 296–312 (2012).
45. Blake, J. A., Thomas, M., Thompson, J. A., White, R. & Ziman, M. Perplexing Pax: from puzzle to paradigm. *Dev. Dyn.* **237,** 2791–2803 (2008).
46. Spijker, H. S. *et al.* Loss of beta-cell identity occurs in type 2 diabetes and is associated with islet amyloid deposits. *Diabetes*, doi: 10.2337/db14-1752 (2015).
47. Yang, J. *et al.* P21cip-overexpression in the mouse beta cells leads to the improved recovery from streptozotocin-induced diabetes. *PLoS One* **4,** e8344, doi: 10.1371/journal.pone.0008344 (2009).
48. Dawkins, R. *The selfish gene*. (Oxford University Oress, 1976).
49. Bernard-Kargar, C., Kassis, N., Berthault, M. F., Pralong, W. & Ktorza, A. Sialylated form of the neural cell adhesion molecule (NCAM): a new tool for the identification and sorting of beta-cell subpopulations with different functional activity. *Diabetes* **50** Suppl 1, S125–130 (2001).
50. Cozar-Castellano, I., Takane, K. K., Bottino, R., Balamurugan, A. N. & Stewart, A. F. Induction of beta-cell proliferation and retinoblastoma protein phosphorylation in rat and human islets using adenovirus-mediated transfer of cyclin-dependent kinase-4 and cyclin D1. *Diabetes* **53,** 149–159 (2004).

Acknowledgements

We thank Dr. Anabel Rojas and Prof. Peter Gruss for kindly providing the R26R reporter mouse and the pPax4-*Cre*-IRES-*Egfp* mouse, respectively. We also thank Jorge Vallejo Ortega, Carmen de Jesus Gil and Noelia Garcia Rodriguez for excellent technical assistance. This work was funded by grants from the Consejeria de Salud, Fundacion Publica Andaluza Progreso y Salud, Junta de Andalucia (PI-0727-2010 to B.R.G. and PI-0085-2013 to P.I.L.), Consejeria de Economia, Innovacion y Ciencia (P10.CTS.6359 to B.R.G.), the Ministerio de Economia y Competitividad, Instituto de Salud Carlos III co-funded by Fondos FEDER (PI10/00871 and PI13/00593 to B.R.G.) and the Fundacion Vencer el Cancer (to B.R.G.). N.C.V. is supported by a JDRF subsidy (17-2013-372 to B.R.G.). A.M.M. is a recipient of a Miguel Servet grant (CP14/00105) from the Instituto de Salud Carlos III co-funded by FEDER whereas E.F.M. is a recipient of a Juan de la Cierva Fellowship from the Ministerio de Economia y Competitividad. Special thank to Luis Casas for his dedication in fund raising and ALUSVI (Asociación Lucha y Sonrie por la Vida de Pilas), a local Andalusia association, for their unconditional financial support.

Author Contributions

P.I.L. generated the bulk of the results. E.F.M., T.B., N.C.V., C.M.J.M., I.G.H.G., L.L.N., J.M.M.G. and A.M.M. contributed to research data. B.S. provided advice, expertise or reagents. P.I.L. and B.R.G. conceived and designed the experiments and wrote the manuscript. All authors reviewed the manuscript. B.R.G. is the guarantor of this work and takes responsibility for the integrity of the data and the accuracy of the data analysis.

Additional Information

Supplementary information accompanies this paper at http://www.nature.com/srep

Competing financial interests: The authors declare no competing financial interests.

How to cite this article: Lorenzo, P. I. *et al.* PAX4 Defines an Expandable β-Cell Subpopulation in the Adult Pancreatic Islet. *Sci. Rep.* **5**, 15672; doi: 10.1038/srep15672 (2015).

Diabetologia (2016) 59:755–765
DOI 10.1007/s00125-016-3864-0

ARTICLE

PAX4 preserves endoplasmic reticulum integrity preventing beta cell degeneration in a mouse model of type 1 diabetes mellitus

José Manuel Mellado-Gil[1] · Carmen María Jiménez-Moreno[1] · Alejandro Martin-Montalvo[1] · Ana Isabel Alvarez-Mercado[1] · Esther Fuente-Martin[1] · Nadia Cobo-Vuilleumier[1] · Petra Isabel Lorenzo[1] · Eva Bru-Tari[2,3] · Irene de Gracia Herrera-Gómez[1] · Livia López-Noriega[1] · Javier Pérez-Florido[4] · Javier Santoyo-López[4,5] · Andreas Spyrantis[6] · Paolo Meda[7] · Bernhard O. Boehm[6,8,9] · Ivan Quesada[2,3] · Benoit R. Gauthier[1]

Received: 24 September 2015 / Accepted: 17 December 2015 / Published online: 26 January 2016

Abstract

Aims/hypothesis A strategy to enhance pancreatic islet functional beta cell mass (BCM) while restraining inflammation, through the manipulation of molecular and cellular targets, would provide a means to counteract the deteriorating glycaemic control associated with diabetes mellitus. The aims of the current study were to investigate the therapeutic potential of such a target, the islet-enriched and diabetes-linked transcription factor paired box 4 (PAX4), to restrain experimental autoimmune diabetes (EAD) in the RIP-B7.1 mouse model background and to characterise putative cellular mechanisms associated with preserved BCM.

Methods Two groups of RIP-B7.1 mice were genetically engineered to: (1) conditionally express either PAX4 (BPTL) or its diabetes-linked mutant variant R129W (mutBPTL) using doxycycline (DOX); and (2) constitutively express luciferase in beta cells through the use of RIP. Mice were treated or not with DOX, and EAD was induced by immunisation with a murine preproinsulin II cDNA expression plasmid. The development of hyperglycaemia was monitored for up to 4 weeks following immunisation and alterations in the BCM were assessed weekly by non-invasive in vivo bioluminescence intensity (BLI). In parallel, BCM, islet cell proliferation and apoptosis were evaluated by immunocytochemistry. Alterations in PAX4- and PAX4R129W-mediated islet gene expression were investigated by microarray profiling. PAX4 preservation of endoplasmic reticulum (ER) homeostasis was assessed using thapsigargin, electron microscopy and intracellular calcium measurements.

José Manuel Mellado-Gil, Carmen María Jiménez-Moreno and Alejandro Martin-Montalvo contributed equally to this work

Electronic supplementary material The online version of this article (doi:10.1007/s00125-016-3864-0) contains peer-reviewed but unedited supplementary material, which is available to authorised users.

✉ Benoit R. Gauthier
benoit.gauthier@cabimer.es

[1] Pancreatic Islet Development and Regeneration Unit, Department of Stem Cells, Andalusian Center for Molecular Biology and Regenerative Medicine (CABIMER), Avda Américo Vespucio, Parque Científico y Tecnológico Cartuja 93, 41092 Seville, Spain

[2] Centro de Investigación Biomédica en Red de Diabetes y Enfermedades Metabólicas Asociadas (CIBERDEM), Spain, http://www.ciberdem.org

[3] Instituto de Bioingeniería, Universidad Miguel Hernandez, Elche, Spain

[4] Medical Genome Project, Genomics & Bioinformatics Platform of Andalusia, Seville, Spain

[5] Present address: Edinburgh Genomics, University of Edinburgh, Edinburgh, UK

[6] Department of Internal Medicine, Ulm University Medical Centre, Ulm, Germany

[7] Department of Cell Physiology and Metabolism, University of Geneva, Geneva, Switzerland

[8] Lee Kong Chian School of Medicine, Nanyang Technological University, Singapore, Republic of Singapore

[9] Imperial College, London, UK

Results PAX4 overexpression blunted EAD, whereas the diabetes-linked mutant variant PAX4R129W did not convey protection. PAX4-expressing islets exhibited reduced insulitis and decreased beta cell apoptosis, correlating with diminished DNA damage and increased islet cell proliferation. Microarray profiling revealed that PAX4 but not PAX4R129W targeted expression of genes implicated in cell cycle and ER homeostasis. Consistent with the latter, islets overexpressing PAX4 were protected against thapsigargin-mediated ER-stress-related apoptosis. Luminal swelling associated with ER stress induced by thapsigargin was rescued in PAX4-overexpressing beta cells, correlating with preserved cytosolic calcium oscillations in response to glucose. In contrast, RNA interference mediated repression of PAX4-sensitised MIN6 cells to thapsigargin cell death.

Conclusions/interpretation The coordinated regulation of distinct cellular pathways particularly related to ER homeostasis by PAX4 not achieved by the mutant variant PAX4R129W alleviates beta cell degeneration and protects against diabetes mellitus. The raw data for the RNA microarray described herein are accessible in the Gene Expression Omnibus database under accession number GSE62846.

Keywords Beta cell degeneration · ER homeostasis · PAX4 · RIP-B7.1 · Type 1 diabetes

Abbreviations

BCL-2	B cell CLL/lymphoma 2
BCM	Beta cell mass
BLI	Bioluminescence intensity
BPTL	RIP-B7.1/*Pax4*/*rtTA*/MIP-*Luc*
CABIMER	Andalusian Center for Molecular Biology and Regenerative Medicine
CALR	Calreticulin
DOX	Doxycycline
DsRed	*Discosoma* sp. red fluorescent protein
EAD	Experimental autoimmune diabetes
EM	Electron microscopy
ER	Endoplasmic reticulum
ERAD	ER-associated protein degradation
GSIS	Glucose-stimulated insulin secretion
KEGG	Kyoto Encyclopaedia of Genes and Genomes
Luc	Luciferase
MIP	Mouse insulin promoter
PAX4	Paired box 4
RER	Rough ER
RIP	Rat insulin II promoter
rtTA	Reverse tetracycline-controlled transactivator
si	Small interfering
STZ	Streptozotocin
Th1	T helper 1
UPR	Unfolded protein response

Introduction

The islet of Langerhans is the core unit of the endocrine pancreas, which regulates blood glucose homeostasis. Regulation is achieved by the release of insulin from beta cells in response to increasing levels of glucose and by the secretion of glucagon from alpha cells under fasting conditions. Imbalance in this circuitry leads to either hyperglycaemia, the hallmark of diabetes mellitus, or hypoglycaemia. Loss of beta cell function coupled to insulin resistance of target tissues, which usually associates with obesity and chronic low-grade inflammation, defines type 2 diabetes [1]; high-grade T lymphocyte inflammation mediating autoimmune beta cell destruction is characteristic of type 1 diabetes [2].

Emerging evidence suggests that alterations in endoplasmic reticulum (ER) function contribute to beta cell disarray in both type 1 and 2 diabetes [3]. In an attempt to restore ER function and prevent apoptosis, cells activate the unfolded protein response (UPR) [4]. The crucial role of the UPR in balancing beta cell death and survival is illustrated in the human Wolfram and Wolcott–Rallison syndromes, in which mutations in UPR genes result in unresolved ER stress, beta cell death and early-onset diabetes [5, 6]. Interestingly, MODY genes such as *Pdx1* and *Hnf1a* regulate UPR-associated genes [7, 8]. These clinical conditions suggest that islet-enriched transcription factors involved in insulin biosynthesis and secretion also preserve the BCM by limiting ER stress.

Paired box (*Pax*) genes encode transcription factors critical for tissue development and cellular differentiation [9]. Paired box 4 (PAX4) is necessary for the generation of pancreatic islet cell progenitors and their differentiation towards beta cells [10, 11]. *Pax4* gene mutations have been associated with type 1 and 2 diabetes as well as with ketosis-prone diabetes, suggesting a key role of PAX4 in mature islets [12, 13]. Accordingly, overexpression of PAX4 in adult beta cells was shown to block streptozotocin (STZ)-induced hyperglycaemia in mice whereas the diabetes-linked variant PAX4R129W was less efficient [14]. Despite differences in nitric oxide synthase 2 (NOS2) levels, both PAX4- and PAX4R129W-expressing islets exhibited similar levels of cytokine-induced NO production, indicating that the nuclear factor-κB (NF-κB) signalling pathway was fully activated and that additional anti-apoptotic pathways are involved in islet survival. Consistent with this premise, PAX4 islets expressed higher levels of B cell CLL/lymphoma 2 (BCL-2) [14]. Nonetheless, overexpression of BCL-2 in islets did not prevent autoimmune-mediated beta cell destruction and development of hyperglycaemia [15]. Thus, although these data highlight the protective function of PAX4 against a chemical acute stress, whether such an effect can also be conveyed in the context of a pathophysiological autoimmune attack and the molecular mechanism involved in this protection remain to be established.

Herein, we investigated whether PAX4 and PAX4R129W could promote beta cell health, preventing the development of hyperglycaemia in the RIP-B7.1 mouse model of experimental autoimmune diabetes (EAD), and sought to characterise the PAX4-regulated pathways implicated in islet survival and expansion.

Methods

Animals and bioluminescence imaging Mouse experiments were approved by the local ethics committee and performed according to the Spanish law on animal use RD 53/2013. The rationale for using RIP-B7.1 (kindly supplied by B. O. Boehm) rather than NOD mice for the current study is provided in the electronic supplementary material (ESM) Methods. BPTL mice were derived as outlined in Fig. 1a, b and maintained on a C57bl/6 background. This mouse harbours four transgenes: (1) RIP-B7.1, a construct coding for the *Cd80* gene under control of the rat insulin promoter (RIP); (2) the tetracycline response element (TRE)/cytomegalo mosaic virus (CMV) *Pax4*, a tetracycline-inducible CMV promoter driving *Pax4* expression; (3) the RIP-reverse tetracycline trans-activator (*rtTA*), a construct allowing selective expression of *Pax4* in beta cells exposed to DOX; and (4) the MIP-Luciferase (*Luc*), a construct that expresses luciferase under the mouse insulin promoter (MIP), allowing assessment of BCM using non-invasive in vivo imaging technology. Induction of *Pax4* or *Pax4*R129W gene expression using doxycycline (DOX) was performed as previously described [14], while EAD was achieved by i.m. immunisation of 9-week-old BPTL animals with 50 μg of pC1/ppins plasmid DNA (1 μg/μl) encoding the murine preproinsulin II. Blood glucose levels were measured using a Precision Xceed glucometer (Abbott, Madrid, Spain). Bioluminescence imaging was performed using a Xenogen IVIS 50 imaging system as previously described [16].

Islet isolation and treatment Islets were isolated and cultured as previously described [14]. Total RNA was extracted using the RNeasy Micro Kit (Qiagen, Madrid, Spain) and quantitative (q)-PCR was performed as described previously [17]. Primer sequences can be obtained on request. For studies on thapsigargin-induced ER stress and apoptosis, islets from either *Pax4*/*rtTA* or *Pax4*R129W/*rtTA* transgenic mice were treated with 1 μg/l DOX for 96 h or left untreated [14]. Fluorescence of the *Discosoma* sp. red fluorescent protein (DsRed) correlating with *Pax4* or *Pax4R129W* expression was monitored using an ImageXpress Micro System (Molecular Devices, Wokingham, UK). Islets were then treated or not with 1 μmol/l thapsigargin for 48 h and apoptosis was assessed by ELISA (Roche Diagnostics, Mannheim, Germany). Glucose-stimulated insulin secretion (GSIS) was performed as previously described [18].

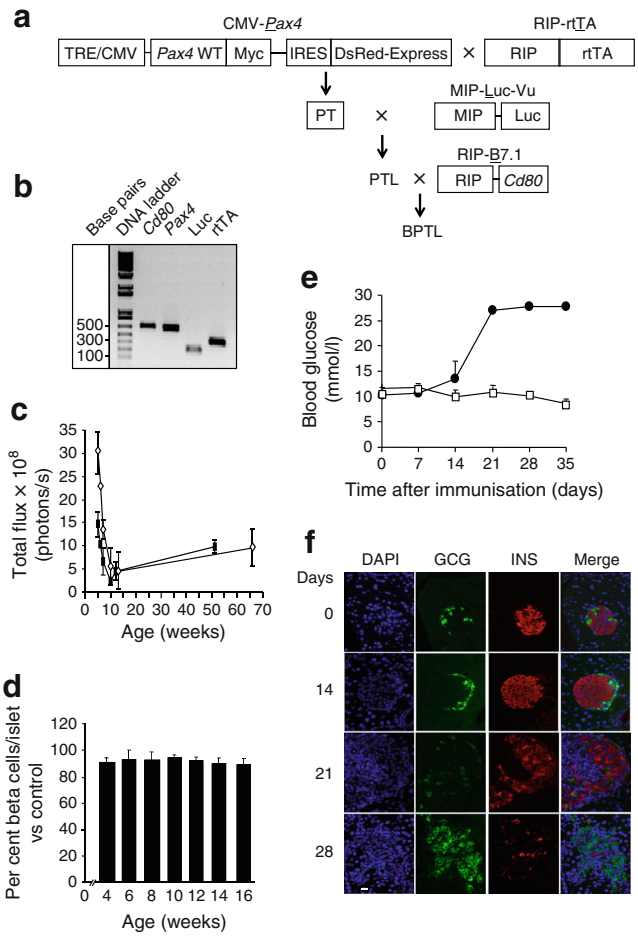

Fig. 1 Characterisation of the BPTL mice. (**a**) Schematic diagram showing the generation of the BPTL mouse. (**b**) Genotyping of BPTL mice by PCR using primer sets for *Cd80*, *Pax4*, *Luc* and *rtTA*. (**c**) The bioluminescent signal was correlated with age in BPTL male (white diamonds, $n=5$) and female (black rectangles, $n=5$) mice. (**d**) BCM calculated as a percentage of total islet cells and compared with 8-week-old animals was assessed in both sexes. On average, cells from at least 25 islets were counted per animal, with each group comprising at least 5–6 mice. (**e**) Blood glucose levels were measured for up to 35 days in BPTL mice ($n=3$) immunised (black circles) or not (control, white squares). (**f**) Pancreatic sections of BPTL mice at the indicated time after immunisation were co-immunostained for glucagon (green) and insulin (red). Nuclei were stained with DAPI (blue). Scale bar, 25 μm. GCG, glucagon; INS, insulin

Intracellular Ca^{2+} measurements Isolated islets were incubated for 1 h at room temperature with 2 μmol/l Fura-2 (Qiagen). Fluorescence recordings were performed using an inverted epifluorescence microscope (Axiovert 200; Zeiss, Jena, Germany) equipped with 360 nm and 380 nm bandpass filters. Recordings were expressed as the ratio of fluorescence at 360 nm and 380 nm (F360/380). Images were taken every 3 s. Intracellular [Ca^{2+}] changes in response to stimuli were analysed as previously described [19].

MIN6 cell culture and RNA interference MIN6 cells were cultured as previously described [20] and transfected with either 50 μmol *Pax4* small interfering (si)RNA (Sigma) or scramble siRNA using Oligofectamine (Life Technologies, Madrid, Spain). Cells were either processed for RNA or treated with thapsigargin (Sigma-Aldrich, Madrid, Spain) to assess apoptosis 48 h after transfection.

Immunohistochemistry and electron microscopy Dissected pancreases were fixed in 4% paraformaldehyde and processed at the Histology Core Facility, Andalusian Center for Molecular Biology and Regenerative Medicine (CABIMER). A detailed immunocytochemistry protocol along with the list of antibodies used is provided in ESM Methods and ESM Table 1. Validation of antibodies was performed on appropriate control samples. The BCM and islet cell number were assessed as described elsewhere [21]. Apoptosis, proliferation and DNA damage were quantified by counting caspase-3-, Ki67- and p53BP1-positive cells, respectively, in at least 20 to 50 islets from three independent pancreatic sections from 3–4 mice per group. Insulitis scoring was performed as previously outlined [22]. For electron microscopy (EM), pancreatic islets were processed using a standard Spurr protocol [23]. Images were acquired with an electron-multiplying charge-coupled device (EMCCD) camera (TRS 2 k × 2 k).

RNA microarray Labelled cRNA samples were prepared from pools of at least 100 islets isolated from either *Pax4*/*rtTA* or *Pax4*R121W/*rtTA* transgenic animals (8-week-old females) treated with DOX or not treated [14]. Three preparations of cRNA per group were then hybridised to the GeneChip Mouse Gene 1.0 ST Array chip (Affymetrix, Santa Clara, CA, USA) using the standard protocols of the Genomic Core Facility, CABIMER. Raw data are accessible in the Gene Expression Omnibus database under accession number GSE62846, while its analysis is described in ESM Methods.

Statistical analysis Results are expressed as mean ± SEM. Statistical differences between two conditions were estimated using the unpaired Student's *t* test. One-way ANOVA was used for comparison of more than two groups with Bonferroni post hoc test or non-parametric Mann–Whitney test (*$p < 0.05$ and **$p < 0.01$).

Results

PAX4 expression blunts EAD in immunised BPTL mice We first monitored in vivo the bioluminescence intensity (BLI) emitted by beta cells of BPTL mice from 4 to 65 weeks of age (Fig. 1c). In 4-week-old mice, the bioluminescence signal was two fold higher in male mice than females. Consistent with a transient wave of beta cell apoptosis and decreased rate of islet growth around weaning [24], both sexes displayed a decline in BLI signal between the fourth and the ninth week (Fig. 1c). Thereafter, this signal did not significantly change with age (Fig. 1c). Morphometric evaluation revealed that the volume density of beta cells was similar in animals aged from 4 to 16 weeks (Fig. 1d). Thus, by 9 weeks of age the bioluminescent signal reflects the mass and function of beta cells, which we hereafter refer to as the functional beta cell mass (BCM). Similar to the RIP-B7.1 animal, immunised BPTL mice developed hyperglycaemia within 21 days (Fig. 1e) due to a gradual loss of beta cells (Fig. 1f), whereas non-immunised mice remained normoglycaemic (Fig. 1e, f).

We next determined whether PAX4 expression could prevent EAD. Five-week-old BPTL mice were treated with DOX for 4 weeks prior to immunisation. Compared with control mice, islets from treated mice revealed a ten fold increase in *Pax4* expression (Fig. 2a), but no change in *Cd80* transcript levels (Fig. 2b). DOX treatment did not alter the BCM or GSIS of PAX4-expressing islets (Fig. 2c, d). Nine-week-old untreated controls remained normoglycaemic and featured no variation in bioluminescent signal for up to 28 days (Fig. 2e). Immunised BPTL mice without DOX revealed a rapid decrease in BLI, reaching undetectable levels by day 28 post-immunisation, which coincided with sustained hyperglycaemia (Fig. 2f). Escalation in blood glucose level observed 21 days after immunisation correlated with a 60% decrease in BLI. DOX-treated and immunised BPTL mice maintained both normoglycaemia and bioluminescent signal (Fig. 2g). Protection was extended up to 63 days (Fig. 2h), at which point 65% of immunised and DOX-treated BPTL mice developed hyperglycaemia, probably because of the robust immune attack conveyed by CD80 overexpression. Immunised and DOX-treated RIP-B7.1 mice developed hyperglycaemia (ESM Fig. 1), excluding a protective effect mediated by the antibiotic through alteration in the gut microbiome [25, 26]. Non-DOX-treated BPTL mice suffered a 40% and 80% reduction in the functional BCM after 21 and 28 days of immunisation, respectively. Such changes were not observed in DOX-treated mice (Fig. 3a, b). By day 63, the latter animals retained approximately 50% of the functional BCM (Fig. 3b).

PAX4 improves beta cell health and mitigates the autoimmune attack Insulitis assessment at 28 days after immunisation revealed that 65% of islets of DOX-treated BPTL mice were insulitis free (grade 0), whereas 90% of islets derived from non-DOX-treated BPTL mice displayed severe insulitis (grades 2–4) (Fig. 4a). Even at 63 days after immunisation only 50% of islets from DOX-treated BPLT mice displayed mild insulitis (Fig. 4a). DOX treatment also diminished the percentage of cleaved CASPASE-3-positive islet cells in immunised animals (Fig. 4b and ESM Fig. 2a). DNA damage induced by NO and reactive oxygen species

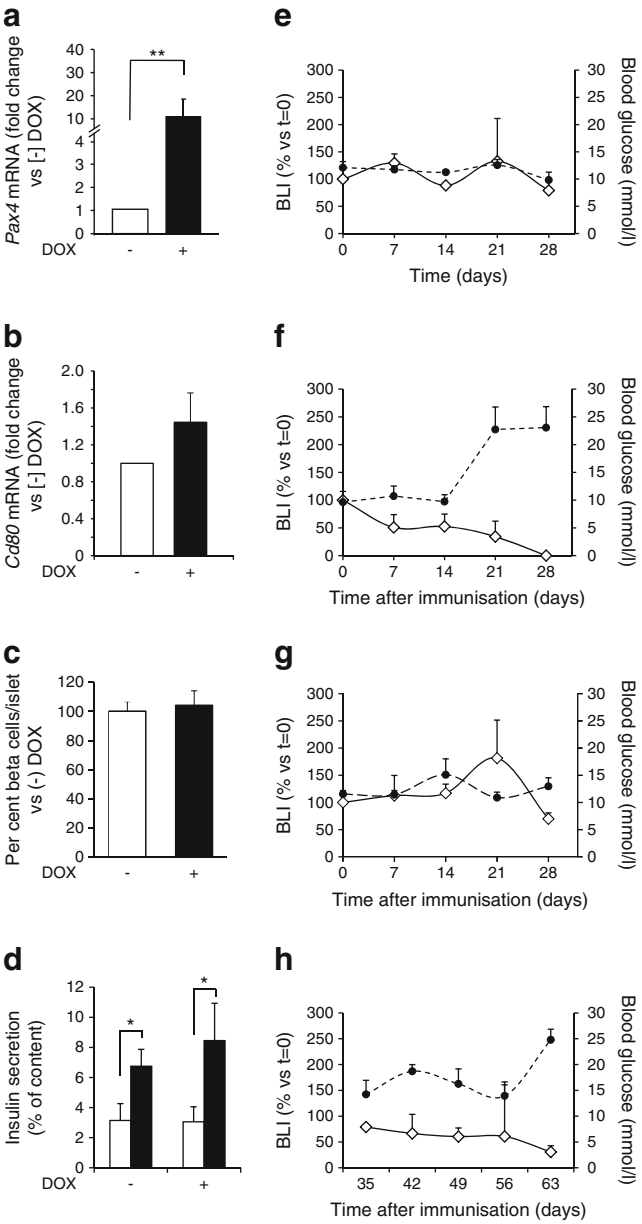

Fig. 2 PAX4 prevents the development of hyperglycaemia in immunised BPTL mice. Islet (**a**) *Pax4* and (**b**) *Cd80* transcript levels in 5-week-old BPTL animals treated with DOX for 1 month or not treated ($n = 4$–6). Relative mRNA levels were normalised to the transcript levels of the housekeeping gene β-actin and/or *Rps29*. Data were calculated as fold change compared with non-DOX-treated mice. $^{**}p < 0.01$. (**c**) BCM was calculated as a percentage of total islet cells and compared with the (−) DOX group. On average, cells from at least 25 islets were counted per animal ($n = 4$–6). (**d**) Insulin secretion by isolated BPTL islets treated or not with DOX was assessed in 30 min static incubations in response to glucose at 2.5 mmol/l (white bars) and 16.5 mmol/l (black bars). Insulin released was quantified by ELISA and expressed as a percentage of total cellular insulin content. $n = 4$–7, $^{*}p < 0.05$. BLI (white diamonds) and blood glucose levels (black circles) was measured weekly for up to 4 weeks in (**e**) control untreated BPTL mice ($n = 4$), (**f**) immunised non-DOX-treated ($n = 6$) and (**g**) immunised DOX-treated BPTL animals ($n = 6$). (**h**) BLI and blood glucose level measurements were extended to 63 days in immunised and DOX-treated BPTL mice ($n = 6$). BLI results are presented as per cent change compared with day 0 ($t = 0$), while blood glucose levels are expressed as means ± SEM

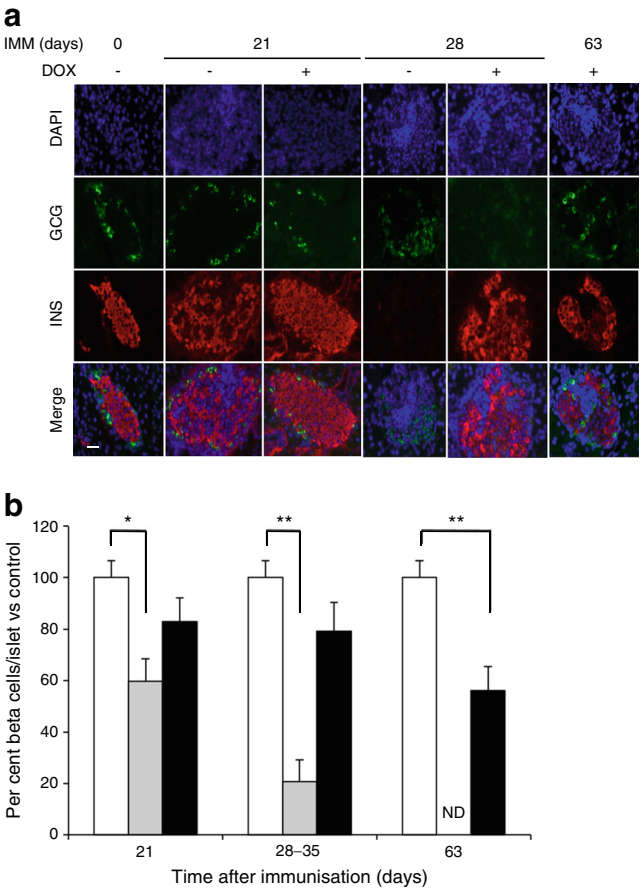

Fig. 3 PAX4 preserves the functional BCM in immunised BPTL mice. (**a**) Immunohistochemical analysis of glucagon (green) and insulin (red) in pancreases from BPTL mice treated or not with DOX and killed at days 0, 21, 28 and 63 post-immunisation. Nuclei are stained blue. Scale bar, 25 μm. (**b**) BCM in control non-immunised and non-DOX-treated (white bars), immunised and non-DOX-treated (grey bars) and immunised and DOX-treated (black bars) mice was calculated as a percentage of total islet cells and compared with the control group at each time point. On average, cells from at least 25 islets were counted per animal ($n = 5$–6). As similar results were obtained for days 28 and 35, the data were combined as a single time point. ND, not determined, as this group was killed at day 35 to comply with animal welfare guidelines. $^{*}p < 0.05$ and $^{**}p < 0.01$. GCG, glucagon; IMM, immunised; INS, insulin

(ROS) contributes to beta cell death [27, 28]. Immunostaining for the double-strand DNA break marker p53BP1 revealed that PAX4 overexpression reduced DNA damage in islets from either immunised BPTL or STZ-treated mice (Fig. 4c). These changes were paralleled by increased cell proliferation in DOX-treated BPLT islets (Fig. 4d and ESM Fig. 2b).

PAX4 regulates genes important for beta cell proliferation and ER homeostasis Transcriptome profiling was conducted on PAX4 and PAX4R129W islets to highlight PAX4 target genes involved in beta cell health, and those altered by the diabetes-linked mutant variant R129W. We initially demonstrated that DOX-treated and immunised mutBPTL mice developed hyperglycaemia (Fig. 5a) with an incidence of

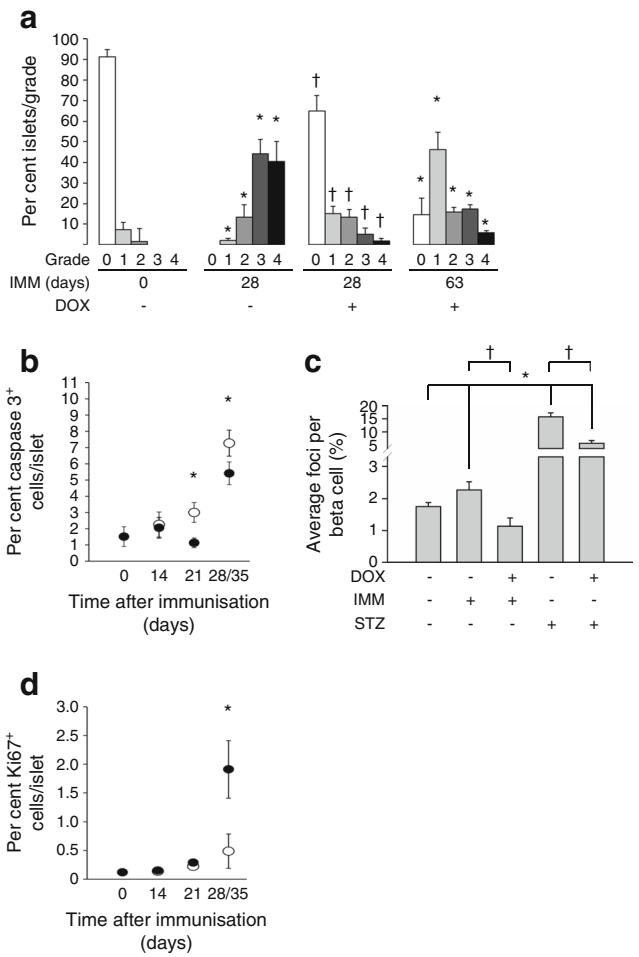

Fig. 4 BPTL mice overexpressing PAX4 display reduced insulitis, correlating with decreased islet apoptosis and DNA damage and increased proliferation. (**a**) Insulitis was scored as grade 0–4 according to the percentage of infiltrated islet area (0: 0%; 1: <10%; 2: >10% and <55%; 3: >55% and <75%; 4: >75%). $n = 5$–6, $^{*}p < 0.05$ vs immunised day 0 and (−) DOX group; $^{\dagger}p < 0.05$ vs immunised day 28 and (−) DOX group. (**b**) Apoptosis was assessed by immunohistochemical analysis of cleaved caspase-3 in pancreatic islets from BPTL mice treated (black ovals) or not (white ovals) with DOX and killed at the time points. As similar results were obtained for days 28 and 35, the data were combined as a single time point. $n = 5$–6, $^{*}p < 0.05$, (+) vs (−) DOX groups within each time point. (**c**) The average number of 53BP1 foci per beta cell was assessed from pancreatic islets of either 14-day-old immunised BPTL mice or 2-day-old STZ-treated PAX4 mice exposed (+) or not (−) to DOX. $n = 5$–6, $^{*}p < 0.05$ vs untreated mice; $^{\dagger}p < 0.05$ vs DOX-untreated immunised or STZ-treated mice. (**d**) Cell proliferation was assessed by the combined immunohistochemical analysis of Ki67 in pancreatic islets from BPTL mice treated (black ovals) or not (white ovals) with DOX and killed at the time points. $n = 5$–6, $^{*}p < 0.05$, (+) vs (−) DOX groups within the time point. IMM, immunised

approximately 75% by day 28 compared with 100% in non-DOX-treated immunised animals (Fig. 5b). Transcriptome analysis revealed that 770 transcripts were upregulated and 449 were downregulated in PAX4 islets, whereas 1437 genes were upregulated and 1136 downregulated in PAX4R129W islets. Genes showing the largest changes are listed in ESM Table 2. Notwithstanding this list, we substantiated by qPCR our previous findings [14] that *Mafa* transcript levels were repressed whereas *Nos2* levels were unchanged in PAX4 islets (ESM Fig. 3). However, *Bcl2* levels were not increased in PAX4-overexpressing islets (ESM Fig. 3), arguing against a role of this factor in protecting from EAD [15].

A functional enrichment analysis disclosed that the cell cycle and the protein processing in ER pathways were among the top upregulated Kyoto Encyclopaedia of Genes and Genomes (KEGG) pathways in islets overexpressing PAX4, but were among the most significantly downregulated pathways in islets overexpressing PAX4R129W (adjusted p values < 0.05) (Fig. 5c, d and ESM Tables 3 and 4). To contrast the expression levels of genes contributing to these pathways, we generated heat maps amenable to statistical analysis (raw p value < 0.05). Several genes associated with cell cycle were increased in PAX4 islets, while remaining unchanged or having lower levels in islets expressing PAX4R129W (Fig. 5e). Genes encoding proteins for peptide folding (*Hspa5* [also known as *Bip*], *Calr*), ER–Golgi translocation (*Lman1*, *Lman2*, *Sec23b* and *Plaa*) and ER-associated protein degradation (ERAD) (*Ufd1l*, *Derl3*, *Pdia4*, *Ssr3*, *Syvn1* and *Dnaja2*/*Hsp40*) were upregulated after overexpression of PAX4, but were downregulated after overexpression of PAX4R129W (Fig. 5f). The UPR-associated genes *Mbtps2*, *Eif2ak3* and *Mapk10* were upregulated in PAX4 islets and were marginally altered in PAX4R129W islets (Fig. 5f).

PAX4 targets ER integrity and calcium homeostasis, protecting cells against apoptosis Given that PAX4 but not PAX4R129W targets genes that are involved in ER homeostasis, we investigated the contribution of ER to PAX4-mediated beta cell health. We initially assessed expression levels of calreticulin (*Calr*), a major Ca^{2+} binding protein of the ER lumen and of galectin-9 (*Lgals9*), a protein involved in immune modulation. Although *Pax4* and *Pax4*R129W transcript levels were increased three fold, *Calr* and *Lgals9* expression levels were only increased in PAX4 islets (Fig. 6a, b). As Ca^{2+} handling by the ER affects the cell sensitivity to apoptosis, we assessed whether PAX4 and PAX4R129W could protect against ER-stress-induced beta cell apoptosis. Islets treated in vitro with DOX exhibited DsRed fluorescence, confirming the expression of the transgenes (Fig. 6c). Thapsigargin exposure prompted a two fold increase in apoptosis in control mice (Fig. 6d). DOX reduced both basal and thapsigargin-induced apoptosis only in PAX4 islets (Fig. 6d). However, *Pax4* siRNA-mediated repression in MIN6 cells caused a 60% decrease in *Calr* transcript levels, with a concomitant sensitisation to thapsigargin-induced apoptosis compared with siControl and thapsigargin-treated cells (Fig. 6e, f).

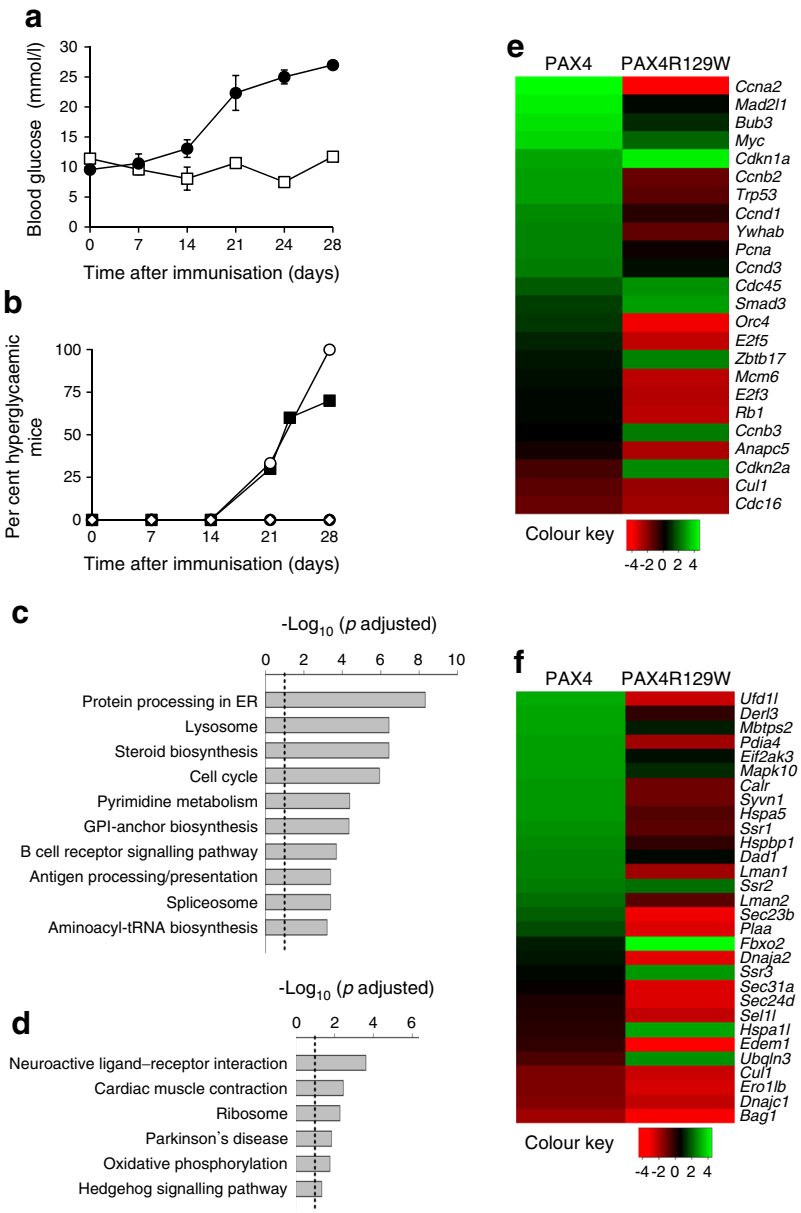

Fig. 5 ER homeostasis and cell cycle are key cellular pathways targeted by PAX4. (**a**) Blood glucose levels were measured for up to 28 days in control non-DOX-treated (control, white squares) and immunised DOX-treated (black circles) mutBPTL mice ($n = 4$). (**b**) Hyperglycaemia incidence was assessed in control non-treated ($n = 5$, white diamonds), immunised and non-DOX-treated ($n = 6$, white circles) and immunised and DOX-treated ($n = 6$, black circles) BPTL mice as well as in immunised and DOX-treated mutBPTL mice ($n = 7$, black squares). (**c**, **d**) Significantly enriched KEGG pathways (adjusted p value <0.05) altered by (**c**) PAX4 and (**d**) PAX4R129W. The dotted line shows the threshold of significance. (**e**, **f**) Heat maps displaying t statistic values of (**e**) cell cycle and (**f**) protein processing in the ER KEGG pathway genes modulated in either PAX4 or PAX4R129W islets vs control. Colours display the t statistic values for all genes within the corresponding KEGG pathway, estimated using the t statistic value from differential expression analysis. GPI, glycosylphosphatidylinositol

Perturbation in beta cell ER homeostasis has been linked to ER dilation [29, 30]. Accordingly, islets from non-DOX-treated *Pax4* transgenic mice exposed in vitro to thapsigargin displayed distension and fragmentation of the rough ER (RER) in beta cells, an effect prevented by PAX4 overexpression (Fig. 7). ER calcium release in response to carbachol was then measured. Calcium release in PAX4-overexpressing beta cells from isolated islets was marginally higher than that of controls cells (Fig. 8a–d). As the higher ER-Ca^{2+}-buffering capacity induced by PAX4 could mask the carbachol-stimulated calcium release, we measured cytosolic Ca^{2+} signals in response to glucose. Glucose-induced calcium oscillations were improved in isolated islets overexpressing PAX4 compared with control islets (Fig. 8e, f). The overall Ca^{2+} signal was also higher in PAX4-overexpressing cells (Fig. 8g–i). Thus, PAX4 overexpression leads to improve ER and Ca^{2+} homeostasis in the face of beta cell stress as encountered during the islet isolation procedure or an immune attack.

Discussion

Inflammation is a common denominator in types 1 and 2 diabetes, and leads to beta cell failure and death, predominantly by apoptosis. As yet, there is no 'unifying hypothesis' for the mechanisms triggering beta cell deterioration [31, 32]; deciphering the molecular roadmap regulated by factors such

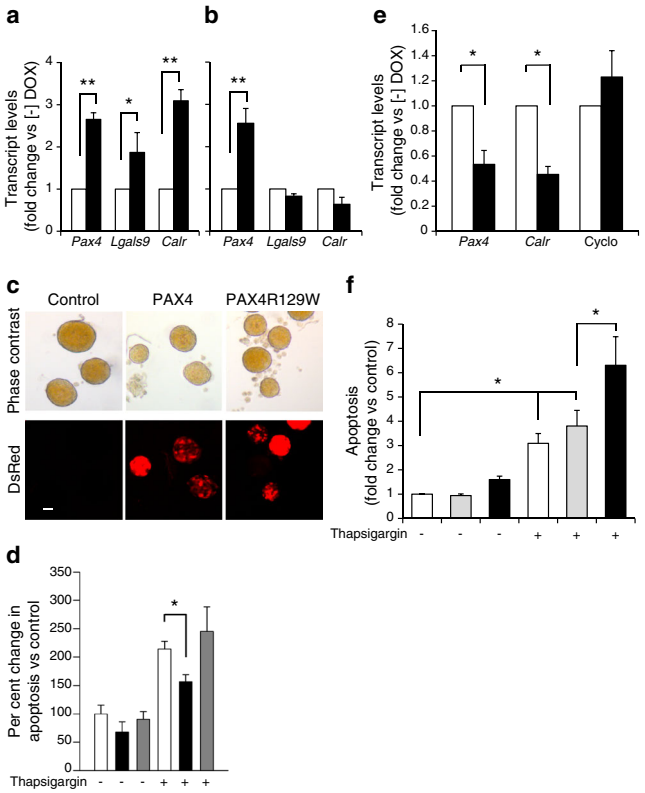

Fig. 6 PAX4-regulated ER homeostasis prevents cell degeneration. Islet PAX4, galectin-9 (*Lgals9*) and calreticulin (*Calr*) transcript levels were assessed in (**a**) PAX4 or (**b**) PAX4R129W transgenic mice treated (black bars) or not treated (white bars) with DOX for 1 month. The relative mRNA levels were normalised to transcript levels of the housekeeping gene β-actin. Data were calculated as fold change compared with the values in control, non-DOX-treated animals. $n = 3$, $^{**}p < 0.01$ and $^{*}p < 0.05$. (**c**) *Pax4* or *Pax4*R129W induction in DOX-treated islets was qualitatively assessed through DsRed fluorescence. Scale bar, 10 μm. (**d**) Control (white bars), PAX4-expressing (black bars) and PAX4R129W-expressing (grey bars) islets were then challenged with 1 μmol/l thapsigargin or not challenged and apoptosis was measured by ELISA. Results expressed as per cent change compared with control non-thapsigargin-treated islets. $n = 5$, $^{*}p < 0.05$. (**e**) *Pax4*, *Calr* and cyclophylin expression levels were measured in MIN6 cells treated with siControl (white bars) and si*Pax4* (black bars). mRNA levels were normalised to the transcript levels of the housekeeping gene β-actin. Data were calculated as fold change compared with the values in siControl-treated cells. $n = 4$, $^{*}p < 0.05$. (**f**) Apoptosis was evaluated in control MIN6 (white bars), and cells treated with siControl (grey bars) or si*Pax4* (black bars), untreated or treated with thapsigargin. Results are expressed as fold change compared with control non-thapsigargin-treated cells. $n = 5$, $^{*}p < 0.05$

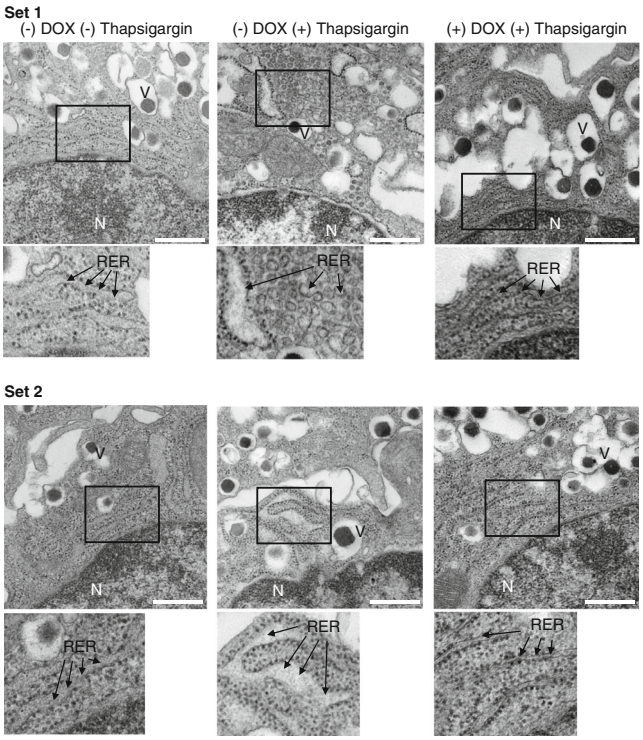

Fig. 7 ER integrity is preserved in PAX4-overexpressing islets. Two sets (upper and lower) of beta cell micrographs from islets isolated from PAX4 transgenic mice, treated with DOX or not treated, and challenged with 1 μmol/l thapsigargin or not challenged. Arrows indicate the RER. Inset is enlarged below each image. Scale bar, 0.5 μm. N, nucleus; V, insulin vesicles

as PAX4—mutations in which are linked to both forms of diabetes—may help identify common pathways. Herein, we provide proof-of-concept that PAX4, but not PAX4R129W, preserves the BCM and delays the development of hyperglycaemia in the RIP-B7.1 mouse model of EAD. This highlights the mechanistic differences between the wild type and mutant variant.

Consistent with previous reports exploiting the RIP-B7.1 model, 90–100% of immunised non-DOX-treated RIP-B7.1 mice bearing either the *Pax4* or *Pax4R129W* transgene developed hyperglycaemia within 3 weeks, correlating with insulitis and beta cell destruction [33]. DOX-mediated induction of *Pax4* prevented hyperglycaemia development in BPTL animals up to 4 weeks after immunisation, whereas *Pax4R129W* induction partially reduced the hyperglycaemic incidence in mutBPTL mice. Thus, PAX4 blunts hyperglycaemia in an autoimmune context, in contrast to several other factors such as caspase-3-generated RAS p21 protein activator 1 (RasGAP) N-terminal fragment (fragment N), cytokine response modifier A (CRMA) or BCL-2 which, despite increasing BCM, could not prevent hyperglycaemia in animal models of type 1 diabetes [15, 22, 34]. Our data imply that in addition to inhibiting apoptosis, PAX4 is involved in additional regulatory pathways, possibly including immune modulation. Correspondingly, insulitis was reduced after PAX4 overexpression, an effect not attributable to a non-specific repression of the *Cd80* transgene that facilitates the immune response. Our observations extend the analogous findings that inhibition of vascular endothelial growth factor receptor 2 (VEGFR-2) in NOD mice reversed hyperglycaemia by abrogating insulitis and restoring islet cell function

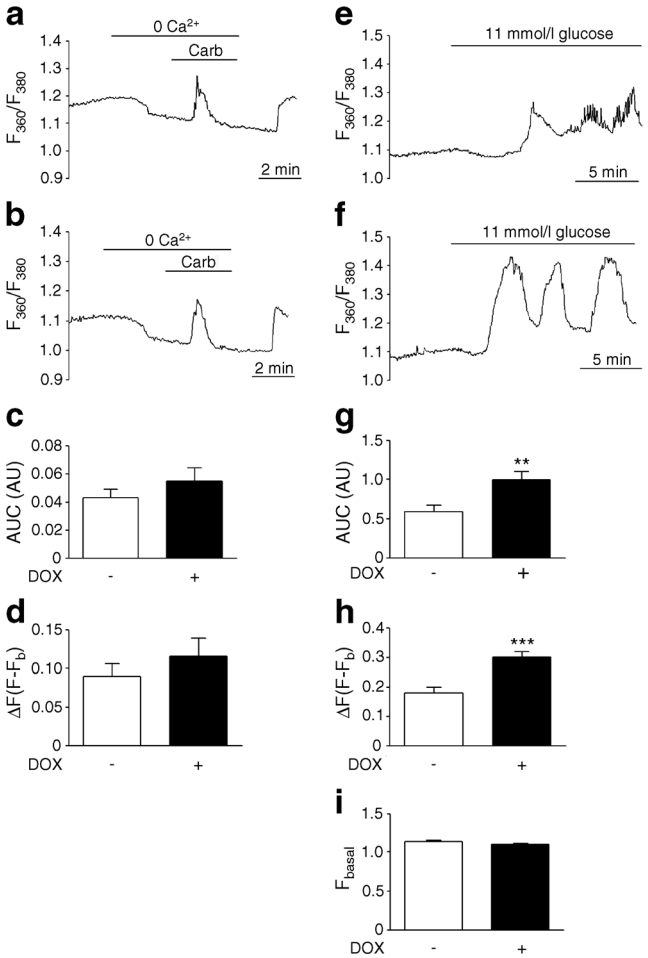

Fig. 8 PAX4-overexpressing islets exhibit normal calcium oscillation in response to glucose. Carbachol-stimulated (100 μmol/l) intracellular release of Ca^{2+} was measured in intact islets (**a**) treated with DOX or (**b**) not treated. As indicated by the bars, islets were exposed to Ca^{2+}-deficient medium containing 2 mmol/l EGTA prior to applying 100 μmol/l carbachol. (**c**) Analysis of the AUC for the time of the stimulus with carbachol from experiments shown in (**a**) and (**b**). (**d**) Analysis of the Ca^{2+} peak amplitude in response to carbachol challenge. ($n = 5$–6). Representative Ca^{2+} signals in response to 11 mmol/l glucose measured in intact islets (**e**) treated with DOX or (**f**) not treated. (**g**) Analysis of the AUC for the last 10 min of the glucose stimulus recording shown in (**e**) and (**f**). (**h**) Analysis of the amplitude of the first Ca^{2+} transient in response to the glucose challenge. (**i**) Analysis of the basal fluorescence during the first minute of the experiments. $n = 9$; $^{**}p \leq 0.01$ and $^{***}p \leq 0.001$. ΔF; fluorescence increase

[35]. Although the mechanism by which PAX4 acts at the interface of beta cells and the immune system to blunt insulitis and improve islet recovery remains undefined, our genetic analysis revealed that *Lgals9* was specifically upregulated in PAX4 islets. This gene induces apoptosis of differentiated T helper 1 (Th1) cells [36], and its overexpression in NOD mice reduced insulitis and hyperglycaemia [37], prolonging the survival of grafts [38]. It is therefore plausible that, by enhancing *Lgals9* expression, PAX4 may downregulate Th1 function, partially impeding insulitis and improving islet survival.

Transcriptome profiling revealed that cell-cycle-associated genes upregulated by PAX4 were downregulated by PAX4R129W, despite comparable expression levels of both transgenes. Specifically, the type 2 diabetes-associated cyclin-dependent kinase inhibitor 2A, which strongly inhibits the proliferative cyclin-dependent kinase 4 (CDK4) [39], was enriched in PAX4R129W islets whereas it was decreased in PAX4 islets. Reciprocally, cyclin D3, which promotes beta cell survival, was increased in PAX4- but not in PAX4R129W-overexpressing islets [40]. These findings provide some molecular insights into the pathogenic effect of the R129W mutation on beta cell plasticity.

Our data also reveal that PAX4, but not PAX4R129W, is a key regulator of ER function by a combined targeting of genes involved in UPR, Ca^{2+} homeostasis, ER–Golgi translocation, and ERAD. The functional importance of the transcriptional changes in these genes was validated by the capacity of PAX4 to prevent thapsigargin-induced ER ultrastructural abnormalities and apoptosis of beta cells, consistent with the finding that PAX4-binding sites are enriched within the promoter region of palmitate-modified ER stress response genes [41]. In contrast, repression of PAX4-sensitised MIN6 cells to thapsigargin cell death correlates with reduced CALR levels. Calreticulin is a Ca^{2+} chaperone of the ER, which contributes to the quality control of protein folding [42]. Overexpression of CALR in MIN6 cells enhances ER Ca^{2+} stores and prevents NO-induced apoptosis [43]. In this context, the production of NO and ROS induced by inflammatory cytokines in the diabetic environment promotes beta cell death by a variety of mechanisms, including the induction of irreversible double-strand DNA breaks [27, 44]. We found that PAX4 blunts DNA damage in two models of experimental diabetes, pointing to a general protective mechanism, possibly through preserved ER homeostasis, implicating CALR [43]. The finding that PAX4-overexpressing islets exhibited improved glucose-induced Ca^{2+} oscillations points to this premise. Loss of oscillatory capacity is associated with diminished islet glucose sensitivity and increased ER dysfunction [45]. Thus, amplified Ca^{2+} content in the CALR-enriched ER of PAX4-overexpressing beta cells may impact cytosolic calcium dynamics [43, 46], thereby preventing activation of downstream apoptotic pathways under stress conditions.

We conclude that PAX4 favours beta cell survival and regeneration in various deleterious inflammatory and high-grade inflammatory environments, such as autoimmunity, through the coordinated regulation of immune modulation, cell cycle, cell survival, ER homeostasis and DNA repair. While both PAX4 and PAX4R129W modulate these pathways, it is the wild-type transcription factor that conveys pro-survival properties by increasing the expression of selected adaptive genes.

Acknowledgements We thank F. Cortes (Department of Stem Cells, CABIMER, Seville, Spain) for kindly providing the 53BP1 antibody as well as his expert advice on DNA damage. We also thank J. Vallejo Ortega (Department of Stem Cells, CABIMER, Seville, Spain), E. Nadujar and M. Pérez (Genomic Core Facility, CABIMER, Seville, Spain) for excellent technical assistance.

Access to research materials The raw data for the RNA microarray described herein are accessible in the Gene Expression Omnibus database under accession number GSE62846.

Funding This work was funded by grants from the Consejeria de Salud, Fundacion Publica Andaluza Progreso y Salud, Junta de Andalucia (PI-0727-2010 to BRG and PI-0085-2013 to PIL), Consejeria de Economia, Innovacion y Ciencia (P10.CTS.6359 to BRG), Ministerio de Ciencia e Innovacion (BFU2013-42789-P to IQ) and the Ministerio de Economia y Competidividad, Instituto de Salud Carlos III co-funded by Fondos FEDER (PI10/00871 and PI13/00593 to BRG). NC-V is supported by a JDRF subsidy (17-2013-372 to BRG.). AM-M is a recipient of a Miguel Servet grant (CP14/00105) from the Instituto de Salud Carlos III co-funded by Fondos FEDER and EF-M is a recipient of a Juan de la Cierva Fellowship. PM is supported by Swiss National Science Foundation grant 310030-141162, and the European Union grant IMIDIA, C2008-T7. BOB is supported by grants from the Lee Kong Chian School of Medicine, Nanyang Technological University, Singapore, Republic of Singapore.

Duality of interest The authors declare that there is no duality of interest associated with this manuscript.

Contribution statement JMMG, CMJ-M and AM-M contributed equally to the conception and design of experiments as well as the acquisition and analysis of data. AIA-M, EF-M, IGHG, LL-N, NC-V, EB-T and IQ were involved in the acquisition and analysis of data. PIL, JS-L, JPF, AS, BOB and PM took part in the analysis and interpretation of data. BRG conceptualised and supervised all experiments and wrote the manuscript. All authors critically reviewed the manuscript for important intellectual content and approved the final version to be published. BRG is the guarantor of this work.

References

1. Donath MY (2014) Targeting inflammation in the treatment of type 2 diabetes: time to start. Nat Rev Drug Discov 13:465–476
2. Tisch R, Wang B (2008) Dysregulation of T cell peripheral tolerance in type 1 diabetes. Adv Immunol 100:125–149
3. Papa FR (2012) Endoplasmic reticulum stress, pancreatic beta-cell degeneration, and diabetes. Cold Spring Harb Perspect Med 2: a007666
4. Cao SS, Kaufman RJ (2014) Endoplasmic reticulum stress and oxidative stress in cell fate decision and human disease. Antioxid Redox Signal 21:396–413
5. Delepine M, Nicolino M, Barrett T, Golamaully M, Lathrop GM, Julier C (2000) EIF2AK3, encoding translation initiation factor 2-alpha kinase 3, is mutated in patients with Wolcott-Rallison syndrome. Nat Genet 25:406–409
6. Inoue H, Tanizawa Y, Wasson J et al (1998) A gene encoding a transmembrane protein is mutated in patients with diabetes mellitus and optic atrophy (Wolfram syndrome). Nat Genet 20:143–148
7. Kirkpatrick CL, Wiederkehr A, Baquie M et al (2011) Hepatic nuclear factor 1alpha (HNF1alpha) dysfunction down-regulates X-box-binding protein 1 (XBP1) and sensitizes beta-cells to endoplasmic reticulum stress. J Biol Chem 286:32300–32312
8. Sachdeva MM, Claiborn KC, Khoo C et al (2009) Pdx1 (MODY4) regulates pancreatic beta cell susceptibility to ER stress. Proc Natl Acad Sci U S A 106:19090–19095
9. Robson EJ, He SJ, Eccles MR (2006) A PANorama of PAX genes in cancer and development. Nat Rev Cancer 6:52–62
10. Greenwood AL, Li S, Jones K, Melton DA (2007) Notch signaling reveals developmental plasticity of Pax4(+) pancreatic endocrine progenitors and shunts them to a duct fate. Mech Dev 124:97–107
11. Sosa-Pineda B, Chowdhury K, Torres M, Oliver G, Gruss P (1997) The Pax4 gene is essential for differentiation of insulin-producing beta cells in the mammalian pancreas. Nature 386:399–402
12. Brun T, Gauthier BR (2008) A focus on the role of Pax4 in mature pancreatic islet beta-cell expansion and survival in health and disease. J Mol Endocrinol 40:37–45
13. Mauvais-Jarvis F, Smith SB, Le May C et al (2004) PAX4 gene variations predispose to ketosis-prone diabetes. Hum Mol Genet 13: 3151–3159
14. Hu He KH, Lorenzo PI, Brun T et al (2011) In vivo conditional pax4 overexpression in mature islet beta cells prevents stress-induced hyperglycemia in mice. Diabetes 60:1705–1715
15. Allison J, Thomas H, Beck D et al (2000) Transgenic overexpression of human Bcl-2 in islet beta cells inhibits apoptosis but does not prevent autoimmune destruction. Int Immunol 12:9–17
16. Park SY, Wang X, Chen Z et al (2005) Optical imaging of pancreatic beta cells in living mice expressing a mouse insulin I promoter-firefly luciferase transgene. Genesis 43:80–86
17. Gauthier BR, Brun T, Sarret EJ et al (2004) Oligonucleotide microarray analysis reveals PDX1 as an essential regulator of mitochondrial metabolism in rat islets. J Biol Chem 279:31121–31130
18. Gauthier BR, Wiederkehr A, Baquie M et al (2009) PDX1 deficiency causes mitochondrial dysfunction and defective insulin secretion through TFAM suppression. Cell Metab 10:110–118
19. Gonzalez A, Merino B, Marroqui L et al (2013) Insulin hypersecretion in islets from diet-induced hyperinsulinemic obese female mice is associated with several functional adaptations in individual beta-cells. Endocrinology 154:3515–3524
20. Semache M, Ghislain J, Zarrouki B, Tremblay C, Poitout V (2014) Pancreatic and duodenal homeobox-1 nuclear localization is regulated by glucose in dispersed rat islets but not in insulin-secreting cell lines. Islets 6, e982376
21. Mellado-Gil J, Rosa TC, Demirci C et al (2011) Disruption of hepatocyte growth factor/c-Met signaling enhances pancreatic beta-cell death and accelerates the onset of diabetes. Diabetes 60: 525–536
22. Bulat N, Jaccard E, Peltzer N et al (2011) RasGAP-derived fragment N increases the resistance of beta cells towards apoptosis in NOD mice and delays the progression from mild to overt diabetes. PLoS One 6, e22609
23. Spurr AR (1969) A low-viscosity epoxy resin embedding medium for electron microscopy. J Ultrastruct Res 26:31–43
24. Scaglia L, Cahill CJ, Finegood DT, Bonner-Weir S (1997) Apoptosis participates in the remodeling of the endocrine pancreas in the neonatal rat. Endocrinology 138:1736–1741
25. Alkanani AK, Hara N, Lien E et al (2014) Induction of diabetes in the RIP-B7.1 mouse model is critically dependent on TLR3 and

MyD88 pathways and is associated with alterations in the intestinal microbiome. Diabetes 63:619–631
26. Angelakis E, Million M, Kankoe S et al (2014) Abnormal weight gain and gut microbiota modifications are side effects of long-term doxycycline and hydroxychloroquine treatment. Antimicrob Agents Chemother 58:3342–3347
27. Oleson BJ, Broniowska KA, Schreiber KH, Tarakanova VL, Corbett JA (2014) Nitric oxide induces ataxia telangiectasia mutated (ATM) protein-dependent gammaH2AX protein formation in pancreatic beta cells. J Biol Chem 289:11454–11464
28. Tornovsky-Babeay S, Dadon D, Ziv O et al (2014) Type 2 diabetes and congenital hyperinsulinism cause DNA double-strand breaks and p53 activity in beta cells. Cell Metab 19:109–121
29. Ravelli RB, Kalicharan RD, Avramut MC et al (2013) Destruction of tissue, cells and organelles in type 1 diabetic rats presented at macromolecular resolution. Sci Rep 3:1804
30. Marroqui L, Masini M, Merino B et al (2015) Pancreatic alpha cells are resistant to metabolic stress-induced apoptosis in type 2 diabetes. EBioMedicine 2:378–385
31. Cnop M, Welsh N, Jonas JC, Jorns A, Lenzen S, Eizirik DL (2005) Mechanisms of pancreatic beta-cell death in type 1 and type 2 diabetes: many differences, few similarities. Diabetes 54(Suppl 2): S97–S107
32. Donath MY, Halban PA (2004) Decreased beta-cell mass in diabetes: significance, mechanisms and therapeutic implications. Diabetologia 47:581–589
33. Karges W, Rajasalu T, Spyrantis A, Wieland A, Boehm B, Schirmbeck R (2007) The diabetogenic, insulin-specific CD8 T cell response primed in the experimental autoimmune diabetes model in RIP-B7.1 mice. Eur J Immunol 37:2097–2103
34. Millet I, Wong FS, Gurr W et al (2006) Targeted expression of the anti-apoptotic gene CrmA to NOD pancreatic islets protects from autoimmune diabetes. J Autoimmun 26:7–15
35. Villalta SA, Lang J, Kubeck S et al (2013) Inhibition of VEGFR-2 reverses type 1 diabetes in NOD mice by abrogating insulitis and restoring islet function. Diabetes 62:2870–2878
36. Zhu C, Anderson AC, Schubart A et al (2005) The Tim-3 ligand galectin-9 negatively regulates T helper type 1 immunity. Nat Immunol 6:1245–1252
37. Chou FC, Shieh SJ, Sytwu HK (2009) Attenuation of Th1 response through galectin-9 and T cell Ig mucin 3 interaction inhibits autoimmune diabetes in NOD mice. Eur J Immunol 39:2403–2411
38. Chou FC, Kuo CC, Wang YL et al (2013) Overexpression of galectin-9 in islets prolongs grafts survival via downregulation of Th1 responses. Cell Transplant 22:2135–2145
39. Scott LJ, Mohlke KL, Bonnycastle LL et al (2007) A genome-wide association study of type 2 diabetes in Finns detects multiple susceptibility variants. Science 316:1341–1345
40. Saavedra-Avila NA, Sengupta U, Sanchez B et al (2014) Cyclin D3 promotes pancreatic beta-cell fitness and viability in a cell cycle-independent manner and is targeted in autoimmune diabetes. Proc Natl Acad Sci U S A 111:E3405–E3414
41. Cnop M, Abdulkarim B, Bottu G et al (2014) RNA sequencing identifies dysregulation of the human pancreatic islet transcriptome by the saturated fatty acid palmitate. Diabetes 63:1978–1993
42. Wang WA, Groenendyk J, Michalak M (2012) Calreticulin signaling in health and disease. Int J Biochem Cell Biol 44:842–846
43. Oyadomari S, Takeda K, Takiguchi M et al (2001) Nitric oxide-induced apoptosis in pancreatic beta cells is mediated by the endoplasmic reticulum stress pathway. Proc Natl Acad Sci U S A 98: 10845–10850
44. Cardozo AK, Ortis F, Storling J et al (2005) Cytokines downregulate the sarcoendoplasmic reticulum pump Ca2+ ATPase 2b and deplete endoplasmic reticulum Ca2+, leading to induction of endoplasmic reticulum stress in pancreatic beta-cells. Diabetes 54:452–461
45. Jahanshahi P, Wu R, Carter JD, Nunemaker CS (2009) Evidence of diminished glucose stimulation and endoplasmic reticulum function in nonoscillatory pancreatic islets. Endocrinology 150:607–615
46. Gilon P, Ravier MA, Jonas JC, Henquin JC (2002) Control mechanisms of the oscillations of insulin secretion in vitro and in vivo. Diabetes 51(Suppl 1):S144–S151

Expert Opinion on Therapeutic Targets

ISSN: 1472-8222 (Print) 1744-7631 (Online) Journal homepage: http://www.tandfonline.com/loi/iett20

Targeting pancreatic expressed PAX genes for the treatment of diabetes mellitus and pancreatic neuroendocrine tumors

Alejandro Martin-Montalvo, Petra I. Lorenzo, Livia López-Noriega & Benoit R. Gauthier

To cite this article: Alejandro Martin-Montalvo, Petra I. Lorenzo, Livia López-Noriega & Benoit R. Gauthier (2017) Targeting pancreatic expressed PAX genes for the treatment of diabetes mellitus and pancreatic neuroendocrine tumors, Expert Opinion on Therapeutic Targets, 21:1, 77-89, DOI: 10.1080/14728222.2017.1257000

To link to this article: https://doi.org/10.1080/14728222.2017.1257000

Accepted author version posted online: 14 Nov 2016.
Published online: 18 Nov 2016.

EXPERT OPINION ON THERAPEUTIC TARGETS, 2017
VOL. 21, NO. 1, 77–89
http://dx.doi.org/10.1080/14728222.2017.1257000

Taylor & Francis
Taylor & Francis Group

REVIEW

Targeting pancreatic expressed PAX genes for the treatment of diabetes mellitus and pancreatic neuroendocrine tumors

Alejandro Martin-Montalvo*, Petra I. Lorenzo*, Livia López-Noriega and Benoit R. Gauthier

Department of Stem Cells, CABIMER-Andalusian Center for Molecular Biology and Regenerative Medicine, Avenida Américo Vespucio, Pancreatic Islet Development and Regeneration Unit/Laboratory of Aging Biology (PIDRU LAB), Sevilla, Spain

ABSTRACT

Introduction: Four members of the PAX family, PAX2, PAX4, PAX6 and PAX8 are known to be expressed in the pancreas. Accumulated evidences indicate that several pancreatic expressed PAX genes play a significant role in pancreatic development/functionality and alterations in these genes are involved in the pathogenesis of pancreatic diseases.

Areas covered: In this review, we summarize the ongoing research related to pancreatic PAX genes in diabetes mellitus and pancreatic neuroendocrine tumors. We dissect the current knowledge at different levels; from mechanistic studies in cell lines performed to understand the molecular processes controlled by pancreatic PAX genes, to *in vivo* studies using rodent models that over-express or lack specific PAX genes. Finally, we describe human studies associating variants on pancreatic-expressed PAX genes with pancreatic diseases.

Expert opinion: Based on the current literature, we propose that future interventions to treat pancreatic neuroendocrine tumors and diabetes mellitus could be developed via the modulation of PAX4 and/or PAX6 regulated pathways.

ARTICLE HISTORY
Received 4 October 2016
Accepted 1 November 2016

KEYWORDS
Diabetes mellitus; pancreatic neuroendocrine tumors; PAX genes; PAX2; PAX4; PAX6; PAX8

1. Introduction: the PAX family

PAX transcription factors, defined by the conserved bipartite paired box DNA-binding domain (PAIRED), are classified into four groups according to the presence/absence of an octapeptide region, and the presence/absence/truncation of a second DNA-binding homeodomain [1,2]. This family of 9 genes in mammals is evolutionarily conserved, with orthologues in worms, flies, frogs, fish, and birds [3,4]. During embryonic development, PAX proteins are involved in cell fate commitment while maintaining cells in a proliferative pre-differentiated status. Their actions include the enhancement of cell proliferation and self-renewal, resistance to apoptosis, and migration of embryonic precursor cells. Mouse models bearing the deletion of individual PAX genes in homozygosis exhibit striking developmental defects causing their death either in the uterus or within few days after birth (Table 1) [5,6]. The expression of several PAX members, such as PAX7 and PAX3, persist in adult progenitor cell populations. In adulthood, these genes are involved in organ/tissue regeneration [7]. The functional role of PAX proteins conveying proliferative phenotypes is also a hallmark of tumorigenic proteins. Indeed, PAX2, PAX3, PAX5, PAX7, and PAX8 are aberrantly expressed in certain cancers and are currently used as tumor markers in kidney, prostate, breast, and ovary cancer among others [8].

To date, PAX2 and PAX8 (group II) as well as PAX4 and PAX6 (group IV) have been directly or indirectly associated to pancreas development or function (Figure 1). More importantly, mutations and/or small-nucleotide polymorphisms (SNPs) in several of these genes have been associated with diabetes mellitus (DM) (Figure 2). The above-mentioned actions of pancreatic expressed PAX genes together with the well-established fact that the diabetic milieu is a risk factor for the development of pancreatic tumors prompted us to review the current knowledge of PAX genes expressed in the pancreas and dissect their physiological and pathophysiological roles with a particularly emphasis on DM and pancreatic neuroendocrine tumors (PNTs). We discuss whether pancreatic-expressed PAX genes, especially PAX6 and PAX4, and their targets have therapeutic potential for the treatment of these terrible diseases.

2. PAX genes and the pancreas

2.1. PAX2; to be or not to be

PAX2 expression is essential for the development of the central nervous system, eye, ear, kidney, and mammary gland [22–24]. Seminal reports detected PAX2 mRNA transcripts in adult rat islets, where two PAX2 isoforms, known as PAX2a and PAX2b, were found [25]. Further *in vitro* functional studies showed that PAX2 interacts with and transactivates the glucagon promoter in islet cell lines and transfected fibroblasts [9]. Based on these data, PAX2 was proposed to be a regulator of islet proglucagon gene expression. PAX2 mRNA is detected

CONTACT Benoit R. Gauthier benoit.gauthier@cabimer.es
*These authors contributed equally to this work.

Article highlights

- Four PAX family members (PAX2, PAX4, PAX6, and PAX8) have been linked to either endocrine pancreas (islets of Langerhans) development or mature function.
- PAX4 and PAX6 control islet cell fate differentiation and survival.
- Small nucleotide polymorphisms/mutations in PAX4, PAX6 and PAX8 were shown to be associated with diabetes mellitus.
- Aberrant expression of PAX4 and PAX6 is associated with either islet malformation or malignancy.
- Changes in the delicate balance PAX4-PAX6 may be involved in the pathogenesis of DM and PNTs.

This box summarizes key points contained in the article.

during murine pancreatic development as early as embryonic day (E) 10.5, reaching its maximal expression around E12.5 (Figure 1). However, PAX2 expression was too low to be detected by immunohistochemistry [10]. Noteworthy, PAX2 mRNA was also detected in human islets [10]. Conversely, an independent report failed to detect PAX2 mRNA either in late embryonic development (E19) or in adult mice islets [9]. In addition, similar proglucagon mRNA expression levels were found in the pancreas of wild type (wt) and homozygous $PAX2^{1Neu}$ mutant mice expressing a truncated nonfunctional variant of PAX2 (Table 1). These results refute the concept that PAX2 is involved in α-cell mature function through regulation of glucagon gene expression. Moreover, the differentiation of α-cells and β cells and islet architecture were not affected in $PAX2^{1Neu}$ mutant mice, raising concerns on the role of PAX2 in islet development or function. However, a detailed analysis of the islets of homozygous and heterozygous $PAX2^{1Neu}$ mutant mice at E18.5 revealed a marked increase in the pancreatic volume occupied by islets [10]. This increase resulted from an increase in the number and size of islets. Even though the total number of islet cells was not quantified, the authors observed an increase in the volume occupied by β-cells, but not by α-cells. Interestingly, the increase in β-cell mass was not associated with a significant increase in total pancreatic insulin content, suggesting a reduction in the insulin content per cell [10]. Based on these data, Zaiko et al. speculated that the absence of PAX2 might favor the expansion of endocrine cells, involving PAX2 in the endocrine/exocrine commitment during embryonic development [10]. Nevertheless, the decrease in insulin content of the β-cells in $PAX2^{1Neu}$ mice pinpoints to an effect of this gene on the functional maturation of the β-cell. In any case, further studies are required to validate this hypothesis. The mild effect of PAX2 deficiency on the pancreas could stem from the compensatory role of other PAX genes expressed in the pancreas. Supporting this hypothesis, several examples have indicated that lack of one PAX gene can be, to some extent, compensated by other members of the PAX family [26]. Humans bearing in heterozygosis the homologous polymorphism of $PAX2^{1Neu}$ mice exhibit a detrimental phenotype that includes optic nerve and kidney failures. However, analyses of associations with glucoregulation or any pancreatic phenotype were not performed in this report [27]. Remarkably, although PAX2 expression has been detected in various types of tumors, this gene has not been associated with any kind of pancreatic tumor and only one study investigated whether PAX2 immunostaining was positive in primary ductal adenocarcinomas of the pancreas. The authors confirmed that none of the samples analyzed expressed PAX2, suggesting that PAX2 is not involved in the pathogenesis of this type of tumor [28]. Therefore, the role of PAX2 in pancreatic physiology and pathophysiology is still uncertain, revealing the need of further studies to validate the implication or not of PAX2 in pancreatic diseases.

2.2. PAX8; An uncertain role in PNTs and DM

PAX8 is expressed during embryogenesis in the thyroid and urogenital system, maintaining its expression in adult kidney and thyroid gland [29–31]. As opposed to other PAX genes expressed in the pancreas, the current scientific literature does not involve the expression of this gene in pancreatic development [32]. PAX8 knock-out (KO) mice exhibit severe growth retardation and die around weaning due to thyroid dysgenesis and subsequent thyroid hormone deficiency. Thyroxine administration can extend the survival of these animals up to at least 6 months of age, indicating that the lack of this hormone is the cause of death of these mice [33]. In humans, detrimental PAX8 polymorphisms in heterozygosis are also associated with thyroid dysgenesis and urogenital malformations [34, 35]. To date, humans harboring deleterious PAX8 variants in homozygosis have not been found, suggesting that the lack of PAX8 is lethal. The compromised survival of homozygous PAX8 KO mice has precluded the evaluation of the plausible physiological role of PAX8 in glucoregulation during adulthood [33, 36]. Interestingly, several reports have suggested that PAX8 may be involved in the control of glucose homeostasis under specific metabolic conditions. The transcriptional profile of islets isolated from pregnant mice revealed a robust induction of PAX8 expression (Figure 1) [37]. Remarkably, under normal conditions (nonpregnant mice fed on a healthy diet), PAX8 mRNA expression is virtually absent in murine pancreatic islets while human islets exhibit very low expression of this transcription factor [38]. These data suggest that transient expression of PAX8 in islets might be required for islet adaptation under situations of increased metabolic demand such as pregnancy. However, there is still a lack of research focused to determine whether homozygous PAX8 KO mice treated or not with thyroxine or heterozygous PAX8 mice suffer alterations in glucose control. Supporting a possible role of PAX8 in islet physiology, SNPs found in the region of chromosome 2 where PAX8 is located show a strong association with type 2 DM (T2DM) in Afro-Americans [39]. Therefore, further investigation is required to define PAX8 function in pancreatic endocrine physiology.

Intriguingly, numerous reports have associated PAX8 expression with PNTs, suggesting the possible use of PAX8 as PNTs marker [40–44]. Unfortunately, the anti-PAX8 polyclonal antibody used in these reports was shown to cross-react with at least PAX5 and PAX6 [38, 45, 46]. Indeed, we found that a monoclonal antibody specific to PAX8 (e.g. raised against a highly divergent sequence not found in other PAX

Table 1. Animal models with depletion and/or mutation of PAX genes with reported impact on islet physiology.

System	Gene	Mouse	Mutation/deletion	Islet morphology	Diabetic phenotype	Viability	Ref
Constitutive	**Pax2**	Pax2 ^{1Neu}	Spontaneous mutation resulting in a truncated 54-aa protein with only the first 21 aa of the wt PAX2. Homologous to a described human mutation	E18.5 and P1 homo and heterozygous animals: Increase in number and size of islets. Normal distribution of endocrine cells within the islets	Not reported	Viable in heterozygosis	[9,10,106]
	Pax4	Pax4$^{-/-}$ (Pax4$^{LacZ/LacZ}$)	Homologous recombination replacing almost the entire paired domain by the β-Gal gene	In homozygosis: Few if any Ins+ and Sts+ cells. Increased Gluc+ cells that appear abnormally clustered. No effect in heterozygosis	Severe hyperglycemia before death	Neonatal death in homozygosis (within 3 days of birth)	[11–13]
	Pax6	Pax6$^{-/-}$ (Pax6$^{LacZ/LacZ}$)	Homologous recombination replacing the start codon and entire paired domain with β-Gal gene	In homozygosis: Few or none Gluc+ cells. β-Gal+ cells expressing Ins, Sts, or PP still detected in the pancreas, but fail to form distinct islets. No effect in heterozygosis	Not reported	Homozygous Pax6$^{-/-}$ mice die at birth	[14]
		Pax6^{Sey}	Spontaneous mutation that generates a truncated protein lacking the homeodomain and the transactivation domain	At E19 reduced number of Ins+ cells and Gluc+ cells in homozygosis.	Not reported	Homozygous Sey mice die at birth	[15,16,107]
		Pax6$^{Sey\ Neu}$	ENU-induced mutation that eliminates the transactivation domain	In homozygosis: Less severe effect vs. Pax6$^{-/-}$, but still strong decrease in Gluc+ cells and Ins+ cells. Sts+ cells and PP+ cells were also decreased. Abnormal distribution of the remaining hormone-producing cells	Reduction in pancreatic insulin and glucagon content	Homozygous SeyNeu mice die at birth	[12,15,17,108]
		Pax6^{m}	ENU-induced mutation in the homeodomain generating a truncated protein lacking the last 5 aa of the homeodomain and the whole transactivation domain	In homozygosis: Decrease in hormone-producing cells, especially Gluc+ cells. In heterozygosis: Normal islet architecture although some Gluc+ cells translocate to the core of the islet	In heterozygosis: Defect in insulin secretion. At 4 months, animals become glucose intolerant and at 14 months develop mild hyperglycemia	Homozygous Pax6$^{m/m}$ mice die soon after birth	[18]
		Pax6$^{flox/flox}$	Mouse line in which the region including the initiation Met and most of the paired domain is flanked by two loxP sequences	Normal islets	Normal glucose homeostasis	Viable and fertile	[109]
		Pax6 $^{flox/flox}$; Le-Cre-GFP or Pax6 $^{flox/LacZ}$; Le-Cre-GFP	Mice generated by crossing Pax6$^{flox/flox}$ or Pax6$^{flox/LacZ}$ animals with Le-Cre-GFP line (expressing CRE under the control of Pax6 regulatory domain)	Perturbed islet morphology with very few Gluc+ cells and reduction in the Ins+ cells. Normal numbers of Sts+ cells and PP+ cells	2–6 days after birth, severe growth retardation, hyperglycemia and hypoinsulinemia	Neonatal death (3–6 days after birth) suffering from an overt diabetic phenotype	[19]
		Pax6 $^{flox/flox}$; Pdx-Cre	Mice generated by crossing Pax6$^{flox/flox}$ animals with Pdx1-Cre line (expressing CRE under the control of Pdx1 promoter)	Similar phenotype as Pax6 $^{flox/flox}$; LeCre. Perturbed islet morphology with very few Gluc+ cells and reduction of Ins+ cells	Not reported	Homozygous mice die after birth	[19]
		Pax6 $^{flox/flox}$; Glu-Cre	Mice generated by crossing Pax6$^{flox/flox}$ animals with Glu-Cre line (expressing CRE under the control of glucagon promoter), resulting in Pax6 depletion in α-cells (68% KO efficiency)	No differences in the number of Gluc+ cells in the mice up to 3 months of age. In 8-month-old animals clear reduction in Gluc+ cells	Not reported	Viable	[110]
		Pax6-R266Stop	ENU-induced mutation that causes a truncation at residue 266. Similar to human Pax6 R240Stop mutation	No obvious structural abnormalities in the pancreas	Heterozygous: Impaired glucose tolerance in animals older than 6 months. Normal response to insulin	All studies were done in heterozygosis	[20]
	Pax4/Pax6	Double KO Pax4$^{-/-}$ Pax6$^{-/-}$	Mice generated by crossing Pax4^{LacZ} animals with Pax6^{LacZ} mice	In homozygosis, lack of any mature endocrine cell	Not reported	Homozygous mice die after birth.	[14]

(*Continued*)

Table1. (Continued).

System	Gene	Mouse	Mutation/deletion	Islet morphology	Diabetic phenotype	Viability	Ref
Conditional	**Pax6**	$Pax6^{flox/flox}$; RIP-CreER	Mice generated by crossing $Pax6^{flox/flox}$ animals with RIP-$CreER^{TM}$ line. Pax6 is depleted in β-cells in adult mice by tamoxifen treatment (95% KO efficiency)	Long term after depletion decrease in Ins+ cells and increase in the other hormone expressing cells of the islet, including Ghr+ cells	Sustained hyperglycemia	Viable	[110]
		$Pax6^{flox/flox}$; CAGCreER^{TM} Or $Pax6^{flox/LacZ}$; CAGCreER^{TM}	Mice generated by crossing $Pax6^{flox}$ or $Pax6^{LacZ}$ animals with CAG-$CreER^{TM}$ line. Pax6 is depleted in the whole body after tamoxifen treatment	Gluc+ cells and Ins+ cells are severely reduced. Sts+ cells and PP+ cells are moderately reduced or not affected. Increase in Ghr+ cells	Polydypsia, polyuria, glycosuria, and elevated fasting blood glucose levels	Viable	[21,110]
		$Pax6^{flox/flox}$; TetO-Cre; Glu-rtTA	Mice generated by crossing $Pax6^{flox/flox}$ mice with TetO-Cre; Glu-rtTA line. Pax6 is depleted in Gluc+ cells by doxycycline treatment (75% KO efficiency)	Decrease in Gluc+ cells and increase in Ghr+ cells	Not reported	Viable	[110]

ENU: N-ethyl-N-nitrosourea; Ins: insulin; Gluc: glucagon; Sts: somatostatin; Ghr: ghrelin. Bold references are the initial report/s describing the animal model.

members) failed to reveal PAX8 expression in PNTs as well as pancreatic tissue. Our results clearly indicated that the high degree of conservation in the N-terminal part of the protein among the different PAX proteins was the underlying cause of the false-positive results associating PAX8 expression with PNTs. Of note, the antibody used in these studies was raised against a region that includes the conserved 128 amino acid paired DNA-binding domain found in all members of the PAX gene family (Figure 2). Notwithstanding the assumptions of the literature using polyclonal PAX8 antibodies, the fact that a PAX gene is expressed in PNTs might be clinically relevant for the diagnosis of this disease [47]. In summary, despite the growing interest aimed at delineating whether PAX8 plays a significant role in diabetogenesis and the formation and progression of PNTs, a definite answer remains to be established.

2.3. PAX4; a crucial role safeguarding β-cell integrity

PAX4 is predominantly expressed in pancreatic β- and δ-cells [11]. During murine embryonic development, PAX4 expression is first detected around E9.5 in the pancreas and the ventral spinal cord, reaching its maximal expression at embryonic E13.5–15.5, when β-cell differentiation is initiated [11]. After birth, and coinciding with the decline in β-cell proliferation, PAX4 expression is decreased, albeit still detectable, in adult rexpression of PAX4 under the control of the Pdx islets (Figure 1) [48–51]. Homozygous PAX4 KO mice, despite being born at Mendelian ratios, die within 3 days after birth with severe hyperglycemia (Table 1) [11, 52, 13]. These animals lack β- and δ-cells, and have an increased α-cell mass [11, 12]. Noteworthy, heterozygous PAX4 KO mice exhibit insulin-producing β-cells and do not develop DM, indicating that a single copy of PAX4 is sufficient to promote normal β-cell development and function [11]. Despite the specific requirement of PAX4 for only β- and δ-cell formation, lineage-tracing analysis demonstrated that all islet cells are derived from PAX4 expressing progenitors [53, 54]. These data suggest that a minimum threshold level of PAX4 is required to determine the commitment of the endocrine cells towards β- and δ-cells. Collombat and coworkers further demonstrated the crucial role of PAX4 in β-cell commitment/differentiation by *in vivo* overexpression of PAX4 under the control of the Pdx1, PAX6, or glucagon promoters. These authors demonstrated that ectopic PAX4 overexpression in murine endocrine precursor cells induces the formation of β-cells at the expense of the other islet cell populations [55]. Moreover, PAX4 overexpression under the control of glucagon promoter during embryonic development or postnatal life results in the trans-differentiation of α-cells toward β-like cells [55, 56], likely through PAX4-mediated transcriptional inhibition of Arx [57]. Similarly, viral-mediated PAX4 expression in human islets induced α-cell-to-β-cell phenotypic conversion [58]. Functional *in vitro* studies conducted to determine PAX4 mechanism of action revealed that PAX4 overexpression in either rodent or human islets stimulates β-cell proliferation and protects β-cells from cytokine-induced apoptosis [50, 59]. These results were validated *in vivo* using a conditional β-cell specific PAX4 overexpression in adult mice. PAX4 overexpression protects against streptozotocin (STZ)-induced DM as well as in a model of experimental autoimmune DM (RIP-B7.1 mice)

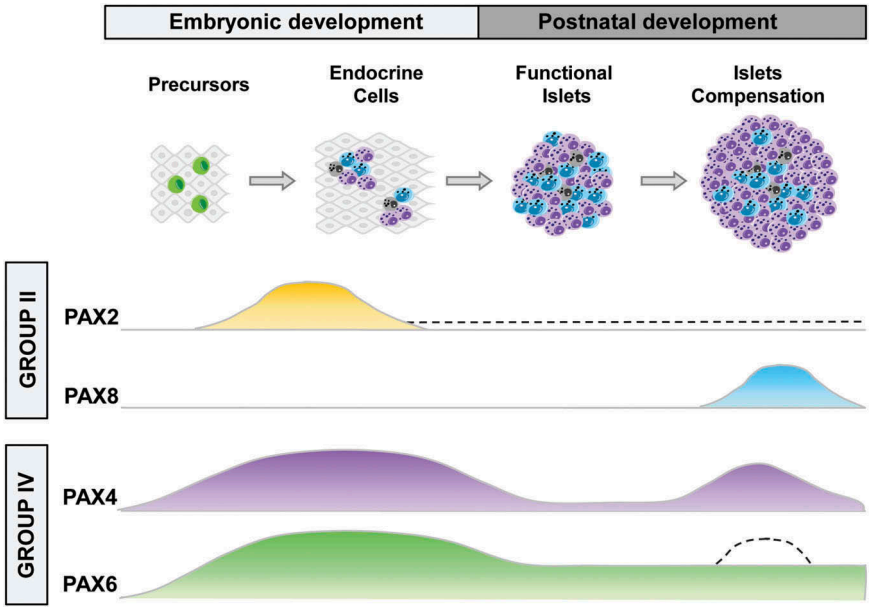

Figure 1. Relative expression of mouse pancreatic PAX genes. Representation of the relative expression of PAX2 and PAX8 (group II) as well as PAX4 and PAX6 (group IV) in mouse islets during embryonic development and postnatal life. In the upper part of the figure the main stages of islet organogenesis and postnatal development are indicated: formation of the precursor cells (E9.5 to E11.5), secondary transition with the formation of the endocrine cells (E12.5 to E 15.5), adult fully functional islet, islet adaptation in response to the increased insulin demand (e.g. during pregnancy). Colored curves underneath indicate the relative expression levels of each PAX gene at the specific time points. The relative expression is not comparable among the four PAX members. Dotted lines indicate probable expression, still not confirmed.

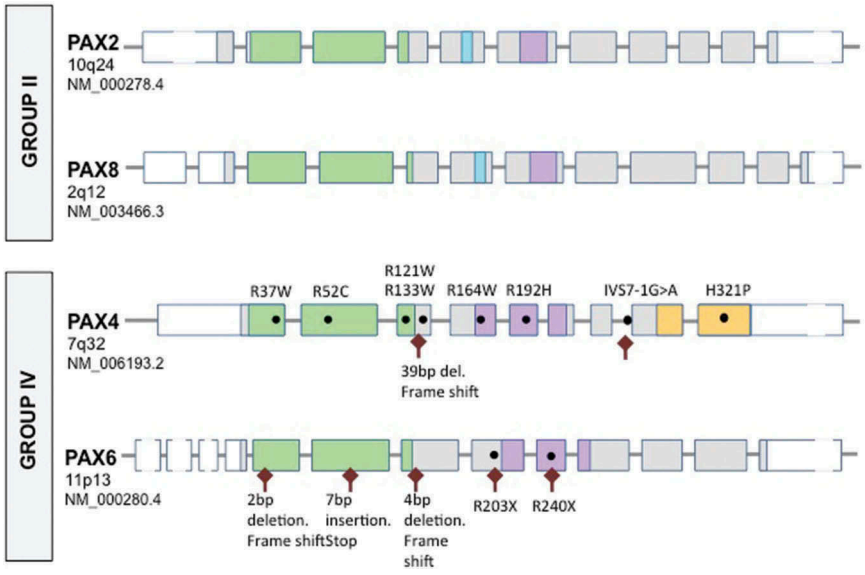

Figure 2. Schematic representation of human pancreatic-expressed PAX genes with annotated mutations associated with impaired glucose homeostasis, DM or pancreatic tumors. Schematic representation of the four human pancreatic PAX genes. Chromosomes location is indicated under the gene name, together with the NCBI reference number. Exons are depicted as rectangles, with the coding region indicated in grey and the specific domains indicated in colors: Paired Domain (green), octapeptide (blue) homedomain (purple) and negative regulatory region (orange). Disease-associated (impaired glucose homeostasis, DM or pancreatic tumors) mutations are indicated in the figure: point mutations are represented by black dots with the resulting amino acid change indicated above. Mutation causing truncated variants of the protein are indicated underneath the gene and represented by brown arrows. Point mutations causing the generation of a stop codon (represented by the 'X' in the amino acid change indication) appear underneath the gene. The relative size of the exons is depicted in the figure. Non-coding exons appear as broken rectangles indicating longer relative size. Full color available online.

[59, 60]. Remarkably, these reports have provided substantial knowledge on the cellular mechanisms orchestrated by PAX4 that protect β-cells. Transcriptome profiling of islets overexpressing PAX4 in β-cells revealed that PAX4 controls the expression of different groups of genes that act at different cellular tasks, conferring multiple layers of protection to promote β-cell survival. Of particular interest, PAX4 preserves the integrity of the endoplasmic reticulum preventing thapsigargin-induced cell death, a treatment that inhibits the sarcoplasmic/endoplasmic reticulum Ca^{2+}-dependent ATPase pump. DNA damage induced

by diabetogenic treatments (STZ and autoimmune attack) was also reduced in PAX4 overexpressing islets [60]. Intriguingly, long-term PAX4 overexpression in these mice resulted in blunted insulin secretion and the appearance of a proliferative $BrDU^{+}/Pdx1^{+}/insulin^{-}$ cell population that suggests that PAX4 promotes the dedifferentiation of mature β-cells [59]. Supporting these data, PAX4 overexpression decreases the expression of MafA and insulin, markers of mature β-cells [59, 61]. Interestingly, β-cell dedifferentiation has been proposed to underlie the functional alterations of pancreatic islets during T2DM development [62, 63]. Based on these data, we hypothesized that, when β-cells are challenged, the induction of PAX4 expression promotes β-cell dedifferentiation to potentiate proliferation and protection in order to recover/protect the β-cell mass. Supporting this hypothesis, an increase in PAX4 expression has been observed in nonobese T2DM patients with a BMI between 22 and 26 [51]. Intriguingly, we and others have demonstrated that PAX4 expression is maintained in adult islets, which might be potentially detrimental for β-cell functionality given the dedifferentiative potential of this gene [48, 54]. However, the use of a transgenic mouse model that expresses GFP under the control of PAX4 promoter allowed us to determine that PAX4 is not homogeneously expressed in all β-cells, but specifically in a β-cell subpopulation. During postnatal development, the expression of PAX4 becomes restricted to a subpopulation of β-cells that decreases with age, correlating with the decrease in the proliferative capacity of pancreatic β-cells [54]. Remarkably, in adult animals, PAX4-expressing cells are more resistant to apoptosis compared to those lacking PAX4 expression when challenged *in vitro* with thapsigargin or *in vivo* with STZ. Moreover, the PAX4-expressing β-cell subpopulation is prone to proliferation during pregnancy, when endogenous PAX4 levels transiently increase correlating with the increase in β-cell proliferation [54]. The fact that PAX4 is only expressed in a subset of β-cells in adult islets is consistent with the proliferative heterogeneity of β-cells [64]. All together, these studies clearly indicate the central role of PAX4 in both development and adult endocrine pancreatic physiology.

The capacity of PAX4 to maintain a β-cell subpopulation in a proliferation-prone status while enhancing resistance to apoptosis suggests a potential role in tumor formation and progression. In this line, high PAX4 expression levels have been reported in human insulinomas [65] as well as in approximately 42% of human PNTs [66]. Noteworthy, in human insulinoma samples, in addition to PAX4 overexpression, a deletion of exon 7 originating a mutated protein that lacks the negative regulatory domain (NRD) has been reported [65]. A similar protein truncation was also detected in a rat insulinoma cell line [67]. Remarkably, the repression of PAX4 in an insulinoma cell line (INS-1E) induces an increase in spontaneous apoptosis, suggesting that PAX4 expression is required for the survival of insulinoma cells [68]. However, long-term PAX4 overexpression (4 months) in mice did not induce PNTs, suggesting that per se PAX4 overexpression does not confer tumorigenic potential [59]. Taken together, these results indicate that high PAX4 expression may not be the root cause of PNT development, but that sustained overexpression of this transcription factor may rather facilitate the dedifferentiation and survival of PNT cells. Accordingly, PAX4 was shown to increase cell cycle activators, including c-myc and cyclin D, as well as inhibitors, such as p21 and Mig6 [54]. These results may support that PAX4-expressing β-cells are prone to proliferation upon alleviation of the cell cycle brakes. It is tenable that chronic hyperglycemia and hyperinsulinemia, known inducers of PAX4 expression, as well as hallmarks of T2DM, could suffice to override these brakes favoring cell proliferation [51].

Taking into consideration the critical role of PAX4 in β-cell formation and plasticity, it is not surprising that detrimental polymorphisms in PAX4 have been associated with type 1 DM (T1DM), T2DM, ketosis-prone DM (KPDM), and maturity onset of the diabetes of the young (MODY) in humans (Figure 2) [31, 69–73]. Genome-wide association studies (GWAS) have identified, in Asian populations, two T2DM susceptibility loci (rs6467136 and rs10229583) located in intergenic regions in the proximity of PAX4 [74, 75]. Further analysis of PAX4 polymorphisms located within the PAX4 gene revealed that, the majority of PAX4 polymorphisms predisposing to DM are located within the evolutionarily conserved DNA-binding domains (amino acids 2 to 222) likely affecting its binding to target genes (Figure 2) [76, 77]. One of the most studied polymorphisms affecting the DNA-binding domain is PAX4 R121W, which has been associated with T2DM in Japanese populations. Patients harboring this polymorphism in homozygosis showed severe defects in first-phase insulin secretion whereas patients harboring the same polymorphism in heterozygosis exhibit impaired insulin secretion. This β-cell dysfunction associated to PAX4 R121W has been correlated with earlier onset of DM [76–79]. Extensive research has been conducted in mice harboring the equivalent polymorphism, the PAX4 R129W variant [59, 60]. *In vitro* studies using primary pancreatic islets overexpressing PAX4 R129W determined that PAX4-mediated protection against cytokine-induced as well as thapsigargin-induced apoptosis is restricted when compared to the overexpression of the wt PAX4. In agreement with these data, *in vivo* overexpression of PAX4 R129W confers only partial protection against STZ as well as in a model of experimental autoimmune DM when compared to the overexpression of wt PAX4 [59, 60]. Besides this well-studied mutation, two PAX4 rare variants, PAX4 R133W and PAX4 R37W, have been found among patients of West African ancestry with KPDM, a rare form of T2DM [72]. These two variants correlated with severe alterations on pancreatic β-cell functionality. Remarkably, PAX4 R133W has been associated with predisposition to KPDM [72]. However, the low incidence of PAX4 R37W has impeded the performance of association analyses for this polymorphism. Interestingly, polymophisms in PAX4, affecting β-cell functionality and survival, have also been associated with DM in Asian families with unknown MODY reinforcing the premise of PAX4 as MODY9. PAX4 R164W variant, associated with DM in Thai MODY families, exhibits compromised PAX4 transcriptional activity resulting in increased glucose-induced apoptosis in INS-1 cells [71, 80]. Another PAX4 polymorphism associated with MODY patients, PAX4 R192H, is located within the homeodomain of the protein. The expression of this variant impairs PAX4 transcriptional repressor activity and reduces β-cell survival under glucotoxic

conditions [71, 81–83]. Additionally, a PAX4 polymorphism affecting the splice acceptor site in intron 7, known as IVS7-1G>A, has been identified in heterozygosis in a MODY family with severe diabetic complications [71]. This isoform results in defective PAX4 protein structure and function, with impaired transcriptional activity and blunted PAX4-mediated protection of INS-1 cells from apoptosis when cells are grown on high glucose [80]. Similarly, a PAX4 polymorphism resulting in a 39-base deletion in exon 3 that causes splicing changes leading to a truncated PAX4 protein that lacks transcriptional repressor activity has been described in a Japanese MODY family [84]. Intriguingly, this polymorphism renders different diabetic phenotypes in different individuals harboring this variant, indicating that other diabetogenic genes or environmental factors might contribute to the phenotype of these patients. In addition to the association of PAX4 detrimental polymorphisms with T2DM, KPDM, and MODY, a polymorphism in PAX4 has also been associated to T1DM. Although it is under debate, the H321P variant in homozygosis was suggested to be a predisposition marker for T1DM in two independent Caucasian populations [70]. However, this correlation was not detected in Finish, Hungarian, and Asian populations [85, 86]. Taken together, substantial clinical evidences indicate that PAX4 is central orchestrating the regulation of molecular networks within the β-cell subpopulation that ensure cell survival and controlled expansion in the adaptation to environmental changes. However, these adaptive mechanisms include at long term the dedifferentiation and proliferation of β-cells, which may under specific conditions benefit the progression of PNTs.

2.4. PAX6; essential and untouchable

During early development, PAX6 is expressed in the eye and brain as well as in pancreatic islet cells. Within the developing murine pancreas, PAX6 is expressed early on throughout the dorsal pancreatic bud. Later on, its expression is restricted to the endocrine cell precursors to promote their differentiation [17, 14, 19]. In adult mice, PAX6 expression is maintained in all the endocrine cells of the pancreas (Figure 1) [19]. PAX6 KO mice as well as mice harboring two independent PAX6 deleterious mutations (Sey^{1Neu} and the naturally occurring Sey^{Sey}) in homozygosis have strong developmental abnormalities and die immediately after birth (Table 1). These animals fail to develop eyes, nasal structures and display abnormal forebrain patterning and altered pancreatic islet morphology [17, 14, 15, 87]. Islets from homozygous null-mutant PAX6 mice are disorganized, lacking α-cells while the other hormone-expressing cell populations are greatly reduced, with the exception of ghrelin expressing cells that are increased [16]. Moreover, these islets exhibit restricted secretion of several pancreatic endocrine hormones [17, 14]. Mice bearing a pancreatic endocrine-specific PAX6 ablation in homozygosis display abnormal glucoregulation [19]. These mice die within 3–6 days after birth exhibiting overt diabetic phenotype, with severe growth retardation, hyperglycemia, and hypoinsulinemia. Immunohistochemical analysis of the pancreas of these mice revealed decreased number of glucagon and insulin expressing cells, but surprisingly, pancreatic peptide and somatostatin expressing cells were not affected [19]. A separated report also indicated that the lack of PAX6 expression specifically in adulthood produces a severe decrease in insulin, glucagon, and somatostatin production [21]. These data clearly demonstrate that PAX6 plays an essential role both during pancreatic embryogenesis as well as in the adult islets. Functional studies determined that, at the molecular level, PAX6 directly regulates the expression of genes required for the maintenance of metabolic homeostasis, such as insulin, incretins, prohormone convertases, glucagon, and somatostatin [17, 88–91]. Consequently, PAX6 was proposed to be involved in hormone production, rather than in the development of endocrine cells. Mice harboring a PAX6 R266Stop mutation (a truncated PAX6 that lacks the transactivation domain) in heterozygosis exhibit normal glucose regulation up to 4 months of age. However, animals older than 6 months exhibit impaired glucose tolerance. These animals were shown to produce less prohormone convertase 1/3, a direct target of PAX6, suggesting that defective proinsulin processing is the cause of the pancreatic phenotype in heterozygous PAX6 mice [20]. Consistent with this premise, heterozygous PAX6 mutant rats rSey, that lack most of the transactivation domain of PAX6, exhibit impaired first phase glucose-induced insulin secretion [92]. PAX6 also regulates production of incretins, which suggest that effects in pancreatic endocrine physiology could stem, at least in part, from the effect of non-pancreatic tissues. In mice, PAX6 is needed for the differentiation of intestine cells producing the gastric inhibitory peptide (GIP), glucagon-like peptide 1 (GLP1) and GLP2 [93]. Circulating GLP1 and its transcript levels in the intestines were markedly reduced in heterozygous mice expressing a PAX6 variant that impairs the homeodomain-binding activity [18]. Interestingly, exendin-4 (a long-lasting GLP1 analog) supplementation in PAX6 heterozygous mice rescued the aberrant phenotype (e.g. abnormal food intake, glycemic excursion, and insulin secretion). Therefore, Ding et al. suggested that the mechanism underlying the detrimental effects on adult PAX6 heterozygous mutant mice was related to the reduced expression of GLP1, an important incretin that potentiates insulin secretion [18].

Heterozygous PAX6 mutations in mice and humans produce microphthalmia, also known as the small eye phenotype, and aniridia [94, 95]. Interestingly, in some instances, aniridia patients harboring in heterozygosis PAX6 variants that impede its transcriptional activity develop abnormal glucose tolerance, impaired insulin secretion, as well as decreased glucagon and GIP concentrations (Figure 2) [96–98]. Patients harboring one copy of the PAX6 R240 stop variant, which lacks the transactivation domain and a small portion of the homeodomain (Figure 2), exhibit reduced insulin secretion upon glucose challenge and impaired proinsulin processing, as reflected by the increased proinsulin/C-peptide ratio [20, 98]. Interestingly, 2 h after the glucose challenge, insulin levels were similar in individuals bearing detrimental PAX6 variants when compared to healthy individuals. In contrast, circulating glucose levels remained high in these patients, suggesting defects in insulin signaling. However, insulin sensitivity was unaffected in an insulin tolerance test, and the proinsulin/C-peptide ratio was higher in patients with PAX6 detrimental polymorphisms [20].

These results suggested that, similar to mice, defective proinsulin processing might be the cause of impaired glucoregulation in humans harboring PAX6 detrimental polymorphisms in heterozygosis. Supporting these data, *in vitro* studies using human islets indicated that islets expressing the impaired glucoregulation-associated PAX6 SNP rs685428 'G' in heterozygosis (known as AG) had lower mRNA levels of PCSK1, the gene encoding prohormone convertase, when compared to islets expressing the fully functional A allele in homozygosis [96].

In addition to mutations directly affecting PAX6 expression, a separated report has indicated that polymorphisms affecting cis-regulatory response elements located in the promoters of direct target genes of PAX6, and possibly PAX4, are associated with the development of DM in humans [99]. Human pancreatic islets harboring in heterozygosis the T2DM-associated rs11603334 SNP, located in the ankyrin repeat and PH domain 1 (ARAP1) promoter (known as 'C' allele), exhibit increased ARAP1 expression. Interestingly, although the mechanism by which ARAP1 expression favors the development of T2DM remains elusive, PAX6 was shown to bind preferentially to the non-T2DM-associated SNP (known as the 'T' allele) in a protein-DNA complex that could also contain PAX4 [99]. The authors speculated that the competitive binding of PAX6, and possibly PAX4, to this site dictates physiological levels of ARAP1 expression, while loss of binding results in aberrantly high expression levels. Supporting this hypothesis, the competition of PAX6 and PAX4 for the same binding sites has been reported in insulin and glucagon promoters [61, 100, 101]. Taken together, these reports indicate that PAX6-mediated ARAP1 expression might be a molecular mechanism contributing to T2DM susceptibility, suggesting that direct targets of PAX genes could have therapeutic potential.

As opposed to the majority of studies investigating the physiological role of PAX6 deficiency, minimal work has been conducted in animal models overexpressing PAX6. Of particular interest is an elegant work published by Yamaoka et al. [102]. This report demonstrated that mice overexpressing PAX6 under the control of the PDX1 promoter exhibited increased proliferation of islet cells. Interestingly, islet neogenesis from ductal epithelial cells was also detected in the vicinity of dilated pancreatic ducts. However, concomitantly with an increased in cell proliferation, many apoptotic cells were detected in islets. As a result, islet hypotrophy was observed due to the simultaneous decrease of β-cell and α-cell area. Moreover, the authors also observed a decrease in whole pancreas weight, indicative of hypoplasia of the exocrine pancreas. However, PAX6 overexpression later in development (driven by the insulin promoter) neither induced islet neogenesis nor increased the proliferation of islet cells. Additionally, a decrease on the β-cell area was detected without any effect on the α-cell area [102]. Interestingly, in PAX6 overexpressing mice, the incidence of hyperglycemia ranged from 22 to 46%, suggesting that additional factors are required to trigger impaired glucoregulation in these mice. Nevertheless, the overexpression of PAX6 under both PDX1 or insulin promoters disturbs the normal development of β-cells. Remarkably, only pPDX1/PAX6 overexpressing mice exhibited an increase in the ductal epithelium and the development of pancreatic cystic adenomas. The authors speculated that PAX6 might play a dual action in pancreatic development controlling on one side the proliferation of primitive ductal epithelia and islet progenitor cells and on the other side the induction of α-cell phenotypes. These findings also indicated that the maintenance of high PAX6 expression is detrimental for the normal development of the endocrine and the exocrine pancreas.

The role of PAX6 in tumor formation and proliferation remains controversial both in animal models and humans. Indirect evidence indicates that high PAX6 expression was found specifically in insulinomas in a transgenic animal model in which the simian virus 40T antigen was under the control of the glucokinase promoter [103]. Interesting studies using human samples have described that 70% of adenocarcinomas, preferentially poorly differentiated, express PAX6 [38, 104]. In differentiated tumors, PAX6 was expressed in the atypical ductules while non-tumorous adjacent pancreatic ducts did not express PAX6. In summary, data in the scientific literature raise concerns regarding the use of strategies aiming to modulate PAX6 expression for the development of novel therapies to treat DM and pancreatic tumors since both the overexpression and restricted expression of PAX6 is associated with impaired glucoregulation and/or the development of different types of pancreatic tumors.

3. Conclusion

Several members of the PAX family of transcription factors orchestrate essential tasks in pancreatic physiology and pathophysiology. Despite discrepancies regarding the role of PAX2 and PAX8 in pancreatic development and function, altered expression of PAX4 and PAX6, has been repeatedly associated with DM and PNTs. Remarkably, while the expression of loss of function variants of both PAX4 and PAX6 is associated with DM, aberrant expression of PAX4 and/or PAX6 is found in certain PNTs. Similar to the pro-proliferative effect of PAX4 and PAX6 during development, increased expression of both PAX4 and PAX6 in PNTs may promote their progression, suggesting that blockage of PAX4/PAX6 expression could represent a promising strategy to treat PNTs. Accumulated evidences indicate that the modulation of PAX6 expression might not be optimal for the treatment of DM since both overexpression and restricted expression of this transcription factor is associated with the development of DM. However, research using transgenic PAX4 overexpressing mice indicates that interventions based on the short-term or intermittent overexpression of PAX4 could be promising to develop novel therapies for the treatment of the different types of DM. In addition, direct targets of PAX4 and PAX6, such as ARAP1, might also be promising candidates for the development for novel therapies to treat these terrible diseases. The data in the scientific literature indicate that increased understanding of the mechanisms controlled by pancreatic PAX genes would offer the potential to develop mechanism-based interventions to prevent and cure DM and PNTs.

4. Expert opinion

Lessons learnt from animal models (Table 1) as well as from human studies have provided sufficient evidence to argue against a role of PAX2 in the pathogenesis of both DM and PNTs. Although the involvement of PAX8 in PNTs has been undoubtedly refuted, punctual expression of this transcription factor under specific conditions indicate a physiological function of PAX8 in the islet of Langerhans, which deserves further investigation. In contrast, there are strong indications that involve changes in expression levels of PAX6 and PAX4 and the occurrence of certain types of pancreatic tumors and DM. Indeed, either gain or loss of PAX6 function results in β-cell death and impaired glucose metabolism while aberrant expression under the control of PDX1 promoter produces pancreatic cystic adenomas [102]. In the case of PAX4, the lack of this gene and the expression of non-fully functional PAX4 variants lead to DM. Long-term PAX4 overexpression prompts β-cell dedifferentiation and hyperglycemia without any apparent development of PNTs [59]. However, research reports indicate that certain insulinomas express high levels of PAX4 and PAX6 [103]. The current scientific literature supports that PAX4 and PAX6 are the main players, within the PAX family, in the development, plasticity, and functionality of the pancreas. Interestingly, PAX4 was originated from duplication of the PAX6 gene early in vertebrate evolution. Such event is usually followed by interplays in their function [105]. However, although of common origin, a striking feature of PAX4 is its sharp repression of PAX6 targets, such as insulin, MAFA, and GLUT2, in the islets of Langerhans. This process involves both direct protein–protein interaction as well as competitive binding to the same cis-regulatory DNA elements within the promoters of their targets. Thus, the ratio of PAX6 to PAX4 likely defines expression levels of common molecular targets that will ultimately dictate the fate of islet β-cell differentiation, proliferation, and/or survival (Figure 3). Such model would reconcile most published data demonstrating that PAX4 is essential for β-cell differentiation yet inhibits most mature β-cell markers. In addition to common islet specific targets, PAX4 and PAX6 also regulate distinct sets of genes. Non-fully functional variants of PAX4, such as the R121W, would result in restricted expression of both direct PAX4 targets such c-myc (cell proliferation) but also in the modulation of the expression of PAX6 interactive targets, resulting in dysfunctional and apoptosis-prone β-cells. Physiological stresses such as obesity-induced insulin resistance and hyperglycemia and/or the presence of non-fully functional variants of these genes may lead to a discontinuity in the balance

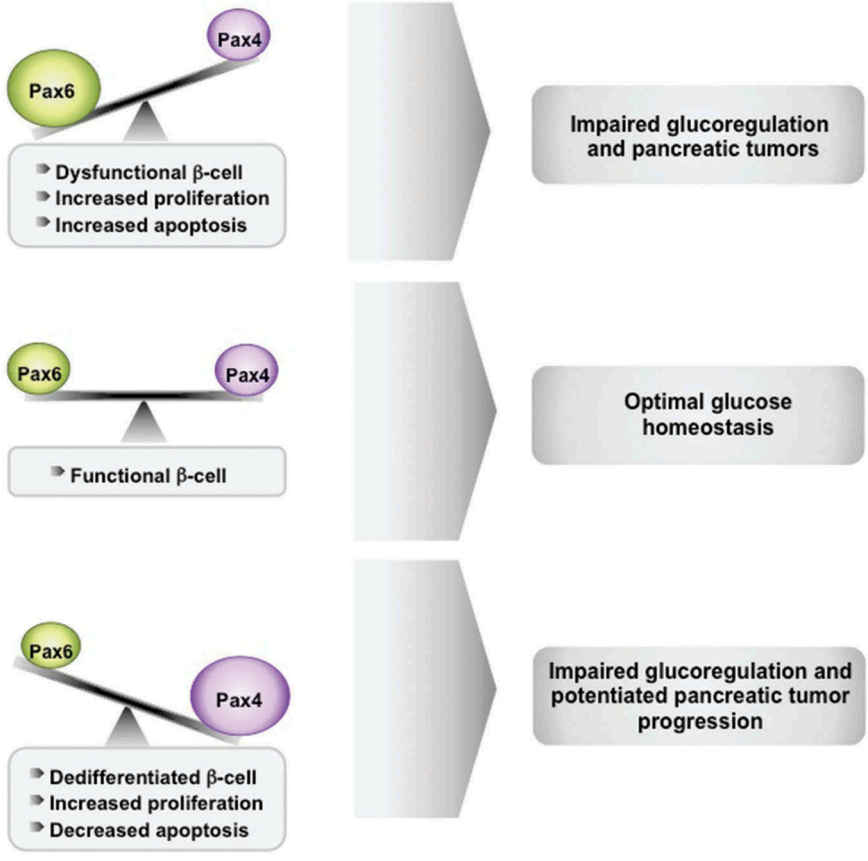

Figure 3. **The PAX6/PAX4 balance dictates islet β-cell fate in health and disease.** Under normal physiological conditions, balanced expression levels in PAX4 and PAX6 specify a healthy and functional β-cell phenotype with low proliferation capacity and minimal apoptosis (middle panel). However, increases in PAX6 or decreases in PAX4 expression levels due to mutations will tilt the balance towards PAX6, resulting in dysfunctional β-cells with impaired insulin processing and increased susceptibility to apoptosis. Sustained Pax6 over-expression may lead to impaired glucoregulation. Pancreatic tumors might be favoured as found in mice over-expressing Pax6 under the control of PDX promotor (upper panel). In contrast, conditions favouring increased PAX4 expression levels to the detriment of PAX6 will impose a protective dedifferentiated phenotype to β-cells with proliferating properties. Sustained Pax4 over-expression may lead to impaired glucoregulation. Although long-term Pax4 over-expression did not cause pancreatic tumors it might favor their progression (lower panel).

between PAX4 and PAX6 [51, 54, 59, 60]. In conclusion, we present arguments indicating that changes in this delicate balance may be involved in the pathogenesis of DM and certain types of pancreatic tumors.

Funding

This work was supported by grants from the Consejería de Salud, Fundación Pública Andaluza Progreso y Salud, Junta de Andalucía; Consejería de Economía, Innovación y Ciencia, Instituto de Salud Carlos III, Fundación Vencer el Cancer and ALUSVI.

Declaration of interest

B. Gauthier receives funding from Fundación Pública Andaluza Progreso y Salud, Junta de Andalucía under grant PI-0727-2010; Consejería de Economía, Innovación y Ciencia under grant P10.CTS.6359; Instituto de Salud Carlos III co-funded by Fondos FEDER under grants PI10/00871 and PI13/00593; Fundación Vencer el Cancer and ALUSVI. A. Martín-Montalvo receives funding from Instituto de Salud Carlos III, co-funded by Fondos FEDER under grant CP14/00105. P. Lorenzo receives funding from Fundación Pública Andaluza Progreso y Salud, Junta de Andalucía under grant PI-0085-2013 and Fundación Vencer el Cancer. The authors have no other relevant affiliations or financial involvement with any organization or entity with a financial interest in or financial conflict with the subject matter or materials discussed in the manuscript apart from those disclosed.

ORCID

Benoit R. Gauthier http://orcid.org/0000-0001-8146-7486

References

Papers of special note have been highlighted as either of interest (•) or of considerable interest (••) to readers.

1. Mayran A, Pelletier A, Drouin J. PAX factors in transcription and epigenetic remodelling. Semin Cell Dev Biol. 2015;44:135–144. Epub 2015 Aug 4.
2. Blake JA, Ziman MR. PAX genes: regulators of lineage specification and progenitor cell maintenance. Development. 2014;141:737–751. Epub 2014 Feb 6.
3. Paixao-Cortes VR, Salzano FM, Bortolini MC. Evolutionary history of chordate PAX genes: dynamics of change in a complex gene family. Plos One. 2013;8:e73560. Epub 2013 Sep 12.
4. Dahl E, Koseki H, Balling R. PAX genes and organogenesis. BioEssays. 1997;19:755–765. Epub 1997 Sep 23.
5. Dohrmann C, Gruss P, Lemaire L. PAX genes and the differentiation of hormone-producing endocrine cells in the pancreas. Mech Dev. 2000;92:47–54. Epub 2000 Mar 8.
6. Wang Q, Fang WH, Krupinski J, et al. PAX genes in embryogenesis and oncogenesis. J Cell Mol Med. 2008;12:2281–2294. Epub 2008 Jul 17.
7. Soleimani VD, Punch VG, Kawabe Y, et al. Transcriptional dominance of PAX7 in adult myogenesis is due to high-affinity recognition of homeodomain motifs. Dev Cell. 2012;22:1208–1220. Epub 2012 Jun 23.
8. Robson EJ, He SJ, Eccles MR. A PANorama of PAX genes in cancer and development. Nat Rev Cancer. 2006;6:52–62. Epub 2006 Jan 7.
9. Flock G, Drucker DJ. PAX-2 activates the proglucagon gene promoter but is not essential for proglucagon gene expression or development of proglucagon-producing cell lineages in the murine pancreas or intestine. Mol Endocrinol. 2002;16:2349–2359.
10. Zaiko M, Estreicher A, Ritz-Laser B, et al. PAX2 mutant mice display increased number and size of islets of Langerhans but no change in insulin and glucagon content. Eur J Endocrinol. 2004;150:389–395. Epub 2004 Mar 12.
• **This report correlates the lack of PAX2 expression with altered islet development and maturation.**
11. Sosa-Pineda B, Chowdhury K, Torres M, et al. The PAX4 gene is essential for differentiation of insulin-producing beta cells in the mammalian pancreas. Nature. 1997;386:399–402.
12. Wang J, Elghazi L, Parker SE, et al. The concerted activities of PAX4 and Nkx2.2 are essential to initiate pancreatic beta-cell differentiation. Dev Biol. 2004;266:178–189. Epub 2004 Jan 20.
13. Collombat P, Hecksher-Sorensen J, Broccoli V, et al. The simultaneous loss of Arx and PAX4 genes promotes a somatostatin-producing cell fate specification at the expense of the alpha- and beta-cell lineages in the mouse endocrine pancreas. Development. 2005;132:2969–2980. Epub 2005 Jun 3.
14. St-Onge L, Sosa-Pineda B, Chowdhury K, et al. PAX6 is required for differentiation of glucagon-producing alpha-cells in mouse pancreas. Nature. 1997;387:406–409.
15. Hill RE, Favor J, Hogan BL, et al. Mouse small eye results from mutations in a paired-like homeobox-containing gene. Nature. 1991;354:522–525. Epub 1991 Dec 19.
16. Heller RS, Stoffers DA, Liu A, et al. The role of Brn4/Pou3f4 and PAX6 in forming the pancreatic glucagon cell identity. Dev Biol. 2004;268:123–134. Epub 2004 Mar 20.
17. Sander M, Neubuser A, Kalamaras J, et al. Genetic analysis reveals that PAX6 is required for normal transcription of pancreatic hormone genes and islet development. Genes Dev. 1997;11:1662–1673. Epub 1997 Jul 1.
18. Ding J, Gao Y, Zhao J, et al. PAX6 haploinsufficiency causes abnormal metabolic homeostasis by down-regulating glucagon-like peptide 1 in mice. Endocrinology. 2009;150:2136–2144. Epub 2009 Jan 1.
19. Ashery-Padan R, Zhou X, Marquardt T, et al. Conditional inactivation of PAX6 in the pancreas causes early onset of diabetes. Dev Biol. 2004;269:479–488. Epub 2004 Apr 28.
20. Wen JH, Chen YY, Song SJ, et al. Paired box 6 (PAX6) regulates glucose metabolism via proinsulin processing mediated by prohormone convertase 1/3 (PC1/3). Diabetologia. 2009;52:504–513. Epub 2008 Nov 27.
21. Hart AW, Mella S, Mendrychowski J, et al. The developmental regulator PAX6 is essential for maintenance of islet cell function in the adult mouse pancreas. Plos One. 2013;8:e54173. Epub 2013 Jan 18.
• **This report correlates the lack of PAX6 expression with altered mature islet function.**
22. Nornes HO, Dressler GR, Knapik EW, et al. Spatially and temporally restricted expression of PAX2 during murine neurogenesis. Development. 1990;109:797–809. Epub 1990Aug 1.
23. Terzic J, Muller C, Gajovic S, et al. Expression of PAX2 gene during human development. Int J Dev Biol. 1998;42:701–707. Epub 1998 Aug 26.
24. Torres M, Gomez-Pardo E, Dressler GR, et al. PAX-2 controls multiple steps of urogenital development. Development. 1995;121:4057–4065. Epub 1995 Dec 1.
25. Ritz-Laser B, Estreicher A, Gauthier B, et al. The paired homeodomain transcription factor PAX-2 is expressed in the endocrine pancreas and transactivates the glucagon gene promoter. J Biol Chem. 2000;275:32708–32715. Epub 2000 Aug 11.
26. Bouchard M, Souabni A, Mandler M, et al. Nephric lineage specification by PAX2 and PAX8. Genes Dev. 2002;16:2958–2970. Epub 2002 Nov 19.
27. Sanyanusin P, Schimmenti LA, McNoe LA, et al. Mutation of the PAX2 gene in a family with optic nerve colobomas, renal anomalies and vesicoureteral reflux. Nat Genet. 1995;9:358–364. Epub 1995 Apr 1.
28. Gnemmi V, Leroy X, Triboulet JP, et al. Pancreatic metastases of renal clear cell carcinoma: a clinicopathological study of 11 cases with special emphasis on the usefulness of PAX2 and mesothelin for the distinction from primary ductal adenocarcinoma of the pancreas. Anal Quant Cytopathol Histopathol. 2013;35:157–162. Epub 2013 Dec 19.
29. Plachov D, Chowdhury K, Walther C, et al. PAX8, a murine paired box gene expressed in the developing excretory system and thyroid gland. Development. 1990;110:643–651. Epub 1990 Oct 1.

30. Poleev A, Fickenscher H, Mundlos S, et al. PAX8, a human paired box gene: isolation and expression in developing thyroid, kidney and Wilms' tumors. Development. 1992;116:611–623. Epub 1992 Nov 1.
31. Sharma R, Sanchez-Ferras O, Bouchard M. PAX genes in renal development, disease and regeneration. Semin Cell Dev Biol. 2015;44:97–106. Epub 2015 Sep 28.
32. Goode DK, Elgar G. The PAX258 gene subfamily: a comparative perspective. Dev Dyn. 2009;238:2951–2974. Epub 2009 Nov 20.
33. Mansouri A, Chowdhury K, Gruss P. Follicular cells of the thyroid gland require PAX8 gene function. Nat Genet. 1998;19:87–90. Epub 1998 May 20.
34. Esperante SA, Rivolta CM, Miravalle L, et al. Identification and characterization of four PAX8 rare sequence variants (p.T225M, p.L233L, p.G336S and p.A439A) in patients with congenital hypothyroidism and dysgenetic thyroid glands. Clin Endocrinol (Oxf). 2008;68:828–835. Epub 2007 Nov 6.
35. Carvalho A, Hermanns P, Rodrigues AL, et al. A new PAX8 mutation causing congenital hypothyroidism in three generations of a family is associated with abnormalities in the urogenital tract. Thyroid. 2013;23:1074–1078. Epub 2013 May 8.
36. Mittag J, Friedrichsen S, Strube A, et al. Analysis of hypertrophic thyrotrophs in pituitaries of athyroid PAX8-/- mice. Endocrinology. 2009;150:4443–4449. Epub 2009 May 30.
37. Rieck S, White P, Schug J, et al. The transcriptional response of the islet to pregnancy in mice. Mol Endocrinol. 2009;23:1702–1712. Epub 2009 Jul 4.

•• **First report of PAX8 being expressed in the endocrine pancreas during gestation.**

38. Lorenzo PI, Jimenez Moreno CM, Delgado I, et al. Immunohistochemical assessment of PAX8 expression during pancreatic islet development and in human neuroendocrine tumors. Histochem Cell Biol. 2011;136:595–607. Epub 2011 Sep 21.

•• **This study determines that PAX8 expression is virtually absent in normal islet and that it is not expressed in PNTs.**

39. Elbein SC, Das SK, Hallman DM, et al. Genome-wide linkage and admixture mapping of type 2 diabetes in African American families from the American Diabetes Association GENNID (Genetics of NIDDM) Study Cohort. Diabetes. 2009;58:268–274. Epub 2008 Oct 9.
40. Long KB, Srivastava A, Hirsch MS, et al. PAX8 expression in well-differentiated pancreatic endocrine tumors: correlation with clinicopathologic features and comparison with gastrointestinal and pulmonary carcinoid tumors. Am J Surg Pathol. 2010;34:723–729. Epub 2010 Apr 24.
41. Sangoi AR, Ohgami RS, Pai RK, et al. PAX8 expression reliably distinguishes pancreatic well-differentiated neuroendocrine tumors from ileal and pulmonary well-differentiated neuroendocrine tumors and pancreatic acinar cell carcinoma. Mod Pathol. 2011;24:412–424. Epub 2010 Oct 5.
42. Ozcan A, Shen SS, Hamilton C, et al. PAX 8 expression in non-neoplastic tissues, primary tumors, and metastatic tumors: a comprehensive immunohistochemical study. Mod Pathol. 2011;24:751–764. Epub 2011 Feb 15.
43. Haynes CM, Sangoi AR, Pai RK. PAX8 is expressed in pancreatic well-differentiated neuroendocrine tumors and in extrapancreatic poorly differentiated neuroendocrine carcinomas in fine-needle aspiration biopsy specimens. Cancer Cytopathol. 2011;119:193–201. Epub 2011 Feb 18.
44. Koo J, Mertens RB, Mirocha JM, et al. Value of Islet 1 and PAX8 in identifying metastatic neuroendocrine tumors of pancreatic origin. Mod Pathol. 2012;25:893–901. Epub 2012 Mar 6.
45. Moretti L, Medeiros LJ, Kunkalla K, et al. N-terminal PAX8 polyclonal antibody shows cross-reactivity with N-terminal region of PAX5 and is responsible for reports of PAX8 positivity in malignant lymphomas. Mod Pathol. 2012;25:231–236. Epub 2011 Nov 1.
46. Moreno CM, Lorenzo PI, Delgado I, et al. PAX8 detection in well-differentiated pancreatic endocrine tumors: how reliable is it? Am J Surg Pathol. 2011;35:1906–1908. Epub 2011 Nov 10.
47. Liau JY, Tsai JH, Jeng YM, et al. The diagnostic utility of PAX8 for neuroendocrine tumors: an immunohistochemical reappraisal. Appl Immunohistochem Mol Morphol. 2016;24:57–63. Epub 2015 Feb 25.
48. Heremans Y, Van De Casteele M, In't Veld P, et al. Recapitulation of embryonic neuroendocrine differentiation in adult human pancreatic duct cells expressing neurogenin 3. J Cell Biol. 2002;159:303–312.
49. Kojima H, Fujimiya M, Matsumura K, et al. NeuroD-betacellulin gene therapy induces islet neogenesis in the liver and reverses diabetes in mice. Nat Med. 2003;9:596–603.
50. Brun T, Franklin I, St-Onge L, et al. The diabetes-linked transcription factor PAX4 promotes {beta}-cell proliferation and survival in rat and human islets. J Cell Biol. 2004;167:1123–1135. Epub 2004 Dec 15.
51. Brun T, He KH H, Lupi R, et al. The diabetes-linked transcription factor PAX4 is expressed in human pancreatic islets and is activated by mitogens and GLP-1. Hum Mol Genet. 2008;17:478–489. Epub 2007 Nov 9.
52. Brink C, Chowdhury K, Gruss P. PAX4 regulatory elements mediate beta cell specific expression in the pancreas. Mech Dev. 2001;100:37–43. Epub 2000 Dec 19.
53. Greenwood AL, Li S, Jones K, et al. Notch signaling reveals developmental plasticity of PAX4(+) pancreatic endocrine progenitors and shunts them to a duct fate. Mech Dev. 2007;124:97–107. Epub 2007 Jan 2.
54. Lorenzo PI, Fuente-Martin E, Brun T, et al. PAX4 defines an expandable beta-cell subpopulation in the adult pancreatic islet. Sci Rep. 2015;5:15672. Epub 2015 Oct 28.

•• **This report determines that PAX4 is expressed in a plastic β-cell subpopulation within the adult islet.**

55. Collombat P, Xu X, Ravassard P, et al. The ectopic expression of PAX4 in the mouse pancreas converts progenitor cells into alpha and subsequently beta cells. Cell. 2009;138:449–462. Epub 2009 Aug 12.

•• **This study reveals the impact of PAX4 overexpression in α to β-cell trans-differentiation.**

56. Al-Hasani K, Pfeifer A, Courtney M, et al. Adult duct-lining cells can reprogram into beta-like cells able to counter repeated cycles of toxin-induced diabetes. Dev Cell. 2013;26:86-100. Epub 2013 Jul 3.
57. Courtney M, Gjernes E, Druelle N, et al. The inactivation of Arx in pancreatic alpha-cells triggers their neogenesis and conversion into functional beta-like cells. PLoS Genet. 2013;9:e1003934. Epub 2013 Nov 10.
58. Zhang Y, Fava GE, Wang H, et al. PAX4 gene transfer induces alpha-to-beta cell phenotypic conversion and confers therapeutic benefits for diabetes treatment. Mol Ther. 2016;24:251–260. Epub 2015 Nov 6.
59. Kh H, Lorenzo PI, Brun T, et al. In vivo conditional PAX4 overexpression in mature islet {beta}-cells prevents stress-induced hyperglycemia in mice. Diabetes. 2011;60:1705–1715. Epub 2011 Apr 28.

•• **This report highlights the protective role of PAX4 overexpression in β-cells.**

60. Mellado-Gil JM, Jimenez-Moreno CM, Martin-Montalvo A, et al. PAX4 preserves endoplasmic reticulum integrity preventing beta cell degeneration in a mouse model of type 1 diabetes mellitus. Diabetologia. 2016;59:755–765. Epub 2016 Jan 28.

•• **This study demonstrates the protective role of PAX4 overexpression in β-cells against experimental autoimmune diabetes and delineates potential therapeutic targets.**

61. Ritz-Laser B, Estreicher A, Gauthier BR, et al. The pancreatic beta-cell-specific transcription factor PAX-4 inhibits glucagon gene expression through PAX-6. Diabetologia. 2002;45:97–107. Epub 2002 Feb 15.
62. Wang Z, York NW, Nichols CG, et al. Pancreatic beta cell dedifferentiation in diabetes and redifferentiation following insulin therapy. Cell Metab. 2014;19:872–882. Epub 2014 Apr 22.
63. Talchai C, Xuan S, Lin HV, et al. Pancreatic beta cell dedifferentiation as a mechanism of diabetic beta cell failure. Cell. 2012;150:1223–1234. Epub 2012 Sep 18.
64. Szabat M, Luciani DS, Piret JM, et al. Maturation of adult beta cells revealed using a Pdx1/insulin dual-reporter lentivirus. Endocrinology. 2009;150:1627–1635. Epub 2008 Dec 20.

65. Miyamoto T, Kakizawa T, Ichikawa K, et al. Expression of dominant negative form of PAX4 in human insulinoma. Biochem Biophys Res Commun. 2001;282:34–40.
66. Zhang L, Smyrk TC, Oliveira AM, et al. KIT is an independent prognostic marker for pancreatic endocrine tumors: a finding derived from analysis of islet cell differentiation markers. Am J Surg Pathol. 2009;33:1562–1569. Epub 2009 Jul 4.
67. Tokuyama Y, Yagui K, Sakurai K, et al. Molecular cloning of rat PAX4: identification of four isoforms in rat insulinoma cells. Biochem Biophys Res Commun. 1998;248:153–156. Epub 1998 Jul 24.
68. Brun T, Duhamel DL, He KHH, et al. The transcription factor PAX4 acts as a survival gene in INS-1E insulinoma cells. Oncogene. 2007;26:4261–4271. Epub 2007 Jan 30.
69. Surapolchai P, Hongeng S, Mahachoklertwattana P, et al. Impaired glucose tolerance and insulin resistance in survivors of childhood acute lymphoblastic leukemia: prevalence and risk factors. J Pediatr Hematol Oncol. 2010;32:383–389. Epub 2010 May 21.
70. Biason-Lauber A, Boehm B, Lang-Muritano M, et al. Association of childhood type 1 diabetes mellitus with a variant of PAX4: possible link to beta cell regenerative capacity. Diabetologia. 2005;48:900–905. Epub 2005 Apr 19.
•• **First study linking a PAX4 mutation to type 1 diabetes mellitus.**
71. Plengvidhya N, Kooptiwut S, Songtawee N, et al. PAX4 mutations in Thais with maturity onset diabetes of the young. J Clin Endocrinol Metab. 2007;92:2821–2826.
72. Mauvais-Jarvis F, Smith SB, Le May C, et al. PAX4 gene variations predispose to ketosis-prone diabetes. Hum Mol Genet. 2004;13:3151–3159.
73. Vernick KD, Collins FH. Association of a Plasmodium-refractory phenotype with an esterase locus in Anopheles gambiae. Am J Trop Med Hyg. 1989;40:593–597. Epub 1989 Jun 1.
74. Cho YS, Chen CH, Hu C, et al. Meta-analysis of genome-wide association studies identifies eight new loci for type 2 diabetes in east Asians. Nat Genet. 2012;44:67–72. Epub 2011 Dec 14.
75. Ma RC, Hu C, Tam CH, et al. Genome-wide association study in a Chinese population identifies a susceptibility locus for type 2 diabetes at 7q32 near PAX4. Diabetologia. 2013;56:1291–1305. Epub 2013 Mar 28.
76. Shimajiri Y, Sanke T, Furuta H, et al. A missense mutation of PAX4 gene (R121W) is associated with type 2 diabetes in Japanese. Diabetes. 2001;50:2864–2869.
•• **First study associating a PAX4 mutation to type 2 diabetes mellitus.**
77. Tokuyama Y, Matsui K, Ishizuka T, et al. The Arg121Trp variant in PAX4 gene is associated with beta-cell dysfunction in Japanese subjects with type 2 diabetes mellitus. Metabolism. 2006;55:213–216.
78. Shimajiri Y, Shimabukuro M, Tomoyose T, et al. PAX4 mutation (R121W) as a prodiabetic variant in Okinawans. Biochem Biophys Res Commun. 2003;302:342–344.
79. Kanatsuka A, Tokuyama Y, Nozaki O, et al. Beta-cell dysfunction in late-onset diabetic subjects carrying homozygous mutation in transcription factors NeuroD1 and PAX4. Metabolism. 2002;51:1161–1165.
80. Sujjitjoon J, Kooptiwut S, Chongjaroen N, et al. Aberrant mRNA splicing of paired box 4 (PAX4) IVS7-1G>A mutation causing maturity-onset diabetes of the young, type 9. Acta Diabetol. 2016;53:205–216. Epub 2015 May 9.
81. Kooptiwut S, Plengvidhya N, Chukijrungroat T, et al. Defective PAX4 R192H transcriptional repressor activities associated with maturity onset diabetes of the young and early onset-age of type 2 diabetes. J Diabetes Complications. 2012;26:343–347. Epub 2012 Apr 24.
82. Chavali S, Mahajan A, Tabassum R, et al. Association of variants in genes involved in pancreatic beta-cell development and function with type 2 diabetes in North Indians. J Hum Genet. 2011;56:695–700. Epub 2011 Aug 5.
83. Sujjitjoon J, Kooptiwut S, Chongjaroen N, et al. PAX4 R192H and P321H polymorphisms in type 2 diabetes and their functional defects. J Hum Genet. 2016. doi:10.1038/jhg.2016.80. Epub 2016 Jun 24.
84. Jo W, Endo M, Ishizu K, et al. A novel PAX4 mutation in a Japanese patient with maturity-onset diabetes of the young. Tohoku J Exp Med. 2011;223:113–118. Epub 2011 Jan 26.
85. Hermann R, Mantere J, Lipponen K, et al. Lack of association of PAX4 gene with type 1 diabetes in the Finnish and Hungarian populations. Diabetes. 2005;54:2816–2819. Epub 2005 Aug 27.
86. Zhang Y, Xiao X, Liu Y, et al. The association of the PAX4 gene with type 1 diabetes in Han Chinese. Diabetes Res Clin Pract. 2008;81:365–369. Epub 2008 Jul 12.
87. Stoykova A, Fritsch R, Walther C, et al. Forebrain patterning defects in Small eye mutant mice. Development. 1996;122:3453–3465. Epub 1996 Nov 1.
88. Dames P, Puff R, Weise M, et al. Relative roles of the different PAX6 domains for pancreatic alpha cell development. BMC Dev Biol. 2010;10:39. Epub 2010 Apr 10.
89. Ritz-Laser B, Estreicher A, Klages N, et al. PAX-6 and Cdx-2/3 interact to activate glucagon gene expression on the G1 control element. J Biol Chem. 1999;274:4124–4132. Epub 1999 Feb 6.
90. Hussain MA, Habener JF. Glucagon gene transcription activation mediated by synergistic interactions of PAX-6 and cdx-2 with the p300 co-activator. J Biol Chem. 1999;274:28950–28957. Epub 1999 Oct 3.
91. Hill ME, Asa SL, Drucker DJ. Essential requirement for PAX6 in control of enteroendocrine proglucagon gene transcription. Mol Endocrinol. 1999;13:1474–1486. Epub 1999 Sep 9.
92. Kuroda A, Kaneto H, Fujitani Y, et al. Mutation of the PAX6 gene causes impaired glucose-stimulated insulin secretion. Diabetologia. 2004;47:2039–2041. Epub 2004 Nov 27.
93. Larsson LI, St-Onge L, Hougaard DM, et al. PAX 4 and 6 regulate gastrointestinal endocrine cell development. Mech Dev. 1998;79:153–159. Epub 1999 Jun 1.
94. Glaser T, Walton DS, Maas RL. Genomic structure, evolutionary conservation and aniridia mutations in the human PAX6 gene. Nat Genet. 1992;2:232–239. Epub 1992 Nov 1.
95. Mirzayans F, Pearce WG, MacDonald IM, et al. Mutation of the PAX6 gene in patients with autosomal dominant keratitis. Am J Hum Genet. 1995;57:539–548. Epub 1995 Sep 1.
96. Ahlqvist E, Turrini F, Lang ST, et al. A common variant upstream of the PAX6 gene influences islet function in man. Diabetologia. 2012;55:94–104. Epub 2011 Sep 17.
97. Nishi M, Sasahara M, Shono T, et al. A case of novel de novo paired box gene 6 (PAX6) mutation with early-onset diabetes mellitus and aniridia. Diabetic Med. 2005;22:641–644. Epub 2005 Apr 22.
98. Yasuda T, Kajimoto Y, Fujitani Y, et al. PAX6 mutation as a genetic factor common to aniridia and glucose intolerance. Diabetes. 2002;51:224–230. Epub 2002 Jan 5.
99. Kulzer JR, Stitzel ML, Morken MA, et al. A common functional regulatory variant at a type 2 diabetes locus upregulates ARAP1 expression in the pancreatic beta cell. Am J Hum Genet. 2014;94:186–197. Epub 2014 Jan 21.
100. Fujitani Y, Kajimoto Y, Yasuda T, et al. Identification of a portable repression domain and an E1A-responsive activation domain in PAX4: a possible role of PAX4 as a transcriptional repressor in the pancreas. Mol Cell Biol. 1999;19:8281–8291. Epub 1999 Nov 24.
101. Petersen HV, Jorgensen MC, Andersen FG, et al. PAX4 represses pancreatic glucagon gene expression. Mol Cell Biol Res Commun. 2000;3:249–254. Epub 2000 Jul 13.
102. Yamaoka T, Yano M, Yamada T, et al. Diabetes and pancreatic tumours in transgenic mice expressing Pa x 6. Diabetologia. 2000;43:332–339. Epub 2000 Apr 18.
•• **This study reports the context dependent impact of PAX6 overexpression in the development of diabetes and pancreatic tumors.**
103. Jetton TL, Moates JM, Lindner J, et al. Targeted oncogenesis of hormone-negative pancreatic islet progenitor cells. Proc Natl Acad Sci U S A. 1998;95:8654–8659.
104. Lang D, Mascarenhas JB, Powell SK, et al. PAX6 is expressed in pancreatic adenocarcinoma and is downregulated during

induction of terminal differentiation. Mol Carcinog. 2008;47:148–156. Epub 2007 Sep 13.

105. Manousaki T, Feiner N, Begemann G, et al. Co-orthology of PAX4 and PAX6 to the fly eyeless gene: molecular phylogenetic, comparative genomic, and embryological analyses. Evol Dev. 2011;13:448–459. Epub 2012 Sep 29.
106. Favor J, Sandulache R, Neuhauser-Klaus A, et al. The mouse Pax2(1Neu) mutation is identical to a human PAX2 mutation in a family with renal-coloboma syndrome and results in developmental defects of the brain, ear, eye, and kidney. Proc Nat Acad Sci USA. 1996;93:13870–13875.
107. Hogan BL, Horsburgh G, Cohen J, et al. Small eyes (Sey): a homozygous lethal mutation on chromosome 2 which affects the differentiation of both lens and nasal placodes in the mouse. J Embryol Exp Morph. 1986;97:95–110.
108. Favor J, Neuhauser-Klaus A, Ehling UH. The effect of dose fractionation on the frequency of ethylnitrosourea-induced dominant cataract and recessive specific locus mutations in germ cells of the mouse. Mut Res. 1988;198:269–275.
109. Ashery-Padan R, Marquardt T, Zhou X, et al. Pax6 activity in the lens primordium is required for lens formation and for correct placement of a single retina in the eye. Genes Dev. 2000;14:2701–2711.
110. Ahmad Z, Rafeeq M, Collombat P, et al. Pax6 inactivation in the adult pancreas reveals Ghrelin as endocrine cell maturation marker. PloS one. 2015;10:e0144597.

British Journal of Pharmacology

British Journal of Pharmacology (2017) **174** 3795–3810 3795

RESEARCH PAPER

Levothyroxine enhances glucose clearance and blunts the onset of experimental type 1 diabetes mellitus in mice

Correspondence Benoit Gauthier and Alejandro Martín-Montalvo, Pancreatic Islet Development and Regeneration Unit/Laboratory of Aging Biology, Centro Andaluz de Biología Molecular y Medicina Regenerativa-CABIMER, Universidad de Sevilla-CSIC-Universidad Pablo de Olavide-Junta de Andalucía, Seville 41092, Spain. E-mail: benoit.gauthier@cabimer.es; alejandro.martinmontalvo@cabimer.es

Received 17 January 2017; **Revised** 26 June 2017; **Accepted** 27 July 2017

Livia López-Noriega[1], Nadia Cobo-Vuilleumier[1], Álvaro Jesús Narbona-Pérez[1], Juan Luis Araujo-Garrido[1], Petra Isabel Lorenzo[1], José Manuel Mellado-Gil[1], José Carlos Moreno[2], Benoit R Gauthier[1,*] and Alejandro Martín-Montalvo[1,*]

[1]*Pancreatic Islet Development and Regeneration Unit/Laboratory of Aging Biology, Centro Andaluz de Biología Molecular y Medicina Regenerativa-CABIMER, Universidad de Sevilla-CSIC-Universidad Pablo de Olavide, Seville, Spain, and* [2]*Thyroid Molecular Laboratory, Institute for Medical and Molecular Genetics (INGEMM), La Paz University Hospital, Autonomous University of Madrid, Madrid, Spain*

*Co-senior authors.

BACKGROUND AND PURPOSE

Thyroid hormones induce several changes in whole body metabolism that are known to improve metabolic homeostasis. However, adverse side effects have prevented its use in the clinic. In view of the promising effects of thyroid hormones, we investigated the effects of levothyroxine supplementation on glucose homeostasis.

EXPERIMENTAL APPROACH

C57BL/6 mice were treated with levothyroxine from birth to 24 weeks of age, when mice were killed. The effects of levothyroxine supplementation on metabolic health were determined. C57BL/6 mice treated with levothyroxine for 2 weeks and then challenged with streptozotocin to monitor survival. Mechanistic experiments were conducted in the pancreas, liver and skeletal muscle. RIP-B7.1 mice were treated with levothyroxine for 2 weeks and were subsequently immunized to trigger experimental autoimmune diabetes (EAD). Metabolic tests were performed. Mice were killed and metabolic tissues were extracted for immunohistological analyses.

KEY RESULTS

Long-term levothyroxine supplementation enhanced glucose clearance and reduced circulating glucose in C57BL/6 mice. Levothyroxine increased simultaneously the proliferation and apoptosis of pancreatic beta cells, promoting the maintenance of a highly insulin-expressing beta cell population. Levothyroxine increased circulating insulin levels, inducing sustained activation of IRS1-AKT signalling in insulin-target tissues. Levothyroxine-treated C57BL/6 mice challenged with streptozotocin exhibited extended survival. Levothyroxine blunted the onset of EAD in RIP-B7.1 mice by inducing beta cell proliferation and preservation of insulin-expressing cells.

CONCLUSIONS AND IMPLICATIONS

Interventions based on the use of thyroid hormones or thyromimetics could be explored to provide therapeutic benefit in patients with type 1 diabetes mellitus.

Abbreviations

BAT, brown adipose tissue; EAD, experimental autoimmune diabetes; GK, glucokinase; GSIS, glucose-stimulated insulin secretion; GSK3β, glycogen synthase kinase 3β; IPPTT, intraperitoneal pyruvate tolerance test; ITT, insulin tolerance test; STZ, streptozotocin; T1DM, type 1 diabetes mellitus; T2DM, type 2 diabetes mellitus; T3, triiodothyronine; T4, levothyroxine; TR, thyroid hormone receptors; THs, thyroid hormones; WAT, white adipose tissue; α-GSU, α-glycoprotein subunit

DOI:10.1111/bph.13975

Introduction

Glycaemic control is exquisitely orchestrated by the hormones secreted by the islets of Langerhans, which exert effects on many target tissues. In the pathogenesis of type 2 diabetes mellitus (T2DM), insulin-target tissues gradually develop insulin resistance. As a result of compromised insulin sensitivity, there is an increased demand of insulin production to maintain circulating glucose concentration within the physiological range. Under these circumstances, pancreatic beta cells overproduce insulin, which in late stages of the disease results in overstimulation of beta cells and their apoptosis. In type 1 diabetes mellitus (T1DM), as opposed to T2DM, there is a direct and specific attack of immune cells that selectively destroys pancreatic beta cells. In both T1DM and T2DM, the lack of a functional beta cell mass produces hyperglycaemia, propelling a vicious cycle of metabolic disorders.

The use of thyroid hormones (THs) and newly generated thyromimetics is promising to improve metabolic homeostasis given their potent effect on weight loss and the reduction of cholesterol levels (de Lange *et al.,* 2011; Lin and Sun, 2011; Moreno *et al.,* 2011). **Triiodothyronine (T3)** and levothyroxine (**T4**), produced in the thyroid gland, are the main THs. T4 is converted into T3 within cells by deiodinases. Interestingly, T4 is less active but more stable (190 h) than T3. The average activity of T3 is about three to five times higher than T4, but the stability is 19 h in euthyroid patients. Other THs or thyromimetics, such as triac, tetrac, thyrinnamines, reverse T3, 3,5-diiodo-l-thyronin and conjugated glucagon/T_3, also exist and are recently attracting attention in the scientific community as promising drugs for the treatment of several pathologies (Ball *et al.,* 1997; Shang *et al.,* 2013; Goglia, 2014; Senese *et al.,* 2014; Finan *et al.,* 2016). One of the main physiological roles of THs is the regulation of basal metabolic rate, defined here as the rate of energy expenditure per time at rest, which accounts for about 60–75% of the calories burned in a healthy subject. Specifically, THs increase oxygen consumption and rates of ATP hydrolysis, while lowering coupled state of the mitochondria and the maximal capacity to produce ATP (Johannsen *et al.,* 2012). Actually, THs are known to induce the catabolism of all types of energy sources (Weinstein *et al.,* 1991). THs induce the reduction of circulating triglycerides and cholesterol containing lipoproteins, as well as the induction of hepatic gluconeogenesis and glycogenolysis (Bahn *et al.,* 2011). Enhanced gluconeogenesis and glycogenolysis support tissues with sufficient fuel to maintain their energy requirements (Dimitriadis and Raptis, 2001; Klieverik *et al.,* 2008).

The mechanistic insights of THs action in cells involve the modulation of gene expression in a process mediated by their binding to **TH receptors (TR)**. TH-TR complexes bound to specific DNA sequences modulate the expression of more than 80 genes (Dong *et al.,* 2009; Shoemaker *et al.,* 2012). In this context, essential cellular processes are orchestrated by THs, such as mitochondrial biogenesis in the nervous system and the contractile apparatus of the endoplasmic reticulum in the heart (Iwen *et al.,* 2013; Vargas-Uricoechea *et al.,* 2014). Additionally, non-genomic effects of TH have also been described (e.g. activation of **Akt** signalling, through the **TR-β**) (Verga Falzacappa *et al.,* 2009; Vicinanza *et al.,* 2013). Moreover, THs play a significant role in the differentiation of the vast majority of somatic cells (Obregon, 2008; Sirakov *et al.,* 2013). Interestingly, during the last years, extensive research has focused on the role of TH in the differentiation, maturation and functionality of metabolic tissues (Mastracci and Evans-Molina, 2014). Thus, T3 supplementation enhanced postnatal pancreatic islet development, *via* the induction of the transcription factor MAFA, and attenuated hyperglycaemia in streptozotocin (STZ)-treated and leptin-receptor deficient mice (Lin and Sun, 2011; Verga Falzacappa *et al.,* 2011; Aguayo-Mazzucato *et al.,* 2013). In addition, T3 administration increased the expression of endocrine markers in acinar and ductal cell lines as well as in pancreatic explants (Misiti *et al.,* 2005; Aiello *et al.,* 2014). Remarkably, newly developed *in vitro* protocols aiming to differentiate human embryonic stem cells towards insulin-secreting beta cells use T3 in specific steps of the differentiation protocol (Pagliuca *et al.,* 2014; Rezania *et al.,* 2014). These data indicate that THs are involved in the differentiation and the maturation of pancreatic precursor cells into functional endocrine cells.

In this report, we set out to investigate whether a long-term supplementation with T4 enhanced glucose clearance in healthy and in STZ-challenged C57BL/6 wild-type mice, as well as improving metabolic homeostasis in the RIP-B7.1 mouse strain, which provides a model of experimental autoimmune diabetes (EAD). We found that T4 improved metabolic control in these murine models *via* the induction of the proliferation of pancreatic beta cells, as well as the production of insulin, which was associated with higher circulating insulin levels and the subsequent activation of the IRS1-Akt axis of insulin signalling in target tissues for insulin.

Methods

Animals

All animal care and experimental procedures complied with national and European Union legislation (Spanish RD 53/2013 and EU Directive 2010/63) for the protection of animals used for scientific purposes. The CABIMER animal facility is an SPF-certified facility. Animal studies are reported in compliance with the ARRIVE guidelines (Kilkenny *et al.,* 2010; McGrath and Lilley, 2015).

Mice were housed in individually ventilated cages (Tecniplast, Buguggiate, Italy). Souralit plus 29/12 bedding (Souralit, Gerona, Spain) was sterilized by autoclave and added to each cage. Mice were group-housed (one to four mice per cage), maintained on a 12 h light/dark cycle and had access to rodent chow TD2914 (Envigo, Barcelona, Spain) and water *ad libitum*.

For experiments in C57BL/6 mice, the offspring of five pairs of mice were used (Janvier, Le Genest-Saint-Isle, France). C57BL/6 mice are considered an optimal model to study glucose homeostasis. Female mice were treated or not with T4 starting at birth (s.c. injection of 18 $ng \cdot g^{-1}$ of body weight daily until weaning). After weaning, mice were supplemented with T4 in drinking water (50 $\mu g \cdot mL^{-1}$) (Spencer and West, 1961; Weinstein *et al.,* 1991; Weinstein *et al.,* 1994; Wistuba *et al.,* 2007; Dong *et al.,* 2010; Mysliwiec

et al., 2011; Buras *et al.,* 2014). Five untreated and six T4-treated animals per group were injected with insulin (0.75 U·kg^{-1} of body weight) before killing. At 24 weeks of age, animals were fasted for 16 h and killed by cervical dislocation.

For experiments related to EAD, transgenic RIP-B7.1 mice were used (Harlan *et al.,* 1994; Mellado-Gil *et al.,* 2016); these mice were supplied by Dr Bernhard. O. Boehm (Ulm University Medical Centre, Ulm, Germany). RIP-B7.1 mice are a well-established model of EAD. T4 supplementation (5 μg·mL^{-1} of T4 in the drinking water) was started at 6 weeks of age. EAD was triggered by intramuscular immunization at 8 weeks of age with 50 μg of pC1/ppins plasmid DNA (1 μg·μL^{-1}) containing the preproinsulin II. At 11 weeks of age, animals were killed by cervical dislocation. For experiments related to chemically induced diabetes mellitus, STZ was used following a previously published protocol (Verga Falzacappa *et al.,* 2011). Briefly, Thirty-four-week-old male C57BL/6 mice were treated with T4 (5 μg·mL^{-1} of T4 in the drinking water). At 2 weeks of T4 treatment, experimental diabetes mellitus was triggered by two injections (one each day for two consecutive days) of STZ (i.p., 150 mg·kg^{-1}), freshly dissolved in 10 mM Na-citrate buffer (pH 4.5). Mice were killed if circulating glucose levels were above 5 g·L^{-1} for more than 96 h.

Blinding, group size and randomization

The data analyst was blinded, whereas the operator was not blind to the group assignment of animals. Mice were selected from the pool eligible for inclusion in the study and were randomly divided into the experimental groups (n = 26 untreated mice and n = 28 T4-treated mice for C57BL/6 mice; n = 8 for the untreated group and n = 9 for the T4-terated group for RIP-B7.1 mice; n = 9 for the untreated group and n = 9 for the T4-treated group for STZ-treated C57BL/6 mice). The number of biological replicates was similar (n untreated-$= n \pm 1$ T4-treated) in the different experiments, experimental loss leading to greater differences in the number of biological replicates within the different experimental groups occurred in the experiments shown in Figures 1L, 2A, B, D, E and 5B and Supporting Information Figure S5B. Quantitative analysis of gene and protein expression was normalized to the mean of the control group to facilitate representation and understanding of the results. Quantitative-PCR data were adjusted by using a reference gene (β-actin). The experiments shown in Supporting Information Figure S1B–E were normalized to glucose levels at time 0 (%) to determine whether differences in metabolic test stem from differences in basal glucose levels (Curtis *et al.,* 2015). Measured glucose values are shown in Figure 1A, E, G, I.

Immunohistochemistry

Dissected tissues were fixed in 4% paraformaldehyde. Pancreatic sections (7 μm thick) were deparaffinized and rehydrated. Antigen retrieval was performed in 0.01 M sodium citrate buffer (pH 6). After 1 h blocking at room temperature, sections were incubated overnight at 4°C with primary antibodies (Supporting Information Table S1). Subsequently, slides were incubated with secondary antibodies (Supporting Information Table S1) for 1 h at room temperature. For immunofluorescence, DAPI-nuclear staining (Life Technologies,Carlsbad, USA) was used. For diaminobenzidine staining, biotinylated secondary antibodies were used (VectorLab, Burlingame, VT, USA). Counterstaining with haematoxylin (Panreac, Barcelona, Spain) was performed. Insulin staining was quantified using Image J as mean value/pixel after background subtraction. Thyroid and pituitary sections were stained with haematoxylin and eosin (Panreac).

Semi-quantitative RT–PCR

Total RNA was extracted from frozen skeletal muscle and liver samples using the Easy-blue RNA extraction kit (Intron Biotechnology, Gyeonggi-doQiagen, Korea). For islet experiments, the RNeasy Micro Kit was used (Qiagen). CDNA was synthesized using the Superscript II (Invitrogen, Carlsbad, CA, USA). The RT-PCR was performed on individual cDNAs using SYBR green (Roche). Primer sequences are presented in Supporting Information Table S2. The mRNA expression was calculated by the $2^{-\Delta\Delta CT}$ method and normalized to the expression of β-actin.

Western blot

Samples were lysed in radioimmunoprecipitation assay buffer (20 mM Tris–HCl (pH 7.5), 150 mM NaCl, 1 mM Na_2EDTA, 1 mM EGTA, 1% NP-40, 1% sodium deoxycholate) with protease, phosphatase and deacetylase inhibitors P0044, P5725, P8340 and SC-362323. Western blots were performed according to standard methods, which involved incubation with a primary antibody of interest, followed by incubation with a horseradish peroxidase-conjugated secondary antibody (Supporting Information Table S1). Blots were quantified with ImageJ, and the bands of interest were normalized to Ponceau S and/or GAPDH staining, as previously validated (Bello *et al.,* 2003).

In vivo insulin and glucose determinations

To determine glucose levels, blood samples were taken by venepuncture using a Precision Xceed glucometer (Abbott, Madrid, Spain) (Martin-Montalvo *et al.,* 2013). Insulin was measured in plasma using ELISA kits (Crystal Chem, Downers Grove, IL, USA). For the oral glucose tolerance test (OGTT), mice were fasted from 6 h at 10 a.m. and received an oral dose of glucose (3 g·kg^{-1}) by gavage. For the intraperitoneal pyruvate tolerance test (IPPTT), mice were fasted for 6 h from 10 a.m. and received aninjection of sodium pyruvate (i.p., 2-g·kg^{-1}) by gavage. For the insulin tolerance test (ITT), mice were fasted for 3 h from 10 a.m. and were injected with insulin (0.75 IU·kg^{-1}, i.p). For glucose determination during a 24 h fasting period, mice were fasted from 8 p.m.

Rotarod

Results from rotarod tests are presented as the time to fall from an accelerating rotarod as previously described (4–40 rpm over 5 min) (Mitchell *et al.,* 2014). Mice were given a 1 min habituation trial at 4 rpm on the day before the experiment. Results shown are the averages of three trials per mouse.

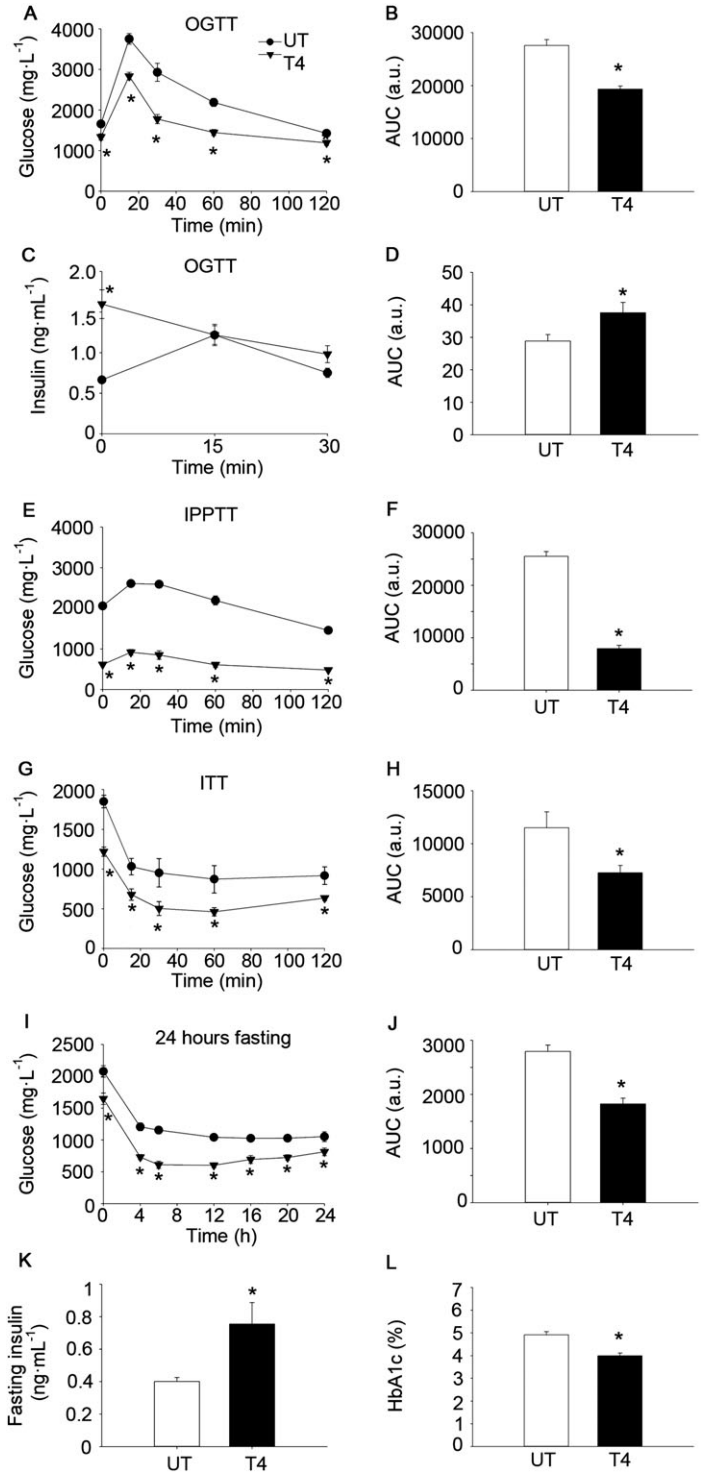

Figure 1

T4 enhances glucose clearance in wild-type C57BL/6 mice. (A) Glucose concentration in blood after oral glucose load (OGTT). Age = 10 weeks. $n = 13$ per group. (B) AUC of glucose levels during the OGTT. (C) Plasma levels of insulin after oral glucose load (OGTT). Age = 9 weeks. $n = 7$ untreated; $n = 8$ T4-treated. (D) AUC of insulin levels during OGTT curve. (E) Glucose concentration in blood after intraperitoneal pyruvate load (IPPTT). Age = 8 weeks. $n = 7$ untreated; $n = 8$ T4-treated. (F) AUC of glucose levels during the IPPTT. (G) Glucose concentration in blood after i.p. insulin injection (ITT). Age = 11 weeks. $n = 12$ untreated; $n = 13$ T4-treated. (H) AUC of glucose levels during the ITT. (I) Glucose concentration in blood during a 24 h fasting period. Age = 12 weeks. $n = 7$ untreated; $n = 8$ T4-treated. (J) AUC of glucose levels during the 24 h fasting period. (K) Sixteen-hour fasting circulating insulin levels. Age = 12 weeks. $n = 7$ untreated; $n = 8$ T4-treated. (L) Percentage of glycated haemoglobin (HbA1c) in blood. Age = 23 weeks. $n = 9$ untreated; $n = 14$ T4-treated. UT, untreated; T4, T4-treated. Data shown are the means ± SEM. *$P < 0.05$, significantly different from untreated mice; two tailed Student's *t*-test.

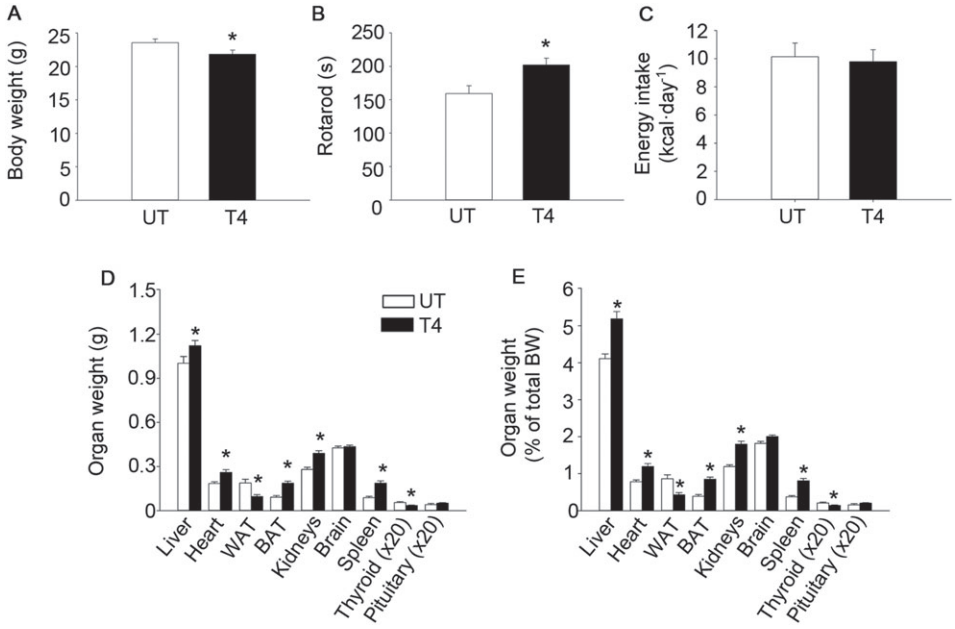

Figure 2

T4 reduces body weight and increases rotarod performance. (A) Body weight. Age = 24 weeks. $n = 12$ untreated; $n = 18$ T4-treated. (B) Time to fall from an accelerating rotarod. Age = 21 weeks. $n = 12$ untreated; $n = 18$ T4-treated. (C) Energy intake. Age = 8 weeks. $n = 7$ untreated; $n = 8$ T4-treated. (D) Organs weight. Age = 24 weeks. For liver, heart, WAT, BAT, kidney, brain and spleen $n = 12$ untreated; $n = 18$ T4-treated. For thyroid and pituitary $n = 6$ untreated; $n = 7$ T4-treated. (E) Organs weight divided by body weight. Age = 24 weeks. For liver, heart, WAT, BAT, kidney, brain and spleen $n = 12$ untreated; $n = 18$ T4-treated. For thyroid and pituitary $n = 6$ untreated; $n = 7$. UT, untreated; T4, T4-treated. Data shown are the means ± SEM. *$P < 0.05$, significantly different from untreated mice; two tailed Student's *t*-test.

Islet isolation, culture and glucose-stimulated insulin secretion (GSIS)

Islets from 24-week-old female wild-type C57BL/6 mice were isolated by intraductal collagenase perfusion as previously described (Jimenez-Moreno *et al.*, 2015). For semi-quantitative RT-PCR purposes, pancreatic islets were processed upon collection. For insulin determination, similar amounts of islet equivalents (10 in each technical replicate) were lysed in HCl-ethanol (5% HCl in 96° ethanol) for 16 h at 4°C. For GSIS studies, islets were cultured overnight in RPMI-1640 medium (2 g·L^{-1} glucose). Then, groups of 10 islets were washed in 500 μL of Krebs-Ringer bicarbonate-HEPES buffer (KRBH) (140 mM NaCl, 3.6 mM KCl, 0.5 mM NaH_2PO_4, 0.5 mM $MgSO_4$, 1.5 mM $CaCl_2$, 2 mM $NaHCO_3$, 10 mM HEPES, 0.1% BSA). Subsequently, fresh KRBH supplemented with 2.8 mM glucose was added, and islets were incubated for 30 min. Next, buffer was harvested ("2.8 mM insulin secretion"), and 500 μL of KRBH supplemented with 22 mM glucose was added. Islets were incubated for an additional 30 min at 37°C, and then, buffer was harvested ("22 mM insulin secretion"). Following the incubations, islets were lysed with HCl-ethanol to obtain the insulin content. In all cases, insulin was measured using ELISA kits (Crystal Chem).

T4 determination

T4 concentration in serum was determined using a T4 commercial kit (MP Biomedicals, Santa Ana,CA, USA).

Homeostasis model assessment of insulin resistance (HOMA-IR)

Insulin resistance was estimated using the HOMA2 Calculator available from the Oxford website (Levy *et al.*, 1998).

Glycated haemoglobin

HbA1c levels were determined in blood samples according to the manufacturer's protocol (CrystalChem).

α-glycoprotein subunit (α-GSU) determination

The α-GSU of pituitary hormones was determined using a commercially available kit following the instructions of the manufacturer (Abbexa, Cambridge, United Kingdom).

TUNEL assay

For the TUNEL staining, the *In Situ* Cell Death Detection Kit, Fluorescein, was used using proteinase K (Sigma-Aldrich, St. Louis, MO, USA).

Data and statistical analysis

The data and statistical analysis in this study comply with the recommendations on experimental design and analysis in pharmacology (Curtis *et al.*, 2015). Data are shown as means ± SEM. Statistical significance was calculated using unpaired, two-tailed Student's *t*-test as two experimental groups (untreated and T4-treated) were compared (Excel 2007, Microsoft). The Mann–Whitney rank sum test was applied when data were normalized to basal glucose levels (SigmaPlot

12.5, Softonic, Barcelona, Spain). A LogRank statistical test was applied for survival curves (SigmaPlot 12.5, Softonic). For all analyses, $P < 0.05$ was considered statistically significant.

Materials

T4, glucose, sodium pyruvate, STZ and the enzyme inhibitors P0044, P5725 and P8340 were purchased from Sigma-Aldrich. SC-362323 was supplied by Santa Cruz Biotechnology (Santa Cruz, CA, USA). Unless otherwise stated, other reagents were purchased from Sigma-Aldrich.

Nomenclature of targets and ligands

Key protein targets and ligands in this article are hyperlinked to corresponding entries in http://www.guidetopharmacology.org, the common portal for data from the IUPHAR/BPS Guide to PHARMACOLOGY (Southan *et al.,* 2016), and are permanently archived in the Concise Guide to PHARMACOLOGY 2015/16 (Alexander *et al.,* 2015a, b).

Results

T4 supplementation enhances glucose clearance in healthy C57BL/6 mice

In order to determine the metabolic effects of T4 supplementation in mice, we treated female wild-type C57BL/6 mice with T4 from postnatal day 1 (18 $ng \cdot g^{-1}$ of body $weight \cdot day^{-1}$; s.c. injections) until weaning, followed by T4 administration in the drinking water (50 $\mu g \cdot mL^{-1}$ *ad libitum*) until 24 weeks of age, when mice were killed (Spencer and West, 1961; Weinstein *et al.,* 1991; Weinstein *et al.,* 1994; Wistuba *et al.,* 2007; Dong *et al.,* 2010; Mysliwiec *et al.,* 2011; Buras *et al.,* 2014). Analysis of serum samples indicated that T4 concentration was increased in T4-treated mice (Supporting Information Figure S1A).

Glucose tolerance was enhanced by T4 supplementation as determined by the lower AUC in an OGTT, even when glucose levels were expressed as the percentage of basal glucose (Figure 1A–B and Supporting Information Figure S1B). Remarkably, basal circulating insulin levels were higher in T4-treated mice in the OGTT, while levels were similar to those of untreated animals at 15–30 min post-glucose load (Figure 1C–D). Glucose levels were also lower at all time points during an IPPTT, indicating that hepatic gluconeogenesis, although significant (e.g. significant increase in glucose levels promoted by pyruvate administration), was not able to normalize glucose levels in T4-treated mice (Figure 1E–F and Supporting Information Figure S1C). In order to determine whether insulin sensitivity was affected, animals were challenged with an ITT. Circulating glucose levels were significantly lower in T4-treated mice at any time point during the ITT, although these differences were related to the lower basal glucose levels, as shown by the lack of significant differences when glucose levels were expressed as the percentage of basal glucose (Figure 1G–H and Supporting Information Figure S1D). We next measured circulating glucose levels during a 24 h fasting period. Glucose levels were significantly reduced in T4-treated mice at any time point during the experiment (Figure 1I–J and Supporting Information Figure S1E). Consistent with the high insulin levels determined during the basal time of the OGTT (6 h fasting), circulating insulin levels were also higher at 16 h of fasting (Figure 1K). Interestingly, despite the lower glucose levels during the ITT, a trend towards increased HOMA-IR was found in T4-treated mice ($P = 0.08$ in two-tailed Student's *t*-test) (Supporting Information Figure S1F). Supporting the long-term reduction of glucose levels in mice treated with T4, the percentage of glycated haemoglobin was lower (note that the untreated group is within the healthy physiological range; ~5%) (Figure 1L). Taken together, these results indicate that T4 supplementation markedly reduced the glucose concentration in blood, which was associated with increased circulating insulin.

We next assessed the effects of T4 supplementation on whole body physiology. Body weight was slightly reduced in T4-treated mice (Figure 2A). Rotarod performance was improved by T4, indicating the overall healthy status of the animals (Figure 2B). Interestingly, energy intake was similar in both experimental groups, even when corrected for changes in body weight (Figure 2C and Supporting Information Figure S2A). Noticeably, at killing, gonadal white adipose tissue (WAT) and thyroid weights were reduced in T4-treated mice (Figure 2D–E). In contrast, several organs, including the brown adipose tissue (BAT), were heavier in T4-treated mice, even when corrected for body weight (Figure 2D–E). Histological examinations of the thyroid and the pituitary revealed no major macroscopic changes in tissue morphology (Supporting Information Figure S2B). Thyroid sections of T4-treated mice had a slightly less intense staining of the colloid in the lumen of the follicle, suggestive of reduced endogenous thyroglobulin content. In addition, serum concentration of the α-GSU of pituitary hormones was concomitantly reduced in T4-treated mice (Supporting Information Figure S2C).

T4 supplementation enhances beta cell turnover and increases beta cell insulin content

T4-mediated increases in circulating insulin levels implied effects of the hormone on pancreatic islets. Accordingly, insulin staining was greater while glucagon was unaffected, in pancreatic sections of T4-treated mice, compared with control mice (Figure 3A–C). Increased insulin content in the islets of T4-treated mice was confirmed by ELISA determination using freshly isolated pancreatic islets (Figure 3D). Determinations of mRNA expression by real-time PCR in pancreatic islets from T4-treated and untreated mice indicated that Akt and **glucokinase (GK)** expression were also significantly increased in the islets of T4-treated mice, whereas no changes were observed in MAFA and FOXO1 gene expression (Supporting Information Figure S3A). Immunohistochemical analysis confirmed that GK expression was increased, while the subcellular localization of FOXO1 and MAFA remained unaffected in T4-treated mice (Figure 3A, E and Supporting Information Figure S3B–C) (Kikuchi *et al.,* 2012; Aguayo-Mazzucato *et al.,* 2013). Remarkably, GSIS assays performed in islets isolated from T4-treated mice showed that insulin secretion was increased, when islets were cultured under low glucose (2.8 mM) conditions (Figure 3F). However, differences in insulin secretion under high glucose (22 mM) conditions did not reach statistical significance. Interestingly, beta cell proliferation, defined here as the percentage of Ki67

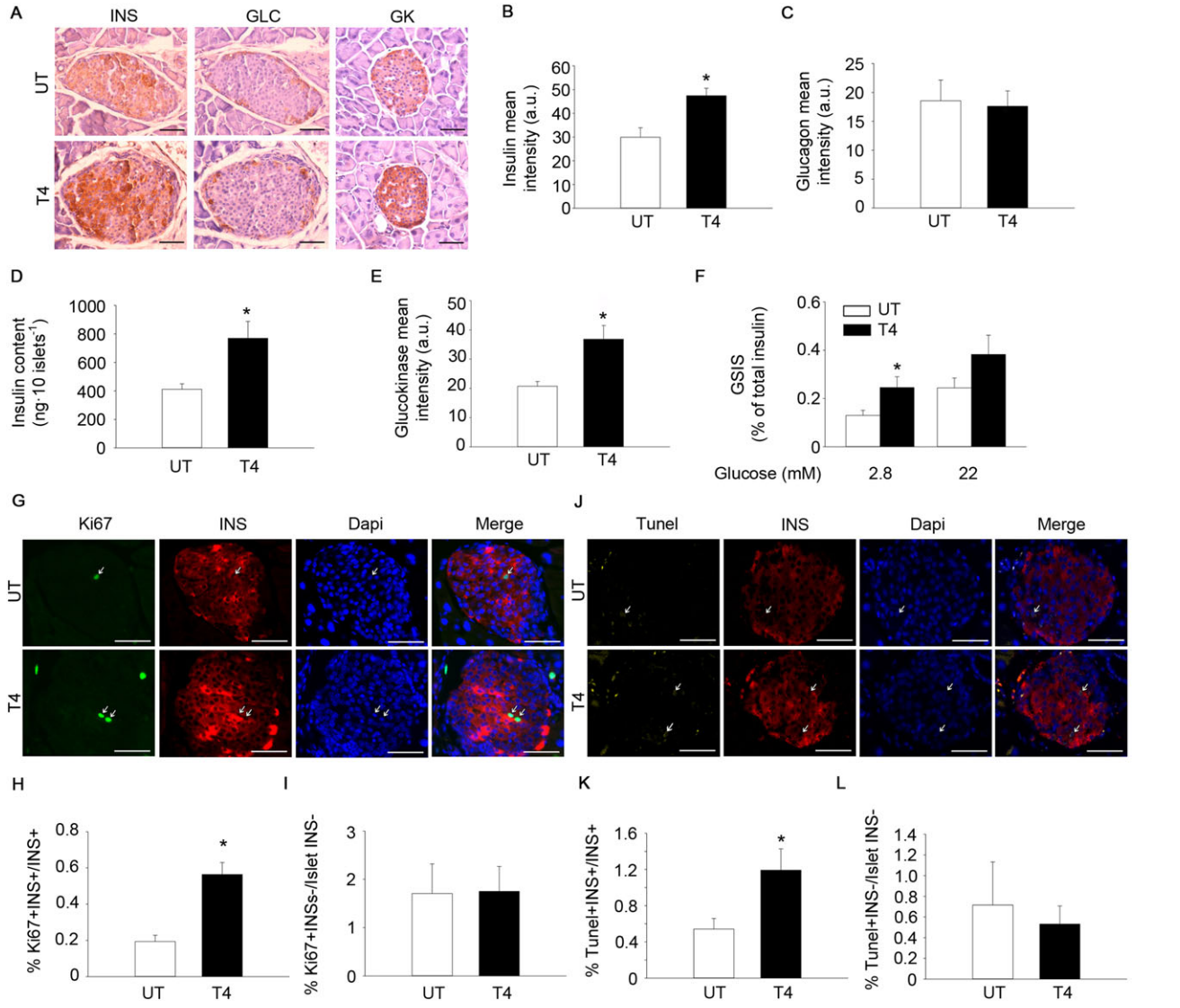

Figure 3

T4 increases insulin expression and enhances the proliferation of pancreatic beta cells. (A) Representative images of insulin (INS), glucagon (GLC) and glucokinase (GK) staining in pancreas from mice treated or not with T4. Diaminobenzidine staining followed by haematoxylin counterstaining. Scale bar = 50 μm. INS; $n = 5$ per group. GLC; $n = 5$ per group. GK; $n = 6$ per group. (B) Quantification of insulin staining (mean intensity). (C) Quantification of glucagon staining (mean intensity). (D) Determination of pancreatic islet insulin content by ELISA. $n = 6$ untreated, $n = 7$ T4-treated. (E) Quantification of glucokinase staining (mean intensity). (F) Determination of GSIS. $n = 6$ untreated, $n = 7$ T4-treated. (G) Representative images of Ki67 and insulin staining in pancreases from mice treated or not with T4. Immunofluorescence followed by DAPI staining. Scale bar, 50 μm. $n = 5$ per group. (H) Percentage of Ki67$^+$-Insulin$^+$ cells over total insulin$^+$ cells. (I) Percentage of Ki67$^+$-Insulin$^-$ cells over total insulin$^-$ cells residing in pancreatic islets. (J) Representative images of TUNEL and insulin staining in pancreas from mice treated or not with T4. Immunofluorescence followed by DAPI staining. Scale bar = 50 μm. $n = 5$ per group. (K) Percentage of TUNEL$^+$-Insulin$^+$ cells over total insulin$^+$ cells. (L) Percentage of TUNEL$^+$-Insulin$^-$ cells over total insulin$^-$ cells residing in pancreatic islets. UT, untreated; T4, T4-treated. Arrows indicate representative positive staining. Data shown are the means ± SEM. *$P < 0.05$ significantly different from untreated mice; two tailed Student's t-test.

positive cells within the insulin-expressing cell population, was increased in T4-treated animals, compared with that in untreated mice (Figure 3G–I). As opposed to beta cells, non-insulin-expressing pancreatic endocrine cells showed similar proliferation (percentage of Ki67 positive cells in islet residing non-insulin expressing cells) (Figure 3G, I). Remarkably, the percentage of apoptotic cells, determined by TUNEL staining, was also increased by T4 administration, specifically in the beta cell population (Figure 3J–L).

T4 induces the activation of IRS1-Akt signalling in insulin-target tissues

In order to determine the underlying mechanism of T4 action in insulin-target tissues, we measured mRNA expression by semi-quantitative real-time PCR. We found that the transcript levels of several members of the insulin signalling pathway were over-expressed in skeletal muscle and in the liver of T4-treated mice (Figure 4A–B). Consistent with these data, protein extracts of both T4-treated liver and skeletal muscle,

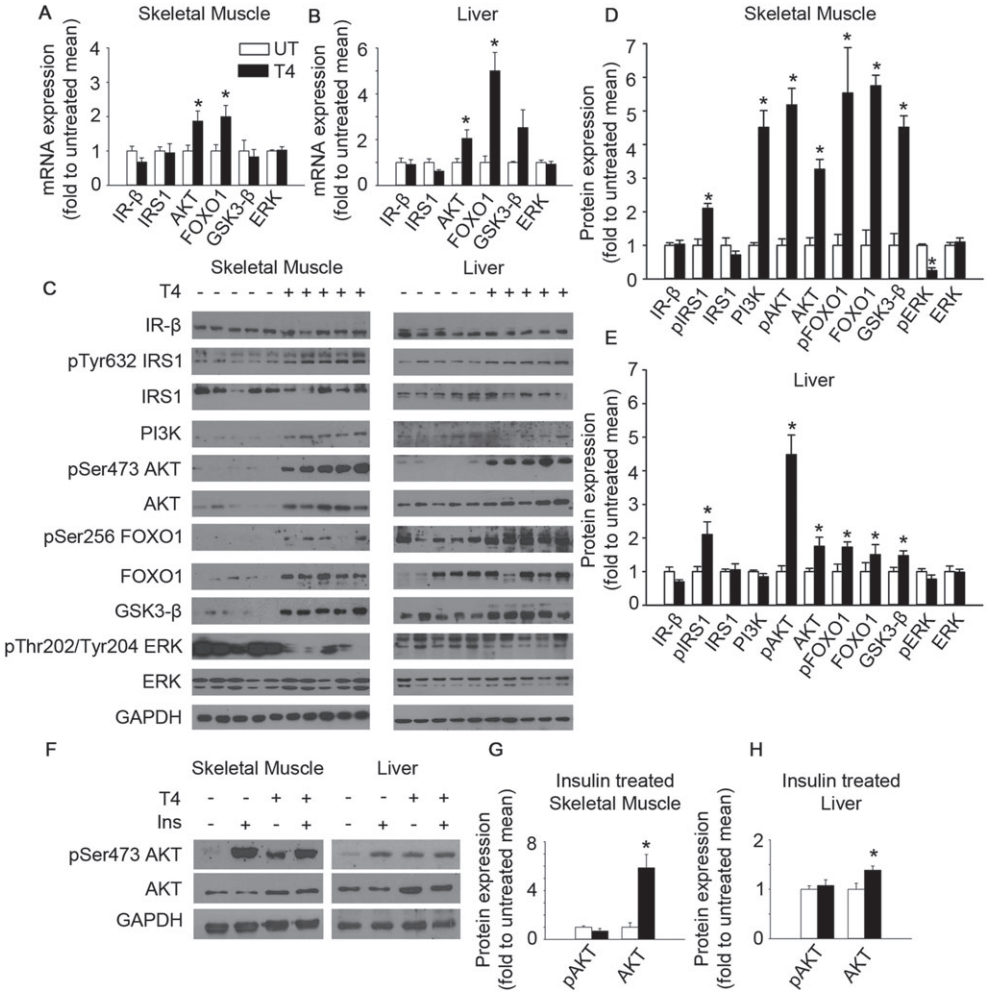

Figure 4

T4 activates insulin signalling in skeletal muscle and liver. (A) Determination of mRNA levels of several members of the insulin pathway in the skeletal muscle of mice treated or not with T4. Mice were fasted for 16 h before they were killed. Values were normalized to untreated mice. IR-β; $n = 5$. IRS1; $n = 6$. Akt; $n = 5$. FOXO1; $n = 6$. GSK3-β; $n = 6$. ERK; $n = 6$. (B) Determination of mRNA levels of several members of the insulin pathway in the liver of mice treated or not with T4. Mice were fasted for 16 h before they were killed. Values were normalized to untreated mice. IR-β; $n = 6$ untreated, $n = 5$ T4-treated. IRS1; $n = 6$ untreated, $n = 5$ T4-treated. AKT; $n = 6$. FOXO1; $n = 6$ untreated, $n = 5$ T4-treated. GSK3-β; $n = 5$. ERK; $n = 6$ untreated, $n = 5$ T4-treated. (C) Western blots indicating activation of insulin signalling in the skeletal muscle and the liver of T4-treated mice. Mice were fasted for 16 h before they were killed. $n = 5$ per group. (D) Densitometric analysis of the Western blots using skeletal muscle extracts shown in panel C. Values were normalized to untreated mice. (E) Densitometric analysis of the Western blots using liver extracts shown in panel C. Values were normalized to untreated mice. (F) Representative images of Western blots showing the maximal activation of insulin signalling in T4-treated and untreated mice challenged with an insulin injection (0.75 U·kg^{-1} of body weight) 15 min prior euthanization. Mice were fasted for 16 h before they were killed. (G) Densitometric analysis of the Western blots using skeletal muscle extracts shown in Supporting Information Figure S4A. $n = 5$ untreated, $n = 6$ T4-treated. Values were normalized to untreated mice. (H) Densitometric analysis of the Western blots using liver extracts shown in Supporting Information Figure S4A. $n = 5$ untreated, $n = 6$ T4-treated. Values were normalized to untreated mice. UT, untreated; T4, T4-treated. Data shown are the means ± SEM. *$P < 0.05$, significantly different from untreated mice; two tailed Student's t-test.

exhibited increased levels of total Akt, FOXO1 and glycogen synthase kinase 3β (GSK3-β) (Figure 4C–E). Moreover, the phosphorylated isoforms of several members of the insulin signalling such as pTyr^{632}-IRS1, pSer^{473}-Akt and pSer^{256}-FOXO1 were significantly increased in both, skeletal muscle and liver lysates isolated from T4-treated mice (Figure 4C–E). Remarkably, ERK phosphorylation at Thr^{202}/Tyr^{204} in skeletal muscle was reduced in T4-treated samples, indicating the specificity of the effect of T4 supplementation in the IRS1-Akt branch of insulin signalling. In order to determine whether T4 supplementation could also increase the maximal activation of the IRS1-AKT axis of insulin signalling, a cohort of mice was treated with insulin (0.75 UI·kg^{-1} of body weight) 15 min before killing (Figure 4F–H and Supporting Information Figure S4A). No differences on insulin-stimulated phosphorylation of Ser^{473}-Akt levels were found, indicating that maximal insulin-induced Akt activation was not affected by T4-treatment. T4 treatment also modulated the expression of genes involved in glucose utilization (e.g. increased glycolysis and gluconeogenesis) and

mitochondrial uncoupling, in both skeletal muscle and liver (Supporting Information Figure S4B–C). Taken together, these results suggest that high circulating levels of insulin, induced by T4, lead to sustained activation of IRS1-Akt signalling and subsequently increased glucose uptake in insulin target tissues, to maintain their high metabolic requirements. Supporting these data, a significant increase of pThr^{172}-**AMPK**, which indicates a starvation-like status, was found in extracts isolated from T4-treated skeletal muscles (Supporting Information Figure S4D–E). Noteworthy, such a change was not detected in liver samples, suggesting that energy metabolism is preferentially affected in tissues with higher metabolic demands (Supporting Information Figure S4D, F).

T4 supplementation improves glycaemic control in the RIP-B7.1 model of EAD and increases survival in STZ-treated mice

Given the effects of T4 supplementation in the promotion of beta cell proliferation and the increase of circulating insulin levels in healthy C57BL/6 mice, we next sought to determine whether T4 supplementation could blunt the onset of T1DM in the RIP-B7.1 model of EAD (Harlan *et al.,* 1994; Mellado-Gil *et al.,* 2016). To this end, RIP-B7.1 mice were treated with T4, (5 $\mu g \cdot mL^{-1}$ in drinking water) starting at 6 weeks of age. RIP-B7.1 mice were immunized at 8 weeks of age to trigger the autoimmune attack on the beta cells. Assay of circulating T4 levels revealed a significant increase in T4-treated RIP-B7.1 immunized mice when compared to untreated RIP-B7.1 immunized mice (Supporting Information Figure S5A).

Noticeably, T4-treated immunized RIP-B7.1 mice gained weight over the course of the experiment, while control (untreated) immunized RIP-B7.1 mice reached a plateau (Figure 5A). Thus, body weights were significantly different from week 4 of T4-treatment. Similar to healthy wild-type C57BL/6 mice (Figure 2D–E), the weight of several organs, including the BAT, was higher at the end of the experiment (5 weeks of T4-treatment; 11 weeks of age) (Figure 5B). However, differences on the weight of gonadal WAT were not apparent, even when corrected for body weight (Figure 5B and Supporting Information Figure S5B).

In order to determine the effect of T4 supplementation in the pathogenesis of EAD, several metabolic tests were performed. An OGTT performed 2 weeks post-immunization revealed enhanced glucose clearance in T4-treated immunized RIP-B7.1 mice (Figure 5C–D). An ITT performed 3 weeks post-immunization indicated that circulating glucose was significantly lower in T4-treated immunized RIP-B7.1 mice at any time point during the experiment (Figure 5E–F). However, these differences seem to stem from the lower basal glucose levels in T4-treated RIP-B7.1 immunized mice. Postprandial glucose determination revealed that, while untreated immunized RIP-B7.1 animals developed hyperglycaemia at 5 weeks of treatment (3 weeks post-immunization), T4-treated immunized RIP-B7.1 mice remained normoglycaemic (Figure 5G). Remarkably, postprandial circulating insulin was dramatically increased in T4-treated RIP-B7.1 immunized mice, which was associated with increased phosphorylation of the IRS1 at Tyr^{632}, in the liver (Figure 5H and Supporting Information Figure S5C–E). In order to determine whether T4 supplementation could improve glucoregulation in a different mouse model of experimental diabetes, STZ chemically induced diabetes mellitus was used. To this end, male wild-type C57BL/6 mice were treated with T4 (5 $\mu g \cdot mL^{-1}$ in the drinking water), starting 2 weeks before injection of STZ (Verga Falzacappa *et al.,* 2011). The average survival of control STZ-treated mice was 8 days, whereas the T4-treated group achieved a mean survival of 34 days, including some mice that survived STZ (Figure 5I; $P < 0.05$, $\chi^2 = 7{,}689$). Postprandial glucose levels showed a trend towards reduced glycaemia in T4-treated mice (Figure 5J). Taken together, our results indicate that treatment with T4 delayed the onset of T1DM in the RIP-B7.1 model of EAD and increased survival in STZ-induced experimental diabetes mellitus.

Immunohistochemical analyses were performed in order to determine the underlying effects of T4 supplementation on the pancreas of immunized RIP-B7.1 mice. Although both immunized untreated and T4-treated RIP-B7.1 mice displayed a similar level of lymphocyte infiltration, T4-treated mice exhibited a marked increase in insulin staining with no significant variation in glucagon staining (Figure 6A–C and Figure S6A–B). We next investigated whether T4 could also increase the proliferation of beta cells in the RIP-B7.1 model of experimental T1DM. Interestingly, the abundance of islet-residing Ki67 positive cells was increased in immunized RIP-B7.1 mice when compared to healthy C57BL/6 mice, indicating that islet-residing immune cells and/or pancreatic endocrine cells proliferate under the immune attack (Figures 3D and 6D). Nonetheless, T4-treated immunized RIP-B7.1 mice exhibited a marked increase in proliferating beta cells when compared to untreated immunized RIP-B7.1 mice (Figure 6D–E). As expected, the immune attack increased the percentage of apoptotic beta cells in both, T4-treated and untreated immunized RIP-B7.1 mice (Figures 3G–H and 6F–G). However, no differences were observed between T4-treated and untreated immunized RIP-B7.1 mice. These results suggest that increased beta cell proliferation might be the underlying mechanism by which T4 blunts the onset of experimental T1DM in mice.

Discussion

Supplementation with THs provides undeniably positive benefits for metabolic health, attenuating hyperglycaemia in STZ-treated and leptin-receptor deficient mice (Lin and Sun, 2011; Verga Falzacappa *et al.,* 2011; Shoemaker *et al.,* 2012). Therefore, THs or their analogues could represent a promising therapeutic approach for the treatment of metabolic complications. However, the detrimental effects of high circulating levels of THs (thyrotoxicosis) are well known. Patients suffering thyrotoxicosis exhibit a pleiotropy of symptoms that include life-threatening disorders such as cardiovascular collapse and thyroid storm, among others (Bahn *et al.,* 2011; Garmendia Madariaga *et al.,* 2014). These risks have precluded the investigation of potential therapies based on the use of THs to treat metabolic disorders.

In this report, we show that a level of T4 supplementation modulates the thyroid-pituitary axis, increases insulin concentration in blood and enhances glucose clearance, while maintaining an overall healthy status in wild-type C57BL/6

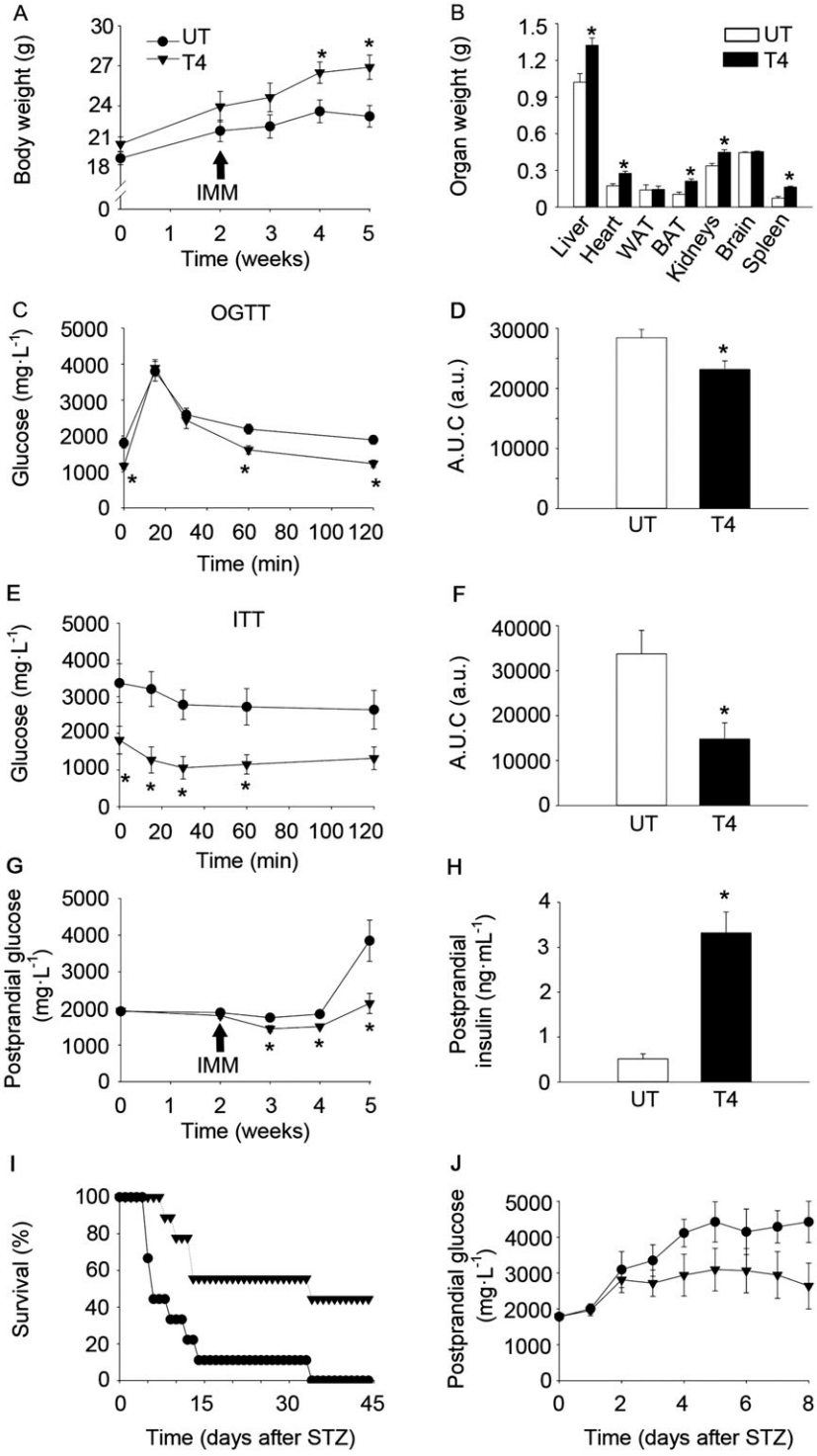

Figure 5

T4 blunts the onset of T1DM in the RIP-B7.1 model of EAD and increases survival in STZ-challenged C57BL/6 mice. (A) Body weight of RIP-B7.1 mice. $n = 8$ untreated; $n = 9$ T4-treated. (B) Organs weight of RIP-B7.1 mice. $n = 6$ untreated; $n = 9$ T4-treated. (C) Glucose concentration in blood during an OGTT at 4 weeks of T4-treatment of RIP-B7.1 mice. $n = 8$ untreated; $n = 9$ T4-treated. (D) AUC of glucose levels during the OGTT. (E) Glucose concentration in blood during and ITT at 5 weeks of T4-treatment of RIP-B7.1 mice. $n = 7$ untreated; $n = 9$ T4-treated. (F) AUC of glucose levels during the ITT. (G) Postprandial glucose concentration in blood on RIP-B7.1 mice. $n = 8$ untreated; $n = 9$ T4-treated. (H) Circulating insulin levels in fed conditions. $n = 7$ untreated; $n = 8$ T4-treated. (I) Survival of C57BL/6 mice challenged with STZ. $n = 9$ per group. (J) Postprandial glucose concentration in blood from C57BL/6 mice challenged with STZ. Alive animals were included (see Figure 5I for n in each time point). UT, untreated; T4, T4-treated; IMM, immunization. Arrows indicate the time of immunization. Data shown are the means ± SEM *$P < 0.05$, significantly different from untreated mice; two tailed Student's t-test. A LogRank survival test was applied to survival curves.

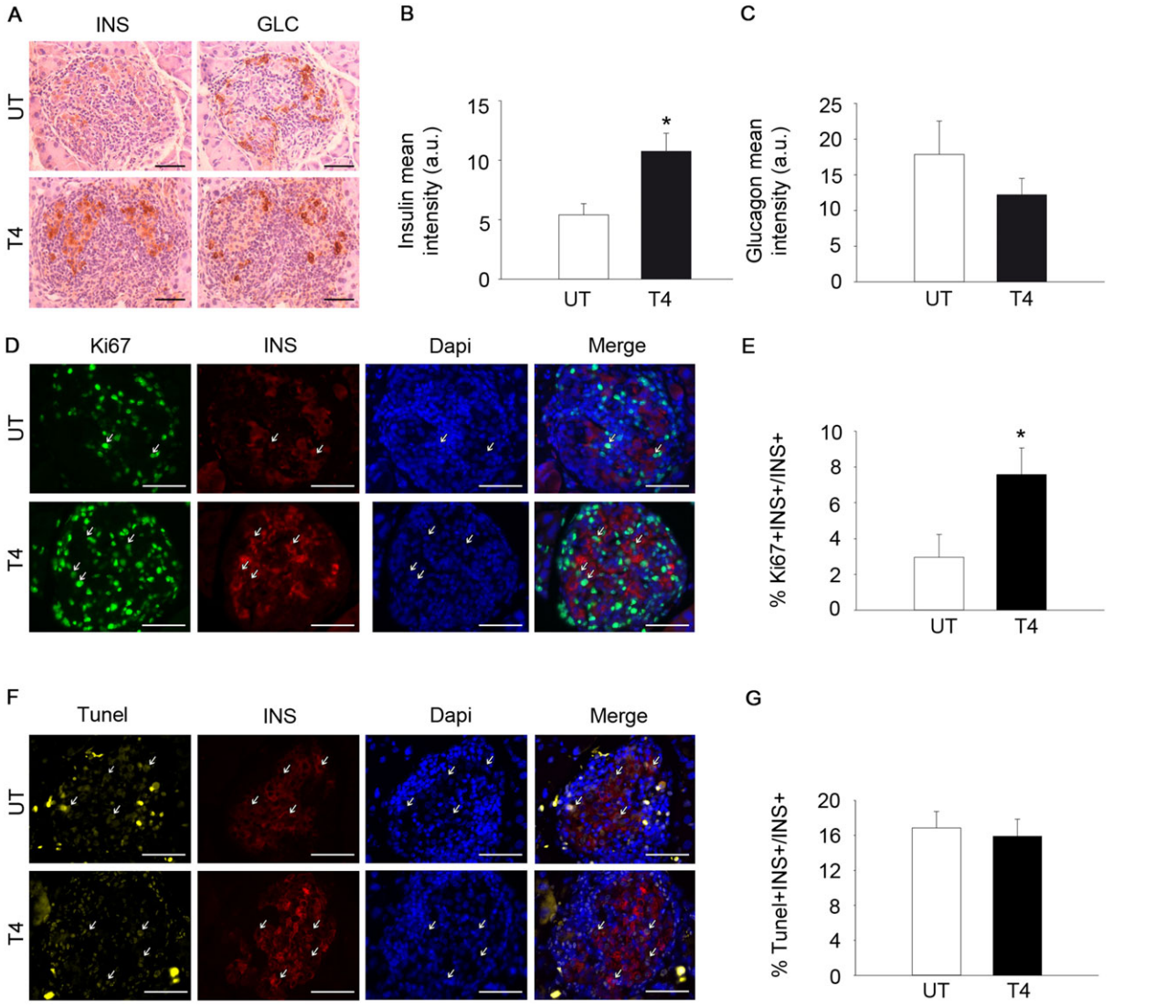

Figure 6

T4 increases insulin expression and enhances beta cell proliferation in the RIP-B7.1 model of EAD. (A) Representative images of glucagon (GLC) and insulin (INS) staining in pancreases from immunized RIP-B7.1 mice, with or without T4. Diaminobenzidine staining followed by haematoxylin counterstaining. Scale bar, 50 μm. $n = 6$ untreated; $n = 5$ T4-treated. (B) Quantification of insulin staining (mean intensity). (C) Quantification of glucagon staining (mean intensity). (D) Representative images of Ki67 and insulin staining in pancreas from immunized RIP-B7.1 mice, with or without T4. Immunofluorescence followed by DAPI staining. Scale bar = 50 μm. $n = 5$ untreated; $n = 5$ T4-treated. (E) Percentage of $Ki67^+$-$Insulin^+$ cells over total $insulin^+$ cells. (F) Representative images of TUNEL and insulin staining in pancreases from immunized RIP-B7.1 mice, with or without T4. Immunofluorescence followed by DAPI staining. Scale bar = 50 μm. $n = 5$ per group. (G) TUNEL $Insulin^+$ cells, as % total $insulin^+$ cells. UT, untreated; T4, T4-treated. Arrows indicate representative positive staining. Data shown are the means ± SEM. *$P < 0.05$, significantly different from untreated mice; two tailed Student's *t*-test.

mice. Our results indicate that T4 supplementation increases insulin content in pancreatic beta cells. The mechanism underlying the increase in insulin content may rely on a TH-dependent regulation of expression of the transcription factor MAFA. Previous reports have demonstrated that the T3-TR complex induces MAFA transcription through direct binding to TH response elements located in the MAFA promoter (Aguayo-Mazzucato *et al.*, 2013). Moreover, MAFA is known to bind to the insulin promoter, inducing insulin expression (Olbrot *et al.*, 2002; Matsuoka *et al.*, 2004), providing a plausible molecular mechanism by which T4 supplementation enhances insulin expression in pancreatic beta cells. However, as opposed to a previous study using 7-day-old mice, our immunohistochemical analysis in pancreatic sections of adult mice indicated that MAFA is predominantly located in the nucleus of pancreatic beta cells and T4 supplementation does not further promote the nuclear localization of MAFA, suggesting that the presence/absence of MAFA in the nucleus of pancreatic beta cells does not control insulin expression in adulthood (Aguayo-Mazzucato *et al.*, 2013). Remarkably, islets isolated from mice treated with T4 exhibited a marked increase in GK gene and protein

expression. Increased GK expression might contribute to the increased insulin secretion under fasting conditions, as observed in GSIS tests, because increased GK activity has been previously shown to lower the glucose threshold that stimulates insulin secretion (Weinhaus *et al.,* 2007; Kassem *et al.,* 2010). Increased circulating insulin activates the IRS1-Akt axis of insulin signalling, suggesting that glucose uptake is increased in insulin target tissues. T4 is known to increase the basal metabolic rate by inducing the expression of several mitochondrial uncoupling proteins, such as UCP2 (Lanni *et al.,* 2003; Ramadan *et al.,* 2011). As a result of increased mitochondrial uncoupling, mitochondrial efficiency is lower (defined here as the amount of nutrients used to produce one molecule of ATP) and heat production is increased (note that BAT weight in T4-treated animals was increased). In order to adapt to this situation, T4-treated cells require higher amounts of nutrients to maintain their metabolism. Therefore, it is tempting to speculate that insulin expression and secretion in pancreatic islets under fasting conditions is enhanced in mice treated with T4 to allow nutrient uptake by insulin-target tissues. Supporting this hypothesis, we found that, as opposed to untreated animals, in which a significant increase in insulin levels was promoted by a glucose bolus, insulin levels in T4-treated mice were already maximal before glucose load, suggesting that the insulin secretion machinery is already active. Moreover, our results also indicate that beta cell proliferation and apoptosis are specifically increased in mice treated with T4. Remarkably, increased GK activity has been associated to increased beta cell proliferation and apoptosis, suggesting that the increase in GK expression induced by T4 administration might contribute to the enhancement of beta cell turnover, promoting the existence of a highly insulin-expressing beta cell population, which actively secretes insulin into the circulation under basal conditions (Kassem *et al.,* 2000; Kassem *et al.,* 2010). Given the age of the animals, the length of the treatment (~24 weeks at the end of th experiment, which represents ~25% of an average lifespan of this mouse strain) and the mouse chow used in this study (a standard healthy diet), we do not believe that the increase of insulin expression in pancreatic beta cells found in T4-treated mice was indicative of over-stimulation of beta cells, as found in pre-diabetic individuals (Martin-Montalvo *et al.,* 2013). The analysis of insulin-target tissues indicates that the higher insulin concentration in blood is able to activate the IRS1-Akt axis of the insulin signalling pathway. Previous reports have indicated that T4 exerts non-genomic effects by activating specifically PI3K and its downstream targets (Lin and Sun, 2011). Although we cannot exclude that non-genomic T4 actions contribute to the activation of PI3K and its downstream targets *in vivo*, we found that T4 supplementation activates insulin signalling as early as the level of IRS1, as shown by the increase in $pTyr^{632}$-IRS1 in skeletal muscles and in livers of T4-treated mice. Remarkably, we found that both T4-supplemented and control mice treated with insulin at the end of the experiment, reached the same level of Akt activation ($pSer^{473}$-Akt levels). Therefore, our results suggest that high insulin levels *per se* are responsible for T4-mediated AKT activation.

In this report, we also show that T4 supplementation blunts the onset of T1DM using the RIP-B7.1 model of EAD and increases survival in STZ-induced experimental diabetes in wild-type C57BL/6 mice. Previous research has determined that during the onset of T1DM, beta cell proliferation is increased in an attempt to compensate beta cell loss (Willcox *et al.,* 2010). We observed that, although immune infiltration and the percentage of apoptotic beta cells is similarly augmented in untreated or T4-treated pancreases during the immune attack, beta cell proliferation is remarkably increased in T4-treated RIP-B7.1 mice. This process presumably leads to compensation for beta cell loss, allowing the production and secretion of enough insulin to maintain normoglycaemia. Our experimental design initiated T4 supplementation 2 weeks prior to induction of diabetes mellitus (immunization or STZ treatment), as these research models (EAD and STZ) are very aggressive and a significant percentage of mice die within the first 2 weeks after the induction of diabetes. In order to evaluate a possible therapeutic benefit, experiments aiming to determine whether T4 supplementation after the onset of T1DM could improve glucoregulation would be required. Our results indicate that interventions based on the use of THs or thyromimetics could open novel venues for the treatment of T1DM. Whereas novel treatments including the use of T4 supplementation might not be optimal for the treatment of metabolic diseases due to side effects, certain newly developed thyromimetics could affect specific cell types or organs that could benefit from these actions of THs, resulting in the improvement of metabolic homeostasis, while avoiding side effects (Shoemaker *et al.,* 2012; Coppola *et al.,* 2014; Finan *et al.,* 2016). Although the profound systemic effects of the T4-administration in mice suggest that THs and thyromimetics might be useful in ameliorating the abnormal metabolism in diabetic patients, the identification of the underlying mechanisms that are critical for the observed improvements on glucose control and potential long-term toxic effects must be addressed before results in mice could be extrapolated to humans.

Acknowledgements

We thank Noelia García-Rodriguez, Victor López-Díaz and Leopoldo Perez-Rosendo for their excellent technical assistance. This work was funded by grants from the Ministerio de Economía y Competitividad, Instituto de Salud Carlos III co-funded by Fondos FEdeR (PI13/00593 to B.R.G.) and (CP14/00105 and PI15/00134 to A.M.-M.) from the Instituto de Salud Carlos III co-funded by Instituto de Salud Carlos III and FEdeR. A.M.-M. and B.R.G. are the guarantors of this work and, as such, had full access to all the data in the study and take responsibility for the integrity of the data and the accuracy of the data analysis.

Author contributions

L.L.-N. performed most of the experiments and contributed to data analysis, discussion and writing the manuscript. N.C.-V. designed and supervised the experiments using the RIP-B7.1 mice and STZ-treated mice. A.J.N.-P. and J.L.A.-G. performed Western blots and semi-quantitative RT-PCRs. P.I.L. and J.M.M.-G. assisted in experimentation. J.C.M. contributed to the experimental design and discussions.

B.R.G. and A.M.-M. designed and supervised the study, secured funding, analysed the data and wrote the manuscript. All authors discussed the results and commented on the manuscript.

Conflict of interest

The authors declare no conflicts of interest.

Declaration of transparency and scientific rigour

This Declaration acknowledges that this paper adheres to the principles for transparent reporting and scientific rigour of preclinical research recommended by funding agencies, publishers and other organisations engaged with supporting research.

References

Aguayo-Mazzucato C, Zavacki AM, Marinelarena A, Hollister-Lock J, El Khattabi I, Marsili A *et al*. (2013). Thyroid hormone promotes postnatal rat pancreatic beta-cell development and glucose-responsive insulin secretion through MAFA. Diabetes 62: 1569–1580. https://doi.org/10.2337/db12-0849.

Aiello V, Moreno-Asso A, Servitja JM, Martin M (2014). Thyroid hormones promote endocrine differentiation at expenses of exocrine tissue. Exp Cell Res 322: 236–248. https://doi.org/10.1016/j.yexcr.2014.01.030.

Alexander SPH, Cidlowski JA, Kelly E, Marrion N, Peters JA, Benson HE *et al*. (2015a). The Concise Guide to PHARMACOLOGY 2015/16: Nuclear hormone receptors. Br J Pharmacol 172: 5956–5978.

Alexander SPH, Fabbro D, Kelly E, Marrion N, Peters JA, Benson HE *et al*. (2015b). The Concise Guide to PHARMACOLOGY 2015/16: Enzymes. Br J Pharmacol 172: 6024–6109.

Bahn RS, Burch HB, Cooper DS, Garber JR, Greenlee MC, Klein I *et al*. (2011). Hyperthyroidism and other causes of thyrotoxicosis: management guidelines of the American Thyroid Association and American Association of Clinical Endocrinologists. Endocr Pract 17: 456–520. https://doi.org/10.4158/EP.17.3.456.

Ball SG, Sokolov J, Chin WW (1997). 3,5-Diiodo-L-thyronine (T2) has selective thyromimetic effects in vivo and in vitro. J Mol Endocrinol 19: 137–147. https://doi.org/10.1677/jme.0.0190137.

Bello RI, Alcain FJ, Gomez-Diaz C, Lopez-Lluch G, Navas P, Villalba JM (2003). Hydrogen peroxide- and cell-density-regulated expression of NADH-cytochrome b5 reductase in HeLa cells. J Bioenerg Biomembr 35: 169–179. https://doi.org/10.1023/A:1023702321148.

Buras A, Battle L, Landers E, Nguyen T, Vasudevan N (2014). Thyroid hormones regulate anxiety in the male mouse. Horm Behav 65: 88–96. https://doi.org/10.1016/j.yhbeh.2013.11.008.

Coppola M, Glinni D, Moreno M, Cioffi F, Silvestri E, Goglia F (2014). Thyroid hormone analogues and derivatives: actions in fatty liver. World J Hepatol 6: 114–129. https://doi.org/10.4254/wjh.v6.i3.114.

Curtis MJ, Bond RA, Spina D, Ahluwalia A, Alexander SP, Giembycz MA *et al*. (2015). Experimental design and analysis and their reporting: new guidance for publication in BJP. Br J Pharmacol 172: 3461–3471. https://doi.org/10.1111/bph.12856.

Dimitriadis GD, Raptis SA (2001). Thyroid hormone excess and glucose intolerance. Exp Clin Endocrinol Diabetes 109 (Suppl 2): S225–S239. https://doi.org/10.1055/s-2001-18584.

Dong H, Paquette M, Williams A, Zoeller RT, Wade M, Yauk C (2010). Thyroid hormone may regulate mRNA abundance in liver by acting on microRNAs. PLoS One 5: e12136. https://doi.org/10.1371/journal.pone.0012136.

Dong H, Yauk CL, Rowan-Carroll A, You SH, Zoeller RT, Lambert I *et al*. (2009). Identification of thyroid hormone receptor binding sites and target genes using ChIP-on-chip in developing mouse cerebellum. PLoS One 4: e4610. https://doi.org/10.1371/journal.pone.0004610.

Finan B, Clemmensen C, Zhu Z, Stemmer K, Gauthier K, Muller L *et al*. (2016). Chemical hybridization of glucagon and thyroid hormone optimizes therapeutic impact for metabolic disease. Cell 167: 843–857 e14. https://doi.org/10.1016/j.cell.2016.09.014.

Garmendia Madariaga A, Santos Palacios S, Guillen-Grima F, Galofre JC (2014). The incidence and prevalence of thyroid dysfunction in Europe: a meta-analysis. J Clin Endocrinol Metab 99: 923–931. https://doi.org/10.1210/jc.2013-2409.

Goglia F (2014). The effects of 3,5-diiodothyronine on energy balance. Front Physiol 5: 528. https://doi.org/10.3389/fphys.2014.00528.

Harlan DM, Hengartner H, Huang ML, Kang YH, Abe R, Moreadith RW*et al*. (1994). Mice expressing both B7-1 and viral glycoprotein on pancreatic beta cells along with glycoprotein-specific transgenic T cells develop diabetes due to a breakdown of T-lymphocyte unresponsiveness. Proc Natl Acad Sci U S A 91: 3137–3141.

Iwen KA, Schroder E, Brabant G (2013). Thyroid hormones and the metabolic syndrome. Eur Thyroid J 2: 83–92. https://doi.org/10.1159/000351249.

Jimenez-Moreno CM, Herrera-Gomez IG, Lopez-Noriega L, Lorenzo PI, Cobo-Vuilleumier N, Fuente-Martin E *et al*. (2015). A simple high efficiency intra-islet transduction protocol using lentiviral vectors. Curr Gene Ther 15: 436–446. https://doi.org/10.2174/1566523215666150630121557.

Johannsen DL, Galgani JE, Johannsen NM, Zhang Z, Covington JD, Ravussin E (2012). Effect of short-term thyroxine administration on energy metabolism and mitochondrial efficiency in humans. PLoS One 7: e40837. https://doi.org/10.1371/journal.pone.0040837.

Kassem S, Bhandari S, Rodriguez-Bada P, Motaghedi R, Heyman M, Garcia-Gimeno MA *et al*. (2010). Large islets, beta-cell proliferation, and a glucokinase mutation. N Engl J Med 362: 1348–1350. https://doi.org/10.1056/NEJMc0909845.

Kassem SA, Ariel I, Thornton PS, Scheimberg I, Glaser B (2000). Beta-cell proliferation and apoptosis in the developing normal human pancreas and in hyperinsulinism of infancy. Diabetes 49: 1325–1333. https://doi.org/10.2337/diabetes.49.8.1325.

Kikuchi O, Kobayashi M, Amano K, Sasaki T, Kitazumi T, Kim HJ *et al*. (2012). FoxO1 gain of function in the pancreas causes glucose intolerance, polycystic pancreas, and islet hypervascularization. PLoS One 7: e32249. https://doi.org/10.1371/journal.pone.0032249.

Kilkenny C, Browne W, Cuthill IC, Emerson M, Altman DG (2010). Animal research: reporting *in vivo* experiments: the ARRIVE guidelines. Br J Pharmacol 160: 1577–1579.

Klieverik LP, Sauerwein HP, Ackermans MT, Boelen A, Kalsbeek A, Fliers E (2008). Effects of thyrotoxicosis and selective hepatic

autonomic denervation on hepatic glucose metabolism in rats. Am J Physiol Endocrinol Metab 294: E513–E520.

de Lange P, Cioffi F, Senese R, Moreno M, Lombardi A, Silvestri E *et al*. (2011). Nonthyrotoxic prevention of diet-induced insulin resistance by 3,5-diiodo-L-thyronine in rats. Diabetes 60: 2730–2739. https://doi.org/10.2337/db11-0207.

Lanni A, Moreno M, Lombardi A, Goglia F (2003). Thyroid hormone and uncoupling proteins. FEBS Lett 543: 5–10. https://doi.org/10.1016/S0014-5793(03)00320-X.

Levy JC, Matthews DR, Hermans MP (1998). Correct homeostasis model assessment (HOMA) evaluation uses the computer program. Diabetes Care 21: 2191–2192. https://doi.org/10.2337/diacare.21.12.2191.

Lin Y, Sun Z (2011). Thyroid hormone potentiates insulin signaling and attenuates hyperglycemia and insulin resistance in a mouse model of type 2 diabetes. Br J Pharmacol 162: 597–610. https://doi.org/10.1111/j.1476-5381.2010.01056.x.

Martin-Montalvo A, Mercken EM, Mitchell SJ, Palacios HH, Mote PL, Scheibye-Knudsen M *et al*. (2013). Metformin improves healthspan and lifespan in mice. Nat Commun 4: 2192. https://doi.org/10.1038/ncomms3192.

Mastracci TL, Evans-Molina C (2014). Pancreatic and islet development and function: the role of thyroid hormone. J Endocrinol Diabetes Obes 2: 1014.

Matsuoka TA, Artner I, Henderson E, Means A, Sander M, Stein R (2004). The MafA transcription factor appears to be responsible for tissue-specific expression of insulin. Proc Natl Acad Sci U S A 101: 2930–2933.

McGrath JC, Lilley E (2015). Implementing guidelines on reporting research using animals (ARRIVE etc.): new requirements for publication in BJP. Br J Pharmacol 172: 3189–3193.

Mellado-Gil JM, Jimenez-Moreno CM, Martin-Montalvo A, Alvarez-Mercado AI, Fuente-Martin E, Cobo-Vuilleumier N *et al*. (2016). PAX4 preserves endoplasmic reticulum integrity preventing beta cell degeneration in a mouse model of type 1 diabetes mellitus. Diabetologia 59: 755–765. https://doi.org/10.1007/s00125-016-3864-0.

Misiti S, Anastasi E, Sciacchitano S, Verga Falzacappa C, Panacchia L, Bucci B *et al*. (2005). 3,5,3′-Triiodo-L-thyronine enhances the differentiation of a human pancreatic duct cell line (hPANC-1) towards a beta-cell-Like phenotype. J Cell Physiol 204: 286–296. https://doi.org/10.1002/jcp.20293.

Mitchell SJ, Martin-Montalvo A, Mercken EM, Palacios HH, Ward TM, Abulwerdi G *et al*. (2014). The SIRT1 activator SRT1720 extends lifespan and improves health of mice fed a standard diet. Cell Rep 6: 836–843. https://doi.org/10.1016/j.celrep.2014.01.031.

Moreno M, Silvestri E, De Matteis R, de Lange P, Lombardi A, Glinni D *et al*. (2011). 3,5-Diiodo-L-thyronine prevents high-fat-diet-induced insulin resistance in rat skeletal muscle through metabolic and structural adaptations. FASEB J 25: 3312–3324. https://doi.org/10.1096/fj.11-181982.

Mysliwiec J, Zbucki R, Nikolajuk A, Mysliwiec P, Kaminski K, Bondyra Z *et al*. (2011). Estrogens modulate RANKL-RANK/osteoprotegerin mediated interleukin-6 effect on thyrotoxicosis-related bone turnover in mice. Horm Metab Res 43: 236–240. https://doi.org/10.1055/s-0031-1271776.

Obregon MJ (2008). Thyroid hormone and adipocyte differentiation. Thyroid 18: 185–195. https://doi.org/10.1089/thy.2007.0254.

Olbrot M, Rud J, Moss LG, Sharma A (2002). Identification of beta-cell-specific insulin gene transcription factor RIPE3b1 as mammalian MafA. Proc Natl Acad Sci U S A 99: 6737–6742.

Pagliuca FW, Millman JR, Gurtler M, Segel M, Van Dervort A, Ryu JH *et al*. (2014). Generation of functional human pancreatic beta cells in vitro. Cell 159: 428–439. https://doi.org/10.1016/j.cell.2014.09.040.

Ramadan W, Marsili A, Larsen PR, Zavacki AM, Silva JE (2011). Type-2 iodothyronine 5'deiodinase (D2) in skeletal muscle of C57Bl/6 mice. II. Evidence for a role of D2 in the hypermetabolism of thyroid hormone receptor alpha-deficient mice. Endocrinology 152: 3093–3102. https://doi.org/10.1210/en.2011-0139.

Rezania A, Bruin JE, Arora P, Rubin A, Batushansky I, Asadi A *et al*. (2014). Reversal of diabetes with insulin-producing cells derived in vitro from human pluripotent stem cells. Nat Biotechnol 32: 1121–1133. https://doi.org/10.1038/nbt.3033.

Senese R, Cioffi F, de Lange P, Goglia F, Lanni A (2014). Thyroid: biological actions of 'nonclassical' thyroid hormones. J Endocrinol 221: R1–12. https://doi.org/10.1530/JOE-13-0573.

Shang G, Gao P, Zhao Z, Chen Q, Jiang T, Zhang N *et al*. (2013). 3,5-Diiodo-l-thyronine ameliorates diabetic nephropathy in STZ-induced diabetic rats. Biochim Biophys Acta 1832: 674–684.

Shoemaker TJ, Kono T, Mariash CN, Evans-Molina C (2012). Thyroid hormone analogues for the treatment of metabolic disorders: new potential for unmet clinical needs? Endocr Pract 18: 954–964. https://doi.org/10.4158/EP12086.RA.

Sirakov M, Skah S, Nadjar J, Plateroti M (2013). Thyroid hormone's action on progenitor/stem cell biology: new challenge for a classic hormone? Biochim Biophys Acta 1830: 3917–3927.

Southan C, Sharman JL, Benson HE, Faccenda E, Pawson AJ, Alexander SPH *et al*. (2016). The IUPHAR/BPS guide to PHARMACOLOGY in 2016: towards curated quantitative interactions between 1300 protein targets and 6000 ligands. Nucl Acids Res 44: D1054–D1068. https://doi.org/10.1093/nar/gkv1037.

Spencer PS, West GB (1961). Sensitivity of the hyperthyroid and hypothyroid mouse to histamine and 5-hydroxytryptamine. Br J Pharmacol Chemother 17: 137–143. https://doi.org/10.1111/j.1476-5381.1961.tb01114.x.

Vargas-Uricoechea H, Bonelo-Perdomo A, Sierra-Torres CH (2014). Effects of thyroid hormones on the heart. Clin Investig Arterioscler 26: 296–309. https://doi.org/10.1016/j.arteri.2014.07.003.

Verga Falzacappa C, Mangialardo C, Madaro L, Ranieri D, Lupoi L, Stigliano A *et al*. (2011). Thyroid hormone T3 counteracts STZ induced diabetes in mouse. PLoS One 6: e19839. https://doi.org/10.1371/journal.pone.0019839.

Verga Falzacappa C, Patriarca V, Bucci B, Mangialardo C, Michienzi S, Moriggi G *et al*. (2009). The TRbeta1 is essential in mediating T3 action on Akt pathway in human pancreatic insulinoma cells. J Cell Biochem 106: 835–848. https://doi.org/10.1002/jcb.22045.

Vicinanza R, Coppotelli G, Malacrino C, Nardo T, Buchetti B, Lenti L *et al*. (2013). Oxidized low-density lipoproteins impair endothelial function by inhibiting non-genomic action of thyroid hormone-mediated nitric oxide production in human endothelial cells. Thyroid 23: 231–238. https://doi.org/10.1089/thy.2011.0524.

Weinhaus AJ, Stout LE, Bhagroo NV, Brelje TC, Sorenson RL (2007). Regulation of glucokinase in pancreatic islets by prolactin: a mechanism for increasing glucose-stimulated insulin secretion during pregnancy. J Endocrinol 193: 367–381. https://doi.org/10.1677/JOE-07-0043.

Weinstein SP, O'boyle E, Haber RS (1994). Thyroid hormone increases basal and insulin-stimulated glucose transport in skeletal muscle. The role of GLUT4 glucose transporter expression. Diabetes 43: 1185–1189. https://doi.org/10.2337/diab.43.10.1185.

Weinstein SP, Watts J, Haber RS (1991). Thyroid hormone increases muscle/fat glucose transporter gene expression in rat skeletal muscle. Endocrinology 129: 455–464. https://doi.org/10.1210/endo-129-1-455.

Willcox A, Richardson SJ, Bone AJ, Foulis AK, Morgan NG (2010). Evidence of increased islet cell proliferation in patients with recent-onset type 1 diabetes. Diabetologia 53: 2020–2028. https://doi.org/10.1007/s00125-010-1817-6.

Wistuba J, Mittag J, Luetjens CM, Cooper TG, Yeung CH, Nieschlag E *et al*. (2007). Male congenital hypothyroid Pax8−/− mice are infertile despite adequate treatment with thyroid hormone. J Endocrinol 192: 99–109. https://doi.org/10.1677/JOE-06-0054.

Supporting Information

Additional Supporting Information may be found online in the supporting information tab for this article.

https://doi.org/10.1111/bph.13975

Figure S1 Glucose levels in metabolic test expressed as percentage of basal glucose. (A) Circulating T4 levels in fed conditions. Age = 13 weeks. n = 7 untreated; n = 8 T4-treated. (B) Glucose concentration in blood during the OGTT expressed as the percentage of basal (time 0) glucose. n = 13 per group. (C) Glucose concentration in blood during the IPPTT expressed as the percentage of basal glucose. n = 7 untreated; n = 8 T4-treated. (D) Glucose concentration in blood during the ITT expressed as the percentage of basal glucose. n = 12 untreated; n = 13 T4-treated. (E) Glucose concentration in blood during a 24-hour fasting period expressed as the percentage of basal glucose. n = 7 untreated; n = 8 T4-treated. (F) Homeostatic assessment of insulin resistance (HOMA-IR) index. Age = 12 weeks. n = 7 untreated; n = 8 T4-treated. UT: Untreated; T4: T4-treated. Data are represented as the mean ± SEM. * $P < 0.05$ significantly different from untreated mice. A two tailed t-test was applied to panels A and F. A Mann–Whitney Rank Sum test was applied to panels B-E.

Figure S2 Energy intake and histology of the thyroid and the pituitary of in T4-treated mice. (A) Energy intake divided by body weight. n = 7 untreated; n = 8 T4-treated. (B) Representative images of the histological analysis o the thyroid and pituitary of T4-treated and untreated mice. Thyroid; n = 6 untreated; n = 7 T4-treated. Pituitary; n = 5 untreated; n = 6 T4-treated. (C) Determination of the α-GSU of pituitary hormones in the serum of T4-treated and untreated mice. n = 7 untreated; n = 8 T4-treated. UT: Untreated; T4: T4-treated. Data are represented as the mean ± SEM. * $P < 0.05$ significantly different from untreated mice (two tailed t-test).

Figure S3 The subcellular localization of MAFA and FOXO1 is not affected by T4 supplementation. (A) Pancreatic islets were isolated from animals treated or not with T4. Determination of messenger RNA (mRNA) levels of genes involved in pancreatic islet metabolism. Values were normalized to islets isolated from untreated mice. n = 6 untreated; n = 5 T4-treated. (B) Representative images of MAFA and insulin (INS) immunofluorescence staining in pancreases from mice treated or not with T4. Scale bar = 50 μm. n = 5 per group. (C) Representative images of FOXO1 and INS immunofluorescence staining in pancreases from mice treated or not with T4. Scale bar = 50 μm. n = 5 per group. UT: 2 Untreated; T3: T3-treated; T4: T4-treated. Data are represented as the mean ± SEM. * $P < 0.05$ significantly different from untreated mice (two tailed t-test).

Figure S4 T4 induces a starvation-like state in the skeletal muscle. (A) Western blots indicating activation of AKT in the skeletal muscle and the liver of T4-treated mice. Mice were fasted for 16 hours and then injected with insulin (0.75 UI.kg-1 of body weight) 15 minutes before the end of the experiment. n = 5 untreated; n = 6 T4-treated. (B) Determination of mRNA levels of genes involved in energy metabolism in the skeletal muscle of mice treated or not with T4. Values were normalized to untreated mice. GLUT2; n = 5 untreated, n = 6 T4-treated. GK; n = 5 untreated, n = 6 T4-treated. G6Pase; n = 5 untreated, n = 6 T4-treated. LPK; n = 5 untreated, n = 6 T4-treated. PEPCK; n = 5 untreated, n = 6 T4-treated. GAPDH; n = 6. LDH; n = 5 untreated, n = 6 T4-treated. PGC1α; n = 6. PGC1β; n = 6. UCP2; n = 5. SREBP1c; n = 5 untreated, n = 6 T4-treated. (C) Determination of mRNA levels of genes involved in energy metabolism in the liver of mice treated or not with T4. Values were normalized to untreated mice. GLUT2; n = 5 untreated, n = 6 T4-treated. GK; n = 5. G6Pase; n = 5 untreated, n = 6 T4-treated. LPK; n = 5 untreated, n = 6 T4-treated. PEPCK; n = 5 untreated, n = 6 T4-treated. GAPDH; n = 6 untreated, n = 5 T4-treated. LDH; n = 5. PGC1α; n = 5 untreated, n = 6 T4-treated. PGC1β; n = 6. UCP2; n = 6 untreated, n = 5 T4-treated. SREBP1c; n = 6 untreated, n = 5 T4-treated. (D) Western blots indicating activation of AMPK in the skeletal muscle and the liver of T4-treated mice. Mice were fasted for 16 hours prior euthanization. n = 5 per group. (E) Densitometric analysis of the western blots using skeletal muscle extracts shown in Supporting Information Figure S4D. Values were normalized to untreated mice. (F) Densitometric analysis of the western blots using liver extracts shown in Supporting Information Figure S4D. Values were normalized to untreated mice. UT: Untreated; T4: T4-treated. Data are represented as the mean ± SEM. * $P < 0.05$ significantly different from untreated mice (two tailed t-test).

Figure S5 T4 supplementation increased circulating T4, alters organs weight and modulates insulin signalling in immunized RIP-B7.1 mice. (A) Circulating T4 levels in fed conditions. n = 9 untreated; n = 8 T4-treated. (B) Organs weight divided by body weight. n = 6 untreated; n = 9 T4-treated. (C) Western blots showing the amount of phosphotyrosine 632 IRS1, total IRS1 and GAPDH, used as loading control, in the skeletal muscle and the liver of T4-treated mice. Skeletal muscle n = 6 untreated, n = 5 T4-treated. Liver n = 6 per group. (D) Densitometric analysis of the western blots using skeletal muscle extracts shown in Supporting 3 Information Figure S5C. Values were normalized to untreated mice. (E) Densitometric analysis of the western blots using liver extracts shown in Supporting Information Figure S5C. Values were normalized to untreated mice. UT: Untreated; T4: T4-treated. Data are represented as the mean ± SEM. * $P < 0.05$ significantly different from untreated mice (two tailed t-test).

Figure S6 T4-treated and untreated immunized RIP-B7.1 mice show similar degree of insulitis. (A) Representative images of immune infiltrations in T4-treated and untreated immunized RIP-B7.1 mice. (B) Insulitis was scored as grade 0–4 according to the percentage of infiltrated islet area (0: 0%; 1: <10%; 2: >10% and <55%; 3: >55% and <75%; 4: >75%). Scale bar = 50 μm. n = 5 per group. UT: Untreated; T4: T4-treated. Data are represented as the mean ± SEM. * $P < 0.05$ significantly different from untreated mice (two tailed t-test).
Table S1 Antibodies used in this study.
Table S2 Primer pair sequences used for quantitative RT-PCR analysis.

Mellado-Gil et al. *Cell Death and Disease* (2018)9:279
DOI 10.1038/s41419-018-0272-z

Cell Death & Disease

ARTICLE Open Access

The type 2 diabetes-associated HMG20A gene is mandatory for islet beta cell functional maturity

Jose M. Mellado-Gil[1], Esther Fuente-Martín[1], Petra I. Lorenzo[1], Nadia Cobo-Vuilleumier[1], Livia López-Noriega[1], Alejandro Martín-Montalvo[1], Irene de Gracia Herrera Gómez[1], Maria Ceballos-Chávez[2], Laura Gómez-Jaramillo[3], Antonio Campos-Caro[3], Silvana Y. Romero-Zerbo[4], Júlia Rodríguez-Comas[5], Joan-Marc Servitja[5,6], Gemma Rojo-Martinez[4,6], Abdelkrim Hmadcha[1,6], Bernat Soria[1,6], Marco Bugliani[7], Piero Marchetti[7], Francisco J. Bérmudez-Silva[4,6], Jose C. Reyes[2], Manuel Aguilar-Diosdado[3,8] and Benoit R. Gauthier[1]

Abstract

HMG20A (also known as iBRAF) is a chromatin factor involved in neuronal differentiation and maturation. Recently small nucleotide polymorphisms (SNPs) in the *HMG20A* gene have been linked to type 2 diabetes mellitus (T2DM) yet neither expression nor function of this T2DM candidate gene in islets is known. Herein we demonstrate that *HMG20A* is expressed in both human and mouse islets and that levels are decreased in islets of T2DM donors as compared to islets from non-diabetic donors. In vitro studies in mouse and human islets demonstrated that glucose transiently increased *HMG20A* transcript levels, a result also observed in islets of gestating mice. In contrast, HMG20A expression was not altered in islets from diet-induced obese and pre-diabetic mice. The T2DM-associated rs7119 SNP, located in the 3′ UTR of the *HMG20A* transcript reduced the luciferase activity of a reporter construct in the human beta 1.1E7 cell line. Depletion of *Hmg20a* in the rat INS-1E cell line resulted in decreased expression levels of its neuronal target gene *NeuroD* whereas *Rest* and *Pax4* were increased. Chromatin immunoprecipitation confirmed the interaction of HMG20A with the *Pax4* gene promoter. Expression levels of *Mafa*, *Glucokinase*, and *Insulin* were also inhibited. Furthermore, glucose-induced insulin secretion was blunted in HMG20A-depleted islets. In summary, our data demonstrate that HMG20A expression in islet is essential for metabolism-insulin secretion coupling via the coordinated regulation of key islet-enriched genes such as *NeuroD* and *Mafa* and that depletion induces expression of genes such as *Pax4* and *Rest* implicated in beta cell de-differentiation. More importantly we assign to the T2DM-linked rs7119 SNP the functional consequence of reducing *HMG20A* expression likely translating to impaired beta cell mature function.

Introduction

Type 2 Diabetes Mellitus (T2DM) is a metabolic disease characterized by impaired insulin secretion and/or action in target organs that leads to elevations in blood glucose levels. Environmental factors as well as strong genetic components contribute to the pathogenesis of T2DM. Thus far, 100–120 susceptibility loci have been associated to T2DM by Genome Wide Association Studies (GWAS)[1–3]. Although functional defects remain to be

Correspondence: Benoit R Gauthier (benoit.gauthier@cabimer.es)
[1]Department of Cell Regeneration and Advanced Therapies, Andalusian Center of Molecular Biology and Regenerative Medicine-CABIMER, Junta de Andalucia-University of Pablo de Olavide-University of Seville-CSIC, Seville, Spain
[2]Department of Genome Biology, Andalusian Center of Molecular Biology and Regenerative Medicine (CABIMER) JA-CSIC-UPO-US, Seville, Spain
Full list of author information is available at the end of the article
These authors contributed equally: Jose M. Mellado-Gil, Esther Fuente-Martín.
Edited by M. Agostini

SPRINGER NATURE CDDpress

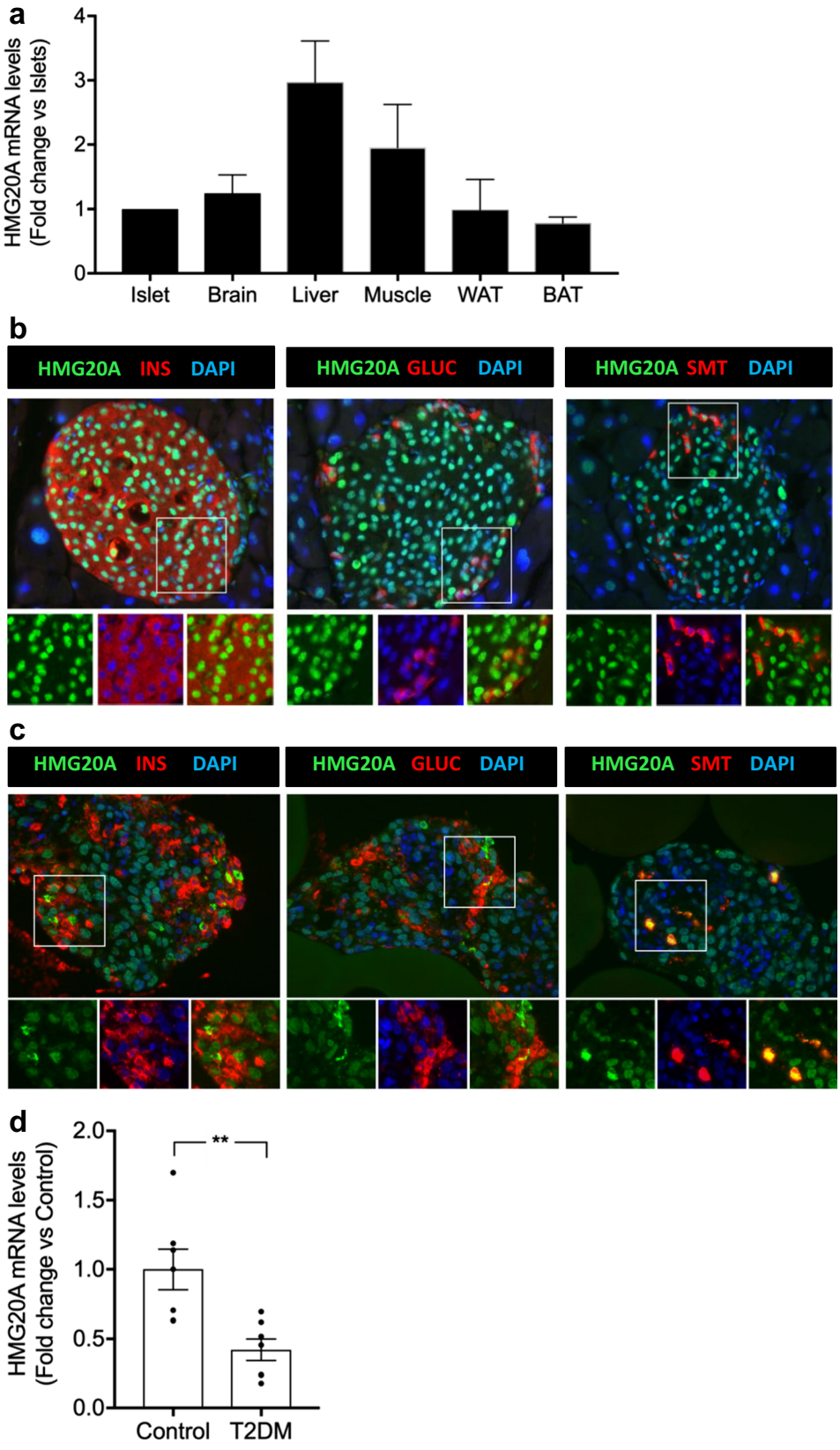

Fig. 1 (See legend on next page.)

(see figure on previous page)
Fig. 1 HMG20A is expressed in both mouse and human islets and is decreased in islets from T2DM donors. a HMG20A transcript levels were assessed by qPCR in islets, brain, liver, muscle, white adipose tissue (WAT), and brown adipose tissue (BAT) from mice ($n = 6$). Representative images of **b** mouse and **c** human islets co-stained for HMG20A (green) along with INSULIN (INS), GLUCAGON (GLUC) or SOMATOSTATIN (SMT) (red). Nuclei are stained using DAPI (blue). Magnification 40×. White boxes define areas enlarged in panels bellow. **d** *HMG20A* mRNA levels were measured by qPCR in human islets isolated from normoglycemic (control) or type 2 diabetic (T2DM) organ donors ($n = 7$). Data are depicted as dot plots with means ± S.E.M. p values were determined using unpaired two-tailed Student's t-test. $^{**}p < 0.01$

assigned, many of these loci point to primary defects in beta cell function rather than to insulin resistance[4]. In this context, several SNPs within the *HGM20A* gene (also known as *iBRAF*) have been associated to T2DM[5–8]. Of particular interest is the rs7119 SNP located within the 3′ UTR of the *HMG20A* transcript. In silico analysis revealed that rs7119 modifies a functional microRNA (miRNA) cis-regulatory element[9]. However, the molecular consequences of this SNP on the expression of *HMG20A* and/or its regulation and impact on islet physiology are still unknown.

HMG20A is a member of the high mobility group (HMG) box-containing genes that binds to chromatin and exerts global genomic changes through establishing active or silent chromatin[10]. HMG20A is highly expressed in mature neurons and plays a key role in promoting neuronal differentiation during development[11]. In this context, HMG20A relieves the transcriptional repression imposed by the complex LSD1–CoREST histone demethylase[12], which function is to silence neuronal genes in non-neuronal tissues through its interaction with the transcription factor REST. In analogy, epigenetic repression of the *Rest* gene in pancreatic precursors was shown to coincide with the activation of the core beta cell program[13]. Mature pancreatic beta cells do not express REST while forced expression results in inhibition of neuronal proteins of the insulin exocytotic machinery such as SNAP25 and SYNAPTOTAGMIN VII (SYT7) leading to impaired glucose-induced insulin secretion[14]. Interestingly, REST was shown to repress expression of key beta cell development genes, such as *NEUROD* and *PAX4*[15,16]. *NEUROD* is a bona fide target gene of HMG20A in neuronal cells[11] and mutations in this gene predispose individuals to maturity onset diabetes of the young 6 (MODY6)[17].

HMG20A is also implicated in epithelial-to-mesenchymal transition (EMT) through interaction with specific key regulators of this process such as SNAIL[18]. EMT is an example of cell plasticity and a key process during embryonic development, and together with the reverse transformation, the mesenchymal-to-epithelial transition (MET), are required for the formation of organs in the final destinations of embryonic migratory cells[19,20]. Both processes occur during pancreatic and islet development and require extensive reorganization of the epigenetic information of the cells. Remarkably, not only in development but also in response to different physiological demands, beta cells may de-differentiate in order to acquire plasticity capabilities and increase survival[21,22], two processes that may implicate PAX4[23,24].

Based on these findings, we hypothesized that HMG20A may contribute to the regulation of key genes such as *NeuroD* and *Pax4* which are essential for beta cell functional maturity as well as survival. Towards this goal, herein we investigate the expression profile and the gene regulatory function of HMG20A in pancreatic islets, as well as determine whether the SNP rs7119 associated with T2DM impacts HMG20A expression. We report that T2DM-associated SNP rs7119 leads to altered HMG20A expression, and that HMG20A regulates metabolism-secretion coupling genes as well as functional maturity of beta cells.

Results

HMG20A is expressed in pancreatic islets and transcript levels are decreased in islets from T2DM donors

As a first step to assign a potential role of the *HMG20A* gene in pancreatic islet physiology, we determined its transcript levels in islets as compared to other tissues. Mouse pancreatic islets displayed comparable expression levels of *Hmg20a* to other organs such as adipose tissue (white and brown), brain and muscle whereas the liver displayed highest levels (Fig. 1a). HMG20A co-stained with INSULIN (beta cells), GLUCAGON (alpha cells) and SOMATOSTATIN (delta cells) whereas its expression was rarely detected in exocrine pancreas (Fig. 1b). A similar endocrine cell expression pattern was detected in human islets (Fig. 1c). We next assessed whether expression levels of *HMG20A* were altered in islets isolated from T2DM donors. The rational was to establish a correlation between *HMG20A* levels and the hyperglycemic environment that may be altered by T2DM-linked SNPs. *HMG20A* transcript levels were decreased by ~60 % in islets from T2DM patients as compared to islets purified from normoglycemic control donors (Fig. 1d).

Metabolic stressors modulate *HMG20A* expression in islets

As *HMG20A* transcript levels were decreased in T2DM islets, we reasoned that lipids and/or glucose might alter its expression. Towards addressing this premise, we used

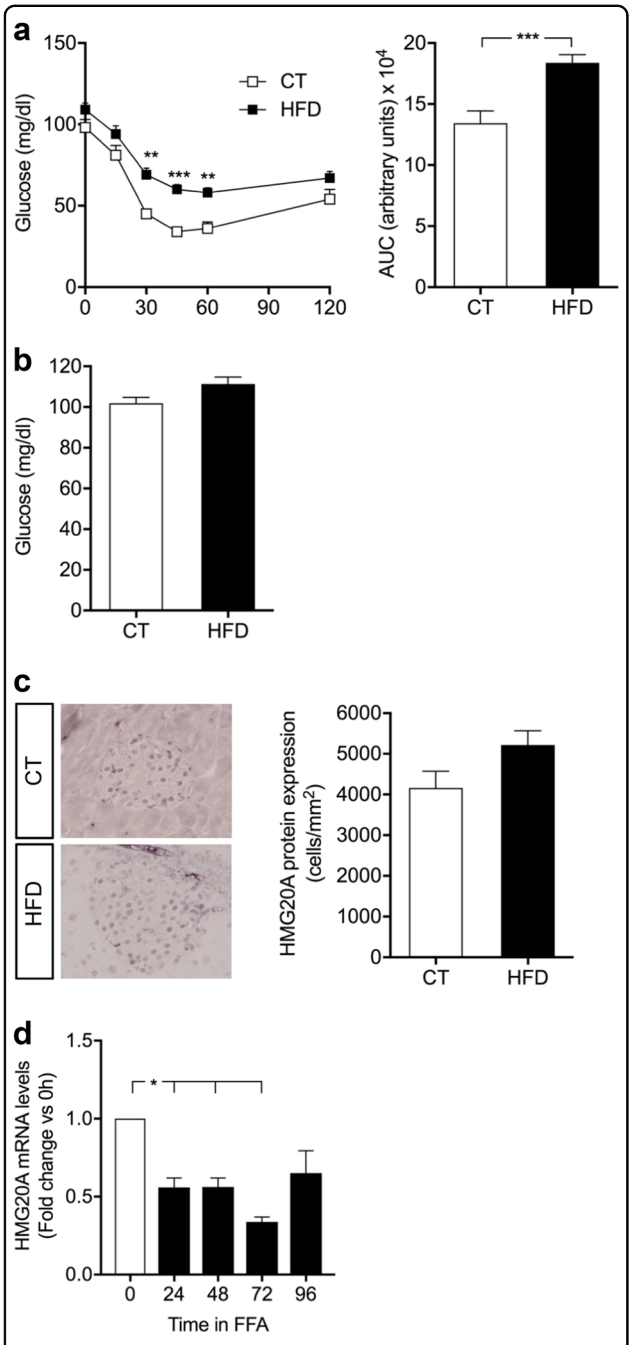

Fig. 2 HMG20A protein expression is not altered in islets of high fat diet (HFD)-induced obesity and pre-diabetic mice. a Insulin tolerance test (ITT) and area under the curve (AUC) analysis in both control (CT) and HFD mice (CT, $n = 10$; HFD, $n = 15$). **b** Fasting blood glucose levels in both control and HFD mice (CT, $n = 10$; HFD, $n = 15$). **c** Representative images of pancreatic sections from HFD and CT mice stained and quantified for HMG20A ($n = 4$). **d** *Hmg20a* mRNA levels were assessed by qPCR in INS-1E cells cultured with 0.05 mM palmitate for 24, 48, 72 or 96 h ($n = 3$ independent experiments performed in triplicates). Data are represented as means + S.E.M. *p* values were determined by ordinary one-way ANOVA. $^{*}p < 0.05$, $^{**}p < 0.01$, $^{***}p < 0.0001$

our mouse model of 45% high fat diet (HFD)-induced obesity and pre-diabetes to assess the contribution of lipids. These mice exhibit a typical 20% increase in body weight, develop glucose intolerance with the concomitant increases in insulin and leptin levels and decreased adiponectin levels[25]. Although these mice developed insulin resistance, glycaemia is normal due to increased insulin levels (Fig. 2a, b). Under these conditions, HMG20A protein levels were not significantly changed in islets as compared to levels in chow-fed control mice (Fig. 2c). In contrast, short-term exposure of INS-1E cells to palmitate resulted in a transient reduction in HMG20A transcript levels (Fig. 2d).

We next assessed the direct action of high glucose on *HMG20A* levels in isolated islets. In human islets, *HMG20A* expression levels were transiently increased by approximately twofold at 72 h returning to basal levels by 96 h (Fig. 3a). A similar transient induction pattern, albeit attaining maximum levels at 48 h, was also observed in mouse islets and in INS-1E beta cells (Fig. 3b,c). Interestingly, a significant decrease was detected INS-1E cells at 72 h of high glucose exposure (Fig. 3c). It is noteworthy that expression levels of *NEUROD*, a bona fide target of HMG20A, mirrored those of *HMG20A* in human islets as well as in INS-1E (Fig. 3d,f), following the same tendency in mouse islets (Fig. 3e). In order to satisfy metabolic demand by fetus and mother, glucose metabolism is altered during pregnancy inducing metabolic stress that, if ill adapted, will lead to gestational diabetes. We therefore pondered whether *Hmg20a* expression levels were modulated during pregnancy. Consistent with this premise, transcript and protein levels of the *Hmg20a* gene were increased reaching a peak of maximum signal at 12.5 and 14.5 days post coitum, respectively, and thereafter declining (Fig. 4a–c). Pregnant females displayed mild glucose intolerance at 14.5 correlating with the peak in HMG20A protein levels (Fig. 4d). Taken together, these data suggest that increased glucose levels both in vitro and in vivo stimulate HMG20A expression.

The rs7119 SNP variant within the 3′ untranslated region (UTR) of human *HMG20A* reduces activity of a luciferase reporter gene

Although GWAS have highlighted a panoply of SNPs correlating with T2DM, few have been assigned a functional consequence to the associated gene. Towards addressing this question, we assessed whether the human *HMG20A* SNPs associated to T2DM may impact HMG20A levels. Of particular interest is the SNP rs7119 located in the 3′ UTR of the *HMG20A* transcript that is encoded in part by exon 10 and the entirety of exon 11 (Fig. 5c). The SNP rs7119 causes a “C” (reference allele “wt”) to “T” (“mut” allele) substitution. In silico analysis of

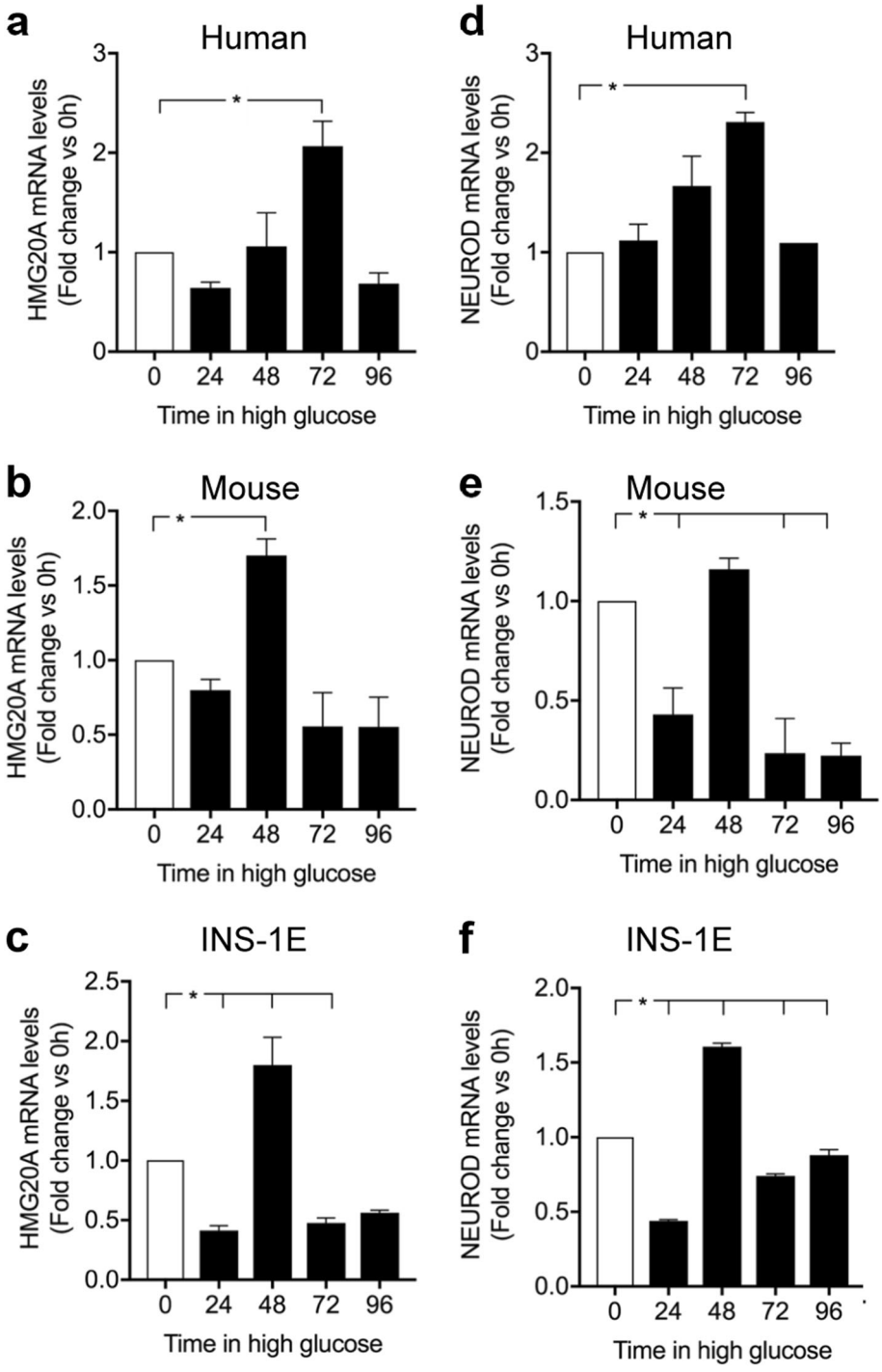

Fig. 3 HMG20A is regulated by glucose. a–c *HMG20A* and **d–f** *NEUROD* mRNA levels were assessed by qPCR in human ($n = 3$ donors performed in triplicates) and mouse islets (three independent preparations of pooled islets from three different isolation) as well as INS-1E cells cultured in 24 mM glucose for 24, 48, 72, or 96 h ($n = 3$ independent experiments of all time points executed in triplicates). Data are represented as means + S.E.M. *p* values were determined by ordinary one-way ANOVA. *$p < 0.05$, compared to the control 0 time point

the *HMG20A* 3′UTR revealed the binding site of a single miRNA (miR-571) to the wt allele whereas the "mut" allele results in the ablation of this miRNA binding site (Table 1). Interestingly expression of miR-571 was not detected in mouse islets as compared to the highly expressed miR375 (data not shown). Notwithstanding, the

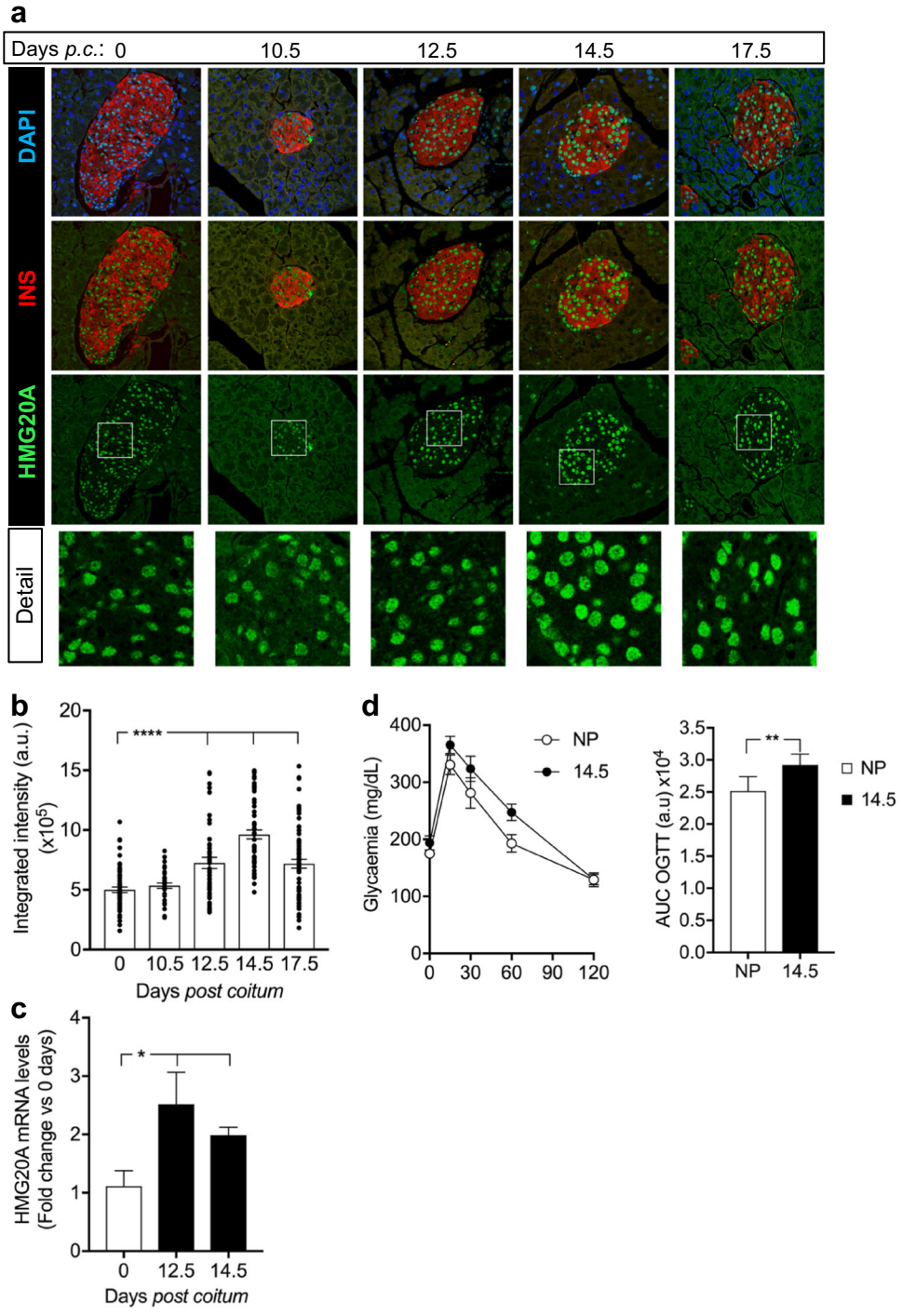

Fig. 4 HMG20A is transiently increased in mouse islets during pregnancy. a Representative images of pancreatic sections from pregnant mice co-stained for HMG20A (green) and INSULIN (INS) (red). Nuclei were stained using DAPI (blue). Magnification 40×. White boxes define areas enlarged in panels below. p.c. post coitum. **b** Quantification of integrated fluorescence intensity for HMG20A in beta cells of islets from pregnant mice ($n = 3$ mice per time point with 35-71 islets counted per time point). Data are depicted as dot plots with means ± S.E.M. **c** HMG20A mRNA levels in islets from pregnant mice ($n = 5$ mice) at 12.5 and 14.5 days of pregnancy. **d** Oral glucose tolerance test (OGTT) and area under the curve (AUC) analysis of non-pregnant (NP) and pregnant (day 14.5 of pregnancy; D14.5) mice (NP, $n = 8$; D14.5, $n = 6$). Data are represented as means ± S.E.M. p values were determined by the unpaired two-tailed Student´s t-test (**d** for AUC and **c**) or ordinary one-way ANOVA with Dunnet's multiple comparison test (**b**). *$p < 0.05$, **$p < 0.01$, ****$p < 0.0001$, compared to the control 0 time point

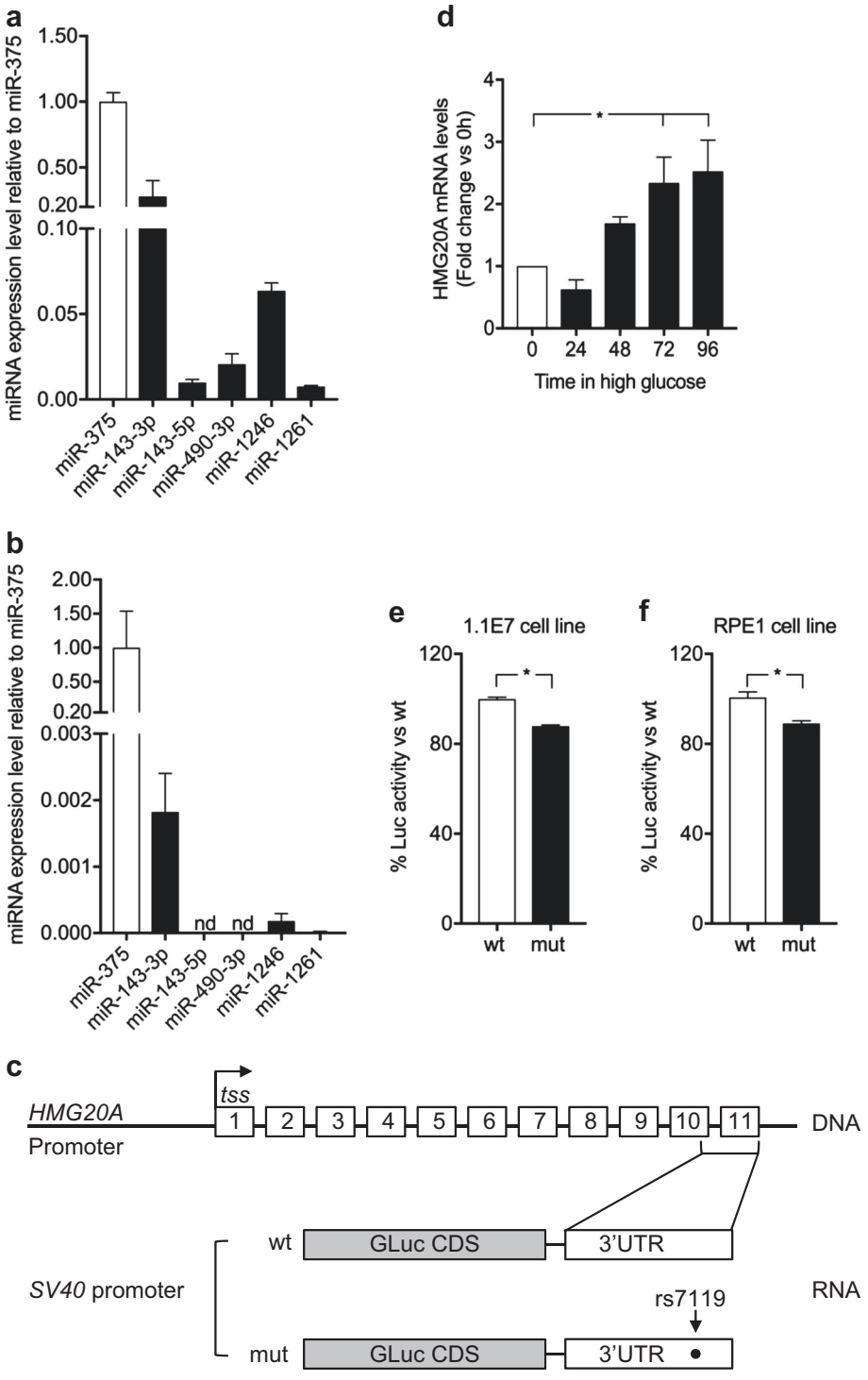

Fig. 5 The rs7119 SNP within the *HMG20A* 3′ UTR decreases protein levels. Expression profile of putative miRNAs binding to the "mut" allele of the HMG20A transcript in **a** human 1.1E7 cells and **b** mouse islets. Data are presented respect to miR375 expression levels. **c** Schematic representation of the *HMG20A* gene depicting the promoter region (*HMG20A* promoter), transcription starting site (tss) and 11 exons. Gaussia luciferase (GLuc) reporter constructs harboring the 3′ UTR corresponding to either wild type (wt) or rs7119 mutant (mut) allele under *pSV40* promoter are shown below. **d** *HMG20A* mRNA levels assessed by qPCR in the human pancreatic beta cell line 1.1E7 cultured in 24 mM glucose for 24, 48, 72, or 96 h ($n = 5$ independent experiments performed in triplicates). **e** Human pancreatic beta 1.1E7 and **f** RPE1 cell lines were transfected with the reporter construct bearing either wt or rs7119 mut variant of the *HMG20*A 3′ UTR. Both the Gaussia Luciferase activity and SEAP activity were determined 24 h post transfection ($n = 3$ independent experiments). Data are represented as means + S.E.M. p values were determined by ordinary one-way ANOVA (**d**) or unpaired Student's t-test (**e**, **f**). *$p < 0.05$

TABLE 1 In silico identification of miRNAs binding sites within the rs7119 SNP located in the 3′UTR of HMG20A

"C" reference alelle	"T" risk allele
(wt)	(mut)
hsa-miR-571	hsa-miR-1261
	hsa-miR-1257
	hsa-miR-1246
	hsa-miR-586
	hsa-miR-490 (5p, 3p)
	hsa-miR-143 (5p, 3p)

"mut" allele generates binding sites for six alternative miRNAs (Table 1) of which four, miR-143 (3p and 5p), miR-490-3p, miR-1246, and miR-1261, were expressed in the human 1.1E7 pancreatic cell line (Fig. 5a). In contrast mouse islets only expressed miR-143 and very low levels of miR-1246 (Fig. 5b). The latter findings suggest that the "mut" variant may alter expression of the *HMG20A* transcript due to the action of those miRNAs. To assess this premise, we generated two Gaussia luciferase (Gluc) reporter constructs harboring either the "wt" or "mut" 3′ UTR of the human *HMG20A* transcript. Expression of these constructs was under the transcriptional regulation of the SV40 basal promoter (Fig. 5c). Transient transfections were then performed in the human pancreatic beta 1.1E7 and retinal pigmented epithelial RPE1 cell lines. The rational of using human cell lines was to maintain species-specific effects targeting the human 3′ UTR of the *HMG20A* transcript, which is distinct than that of the mouse *Hmg20a* transcript. We initially confirmed that glucose also stimulated *HMG20A* expression in 1.1E7 beta cells (Fig. 5d). The "mut" variant displayed significantly less Gluc activity as compared to the construct bearing the "wt" variant 48 h post transfection in either cell lines (Fig. 5e, f). These results suggest that the diabetes-linked SNP rs7119 alters expression of the human *HMG20A*.

HMG20A regulates the expression of beta cell genes involved in metabolism-secretion coupling and beta cell maturity

To determine the specific contribution of HMG20A to islet beta cell function and the impact of its reduced levels in T2DM islets, we silenced *HMG20A* expression by RNA interference and then assessed transcript levels of key factors involved in beta cell identity and function. A 60% depletion of *Hmg20a* in INS-1E cells (Fig. 6a, b) resulted in a concomitant 60% inhibition of *NeuroD* transcript levels (Fig. 6c). *Mafa*, which is essential to maintain the beta cell phenotype, was decreased by 50% whereas *Pdx1* was unaltered. Interestingly, *Pax4* as well as *Rest* were increased by 1.8- and 1.5-fold, respectively, subsequent to *Hmg20a* silencing (Fig. 6c). We previously demonstrated that chronic overexpression of *Pax4* leads to loss of beta cell identity characterized by decreased *Mafa* and *Insulin* expression[23]. We thus, pondered whether HMG20A could directly regulate *Pax4* thereby maintaining its expression within a range that would not interfere with beta cell function. To validate this premise, chromatin immunoprecipitation (ChIP) experiments were performed using the islet specific *Pax4* gene promoter[24]. As expected H3K4me2, a marker for active promoters and enhancers specifically occupied this region (Fig. 6d)[26]. More importantly, HMG20A also occupied the *Pax4* gene promoter region as well as exon 1 while control anti-IgG exhibited no binding (Fig. 6e). Since NEUROD and MAFA are involved in metabolism-secretion coupling in beta cell, genes implicated in this process were assessed after *Hmg20a* silencing. *Glucokinase* (*Gck*) and *Insulin* transcript levels were significantly repressed by 30% (Fig. 6f). In contrast, *Pi3k* and *Glut2* levels were increased 1.8 and 2.6-fold, respectively (Fig. 6f). Transcript levels of *Syt7* and *Snap25*, two factors involved in insulin granule membrane docking and fusion were not altered in *Hmg20a*-repressed INS-1E cells (Fig. 6f). The modulation of key HMG20A target genes was validated using a second independent siHMG20A (Fig. 6g). Taken together our results indicate that HMG20A coordinates expression of genes that will establish the mature beta cell phenotype.

Glucose-stimulated insulin secretion is impaired by *Hmg20a* depletion

We next assess the cellular and functional consequences of *Hmg20a* depletion in beta cells. Neither cell death nor proliferation was altered by HMG20A depletion in INS-1E cells (Fig. 7a, b). In contrast, glucose-stimulated insulin secretion (GSIS) was blunted in these cells (Fig. 7c). Similarly, subsequent to a 40% depletion of *Hmg20a* in mouse islets (Fig. 7d), cell proliferation was unaltered while GSIS was drastically decreased as compared to control islets (Fig. 7e, f). Taken together, *Hmg20a* expression is essential for insulin secretion.

Discussion

The overall aim of the current study was to assign a functional role of the putative diabetes-linked *HMG20A* gene to islet physiology, and determine the pathophysiological consequence of the rs7119 SNP associated with this disease. We find that: (1) *HMG20A* is expressed in pancreatic islet beta cells, (2) HMG20A levels are decreased in T2DM islets, (3) high glucose stimulates HMG20A expression, (4) the T2DM-associated SNP within the 3′ UTR of the HMG20A transcript decreases luciferase activity, (5) HMG20A regulates key genes in beta cell function and maturity, and (6) HMG20A

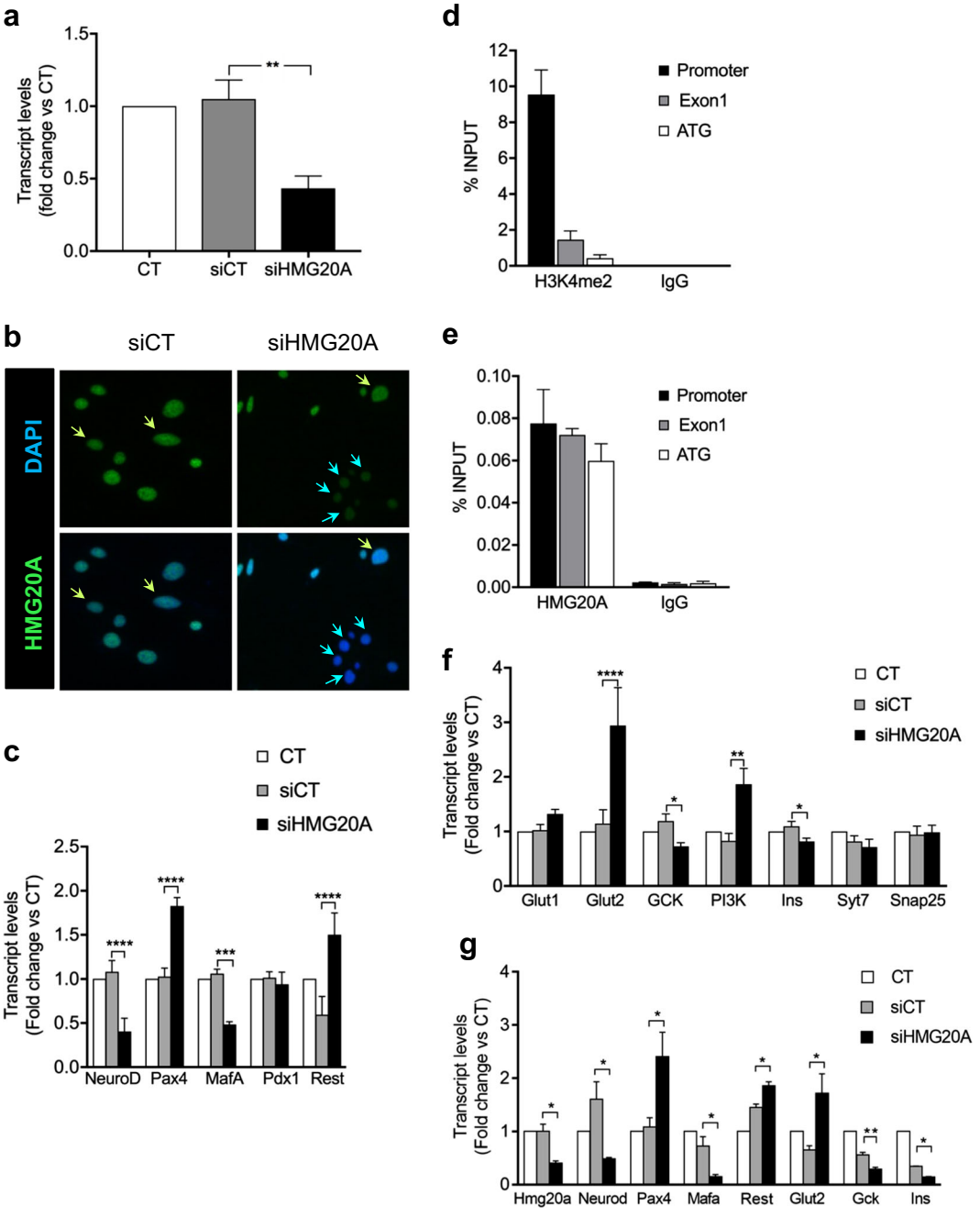

Fig. 6 HMG20A regulates metabolism-secretion coupling genes in INS-1E cells. a *Hmg20a* was silenced by specific siRNA in INS-1E cells ($n = 6$ independent experiments, each performed in triplicates). **b** Representative images of INS-1E cells immuno-stained for HMG20A (green) and DAPI (blue) confirming decreased protein level after treatment with siHMG20A. Magnification 40×. **c** Beta cell development and maturity genes, as *Neurod*, *Pax4*, *Mafa, Pdx1*, and *Rest* transcripts levels after silencing of *Hmg20a* in INS-1E cells ($n = 4$ independent experiments performed in triplicates). **d** H3K4m2 and **e** HMG20A occupancy of promoter, exon 1 and ATG regions of the *Pax4* gene after chromatin immunoprecipitation using anti-H3K4m2 or anti-HMG20A antibodies, with IgG as a control for non-specific interactions ($n = 4$ independent experiments performed in triplicates). **f** Beta cell metabolism-secretion coupling genes transcripts levels after silencing of *Hmg20a* in INS-1E cells ($n = 4$ independent experiments, performed in triplicates). **g** Alteration in the expression of key genes was confirmed in INS-1E cells using a second siHMG20A ($n = 4$ independent experiments performed in triplicates). Data are represented as means + S.E.M. *p* values were determined by one-way ANOVA with Tukey's multiple comparisons test (**a, c, f, g**). $^{*}p < 0.05$, $^{**}p < 0.01$, $^{***}p < 0.001$, $^{****}p < 0.0001$

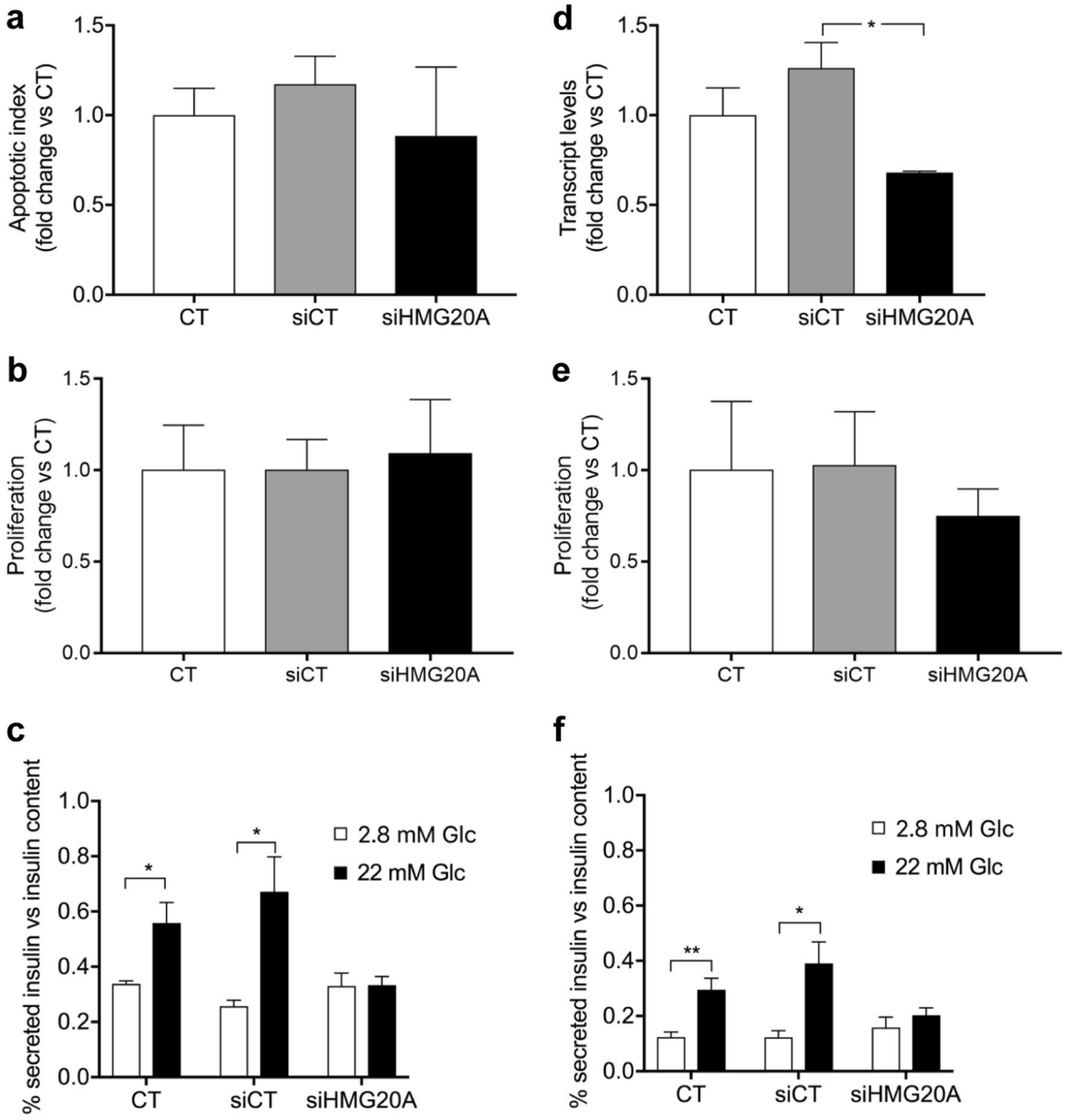

Fig. 7 *Hmg20a* silencing impairs insulin secretion in INS-E1 cells as well as in mouse islets without affecting cell death or proliferation. a Cell death ($n = 3$), **b** proliferation ($n = 3$), and **c** glucose-induced insulin secretion (GSIS, $n = 4$) were assessed subsequent to siRNA-mediated HMG20A depletion in INS-1E cells. **d** Effect of siRNA-mediated HMG20A depletion on **e** cell proliferation ($n = 6$ islet preparations) and **f** GSIS in mouse islets ($n = 6$ islet preparations). Data are represented as mean + S.E.M. *p* values were determined by unpaired two-tailed Student's *t*-test. $^{*}p < 0.05$, $^{**}p < 0.01$

depletion impairs GSIS. Therefore, we provide first evidence that *HMG20A* is a key regulator of mature beta cell function.

Our results indicate that variations in glucose levels are a main rheostat of islet HMG20A expression, which in turn appears to modulate islet adaptive measures by increasing insulin biosynthesis. The latter premise is supported by our findings that *NEUROD* expression levels mirrored those of *HMG20A*, being stimulated by high glucose and inhibited under siRNA-mediated *Hmg20a* downregulation. Mutations in the *NEUROD* gene predispose individuals to develop maturity onset diabetes of the young (MODY6)[17] while adult mouse islets lacking *Neurod* respond poorly to glucose[27]. We also found reduced expression levels of *Mafa* as a consequence of *Hmg20a* depletion. This transcription factor along with NEUROD activates expression of the *Gck* and *Insulin* gene[27–29], consistent with reduced levels of both transcripts in Hmg20A-silenced cells. Intriguingly, *Glut2* was increased following *Hmg20a* repression perhaps as a compensatory mechanism to increase cellular glucose influx due to decreased GCK-mediated phosphorylation

and glycolysis[30]. Thus, the coordinated regulation of *NeuroD* and *Mafa* by HMG20A may be a key molecular hub essential for beta cell function and adaptation to physiological stress such as during pregnancy in which glucose metabolism is altered. Interestingly, although HMG20A was repressed by palmitate *in vitro*, expression levels were not significantly altered in islets of a mouse model of high fat diet-induced obesity and pre-diabetes. Thus, it is tempting to speculate that *in vivo*, glucose and lipids may have opposite effect on HMG20A expression nullifying any significant increased in expression, which may in long-term hinder islet adaptation, precipitating beta cell dysfunction and T2DM. The latter hypothesis may rationalize the observed association of HMG20A risk variants with T2DM in obese cases[8].

Our study also identifies the *Pax4* gene as a direct target repressed by HMG20A. Although the *Pax4* gene promoter was shown to interact with REST[15], the absence of this "disallowed" gene in beta cells suggest that HMG20A acts independent of the LSD1–coREST complex that requires REST to be recruited onto DNA[14]. Rather, our results are in agreement with recent findings that HMG20A in cohort with LSD1 is sufficient to repress *Snail1* and induce TGF beta-triggered EMT, demonstrating a mechanism independent of REST as well as the capacity of HMG20A for binding directly to DNA[18]. Notwithstanding, *Hmg20a* silencing also evoked REST re-expression indicating that in cohort with PAX4, these two factors may promote de-differentiation of beta cells conveying increased survival under unfavorable physiological conditions such as chronic hyperglycemia.

To date, regulation of the endogenous *Pax4* gene in mature islets conveying protection and adaptation in response to physiological or pathophysiological conditions has remained obscure. Our data suggest that HMG20A may be an important epigenetic regulator of *Pax4* gene expression that will dictate the faith of beta cells under stress conditions such as in T2DM. In accord with this premise, we previously demonstrated that PAX4 expression was increased in islets derived from T2DM patients[31]. We now demonstrate that HMG20A levels are repressed in T2DM islets. These combined human data are in line with increased expression of *Pax4* subsequent to *Hmg20a* silencing in either islets or INS-1E cells without altering apoptosis and proliferation. Accumulating evidence suggest that the main characteristic event in T2DM is not massive beta cell death but rather beta cell de-differentiation[32]. We previously demonstrated that chronic expression of *Pax4* is implicated in this process through downregulation of *Mafa* and *Insulin* expression[33]. Our current data substantiate these findings as we detected a decrease in *Mafa* expression after *Hmg20*a silencing. Thus, the role of HMG20A may be to supress *Pax4* transcription thereby permitting expression of *Mafa* as well as *Insulin*. Such cross talk between the two factors is highlighted also during pregnancy. Indeed, we previously found a peak of *Pax4* expression and beta-cell proliferation at 10.5 days and 12.5 days of pregnancy respectively[24]. Herein, we now find that HMG20A expression in islets is increased at 14.5 days of pregnancy, just after the peak of proliferation and correlating with decreased *Pax4* and increased *Mafa* expression levels. These findings are consistent with the premise that beta cells after proliferation have to re-differentiate to reach their metabolic mature phenotype and adequately secrete insulin, a process requiring MAFA[34]. A similar regulatory cross talk between HMG20A and PAX4 may also be operative in early stages of hyperglycemia, which is characterized by active beta cell adaptation. Nonetheless, long-term exposure may favor de-differentiation and survival (without altering proliferation) to the detriment of function, as we observed *in vitro* in which *HMG20A* expression was transiently increased but then inhibited by glucose. Although further studies will be needed to specify the mechanism by which HMG20A regulates those islet-enriched genes, our work provides the basis for the involvement of a non-mutually exclusive cross regulation of HGM20A and PAX4 in islet/beta cell physiology.

A significant finding of our study is the potential decreased in HMG20A levels associated with the diabetes-linked rs7119 SNP within the 3′ UTR of the transcript. This SNP opens the putative binding site of several new miRNAs as compared to the normal wild type allele. Although a previous study has linked T2DM-associated genes to islet-expressed miRNA[35], our study, to the best of our knowledge, provides first evidence that a diabetes-linked SNP alters the putative binding site for miRNAs resulting in the deregulate repression of the target transcript. Further indication for a dysfunctional role of the rs7119 variant in aberrant HMG20A repression was highlighted by the expression of SNP-associated miRNAs, the most abundant being miR-143 and 1246, in human 1.1E7 cells and mouse islets. In contrast, miR-571 associated with the wild type allele miRNA binding site was not express suggesting the potential absence of post-transcriptional regulation conveyed by the normal allele. Although scarce details are available on the role of miR-143 and 1246 in islet function, miR-143 was shown to be among the ten most abundant miRNAs expressed in human islets beta cells whereas miR-1246 was predominantly expressed in other islet cell types[35]. Elsewhere, miR-143 expression was found to be essential for human pre-adipocyte differentiation partly through repression of its target gene ERK5 involved in cell growth and proliferation[36]. Although it remains to be validated, the potential serendipitous binding of miR-143 to the HMG20A rs7119 gene variant may induce aversely de-differentiation through activation of *Pax4* and *Rest*.

The overall data presented in this work clearly describes a functional link between HMG20A and islet physiology. HMG20A regulates metabolism-secretion coupling genes in beta cells and could be also involved in beta cell plasticity through PAX4 and REST, regulating phenotypic changes needed for beta cells in order to respond to different physiological situations as pregnancy and obesity. Failure on those HMG20A-mediated processes could lead to the development and establishment of T2DM. As consequence, our study opens a venue to consider targeting of HMG20A expression and/or regulation as potential therapies for T2DM.

Materials and methods

Animals

The experimental mouse procedures were approved by the Institutional Animal Care Committee of the Andalusian Center of Molecular Biology and Regenerative Medicine (CABIMER) and by the ethic committee of the University of Malaga, Biomedical Research Institute of Málaga (IBIMA) and performed according to the Spanish law on animal use RD 53/2013. Animal studies were performed in compliance with the ARRIVE guidelines[37]. Mice were housed in ventilated plastic cages and maintained on a 12-h light–dark cycle with ad libitum access to pelleted chow and water. C57BL/6J of both genders were used to obtain pancreatic islets and other tissues (liver, adipose tissue, skeletal muscle, and brain) and females for pregnancy studies. For diet-induced obesity studies, 8-weeks-old male C57BL/6J mice (Janvier Labs, Saint-Berthevin Cedex, France) were housed in individual cages under a 12 h light/dark cycle (8:00 pm light off) in a room with controlled temperature (21 ± 2 °C) and humidity ($50 \pm 10\%$). For induction of obesity, groups of ten mice were fed a high fat diet (D12451 Research Diets Inc., New Brunswick, NJ, USA), containing 45% of Kcal from saturated fat, for 15 weeks. In parallel, groups of ten age-matched mice were fed a control diet containing 10% of Kcal from fat (D12450 Research Diets Inc.). Circulating glucose levels were measured from tail vein blood samples using an Optium Xceed glucometer (Abbott Scientifica SA, Barcelona, Spain). Insulin tolerance tests (ITT) and glucose tolerance test (OGTT) were performed as previously described[38]. At 15 weeks, mice were sacrificed by cervical dislocation and pancreas extracted for histological processing.

Pancreatic islet and cell line cultures

Mouse pancreatic islets were isolated from 2 to 4-months-old C57BL/6J mice by intraductal collagenase as previously described[24,39] . After isolation, mouse islets were cultured in 5.5 mM glucose/RPMI 1640 medium (Life Technologies, Madrid, Spain) supplemented with 10 % Fetal bovine serum (FBS, Sigma-Aldrich, Madrid, Spain), 100 U/ml penicillin, 100 µg/ml streptomycin (Sigma-Aldrich), 2 mM L-glutamine (Life Technologies), 1 mM sodium pyruvate (Sigma-Aldrich), 50 µM β-mercaptoethanol (Life Technologies), and 10 mM HEPES (Life Technologies) prior to different experimental treatments. Islets from non-diabetic or T2DM organ donors were obtained in Pisa or purchased from Tebu-Bio (Barcelona, Spain). After reception, human islets were cultured in CMRL-1066 (Gibco) medium containing 5.5 mM glucose and supplemented with 10% FBS, 100 U/ml penicillin, 100 µg/ml streptomycin, 2 mM L-glutamine, and 100 µg/ml gentamycin. To assess glucose influence in HMG20A expression, both human and mice islets were cultured in normal (5.5 mM) or high (24.4 mM) glucose concentrations for 24, 48, 72, and 96 h, and lately harvested for RNA extraction.

The rat insulinoma INS-1E beta cell line (kindly provided by Dr. P Maechler, Geneva, CH) was cultured between passages 50–90 and maintained in 11.1 mM glucose/RPMI 1640 medium (Life Technologies) supplemented with 10% FBS, 100 U/ml penicillin, 100 µg/ml streptomycin, 2 mM L-glutamine, 1 mM sodium pyruvate, 50 µM β-mercaptoethanol, and 10 mM HEPES. Following overnight glucose deprivation (3 mM), cells were cultured in 11.1 mM or 24.4 mM glucose RPMI 1640 medium for 24, 48, 72, and 96 h. Alternatively INS-1E cells were also exposed to 0.5 mM palmitate for up to 96 h. Cells were harvested at each time point for RNA extraction.

The human retinal pigmented epithelial RPE1 (ATCC, CRL-4000) and the islet beta 1.1E7 cell lines (The European Collection of Authenticated Cell Cultures) were cultured in F-12 Ham and RPMI media, respectively, prior to luciferase reporter assays. The 1.1E7 cell line was also cultured in the presence of either 11.1 or 24.4 mM glucose for up to 96 h. RNA was extracted at 24, 48, 72, and 96 h post treatment.

RNA interference

Mouse pancreatic islets and INS-1E cells were cultured as previously described[40] and transfected with either 50 µmol of two independent *HMG20A* small interfering (si) RNAs (5′-AGGCAAAUCUCAUAGGCAA-3′ and 5′-UCACAAGGAUGUUGGGCAA-3′) or scramble siRNA (Sigma-Aldrich) using Oligofectamine (Life Technologies). Samples were processed for RNA, immunofluorescence, GSIS, cell proliferation and death assessment 72 h after transfection.

RNA extraction and quantitative-PCR expression analysis

Qiagen RNeasy Micro and Mini kits (Qiagen, Madrid, Spain) were used for the extraction of total RNA from the different tissues, islets and cell line samples. After quantification of the RNA concentration using a NanoDrop 1000 Spectrophotometer (Wilmington, DE, USA), single-stranded cDNA was synthesized with the Superscript II

First-Strand cDNA synthesis kit (Invitrogen, Carlsbad, CA, USA) and Anchored OligodT as primers (Sigma-Aldrich). Quantitative PCR was performed on a 7500 Real-Time PCR System (Applied Biosystems). Gene-specific primers (*HMG20A, NEUROD1, PDX1, PAX4, REST, GLUKOKINASE, INSULIN, PI3K, MAFA, GLUT1, GLUT2, SNAP25*, and *SYT7*) were designed using Power Primer3 (Supplementary Table 1, 2 and 3). Expression levels of the housekeeping genes *β-ACTIN* or *CYCLOPHILIN* were used for normalization. The relative gene expression was calculated using the $2^{-\Delta\Delta Ct}$ method[24]. For miRNA expression profiling, microRNAs were extracted from the 1.1E7 beta cell line and mouse pancreatic islets using the miRNAeasy kit (Qiagen) and cDNA synthesis was conducted using the Universal cDNA Synthesis Kit (Exiqon) as previously described[41]. ExiLENT SYBR Green Master Mix Kit and primers for each assay to perform quantitative-PCR (qPCR) were obtained from Exiqon.

Immunofluorescence and immunohistochemistry studies

Dissected pancreases were fixed overnight in 4% paraformaldehyde at 4 °C and processed for embedding in paraffin at the Histology Core Facility, CABIMER. Pancreatic sections from non-pregnant/pregnant mice sacrificed at 10.5, 12.5, 14.5, and 17.5 days post coitum were analyzed by immunohistochemistry using specific antibodies against HMG20A, insulin, glucagon, and somatostatin (Supplemental Table 4). Counterstaining was performed with 5 µg/ml DAPI (Life Technologies) to stain the nuclei and slides were mounted using fluorescent mounting medium (DAKO). Images were acquired using either the epifluorescence (Leica AF6000, Leica, England) or confocal (Leica TCS SP5) microscopes. Expression of HMG20A in beta cells was quantified using Metamorph Analysis Software (Molecular Devices). Single frames were acquired using a confocal TCS SP5 microscope (Leica). Same illumination settings were applied for all the samples (image parameters including pinhole size, photomultiplier offset and gain, and laser intensity were first set for non-pregnant control samples, and then, the same settings were used for all conditions). For Image analysis/quantification, the integrated intensity values (∑ pixel intensity at region of interest) were measured as previously described[42–44]. Integrated intensity of nuclear HMG20A in islet cells co-expressing insulin were measured, and the average of intensity per islet was calculated. Three independent animals and an average of 50 islets were used for each time point. Pancreatic sections from control and HFD mice were performed and analyzed as previously described[25].

Luciferase 3′ UTR reporter assays

The effect of the 3′ UTR SNP rs7119, previously linked to T2DM was evaluated by luciferase reporter assays. 3′ UTR constructs containing the wt allele (reference allele) "C" or the DMT2-linked allele ("mut" allele) "T" cloned downstream of the luciferase gene were obtained from GeneCopoeia. Luciferase contained in these constructs is a secreted one; therefore luciferase activity can be measured in the medium. These constructs also have a secreted embryonic alkaline phosphatase (SEAP) gene driven by a constitutive promoter, used as internal control. The Secrete-Pair TM Dual Luminescence Assay Kit (GeneCopoeia) was used as luciferase reporter system according to manufacturer's instructions. RPE1 and 1.1E7 cell lines were chosen for transfection studies using those constructs. Both are cell lines of human origin and from different tissues. RPE1 are cells from retina pigmentosum ephitelia[45] meanwhile 1.1E7[46] is a human beta cell line. The RPE1 and 1.1E7 cell lines were transfected and luciferase activity was measured 48 h after in the collected culture media.

Glucose-stimulated insulin secretion assays

Insulin secretion in response to 2.8 mM or 22 mM glucose was measured in static incubations as previously described[47,48] in both mouse pancreatic islets and INS-1E cells. Following the incubations, supernatants were collected and islets and cells were lysated with HCl-ethanol to obtain the insulin content. Insulin from supernatants and cell contents was measured by ELISA (Mercodia, Uppsala, Sweden). All experiments were run in triplicate.

Cell death and proliferation

Cell death (apoptosis) and proliferation was measured using either the Cell Death Detection ELISA kit or the 5-Bromo-2′-deoxy-uridine labeling and detection kit (Roche Diagnostics, Madrid, Spain) as described by the manufacturer.

ChIP assays

ChIP assays were performed as previously described[12,18]. INS-1E cells were treated with 1% formaldehyde for 15 min at 37 °C for crosslinking. Chromatin was sonicated to an average fragment size of 400 to 500 bp using the Diagenode Bioruptor. Immunoprecipitations were performed using the following reagents: Dynabeads Protein A (Invitrogen), rabbit polyclonal anti-HMG20A (Sigma-Aldrich) and rabbit monoclonal to Histone H3 (di methyl K4) (Abcam). Rabbit IgG (Sigma) was used as a control for non-specific interactions. Input was prepared with 10% of the chromatin used for immunoprecipitation. Quantification of immunoprecipitated DNA was performed by real-time PCR with the Applied Biosystems 7500 FAST real-time PCR system, using Applied Biosystems Power SYBR green master mix. Each sample was quantified in triplicate. Provided data are the average of at least three independent experiments.

Statistical analysis

The Ruth Lenth's power of analysis was applied to the different animal models to ensure that adequate numbers of animals had been studied to detect significant changes. Results are expressed as mean ± SEM (line plots as a function of time) or as mean + SEM (bar graphs). Statistical analyses were performed using the GraphPad Prism software version 7 (GraphPad Software, La Jolla, USA).

Acknowledgements

This work was supported by the Consejería de Salud, Fundación Pública Andaluza Progreso y Salud, Junta de Andalucía (PI-0727-2010 to B.R.G., PI-0085-2013 to P.I.L., PI-0006-2016 to E.F.-M. and PI-0574-2012 to S.Y.R.-Z.), the Consejería de Economía, Innovación y Ciencia (P10.CTS.6359 to B.R.G. and P09-CTS-5445 to A.C.-C.), the Ministerio de Economía y Competitividad, Instituto de Salud Carlos III co-funded by Fondos FEDER (PI10/00871 and PI13/00593 to B.R.G., and BFU2014-5343-P to J.C.R.) and the Red TerCel program (RD12/0019/0028 to B.S. and K.H.). E.F.M. is recipient of a Juan de la Cierva Incorporación Fellowship from the Ministerio de Economía y Competitividad (IJCI-2015-26238). S.Y.R.Z is a recipient of a postdoctoral fellowship from Consejería de Salud, Junta de Andalucía (RH-0070-2013). F.J.B.S. is recipient of a "Nicolás Monardes" research contract from Consejería de Salud Junta de Andalucía, (C-0070-2012). A.M.M. is supported by CP14/00105 and PI15/00134 from the Instituto de Salud Carlos III co-funded by Fondes FEDER. CIBERDEM is an initiative of the Instituto de Salud Carlos III. We thank Noelia García-Rodriguez, Lourdes Sanchez-Salido, and Leopoldo Perez-Rosendo for their excellent technical assistance. B.R.G. is the guarantor of this work and, as such, had full access to all the data in the study and takes responsibility for the integrity of the data and the accuracy of the data analysis.

Author details

[1]Department of Cell Regeneration and Advanced Therapies, Andalusian Center of Molecular Biology and Regenerative Medicine-CABIMER, Junta de Andalucia-University of Pablo de Olavide-University of Seville-CSIC, Seville, Spain. [2]Department of Genome Biology, Andalusian Center of Molecular Biology and Regenerative Medicine (CABIMER) JA-CSIC-UPO-US, Seville, Spain. [3]Research Unit, University Hospital "Puerta del Mar", Instituto de Investigación e Innovación en Ciencias Biomédicas de la Provincia de Cádiz (INiBICA), Cádiz, Spain. [4]Unidad de Gestión Clínica Intercentros de Endocrinología y Nutrición, Instituto de Investigación Biomédica de Málaga (IBIMA), Hospital Regional Universitario de Málaga, Universidad de Málaga, Málaga, Spain. [5]Diabetes & Obesity Research Laboratory, Biomedical Research Institute August Pi I Sunyer (IDIBAPS), Barcelona, Spain. [6]Centro de Investigación Biomédica en Red de Diabetes y Enfermedades Metabólicas Asociadas (CIBERDEM), Madrid, Spain. [7]Department of Translational Research and of New Surgical and Medical Technologies, University of Pisa, Pisa, Italy. [8]Endocrinology and Metabolism Department University Hospital "Puerta del Mar", Instituto de Investigación e Innovación en Ciencias Biomédicas de la Provincia de Cádiz (INiBICA), Cádiz, Spain

Conflict of interest

The authors declare that they have no conflict of interest.

Supplementary Information accompanies this paper at (https://doi.org/10.1038/s41419-018-0272-z).

Received: 4 August 2017 Revised: 20 December 2017 Accepted: 27 December 2017
Published online: 15 February 2018

References

1. Frayling, T. M. & Hattersley, A. T. Physiology helps GWAS take a step closer to mechanism. *Diabetes* **63**, 1836–1837 (2014).
2. Prasad, R. B. & Groop, L. Genetics of type 2 diabetes-pitfalls and possibilities. *Genes (Basel)* **6**, 87–123 (2015).
3. Mohlke, K. L. & Boehnke, M. Recent advances in understanding the genetic architecture of type 2 diabetes. *Hum. Mol. Genet.* **24**, R85–R92 (2015).
4. Perry, J. R. & Frayling, T. M. New gene variants alter type 2 diabetes risk predominantly through reduced beta-cell function. *Curr. Opin. Clin. Nutr. Metab. Care* **11**, 371–377 (2008).
5. Kooner, J. S. et al. Genome-wide association study in individuals of South Asian ancestry identifies six new type 2 diabetes susceptibility loci. *Nat. Genet.* **43**, 984–989 (2011).
6. Sim, X. et al. Transferability of type 2 diabetes implicated loci in multi-ethnic cohorts from Southeast Asia. *PLoS Genet.* **7**, e1001363 (2011).
7. Fukuda, H. et al. A single nucleotide polymorphism within DUSP9 is associated with susceptibility to type 2 diabetes in a Japanese population. *PLoS ONE* **7**, e46263 (2012).
8. Perry, J. R. et al. Stratifying type 2 diabetes cases by BMI identifies genetic risk variants in LAMA1 and enrichment for risk variants in lean compared to obese cases. *PLoS Genet.* **8**, e1002741 (2012).
9. Arnold, M., Ellwanger, D. C., Hartsperger, M. L., Pfeufer, A. & Stumpflen, V. Cis-acting polymorphisms affect complex traits through modifications of microRNA regulation pathways. *PLoS ONE* **7**, e36694 (2012).
10. Bianchi, M. E. & Agresti, A. HMG proteins: dynamic players in gene regulation and differentiation. *Curr. Opin. Genet. Dev.* **15**, 496–506 (2005).
11. Wynder, C., Hakimi, M. A., Epstein, J. A., Shilatifard, A. & Shiekhattar, R. Recruitment of MLL by HMG-domain protein iBRAF promotes neural differentiation. *Nat. Cell Biol.* **7**, 1113–1117 (2005).
12. Ceballos-Chavez, M. et al. Control of neuronal differentiation by sumoylation of BRAF35, a subunit of the LSD1-CoREST histone demethylase complex. *Proc. Natl Acad. Sci. USA* **109**, 8085–8090 (2012).
13. van Arensbergen, J. et al. Derepression of polycomb targets during pancreatic organogenesis allows insulin-producing beta-cells to adopt a neural gene activity program. *Genome Res.* **20**, 722–732 (2010).
14. Martin, D. & Grapin-Botton, A. The importance of REST for development and function of beta cells. *Front. Cell Dev. Biol.* **5**, 12 (2017).
15. Kemp, D. M., Lin, J. C. & Habener, J. F. Regulation of Pax4 paired homeodomain gene by neuron-restrictive silencer factor. *J. Biol. Chem.* **278**, 35057–35062 (2003).
16. Martin, D. et al. REST represses a subset of the pancreatic endocrine differentiation program. *Dev. Biol.* **405**, 316–327 (2015).
17. Malecki, M. T. et al. Mutations in NEUROD1 are associated with the development of type 2 diabetes mellitus. *Nat. Genet.* **23**, 323–328 (1999).
18. Rivero, S., Ceballos-Chavez, M., Bhattacharya, S. S. & Reyes, J. C. HMG20A is required for SNAI1-mediated epithelial to mesenchymal transition. *Oncogene* **34**, 5264–5276 (2015).
19. Lamouille, S., Xu, J. & Derynck, R. Molecular mechanisms of epithelial-mesenchymal transition. *Nat. Rev. Mol. Cell Biol.* **15**, 178–196 (2014).
20. Nieto, M. A. Epithelial plasticity: a common theme in embryonic and cancer cells. *Science* **342**, 1234850 (2013).
21. Talchai, C., Xuan, S., Lin, H. V., Sussel, L. & Accili, D. Pancreatic beta cell dedifferentiation as a mechanism of diabetic beta cell failure. *Cell* **150**, 1223–1234 (2012).
22. Wang, Z., York, N. W., Nichols, C. G. & Remedi, M. S. Pancreatic beta cell dedifferentiation in diabetes and redifferentiation following insulin therapy. *Cell Metab.* **19**, 872–882 (2014).
23. Hu, He. K. H. et al. In vivo conditional Pax4 overexpression in mature islet beta-cells prevents stress-induced hyperglycemia in mice. *Diabetes* **60**, 1705–1715 (2011).
24. Lorenzo, P. I. et al. PAX4 defines an expandable beta-cell subpopulation in the adult pancreatic islet. *Sci. Rep.* **5**, 15672 (2015).
25. Romero-Zerbo, S. Y. et al. The cannabinoid ligand LH-21 reduces anxiety and improves glucose handling in diet-induced obese pre-diabetic mice. *Sci. Rep.* **7**, 3946 (2017).
26. Wang, Z. et al. Combinatorial patterns of histone acetylations and methylations in the human genome. *Nat. Genet.* **40**, 897–903 (2008).

27. Gu, C. et al. Pancreatic beta cells require NeuroD to achieve and maintain functional maturity. *Cell. Metab.* **11**, 298–310 (2010).
28. Moates, J. M., Nanda, S., Cissell, M. A., Tsai, M. J. & Stein, R. BETA2 activates transcription from the upstream glucokinase gene promoter in islet beta-cells and gut endocrine cells. *Diabetes* **52**, 403–408 (2003).
29. Wang, H., Brun, T., Kataoka, K., Sharma, A. J. & Wollheim, C. B. MAFA controls genes implicated in insulin biosynthesis and secretion. *Diabetologia* **50**, 348–358 (2007).
30. Remedi, M. S. & Nichols, C. G. Hyperinsulinism and diabetes: genetic dissection of beta cell metabolism-excitation coupling in mice. *Cell. Metab.* **10**, 442–453 (2009).
31. Brun, T. et al. The diabetes-linked transcription factor Pax4 is expressed in human pancreatic islets and is activated by mitogens and GLP-1. *Hum. Mol. Genet.* **17**, 478–489 (2008).
32. Hunter, C. S. & Stein, R. W. Evidence for loss in identity, de-differentiation, and trans-differentiation of islet beta-cells in type 2 diabetes. *Front. Genet.* **8**, 35 (2017).
33. Lorenzo P. I., Juarez-Vicente F., Cobo-Vuilleumier N., Garcia-Dominguez M., Gauthier B. R. The diabetes-linked transcription factor PAX4: from gene to functional consequences. *Genes (Basel)* **8**, E101 (2017).
34. Kaneto, H. et al. Role of MafA in pancreatic beta-cells. *Adv. Drug Deliv. Rev.* **61**, 489–496 (2009).
35. van de Bunt, M. et al. The miRNA profile of human pancreatic islets and beta-cells and relationship to type 2 diabetes pathogenesis. *PLoS ONE* **8**, e55272 (2013).
36. Esau, C. et al. MicroRNA-143 regulates adipocyte differentiation. *J. Biol. Chem.* **279**, 52361–52365 (2004).
37. Kilkenny, C., Browne, W. J., Cuthill, I. C., Emerson, M. & Altman, D. G. Improving bioscience research reporting: the ARRIVE guidelines for reporting animal research. *PLoS Biol.* **8**, e1000412 (2010).
38. Lopez-Noriega, L. et al. Levothyroxine enhances glucose clearance and blunts the onset of experimental type 1 diabetes mellitus in mice. *Br. J. Pharmacol.* **174**, 3795–3810 (2017).
39. Mellado-Gil, J. M. et al. PAX4 preserves endoplasmic reticulum integrity preventing beta cell degeneration in a mouse model of type 1 diabetes mellitus. *Diabetologia* **59**, 755–765 (2016).
40. Brun, T., Duhamel, D. L., Hu He, K. H., Wollheim, C. B. & Gauthier, B. R. The transcription factor PAX4 acts as a survival gene in INS-1E insulinoma cells. *Oncogene* **26**, 4261–4271 (2007).
41. Rodriguez-Comas, J. et al. Stress-induced microRNA-708 impairs beta-cell function and growth. *Diabetes* **66**, 3029–3040 (2017).
42. Mahoney, E. et al. ER stress and autophagy: new discoveries in the mechanism of action and drug resistance of the cyclin-dependent kinase inhibitor flavopiridol. *Blood* **120**, 1262–1273 (2012).
43. Monteiro, P. et al. Endosomal WASH and exocyst complexes control exocytosis of MT1-MMP at invadopodia. *J. Cell Biol.* **203**, 1063–1079 (2013).
44. Wheelock, M. S., Wynne, D. J., Tseng, B. S. & Funabiki, H. Dual recognition of chromatin and microtubules by INCENP is important for mitotic progression. *J. Cell Biol.* **216**, 925–941 (2017).
45. Rambhatla, L., Chiu, C. P., Glickman, R. D. & Rowe-Rendleman, C. In vitro differentiation capacity of telomerase immortalized human RPE cells. *Invest. Ophthalmol. Vis. Sci.* **43**, 1622–1630 (2002).
46. McCluskey, J. T. et al. Development and functional characterization of insulin-releasing human pancreatic beta cell lines produced by electrofusion. *J. Biol. Chem.* **286**, 21982–21992 (2011).
47. Gauthier, B. R. et al. PDX1 deficiency causes mitochondrial dysfunction and defective insulin secretion through TFAM suppression. *Cell. Metab.* **10**, 110–118 (2009).
48. Jimenez-Moreno, C. M. et al. A simple high efficiency intra-islet transduction protocol using lentiviral vectors. *Curr. Gene Ther.* **15**, 436–446 (2015).

nature COMMUNICATIONS

ARTICLE

DOI: 10.1038/s41467-018-03943-0 OPEN

LRH-1 agonism favours an immune-islet dialogue which protects against diabetes mellitus

Nadia Cobo-Vuilleumier[1], Petra I. Lorenzo[1], Noelia García Rodríguez[1], Irene de Gracia Herrera Gómez[1], Esther Fuente-Martin[1], Livia López-Noriega[1], José Manuel Mellado-Gil[1], Silvana-Yanina Romero-Zerbo[2,3], Mathurin Baquié[4], Christian Claude Lachaud[1], Katja Stifter[5], German Perdomo[6], Marco Bugliani[7], Vincenzo De Tata[8], Domenico Bosco[9], Geraldine Parnaud[9], David Pozo[10], Abdelkrim Hmadcha[1,3], Javier P. Florido[11], Miguel G. Toscano[12], Peter de Haan[12], Kristina Schoonjans[13], Luis Sánchez Palazón[14], Piero Marchetti[7], Reinhold Schirmbeck[5], Alejandro Martín-Montalvo[1], Paolo Meda[15], Bernat Soria[1,3], Francisco-Javier Bermúdez-Silva[2,3], Luc St-Onge[16] & Benoit R. Gauthier[1]

Type 1 diabetes mellitus (T1DM) is due to the selective destruction of islet beta cells by immune cells. Current therapies focused on repressing the immune attack or stimulating beta cell regeneration still have limited clinical efficacy. Therefore, it is timely to identify innovative targets to dampen the immune process, while promoting beta cell survival and function. Liver receptor homologue-1 (LRH-1) is a nuclear receptor that represses inflammation in digestive organs, and protects pancreatic islets against apoptosis. Here, we show that BL001, a small LRH-1 agonist, impedes hyperglycemia progression and the immune-dependent inflammation of pancreas in murine models of T1DM, and beta cell apoptosis in islets of type 2 diabetic patients, while increasing beta cell mass and insulin secretion. Thus, we suggest that LRH-1 agonism favors a dialogue between immune and islet cells, which could be druggable to protect against diabetes mellitus.

[1] Department of Cell Regeneration and Advanced Therapies, Andalusian Center for Molecular Biology and Regenerative Medicine-CABIMER, Junta de Andalucia-University of Pablo de Olavide-University of Seville-CSIC, Seville 41092, Spain. [2] Unidad de Gestión Clínica Intercentros de Endocrinología y Nutrición, Instituto de Investigación Biomédica de Málaga (IBIMA) Hospital Regional Universitario de Málaga Universidad de Málaga, Málaga 29010, Spain. [3] Centro de Investigación Biomédica en Red de Diabetes y Enfermedades Metabólicas Asociadas (CIBERDEM), Madrid 28029, Spain. [4] Neurix SA, Geneva 1228, Switzerland. [5] Ulm University Hospital, Ulm 89081, Germany. [6] Facultad de Ciencias de la Salud, Universidad de Burgos, Burgos 09001, Spain. [7] Department Clinical and Experimental Medicine, University of Pisa—AOUP University Hospital, Pisa 56126, Italy. [8] Department of Translational Research and of New Surgical and Medical Technologies, University of Pisa, Pisa 56126, Italy. [9] Cell Isolation and Transplantation Centre, University Hospital, Geneva 1211, Switzerland. [10] Department of Cell Dynamics and Signalling, CABIMER-Andalusian Center for Molecular Biology and Regenerative Medicine, Seville 41092, Spain. [11] Clinical Bioinformatics Area, Fundación Progreso y Salud, Consejería de Salud, Seville 41013, Spain. [12] Amarna Therapeutics, Seville 41092, Spain. [13] Laboratory of Metabolic Signaling, EPFL, Lausanne 1015, Switzerland. [14] Biological Resources, CABIMER-Andalusian Center for Molecular Biology and Regenerative Medicine, Seville 41092, Spain. [15] Department of Cell Physiology and Metabolism, University of Geneva, Geneva 1211, Switzerland. [16] Neuried Munich 82061, Germany. Correspondence and requests for materials should be addressed to B.R.G. (email: benoit.gauthier@cabimer.es)

Type 1 diabetes mellitus (T1DM) is a $CD4^+$ and $CD8^+$ T-cell-dependent autoimmune disease that targets beta cell destruction, ultimately leading to hyperglycemia and insulin dependence. The collapse in tolerance to self-antigens, such as insulin, is precipitated by genetic and environmental factors[1,2]. To date, therapies aimed at inhibiting the immune system using anti-CD3 monoclonal antibodies or at neutralizing pro-inflammatory cytokines, have had limited success[3,4]. One of the reasons may be that inhibiting the immune and inflammatory reactions in the pancreas impairs the repairing and regeneration capabilities of a functional beta cells mass[5,6], as observed during wound healing[7]. Novel agents that could guide a pro-inflammatory autoimmune destructive environment toward an anti-inflammatory milieu facilitating islet regeneration, would define a novel class of antidiabetic therapies.

The liver receptor homolog-1 (LRH-1, or NR5A2) is a member of the NR5A family of nuclear receptors, which plays a pivotal role in early embryonic development, and specifies the endodermal lineage[8]. In the liver, LRH-1 modulates the expression of genes involved in cholesterol and bile acid metabolism, as well as in glucose homeostasis[9], attenuates the hepatic acute phase response, which is triggered upon increases of pro-inflammatory cytokines, and protects against endoplasmic reticulum stress[10,11]. In the intestine, LRH-1, modulates the enterocyte renewal and regulates the local immune system via production of glucocorticoids[12]. In the pancreas, LRH-1 regulates the expression of genes involved in digestive functions, and protects the endocrine islets against cytokine- and streptozotocin-induced apoptosis[13,14], while stimulating the production of enzymes involved in glucocorticoids biosynthesis[14]. In view of the above, specifically of the possibility that LRH-1 could elicit an islet-driven anti-inflammatory micro-environment, we posited that upregulating LRH-1 activity could have beneficial therapeutic effects in diabetes mellitus (DM).

Natural phospholipids physiologically stimulates LRH-1 activity[15,16], decreasing hepatic steatosis and improving glucose homeostasis in animal models of insulin resistance[17]. Given that LRH-1 can also be activated by smaller, non-polar bicyclic compounds[18], we have synthesized a compound termed BL001, which we have tested in mouse models of T1DM, as well as in pancreatic islets from patients affected by Type 2 DM (T2DM). Here we report that the long-term in vivo administration of BL001 prevents the development of diabetes in mice, through the combined maintenance of a functional islet beta cell mass and the release of anti-inflammatory factors, which contribute to the islet regeneration effect. We further report that BL001 also protects human islet cells from apoptosis and improves impaired insulin secretion as well as beta cell survival in the pancreatic islets of T2DM patients. The data define LRH-1 as a novel therapeutic target for the treatment of T1DM.

Results

BL001 activates LHR-1 without cytotoxic or metabolic effects. The chemical structure of BL001, which specifically binds to and activates LRH-1[18], is depicted in Supplementary Fig. 1a. The effects of the drug on LRH-1 activity, cell viability, and toxicity are described in Supplementary Fig. 1b–e. Pharmacokinetic and safety profiling of BL001 were studied in C57BL/6 and RIP-B7.1 mice, respectively. An i.p. injection of 10 mg/kg b.w. BL001 led to peak plasma concentrations of 3.6 µg/ml (≈8 µM) after 0.2 h, and a half-life of 9.4 h. Daily injections during 24 weeks did not reveal macroscopic organ alterations in BL001-treated RIP-B7.1 mice (Supplementary Fig. 2a, b), which also featured normal plasma levels of total cholesterol and triglycerides up to 8 weeks of treatment (Supplementary Fig. 3a, b). Insulin sensitivity was not altered by this BL001 treatment (Supplementary Fig. 3c).

BL001 blunts apoptosis and attenuates diabetes in mice. To assess the anti-apoptotic effect of BL001, mouse islets were exposed to 10 µM BL001 in the presence of 2 ng/ml IL1beta, 28 ng/ml TNFalpha and 833 ng/ml IFNgamma. The drug prevented the cytokine-induced islet cell death (Fig. 1a). A substantial loss of LRH-1 transcript and protein by RNAi, sensitized BL001-treated islets to the cytokine-induced apoptosis (Fig. 1b–d). The anti-diabetic role of BL001 was next evaluated in animal models of T1DM. C57BL/6 male mice that received 150 mg/kg b.w. streptozotocin (STZ) developed diabetes within 4 weeks (Fig. 1e, Supplementary Fig. 4a). The incidence of diabetes was decreased after a 5 day pre-treatment with 10 mg/kg b.w. BL001 (Fig. 1e, Supplementary Fig. 4a), which decreased the loss of insulin-containing beta cells (Fig. 1g), and increased the proportion of cells staining for both insulin and glucagon (Fig. 1h, i). Moreover, 30% of the mice that developed diabetes returned to normoglycemia 4 weeks after a daily injection of 10 mg/kg b.w. BL001, starting 1 week after the STZ injection (Fig. 1f, Supplementary Fig. 4b).

To evaluate the effect of BL001 against an autoimmune attack, we studied RIP-B7.1 mice, a model mimicking the etiology of T1DM[19], without gender influence[20]. Eighty percent of RIP-B7.1 mice immunized against insulin developed diabetes within 8 weeks (Fig. 1j, Supplementary Fig. 4c), when receiving only a vehicle solution. This proportion dropped to 43% in mice treated with 10 mg/kg b.w. BL001 for 5 days prior to immunization (Fig. 1j, Supplementary Fig. 4c). Still, a similar increase in the proliferation of T cells in response to insulin was also detected in the splenocytes of mice treated or not with BL001, both 4 and 8 weeks after the insulin immunization (Fig. 1k), confirming that all mice had mounted an in vivo autoimmune attack. At these time points, immunostaining showed a near-complete destruction of beta cells in the islets of the control immunized mice, and the persistence of sizable numbers of these cells in the immunized mice treated with BL001 (Fig. 1l). In the presence of hyperglycemia, the latter animals also featured islets with a significant increase in the number of $PDX1^+$ cells as compared to immunized mice (Fig. 1m, n).

Mice in which the BL001 treatment was initiated 5 days after the immunization, featured an incidence of diabetes similar to that of controls for the first 5 weeks (Fig. 1o, Supplementary Fig. 4d). Thereafter, however, the incidence of diabetes was lower (~30%) in the BL001-treated mice than in immunized controls (~80%; Fig. 1o, Supplementary Fig. 4d). A similar decrease in diabetes incidence was observed in female NOD mice treated with BL001 from week 12 (Fig. 1p), an age at which these animals feature an ongoing autoimmune attack, and reduced insulin content. To establish whether the in vivo effects of BL001 were mediated via LRH-1, we generated mice in which the *Lrh1* gene was selectively disrupted in beta cells. To this end, Lrh1 lox/lox mice were crossed with RIP-Cre mice. We found that all mice carrying two deleted alleles (βLRH-$1^{-/-}$), and 75% of the progenies carrying one normal allele (βLRH-$1^{-/+}$) died within 3 weeks of life (Supplementary Fig. 5a). Immunofluorescence staining of islets from day 1 neonatal pups, showed an atypical islet morphology, with a normal proportion of insulin-containing beta cells surrounded by an increased proportion of glucagon-containing alpha cells in homozygous mice (Supplementary Fig. 5b–e).

BL001 inhibits insulitis and alters serum cytokine profile. To unravel the mechanism whereby BL001 impedes the progression of diabetes, we evaluated the lymphocytic infiltration of islets (insulitis) in mice pre-treated or not with BL001. Four weeks after immunization, a sizable insulitis was detected in the pancreas of

both BL001-treated and control mice (Fig. 2a, b). However, 4 weeks later, the normoglycemic BL001-treated mice were nearly free of insulitis, in contrast to controls which displayed strong infiltration (Fig. 2c, d). Accordingly, no $CD4^+$ or $CD8^+$ T cells were found in the islets of the former animals (Supplementary Fig. 6), which also showed significantly higher levels of circulating IL10, IL5, IL6 (Fig. 2e, f), CCL2, CCL4 (Fig. 2g, h), and TGFbeta (Fig. 2i, j) than immunized controls at 8 but not 4 weeks. In contrast, no significant differences were observed in levels of INFgamma (0.6965 ± 0.0931 versus 0.4989 ± 0.0733 $p = 0.1072$, unpaired Student's t test), TNFalpha (5.925 ± 0.815 versus 6.648 ± 0.659 $p = 0.4982$, unpaired Student's t test), IL1beta ($0.5267 \pm$

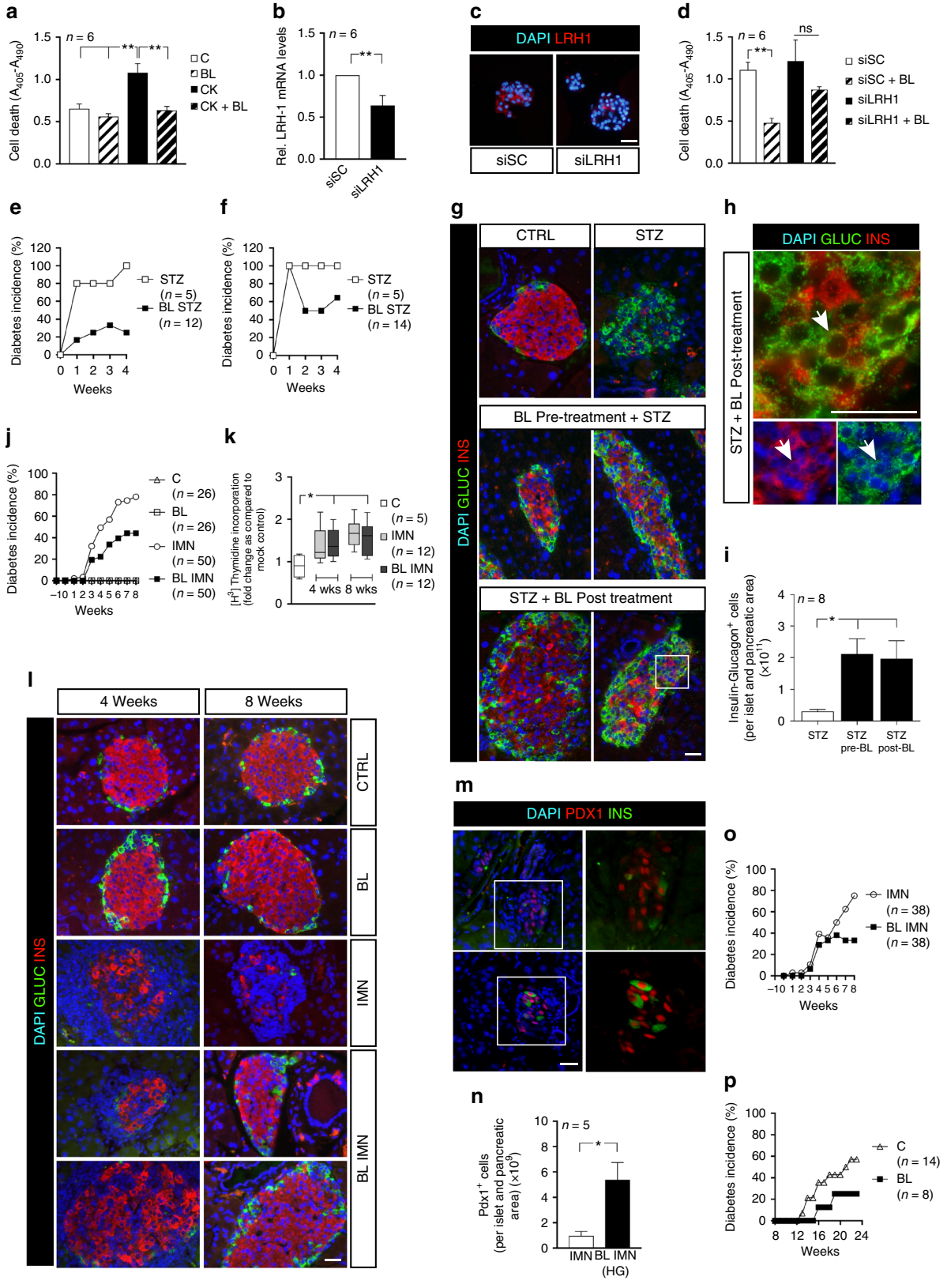

0.0913 versus 0.3461 ± 0.0579 $p = 0.1092$, unpaired Student's t test) and IL2 (1.306 ± 0.181 versus 1.111 ± 0.154 $p = 0.4221$, unpaired Student's t test) between immunized untreated and BL001-treated mice at 8 weeks.

BL001 elicits a tolerogenic environment within the pancreas. To analyze how BL001 remodeled the immune cell environment, we performed flow cytometry studies on pancreatic cell suspensions (gating strategy shown in Supplementary Fig. 7). The proportions of $CD4^+/CD25^+/FoxP3^+$ Tregs and $CD4^+/IL4^+$ Th2 cells were higher in the pancreas of the immunized and BL001-treated RIP-B7.1 mice than in the cognate controls (Fig. 3a, c), whereas $CD4^+$/IFN gamma$^+$ Th1 cells were decreased, and $CD4^+/IL17^+$ Th17 cells were unaffected (Fig. 3b, d). Furthermore, the number of $CD103^+/IDO^+$ tolerogenic dendritic cells, $F4/80^+/CD11b^+$ macrophages, and their M2-like anti-inflammatory subtype ($F4/80^+/CD11b^+/CD206^+$) were also increased in BL001-treated mice (Fig. 3e–g). Accordingly, transcriptome profiling revealed that BL001 significantly increased the expression of key genes associated with the M2 genetic signature, including, *Clec7a* (Dectin-1), *Clec10a* (CD301), *Chst7*, *Tiam1*, *Cd300ld*, and *Olfm1* (Noelin-1 or Pancortin)[21] (Fig. 3h).

BL001 favors a M2 macrophage phenotype via LRH-1. To further delineate the role of BL001 in promoting a M2 macrophage phenotype resulting in increased IL10 secretion, peritoneal macrophages were isolated and treated in vitro with the compound. BL001 dose-dependently increased transcript levels and the secretion of IL10 and TGFbeta (Fig. 4a–d). Exposure to LPS, also enhanced the expression and secretion of IL10, but not of TGF beta by these cells (Fig. 4e–h). To substantiate that BL001-mediated M2 polarization was conveyed by direct LRH-1 activation, the latter receptor was knock down using siRNA. Silencing of LRH-1 transcript and protein levels by ~70% in primary macrophages (Fig. 4i, j), significantly blunted the BL001-mediated increase in expression of the M2 signature genes, *Clec7a*, *Clec10a*, and *Olfm1* as well as *Il10* (Fig. 4k, l, p, q), independent of LPS treatment. Transcript levels of *Chst7*, *Tiam1*, and *Cd300ld* were also repressed, albeit in macrophages either treated or not with LPS (Fig. 4m–o). In contrast, TGFbeta expression was not altered in LRH-1 silenced cells (Fig. 4r). As IL10 biosynthesis and secretion in alternatively activated macrophage has been linked to *Clec7a* stimulation[22,23], secretion levels of this cytokine was next evaluated in LRH-1 knockdown cells. Accordingly, IL10 secretion was decreased in BL001-treated macrophages independent of LPS treatment (Fig. 4s) indicating that LRH-1 is involved in the BL001-dependent polarization and cytokine secretory function of M2 macrophages.

BL001 increases the number of bi-hormonal cells in islets. To assess whether the BL001 treatment favored the survival and replenishment of islet cells, we morphometrically evaluated the mass of beta and alpha cells, as well as islet numbers and sizes. Eight weeks after immunization, all these parameters were increased in the BL001-treated mice (Fig. 5a–d, Supplementary Fig. 8a–c). This increase was not associated to enhanced proliferation or decreased apoptosis of beta cells, as assessed using different methods (Fig. 5e–h, Supplementary Fig. 9a, b). In contrast, the immunized mice, which did not receive BL001, featured higher levels of beta cell proliferation and apoptosis as a result of the ongoing autoimmune attack (Fig. 5e–h). Eight weeks after immunization, the mass of alpha cells was also increased in BL001-treated mice in the absence of enhanced proliferation (Fig. 5c, d, i, j, Supplementary Fig. 9c). At this time point, islets of these mice, also contained increased numbers of cells co-expressing insulin and glucagon, as well as PDX1 and glucagon (Fig. 5k–n and supplementary Fig. 10). Since the data suggest the potential activation of a genetic beta cell program in alpha cells, we investigated whether a 48-h BL001 treatment could suppress the expression of ARX, whose down-regulation triggers beta-to-alpha cell trans-differentiation[24]. Accordingly, a 2-day exposure to BL001 decreased the expression of ARX, glucagon, and MafB transcripts in the alpha cell-derived TC1–6 cell line (Fig. 5o).

BL001 protects human islet from apoptosis improving function. Having validated the proof-of-concept in mice that BL001 protects islets and prevents both chemically and autoimmune-induced diabetes, we next sought to determine whether these beneficial effects were translated to human islets under stress conditions. Ten to twenty μM BL001 did not reveal any cytotoxic effects on islets obtained from normoglycaemic donors (Supplementary Fig. 11a). In the same islets, the expression levels of LRH-1 were also unchanged, whereas that of its target gene *shp* was increased (Supplementary Fig. 11b). However, 10 μM BL001 decreased the apoptosis of islet beta cells, 24 and 72 h after an exposure to either cytokines (Fig. 6a, c) or streptozotocin (Fig. 6b, d). Glucose-stimulated insulin secretion (GSIS) of islets from non diabetic donors (Supplementary Table 1) was not modified by BL001 (Fig. 6e). In contrast, GSIS of islets from type 2 diabetic donors (Supplementary Table 2) was significantly increased after exposure to BL001 (Fig. 6f). Under these conditions, the proportion of apoptotic beta cells was significantly decreased (Fig. 6g,

Fig. 1 BL001 improves islet survival and blunts development of diabetes in three mouse models. **a** Exposure to 10 μM BL001 (BL) for 72 h blocked cytokine-induced apoptosis (CK; 2 ng/ml IL1beta, 28 ng/ml TNFalpha and 833 ng/ml IFNgamma) in mouse islets. Cell death was assessed by ELISA quantification of mono and oligonucleosomes released by apoptotic cells. This blockade was blunted in islets transfected with siRNAs (**d**) which decreased LRH-1 transcript (**b**) and protein levels (LRH1, red; scale bar: 25 μM) (**c**). Data are means + s.e.m. values of six independent experiments using six different islet preparations and performed in triplicates. siSC, pool of siRNAs against scrambled sequence. BL001 (10 mg/kg b.w.) also decreased the incidence of diabetes in C57Bl/6 male mice treated with a single dose of streptozotocin (STZ;150 mg/kg b.w.), irrespective of whether the former drug was given prior to (**e**) or 1 week after (**f**) STZ. Values are means ± s.e.m. of $n = 5$ (STZ)-14 mice (BL/STZ). After these 2 protocols, insulin-containing beta cells (red) and glucagon-containing alpha cells (green) were preserved in islets of STZ and BL001-treated mice (**g**), which also featured an increase number of cells containing both hormones (**h**, arrowheads). Nuclei were stained with DAPI (blue). Scale bars: 25 μM. **i** Quantification of insulin- and glucagon-positive cells. **j** A 5-day BL001 pre-treatment of RIP-B7.1 mice prior to immunization decreased the diabetes incidence. Values are means ± s.e.m. C (vehicle treated, $n = 26$ male and female mice); BL (BL001, $n = 26$ male and female mice); IMN (immunized, $n = 50$ male and female mice), and BL IMN (BL001-treated and immunized, $n = 50$ male and female mice). **k** Immunization increased the proliferation of RIP-B7.1 splenocytes, an effect that was not modified by the BL001 treatment. Values are median (lines in the boxes) ± median errors of 5–12 preparations. **l** The 8-week-long BL001 treatment preserved insulin- (red) and glucagon-containing cells (green) in islets of immunized RIP-B7.1 mice (scale bar: 25 μM). **m**, **n** BL001-treated and immunized RIP-B7.1 mice that developed hyperglycemia contained a higher number of $PDX1^+$ cells as compared to untreated and immunized animals (scale bar: 25 μM). **o** Diabetes incidence of RIP-B7.1 mice that were immunized at days 0 and 7 and subsequently injected daily, starting at week 1 and for up to 8 weeks, with either vehicle (IMN, $n = 38$ male and female mice) or BL001 (BL IMN, $n = 38$ male and female mice). **p** Diabetes incidence in female NOD mice receiving (BL, $n = 8$) or not (C, $n = 14$) BL001 from 12 weeks. *$p < 0.05$, **$p < 0.01$, ***$p < 0.001$, and ****$p < 0.0001$, one-way ANOVA (**a**, **d**, **k**, **i**) or Student's t test (**b**, **n**)

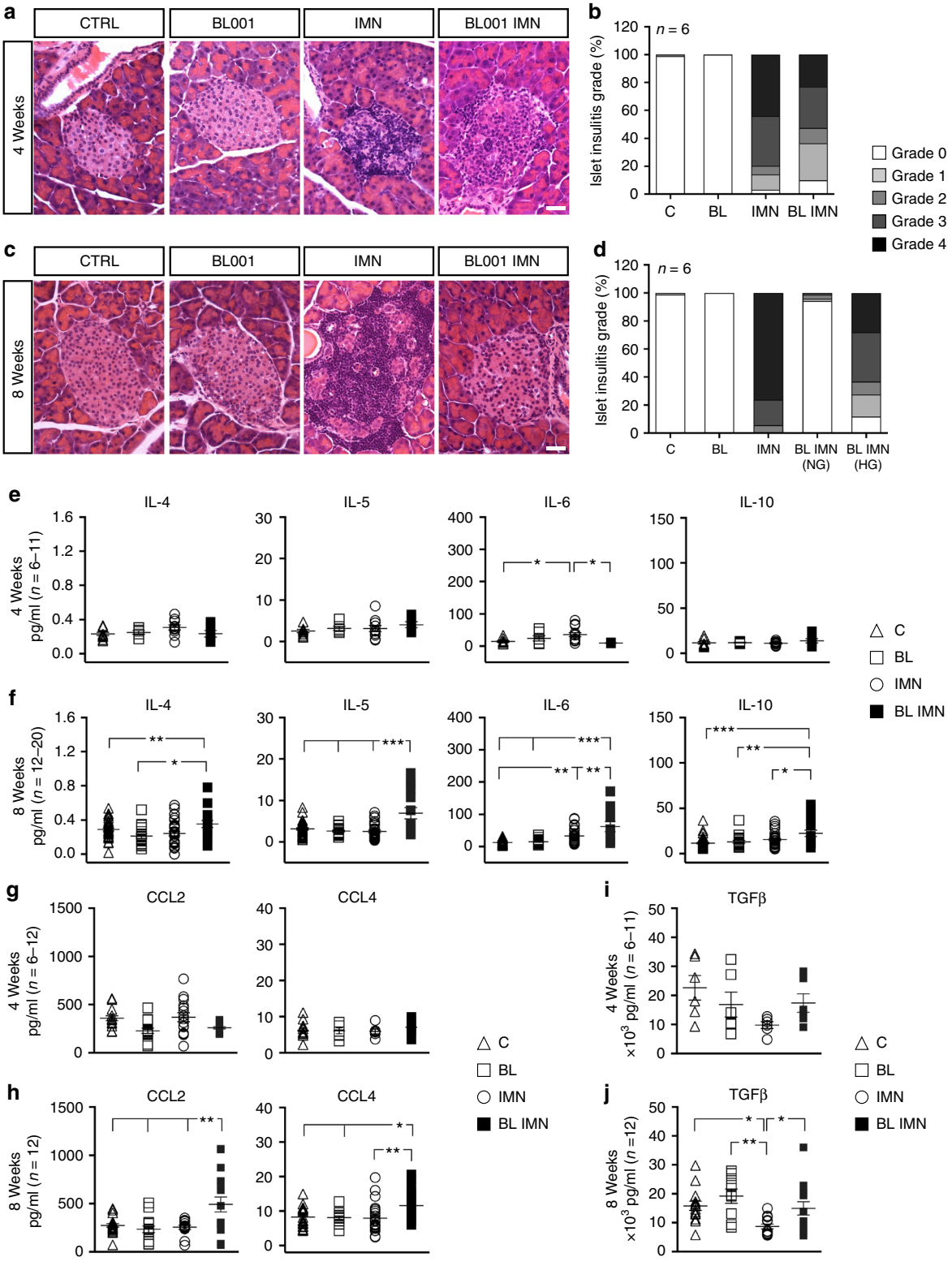

Fig. 2 BL001 decreases insulitis and modulates the blood cytokine profile. Histology (representative images, scale bar: 25 μM) and morphometry at **a**, **b** 4 and **c**, **d** 8 weeks revealed that treatment with 10 mg/kg b.w. BL001 decreased the incidence and severity of insulitis in immunized RIP-B7.1 mice. At 8 weeks, BL001-treated and immunized mice that developed hypeglycemia exhibited a similar degree of insulitis to the BL001-treated and immunized mice that were normoglycemic at 4 weeks. Impact of BL001 treatment on the profile of cytokines, chemokines and TGFbeta at 4 weeks (**e**, **g**, **i**) and 8 weeks (**f**, **h**, **j**). Plots show individual mice values. $^{*}p < 0.05$, $^{**}p < 0.01$, and $^{***}p < 0.001$, one-way ANOVA

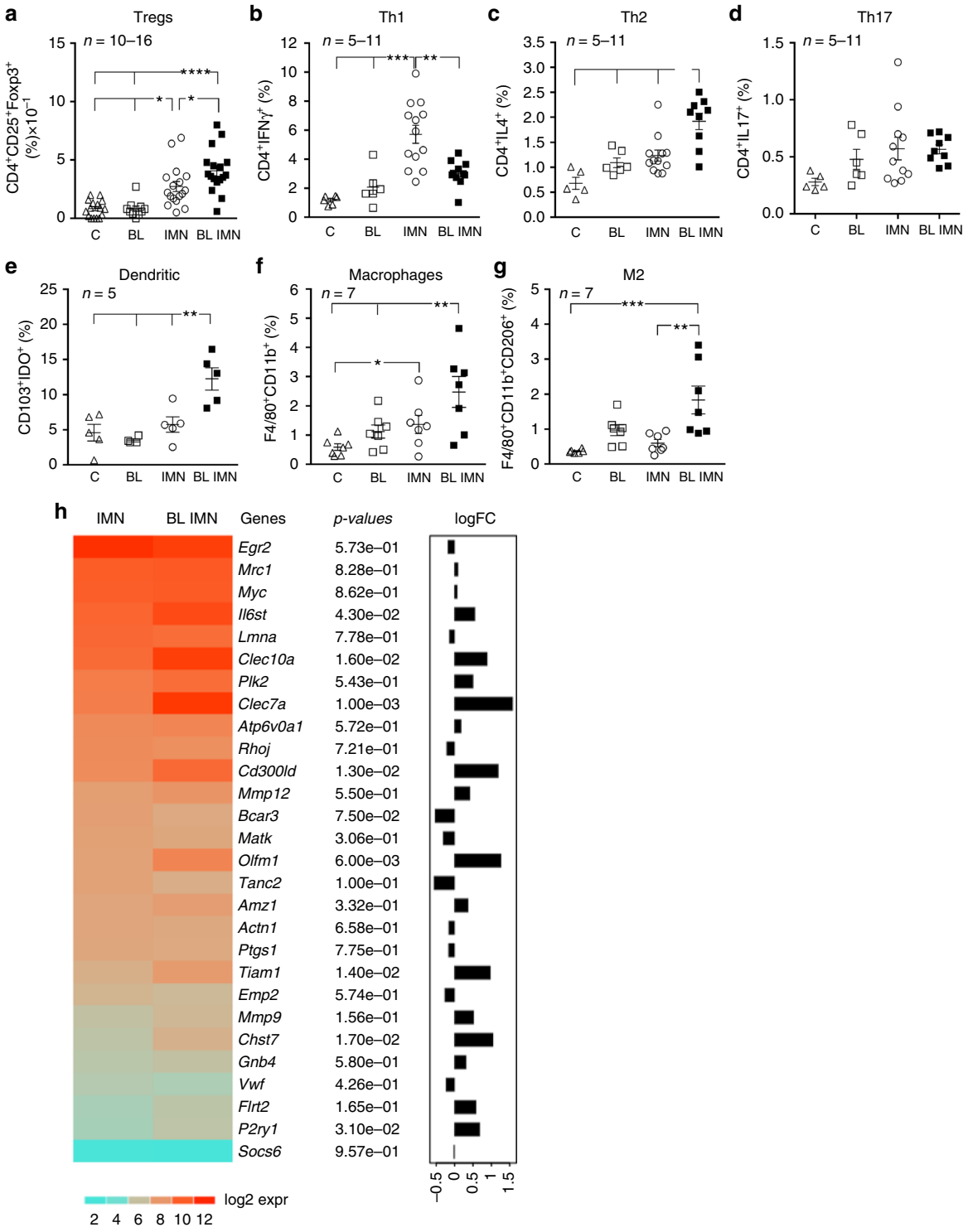

Fig. 3 BL001 promotes a pancreatic anti-inflammatory/tolerogenic environment. RIP-B7.1 male and female mice were pre-treated or not with BL001 for 5 days and then immunized. Treatment with BL001 was pursued for an additional 8 weeks at which point animals were sacrificed and pancreas extracted and processed for flow cytometry quantification of **a** Tregs ($n = 10$–16 mice), **b** Th1 ($n = 5$–11 mice), **c** Th2 ($n = 5$–11 mice), **d** Th17 ($n = 5$–11 mice), **e** dentritic cells ($n = 5$ mice), **f** macrophages ($n = 7$ mice), and **g** M2-like macrophages ($n = 7$ mice). **h** Heatmap displaying expression values of a subset of M2 macrophage genes in F4/80$^+$/CD11b$^+$/CD206$^+$ pancreatic subpopulations isolated from immunized mice treated or nor with BL001 (IMN and IMN BL). Also depicted are raw *p*-values and the graphical representation of logFC from the differential expression analysis (IMN BL versus IMN). *$p < 0.05$, **$p < 0.01$, ***$p < 0.001$, and ****$p < 0.0001$, one-way ANOVA (**a**–**g**)

h) and paralleled by reduced cleaved caspase-3 activity (Fig. 6i, j and Supplementary Fig. 12).

To assess whether comparable effects could be observed during an ongoing, in vivo immune attack, mimicking a T1DM environment, we transplanted human islets under the kidney capsule of immune competent C57BL/6 mice, treated or not with BL001. Two days after xenotransplantation, mice were treated with daily injections of BL001 or vehicle for 7 days. At this time point, rejection of the human islets is anticipated[25,26]. Consistent with the protective effect of BL001, grafts from BL001-treated

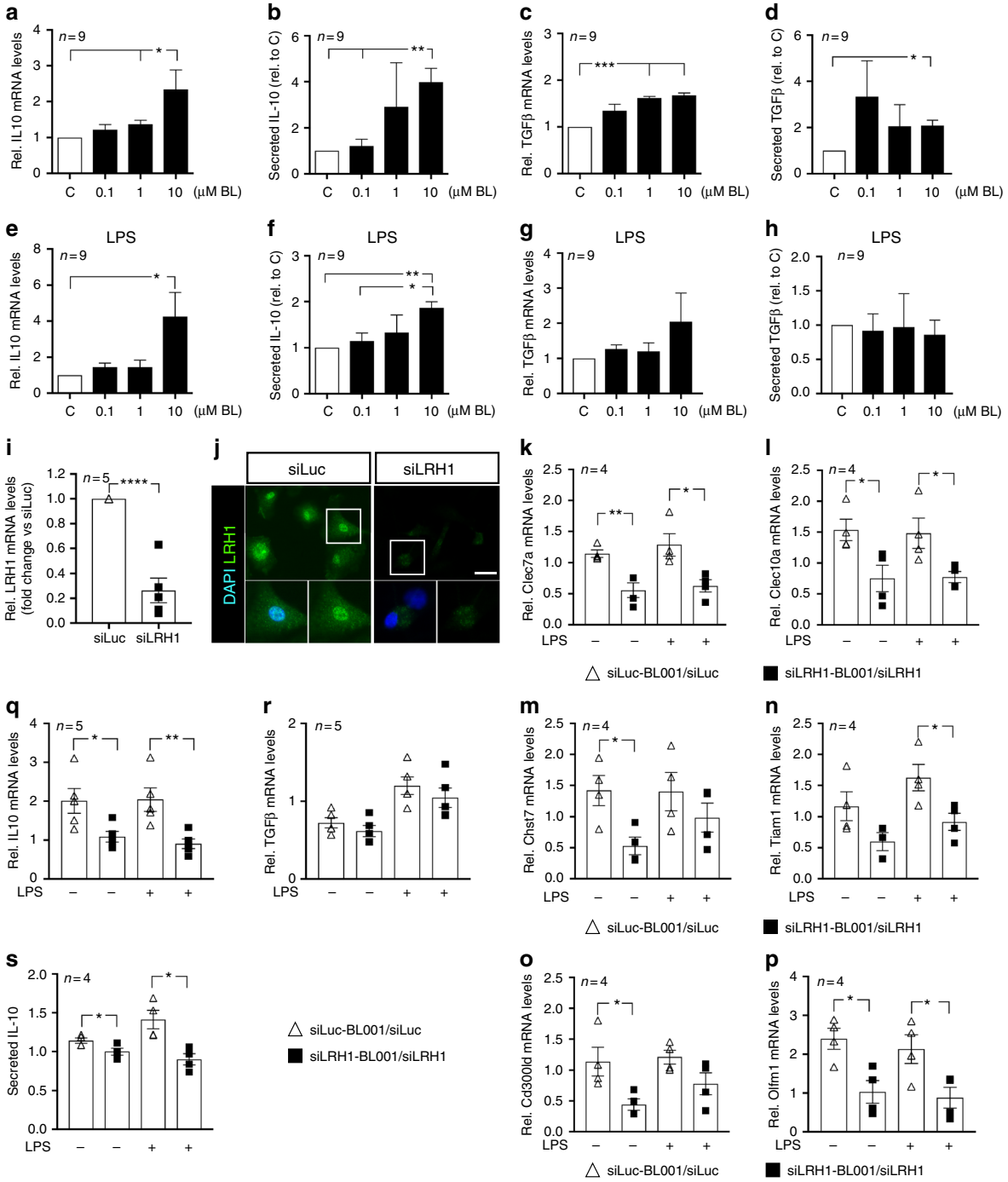

Fig. 4 LRH-1 is required for BL001-mediated M2 polarization. Primary macrophages were exposed in culture to increasing concentration of BL001 for 24 h. Media was collected and RNA isolated to perform QT-PCR. Transcript and secreted levels of **a**, **b** Il10 and **c**, **d** Tgfb were then determined ($n = 9$ mice). **e**–**h** Primary macrophages were incubated for 24 h with increasing concentrations of BL001 alone or in combination with 1.0 μg/ml lipopolysaccharide (LPS). Transcript and secreted levels of **e**, **f** IL10 and **g**, **h** TGFbeta were then measured ($n = 9$ mice). **i** siRNA-mediated repression of LRH-1 transcript and **j** protein levels in mouse primary macrophages as assessed by QT-PCR and immunostaining (LRH-1, green; scale bar: 25 μM). Relative expression levels of M2 signature genes, **k** *Clec7a*, **l** *Clec10a*, **m** *Chst7*, **n** *Tiam1*, **o** *Cd300ld*, and **p** *Olfm1* in control or LRH-1-silenced macrophages treated or not with 10 μM BL001 and LPS ($n = 4$). **q** *Il10* and **r** *Tgfb* transcript levels in siLRH1-treated or not macrophages in the presence or absence of 10 μM BL001 and LPS ($n = 5$). **s** Secreted levels of IL10 in silenced or not macrophages. Results are expressed as the averages + s.e.m. (**a**–**i** and **k**–**s**). *$p < 0.05$, **$p < 0.01$, ***$p < 0.001$, and ****$p < 0.0001$, one-way ANOVA (**a**–**h**) and Student's *t* test (**i**, **k**–**s**)

mice showed greater numbers of beta cells than the controls (Fig. 6k, l).

Immune-related biological processes are targeted by BL001. To evaluate the effects of BL001 on a larger scale, we profiled gene expression via DNA microarray analysis in mouse islets exposed to BL001 for 2 days. We found that 277, 23, and 195 gene ontology (GO) terms were enriched in islets exposed to 0.1, 1.0, and 10 μM BL001, respectively (Fig. 7a). Seven of these GO terms were common to all conditions, whereas no common down-regulated GO terms was found in the same samples (Fig. 7a). The seven enriched GO terms were related to genes involved in

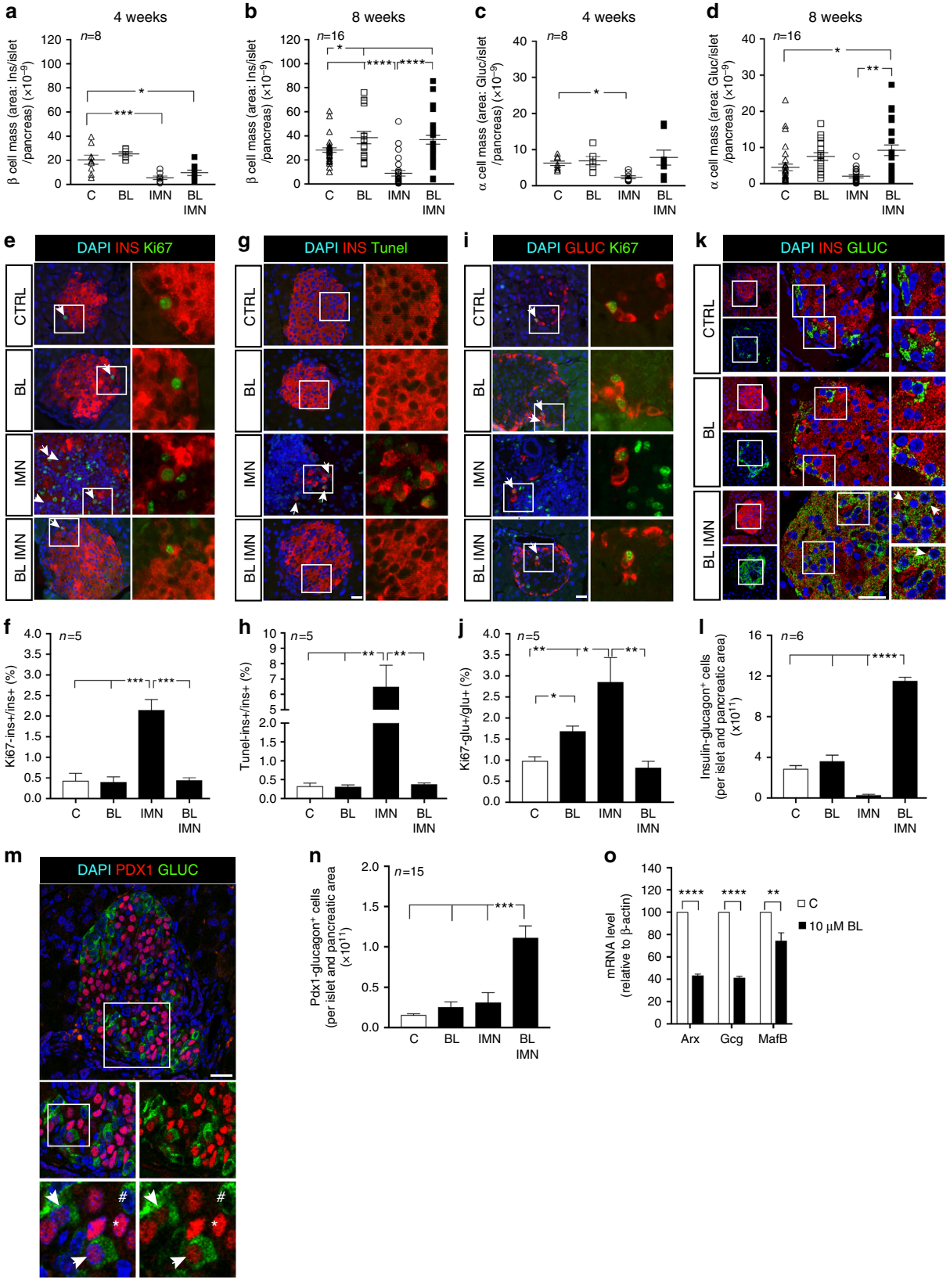

immune functions (Fig. 7b). Heat maps of those genes which were consistently modified, identified 33 genes (Fig. 7c). Those encoding for the CCL2, CCL3, CCL7 chemokines, the cytokine IL6 and the prostaglandin-endoperoxide synthase-2 (PTGS2) were the most induced by the BL001 exposure, whereas the gene coding for the IL1 beta receptor (IL1R1) was the most downregulated (Fig. 7c). Quantitative PCR of these genes, confirmed that the CCL2, CCL3, and PTGS2 transcripts were upregulated by the BL001 exposure (Fig. 7d–f), whereas the IL1R1 transcript was downregulated under the same conditions (Fig. 7g).

Discussion

In spite of major efforts, the available strategies to restore/preserve a functional beta cell mass through immunomodulation and/or beta cell regeneration/replacement treatments have so far shown limited efficacy for the long-term improvement of glycaemia in T1DM patients[27]. This frustrating situation calls for innovative approaches to this complex problem; identify novel "druggable" targets that could promote the regeneration of a functional beta cell mass, while attenuating the autoimmune attack, and preserving the anti-inflammatory locale that appears necessary for beta cell renewal. Here, we show that BL001, a small agonist of the LRH-1 receptor, has such characteristics, which prevent and revert diabetes in three different mouse models of T1DM.

Our data first document that, by activating LRH-1, BL001 primes macrophages toward the anti-inflammatory M2 phenotype (as revealed by the enhanced M2 genetic signature) resulting in direct stimulation of IL10 expression and secretion[23]. BL001-treated mice also featured increased numbers of pancreatic Tregs, whose expansion is induced by IL10[28], and which are essential in maintaining self-immune tolerance including in T1DM[29]. Circulating levels of CCL2 as well as its expression in islets were increased in BL001-treated and immunized RIP-B7.1 mice. Although the impact of CCL2 as a pro or anti-inflammatory chemokine is disease- and cell-dependent[30], our results suggest that in the context of autoimmune diabetes, increased levels of local CCL2 appears to be associated with the recruitment of macrophages to the pancreas which, in turn are further polarized towards the M2-like subtype under the influence of IL10 production. CCL2 through enhanced IL4 production also fosters an environment that favors expansion of Th2[31], a cell type and cytokine that were increased in the pancreas and in the circulation of immunized, BL001-treated RIP-B7.1 mice. Immunized mice treated with BL001 also displayed increased circulating TGFbeta levels correlating with the presence of a larger number of $CD103^+/IDO^+$ dentritic cells, which convey immunosuppressive and tolerogic functions[32,33]. Given that the adoptive transfer of M2 macrophages as well as the upregulation of CCL2 enhance beta cell survival in NOD mice[34,35] and that the autologous transfer of Tregs improves islet survival and function in T1DM patients[36], the immune changes we observed converge to demonstrate that BL001 significantly inhibits the aggressive autoimmune process favoring tolerance, which presumably contributes to its beneficial effects. In this context, BL001-treated and immunized mice that develop diabetes retained islets with a significant number of $PDX1^+$ cells and reduced insulitis at 8 weeks as compared to immunized mice. Although speculative, the latter results indicate that BL001 dosage or activity was suboptimal in favoring an anti-inflammatory and tolerogenic environment resulting in beta cell destruction and hyperglycemia in these animals.

Blood analysis further showed that BL001 increased circulating levels of the IL5 and IL6 cytokines, and of the chemokine CCL4, which have anti-inflammatory actions. IL6 enhances insulin secretion via the release of GLP1 by alpha cells[37,38] while IL5 and CCL4 shift pro-inflammatory Th1 cells towards the anti-inflammatory Th2 subset and stimulate expansion of Tregs[39,40]. Accordingly, we found reduced numbers of Th1 cells but increased numbers of Th2 and Tregs cells in the pancreas of the immunized and BL001-treated mice. In contrast, circulating levels of IFNgamma, TNFalpha, IL1beta and IL2 remained constant suggesting that production of these cytokines were not directly impacted by the compound. BL001 treatment also stimulated the islet expression of PTGS2, an inducible prostaglandin synthase, whose PGE_2 metabolite also inhibits Th1 cells and protects against T1DM[41–43]. In addition, IL6 and the potential secretion of PTGS2-derived PGE_2 by islets along with IL4 and IL10 released by Th2 as well as Tregs, will further contribute to M2 polarization within the pancreas independent of the direct activation of LRH-1 in macrophages by BL001[44–47]. These data highlight that, in addition to a direct sizable action on the immune system, BL001 also promotes the release of pancreatic islet-derived factors favoring an anti-inflammatory environment that will further induce tolerogenecity. Future work will focus on dissecting the mechanism whereby the BL001/LRH-1 signaling pathway achieves these beneficial effects.

Our study further documents that the LRH-1 receptor is essential for the proper organization of pancreatic islets. Thus, the beta cell loss of the LHR-1 receptor modifies the proportion of islet cells characterized by an increase in the number of alpha cells, and the retention of a sizable beta cell mass, which associate with a rapid, post-natal death of transgenic mice. Our parallel experiments also show that BL001-mediated activation of LRH-1 stimulates the regeneration of beta cells, in the islets of both control and diabetic mice, an effect which is not attributable to a change in the proliferation and apoptosis of these

Fig. 5 BL001 promotes beta and alpha cell mass expansion in immunized RIP-B7.1 mice. The control (C) mass of beta (**a**, **b**) and alpha cells (**c**, **d**) of RIP-B7.1 mice was decreased after immunization (IMN), an alteration that was prevented by 10 mg/kg b.w. BL001 daily treatment for 8 weeks (BL IMN). Dot plots show the results from 8 (4 weeks) and 16 (8 weeks) pancreas per group, each dot corresponding to the cell mass of an entire pancreatic section. **e**–**j** Representative immunofluorescence images of islets co-stained and quantified for **e**, **f** insulin (INS, red) and Ki67 (green), **g**, **h** insulin (red) and Tunel (green), **i**, **j** glucagon (GLUC, red) and Ki67 (green). All values are means of 5 mice per group. Scale bars: 25 µM. Right panels are enlargements of boxed area, and arrow heads point to example of cells simultaneously stained for 2 proteins. **k** Representative confocal images showing the distribution of the insulin- (red) and glucagon-bihormonal cells (green) as well as **l** quantification in islets of the different animal groups. Nuclei were stained with DAPI (blue). Scale bar: 25 µM. Right panel show enlargements of boxed areas. Arrow heads point to cells co-stained for the two depicted markers. **m** A representative image depicting co-immunostaining of PDX1 (red) and glucagon (green) in a pancreas of a normoglycemic immunized BL001-treated mouse, and **n** quantification of such cells in the various groups. Bottom left panels are enlargements of boxed area. Bottom right panels, are without DAPI staining. White arrows point to $PDX1^+/GLUC^+$ cells, # identifies a $PDX1^-/GLUC^+$ cell and * highlights a $PDX1^+/GLUC^-$ cell. $n = 15$ pancreatic slices obtained from five independent mice per group. Scale bar: 25 µM. **o** After a 24-h exposure to 10 µM BL001 (BL), alpha TC-1.6 cells featured decreased expression of the Arx, glucagon (Ggc) and MafB transcripts. Six independent experiments were performed and subsequent QT-PCR conducted in triplicates. Values are means + s.e.m. (**f**, **h**, **j**, **l**, **n**, **o**). $^*p < 0.05$, $^{**}p < 0.01$, $^{***}p < 0.001$, and $^{****}p < 0.0001$, one-way ANOVA (**a**–**d**, **f**, **h**, **j**, **l**, **n**) and the Student's *t* test as compared to control (**o**)

cells. The underlying mechanism may or may not directly target beta cells, and remains to be ascertained. A possible explanation may be an alpha-to-beta cell trans-differentiation[48], as suggested by (1) the frequent occurrence of cells containing both insulin and glucagon after the BL001 administration, (2) repression of the alpha genetic program by BL001, and (3) increased alpha cells subsequent to LRH-1 beta cell-specific deletion. However, this possibility still needs to be validated by specific lineage tracing studies. The fact that BL001 and STZ-treated mice displayed fewer bi-hormonal cells suggest that such trans-differentiation may be facilitated by the increase in Tregs and M2 macrophages and/or by IL6 and IL10[49,50]. Antecedents for such immune-regenerative mechanism have been described in salamander and zebrafish[51,52]. Furthermore, Tregs and M2 macrophages are key remodeling players in mouse tissue repair (muscle, bone and vasculature) promoting cell differentiation and expansion[53,54].

In summary, our data define LRH-1 as a novel target for the treatment of diabetes, which can be modulated by BL001. The inhibitory effect of the drug on the immune system, its tolerogenic action and its effects on beta cells survival and regeneration combine to account for the beneficial effects observed in rodent

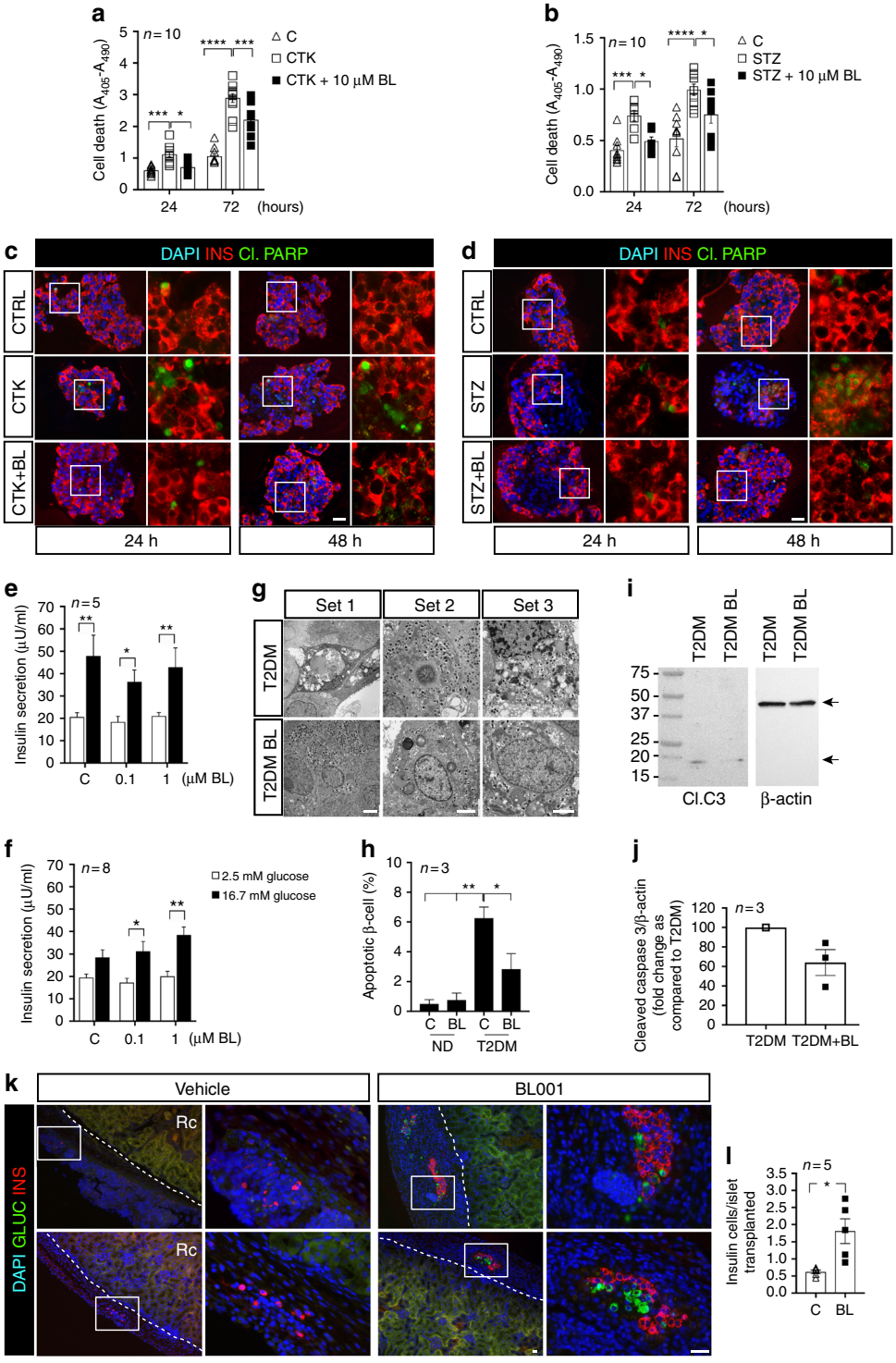

models (Fig. 8). The finding that the drug also decreases beta cell apoptosis in islets from patients with T2DM, and improves their insulin secretion as well as improves beta cell survival in xeno-transplantation, opens the exciting perspective that it could be of value also in the human clinic. In this perspective, the development of new LRH-1 agonists, more stable than BL001 and adapted to oral administration is an urgent need.

Methods

BL001 synthesis and formulation. BL001 [(3a*S*,6a*R*)-1,2,3,3a,6,6a-hexahydro-4-(3-methoxyphenyl)-5-((*E*)-oct4-en-4-yl)-*N*-phenylpentalen-3a-amine] was synthesized by Sreeni Labs Private Limited (India), at a HPLC purity >98%. The semi-solid compound was dissolved in 100% DMSO, at 0.5 mg/ml and 100 µg/ml stock concentrations for in vitro and in vivo studies, respectively. The optimal formulation for in vivo administration (hereafter referred to as vehicle) was: 1% DMSO, 40% WellSolve (Celeste Corporation, Japan) and 59% water. In vitro pharmacology activity assay and ADME-Tox studies were outsourced to Cerep/Eurofins (http://www.cerep.fr); pharmacokinetic studies were performed by GVK Biosciences Pvt. Ltd. (http://www.gvkbio.com/).

Mice. RIP-B7.1[19], LRH-1 Lox/Lox (kindly provided by Dr. K. Schoonjans, EPFL, Switzerland), RIP-Cre[55], C57BL/6 mice (purchased from Janvier Labs, France), and NOD mice (Charles River, Calco Italy) were housed in ventilated plastic cages under a 12-h light/dark cycle, and were given food and water ad libitum. Mice experimentations were approved by the CABIMER Ethics Committee for Animal Experimentation, and performed in accordance with the Spanish law on animal use RD 53/2013. NOD mice studies were carried out in strict accordance with the recommendations in the Guide for the Care and Use of Laboratory Animals of the German Federal Animal Protection Law. Protocols were approved by the Committee on the Ethics of Animal Experiments of the University of Ulm (Tierforschungszentrum Ulm, Oberberghof) and the Regierungspräsidium Tübingen (Permit Numbers: 1199 and 1327 to R.S.). Mice were randomly distributed for all experiments and not subject to blind analysis. Seven- to eight-week-old males and females RIP-B7.1 mice were injected daily i.p. with 10 mg/kg b.w. BL001, starting either 5 days prior to or after immunization. Immunization was achieved by injection of 50 µg preproinsulin (ppINS) expression plasmid (PlasmidFactory GmbH, Germany) into the two anterior tibialis muscles. Mice were euthanized 4 and 8 weeks after immunization, and pancreases and spleens were extracted for immunocytochemistry and proliferation assays, respectively. In addition, 8-week-old male C57BL/6 mice were treated with BL001 for 5 days prior or after an i.p. injection of 150 mg/kg b.w. streptozotocin (STZ) prepared in 0.01 M sodium citrate at pH 4.5. Twelve-week-old female NOD mice were injected daily i.p. with 10 mg/kg b.w. BL001, for up to 25 weeks. Circulating glucose levels were measured from tail vein blood samples using an Optium Xceed glucometer (Abbott Scientifica SA, Barcelona, Spain). Non-fasting blood glucose ≥13.8 mmol/l for two consecutive measurements was considered to indicate overt diabetes. For insulin tolerance tests (ITT), animals were fasted for 5 h, and then i.p. injected with 0.5 U/kg b.w. Actrapid Insulin. Glycemia was measured at 0, 30, 60, 90, and 120 min after this injection. Cytokine levels were assessed in blood and culture media using the mouse V-PLEX ProInflammatory Panel 1 kit 10-Plex (Meso Scale Discovery, Rockville, USA). Detection was performed by electrochemiluminescence technology, and data acquired on a MSD MESO^{TM} QuickPlex SQ120. Blood triglyceride and cholesterol levels were measured using an Accutrend Plus apparatus (Roche Diagnostics, Mannheim, Germany), using the appropriate strips. Temporal MRI scan of mice were acquired using a Bruker BioSpec 9.4 T/20 animal MRI system, equipped with 400 mT/m gradients and a 40 mm quadrature resonator. Images were acquired using a Turbo-RARTE sequence with respiratory gating (TEeff = 24 ms, TR = 1400 ms, Rare Factor = 4, slice thickness = 0.75 mm, in-plane resolution = 78 × 78 µm).

Mouse islet isolation. Mouse islets were isolated by collagenase dissociation, handpicked, and maintained in 11.1 mM glucose/RPMI-1640 (ThermoFisher Scientific, Madrid, Spain) supplemented with 10% fetal bovine serum (FBS; Sigma-Aldrich, Madrid, Spain), 100 U/ml penicillin (Sigma-Aldrich) and 100 mg/ml streptomycin (Sigma-Aldrich)[56].

Human islet isolation, procuration and treatment. Human islets were either obtained from The Cell Isolation and Transplantation Center (Department of Surgery, Geneva; Switzerland) or purchased from Tebu-Bio (Barcelona, Spain). Islets from non-diabetic or T2DM organ donors were obtained in Pisa or purchased from Tebu-Bio (Barcelona, Spain). Signed informed consents were obtained from the families of organ donors. The ethical and investigation committee of the University Hospital of Virgen Macarena and Virgen del Rocio approved all procedures (#2013-04398 to B.R.G.). Human islet preparations were washed, handpicked, and subsequently maintained in CMRL-1066 (ThermoFisher Scientific) containing 5.6 mM glucose, and supplemented with 10% FCS, 100 U/ml penicillin, 100 µg/ml streptomycin, and 100 µg/ml gentamycin (all purchased from Sigma-Aldrich). Human and mouse islets were either untreated or exposed to various concentrations of BL001 for 24–48 h prior to (1) addition of 2 ng/ml IL1beta, 28 ng/ml TNFalpha and 833 ng/ml IFNgamma; (2) addition of 1 mM streptozotocin; (3) assessment of glucose-induced insulin secretion; (4) measurement of apoptosis. In some experiments, LRH1 was repressed in mouse islets and primary peritoneal macrophages by RNA interference. To this end, On-target plus NR5A2 siRNA-smart pool (Dharmacon, cat number L-047044-01) along with either control on-target plus non-targeting pool (Dharmacon, cat number D00181010) for islets or siLuciferase (5′-CGUACGCGGAAUACUUCGA-3′) for macrophages were used in these studies. Fifty nM of siRNAs were pre-mixed with Lipofectamine (ThermoFisher Scientific) and subsequently added to cells for 24 h. Fresh medium was then added and cells cultured under various treatments. Apoptosis was measured at 24 and 72 h using the Roche Cell Death Detection ELISA kit (Roche Diagnostics, Mannheim, Germany). This assay is based in the quantitative sandwich-enzyme immunoassay principle using monoclonal antibodies against DNA and histones, respectively, that allow specific detection of mono- and oligonucleosomes in apoptotic cells. Islet viability was assessed using the MTT assay, according to the manufacturer's recommendations (Roche, Spain). In some instance, protein extracts were prepared from T2DM islets and cleaved-caspase-3 activity was assessed by western blot analysis[57].

Human islet transplantation. Human islet transplantations were performed using a modified protocol from Robertson and Szot[58,59]. Briefly, 10-week-old immunocompetent C57BL/6 male mice were anesthetized by an i.p. injection of 100 mg/kg ketamine and 10 mg/kg xylazine, 150–200 islets were collected without centrifugation in a minimum of medium, and transplanted under the kidney capsule using flame-polished borosilicate glass capillaries (Harvard Apparatus, GC100T-10). Upon termination of the experiment, animals were sacrificed and transplanted kidneys extracted, fixed and embedded for further histology analysis. In order to accurately assess transplant reject/engraftment the entire kidney was sectioned and insulin/glucagon co-immunostaining for was performed at every 15th slice, an interval of ~75–150 µm that corresponds to the median size of the majority of islets.

Cell culture and assays. The mycoplasma-free alpha TC1–6 cell line was purchased from ATCC (CRL-2934; Barcelona), and maintained in DMEM (ThermoFisher Scientific) supplemented with 10% FBS, 15 mM HEPES, 0.1 mM non-essential amino acids, 0.02% BSA, 2 g/l glucose, 1.5 g/l sodium bicarbonate and 5

Fig. 6 BL001 protects human islets against apoptosis and rescues insulin secretion in islets of type 2 diabetic donors. **a** A 24 and 72 h exposure to cytokines (CTK) or **b** streptozotocin (STZ) increased cell death in human islets. This effect was prevented by 10 µM BL001 (BL). $n = 10$ independent islet preparations, performed in either duplicates or triplicates. Double immunostaining for insulin (INS) and cleaved PARP (Cl.PARP) in sections from human isolated islets exposed to either **c** cytokine (CTK) or **d** streptozotocin (STZ) and treated or not with 10 µM BL001 (BL). Scale bars: 25 µM. Right panels of each time point are enlargements of boxed area in left panel. **e** After a 24-h exposure to 0 (C) −1 µM BL001, islets from normoglycemic donors ($n = 5$ independent donors) were similarly stimulated by glucose to release insulin. **f** In contrast 0.1–1 µM BL001 increased glucose-stimulated insulin secretion in islets of type 2 diabetic donors ($n = 8$ independent donors). Data are means + s.e.m. **g** Electron micrographs show apoptotic beta cells in islets of type 2 diabetic donors (T2DM), which were unfrequent when these islets were exposed to 1 µM BL001 (T2DM BL). Scale bars: 2 µM. **h** Quantification shows that the percentage of apoptotic beta cells decreased after exposure to 1 µM BL001, in three independent donors. **i** Western blot of cleaved caspase-3 (Cl.C3) and actin in protein extracts isolated from control (T2DM) and BL001 treated T2DM islets (T2DM BL) along with **j** densitometric analysis. $n = 3$ independent donors. **k** 10-week-old C57BL/6 male mice were transplanted with 150–200 human islets under the kidney capsule. Two days after transplantation, mice were treated daily with BL001 or vehicle for seven days. Kidneys were harvested and processed for immunofluorescence. Two independent representative image sets of kidney sections immunostained with sera against insulin (red) and glucagon (green). DAPI nuclear counterstaining is used. Scale bar: 25 µM. Right panels correspond to the white squares indicated in the left panels. Rc Renal cortex. **l** Quantification of insulin-positive cells in islets transplanted under the kidney capsule. $n = 5$ independent transplantations. $^{*}p < 0.05$, $^{**}p < 0.01$, $^{***}p < 0.001$, and $^{****}p < 0.0001$, two-way ANOVA (**a**, **b**) and Student's *t* test (**e**, **f**, **h**, **j**, **l**)

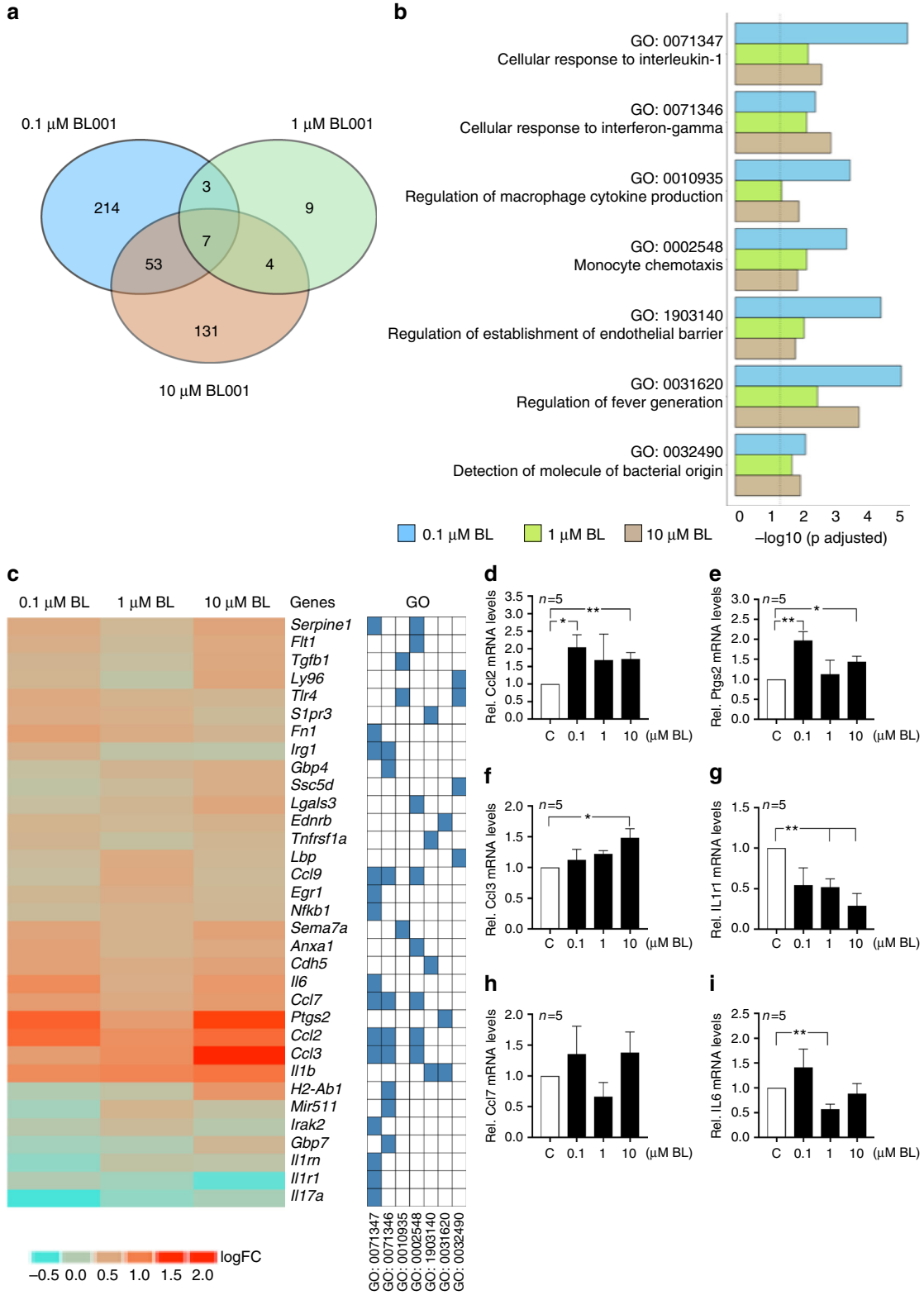

Fig. 7 BL001 potentiates islet genes involved in immunomodulation. Isolated mouse islets were treated with 0.1–10 μM BL001 for 24 h and RNA isolated for DNA microarray analysis ($n = 3$ independent islet preparations per BL001 concentrations). **a** Venn diagram depicting the number of GO terms significantly enriched after three different BL001 treatment. **b** Enrichment plot for the seven GO terms common to all three BL001 concentrations. **c** Heatmaps displaying logFC values of transcripts modulated by BL001, and their association with common GO processes. Blue cells reflect the membership of a gene to a given GO BP term. Validation by QT-PCR of **d** Ccl2, **e** Ptgs2, **f** Ccl3, **g** Il1r1, **h** Ccl7, and **i** Il6 transcript levels in mouse islets treated with BL001. $n = 5$ independent islet preparations. $^{*}p < 0.05$ and $^{**}p < 0.01$, Student's t test versus control untreated (C)

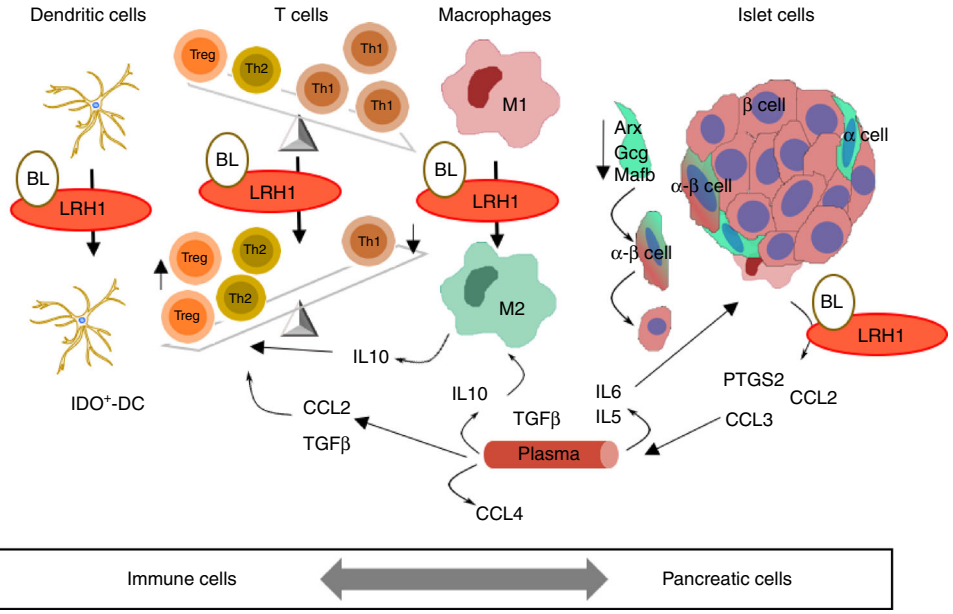

Fig. 8 Proposed model of BL001/LRH-1 cellular action. Schematic view of the effects of BL001 in changing the pancreas pro-inflammatory immune environment toward an anti-inflammatory environment, which promotes beta cell regeneration, possibly through alpha-to-beta cell trans-differentiation

μM beta mercaptoethanol (all purchased from Sigma-Aldrich). The proliferation of splenocytes isolated from mouse spleens was assessed after a 3-day culture in RPMI 1640 medium supplemented with 8% FBS, 20 mM L-glutamine, 1% sodium pyruvate, 1% nonessential amino acids, and 1% penicillin/streptomycin (all from Invitrogen), in the presence or absence of the insulin peptide SLYQLENYCA. Cells were pulsed with [^{3}H]-thymidine for the last 24 h of culture, harvested and lysed onto membranes prior to liquid scintillation counting using a Beckman Coulter LS 6500 counter. Mouse primary macrophages were isolated from the peritoneal cavity, and cultured in DMEM/F12–10 (ThermoFisher Scientific) supplemented with 10% FBS, 2 mM L-glutamine, 100 U/ml penicillin, 100 μg/ml streptomycin (all purchased from Sigma-Aldrich). Cells were stimulated with 1 μg/ml LPS (in DMSO), in the absence or presence of 0.1, 1, or 10 μM BL001 for 24 h. The secretion of cytokines was measured in the culture medium by electrochemiluminescence technology from MesoScale Discovery (Rockville, USA), and RNA was extracted from cells.

Flow cytometry. Subpopulations of T helper cells extracted from mouse pancreas, were characterized by flow cytometry (FACSCalibur, BD Biosciences, Madrid, Spain), using the following antibodies (Supplementary Table 3): FITC-conjugated anti-mouse CD4; Alexa fluor 647-conjugated anti-mouse IL17; Alexa fluor 647-conjugated anti-mouse IL4; PE-Cy7-conjugated anti-mouse IFNgamma. Regulatory T cells were evaluated using FITC-conjugated anti-mouse CD4, in combination with APC-conjugated anti-mouse CD25, and PE-conjugated anti-mouse FoxP3 antibodies. Pancreatic macrophage subpopulations were assessed using Alexa fluor 488 anti-mouse CD45, BV421 anti-mouse CD11b, APC anti-mouse F4/80 and PE anti-mouse CD206. Dendritic cells were evaluated using Alexa fluor 488 anti-mouse CD45, PE anti-mouse CD103 and Alexa fluor 647 anti-IDO. Data were analyzed using FlowJo V9 software (Tree Star). Cell sorting was performed using a FACSAria I (BD).

Immunohistochemistry and electron microscopy. Pancreases and isolated islets were fixed and embedded as previously detailed[56]. Primary and secondary antibodies are listed in Supplementary Table 3. Nuclear counterstaining was performed by DAPI, and sections were mounted using DAKO fluorescent mounting medium. Islet cell apoptosis was measured using a TUNEL assay (In Situ Cell Death Detection Kit, Roche, Madrid, Spain). Images were acquired using either a Leica DM6000B or a Leica TCS SP5 confocal microscope. For the assessment of beta- and alpha-cell mass, images of pancreatic sections were automatically acquired using a software (NIS-Elements imaging)-controlled data acquisition Nikon eclipse Ti-e microscope (Nikon). Morphometric quantification was performed using the Fiji/ImageJ software. Insulitis was scored in paraffin sections of pancreas, stained with H&E. Cells with small nuclei were considered of haematopoietic origin. Insulitis scoring was performed as a grade of 0 to 4 according to percentage of infiltrated islet area (0, 0%; 1<10%; 10%<2>55%; 55%<3>75%; 4>75%). For electron microscopy, pancreatic islets were processed using a standard Spurr protocol[60]. Electron microscopy images were acquired with an EMCCD camera (TRS 2kx2k). The number of non-apoptotic and apoptotic (visualized by blebbing and nuclear condensation) beta cells was counted and the respective percentage of dying cells was expressed as the number of apoptotic cell type over the total number of beta cells.

DNA microarray. Labeled cRNA samples were prepared from pools of at least 100 islets isolated from 8-week-old C57BL/6 female mice, treated or not with increasing concentrations of BL001, and subpopulations of M2-like macrophages (CD45+/F4/80+/CD11b+/CD206+) purified from the pancreas of either vehicle- or BL001-treated and immunized C57BL/6 mice. Three independent preparations of cRNA were prepared per group, and hybridized to the GeneChip Mouse Gene 2.0 ST Array (islets) and to the Clariom S Assay Mouse Array (M2-like macrophages) (Affymetrix, Santa Clara, CA), using standard protocols of the Genomic Core Facility of CABIMER. For each microarray experiment, the Robust Multiarray Analysis (RMA) method was applied on a per-chip basis for background correction[61]. Subsequent normalization across arrays, and summarization were performed using a quantile algorithm and median-polish, respectively[62], via oligo package from Bioconductor (http://www.bioconductor.org). A differential gene expression analysis was then performed using the limma package[63]. Computed p values were corrected using the false discovery rate (FDR) method, to harmonize for the multiple comparisons of all genes[64].

For the islet samples, gene set analysis was performed using the logistic regression model[65], while GO annotation for genes in the microarrays were extracted from Bioconductor GO.db annotation package[66]. Heatmaps of logFC values from differential expression analyses (different concentrations of BL001 versus control) were generated for those genes which were expressed in all groups (raw p-value < 0.05), and associated to the statistically enriched (p-adjusted <0.05) seven GO terms identified at all drug concentrations.

For the M2-like macrophages, a heatmap of log2 expression values of a subset of M2 gene signatures[21], was generated for the CD45$^+$/F4/80$^+$/CD11b$^+$/CD206$^+$ subpopulation isolated from either untreated (IMN) or BL001-treated immunized (IMN BL) mice. LogFC values from differential expression analyses (IMN BL versus IMN) were generated for these genes (raw p-value < 0.05).

RNA isolation and quantitative PCR (QT-PCR). Total RNA was extracted using the RNeasy Micro Kit (Qiagen). Complementary DNA using 0.5 to 1 μg RNA was synthesized using the Superscript II (ThermoFisher Scientific). The RT-PCR was performed on individual cDNAs using SYBR green (Roche)[56]. Primers can be obtained upon request.

Statistical analysis. The Ruth Lenth's power of analysis was applied to the different animal models to ensure that adequate numbers of animals had been studied to detect significant changes. Results are expressed as mean ± s.e.m. (line plots as a function of time) or as mean + s.e.m. (bar graphs). Statistical analysis were performed using the GraphPad Prism software (GraphPad Software, La Jolla, USA). Statistical differences were estimated by one- or two-way ANOVA, with Bonferroni post hoc tests, Student's t test or non-parametric Mann–Whitney test, whichever was appropriate.

Data availability. The Microarray raw data that support the findings of this study have been deposited in the Gene Expression Omnibus repository with the super-series accession number GSE94505 and subseries numbers GSE94505 and GSE104322.

Received: 10 November 2017 Accepted: 23 March 2018
Published online: 16 April 2018

References

1. Pociot, F. & Lernmark, A. Genetic risk factors for type 1 diabetes. *Lancet* **387**, 2331–2339 (2016).
2. Rewers, M. & Ludvigsson, J. Environmental risk factors for type 1 diabetes. *Lancet* **387**, 2340–2348 (2016).
3. Vudattu, N. K. & Herold, K. C. Treatment of new onset type 1 diabetes with teplizumab: successes and pitfalls in development. *Expert. Opin. Biol. Ther.* **14**, 377–385 (2014).
4. Moran, A. et al. Interleukin-1 antagonism in type 1 diabetes of recent onset: two multicentre, randomised, double-blind, placebo-controlled trials. *Lancet* **381**, 1905–1915 (2013).
5. Sherry, N. A. et al. Effects of autoimmunity and immune therapy on beta-cell turnover in type 1 diabetes. *Diabetes* **55**, 3238–3245 (2006).
6. Hajmrle, C. et al. Interleukin-1 signaling contributes to acute islet compensation. *JCI Insight* **1**, e86055 (2016).
7. Godwin, J. W., Pinto, A. R. & Rosenthal, N. A. Chasing the recipe for a pro-regenerative immune system. *Semin. Cell Dev. Biol.* **61**, 71–79 (2016).
8. Fayard, E., Auwerx, J. & Schoonjans, K. LRH-1: an orphan nuclear receptor involved in development, metabolism and steroidogenesis. *Trends Cell. Biol.* **14**, 250–260 (2004).
9. Lee, Y. K. & Moore, D. D. Liver receptor homolog-1, an emerging metabolic modulator. *Front. Biosci.* **13**, 5950–5958 (2008).
10. Venteclef, N., Jakobsson, T., Steffensen, K. R. & Treuter, E. Metabolic nuclear receptor signaling and the inflammatory acute phase response. *Trends Endocrinol. Metab.* **22**, 333–343 (2011).
11. Mamrosh, J. L. et al. Nuclear receptor LRH-1/NR5A2 is required and targetable for liver endoplasmic reticulum stress resolution. *eLife* **3**, e01694 (2014).
12. Fernandez-Marcos, P. J., Auwerx, J. & Schoonjans, K. Emerging actions of the nuclear receptor LRH-1 in the gut. *Biochim. Biophys. Acta* **1812**, 947–955 (2011).
13. Mellado-Gil, J., Cobo-Vuilleumier, N. & Gauthier, B. R. Islet β-cell mass preservation and regeneration in diabetes mellitus: four factors with potential therapeutic interest. *J. Transplant.* **2012**, 230870 (2012).
14. Baquie, M. et al. The liver receptor homolog-1 (LRH-1) is expressed in human islets and protects {beta}-cells against stress-induced apoptosis. *Hum. Mol. Genet.* **20**, 2823–2833 (2011).
15. Ortlund, E. A. et al. Modulation of human nuclear receptor LRH-1 activity by phospholipids and SHP. *Nat. Struct. Mol. Biol.* **12**, 357–363 (2005).
16. Krylova, I. N. et al. Structural analyses reveal phosphatidyl inositols as ligands for the NR5 orphan receptors SF-1 and LRH-1. *Cell* **120**, 343–355 (2005).
17. Lee, J. M. et al. A nuclear-receptor-dependent phosphatidylcholine pathway with antidiabetic effects. *Nature* **474**, 506–510 (2011).
18. Whitby, R. J. et al. Identification of small molecule agonists of the orphan nuclear receptors liver receptor homolog-1 and steroidogenic factor-1. *J. Med. Chem.* **49**, 6652–6655 (2006).
19. Mellado-Gil, J. M. et al. PAX4 preserves endoplasmic reticulum integrity preventing beta cell degeneration in a mouse model of type 1 diabetes mellitus. *Diabetologia* **59**, 755–765 (2016).
20. Mauvais-Jarvis, F., Arnold, A. P. & Reue, K. A guide for the design of pre-clinical studies on sex differences in metabolism. *Cell. Metab.* **25**, 1216–1230 (2017).
21. Jablonski, K. A. et al. Novel markers to delineate murine M1 and M2 macrophages. *PLoS ONE* **10**, e0145342 (2015).
22. Goodridge, H. S., Simmons, R. M. & Underhill, D. M. Dectin-1 stimulation by *Candida albicans* yeast or zymosan triggers NFAT activation in macrophages and dendritic cells. *J. Immunol.* **178**, 3107–3115 (2007).
23. Lefevre, L. et al. LRH-1 mediates anti-inflammatory and antifungal phenotype of IL-13-activated macrophages through the PPARgamma ligand synthesis. *Nat. Commun.* **6**, 6801 (2015).
24. Courtney, M. et al. The inactivation of Arx in pancreatic alpha-cells triggers their neogenesis and conversion into functional beta-like cells. *PLoS Genet.* **9**, e1003934 (2013).
25. Brandhorst, D., Brandhorst, H., Maataoui, V., Maataoui, A. & Johnson, P. R. Anti-caspase-3 preconditioning increases proinsulin secretion and deteriorates posttransplant function of isolated human islets. *Apoptosis* **18**, 681–688 (2013).
26. Qi, M. et al. Survival of human islets in microbeads containing high guluronic acid alginate crosslinked with Ca2+ and Ba2+. *Xenotransplantation* **19**, 355–364 (2012).
27. Ludvigsson, J. Therapies to preserve beta-cell function in type 1 diabetes. *Drugs* **76**, 169–185 (2016).
28. Schmidt, A. et al. Human macrophages induce CD4(+)Foxp3(+) regulatory T cells via binding and re-release of TGF-beta. *Immunol. Cell. Biol.* **94**, 747–762 (2016).
29. Salomon, B. et al. B7/CD28 costimulation is essential for the homeostasis of the CD4 + CD25 + immunoregulatory T cells that control autoimmune diabetes. *Immunity* **12**, 431–440 (2000).
30. Luther, S. A. & Cyster, J. G. Chemokines as regulators of T cell differentiation. *Nat. Immunol.* **2**, 102–107 (2001).
31. Gu, L. et al. Control of TH2 polarization by the chemokine monocyte chemoattractant protein-1. *Nature* **404**, 407–411 (2000).
32. Pallotta, M. T. et al. Indoleamine 2,3-dioxygenase is a signaling protein in long-term tolerance by dendritic cells. *Nat. Immunol.* **12**, 870–878 (2011).
33. Grohmann, U. et al. A defect in tryptophan catabolism impairs tolerance in nonobese diabetic mice. *J. Exp. Med.* **198**, 153–160 (2003).
34. Parsa, R. et al. Adoptive transfer of immunomodulatory M2 macrophages prevents type 1 diabetes in NOD mice. *Diabetes* **61**, 2881–2892 (2012).
35. Takada, Y. et al. Monocyte chemoattractant protein-1 contributes to gut homeostasis and intestinal inflammation by composition of IL-10-producing regulatory macrophage subset. *J. Immunol.* **184**, 2671–2676 (2010).
36. Marek-Trzonkowska, N. et al. Therapy of type 1 diabetes with CD4(+)CD25 (high)CD127-regulatory T cells prolongs survival of pancreatic islets—results of one year follow-up. *Clin. Immunol.* **153**, 23–30 (2014).
37. Ellingsgaard, H. et al. Interleukin-6 enhances insulin secretion by increasing glucagon-like peptide-1 secretion from L cells and alpha cells. *Nat. Med.* **17**, 1481–1489 (2011).
38. Yusta, B. et al. GLP-1 receptor activation improves beta cell function and survival following induction of endoplasmic reticulum stress. *Cell Metab.* **4**, 391–406 (2006).
39. Tran, G. T. et al. IL-5 promotes induction of antigen-specific CD4+ CD25+ T regulatory cells that suppress autoimmunity. *Blood* **119**, 4441–4450 (2012).
40. Meagher, C. et al. CCL4 protects from type 1 diabetes by altering islet beta-cell-targeted inflammatory responses. *Diabetes* **56**, 809–817 (2007).
41. Chan, M. M. & Moore, A. R. Resolution of inflammation in murine autoimmune arthritis is disrupted by cyclooxygenase-2 inhibition and restored by prostaglandin E2-mediated lipoxin A4 production. *J. Immunol.* **184**, 6418–6426 (2010).
42. Oikawa, Y. et al. Protective role for cytosolic phospholipase A2alpha in autoimmune diabetes of mice. *FEBS Lett.* **579**, 3975–3978 (2005).
43. Vennemann, A. et al. PTGS-2-PTGER2/4 signaling pathway partially protects from diabetogenic toxicity of streptozotocin in mice. *Diabetes* **61**, 1879–1887 (2012).
44. Gordon, S. & Martinez, F. O. Alternative activation of macrophages: mechanism and functions. *Immunity* **32**, 593–604 (2010).
45. Luan, B. et al. CREB pathway links PGE2 signaling with macrophage polarization. *Proc. Natl Acad. Sci. USA* **112**, 15642–15647 (2015).
46. Sanmarco, L. M. et al. IL-6 promotes M2 macrophage polarization by modulating purinergic signaling and regulates the lethal release of nitric oxide during Trypanosoma cruzi infection. *Biochim. Biophys. Acta* **1863**, 857–869 (2017).
47. Roncarolo, M. G. et al. Interleukin-10-secreting type 1 regulatory T cells in rodents and humans. *Immunol. Rev.* **212**, 28–50 (2006).
48. Thorel, F. et al. Conversion of adult pancreatic alpha-cells to beta-cells after extreme beta-cell loss. *Nature* **464**, 1149–1154 (2010).
49. Riley, K. G. et al. Macrophages are essential for CTGF-mediated adult beta-cell proliferation after injury. *Mol. Metab.* **4**, 584–591 (2015).
50. Dirice, E. et al. Soluble factors secreted by T cells promote beta-cell proliferation. *Diabetes* **63**, 188–202 (2014).
51. Godwin, J. W., Pinto, A. R. & Rosenthal, N. A. Macrophages are required for adult salamander limb regeneration. *Proc. Natl Acad. Sci. USA* **110**, 9415–9420 (2013).
52. Li, L., Yan, B., Shi, Y. Q., Zhang, W. Q. & Wen, Z. L. Live imaging reveals differing roles of macrophages and neutrophils during zebrafish tail fin regeneration. *J. Biol. Chem.* **287**, 25353–25360 (2012).
53. Ogle, M. E., Segar, C. E., Sridhar, S. & Botchwey, E. A. Monocytes and macrophages in tissue repair: Implications for immunoregenerative biomaterial design. *Exp. Biol. Med.* **241**, 1084–1097 (2016).
54. Schiaffino, S., Pereira, M. G., Ciciliot, S. & Rovere-Querini, P. Regulatory T cells and skeletal muscle regeneration. *FEBS J.* **284**, 517–524 (2016).
55. Hu, He. K. H. et al. In vivo conditional Pax4 overexpression in mature Islet beta cells prevents stress-induced hyperglycemia in mice. *Diabetes* **60**, 1705–1715 (2011).
56. Lorenzo, P. I. et al. PAX4 defines an expandable beta-cell subpopulation in the adult pancreatic islet. *Sci. Rep.* **5**, 15672 (2015).

57. Lopez-Noriega, L. et al. Levothyroxine enhances glucose clearance and blunts the onset of experimental type 1 diabetes mellitus in mice. *Br. J. Pharmacol.* **174**, 3795–3810 (2017).
58. Robertson, N. J., Fairchild, P. J. & Waldmann, H. Ectopic transplantation of tissues under the kidney capsule. *Methods Mol. Biol.* **380**, 347–353 (2007).
59. Szot, G. L., Koudria, P. & Bluestone, J. A. Murine pancreatic islet transplant. *J. Vis. Exp.* **7**, e255 (2007).
60. Spurr, A. R. A low-viscosity epoxy resin embedding medium for electron microscopy. *J. Ultrastruct. Res.* **26**, 31–43 (1969).
61. Irizarry, R. A. et al. Exploration, normalization, and summaries of high density oligonucleotide array probe level data. *Biostatistics* **4**, 249–264 (2003).
62. Carvalho, B. S. & Irizarry, R. A. A framework for oligonucleotide microarray preprocessing. *Bioinformatics* **26**, 2363–2367 (2010).
63. Smyth, G. K. Linear models and empirical bayes methods for assessing differential expression in microarray experiments. *Stat. Appl. Genet. Mol. Biol.* **3**, Article3 (2004).
64. Benjamini, Y. & Hochberg, Y. Controlling the false discovery rate: a practical and powerful approach to multiple testing. *J. Roy. Stat. Soc. Ser. B* **57**, 289–300 (1995).
65. Montaner, D. & Dopazo, J. Multidimensional gene set analysis of genomic data. *PLoS ONE* **5**, e10348 (2010).
66. Carlson, M. G. O. db: a set of annotation maps describing the entire Gene Ontology. Bioconductor https://bioconductor.org/packages/release/data/annotation/html/GO.db.html (2017).

Acknowledgements

We thank Maria Torres, Evie Egelmeers, and Daniel Parras Molina for excellent technical assistance as well as Drs. Maria José Quintero, Paloma Dominguez, Marta Cejudo Guillén, and Soledad López Enriquez for analysis support. This work was funded by grants from the Juvenile Diabetes Research Foundation (17-2013-372 to B.R.G.), the Consejeria de Salud, Fundacion Publica Andaluza Progreso y Salud, Junta de Andalucia (PI-0727-2010 to B.R.G. and P10CTS6505 to B.S.), Consejeria de Economia, Innovacion y Ciencia (P10.CTS.6359 to B.R.G.), the Ministerio de Economia y Competidividad co-funded by Fondos FEDER (PI10/00871, PI13/00593, and BFU2017-83588-P to B.R.G.; PI14/01015, RD12/0019/0028, and RD16/0011/0034 to B.S.; PI16/00259 to A. H.) and Deutsche Forschungsgemeinschaft (GRK-1789 ´CEMMA´ and DFG SCHI-505/6-1 to R.S.). Special thanks to the families of the DiabetesCero Foundation that graciously supported this work (to B.R.G.). A.M.M. is a recipient of a Miguel Servet grant (CP14/00105) from the Instituto de Salud Carlos III co-funded by Fondos FEDER whereas E.F. M. is a recipient of a Juan de la Cierva Fellowship. I.G.H.G. is supported by a fellowship from Amarna Therapeutics. In some instances, human islets were procured through the European Consortium for Islet Transplantation funded by Juvenile Diabetes Research Foundation (3-RSC-2016-162-I-X).

Author contributions

N.C.V. and B.R.G. conceptualized the study. N.C.V., B.R.G., and P.M. wrote the manuscript. N.C.V., P.I.L., P.M., L.S.P., L.S.O., F.J.B.S., and B.R.G. designed the study and analyzed the data. N.G.R., I.G.H.G., E.F.M., L.L.N., S.Y.R.Z., M.B., C.C.L., K.S., M.B., D. B., G.P., D.P., M.G.T, V.dT., R.S., G.P., L.S.P., P.dH., A.H., J.M.M.G., B.S., and A.M.M. were involved in the acquisition and analysis of data. K.Sc. supplied transgenic mice. Bioinformatics analysis was performed by J.P.F. All authors critically reviewed the manuscript for important intellectual content and approved the final version to be published. B.R.G. is the guarantor of this work.

Additional information

Supplementary Information accompanies this paper at https://doi.org/10.1038/s41467-018-03943-0.

Competing interests: Two patents (WO 2011 144725 A2 and WO 2016 156531 A1) related to BL001 have been published, of which B.R.G., N.C.V., D.P., L.S.O., and M.B. are inventors. These patents have been licensed to ARIDDAD Therapeutics, a Biotech spinoff co-founded by B.R.G., N.C.V., L.St.-O., and P.dH. The remaining authors declare no competing interests.

Reprints and permission information is available online at http://npg.nature.com/reprintsandpermissions/

Publisher's note: Springer Nature remains neutral with regard to jurisdictional claims in published maps and institutional affiliations.